IN VITRO CHROMATIN RECONSTITUTION AS A TOOL TO STUDY H2A.V AND THE DNA DAMAGE RESPONSE

DISSERTATION

ZUM ERWERB DES DOKTORGRADES DER NATURWISSENSCHAFTEN AN DER

MEDIZINISCHEN FAKULTÄT DER LUDWIG-MAXIMILIANS-UNIVERSITÄT ZU MÜNCHEN

vorgelegt von Lisa Harpprecht aus Reutlingen

2018

Aus dem Adolf-Butenandt-Institut, Lehrstuhl: Molekularbiologie

Im Biomedizinischen Centrum der Ludwig-Maximilians-Universität München

Vorstand: Prof. Dr. rer. nat. Peter B. Becker

Mit Genehmigung der Medizinischen Fakultät der Universität München

Betreuer: Prof. Dr. Peter B. Becker

Zweitgutachter: Priv. Doz. Dr. Anna A. Friedl

Dekan: Prof. Dr. med. dent. Reinhard Hickel

Tag der mündlichen Prüfung: 19.12.2018

EIDESSTATTLICHE VERSICHERUNG

Harpprecht, Lisa

Ich erkläre hiermit an Eides statt, dass ich die vorliegende Dissertation mit dem Thema

IN VITRO CHROMATIN RECONSTITUTION AS A TOOL TO STUDY H2A.V AND THE DNA DAMAGE RESPONSE

selbständig verfasst, mich außer der angegebenen keiner weiteren Hilfsmittel bedient und alle Erkenntnisse, die aus dem Schrifttum ganz oder annähernd übernommen sind, als solche kenntlich gemacht und nach ihrer Herkunft unter Bezeichnung der Fundstelle einzeln nachgewiesen habe.

Ich erkläre des Weiteren, dass die hier vorgelegte Dissertation nicht in gleicher oder in ähnlicher Form bei einer anderen Stelle zur Erlangung eines akademischen Grades eingereicht wurde.

Planegg, den 09.01.2018 — Lisa Harpprecht

_____ _____

Ort, Datum — Unterschrift Doktorandin/Doktorand

Eidesstattliche Versicherung Stand: 31.01.2013

TABLE OF CONTENTS

I. SUMMARY

To protect genome integrity, the cell needs to respond to DNA damage instantly. However, investigations of these events are not straightforward, as damage has to be induced in a locus- and time-resolved manner to study subsequent changes around the damage site.

In addition to this, DNA damage factors often play major roles in cell cycle regulation. Hence, the possibilities to study function of DNA damage factors in mutant backgrounds is often limited to the viability of the mutant organism.

To dissect damage-associated processes in the context of chromatin, I applied an *in vitro* system, where chromatin was reconstituted by *Drosophila* embryo extract and DNA double strand breaks were simulated by free DNA ends of recombinant DNA fragments. This system allows the purification of chromatin for detailed analysis by mass spectrometry and Western blot analysis after distinct time points by immobilization to paramagnetic beads. Furthermore, reconstitution of chromatin with defined properties, including nucleosomes with histone variant or mutant histones could be used to better understand the DNA damage response. In addition to this, the biochemical analysis allowed to modify reaction conditions, for example by omitting ATP.

I demonstrated that *Drosophila* embryo extract is able to mount a DNA damage response with endogenous factors. This DNA damage response is characterized by the recruitment of DNA damage-associated factors like the Ku and RPA complexes and phosphorylation of the histone variant H2A.V (γH2A.V) at its H2A.X-like C-terminal motif. This phosphorylation mark has been shown to spread along DNA including free DNA ends.

I was able to dissect this spreading event and showed that phosphorylation of H2A.V initiated very rapidly and spread over long distances in *cis*. However, H2A.V phosphorylation did not spread in *trans* to circular DNA molecules, unless DNA-DNA bridging proteins were added. In these cases, spreading of H2A.V to circular DNA fragments was observed. Furthermore, phosphorylation of H2A.V was not initiated by nucleosomes including the phospho-mimic form of H2A.V in the absence of DNA damage.

I furthermore showed that the recruitment of Ku is independent from the phosphorylation of H2A.V, or even the presence of H2A.V in general.

In addition to this, I applied the *in vitro* system to investigate the role of the chromatin remodeling complex ACF in the incorporation and turnover processes of H2A.V and to address the role of ACF in the DNA damage response.

To summarize, this study established a cell-free system that can be used to study the DNA damage response of *Drosophila* at a mechanistic level and demonstrated its potential by monitoring the spreading of the damage-associated γH2A.V mark along extended chromatin regions.

II. ZUSAMMENFASSUNG

Um ihre Genomintegrität zu schützen, muss die Zelle umgehend auf Zellschäden reagieren. Die Analyse dieser Prozesse ist jedoch nicht trivial, da dazu ein zeitlich und räumlich definierter DNA-Bruch induziert werden muss, um die darauffolgenden Prozesse am Bruch zu erfassen.

Außerdem haben DNA-Reparaturfaktoren häufig wichtige Funktionen in der Regulation des Zellzyklus. Darum sind die Möglichkeiten zur Analyse derer Funktionen durch die Überlebensfähigkeit der Mutanten limitiert.

Zur Erforschung der Vorgänge nach Induzieren des DNA-Bruchs habe ich ein *in vitro*-System verwendet, in welchem Chromatin mithilfe eines *Drosophila* Embryonen-Extrakts assembliert und DNA-Brüche durch freie DNA-Enden simuliert werden. Durch Immobilisieren der DNA an paramagnetische Partikeln wird eine Aufreinigung des Chromatins für differenzierte Analysen bestimmter Zeitpunkte mithilfe von Massenspektrometrie oder Western Blots ermöglicht. Außerdem ermöglicht das System die Herstellung von Chromatin mit definierten Eigenschaften, zum Beispiel aus Nukleosomen mit Histon-Varianten oder -Mutanten, um Vorgänge nach Erkennen eines DNA-Schadens besser zu verstehen. Schließlich ermöglicht diese biochemische Analyse die Modifikation von Reaktionsbedingungen, etwa durch den Verzicht von ATP.

Ich konnte zeigen, dass *Drosophila* Embryonen-Extrakt mithilfe endogener Faktoren eine Antwort auf DNA-Schäden initiieren kann. Diese Reaktion zeichnet sich durch die Rekrutierung von DNA-Schaden-assoziierten Faktoren aus, wie den Ku- und den RPA-Komplex, und durch die Phosphorylierung der Histon-Variante H2A.V (γH2A.V) an ihrem H2A-X-ähnlichen C-terminalen Motiv. Diese Phosphorylierung wandert entlang der DNA, welche freie DNA-Enden beinhaltet.

Zudem konnte ich den Ausbreitungsprozess der Phosphorylierung aufgliedern und zeigen, dass die Phosphorylierung rapide initiiert wird und sich in *cis* über lange Distanzen ausbreitet. Diese Ausbreitung erfolgte jedoch nicht in *trans*, solange keine DNA-DNA-verknüpfenden Proteine zugegeben wurden. Diese konnten dann eine Ausbreitung der Phosphorylierung auf zirkuläre DNA-Fragmente ermöglichen. Des Weiteren wurde in Abwesenheit von DNA-Brüchen keine Phosphorylierung durch Nukleosome initiiert, welche eine Phospho-Mimik-Mutante besaßen.

Schließlich konnte ich demonstrieren, dass die Rekrutierung von Ku unabhängig von der H2A.V-Phosphorylierung, und von H2A.V selbst stattfindet.

So konnte ich schließlich das *in vitro*-System zur Untersuchung der Rolle des Chromatin-Remodeling-Komplexes ACF im Einbau und Umbau von H2A.V und in der Antwort auf DNA-Schäden verwenden.

Zusammenfassend wurde mit dieser Studie ein zellfreies System etabliert, welches zur Analyse der Antwort auf DNA-Schäden in *Drosophila* auf mechanistischer Ebene verwendet werden kann und welches sein Potential zur Veranschaulichung der DNA-Bruch-abhängigen Phosphorylierungs-Ausbreitung entlang der DNA beweisen konnte.

III. INTRODUCTION

A. CHROMATIN

1. THE COMPOSITION OF CHROMATIN

The human genome consists of $3.2*10^9$ base pairs resulting in about 2 m double-stranded DNA, which needs to be packed and organized in the nucleosome of about 6 µm diameter in size (Alberts 2017). The first level of organization is achieved by nucleosomes, which are repetitive building blocks composed of histone octamers with 147 bp of DNA wrapped around in a left-handed helical turn (Kornberg 1974), forming a so-called beads-on-a-string-structure (P. Zhu & G. Li 2016; Cutter & Hayes 2015; Khorasanizadeh 2004; Luger et al. 2012). The octamer, in turn, is comprised of a tetramer with two histones H3 and H4 and two associated dimers of histones H2A and H2B (Luger et al. 1997). On top of this, the beads-on-a-string-structure is organized into chromatin loops and tertiary structures (Dixon et al. 2016; Hansen et al. 2018). According to the current state of knowledge, DNA loops are often formed to regulate the expression of chromatin and are mediated by cohesin, which brings together different regions on the genome (reviewed in Hansen et al. 2018). Chromatin structure is not only regulated by the histones forming the nucleosome, but also by high-mobility group proteins, which can bind and modify specific DNA structures and thereby affect transcription (Reeves 2015). Finally, chromatin structure is also regulated by long non-coding RNA, which has been shown to be able to act on nucleosome positioning and loop formation (reviewed in Böhmdorfer & Wierzbicki 2015). Chromatin fibers are organized into chromosomes (reviewed in Gilbert et al. 2005). A simplified illustration of chromatin composition is shown in Figure 1.

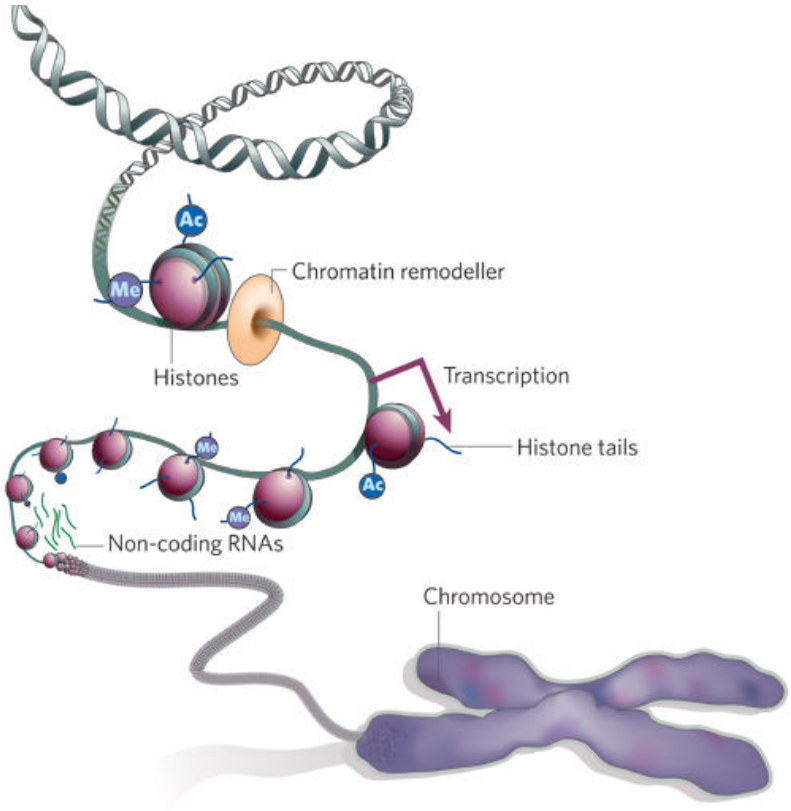

FIGURE 1: CHROMATIN IS COMPOSED OF DNA WRAPPED AROUND HISTONES AND OTHER ASSOCIATED NON-HISTONE PROTEINS LIKE CHROMATIN REMODELERS AND OTHER COMPONENTS LIKE NON-CODING RNA (FIGURE ADAPTED FROM AMERICAN ASSOCIATION FOR CANCER RESEARCH HUMAN EPIGENOME TASK FORCEEUROPEAN UNION, NETWORK OF EXCELLENCE, SCIENTIFIC ADVISORY BOARD 2008).

2. CHROMATIN ORGANIZATION

Binding of chromatin components is highly regulated and results in the formation of chromatin domains, which are characterized by the abundance of histone modifications, structural proteins, enzymes, and non-coding RNA, which determine the functional state of this chromatin domain. According to this observation, five chromatin states have been described: Blue and black chromatin states have been described as transcriptionally inactive, with black as repressed "void" chromatin, and blue as Polycomb Group Protein (PcG)-regulated chromatin. PcG proteins in turn are essential during the development of *Drosophila* to keep developmental genes in a repressed state in tissues where they should not be expressed (reviewed in Schuettengruber et al. 2017; Dorafshan et al. 2017; Kassis et al. 2017).

Red and yellow were described as highly transcribed, but differently regulated chromatin, and green as HP1-bound chromatin (Filion, van Bemmel, Braunschweig, Talhout, Kind, L. D. Ward, Brugman, de Castro, Kerkhoven, Bussemaker & van Steensel 2010). The chromosome is organized in topologically associated domains (TADs), resulting in the formation of regulatory units of chromatin domains composed of similar chromatin components (Figure 2).

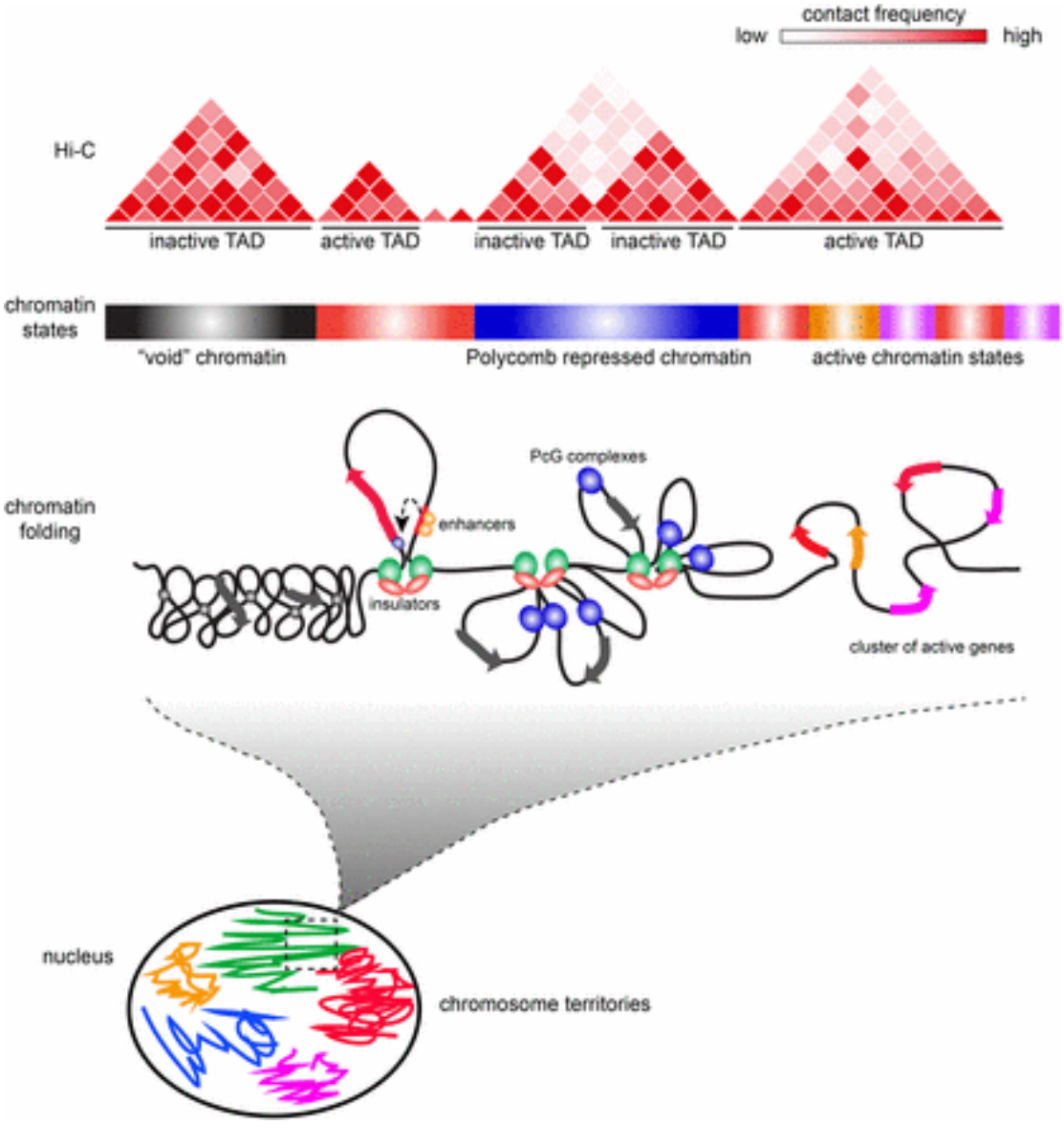

FIGURE 2: ORGANIZATION OF CHROMATIN INTO TOPOLOGICALLY ASSOCIATED DOMAINS (TADS) (FIGURE ADAPTED FROM SCHWARTZ & CAVALLI 2017). CHROMATIN REGIONS ARE CHARACTERIZED ACCORDING TO THEIR EPIGENETIC MODIFICATIONS, WHICH DEFINE THEIR CHROMATIN STATE. THESE CHROMATIN STATES WERE DESCRIBED AS TRANSCRIPTIONALLY INACTIVE, WITH "BLACK" AS REPRESSED "VOID" CHROMATIN, AND "BLUE" AS POLYCOMB GROUP PROTEIN (PCG)-REGULATED CHROMATIN, OR AS HIGHLY TRANSCRIBED WITH "RED" AND "YELLOW", AND "GREEN" AS HP1-BOUND CHROMATIN (FILION, VAN BEMMEL, BRAUNSCHWEIG, TALHOUT, KIND, L. D. WARD, BRUGMAN, DE CASTRO, KERKHOVEN, BUSSEMAKER & VAN STEENSEL 2010). THESE CHROMATIN STATES ARE ORGANIZED WITHIN TOPOLOGICALLY ORGANIZED DOMAINS (TADS) BY BINDING OF INSULATORS. TADS CAN BE MEASURED BY HI-C, A METHOD, WHICH DETERMINES THE CONTACT FREQUENCIES OF DNA REGIONS WITH OTHER DNA REGIONS.

Processes like transcription require transient access to DNA regions and therefore, nucleosomes need to be remodeled in an ATP-dependent process. This task is mediated by chromatin remodeling complexes, which are, according to their ATPase subunits, divided into different subclasses with specific functions: The Swi/Snf family, the Iswi family, the Chd family,

and the Ino80 family (reviewed in Clapier & Cairns 2009). Depending on situation and requirements, they can modify chromatin by sliding or evicting nucleosomes or by exchange of histones (reviewed in Becker & Workman 2013). To avoid an unintended DNA damage response at the ends of the chromosomes, the telomeres, these DNA ends form specific structures consisting of typical repeat sequences and a telomeric loop (T-loop), which are bound by telomere-specific proteins (reviewed in O'Sullivan & Karlseder 2010).

3. TECHNIQUES TO INVESTIGATE CHROMATIN COMPOSITION AND ORGANIZATION

In the last decades, many techniques have been developed to investigate protein-DNA contacts or DNA-DNA contacts, to better understand the 3-dimensional organization of chromatin by DNA-binding proteins.

The most common method to map protein-DNA contacts is by chromatin immunoprecipitation (ChIP). Here, protein binding to DNA is captured by cross-linking reagents (e.g. formaldehyde), and after fragmentation of chromatin by either sonication or micrococcal nuclease (MNase) treatment, the cross-linked protein-DNA complex is purified by immunoprecipitation with antibodies against the target of interest. After de-crosslinking, the isolated DNA fragments are purified and analyzed by qPCR or sequencing to identify the sequences to which the protein of interest had been bound.

Other indirect ways to investigate binding of chromatin-associated factors test for the accessibility of chromatin. Examples are MNase-Seq and DNase-Seq, in which DNA not protected by protein binding are digested and the remaining DNA is purified and sequenced to identify regions, which are occupied by nucleosomes and other DNA binding proteins. ATAC-Seq, another approach to investigate DNA accessibility, utilizes transposases, which integrate adapters into accessible chromatin regions, that can be identified by sequencing. Finally, FAIRE-Seq identifies accessible chromatin regions by isolation of free DNA from protein-associated DNA by phenol-chloroform extraction after fragmentation. The listed techniques are reviewed in P. J. Park 2009; Furey 2012; Tsompana & Buck 2014.

To capture the three-dimensional chromatin organization, different techniques called chromosome conformation capture (3C) and variants thereof called 4C, 5C, Capture C, Hi-C, or Capture Hi-C have been developed. The common principle of these techniques is the cross-linking of DNA regions, which are in close proximity to each other in the nucleus through DNA-interacting proteins. After cross-linking, DNA is fragmented by DNA restriction enzymes and the cross-linked DNA fragments are ligated in a highly diluted reaction, resulting in ligation products of the proximal DNA regions. Depending on the variations of these techniques, these ligation products are processed and analyzed in different ways to identify the chromosome conformation. A similar approach, but with an additional chromatin immunoprecipitation step to isolate the DNA-interacting protein, is ChIA-PET. An overview of the methods described can be found in de Wit & de Laat 2012; Denker & de Laat 2016; Sati & Cavalli 2016.

B. HISTONE VARIANTS

1. PROPERTIES OF HISTONE VARIANTS

Besides canonical histones H2A, H2B, H3 and H4, several histone variants have been described, predominantly of histone H2A and H3. Histone variants differ from their canonical part in their amino acid sequence and often include additional protein domains. In addition to this, transcription of canonical histones differs from transcription of variant in many ways: genes of canonical histones do not contain intron sequences, are only expressed in S-phase and their mRNA is not polyadenylated. Instead, its mRNA contains a stabilizing loop structure at its 3'end. In contrast to this, histone variant genes may contain introns and their mRNA is generally polyadenylated. In addition to this, expression of histone variant genes is not limited to S-phase (reviewed in Bönisch & Hake 2012; Buschbeck & Hake 2017). Histone variants can influence the chromatin structure and recruit factors involved in the regulation of transcription, DNA repair or cell cycle control (reviewed in Bönisch et al. 2008; Zink & Hake 2016).

2. H2A VARIANTS

H2A contributes the largest number of histone variants. Among those, two variants are common in most organisms (reviewed in Bönisch & Hake 2012). These are H2A.X, a variant mainly involved in the DNA damage response, and H2A.Z, which has important roles in the regulation of transcription (reviewed in Talbert & Henikoff 2010).

H2A.X contains a characteristic C-terminal SQ motif, which is conserved from fly and frog to mouse and human and is phosphorylated in response to DNA double-strand breaks (DSBs) by DNA damage-associated kinases (reviewed in Kinner et al. 2008, also see III.B.5).

Similarly, H2A.Z can be found in nearly all species, from yeast to human, and is essential in many organisms like fly, frog and mouse (reviewed in Zlatanova & Thakar 2008).

In yeast and mammals, the incorporation of H2A.Z has been shown to depend on the remodeling complexes SWR1 (Kobor et al. 2004; G. Mizuguchi 2004), or p400/SRCAP (Ruhl et al. 2006), respectively. These SWR1-llike remodeling complexes are large multi-subunit complexes, which are not only required to regulate transcription, but also to maintain the genome integrity (reviewed in Morrison & Shen 2009). Another complex in turn, Ino80, regulates the incorporation of H2A.Z and replaces H2A.Z for its canonical counterpart (Brahma et al. 2017; Lademann et al. 2017; Papamichos-Chronakis et al. 2011). In contrast to this, incorporation of H2A.X is not well understood and seems to be performed in a more random manner and similar to the incorporation of H2A.

3. H2A.V AND ITS FUNCTION IN *DROSOPHILA*

H2A.V is an essential histone variant in *Drosophila melanogaster* (van Daal & Elgin 1992; Clarkson et al. 1999) and particularly highly expressed in early stages during development, but the protein is present in all stages (van Daal & Elgin 1992). In contrast to mammals, H2A.V is the only H2A variant in flies. This means, that H2A.V needs to combine functions of H2A.X and H2A.Z (reviewed in Baldi & Becker 2013). Like other histones, H2A.V bears the typical histone fold, a motif composed of three alpha-helices (Clarkson et al. 1999; Chakravarthy et al. 2004). In addition to this, two additional alpha-helices are flanking the three alpha-helices, an N-terminal and a C-terminal helix. Clarkson et al performed rescue experiments with H2A.V constructs, in which different H2A.V regions were replaced for its counterparts in H2A in a H2A.V mutant background. Strikingly, the construct lacking the C-terminal alpha-helix was not able to rescue the H2A.V mutant lethality (Clarkson et al. 1999). This C-terminal helix is located in the inside of the nucleosome and might be important for the stability of the core particle rather than for interactions with DNA or other proteins.

Interestingly, H2A.V shows a very high sequence similarity with H2A.Z in many organisms ranging from *Homo sapiens* with 98% identity to Saccharomyces cerevisiae with 76% identity (protein-protein BLAST on https://blast.ncbi.nlm.nih.gov). However, besides its high sequence similarity to H2A.Z, H2A.V exhibits the typical C-terminal motif found in H2A.X (Talbert & Henikoff 2010), which consists of the four amino acids SQAY and whose serine residue is phosphorylated by DNA damage activated kinases like ATM and ATR to convey the DNA damage response (Joyce et al. 2011; Ravi et al. 2009). Truncations of the H2A.X-like C-terminus of H2A.V were not lethal, suggesting that the H2A.X-function including the SQAY motif is not essential (Clarkson et al. 1999).

Another modification of H2A.V, which is implicated in the DNA damage response, is acetylation at lysine 5. Kusch et al showed, that this acetylation mark is important to remove phosphorylated H2A.V from sites of damage (Kusch 2004, see also chapter III.B.5).

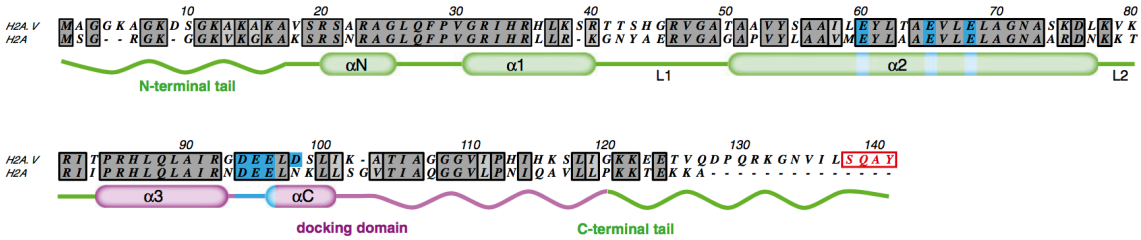

FIGURE 3: COMPARISON OF H2A AND H2A.V. H2A.V CONTAINS, LIKE H2A, A HISTONE FOLD AND IN ADDITION TO THIS THE H2A.X-LIKE PHOSPHORYLATION MOTIF SQAY. THE SERINE (S) RESIDUE OF THIS MOTIF IS PHOSPHORYLATED BY ATM AND ATR KINASES DURING THE DNA DAMAGE RESPONSE. IN ADDITION TO THE C-TERMINAL PHOSPHORYLATION, H2A.V CAN BECOME ACETYLATED ON ITS N-TERMINAL LYSINE (K) 5 BY TIP60 (FIGURE ADAPTED FROM BALDI & BECKER 2013).

H2A.V is distributed along the entire genome and can be found in eu- and heterochromatin (Leach et al. 2000), supporting its role as a damage sensor, which is spread over the entire genome to sense DNA damage. Furthermore, H2A.V is enriched at boundaries of transposons and of genes in heterochromatic regions (Zhang & Pugh 2011).

In addition to that, H2A.V is enriched at promotors, pointing to its H2A.Z-like role as a transcriptional regulator (Weber et al. 2010), which will be addressed in the next chapter.

4. THE ROLE OF H2A.V IN TRANSCRIPTIONAL REGULATION

In most cases, histone variants are incorporated into chromatin in a cell cycle-independent manner to influence chromatin structure and function, either by site-specific replacement of canonical histones or to replenish nucleosomes that are evicted, for example by transcription (reviewed in Weber et al. 2014).

Interestingly, H2A.V has opposing effects on transcription depending on context as roles of H2A.V as an activator and as a repressor of transcription have been described (reviewed in Baldi & Becker 2013). On one hand, H2A.V has been shown to facilitate transcription of heat shock genes (Kusch et al. 2014). On the other hand, the H2A.V gene has been classified as a polycomb group gene and thus somehow contributes to developmental silencing (Swaminathan 2005). In addition to that, H2A.V has also been reported to be involved in the establishment of heterochromatin (Swaminathan 2005; Hanai et al. 2008).

H2A.V is incorporated into promotor regions similarly to H2A.Z, with particularly high abundance in the first nucleosomes after the nucleosome-free region (NFR), but absent in the -1 nucleosome upstream of the NFR, where it might facilitate nucleosome disruption to facilitate gene transcription (Mavrich et al. 2008; Weber et al. 2010).

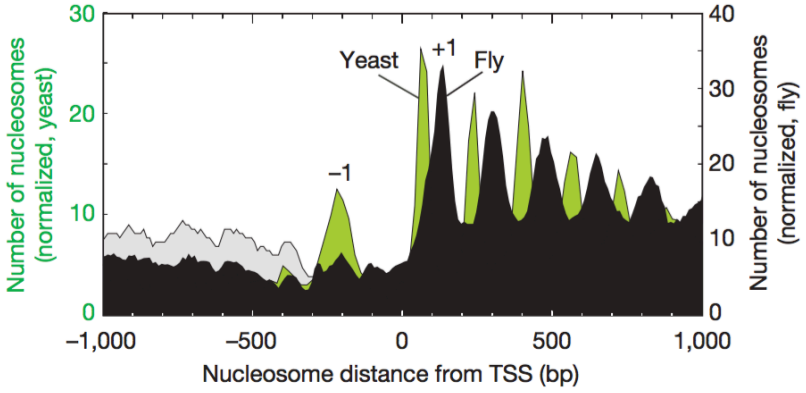

FIGURE 4: DISTRIBUTION OF H2A.V NUCLEOSOMES IN *DROSOPHILA* (BLACK) AND H2A.Z NUCLEOSOMES IN SACCHAROMYCES (GREEN) AROUND TRANSCRIPTION START SITES (TSS) (FIGURE ADAPTED FROM MAVRICH ET AL. 2008).

However, to date, it is controversially discussed whether homotypic nucleosomes consisting of two H2A.V molecules are more or less stable than nucleosomes consisting of H2A. Tremethick

et al suggest that H2A.V nucleosomes are more stable and less prone to disassembly than canonical nucleosomes (Y.-J. Park et al. 2004). In contrast to that, Henikoff's lab showed, that incorporation of H2A.V into nucleosomes downstream of the transcription start site reduces the barrier created by nucleosomes and facilitates transcription (Weber et al. 2014).

5. THE ROLE OF H2A.V IN THE DNA DAMAGE RESPONSE

It has been shown that C-terminal phosphorylation of H2A.V is essential for the DNA damage response in *Drosophila*, equivalent to C-terminal H2A.X phosphorylation in mammals. This phosphorylation is mediated by ATM and ATR, or their *Drosophila* homologues Tefu and Mei-41, respectively (Madigan et al. 2002; Zou & Elledge 2003). Tefu (from telomere fusion) is required to prevent the fusion of Drosophila telomeres during mitosis and meiosis. Mei-41, in turn, is required for the crossover process during meiosis (Sibon et al. 1999). In absence of the checkpoint proteins Tefu, Mei-41, or the MRN complex, telomeres can fuse, maybe due to the impaired recruitment of capping proteins to the telomeres. Strikingly, this phenotype can be rescued in H2A.V mutants (Rong 2008). However, the role of H2A.V in this observation is still elusive.

H2A.V has been shown to be important for the recruitment of Parp1, an enzyme that transfers poly(ADP-ribose) residues to chromatin components to decondense chromatin structure and facilitate DNA repair. Phosphorylation of H2A.V in turn then leads to the activation of Parp1 (Kotova et al. 2011). Interestingly, this phosphorylation mark was reported to be mediated by Jil1 (Thomas et al. 2014), a kinase that was reported to phosphorylate serine 10 of H3 to regulate chromatin structure (Jin et al. 1999; Y. Wang et al. 2001). Unlike ATM and ATR, Jil1 was not implicated in the DNA damage response so far, but in transcriptional regulation and dosage compensation (Jin et al. 1999). Phosphorylated H2A.V is a target of the Domino (Dom)/Tip60 complex, which acetylates H2A.V on its N-terminal lysine 5 by the histone acetyl transferase subunit Tip60 (Kusch 2004).

6. H2A.V INCORPORATION AND THE ROLE OF REMODELERS

How H2A.V is incorporated, is still barely understood. However, Kusch et al showed that the Dom/Tip60 complex, a SWR1-like complex in *Drosophila*, is involved in the incorporation of H2A.V at heat shock promotors (Kusch et al. 2014) and at the promotor of the E2f gene (Lu et al. 2007). Furthermore, a former PhD student in our lab, Kenneth Börner, discovered that the two splice variants of the Domino (Dom) remodeling ATPase, DomA and DomB, have distinct functions in the incorporation of H2A.V during oogenesis in *Drosophila*. For example, H2A.V incorporation into the germline chromatin of the germarium is DomB-dependent, whereas DomA mediates the eviction of H2A.V from germline cells (Börner & Becker 2016).

In addition to that, the Iswi-containing chromatin remodeling factors, ACF and RSF, have also been implicated in H2A.V incorporation. For instance, Chioda et al. showed that heterochromatic localization of H2A.V is diminished in acf1 mutants (Chioda et al. 2010). Other unpublished data from our lab suggested a role of Acf1 in the removal of phosphorylated H2A.V after DNA damage (preliminary observation from Natascha Steffen and Alessandro Scacchetti). Finally, Rsf1, a component of the Iswi remodeling component RSF, was shown to be required for the incorporation of H2A.V during the establishment of heterochromatin (Hanai et al. 2008).

C. POST-TRANSLATIONAL HISTONE MODIFICATIONS

Besides incorporation of histone variants, another mode to alter chromatin structure and to regulate chromatin-associated processes is the deposition of post-translational histone modifications by "writers" like histone acetyltransferases, kinases and methyltransferases. These combinations of histone modifications build a histone code, which can be recognized by "readers", to influence and regulate the structure of chromatin (Prakash & Fournier 2018). The most common post-translational histone modifications addressed in this thesis, which are deposited by so-called writers: phosphorylation is mediated by kinases, acetylation by histone acetyl transferases, and methylation by histone methyl transferases. These modifications can be recognized by readers to regulate processes like transcription or DNA repair and modify chromatin structure (Rothbart & Strahl 2014; Prakash & Fournier 2018).

In this thesis, I will mainly focus on histone modifications, which are involved in the DNA damage response.

D. DNA DAMAGE SIGNALING AND REPAIR

In the following chapter, I mainly refer to events described in mammals, unless stated otherwise. Chapter III.D.7 summarizes the state of knowledge of the DNA damage response in *Drosophila*.

1. REPAIR OF DNA DSBS

DSBs are hazardous to the genomic integrity and need to be repaired immediately. There are two main pathways to repair DNA DSBs, namely Non-Homologous End Joining (NHEJ) and Homologous Repair (HR). The pathway choice depends on different factors, including cell cycle state, cell type and organism. For example, HR depends by its nature on a homologous region and is therefore restricted to late S- or G2-phase, when sister chromatids can serve as homology partners. In yeast, HR is the predominant pathway, possibly because yeast cells rely

more on error-free repair than multicellular organisms, which generally prefer the NHEJ pathway (Shrivastav et al. 2008; Kinner et al. 2008).

In *Drosophila*, HR is assumed to be the preferred pathway as well (Rong & Golic 2003; Preston et al. 2006; Marin-Vicente et al. 2015), even in heterochromatin, with its high density of repetitive sequences (Chiolo et al. 2011; P. C. Caridi et al. 2017; C. P. Caridi et al. 2018), also see III.D.7).

To initiate the DNA break repair via NHEJ, a Ku complex is tethered to the broken ends, forming a ring around the DNA and diffusing to the inside to enable other repair factors to bind. Ku binding facilitates the fusion of the broken ends and supports the recruitment of additional factors, like DNA-PK, which in turn recruits Artemis, a nuclease that can process DNA ends before ligation by a complex consisting of Lig4, Xrcc4 and Xlf. Besides the classical NHEJ pathway, there is an alternative, Ku-independent NHEJ pathway. In this error-prone pathway, repair is mediated with the help of very short homology sequences of only few base pairs and in dependence of MRN and CtIP, components, which are also relevant in HR (reviewed in H. H. Y. Chang et al. 2017). If damage is repaired by HR, MRN is recruited to the break site together with CtIP, leading to a long-range resection of DNA resulting in 3' overhangs. These overhangs are rapidly bound by RPA, which is later replaced by Rad51, supported by Brca2. This filament then initiates the homology search forming heteroduplex DNA with the homologous DNA molecule of the intact sister chromatid to enable the replication of the damaged DNA filament. Afterwards, the invading strands are resolved and ligated (reviewed in Hiom 2010).

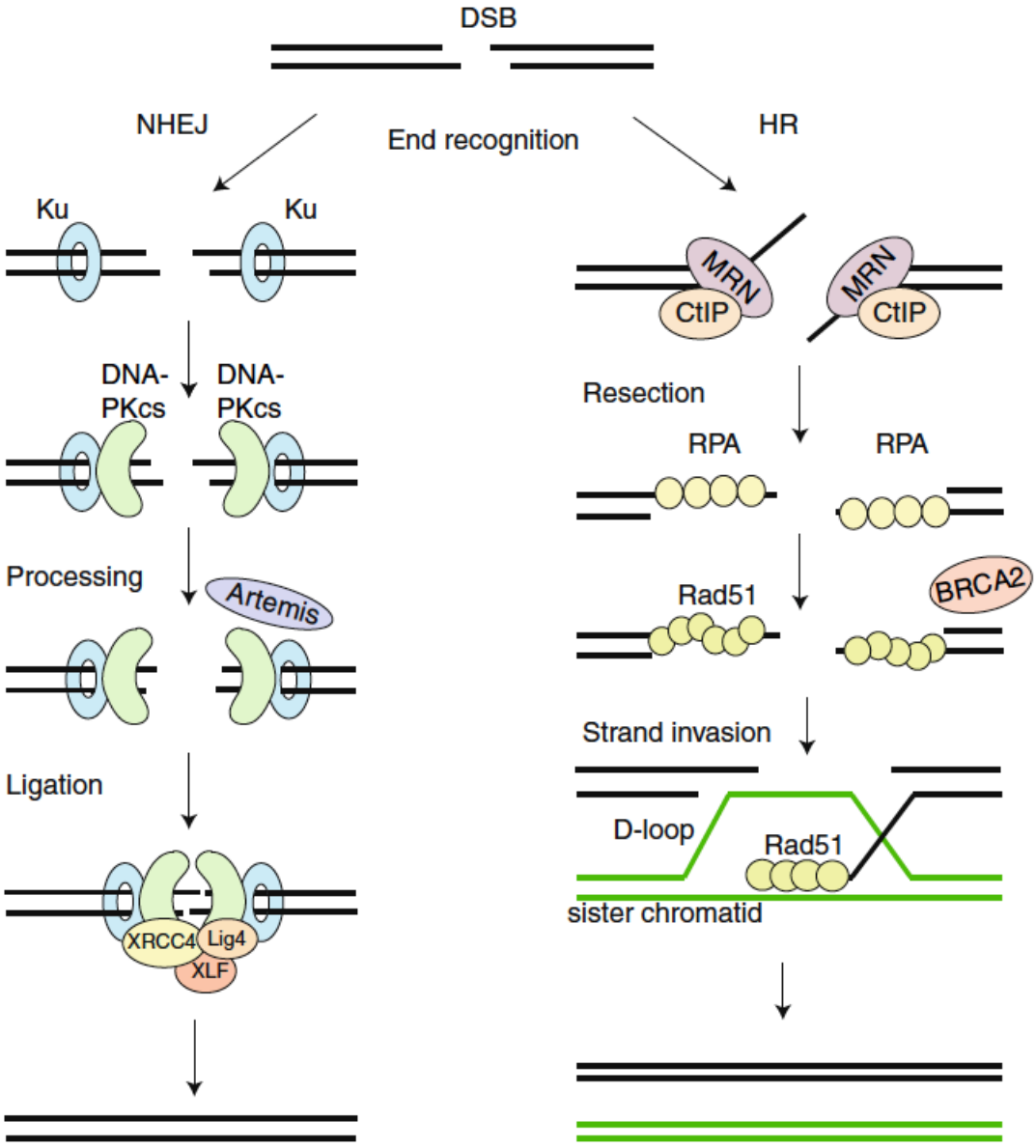

FIGURE 5: REPAIR OF DNA DSBS BY HOMOLOGOUS REPAIR (HR) OR NON-HOMOLOGOUS END JOINING (NHEJ). IN BOTH CASES, THE DNA DAMAGE RESPONSE IS INITIATED BY PHOSPHORYLATION OF H2A.X BY ATM. FOR HR, DNA ENDS ARE BOUND BY THE MRN COMPLEX AND LATER ON PROCESSED TO 3'OVERHANGS, WHICH ARE BOUND BY RPA AND REQUIRED BY AN HOMOLOGY-DEPENDENT DNA REPAIR PROCESS. FOR NHEJ, THE KU COMPLEX IS RECRUITED TO THE BREAK SITE, FOLLOWED BY THE RECRUITMENT OF DNA-PKCS. DNA ENDS ARE THEN PROCESSED AND LIGATED IN A FAST, BUT ALSO ERROR-PRONE MANNER (FIGURE ADAPTED FROM BRANDSMA & GENT 2012).

2. RECOGNITION OF DSBS

DNA damage can occur in response to endogenous factors or exogenous factors. Examples for endogenous factors could be the generation of reactive metabolic substances, like reactive oxygen species (ROS). ROS are oxygen-containing reactive molecules, which can be generated during metabolic processes and which can lead to the oxidation of DNA (Dickinson & C. J. Chang 2011). Other substances could also lead to alkylation of DNA, to the formation of DNA adducts or to the loss of DNA bases. Examples for exogenous factors could be reactive substances in the environment or irradiation by UV light, which can lead to the modification or loss of nucleotides or to the breakage of the DNA backbone in either one strand (nick) or in both strands (DSB) (reviewed in Ciccia & Elledge 2010; De Bont 2004). Due to the disconnection of the DNA strand, DSBs are particularly harmful to the genome integrity and have to be recognized and repaired immediately. One of the first events after DSB occurrence is the recruitment of the MRN complex, which is composed of Mre11, Rad50 and Nbs1 and which recruits and activates ATM. In addition to MRN, other DSB sensor proteins, which are rapidly recruited to breaks, are Parp1, Ku70/Ku80, and, in case of ssDNA, RPA (Ciccia & Elledge 2010). ATM, in turn, phosphorylates many other damage-associated proteins like H2A.X, Mdc1, 53BP1, Brca1, Mre11, Rad50 and Nbs1 (Shiloh 2014; Tripathi et al. 2018; Ranjha et al. 2018). Besides ATM, other DNA damage kinases have been identified, namely ATR and DNA-PK. Even though they can act redundantly, each of them has specific roles. ATM, for example, is recruited by Nbs1 of the MRN complex and is the major kinase during HR. In contrast to this, DNA-PK is recruited by Ku and predominates in NHEJ. ATR recruitment is, in contrast to ATM and DNA-PK, not limited to damage caused by DSBs and occurs in presence of RPA-coated ssDNA by Atrip. Here, ATR is activated in response to replicational stress by arrested replication forks (I. M. Ward & Chen 2001; Blackford & Jackson 2017; Saldivar et al. 2017).

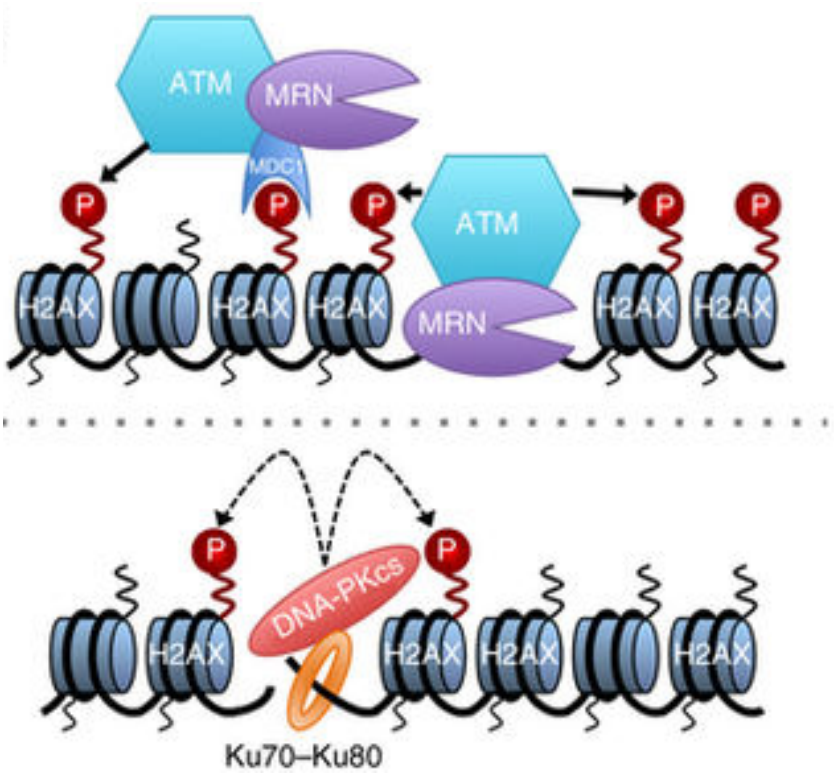

FIGURE 6: EARLY EVENTS AFTER DNA DAMAGE RECOGNITION (FIGURE ADAPTED FROM HARTLERODE ET AL. 2012). IF THE DSB IS REPAIRED BY HR, THE MRN IS RECRUITED FIRST, LEADING TO THE ACTIVATION OF ATM AND SUBSEQUENT PHOSPHORYLATION (P) OF H2A.X. THIS LEADS TO THE RECRUITMENT OF MDC1 AND FURTHER RECRUITMENT AND ACTIVATION OF ATM (UPPER PANEL). IF THE DSB IS REPAIRED BY NHEJ, THE KU COMPLEX CONSISTING OF KU70 AND KU80 IS RECRUITED TO THE BREAK, LEADING TO THE RECRUITMENT OF DNA-PKCS, WHICH PHOSPHORYLATES (P) H2A.X (LOWER PANEL).

This C-terminal phosphorylation of H2A.X (H2A.V in *Drosophila*) by DNA damage-activated kinase ATM, but also by ATR or DNA-PK then recruits additional Mdc1 (mu2 in *Drosophila*) to the break site, which in turn leads to an enrichment of MRN at the break site and further recruitment and activation of ATM and subsequent phosphorylation of H2A.X. This feedback loop leads to an amplification and expansion of the signal (Savic et al. 2009; Podhorecka et al. 2010; Georgoulis et al. 2017). In total, H2A.X contributes with about 2-25% to the mammalian H2A pool, and is distributed along the whole genome (Rogakou et al. 1998; Kinner et al. 2008), therefore, the phosphorylation signal can be amplified and distributed over long distances.

Besides the role of H2A.X in DNA damage, studies in mammals showed, that H2A.Z is incorporated into regions spanning few kilobases around the DSB in a p400-depenent manner. This was shown to have critical functions in repair-associated processes like the formation of open chromatin conformation, the deposition of post-translational histone modifications, the recruitment of complexes like BRCA and Ku and the regulation of DNA resection prior to HR (Xu et al. 2012). Another study in yeast showed, that incorporation of H2A.Z at sites around DSBs is also required to translocate the DSB to the periphery of the nucleus to enable efficient DNA repair (Horigome et al. 2014). To facilitate the exchange at break sites, H2A.Z is marked by

SUMOylation in yeast and mammals, which is the conjugation to a small ubiquitin-like protein (Kalocsay et al. 2009; Fukuto et al. 2018).

To investigate the dynamics of factors recruited to sites of DNA damage, an extensive real-time immunofluorescence analysis was performed on HeLa cells with EGFP-tagged DNA repair proteins under their own regulatory sequences. In this study, they identified clusters of proteins according to their kinetics after induction of DNA damage. Among the first cluster, which was recruited within the first seconds, were proteins involved in early steps of DSB repair (Ku70, Lig4, Rad50, ATM, Mdc1), Parp1 and proteins binding to the PARylation mark, histone deacetylases, and chromatin remodelers (Smarca5, Smarcad1). Only 10 to 20 min after damage induction, proteins involved in the HR pathway were recruited (Rpa1, Rad51) (Aleksandrov et al. 2018). This order of events has important implications in the regulation of DNA damage. For example, in the first seconds, factors to prime chromatin for repair are recruited and deposit post-translational modifications or remodel chromatin. Only lateron, the repair machinery for the complex and highly regulated repair pathways like HR are recruited. In addition, they were able to show that early events regulate the onset of later events (e.g. the removal of Parp1 is connected to the initiation of HR (Aleksandrov et al. 2018). The first changes in the DNA damage response have also been described in an "access–repair–restore" model (Soria et al. 2012) which will be discussed in III.D.3.

3. THE "ACCESS–REPAIR–RESTORE" (ARR) MODEL

Chromatin undergoes various changes in response to damage to maintain genomic integrity and to enable proper DNA repair.

To overcome the chromatin barrier composed of nucleosomes and chromatin-associated proteins, and to allow repair factors to access the break, it has been proposed that chromatin is first subject to a local remodelling process, which renders it more accessible for the repair machinery. This process was first observed in 1991 (Smerdon 1991) and further studied later in the lab of Geneviève Almouzni, where it was termed the "access–repair–restore" model (Soria et al. 2012). Interestingly, increasing numbers of studies showed that one of the earliest steps is the recruitment of histone deacetylases like the NuRD complex (Smeenk et al. 2010) and histone methyltransferases like Suv39h1 (Ayrapetov et al. 2014), which presumably lead to the establishment of repressive chromatin in proximity to the break site. This step, which occurs already in the very first minutes after DSB recognition prior to the decondensation step described before, might be important to block transcription of genes affected by the break. After that, repressive marks are released, and chromatin is then turned into a more open state to facilitate the association of repair factors.

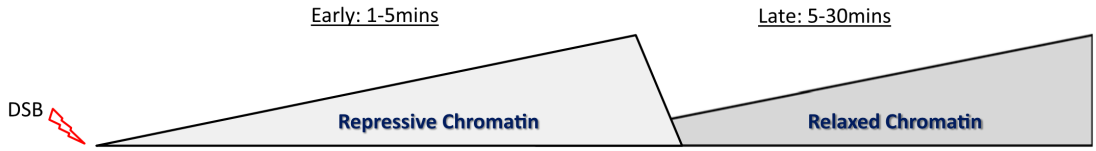

FIGURE 7: CHROMATIN STRUCTURE AFTER DSB RECOGNITION (FIGURE ADAPTED FROM GURSOY-YUZUGULLU, HOUSE & PRICE 2016). WITHIN THE FIRST MINUTES, CHROMATIN BECOMES COMPACTED AND REPRESSIVE TO INHIBIT TRANSCRIPTION FROM DAMAGED REGIONS. THIS CHROMATIN STATE IS CHARACTERIZED BY THE RECRUITMENT OF FACTORS THAT DEACETYLATE AND DEMETHYLATE CHROMATIN, DEPOSIT REPRESSIVE HISTONE MARKS LIKE DI- AND TRI-METHYLATION OF LYSINE 9 ON HISTONE H3 AND BY THE DEPOSITION OF H2A.Z. AFTERWARDS, A MORE RELAXED CHROMATIN ORGANIZATION IS ESTABLISHED TO ALLOW THE RECRUITMENT OF REPAIR FACTORS AND TO FACILITATE THE REPAIR PROCESS, WHICH IS ACHIEVED BY REMOVAL OF H2A.Z AND ACETYLATION OF H4.

4. SPREADING OF THE H2A.X PHOSPHORYLATION MARK

Phosphorylation of H2A.X is first initiated at the DSB and then propagates along the DNA. Over time, the phosphorylation signal is not only amplified, but also spreads over long distances. This process is mediated through a feedback mechanism illustrated in Figure 8. In this feedback loop, Mdc1, a DNA damage checkpoint mediator (Stewart et al. 2003) is recruited by phosphorylated H2A.X, leading to further recruitment of the MRN complex, which in turn enhances the phosphorylation of H2A.X by ATM.

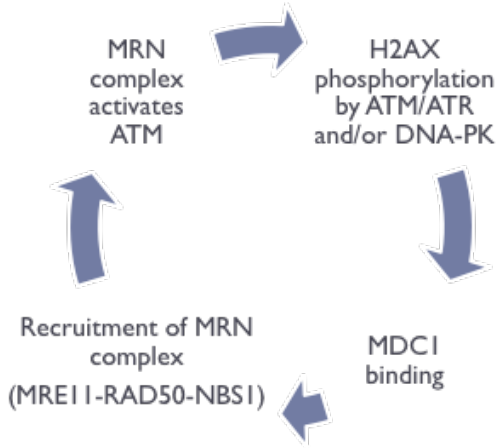

FIGURE 8: FEEDBACK LOOP OF DAMAGE SIGNALING MEDIATED BY H2A.X PHOSPHORYLATION: RECOGNITION OF DNA DSBS LEADS TO THE RECRUITMENT OF MRN, WHICH RECRUITS AND ACTIVATES KINASES LIKE ATM. ATM PHOSPHORYLATES H2A.X, LEADING TO THE BINDING OF MDC1 AND THE MRN COMPLEX, WHICH, IN TURN, LEADS TO RECRUITMENT AND AMPLIFICATION OF MORE ATM, RESULTING IN THE SPREADING AND AMPLIFICATION OF THE PHOSPHORYLATION MARK AROUND DSBS.

Remarkably, the phosphorylation mark can spread over long distances from the break, up to 300 kb in yeast and up to 2 MB in mammals (C.-S. Lee et al. 2014; Iacovoni et al. 2010), however, the mechanism of spreading is not yet understood. The spreading event is not uniformly along the chromosome, but may appear rather discontinuous and asymmetrical (Shroff et al. 2004; Iacovoni et al. 2010, see Figure 9).

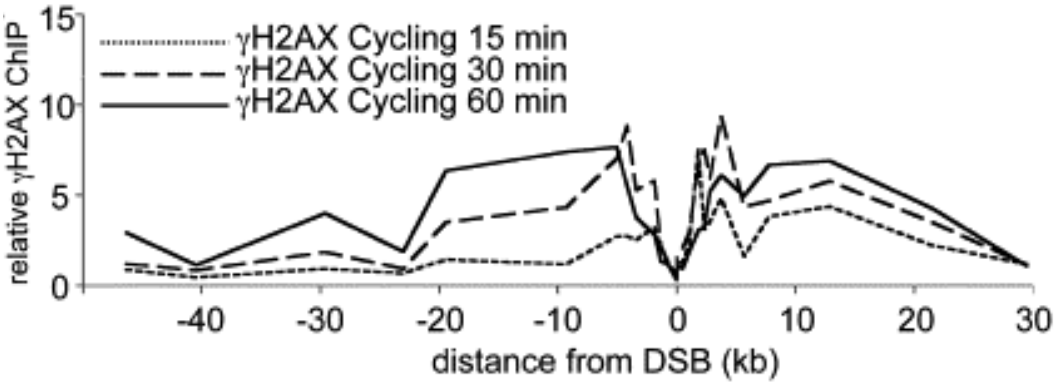

FIGURE 9: TIME COURSE OF H2A.X PHOSPHORYLATION IN MAMMALIAN CELLS FROM 15 MIN TO 60 MIN 30 TO 40 KB AROUND THE DSB. THE PHOSPHORYLATION SIGNAL INCREASES IRREGULARLY AT REGIONS CLOSE TO THE BREAK SITE AND WITH SOME DELAY AT REGIONS MORE DISTAL FROM THE BREAK SITE. FIGURE FROM SHROFF ET AL. 2004.

In addition to this, spreading of H2A.X phosphorylation overlap with TADs and spreading seems to be controlled and limited by cohesion, which usually defines the borders of TADs (Caron et al. 2012). In addition to this, spreading of H2A.X phosphorylation signaling has also been observed in trans on centromeric regions in yeast, which were analyzed after introducing DSBs into specific sites of the chromosome. Interestingly, an increase of phosphorylated H2A.X was observed on intact chromosomes, which might be due to clustering of centromeres in yeast nuclei (C.-S. Lee et al. 2014), which are generally clustered at the periphery of the nucleosome (T. Mizuguchi et al. 2015).

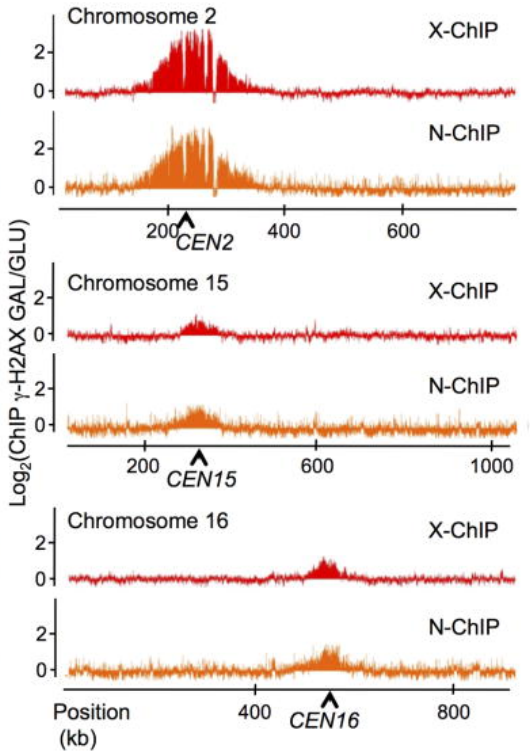

FIGURE 10: H2A.X PHOSPHORYLATION IN YEAST. A DSB WAS INSERTED IN CHROMOSOME 2 CLOSE TO THE CENTROMERIC REGION. FROM THIS, SPREADING OF THE PHOSPHORYLATION SIGNAL WAS OBSERVED TO CENTROMERIC REGIONS OF OTHER CHROMOSOMES. CHROMATIN IMMUNOPRECIPITATION WAS PERFORMED WITH CROSSLINKING (X-CHIP) AND UNDER NATIVE CONDITIONS WITHOUT CROSS-LINKING (N-CHIP). FIGURE ADAPTED FROM C.-S. LEE ET AL. 2014.

To date, two possible models of spreading are discussed: either by moving along the DNA in *cis*, continuously adding additional marks to the neighboring H2A.X containing nucleosomes, or by establishing transient chromosomal contacts through dynamic loop formation, which leads to the spreading of the phosphorylation mark to spread over distances. In principle, these scenarios should be distinguishable in time-resolved analyses of the signal development: in the first model, the signal would be expected to increase laterally from the break site towards the periphery, mediated by the feedback mechanism described in Figure 8. In the second case, the signal would augment more globally (Erdel 2017), see Figure 11) by a not yet identified mechanism. To investigate these possibilities in more detail, mathematical models for the spreading behavior of post-translational histone modifications have been developed (Tommasino et al. 2015; Erdel & Greene 2016; Jost & Vaillant 2018). After comparison of experimental data with the model, calculations including the spreading over three-dimensional DNA loops were more close to the measured data, supporting the model of spreading by DNA looping (Tommasino et al. 2015). This model would include the activity of activated ATM, which could diffuse away from the damage region to close intact DNA regions, facilitated by the formation of repair clusters. The formation of these clusters is not yet well understood, but could be mediated by cohesin, a complex with the ability to connect DNA strands using its ring structure. It has been shown that cohesion is recruited to DSBs in yeast and human (Ünal et al. 2004; Ström et al. 2004; S.-H. Lee & C.-H. Kim 2002) and that ATM phosphorylates a subunit of cohesin upon damage induction (S.-T. Kim et al. 2002).

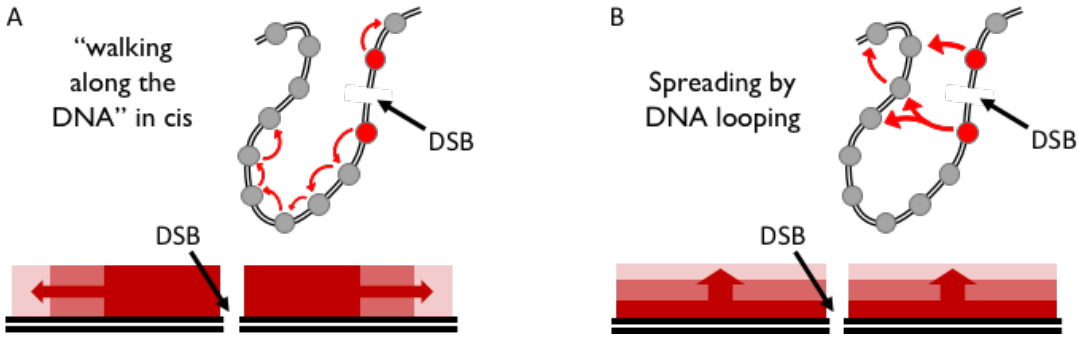

FIGURE 11: POSSIBLE SPREADING MECHANISMS OF THE H2A.V PHOSPHORYLATION SIGNAL: IN MODEL A THE PHOSPHORYLATION SIGNAL IS TRANSMITTED ALONG THE DNA, LEADING TO AN AMPLIFICATION OF THE SIGNAL FROM THE BREAK TO THE PERIPHERY BY THE PREVIOUSLY DESCRIBED FEEDBACK MECHANISM. IN MODEL B THE PHOSPHORYLATION SIGNAL IS TRANSMITTED IN *TRANS*, TO DNA REGIONS, WHICH WERE BROUGHT IN CLOSE PROXIMITY BY DNA LOOPING. RED CIRCLES INDICATE PHOSPHORYLATED H2A.X-CONTAINING NUCLEOSOMES, GREY CIRCLES INDICATE NON-PHOSPHORYLATED H2A.X-CONTAINING NUCLEOSOMES; ARROWS INDICATE THE SPREADING OF THE PHOSPHORYLATION SIGNAL. THE LOWER PANEL SHOWS THE SPREADING DIRECTION OF PHOSPHORYLATION WITH INTENSITIES EITHER INCREASING FROM THE DSB TO THE PERIPHERY (LEFT) OR MORE EVENLY DISTRIBUTED ALONG THE DNA (RIGHT).

All these points could argue for a combination of both models, where the phosphorylation mark might spread along the chromosome fiber but could also be amplified by spatial contacts of chromosomal domains, leading to an increased signal at regions, which are more frequently close to other DNA regions due to sequences bound by DNA linking proteins like cohesion, which also limits and defines regions of H2A.X phosphorylation spreading. Figure 9 shows an example of an H2A.X phosphorylation time course in mammalian cells, where phosphorylation

signals increase from the break site towards the periphery, but also show irregular signal amplifications of regions with higher or lower phosphorylation signals.

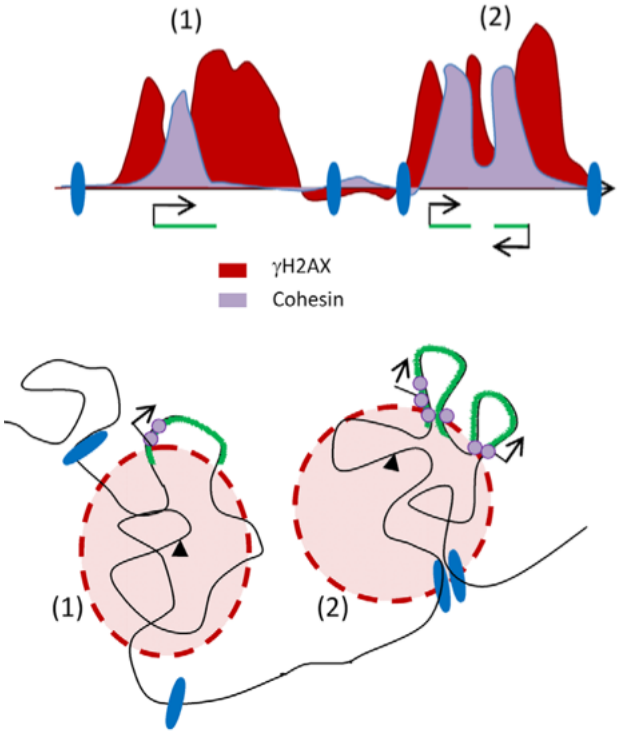

FIGURE 12: MODEL OF H2A.X PHOSPHORYLATION SPREADING WITHIN DNA DAMAGE FOCI, WHICH ARE REGULATED BY BINDING OF COHESIN (FIGURE ADAPTED FROM CARON ET AL. 2012). THE UPPER BINDING PROFILES OF COHESIN (PURPLE) TOGETHER WITH ANTAGONIZING PROFILES OF H2A.X PHOSPHORYLATION (RED), WHICH COULD BE DELIMITED BY CHROMATIN-ASSOCIATED FACTORS (BLUE). THESE PROFILES RESULT FROM THE ORGANIZATION OF DNA INTO DNA DAMAGE FOCI, WHICH INCLUDE THE DNA DSB (BLACK TRIANGLE) AND ADDITIONAL LOOPS OF DNA, AND WHICH ARE ACCOMPLISHED THROUGH BINDING OF COHESIN (PURPLE CIRCLES) (RED CIRCLES, LOWER PANEL). TRANSCRIBED REGIONS (IN GREEN) ARE OUTSIDE OF THE DNA DAMAGE FOCI AND EXCLUDED FROM THE SPREADING EVENT OF H2A.X PHOSPHORYLATION.

5. DEPHOSPHORYLATION OF H2A.X

Several studies in yeast and mammals showed that γH2A.X appear about 15 min after DSB induction and is removed again after approximately one to two hours (Kinner et al. 2008). This is accomplished by protein phosphatase 2A (PP2A) in mammals, and dephosphorylation can occur on monomeric H2A.X, as a dimer with H2B or incorporated into nucleosomes (Chowdhury et al. 2005).

However, it is still under debate whether dephosphorylation of H2A.X is performed on chromatin or after removal from the break site. However, considering the observation, that PP2A colocalizes at damage sites together with γH2A.X, it seems probable that PP2A dephosphorylates H2A.X directly at the site of damage (Chowdhury et al. 2005). Furthermore, photobleaching experiments of GFP-labeled H2A.X showed, that the mobility of incorporated H2A.X is not particularly high, indicating that turnover is not a predominant process in cells (Siino et al. 2002). In contrast to this, phosphorylated H2A.V in flies is believed to be removed by the Dom/Tip60 histone exchange complex, that was first shown to acetylate γH2A.V followed by exchange of H2A.V/H2B dimers by unphosphorylated H2A.V/H2B (Kusch 2004). Similarly, in yeast, Ino80 has been shown to remove phosphorylated H2A.X from chromatin (Bao 2011).

6. OTHER DNA DAMAGE-ASSOCIATED POST-TRANSLATIONAL HISTONE MODIFICATIONS

In addition to γH2A.X, other DNA damage-associated post-translational histone modifications have been described. The following table summarizes the modifications that have been linked to DSBs in mammals.

TABLE 1: DNA DAMAGE-ASSOCIATED POST-TRANSLATIONAL HISTONE MODIFICATIONS IN MAMMALS; S: SERINE, K: LYSINE, P: PHOSPHORYLATION, UB: UBIQUITINOYLATION, ME: METHYLATION, ME2/ME3: DI-/TRI-METHYLATION, AC: ACETYLATION

Modification	Enzyme	Reference
H2A.XS139p	ATM, ATR, DNA-PKcs	Blackford & Jackson 2017
H2A.X	Tip60	Chailleux et al. 2010
H2A/H2A.Xub	Rnf8/Rnf168	Huen et al. 2007; Kolas et al. 2007; Mailand et al. 2007; Doil et al. 2009
H2AXK119ub	Ring1B/Ring2 Brca1	Xie et al. 2010; Q. Zhu et al. 2011
H2BK120ub	Rnf20-Rnf40	Moyal et al. 2011
H3ub and H4ub	Cul4-Ddb-Roc1	H. Wang et al. 2006
H3K36me2	Metnase/SETMAR	Fnu et al. 2011
H3K79me	Dot1	Wakeman et al. 2012
H3K9me3	Suv39h1	Ayrapetov et al. 2014
H4K5ac H4K8ac H4K12ac H4K16ac	Hat1, Tip60, Atf2, Hpa2, p300 HAT, Gcn5, Pcaf, Elp3, Sas2	reviewed in Dhar et al. 2017
H4K16ac	Mof	X. Li et al. 2010
H4K20me2	Set8/Suv4-20	Jorgensen et al. 2013

7. DNA REPAIR IN *DROSOPHILA*

In *Drosophila*, DSB can be repaired via both pathways, HR and NHEJ, depending on the cell cycle state and cell type. In *Drosophila* tissues, whose cells are predominantly in G1, NHEJ is the preferred pathway in heterochromatic regions. In contrast to this, HR is preferred in heterochromatin of *Drosophila* cell culture cells, which are predominantly in S/G2 (reviewed in P. C. Caridi et al. 2017). Rong et al studied the repair of DSBs in the *Drosophila* premeiotic germline, which were induced by the expression of a specific endonuclease SceI (Rong & Golic 2000) and repaired by HR using the homologous chromosome as repair template (Rong & Golic 2003). The preference of DSB repair via homology search in *Drosophila* was also observed in several other studies (Adams et al. 2003; LaRocque et al. 2007; Do et al. 2014).

Another study using SceI to introduce DSBs was performed to investigate repair pathway choice in different developmental stages of the germ line, revealing that NHEJ only becomes

predominant at late stages before meiosis, whereas single-strand annealing, a pathway relying on homology search similar to HR, is more prevalent at very early stages and less frequent lateron (Preston et al. 2006).

For HR, resection of DNA ends is first initiated by the MRN complex and carried on by CtIP/Sae2 and later by Exo1 or Dna2/Blm (reviewed in Symington & Gautier 2011). The resected 3' ends are then bound by the Rad51 orthologue spn-A and after homology search and synthesis of the broken DNA strand, the Holliday junctions are resolved (Sekelsky 2017). In *Drosophila*, DSBs induced by X-rays into heterochromatic regions are repaired by HR but are translocated out of the heterochromatic domain before Rad51 binding to the resected DNA strand (Chiolo et al. 2011). Repair by NHEJ, on the other hand, is initiated by the recruitment of the Ku complex consisting of Ku70 and Ku80, or the *Drosophila* orthologues Irbp and Ku80, respectively. However, unlike in mammals, the catalytic subunit of the complex, DNA-dependent protein kinase (DNA-PK), does not exist in *Drosophila*. Then, end processing is performed by Artemis and ligated by Lig4, Xrcc4, and Xlf, which have all been identified in *Drosophila* (reviewed in Sekelsky 2017).

Besides the repair of DNA DSBs, other pathways have been investigated in *Drosophila*. For example, *Drosophila* embryo extract (see III.E) was used to investigate the nucleotide excision repair (NER) pathway (Gaillard et al. 1997), which is generally used to remove UV-induced damage and bulky adducts (Luijsterburg & van Attikum 2011). In this assay, chromatin was assembled *in vitro* on UV-irradiated DNA. Interestingly, nucleosomes were not only assembled in regular arrays starting from the NER target site, but also the plasmid was repaired by extract components (Gaillard et al. 1997).

8. THE CHROMATIN REMODELING SUBUNIT ACF1 AND ITS ROLE IN DNA DAMAGE

In general, Iswi-containing chromatin remodeling factors are responsible for the regular spacing of nucleosomes by sliding nucleosomes along the DNA (reviewed in Längst & Becker 2001). Besides this, Iswi remodelers, and in particular ACF with the mammalian Acf1 orthologue BAZ1A were shown several times to be involved in DNA damage (Lan et al. 2010; Sánchez-Molina et al. 2011; Aydin et al. 2014; Oppikofer et al. 2017). It has been shown that CHRAC accumulates at DSBs and interacts with the Ku complex, which is recruited to DNA ends as a component of the NHEJ pathway. In fact, it has been postulated that CHRAC assists the accumulation of Ku at the break site (Lan et al. 2010).

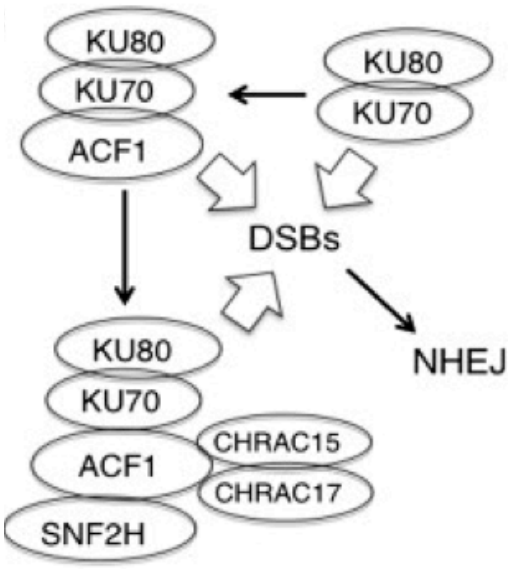

FIGURE 13: ACF1 CAN INTERACT WITH SUBUNITS OF THE KU COMPLEX (FIGURE ADAPTED FROM LAN ET AL. 2010). THE KU COMPLEX, CONSISTING OF KU70 AND KU80, WAS SHOWN TO HAVE THE ABILITY TO INTERACT WITH ACF1, A COMPONENT OF THE CHRAC COMPLEX CONSISTING OF ACF1, THE MAMMALIAN ISWI HOMOLOG SNF2H, AND CHRAC17 AND CHRAC15, WHICH ARE THE MAMMALIAN HOMOLOGUES OF *DROSOPHILA* CHRACH14 AND CHRAC16. THIS INTERACTION WAS SHOWN TO BE IMPORTANT FOR EFFICIENT RECRUITMENT OF KU TO THE DSB, WHICH IS NECESSARY FOR EFFICIENT REPAIR BY NHEJ.

Acf1 contains a WAC domain, a DDT domain and a PHD finger domain, required for interaction with DNA, with Iswi, and with core nucleosomes, respectively (Fyodorov & Kadonaga 2002; Hogan & Varga-Weisz 2007). Analysis with Acf1 mutant constructs showed that the N-terminal part including the WAC and DDT domain is responsible for the accumulation at DNA break sites after damage (Lan et al. 2010).

E. CHROMATIN RECONSTITUTION *IN VITRO*

In the past, various approaches to assemble nucleosomes *in vitro* have been performed at different levels of complexity. The simplest system is salt gradient-mediated assembly, which can be performed in the absence of any additional assembly factors. Here, histones are either purified or recombinantly expressed and histone octamers are stabilized in high salt buffer, which covers the positive charge of the highly basic histones. In the presence of DNA, nucleosomes can be formed by gradually decreasing the salt concentration, which leads to the transfer of the positively charged octamers onto negatively charged DNA. A less efficient approach to assemble nucleosomes is the careful titration of histones to DNA in low salt buffer (Ruiz-Carrillo et al. 1979; Stein et al. 1979).

In addition to this, assembly can be performed by addition of purified histone chaperones to the octamers, like nucleoplasmin (Laskey et al. 1977; Earnshaw et al. 1980), polyglutamic acid (Stein et al. 1979) or other negatively charged supplements, to improve nucleosome formation by shielding the positive charge of histones and prevent unspecific aggregations at physiological salt concentrations (reviewed in Laskey & Earnshaw 1980).

Finally, chromatin can be reconstituted by crude cell extracts. Chromatin *in vitro* reconstitution by cell extracts is a cell-free tool developed in 1977 by Laskey et al using *Xenopus* embryo extract to study chromatin assembly and transcription (Laskey et al. 1977). In parallel to this, a

similar approach was developed using *Drosophila* embryo extract (Nelson et al. 1979). Obtaining sufficient amounts of *Drosophila* embryos for extract preparation is straight forward, as *Drosophila* cultures can be maintained in large amounts and availability is not season-dependent, as it is for *Xenopus* embryos (Rodriguez-Campos et al. 1989).

In addition to this, extract from mammalian cells was used to reconstitute chromatin *in vitro* (Krude et al. 1993). Compared to the other *in vitro* systems, in mammalian cell extract, chromatin reconstitution is coupled to replication (Krude & Knippers 1993), whereas with *Xenopus* extract, replication-dependent and -independent chromatin assembly can occur (Almouzni & Méchali 1988; Almouzni et al. 1990). However, the preparation of *Xenopus* and mammalian extracts are laborious and material is limited (Rodriguez-Campos et al. 1989). In addition to this, *in vitro* systems using mammalian extract had to be supplied with additional histones to enable proper chromatin assembly. Therefore, Becker and Wu developed 1992 a protocol for chromatin assembly *in vitro* using *Drosophila* extract from preblastoderm embryos (Becker & Wu 1992), which results in very stable and reproducible extracts producing nucleosomes with physiological spacing. Due to the high demand of protein during the first very rapid cell division cycles in *Drosophila* embryos, this extract contains massive amounts of maternally deposited factors and provides sufficient amounts of histones and remodeling factor to reconstitute chromatin. These factors are deposited in specific reservoirs until required. H2A, H2B and H2A.V, for example, have been shown to be gathered in lipid droplets (Z. Li et al. 2012; Z. Li et al. 2017). However, extracts prepared from preblastoderm embryos are not capable of transcription, unlike extracts from postblastoderm embryos.

Figure 14 shows a simplified scheme of the embryo extract preparation, which is used in this thesis to reconstitute chromatin on recombinant DNA. Embryos during the first 1.5 h after egg laying (AEL) are collected and dechorionated. After several washing steps (not shown), the embryos are homogenized, and the homogenate is separated by ultracentrifugation into a lipid layer, a nuclei-containing pellet and a clear cytoplasmic extract, which is collected and frozen in liquid nitrogen until used for chromatin assembly on recombinant DNA. In this case, DNA was coupled to paramagnetic beads to facilitate isolation of reconstituted chromatin for analysis by Western blot or mass spectrometry.

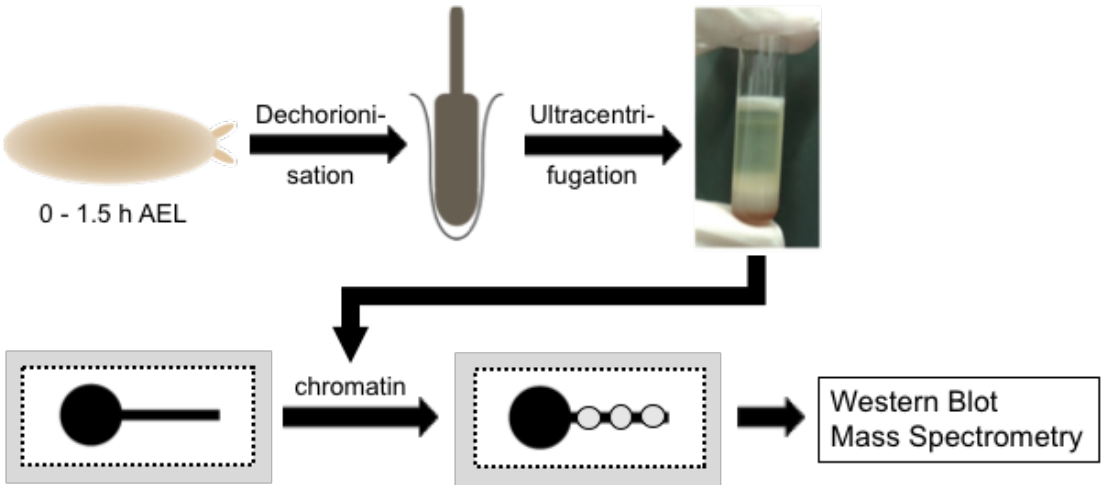

FIGURE 14: PRINCIPLE OF EMBRYO EXTRACT PREPARATION FROM PREBLASTODERM 0 TO 1.5 H OLD EMBRYOS AS PREVIOUSLY DESCRIBED IN BECKER & WU 1992 AND CHROMATIN *IN VITRO* RECONSTITUTION. DECHORIONIZED EMBRYOS ARE HOMOGENIZED AND EXTRACT IS SEPARATED BY ULTRACENTRIFUGATION. RECOMBINANT DNA (HERE IMMOBILIZED ON PARAMAGNETIC BEADS) IS USED FOR CHROMATIN *IN VITRO* RECONSTITUTION BY THE EXTRACT.

F. OBJECTIVE OF THIS THESIS

In this thesis, I employed the chromatin *in vitro* reconstitution system to establish a tool for DNA damage-associated investigations *in vitro*.

The project is structured into three parts: In the first part, I characterized the *in vitro* reconstituted chromatin. In the second part, I explored the recruitment of factors to sites of damage by isolating chromatin immobilized on solid phases, dissected rapid events in a time- and location-resolved manner and investigated DNA damage-associated events on predefined nucleosomes composed of canonical, variant, or mutated histones. In the third part I explored the role of Iswi-containing remodelers, in particular ACF and RSF, in the incorporation and turnover of H2A.V

IV. MATERIALS

A. CHEMICALS

4-OHT (Sigma)
Acetic acid (VWR)
Acetyl-CoA (Sigma)
Acrylamide Rotiporese Gel 30 (Roth)
Agarose (Bio & Sell)
Ammonium acetate (Roth)
Ammonium bicarbonate (Sigma)
Ammonium sulfate (VWR)
Ampicillin (Roth)
Aprotinin (Genaxxon)
ATP (Roche)
Bromophenol blue (Serva)
BSA (Sigma or New England Biolabs)
Calcium chloride (Sigma)
Chloramphenicol (Roth)
Complete Protease Inhibitor Cocktail Tablets (Roche)
Coomassie Brilliant Blue (Sigma)
Creatine Phosphate (Sigma)
DAPI (Invitrogen)
DMSO (Sigma)
DTT (Roth)
ECL Advance Western Blotting Detection Kit (VWR)
EDTA (Sigma)
Effectene Transfection Reagent (Qiagen)
EGTA (Sigma);
Ethanol (Sigma)
Ethidium bromide (Sigma)
FBS (Sigma)
Glycerol (VWR)
Glycine (Diagonal)
Glycogen (Roth)
Guanidine hydrochloride (Sigma)
Hepes (Roth)
HEPES (Serva)
Hydroxyurea (Sigma)
IPTG (Roth)
Isopropanol (Sigma)
L-lysine monohydrochloride (Sigma)
LB Agar (Serva)
Leupeptin (Genaxxon)
Magnesium chloride (VWR)
Methanol (Sigma)
N-Lauroylsarcosine (Sigma)
NDS (Dianova)

NGS (Dianova)
NP-40 (Igepal CA-630) (Sigma)
Orange G (Sigma)
Paraformaldehyde (Life Technologies)
Penicillin/Streptomycin (Sigma)
Pepstatin (Genaxxon)
PMSF (Sigma)
Potassium chloride (VWR)
Power up SYBR Green (Life technologies)
Rotiporese® Gel 30 (Roth)
Schneider's *Drosophila* medium (Life Technologies)
SDS (Serva)
Sodium bicarbonate (Sigma)
Sodium carbonate (Sigma)
Sodium chloride (Neolab or Serva)
Sodium deoxycholate (Sigma)
Sodium hypochlorite solution (VWR)
Spermidine (Sigma)
Spermine (Sigma)
TEMED (Sigma)
Thiourea (Sigma)
Tris (Diagonal)
Triton X-100 (Sigma)
Tween 20 (Sigma)
Wortmannin from Penicillium Fumiculosum (Sigma)
β-glycerophosphate (Sigma)
β-mercaptoethanol (Sigma)

B. ENZYMES

Apyrase (New England Biolabs)
Creatine Kinase (Sigma)
DNA Polymerase I, Large (Klenow) Fragment (New England Biolabs)
LysC (Wako)
Micrococcal Nuclease (Sigma)
Pfu Turbo DNA Polymerase (Agilent)
Phusion High-Fidelity DNA Polymerase (New England Biolabs)
PmlI (Life technologies)
Proteinase K (Diagonal)
Restriction enzymes (New England Biolabs, unless specified otherwise)
RNase A (Sigma)
SgrDI (Life technologies)
T4 DNA Ligase (New England Biolabs)
Trypsin (Promega)

C. KITS

Biotin-Nick Translation Mix (Sigma)
DNeasy Blood & Tissue Kit (Qiagen)
ECL Advance Western Blotting Detection Kit (VWR)
ENLITEN rLuciferase/rLuciferin Reagent A (Promega)
Genelute PCR Clean-Up Kit (Sigma)
Gibson Assembly Master Mix (Biolabs)
Immobilon Western Chemiluminescent HRP Substrate (Merck Millipore)
MEGAscrip T7 Transcription Kit (Thermo)
NEBNext Ultra II DNA Library (New England Biolabs)
Nucleobond PC 500 (Macherey-Nagel)
NucleoSpin Gel and PCR Clean-up (Macherey-Nagel)
NucleoSpin Plasmid Mini Kit (Macherey-Nagel)
RNeasy Mini Kit (Qiagen)

D. CONSUMABLES

Amicon Ultra-4 (Merck Millipore)
Complete, Mini EDTA-free (Sigma)
Membrane filters nitrocellulose (Roth)
Membrane filters pore size 0.2 µm and 0.45 µm (Roth)
Milles-HPF HV Filter, 0.45 µm (Merck Millipore)
Miracloth (VWR)
Protran membran BA85 (VWR)
Slide-A-Lyzer Mini Dialysis Unit (Life technologies)
Spectra/Por 3 MWCO 3.5 kDa dialysis membranes (VWR)
Whatman cellulose chromatography paper (Sigma)

E. FLY POPULATION

Agar-Agar (Die Gewürzmühle Brecht)
Apple juice (Discounter)
Cellulose (Arndt)
Dry yeast, Fermipan rot (Hobbybäcker)
Styrofoam dishes (Margret Lutz)
Yeast extract (BD Biosciences)

F. MARKERS

DNA Ladder 1 kb (New England Biolabs)
DNA Ladder 100 bp (New England Biolabs)
Protein-Marker IV (VWR)

G. COLUMNS AND RESINS

Agencourt AMPure XP beads (Beckman Coulter)
Anti-FLAG M2 Agarose beads (Sigma)
Dynabeads M280 Streptavidin (Life technologies)
HiTrap Q HP (VWR)
HiTrap SP Colums (VWR)
Mini quick spin DNA columns (Sigma)
Protein A or G Sepharose, beads (Elisabeth Kremmer, Helmholtz Center Munich)
TopTip C18 stage tips (Glygen)

H. NUCLEOTIDES

2'-Deoxyguanosine-5'-O-(1-thiotriphosphate) (Enzo Life Sciences)
5'-Adenylylimodiphosphat AMPPNP (Sigma)
Biotin-14-dATP (Life technologies)
Biotin-16-dUTP (Sigma)
dATP, dTTP, dCTP, dGTP (Bioline)
dNTP mix (NEB)
Thymidine-5´O-(1-thiotriphosphate) (Enzo Life Sciences)

I. PLASMIDS AND FOSMIDS

FlyFosmids 019611 and 019829 (Pawel Tomancak, MPI Dresden, Germany, published in Ejsmont et al. 2009)
pBluescript-13x5SrRNA (kind gift from Axel Imhof, BMC Martinsried, Germany, published in Völker-Albert et al. 2016)
pET15b-H2A, pET15b-H2B (kind gift from Felix Müller-Planitz, BMC Martinsried, Germany, published in Klinker, Haas, et al. 2014)
pFBDM-6xHis-Iswi-Acf1-Flag (generated by Silke Krause, BMC Martinsried, Germany)
pRM-3xHA-AsiSI-ER (kind gift from Gaelle Legube, Toulouse, France, published in Massip et al. 2010)
pRSET-A-H2A.V (kind gift from Jürg Müller, MPI Martinsried, Germany, sequence listed in XI.A.
pRSET-A-H2A.VE, pRSETA-H2A.V-3xFlag, pRSETA-H2A.VΔC, pRSETA-H2A.VE-3xFlag, pRSETA-3xFlag-H2A.V, pRSETA-3xFlag-H2A.VΔC, pRSETA-3xFlag-H2A.VE (generated in this thesis using site-directed mutagenesis, see IV.J.1 and V.E.3)
pUC18 (published in Yanisch-Perron et al. 1985)
pUC18-25x601 (published in Klinker, Mueller-Planitz, et al. 2014)

J. OLIGONUCLEOTIDES

1. OLIGONUCLEOTIDES TO INSERT POINT MUTATIONS

(ordered at Biomers, Germany)

Introduction of stop codon to produce ΔC-term H2A.V

Fw: GGCAAAAAAGAAGAAACCGTTCAGTAGCCGCAGCGTAAAGG

Rv: CCTTTACGCTGCGGCTACTGAACGGTTTCTTCTTTTTTGCC

S → E exchange in N-term 3xFlag H2A.V and untagged H2A.V

Fw: GCGTAAAGGTAATGTTATTCTGGAACAGGCCTATTAAGGATCCG

Rv: CGGATCCTTAATAGGCCTGTTCCAGAATAACATTACCTTTACGC

S → E exchange in C-term 3xFlag H2A.V

Fw: GCGTAAAGGTAATGTTATTCTGAGCCAGGCCTATGATTATAAGGATCACG

Rv: CGTGATCCTTATAATCATAGGCCTGGCTCAGAATAACATTACCTTTACGC

2. INSERTS TO INTRODUCE 3XFLAG TAGGED H2A.V

Sequence to introduce N-terminal 3xFLAG into pRSET-A-H2A.V (GeneCust):

TCTAGAAATAATTTTGTTTAACTTTAAGAAGGAGATATACATATGGATTATAAAGATCATGAT
GGTGATTATAAAGATCATGATATTGATTATAAAGATGATGATGATAAAGCAGGCGGTAAAG
CAGGTAAAGATAGCGGTAAAGCAAAAGCAAAAGCCGTTAGCCGTAGCGCACGTG

Sequence to introduce C-terminal 3xFLAG into pRSET-A-H2A.V (GeneCust):

AGGCCTATGATTATAAAGATCATGATGGTGATTATAAAGATCATGATATTGATTATAAAGAT
GATGATGATAAATAAGGATCCGAGCTC

3. OLIGONUCLEOTIDES FOR QPCR AMPLIFICATION

FlyFos019611

Control region 1 fw: GGACCTGCTAGTGTCCTGCG
Control region 1 rv: GCAGATGGAACATTCCGTTCTGCG
Control region 2 fw: GGCAGGCGACTGTTTGCC
Control region 2 rv: GCCAACACGTTGGAGGCG
Distance 500 bp 1 fw: GGCTGCGCCCTGTGC
Distance 500 bp 1 rv: GCTGTTCCCTGGTGCTTC
Distance 1500 bp 1 fw: CCGGATGGCTCAGGCATCG
Distance 1500 bp 1 rv: GCAGGAAGCGGCGGC
Distance 3000 bp 1 fw: GGGTGATAGTGTTGAGAAGACCTCTCG
Distance 3000 bp 1 rv: CCAGATACTCTTCGACCGAACGCC
Distance 500 bp 2 fw: CGGACGAGAAGTGGTAAGAGGAGC
Distance 500 bp 2 rv: CGACATAGAAACGTGTGCGTGGC
Distance 1500 bp 2 fw: CCAATGCACACACTCGAACTCACC
Distance 1500 bp 2 rv: CCACGAAGATGTCGGTAAACATTTGCG
Distance 3000 bp 2 fw: CCAGGGACCATCTCCACCTCC
Distance 3000 bp 2 rv: CGGCACACAAACTGTTTCGCC

FlyFos019829

Control region 1 fw: GGGCTACGTGTTTTGCTCGTGG
Control region 1 rv: CGTCCTTTTCCCCAAGATAGAAAGGC
Control region 2 fw: GGCCCGTTTGTCAGAAAAAGAGCC
Control region 2 rv: GCCAGTCCAAGACGGTAACGC

4. Oligonucleotides to amplify DNA from genomic DNA to generate RNAi

Tip60

Fw: TAATACGACTCACTATAGGGGAA CTC TGT CAT TAC GTA GAA GAG AAA C
Rv: TAATACGACTCACTATAGGGCCTACAACTCCGCAGACAC

Ku70

Fw: TAATACGACTCACTATAGGGCCCCAGATAATGGGGAAGATAAG
Rv: TAATACGACTCACTATAGGGTCT ATG CGC TTG TCC TGT TG

Ku80

Fw: TAATACGACTCACTATAGGGCAA TTA AGC CCA CAC CG
Rv: TAATACGACTCACTATAGGGAAA TGG TTG TGC TAC TGC

K. Antibodies

1. Monoclonal primary antibodies

(from Elisabeth Kremmer, Helmholtz Center Munich)

a-Ku70 Peptide 1, 6B2	rat, WB 1:5
a-Ku70 Peptide 1, 12B8	rat, WB 1:5
a-Ku70 Peptide 2, 5H4	rat, WB 1:5
a-Ku80 Peptide 1, 8E7	rat, WB 1:5
a-Ku80 Peptide 2, 8B11	rat, WB 1:5
a-Acf1, 3F1	rat, WB 1:5
a-Acf1, 8E3	rat, WB 1:5
a-HA, 12CA5	mouse, WB 1:5
a-Chrac14, 5C7	rat, WB 1:5
a-Chrac16, 6G6	rat, WB 1:5
a-DomA+B, 2G5	rat, WB 1:5
a-DomA, 24C10	rat, WB 1:5
a-DomB, 4H4	mouse, WB 1:5
a-Tip60, 2C4	mouse, WB 1:5
a-Tip60, 6H1	rat, WB 1:5

2. COMMERCIAL PRIMARY ANTIBODIES

a-H2AvD p S 137 (Biomol)	rabbit, WB 1: 5000
a-H3 antibody ab1791 (Abcam)	rabbit, WB 1: 20000
a-H4 antibody ab10158 (Abcam)	rabbit, WB 1: 5000
a-H4K16ac (Millipore)	rabbit, WB: 1:10.000
a-H4K16ac (Active Motif)	rabbit, WB: 1:500
a-poly(ADP-ribose) antibody ab14459 (Abcam)	mouse, WB: 1:1000

3. PRIMARY ANTIBODIES GENERATED IN OUR LABORATORY OR IN OTHERS

a-Acf1 rb2 (Jain, Baldi, Zabel, Straub & Becker 2015)	rabbit, WB 1:2500
a-H2A (kind gift from Jürg Müller, MPI Martinsried, Munich, Germany)	rabbit, WB 1: 2000
a-H2A.V (Börner & Becker 2016)	rabbit, WB 1:500
a-H2AvDpS137 (kind gift from R. Scott Hawley, Kansas, USA, (Lake et al. 2013)	mouse, WB 1: 20000
a-Iswi rb2 (unpublished)	rabbit, WB 1:2500
a-Rsf1 (Jain, Baldi, Zabel, Straub & Becker 2015)	rabbit, WB 1:2000

4. SECONDARY ANTIBODIES AND STAINING REAGENTS

a-mouse Cy3	donkey, IF: 1:2500
a-mouse IgG-HRP-linked Whole AB (VWR)	sheep, WB: 1:20 000
a-mouse IRDye 680RD (LI-COR Biosciences)	goat, WB: 1:10 000
a-rabbit Alexa488	donkey, IF: 1:2500
a-rabbit IgG-HRP-linked Whole AB (VWR)	donkey, WB: 1:20 000
a-rabbit IRDye 800CW (LI-COR Biosciences	goat, WB: 1:10 000
a-rat IgG-HRP-linked Whole AB (VWR)	goat, WB: 1:20 000
a-rat IRDye 800CW (LI-COR Biosciences)	goat, WB: 1:10 000
DAPI (Invitrogen)	IF: 1:500

V. METHODS

A. *DROSOPHILA* POPULATION

1. PREPARATION OF APPLE JUICE AGAR PLATES AND YEAST PASTE

Apple juice agar plates (about 200 plates): 1460 g agar was dissolved in 32 L deionized water, then 14 L apple juice and 2 L molasses were slowly added while stirring. The agar was stirred to chill down to less than 70°C and 1120 mL 10% (w/v) Nipagin (dissolved in ethanol) were added. Plates were then poured using styrofoam dishes of 225 cm x 175 cm x 25 cm size (Margret Lutz GmbH & Co. KG) with about 1 cm of agar, and stored after polymerization of the agar in clean plastic bags at 4°C. 500 g dry yeast were dissolved in 750 mL ddH_2O and 4.2 mL propionic acid (Sigma) and stored at 4°C.

2. PREPARATION OF EMBRYO BOXES TO MAINTAIN THE *DROSOPHILA* POPULATION

Embryos from overnight plates were collected, washed in 70% EtOH and transferred to small Whatman papers to dry. Meanwhile, cellulose tissues were distributed to plastic boxes of about 30 cm x 30 cm x 10 cm and soaked with 425 mL - 450 mL of an embryo nutrition suspension composed of 77 g inactivated yeast, 50 g sugar, 12 mL 10% (w/v) Nipagin (dissolved in ethanol), 4.8 mL ortho-phosphoric acid, 0.6 mL propionic acid and 430 mL water. The Whatman papers with embryos were transferred onto the soaked cellulose tissues and the boxes with embryos were closed with lids consistent of grids to allow air circulation. The boxes were then kept at 25°C and appropriate humidity for 10 days until the embryos reached the adult stage. After hatching, flies in the boxes were transferred in to collection cages and kept at 25°C and appropriate humidity. Agar plates stocked with yeast paste were added and changed regularly.

B. SAMPLE PREPARATION FOR CHROMATIN *IN VITRO* RECONSTITUTION

1. *DROSOPHILA* EMBRYO EXTRACT (DREX) PREPARATION

DREX was prepared from preblastoderm Oregon-R embryos 0-90 min AEL according to Becker & Wu 1992 with the following modifications:

After collection of 0-90 min old embryos, the embryos were dechorionated in 200 mL embryo wash buffer and 60 mL 13% sodium hypochlorite (VWR) for 3 min at room temperature while stirring. Embryos were rinsed for 5 min with cold water and transferred into a glass cylinder with embryo wash buffer. After settling of the embryos, the buffer was decanted, and the embryos were washed first in 0.7% NaCl and then in extract buffer EX10.

After the last wash, embryo wash buffer was decanted, and embryos were homogenized with one stroke at 3000 rpm and 10 strokes at 1500 rpm using Schuett homgenplus, (Schuett-biotec). The homogenate was adjusted to a final $MgCl_2$concentration of 5 mM and centrifuged for 15 min at 27000 g at 4°C. The white lipid layer was discarded, and the supernatant was centrifuged for 2 h at 245000 g at 4°C. The clear supernatant was isolated with a needle and syringe, leaving the lipid layer and pelleted nuclei in the tube.

embryo wash buffer
0.7% NaCl
0.04% Triton X-100

EX-10
10 mM KCl
10 mM HEPES pH 7.6
1.5 mM $MgCl_2$
0.5 mM EGTA
10% glycerol
10 mM β-glycerophosphate
1 mM DTT
0.2 mM PMSF
1 mM aprotinin
1 mM leupeptin
1 mM pepstatin

2. DEPLETION OF DREX

For depletion of DREX from Acf1, monoclonal Acf1 8E3 or 3F1 antibodies were pre-coupled to protein G beads washed in PBS overnight on a rotating wheel at 4°C using 15 mL antibody per 200 µL protein G beads. Beads were then blocked in 5% BSA in PBS for 1h on a rotating wheel at 4°C and washed 5 times in EX10 buffer on a rotating wheel at 4°C. For depletion, 100 µL beads were added to 200 µL of extract and incubated for 3 h on a rotating wheel at 4°C. Afterwards, beads were pelleted for 2 min at 500 g and the supernatant was transferred to another 100 µL fresh blocked and antibody coupled beads for a second round of depletion for 3 h on a rotating wheel at 4°C. Afterwards, the supernatant was transferred to fresh tubes, snap frozen and stored at -80°C. Protein concentrations were in the range of about 30 mg/mL.

3. *DROSOPHILA* TRANSCRIPTION EXTRACT PREPARATION (TRAX)

For *Drosophila* transcription extract preparations, embryos from 0 to 12 h after egg laying were collected and stored at 4°C until 76 g were collected. Embryos were dechorionated as described in V.B.1 and rinsed with 1L embryo wash solution, then with distilled tap water and then dried with paper towel. Then, the embryos were resuspended in about 2 mL/g embryos of Buffer 1 and homogenized using the Yamato LH-21 homogenizer at 1000 rpm two passes. The homogenate was then passed through a funnel with a single layer miracloth and diluted with additional buffer 1 to a final volume of 5 mL/g embryos. Nuclei were then pelleted at 10 000 g for 15 min at 4°C, supernatants and lipids were removed and the outer layer of the

pellet was resuspended with buffer AB to a final concentration of 1 mL/g embryos without resuspending the lower layer of the pellet consisting of lipids. The last centrifugation step was repeated, and the pellet was then dissolved using a 40 mL B Dounce homogenizer. Then, 1/10 of the homogenate volume of room temperature ammonium sulfate pH 7.9 was added and the homogenate was mixed by inversion and centrifuged first for 20 min at 25 000 g and then for 2 h at 140 000, each time at 4°C. The supernatant beyond the lipid layer was removed with a syringe and a needle and supplied with 0.3 g per mL supernatant of finely grounded ammonium sulfate powder while stirring. After that, the supernatant was centrifuged for 20 min at 4°C at 25 000 g. The pellet was then resuspended in buffer C to a final concentration of 0.2 mL/g embryos using a dounce homogenizer and dialyzed for 4 h against 2 L of buffer C. The protein concentration was 14 mg/ml.

Buffer 1
15 mM HEPES pH 7.6
10 mM KCl
2 mM $MgCl_2$
0.5 mM EGTA
0.1 mM EDTA
350 mM sucrose
1 mM DTT
0.2 mM PMSF
1 mM NaMBS
1x Roche complete protein inhibitors

Buffer AB
15 mM HEPES pH 7.6
110 mM KCl
2 mM $MgCl_2$
0.1 mM EDTA
1 mM DTT
0.2 mM PMSF
1 mM NaMBS
1x Roche complete protein inhibitors

Buffer C
20% glycerol
25 mM HEPES pH 7.6
100 mM KCl
2 mM $MgCl_2$
0.1 mM EDTA
1 mM DTT
0.2 mM PMSF
1 mM NaMBS
1x Roche complete protein inhibitors

4. Preparation of immobilized DNA

Depending on the assay, either free (circular or linearized) DNA or immobilized DNA was used. As free DNA, pUC18 or FlyFosmids 019829 and 019611 were used. For linearization, pUC18 or FlyFosmid 019611 were restricted with XbaI, or FseI, respectively. For immobilization, 5' overhangs generated after restriction were filled up with biotinylated nucleotides by Klenow (exo^-) in the following reaction: 50 µM biotinylated dATP and/or dUTP were used together with 200 µM of the remaining dNTPs. To avoid unspecific degradation by nucleases in the extract, one unbiotinylated nucleotide was replaced by thio-dTTP or thio-dGTP, at 200 µM final concentration. The fill-up reaction was performed with 0.3 U/µL Klenow (exo^-) in 1x NEB2 for 1h at 37°C. To introduced biotinylated nucleotides by nick translation, circular pUC18 DNA was incubated in different ratios with Biotin-Nick Translation Mix (Sigma) for 90 min at 15°C (either

2 µg DNA in 32 µL ddH_2O supplied with 8 µL mix or 10 µg DNA in 16 µL ddH_2O supplied with 4 µL mix). To remove unincorporated nucleotides, DNA was either purified over G50 Sepharose columns (Roche) or with the NucleoSpin Gel and PCR Clean-up kit (Macherey-Nagel).

For immobilization of biotinylated DNA, a coupling mix was prepared as follows: 30 ng/µL biotinylated DNA in 1x binding and washing buffer were added to Dynabeads M-280 Streptavidin beads (Life technologies), which were prewashed once with PBS-BSA-NP40 and twice with 2x Binding and washing Buffer. The optimal binding ratio of beads : biotinylated DNA was determined in a previous titration to be 30 µL slurry : 1 µg DNA. Beads and coupling mix were incubated over night at 4°C while rotating. The efficiency of biotinylation was tested in a missing band test with 300 ng of input DNA and 10 µL of coupling mix after biotinylation (corresponding to 300 ng DNA before immobilization) analyzed on a 1% (w/v) agarose gel (0.5x TAE buffer, 0.5 µg/mL ethidium bromide).

2x binding and washing buffer
2 M NaCl
50 mM Tris–HCl pH 8.0
1 mM EDTA

0.5x TAE buffer
20 mM Tris pH 7.6
10 mM acetic acid
0.5 mM EDTA

5. HISTONE EXPRESSION AND PURIFICATION

Arrays were reconstituted from recombinant *Drosophila* histones purified according to Klinker, Haas, et al. 2014 with the following modifications: due to the lower pI, histone H2A.V and its tagged versions were purified in buffer Sau-0 instead of Sau-200. Histone H3 and H4 were kind gifts from Catherine Regnard (prepared by the purification of inclusion bodies).

Sau-0
40 mM sodium acetate pH 5.2
1 mM EDTA pH 8
10 mM lysine
Add fresh
7.5 M urea
5 mM DTT

Sau-1000
40 mM sodium acetate pH 5.2
1 mM EDTA pH 8
10 mM lysine
1 M NaCl
Add fresh
7.5 M urea
5 mM DTT

6. OCTAMER RECONSTITUTION

For octamer reconstitution, ratios of the corresponding histones were titrated to reach final ratios of H2A:H2B:H3:H4 1.2:1.2:1:1. After titration, histones were pooled, lyophilized and resuspended in Unfolding buffer to final concentrations of 4.7 mg/mL for H2A and H2B, and 4.0 mg/mL for H3 and H4, respectively. The histones were dialyzed against Refolding buffer at 4°C overnight. Octamers were purified by Size exclusion chromatography in Refolding buffer on a Hiload 16/600 Superdex 200 column (Sigma).

Unfolding buffer
7 M guanidine hydrochloride
20 mM Tris pH 7.5
10 mM DTT

Refolding buffer
10 mM Tris pH 7.5
2 M NaCl
1 mM EDTA
5 mM DTT

7. RECONSTITUTION OF RECOMBINANT NUCLEOSOME ARRAYS

Nucleosomes were reconstituted by salt gradient dialysis as follows: 100 µL reactions consistent of 10 µg DNA, around 10 µg octamer (optimal octamer amounts were determined after titration), 20 µg BSA, 0.1% Igepal CA-630, 10 mM Tris pH 7.6, 2 M NaCl, 1 mM EDTA were transferred into dialysis cups (Slide-A-Lyzer; MWCO 3500, Thermo Fisher) and placed in 300 mL high salt buffer. Salt concentration was decreased constantly at room temperature by pumping 3L of low salt buffer into the 300 mL high salt buffer using a peristaltic pump (Minipulse evolution, Gilson, mode 8.4 rpm). After the gradient, the dialysis cups were dialyzed 2 h at room temperature against low salt buffer. Quality of nucleosome assembly was assessed by limited MNase digestion.

low-salt buffer
10 mM Tris pH 7.6
50 mM NaCl
1 mM EDTA
0.05% Igepal CA-630
0.01% β-mercaptoethanol

high-salt buffer
10 mM Tris-HCl pH 7.6
2 M NaCl
1 mM EDTA pH 8.0
0.05% Igepal CA-630
0.1% β-mercaptoethanol

C. *IN VITRO* CHROMATIN ASSEMBLY AND ANALYSIS

1. STANDARD CHROMATIN ASSEMBLY REACTION

When chromatin assembly was performed on immobilized DNA, beads with DNA were first blocked for 1 h on a rotating wheel at 4°C in PBS-BSA-NP40 buffer and washed twice in EX-50 buffer supplied with 0.05% Igepal. For chromatin assembly, 1 µg of free or immobilized recombinant DNA or recombinant nucleosome arrays were incubated with 40 µL (for γH2A.V spreading reactions) or 60 µL DREX supplied with 10 mM β-glycerophosphate and ATP regenerating buffer and filled up to a total volume of 120 µL with EX50 buffer and incubated at 26°C.

PBS-BSA-Igepal
PBS with 0.05% BSA (w/v)
and 0.05% Igepal (v/v)

ATP regenerating buffer
3 mM ATP
30 mM creatine phosphate
10 µg/mL creatine kinase
3 mM $MgCl_2$
1 mM DTT

EX-50
50 mM KCl
10 mM HEPES pH 7.6
1.5 mM $MgCl_2$
0.5 mM EGTA
10% glycerol
10 mM β-glycerophosphate
1 mM DTT
0.2 mM PMSF
1 mM aprotinin
1 mM leupeptin
1 mM pepstatin

2. LIMITED MNASE DIGESTION AND SUPERCOILING ASSAY

To assess chromatin assembly by limited MNase digestion, 1 µg DNA was supplied with 40 µL to 80 µL DREX supplied with ATP regenerating buffer and filled up to a total volume of 140 µL with EX50 buffer. Chromatin assembly was then performed for 6 h at 26°C. Then, 200 µL MNase mix was added to each reaction and 110 µL aliquots were removed after 15 s, 30 sec and 90 s and transferred to fresh tubes with 40 µL MNase stop solution to stop MNase digest by chelating Ca^{2+} ions in the reaction. Afterwards, the tubes were supplied with 2 µL RNase and incubated for 30 min at 37°C. Then, SDS up to a final concentration of 0.2% (w/v) and 10 µL proteinase K was added and protein digest was performed overnight at 37°C. On the next day, DNA was pelleted by ethanol precipitation, eluted in TE buffer and supplied with DNA sample buffer including Orange G, and separated on 1.5% agarose (w/v) in 0.5x TAE buffer at 100 volts. DNA was then stained with 12.5 µg ethidium bromide / 100 mL TAE buffer for 20 min at room temperature.

For the supercoiling assay, 1.5 µg DNA was supplied with 60 µL to 90 µL DREX supplied with ATP regenerating buffer and filled up to a total volume of 200 µL with EX50 buffer. Chromatin

assembly was then performed at 26°C and stopped after 10 min, 30 min, 60 min, and 180 min by transferring 40 µL of the reaction to 10 µL MNase stop solution. Afterwards, samples were treated with RNase and proteinase K and DNA was purified as described before. Gel electrophoresis after DNA elution in TE buffer and addition of DNA sample buffer including Orange G or bromophenol blue was then performed on 1.2% agarose (w/v) in 1x in Tris/glycine buffer at 100 volts. DNA was then stained with 12.5 µg ethidium bromide / 100 mL TAE buffer for 20 min at room temperature.

MNase mix
5 mM CaCl2 and 12 U/mL MNase in EX50

MNase stop solution
100 mM EDTA pH 8.0
2.5% N- lauroylsarcosine

RNase A (10mg/mL)
10 mM Tris pH 7.5
15 mM NaCl
heated to 100°C for 15 min

Proteinase K (10 mg/mL)
in 50 mM Tris pH 8.0, 5 mM $CaCl_2$ and 50% glycerol

TE buffer
10 mM Tris pH 7.5
1 mM EDTA pH 8

6x DNA sample buffer
60% glycerol (v/v), filled up with TE buffer
add spatula tip of Orange G or bromophenol blue

0.5x TAE buffer
20 mM Tris pH 7.6
10 mM acetic acid
0.5 mM EDTA

1x in Tris/glycine buffer
25 mM Tris
200 mM glycine

3. Chromatin Immunoprecipitation

Chromatin immunoprecipitation was performed on standard chromatin assembly reactions, unless indicated otherwise. Formaldehyde crosslinking was performed for 10 min at 26°C with concentrations of 0.01% or 0.1% formaldehyde, for histones, or chromatin remodeling factors, respectively.

To capture fast spreading events, formaldehyde crosslinking was performed with 0.1% formaldehyde for 3 min at 26°C. Crosslinking was quenched by addition of 125 mM glycine for 5 min at 26°C. Then, after addition of 1.5 mM $CaCl_2$, chromatin was fragmented by MNase treatment for 15 min at 30°C, with 1.2 U per µg DNA for chromatin assembled from endogenous nucleosomes, and 2.4 U per µg DNA for chromatin assembled from recombinant nucleosomes, respectively. MNase digestion was stopped by chelating the Ca^{2+} ions with 10 mM EDTA. Chromatin was then filled up with RIPA to 500 µL per 1 µg DNA. Then, pre-clearing was performed by incubation with 30 µL slurry of protein A or G beads (depending on which was used for the immunoprecipitation later) washed with RIPA for 1 h on a rotating wheel at 4°C. Then, beads were pelleted after centrifugation at 500 g for 2 min, the supernatant was transferred into fresh tubes, split for immunoprecipitation and supplied with the

corresponding antibody. Amounts of chromatin and antibody used per ChIP as well as usage of protein A or G beads are listed in Table 2. For monoclonal rat antibodies, protein G beads were washed with PBS and precoupled to antibody overnight on a rotating wheel at 4°C (1.5 mL antibody per 30 µL beads).

TABLE 2: ANTIBODY CONCENTRATIONS AND BEADS USED FOR CHROMATIN IMMUNOPRECIPITATION

antibody	Amount per µg DNA	Beads used for pre-clean and IP
a-H2A.V (Anton Eberharter)	4 µL per 0.5 µg	A:G mix 50:50
a-γH2A.V (Rockland)	3 µL per 0.5 µg	A:G mix 50:50
a-H4K16ac (Active motif)	6 µL per 1 µg	A:G mix 50:50
a-H2A (Müller laboratory)	8 µL per 1 µg	A:G mix 50:50
a-H3 (Abcam)	3 µL per 1 µg	A:G mix 50:50
a-Acf1 rb2	15 µL per 1 µg	A:G mix 50:50
a-Iswi rb2	15 µL per 1 µg	A:G mix 50:50
a-Ku70 (mix of 6B2, 12B8 and 5H4)	precoupled	G
a-Ku80 (mix of 8E7 and 8B11)	precoupled	G
a-Acf1 8E3	precoupled	G

a-Ku70 Peptide 1, 6B2, rat, WB 1:5
a-Ku70 Peptide 1, 12B8, rat, WB 1:5
a-Ku70 Peptide 2, 5H4, rat, WB 1:5
a-Ku80 Peptide 1, 8E7, rat, WB 1:5
a-Ku80 Peptide 2, 8B11, rat, WB 1:5

Chromatin samples including the antibody were incubated overnight on a rotating wheel at 4°C, supplied with 30 µL protein A or G beads according to Table 2 and incubated for 3 h on a rotating wheel at 4°C. Then, beads were washed 5 times with RIPA, each for 10 min on a rotating wheel at 4°C and then, after removal of supernatant, supplied with 100 µL TE including 10 µg RNaseA. After incubation of 30 min at 37°C while shaking, samples were supplied with 0.5% SDS and 100 µg proteinase K. De-crosslinking was then performed at 68°C and 800 rpm for 2 h, followed by 37°C and 800 rpm overnight. DNA was then purified using the Genelute PCR Clean-Up Kit (Sigma) and eluted in 30 µL TE buffer.

RIPA buffer (adapted from Abcam)
150 mM sodium chloride
1.0% NP-40 (or Triton X-100)
0.5% sodium deoxycholate
0.1% SDS
50 mM Tris pH 8.0

TE buffer
10 mM Tris pH 7.5
1 mM EDTA pH 8

RNase A (10mg/mL)
10 mM Tris pH 7.5
15mM NaCl
heated to 100°C for 15 min

Proteinase K (10 mg/mL)
50 mM Tris pH 8.0
5 mM $CaCl_2$
50% glycerol

4. Quantitative real-time PCR and DNA Sequencing

For qPCR, DNA purified after chromatin immunoprecipitation was diluted 1:30 in ddH_2O. All measurements were performed in triplicates using 2 µL of diluted DNA, 5 µM of each, forward and reverse primer, and Power up SYBR Green in 10 µL total volume. Concentrations were determined in reference to a standard curve of input DNA of 0.00025 ng, 0.0025 ng, 0.025 and 0.25 ng. For next generation sequencing, libraries were prepared using NEBNext Ultra II DNA Library (New England Biolabs) according to manufacturer's instructions and sequenced by the Laboratory for Functional Genome Analysis (LAFUGA) platform, Gene Center Munich, Germany using an Illumina HiSeq1500 sequencer in approximately 1 million single-end reads for FlyFosmid DNA and 40 million single-end reads for genomic DNA. Mapping and normalization was performed by Tamás Schauer as follows: Reads were mapped using bowtie2 (version 2.2.9) against the reference genome (version dm6) and multi-mapping reads were excluded (MAPQ > 1). Read coverages were calculated using R/Bioconductor packages (version 3.6) and were normalized by the total number of reads mapped to the control FlyFosmid (unless indicated otherwise). The normalized profiles were visualized in the IGV browser (version 2.3.82).

5. Mass spectrometry Analysis

For Acf1 depletion, 70 µL protein G sepharose beads pre-coupled to 8E3 or 3F1 antibody, blocked with BSA and washed with EX10, were incubated with 140 µL extract for 3 h at 4°C on a rotating wheel. Afterwards, beads were washed 5 times with EX50 buffer supplied with 2 mM DTT and prepared for mass spectrometry analysis as follows:

100 µL 4 M urea in 100 mM Tris pH 8 supplied with 1 µg LysC was added to the beads and incubated for 1.5 h at 28°C while shaking. The supernatant was transferred into a new vial and beads were washed twice with 200 µL 100 mM ammonium bicarbonate and both supernatants were combined with the first supernatant to obtain 500 µL per tube. Then, DTT was added to a final concentration of 2 mM and trypsin digestion was performed with 2 µg trypsin per tube overnight at 30°C. On the next day, iodoacetamide was added to a final concentration of 10 mM and samples were incubated for 30 min at room temperature in the dark. Samples were then acidified with 5% trifluoroacetic acid (v/v) and desalted with TopTip C18 stage tips (Glygen) as follows: tips were prepared by washing twice with 50 µL methanol and 5 times with 70 µL 0.2% (v/v) trifluoroacetic acid. Then, samples were loaded onto the C18 stage tips, washed twice with 70 µL 0.2% (v/v) formic acid and dried by an additional round of centrifugation. Elution was performed with 2x 100 µL 70% (v/v) acetonitrile and 0.1% (v/v) formic acid. Samples were then vacuum dried, dissolved in 20 µL 0.2% (v/v) formic acid and analyzed by Andreas Schmidt (Protein Analysis Unit ZfP, LMU Munich) with LC MS/MS using the Triple TOF 6600 system (Sciex).

For chromatin samples on immobilized DNA, standard chromatin assembly reactions were prepared as described. After assembly for 15 min or 3 h, beads were washed with EX50 buffer (w/o proteinase inhibitors) supplied with 2 mM DTT and beads and input samples were filled

up with the same buffer up to 20 µL. Then, samples were incubated at 56°C for 35 min to reduce disulfide bonds, cooled down to room temperature and supplied with urea in 100 mM Tris pH 8 and iodoacetamide to final concentrations of 5 M, or 10 mM, respectively, and incubated for 35 min in the dark at room temperature while shaking. Samples were then diluted with 100 mM ammonium bicarbonate to a final concentration of 1 M urea and 5 µg trypsin was added to each SN or input sample and 1 µg trypsin to each beads sample and incubated overnight at 30°C. Beads were then collected on paramagnetic devices and supernatants were transferred to fresh vials. Beads were washed twice with 70 µL 0.2% formic acid (v/v) and supernatants from washing were combined with the previous supernatant from digestion. Samples were then acidified with trifluoroacetic acid to pH 2-3 and desalted with C18 stage tips as described before. The eluate was again vacuum dried, dissolved in 20 µL 0.2% (v/v) formic acid and analyzed by Andreas Schmidt (Protein Analysis Unit ZfP, LMU Munich) with LC MS/MS using the Triple TOF 6600 system (Sciex).

For the analysis of post-translational histone modifications, the following modified chromatin assembly reactions were set-up to decrease the abundance of free unincorporated histones: 1 µg of free linearized or circular DNA or preassembled arrays of H2A.V or H2A.VΔC nucleosomes on linearized or circular DNA were incubated with 8 µL DREX supplied with 10 mM β-glycerophosphate and ATP regenerating buffer and filled up to a total volume of 40 µL with EX50 buffer and incubated at 26°C for 15 min or 3 h. Samples were then snap frozen in liquid nitrogen and analyzed by Christian Feller, ETH Zurich, Switzerland.

D. CELL CULTURE METHODS

1. MAINTENANCE AND MODIFICATION OF *DROSOPHILA* SCHNEIDER CELLS

Stable transfection with AsiSI was performed using *Drosophila* S2_DGRC cells maintained in Schneider's *Drosophila* medium supplemented with penicillin, streptomycin and 10% (v/v) fetal calf serum at 26°C. Stable transfection was performed with Effectene Transfection Reagent (Qiagen) according to manufacturer's instructions. 2-3 days after transfection, 10 µg/mL puromycin was added to select for cells, which incorporated the construct including a puromycin resistance gene. In parallel, a control transfection without DNA was performed and treated with puromycin-containing medium in parallel. When the cells of the control transfection died due to the lacking resistance, AsiSI-transfected cells were transferred to Schneider's *Drosophila* medium supplemented with penicillin, streptomycin and 10% (v/v) fetal calf serum and maintained at 26°C. For SDS-PAGE, cells were washed with PBS, resusupended in 100 µL urea sample buffer per $2*10^6$ cells and boiled at 95°C for 5 min.

PBS
140 mM NaCl
3 mM KCl
10 mM Na_2HPO_4
2 mM KH_2PO_4

Urea sample buffer
9M urea
1% SDS
25 mM Tris pH 6.8
1 mM EDTA
0.02% bromophenol blue
100 mM DTT

2. INDUCTION OF DSBS INTO THE GENOME OF STABLY TRANSFECTED ASISI CELLS

$1*10^6$ SL2 cells were supplied with $CuSO_4$ to a final concentration of 5 mM and incubated for 24 h at 26°C. Then 4-OHT was added to a final concentration of 300 nM and cells were incubated for additional 4 h at 26°C.

3. KNOCK DOWN OF TIP60, KU70, AND KU80

Appropriate target regions for RNAi against Tip60, Ku70 and Ku80 were determined using http://www.flyrnai.org/cgi-bin/DRSC_gene_lookup.pl. The following amplicons were used: Tip60 RNAi: DRSC18661; Ku70 RNAi: DRSC29386; Ku80 RNAi: DRSC26861. The genomic region of interest was amplified from genomic DNA isolated from W1118 flies by Phusion High-Fidelity DNA Polymerase (New England Biolabs) according to manufacturer's instructions with the following PCR program:

2 min	99°C	
10 sec	99°C	
20 sec	50°C	
15 sec	72°C	(30 cycles)
5 min	72°C	

4 µL of the PCR product were analysed by gel electrophoresis to confirm successful PCR amplification. To generate dsRNA, *in vitro* transcription was performed with the MEGAscrip T7 Transcription Kit (Thermo) and purified using the RNeasy Mini Kit (Qiagen) according to manufacturer's instructions.

For knock down, $1*10^6$ cells were resuspended in 1 mL Schneider's *Drosophila* medium (Life Technologies) supplemented with penicillin, streptomycin and incubate with 10 µg dsRNA for 30 min at room temperature while shaking. Then 3 mL Schneider's *Drosophila* medium supplemented with penicillin, streptomycin and 10% (v/v) fetal calf serum was added and incubated for 4 days at 26°C.

4. IF STAINING OF AsiSI TRANSFECTED SL2 CELLS

First, DSBs were induced as described in V.D.2 using 1*106 cells in 5 mL Schneider's *Drosophila* medium supplemented with penicillin, streptomycin and 10% (v/v) fetal calf serum. After resuspension of cells, 100 µL were transferred to 3-well coverslips and left for 1 h to allow them settling. Then cells were washed in a coplin jar with PBS for 5 min at room temperature, fixed by adding 100 µL 3.7% (v/v) formaldehyde in PBS for 10 min, and washed again twice in PBS for 5-10 min. Afterwards, cells were permeabilized in a coplin jar with ice-cold PBS with 0.25% Triton for 6 min on ice. After washing again twice in PBS for 5-10 min, the coverslips were dried with Whatman paper and 100 µL PBS with 0.1% Triton and 5% NDS was added for blocking. After 2 h of incubation at room temperature, the slides were washed in PBS and 100 µL antibody solution (polyclonal rabbit-H2A.V and monoclonal mouse-γH2A.V, both diluted in PBS with 0.1% Triton, 5% NDS and 5% non-fat milk) were added to the cover slips. Slides were incubated in a wet chamber (consisting of a wet towel in a closed box) overnight at room temperature), and then washed again twice in PBS with 0.1% Triton for 5-10 min and dried with Whatman paper. Then 100 µL of antibody solution (donkey-anti-mouse Cy3 and donkey-anti-rabbit Alexa488 diluted in PBS with 0.1% Triton, 5% NDS and 5% non-fat milk) was added and incubated in a slide holder for 1-2 h protected from light. Then, slides were washed again twice in PBS with 0.1% Triton, stained with DAPI in PBS for 10 min, washed with PBS for 5-10 min and dried by gently tapping the slides onto a paper towel. Afterwards, 1 drop of Vectashield mounting medium was applied to the cells and covered with a coverslip. After slightly pressing the coverslip onto the slide, the coverslip was sealed with clear nail polish and dried for 30 min at room temperature and protected from light. The slides were stored in the dark at 4°C.

E. STANDARD LABORATORY METHODS

1. SDS-PAGE AND WESTERN BLOT ANALYSIS

Samples were supplied with LaemmLi buffer, heated up to 95°C for 5 min, and separated on SERVAGel TG PRiME precast gels in running buffer according to the manufacturer's instructions. As a size standard, 5 µL of Protein-Marker IV was loaded. Then, gels were either analyzed by Coomassie staining or processed for Western blot analysis. For Coomassie staining, the gel was fixed for 15 min in SDS Gel fix solution and then stained in 15 mL SDS Gel Coomassie staining solution supplied with 500 µL Coomassie staining. For Western blot, proteins were transferred onto nitrocellulose membranes (Protran membran BA85) using the Mini Trans-Blot® Electrophoretic Transfer Cell (BioRad) for 90 min at 400 mA according to the manufacturer's instructions. After transfer, membranes were blocked in 5% BSA in TBS-T for 30-60 min on a shaker at room temperature and then incubated overnight on a shaker at 4°C. Antibody concentrations are listed in IV.K. The next day, membranes were washed three times in TBS-T for 5 min at room temperature and then incubated for 1-2 h with secondary antibodies on a shaker at room temperature. Secondary antibodies coupled to Horseradish Peroxidase for

chemiluminescence detection using the ECL system or secondary antibodies coupled to infrared dyes were used. The former were diluted 1:20 000 in 5% BSA in TBS-T, the latter 1:10 000 in TBS-T. After washing five times in TBS-T for 10 min at room temperature, signal was either detected by the ECL detection system using Immobilon Western Chemiluminescent HRP Substrate (Merck Millipore) according to the manufacturer's instructions and scanned by the ChemiDoc (BioRad) or by the Licor detection system.

5x LaemmLi buffer
250 mM Tris-HCl pH 6.8
10% SDS(w/v)
50% glycerol (v/v)
0.1% bromophenol blue (w/v)
10% β-mercaptoethanol (v/v)

SDS Gel fix solution
50% ethanol (v/v)
10% acetic acid (v/v)

SDS Gel Coomassie staining solution
5% ethanol
7.5% acetic acid

Coomassie staining
0.25% Coomassie B G250

Running buffer
25 mM Tris
200 mM glycine
0.1% SDS

Transfer buffer
25 mM Tris
200 mM glycine

TBS
25 mM Tris pH 8
3 mM KCl
140 mM NaCl

TBS-T
TBS with 0.1% Tween-20

2. OBTENTION OF FLYFOS DNA

FlyFosmids of the genomic fosmid libraries of *Drosophila melanogaster* were obtained from the Tomancak laboratory in Dresden (Ejsmont Nature Methods 2009). DNA containing *E.coli* cultures transformed with FlyFos019611 or FlyFos019829 were stored in 30% glycerol stocks at -80°C. For FlyFosmid amplification, few cells from the glycerol stocks were transferred with a spatula into LB medium and 17 µg/mL chloramphenicol and incubated 8h in a shaker at 37°C. Then, 5 mL of the culture where transferred into 500 mL flasks with LB medium and 17 µg/mL chloramphenicol, supplied with arabinose to a final concentration of 0.1% (w/v) and incubated overnight in a shaker at 37°C. The cells were then harvested by centrifugation at 2800 g for 15 min and FlyFosmid DNA was purified using the Nucleobond PC 500 kit (Macherey-Nagel).

LB medium
1% peptone (w/v)
0.5% yeast extract (w/v)
1% NaCl (w/v)

3. INTRODUCTION OF POINT MUTATIONS INTO H2A.V CONSTRUCTS

Introduction of point mutations were performed according to a protocol adapted from the QuikChange Site-Directed Mutagenesis Kit (Agilent) and mutagenesis primers were designed according to the guidelines of this manual.

After incubation with 1 µL DpnI for 1 h at 37°C to degrade the methylated non-mutated DNA template, competent *E.coli* DH5a cells were transformed with 2 µL of the PCR reaction and plated onto Ampicillin containing LB agar plates. After overnight incubation of the plates at 37°C, colonies were picked, and cells were amplified in 5 mL ampicillin containing overnight cultures for subsequent DNA purification using the NucleoSpin Plasmid Mini Kit. The success of introducing the desired point mutations was assessed by sequencing at Eurofins Genomics GmbH with appropriate primers offered by the company.

Agar plates

LB medium
2% Agar (w/v)

VI. RESULTS

A. CHARACTERIZATION OF *IN VITRO* RECONSTITUTED CHROMATIN

1. CHARACTERIZATION OF *IN VITRO* RECONSTITUTED CHROMATIN

In this thesis, extract obtained from preblastoderm *Drosophila* embryos as described in III.E was used to reconstitute chromatin *in vitro* from endogenous factors. To this end, DNA with various volumes of extract was incubated in presence of an ATP regenerating system to ensure sufficient energy supply during the ATP-dependent remodeling processes.

To confirm the formation of regular nucleosome arrays with physiological spacing, chromatin was treated with micrococcal nuclease (MNase), which targets linker DNA between nucleosomes, and digestion was stopped after various time points. Then, DNA was purified and analyzed by gel electrophoresis.

Limited MNase digests resulted in the formation of characteristic DNA fragment ladders, which represent the DNA associated with mono-, di-, tri-, or oligo-nucleosomes, depending on the extend of digestion. From this ladder, a repeat length of approximately 170 bp was determined, leading to a linker length of about 20 bp. In addition to this, limited MNase digestion was used to assess the quality of chromatin assembly using different ratios of extract to DNA, which was titrated accordingly for every extract preparation. Here, the extend of the 'MNase ladder' reflecting more complete chromatin assembly improved by increasing the amount of extract, resulting in more defined nucleosome arrays and increasing numbers of oligo-nucleosomes (n, see Figure 15).

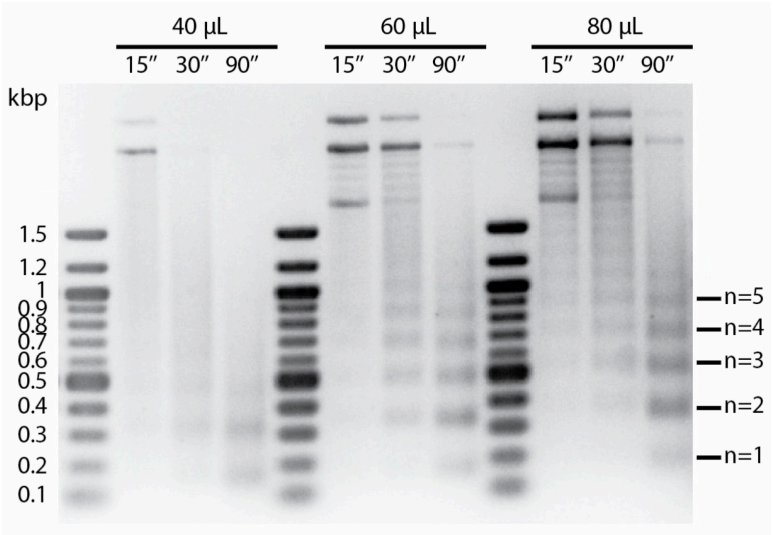

FIGURE 15: LIMITED MNASE DIGESTION FOR 15 SEC, 30 SEC, AND 90 SEC AFTER *IN VITRO* CHROMATIN RECONSTITUTION WITH 40 µL, 60 µL, AND 80 µL EXTRACT PER 1 µG DNA AND ANALYSIS OF PURIFIED DNA AFTER GEL ELECTROPHORESIS (N INDICATES THE NUMBER OF OLIGO-NUCLEOSOMES, WITH N=1: MONO-NUCLEOSOMES, N=2: DI-NUCLEOSOMES, ETC.).

To assess proper formation of nucleosomes with left-handed DNA wrapped around the histone octamer (see III.A.1), Supercoiling Assays were performed. Nucleosome assembly introduces

DNA negative toroidal supercoils into circular DNA. The compensatory positive plectonemic supercoils are relaxed by endogenous topoisomerases in the extract. After removal of the nucleosomes by proteinase digestion, the toroidal supercoils are converted in their plectonemic forms. For each nucleosome one superhelical turn is introduced in the plasmid, which can be resolved on agarose gels (Keller 1975; Becker & Wu 1992). Here, chromatin was assembled *in vitro* on supercoiled plasmid DNA using *Drosophila* embryo extract for 10 min, 30 min, 60 min, and 180 min and after assembly, DNA was purified and analyzed by gel electrophoresis (see V.C.2).

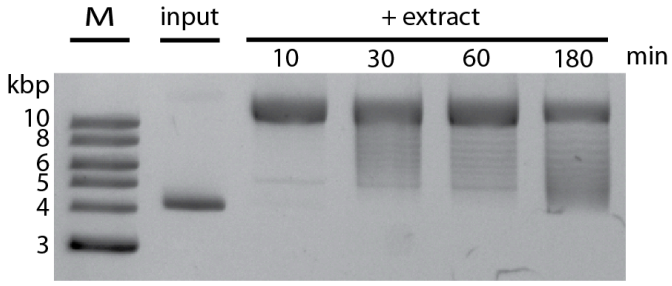

FIGURE 16: SUPERCOILING ASSAY AFTER *IN VITRO* CHROMATIN ASSEMBLY WITH *DROSOPHILA* EMBRYO EXTRACT FOR 10 MIN, 30 MIN, 60 MIN, AND 180 MIN. FOR INPUT, SUPER-COILED PLASMID DNA WAS USED. AFTER 10 MIN, PLASMID DNA IS IN A RELAXED STATE DUE TO TOPOISOMERASES IN THE EXTRACT. OVER TIME, SUPERCOILS ARE INTRODUCED BY NUCLEOSOME ASSEMBLY, WHICH CAN BE RESOLVED BY GEL ELECTROPHORESIS.

Due to its compact conformation, supercoiled input DNA (purified from bacteria) runs faster in an agarose gel than the relaxed plasmid after addition of extract. However, for each assembled nucleosome, a positive supercoil is introduced. As a conclusion, the supercoiling assay can be used to visualize the assembly of nucleosomes on supercoiled plasmid DNA, with increasing numbers of nucleosomes from 30 to 180 min.

To enable purification of *in vitro* reconstituted chromatin for analysis, recombinant DNA was immobilized to paramagnetic beads by biotin-streptavidin coupling. For this, DNA ends with 5' overhangs were filled up with biotinylated nucleotides at either one end or both ends for subsequent immobilization to streptavidin-coupled beads at either one end, or both ends, respectively (Sandaltzopoulos et al. 1994). It has been shown earlier that DNA ends bound to a bead surface by biotin-streptavidin interaction are not recognized as 'free ends' (Postow et al. 2008). Immobilization was controlled by the 'missing band' test, in which DNA in the supernatant after immobilization to paramagnetic beads was analyzed in comparison to input DNA before immobilization. Correct immobilization was then confirmed with restriction enzymes, which detach DNA fragments in the case of one-sided immobilized DNA but not in the case of both-sided immobilized DNA (see Figure 17).

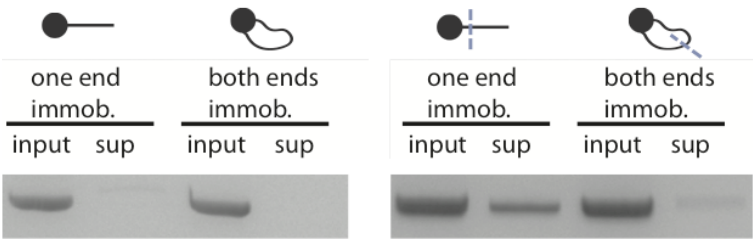

FIGURE 17: MISSING BAND TEST TO CONFIRM COMPLETE AND CORRECT IMMOBILIZATION OF BIOTINYLATED DNA TO PARAMAGNETIC STREPTAVIDIN BEADS. LEFT: INPUT DNA BEFORE IMMOBILIZATION IN COMPARISON TO DNA IN SUPERNATANT (SUP) FOR DNA IMMOBILIZED AT ONE END OR BOTH ENDS. RIGHT: TREATMENT OF IMMOBILIZED DNA WITH RESTRICTION ENZYMES LEADING TO EITHER DETACHMENT OF DNA FROM BEADS (IN CASE OF ONE END IMMOBILIZED DNA) OR LEAVING BOTH FRAGMENTS ATTACHED (IN CASE OF BOTH ENDS IMMOBILIZED DNA). PURPLE DASHED LINES. INDICATE SITES OF RESTRICTION).

To confirm the proper assembly of nucleosomes on immobilized DNA, chromatin was assembled *in vitro* as described in III.E and analyzed by SDS gel electrophoresis followed by Coomassie staining. The bands of the histone octamer are visible on both fragments, with one end or both ends immobilized. However, the band of streptavidin runs at the same height than H4. In addition to this, the band of H2A.V runs at the same height than H2B. Beads without immobilized DNA did not show histones or extract proteins, but the streptavidin band only (compare Figure 23).

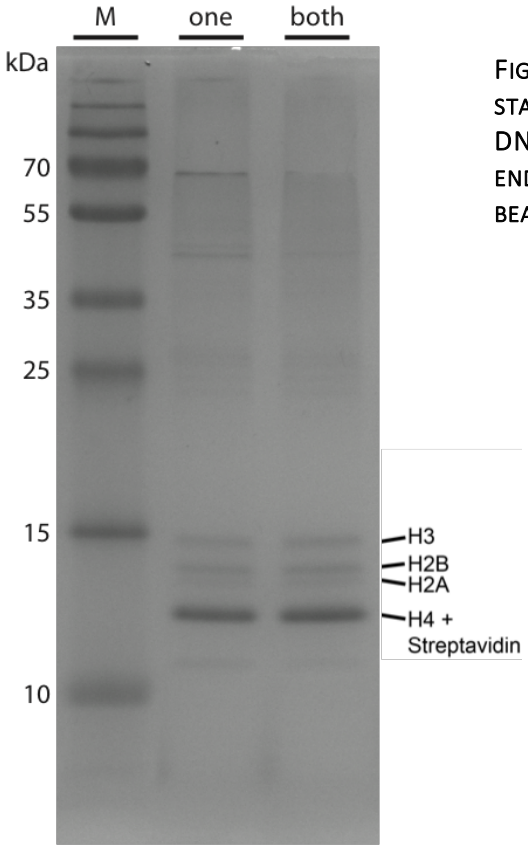

FIGURE 18: SDS GEL ELECTROPHORESIS AND COOMASSIE STAINING OF *IN VITRO* RECONSTITUTED CHROMATIN ON DNA IMMOBILIZED AT EITHER ONE END (ONE) OR BOTH ENDS (BOTH) AFTER PURIFICATION VIA PARAMAGNETIC BEADS.

To furthermore verify the formation of nucleosomes, limited MNase digestion was performed on immobilized chromatin after chromatin *in vitro* reconstitution on DNA immobilized at either one end or both ends (see Figure 19). After purification of DNA and gel electrophoresis, bands corresponding to mono- and di-nucleosomes were detected, demonstrating the formation of nucleosomes on immobilized DNA fragments.

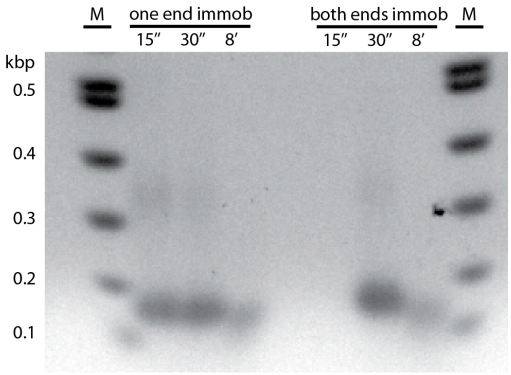

FIGURE 19: LIMITED MNASE DIGESTION ON IMMOBILIZED CHROMATIN. CHROMATIN ASSEMBLY WAS PERFORMED AT ONE END OR BOTH END IMMOBILIZED DNA AND TREATED WITH MNASE FOR 15 SEC, 30 SEC, OR 8 MIN. DNA WAS THEN PURIFIED AND ANALYZED BY GEL ELECTROPHORESIS.

2. DETERMINATION OF *IN VITRO* INCORPORATED H2A.V BY *DROSOPHILA* EMBRYO EXTRACT

To determine the amount of incorporated H2A.V in comparison to canonical H2A, I performed Western blot analysis on chromatin assembled on recombinant DNA next to nucleosomes reconstituted with either only H2A or H2A.V. These were used as reference, as the ratio of H2A or H2A.V to H4 was assumed to be 1. The double band detected with antibody against H2A.V in the chromatin samples results from the phosphorylated and unphosphorylated form of H2A.V, which will be investigated in more detail in VI.B.

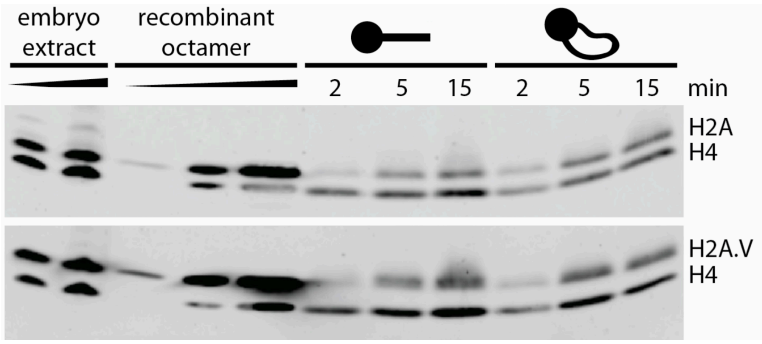

FIGURE 20: WESTERN BLOT ANALYSIS OF HISTONES H2A AND H4 (UPPER PANEL) AND HISTONES H2A.V AND H4 (LOWER PANEL) OF CHROMATIN ASSEMBLED ON DNA IMMOBILIZED AT ONE END IN COMPARISON TO RECOMBINANT HISTONE OCTAMERS CONSISTING OF EITHER H2A (UPPER PANEL) OR H2A.V (LOWER PANEL) AND *DROSOPHILA* EMBRYO EXTRACT.

Western blot analysis of reconstituted chromatin revealed that about a quarter of H2A is replaced by H2A.V, similar to what has been described *in vivo* (H2A.V in 25% of nucleosomes,

www.flybase.org, 27.04.2018). Unexpectedly, similar values were obtained for the canonical histone H2A, suggesting that H2A contributes with only about a quarter to the constitution of *in vitro* reconstituted nucleosomes. However, H2A and H2A.V are the only H2A-like histones known in *Drosophila*, which could contribute to the formation of nucleosomes and no other H2A variants are known so far. Furthermore, Coomassie staining of nucleosomes after *in vitro* reconstitution showed octamers in comparable ratios, excluding the formation of tetramers instead of octamers. An explanation for this conflicting result might be differences in Western blot detection between endogenous histones from embryo extract, e.g. due to post-translational modifications, and recombinant histones purified from bacteria cultures.

TABLE 3: SIGNAL INTENSITIES OF H2A, H2A.V AND H4 FROM FIGURE 20 QUANTIFIED BY IMAGE STUDIO™ LITE SOFTWARE, LI-COR BIOSCIENCES. INTENSITY RATIOS OF H2A AND H2A.V AGAINST H4 FROM ASSEMBLED CHROMATIN IMMOBILIZED AT ONE END (OEB) OR BOTH ENDS (BEB) FOR 2 MIN, 5 MIN, OR 15 MIN AND EMBRYO EXTRACT WERE NORMALIZED TO THE RATIO OF RECOMBINANT OCTAMER WITH EITHER H2A OR H2A.V TO DETERMINE THE CONTRIBUTION OF H2A OR H2A.V, SHOWN IN PERCENT.

	Intensity H2A	Intensity H4	Normalized to H4	Average	Normalized to recombinant octamer ratio
embryo extract	277000	337000	0.82	0.74	27%
	423000	651000	0.65		
recombinant octamer	71900	48700	1.48	2.72	100%
	357000	178000	2.01		
	858000	183000	4.69		
oeb 2 min	108000	211000	0.51		19%
oeb 5 min	179000	239000	0.75		27%
oeb 15 min	216000	294000	0.73		27%
beb 2 min	121000	160000	0.76		28%
beb 5 min	222000	220000	1.01		37%
beb 15 min	254000	246000	1.03		38%
	Intensity H2A.V	Intensity H4	Normalized to H4	Average	Normalized to recom-binant octamer ratio
embryo extract	520000	327000	1.59	1.41	44%
	726000	588000	1.23		
recombinant octamer	287000	110000	2.61	3.18	100%
	955000	196000	4.87		
	1970000	964000	2.04		
oeb 2 min	418000	496000	0.84		27%
oeb 5 min	414000	542000	0.76		24%
oeb 15 min	566000	788000	0.72		23%
beb 2 min	221000	329000	0.67		21%
beb 5 min	507000	545000	0.93		29%
beb 15 min	459000	430000	1.07		34%

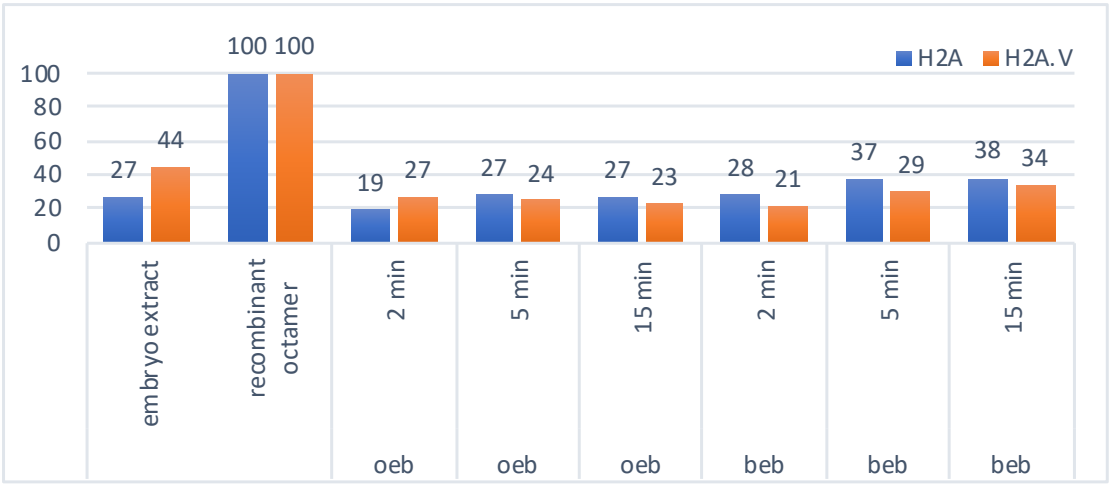

FIGURE 21: CONTRIBUTION OF H2A OR H2A.V DETERMINED IN TABLE 2 FROM ASSEMBLED CHROMATIN IMMOBILIZED AT ONE END (OEB) OR BOTH ENDS (BEB) FOR 2 MIN, 5 MIN, OR 15 MIN AND EMBRYO EXTRACT (IN PERCENT).

3. EVALUATION OF ATP DEPENDENCY IN CHROMATIN RECONSTITUTION

To evaluate the role of ATP on chromatin reconstitution, I performed chromatin assembly reactions in the absence of ATP. To remove endogenous ATP, apyrase was added to the extract before assembly. Quantification of ATP concentrations before and after addition of apyrase using a bioluminescence detection reagent (ENLITEN rLuciferase/rLuciferin Reagent A, Promega) revealed an approximate 100-fold decrease of ATP from 41 µM to 0.3 µM.

TABLE 4: ATP CONCENTRATIONS OF *DROSOPHILA* EMBRYO EXTRACT BEFORE AND AFTER TREATMENT WITH APYRASE DETERMINED BY CHEMILUMINESCENCE.

	nM ATP
Extract before apyrase treatment	40716
Extract after apyrase treatment	342

As in VI.A.1, supercoiling assays were performed to investigate nucleosome formation in presence and absence of ATP after 10 min, 30 min, 60 min, and 180 min assembly time (see Figure 22). In presence of ATP, the formation of nucleosomes led to the formation of supercoiled plasmid DNA over time (compare also VI.A.1, Figure 16). However, in absence of ATP, no supercoiling of the plasmid was observed. Instead, a DNA band presumably resulting from nicked DNA was observed in all samples. It is possible, that these nicks were introduced by topoisomerases, which could not be ligated in the absence of ATP. Therefore, the question, if nucleosomes formed in the absence of ATP, was not addressable with this approach. However, it has been shown, that prior to proper nucleosome formation, histones associate

with DNA in a "non-nucleosomal histone-DNA intermediate" (Torigoe, Urwin, Ishii, Smith & Kadonaga 2011), which is lateron transform into a mature nucleosome in an Acf1- (and therefore presumably ATP-) dependent manner. It can be assumed, that in the absence of ATP, no mature nucleosomes are formed, but rather premature assemblies of histone proteins to DNA, which are processed in presence of ATP.

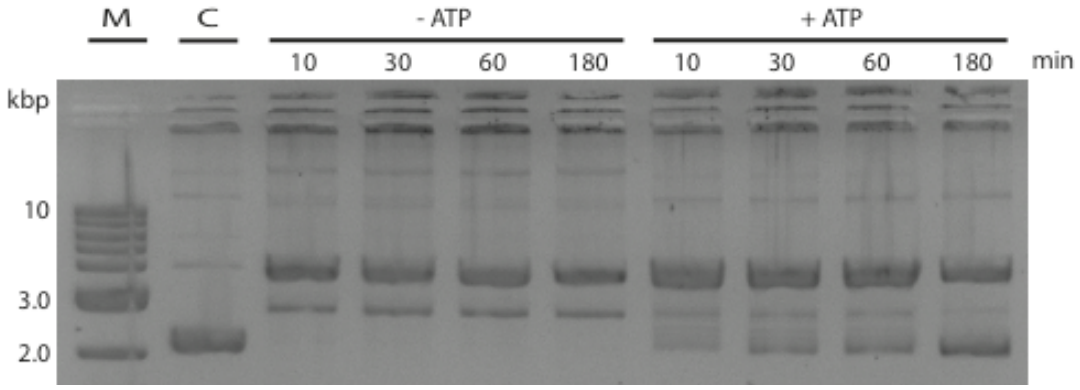

FIGURE 22: SUPERCOILING ASSAY AFTER *IN VITRO* CHROMATIN ASSEMBLY WITH *DROSOPHILA* EMBRYO EXTRACT FOR 10 MIN, 30 MIN, 60 MIN, AND 180 MIN IN PRESENCE AND ABSENCE OF ATP. FOR INPUT, SUPERCOILED PLASMID DNA WAS USED. AFTER 10 MIN, PLASMID DNA IS IN A RELAXED STATE DUE TO TOPOISOMERASES IN THE EXTRACT. OVER TIME, SUPERCOILS ARE INTRODUCED BY NUCLEOSOME ASSEMBLY, WHICH CAN BE RESOLVED BY GEL ELECTROPHORESIS.

In addition to the supercoiling assay, limited MNase digestion was performed as described in VI.A.1. However, no MNase ladders were obtained in the absence of ATP, except of a blurry mono-nucleosomal band. Instead, a smear of fragmented DNA was detected (not shown). This observation might be explained by the missing Acf1 activity, which is required for the establishment of spaced nucleosomes, a prerequisite of distinct MNase ladders. In addition to this, as mentioned before, the establishment of mature nucleosomes was also shown to depend on Acf1 (Varga-Weisz et al. 1997; Torigoe, Urwin, Ishii, Smith & Kadonaga 2011). When analyzing chromatin assembled in absence of ATP by SDS-PAGE followed by Coomassie staining, histones were detected similar to the control experiment in presence of ATP. However, as discussed before, it is not clear if these octamers are assembled into nucleosomes.

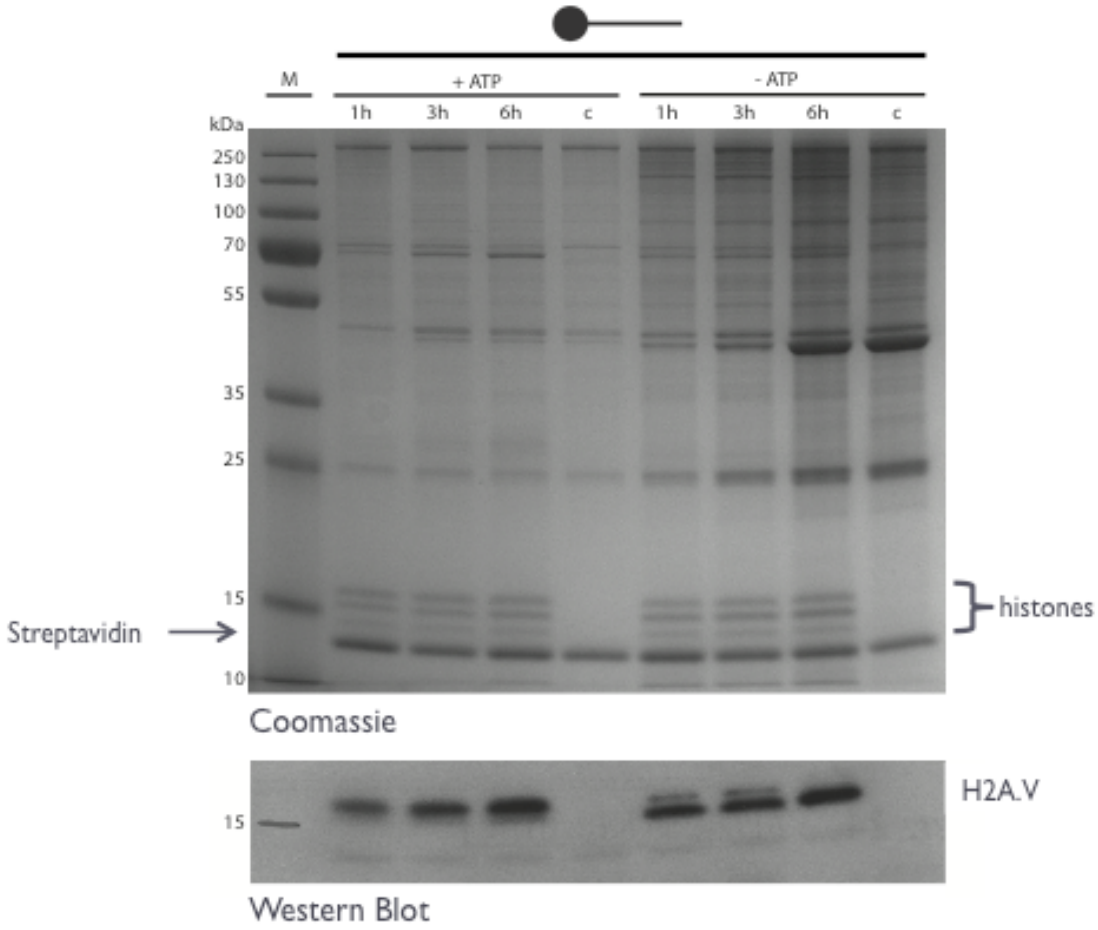

FIGURE 23: CHROMATIN ASSEMBLED IN PRESENCE AND ABSENCE OF ATP. UPPER PANEL: COOMASSIE STAINING AFTER SDS-PAGE OF CHROMATIN ASSEMBLED IN PRESENCE OR ABSENCE OF ATP FOR 1 H, 3 H, OR 6 H. AS A NEGATIVE CONTROL, ASSEMBLY WAS PERFORMED FOR 6 H WITH BEADS ONLY (C). LOWER PANEL: SAMPLES OF UPPER PANEL WERE BLOTTED AND THE MEMBRANE WAS PROBED WITH ANTI-H2A.V ANTIBODY.

Western blot analysis revealed that in the absence of ATP, H2A.V can still be detected on chromatin assembled in the absence of ATP (Figure 23). However, it is not clear whether H2A. V is incorporated into nucleosomes or only associated to be incorporated by ATP-dependent remodeling complexes like Dom/Tip60. However, considering the bivalent role of H2A.V comprising H2A.X and H2A.Z function, it is possible that part of H2A.V is randomly incorporated into nascent chromatin like H2A.X, to serve as an evenly distributed DNA damage sensor, whereas additional H2A.V is specifically incorporated into specific regions to regulate gene expression in an ATP-dependent manner. Due to the free end of DNA immobilized at one end and the resulting DNA damage response (see III.B.3 and III.B.5), incorporated H2A.V was phosphorylated in presence of ATP, which can be detected by an antibody specific for the C-terminal phosphorylation mark and by the double band detected by the antibody against H2A.V, which is able to detect the unphosphorylated, as well as the phosphorylated form (Figure 23, Figure 27).

To investigate, if H2A.V incorporation into preassembled nucleosome arrays by histone exchange can be observed in this *in vitro* system, I incubated H2A arrays with extract, which was either depleted of ATP with apyrase as described before or supplied with an ATP regenerating system. These H2A arrays consist of recombinant nucleosomes on immobilized arrays of 25 601 Widom sequences (Klinker, Mueller-Planitz, et al. 2014), which exhibit a nucleosome positioning sequence to favor the generation of regular nucleosome arrays (Lowary & Widom 1998, see Figure 24).

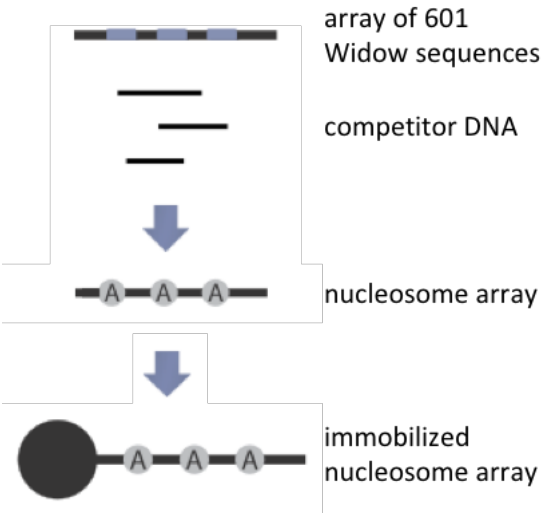

FIGURE 24: GENERATION OF IMMOBILIZED ARRAYS OF RECOMBINANT NUCLEOSOMES CONSISTING OF EITHER H2A OR H2A.V OR H2A.VE. NUCLEOSOMES WERE ASSEMBLED BY SALT-GRADIENT DIALYSIS FROM RECOMBINANT OCTAMERS ONTO BIOTINYLATED DNA FRAGMENTS CONSISTING OF WIDOM 601 SEQUENCES (PURPLE) AND THEN IMMOBILIZED TO STREPTAVIDIN-COUPLED PARAMAGNETIC BEADS. FRAGMENTS RESULTING FROM THE PLASMID BACKBONE WERE NOT IMMOBILIZED AND REMAINED IN THE SUPERNATANT. DURING NUCLEOSOME ASSEMBLY, THESE BACKBONE FRAGMENTS WERE USED AS COMPETITOR DNA, WITH LOWER NUCLEOSOME AFFINITY THAN THE WIDOM 601 SEQUENCE ARRAYS TO BIND EXCESS NUCLEOSOMES.

To assure, that detected H2A.V after incubation with extract results from nucleosome turnover instead of incorporation on gaps between recombinant nucleosomes, quality controls prior to immobilization to the beads were performed, to aim for complete occupation of all 601 Widom sequences with recombinant nucleosomes.

The extend of nucleosome formation was probed by restriction enzyme digestion of target sites either within the Widom 601 sequence (Figure 25) or with target sites in the linker DNA between the Widom 601 sequences (Figure 26) as described in Klinker, Mueller-Planitz, et al. 2014; Maier et al. 2008. In the former case, the target site was only accessible in cases, where nucleosome assembly was not complete, leading to fragmented Widom 601 arrays, which were not occupied by nucleosomes.

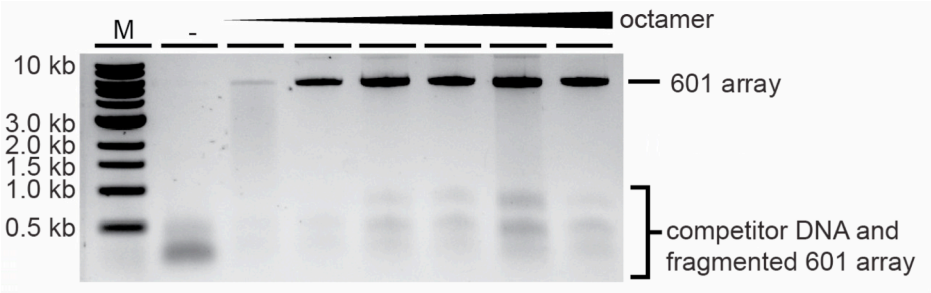

FIGURE 25: QUALITY CONTROL OF NUCLEOSOME ASSEMBLY ON WIDOM 601 SEQUENCES BY ALUI RESTRICTION PRIOR TO IMMOBILIZATION. THE TARGET SITE OF ALUI IS WITHIN THE WIDOM 601 SEQUENCE AND HENCE ONLY ACCESSIBLE IN THE ABSENCE OF NUCLEOSOMES. THEREFORE, WITH INCREASING ASSEMBLY DEGREE ACCOMPLISHED BY INCREASING AMOUNTS OF NUCLEOSOMES, LESS OF THE 601 ARRAY IS DEGRADED. IN ADDITION, FRAGMENTS RESULTING FROM THE BACKBONE OF THE VECTOR INCLUDING THE WIDOM 601 ARRAY, ARE DETECTABLE IN THE GEL (COMPETITOR DNA). NUCLEOSOME-FREE DNA (-) WAS ADDED AS A CONTROL AND IS COMPLETELY DEGRADED BY ALUI.

In the latter case, restriction enzyme digestion resulted in mono-nucleosomes, which were analyzed by native gel electrophoresis (Figure 26). Incomplete assembly led to the formation of protein-free 601 fragments, which run faster than mono-nucleosomes, as demonstrated by the control sample with free Widom 601 arrays (-).

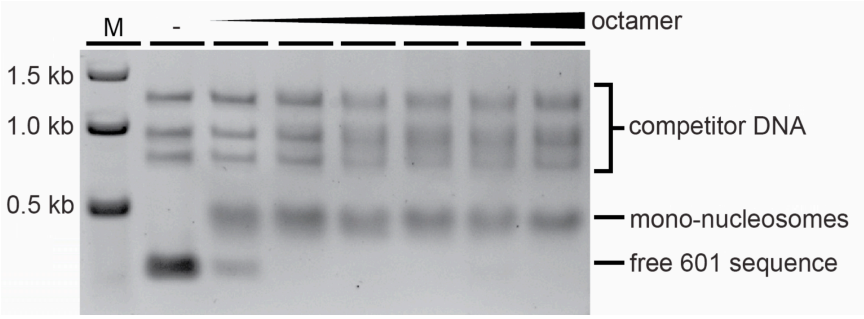

FIGURE 26: QUALITY CONTROL OF NUCLEOSOME ASSEMBLY ON WIDOM 601 SEQUENCES BY AVAI RESTRICTION PRIOR TO IMMOBILIZATION. THE TARGET SITE OF AVAI IS IN BETWEEN THE WIDOM 601 SEQUENCES GENERATING EITHER FREE WIDOM 601 SEQUENCES OR MONO-NUCLEOSOMES, WHICH CAN BE SEPARATED BY NATIVE GEL ELECTROPHORESIS. NUCLEOSOME-FREE DNA (-) WAS ADDED AS A CONTROL AND IS DIGESTED INTO FREE WIDOM 601 SEQUENCES AND FRAGMENTS RESULTING FROM THE BACKBONE OF THE VECTOR INCLUDING THE WIDOM 601 ARRAY (COMPETITOR DNA). WITH INCREASING ASSEMBLY DEGREE, FIRST THE WIDOM 601 SEQUENCES, AND THEN THE COMPETITOR DNA BECOMES OCCUPIED BY NUCLEOSOMES, AS VISIBLE FROM THE SIZE SHIFT.

After the quality controls, arrays were immobilized to paramagnetic beads and used for chromatin *in vitro* assembly. However, only low amounts of H2A.V were incorporated in presence or absence of ATP, suggesting that exchange of H2A by H2A.V was not accomplished to a high extent in either case.

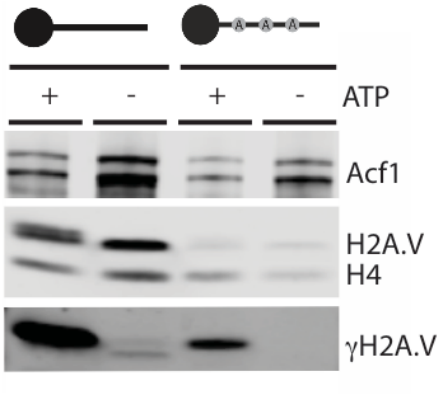

FIGURE 27: CHROMATIN ASSEMBLED IN PRESENCE AND ABSENCE OF ATP ON EITHER FREE DNA OR ON PREASSEMBLED RECOMBINANT H2A NUCLEOSOMES. AFTER SDS-PAGE, PROTEINS WERE BLOTTED AND THE MEMBRANE WAS PROBED WITH ANTIBODIES AGAINST ACF1, H2A.V, H4 AND γH2A.V.

Interestingly, we observed that in absence of ATP, Acf1 was enriched on chromatin. This observation was also made for other remodeling factors like Iswi, the ATPase subunit of ACF (Figure 27).

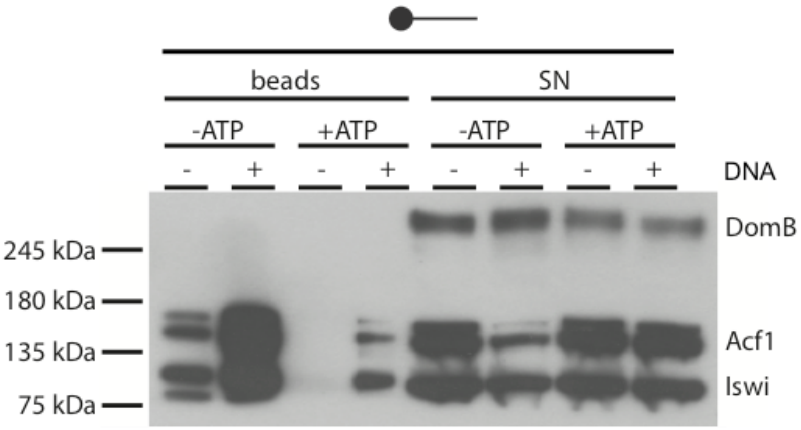

FIGURE 28: CHROMATIN ASSEMBLED IN PRESENCE AND ABSENCE OF ATP. IN ADDITION TO THE BEAD SAMPLES, ABOUT 14% OF SUPERNATANT (SN) WAS LOADED. AFTER SDS-PAGE, PROTEINS WERE BLOTTED AND THE MEMBRANE WAS PROBED WITH ANTIBODIES AGAINST DOMB, ACF1 AND ISWI.

To investigate, if this enrichment was physiological or due to unspecific "sticking" of protein to beads or DNA, assembly reactions were performed with changing environments in presence and absence of ATP. If the enrichment was caused by unspecific binding, the effect would most likely not be reversed in presence of ATP. However, if the enhanced binding is caused by trapping of Acf1, which was recruited to nucleosomes to catalyze their sliding reaction but cannot perform this reaction in absence of ATP, this enrichment should be reversible in presence of ATP. Indeed, when chromatin was assembled first in absence of ATP and then ATP was added, (Figure 29, lane 3), Acf1 levels were reduced again to levels comparable to those, where chromatin was assembled in presence of ATP from the beginning (Figure 29, lane 4 and 5). In contrast, Acf1 levels in chromatin assemblies in absence of ATP remained higher (Figure 29, lane 1 and 2), and increased after removal of ATP (Figure 29, lane 6 compared to lane 4). This observation supports the hypothesis of trapped Acf1. However, it cannot be excluded, that the enrichment of protein binding is caused by the inhibition of chromatin bound proteasome, which have been reported to remove protein aggregates from chromatin (doctoral thesis Moritz Völker Albert, BMC Munich, Germany).

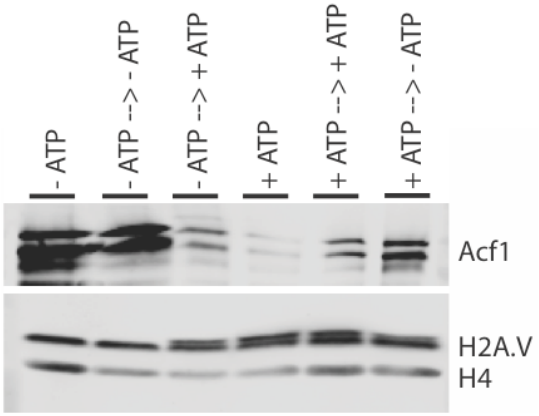

FIGURE 29: CHROMATIN ASSEMBLED IN PRESENCE AND ABSENCE OF ATP. CHROMATIN WAS ASSEMBLED ON IMMOBILIZED DNA IN EITHER PRESENCE OR ABSENCE OF ATP FOR 3 H EACH AND THEN TRANSFERRED INTO REACTIONS WITH OR WITHOUT ATP OR DIRECTLY PREPARED FOR SDS-PAGE (SEE DESCRIPTION). AFTER BLOTTING, THE MEMBRANE WAS PROBED WITH ANTIBODIES AGAINST ACF1, H2A.V AND H4.

4. STABILITY OF CHROMATIN REMODELERS IN RECONSTITUTED CHROMATIN

To investigate the stability of chromatin-associated factors after assembly, I analyzed the immobilized chromatin samples after washes with different stringencies, using wash buffers including 50 mM, 100 mM and 200 mM KCl. Acf1 remained associated with chromatin after washing with 50 mM and 100 mM KCl but dissociated substantially after washing with 200 mM KCl. A similar behavior was observed for Iswi, suggesting that both components dissociate as a complex. Furthermore, DomB displayed the weakest association, which was already considerably decreased after washing with 100 mM KCl (not shown here).

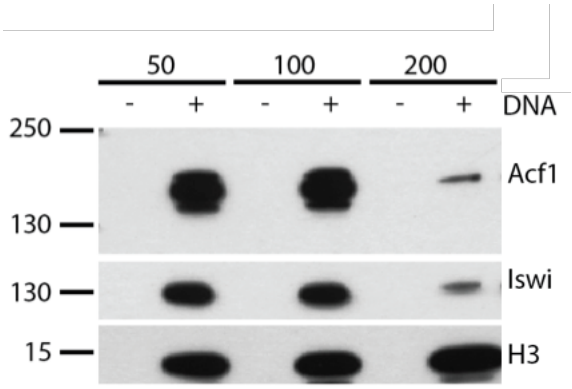

FIGURE 30: STABILITY OF *IN VITRO* ASSOCIATED CHROMATIN REMODELING FACTORS AFTER CHROMATIN *IN VITRO* ASSEMBLY. CHROMATIN WAS ISOLATED VIA PARAMAGNETIC BEADS AND WASHED WITH BUFFERS OF 50 MM, 100 MM, OR 200 MM KCL AND ANALYZED BY SDS-PAGE. AS NEGATIVE CONTROLS, CHROMATIN ASSEMBLY WAS PERFORMED WITH BEADS ONLY (- DNA). AFTER BLOTTING, THE MEMBRANE WAS PROBED WITH ANTIBODIES AGAINST ACF1, ISWI AND H3.

5. EXCHANGE OF H2A.V IN NUCLEOSOMES

As already mentioned in III.B.5 and 0, Kusch et al showed, that exchange of phosphorylated H2A.V by unmodified variant histone was mediated by the Dom/Tip60 complex, to remove the phosphorylation mark upon repair of DNA damage. Prior to phosphorylation, H2A.V becomes acetylated by Tip60, the HAT subunit of the complex, on lysine 5 (Kusch 2004). In addition to this, they show that exchange of H2A.V is enhanced in the presence of acety-CoA. Kusch et al. also showed, that nucleosomal H2A is replaced by H2A.V at heat shock promoters (Kusch et al.

2014). To investigate, if histone exchange can also occur *in vitro*, I preassembled arrays of recombinant nucleosomes with octamers consisting of H2A or H2A.V or a phosphomimic mutant of H2A.V (H2A.VE), with its serine of the C-terminal SQAY-motif replaced by negatively charged glutamine to mimic the phosphorylation, as described in VI.A.3 (also see Figure 24).

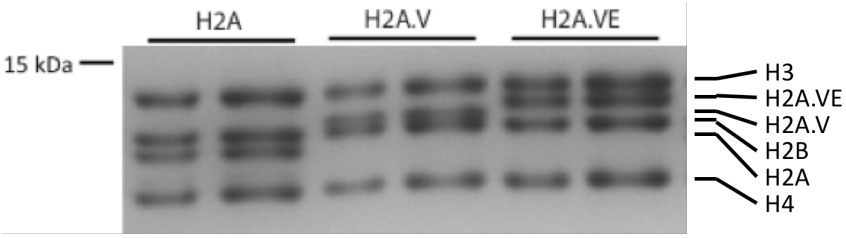

FIGURE 31: SDS-PAGE FOLLOWED BY COOMASSIE STAINING OF RECOMBINANT NUCLEOSOMES ASSEMBLED ACCORDING TO FIGURE 24. FOR EACH TYPE OF NUCLEOSOME, TWO DIFFERENT CONCENTRATIONS WERE LOADED.

Indeed, as shown in Figure 32, H2A.V incorporation into H2A arrays, which had been assembled to lower saturation (leaving free DNA between nucleosomes) was higher, suggesting that either histone exchange is more efficient under those circumstances or, more likely, nucleosomes containing endogenous H2A.V were assembled between recombinant nucleosomes on the array. As turnover of H2A and H2A.V is reported to be an acetylation-dependent process, I performed the turnover reactions in presence of acetyl-CoA and butyrate, a histone deacetylase inhibitor, to promote turnover.

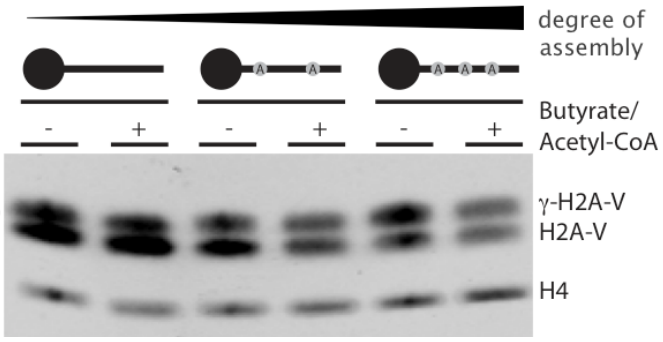

FIGURE 32: CHROMATIN ASSEMBLY ON PREASSEMBLED RECOMBINANT H2A NUCLEOSOMES WITH INCREASING ASSEMBLY DEGREE AND IN PRESENCE OR ABSENCE OF ACETYL-COA AND BUTYRATE. AFTERWARDS, CHROMATIN WAS ANALYZED BY SDS-PAGE, PROTEINS WERE BLOTTED AND MEMBRANES WERE PROBED WITH ANTIBODIES AGAINST γH2A.V, H2A.V AND H4.

However, addition of acetyl-CoA and butyrate did not improve incorporation of H2A.V (Figure 32 and Figure 33) suggesting that the coenzyme was not limiting the reaction. Conceivably, a lack of histone exchange is due to the fact that the DOM-A complex containing DomA and the acetyltransferase Tip60 (Kusch 2004; Kusch et al. 2014) is not abundant in preblastoderm embryos (Ruhf et al. 2001). In support of this notion, DomA was not detected in the chromatin assembly extracts by Western blot or mass spectrometry.

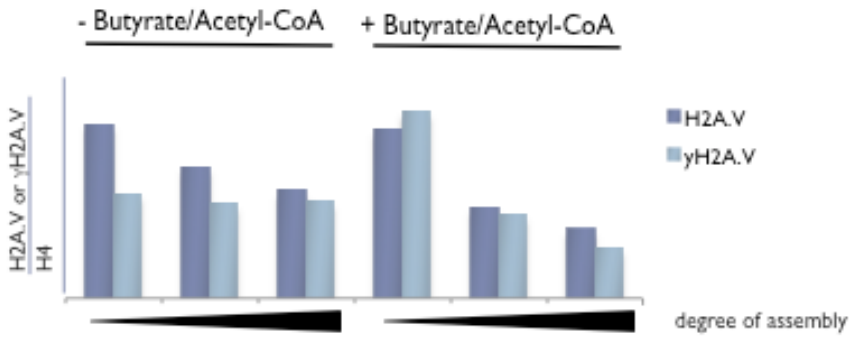

FIGURE 33: QUANTIFICATION OF SIGNAL INTENSITIES OF FIGURE 32 BY IMAGE STUDIO™ LITE SOFTWARE, LI-COR BIOSCIENCES. INTENSITIES OF H2A.V AND γH2A.V WERE NORMALIZED TO H4.

To circumvent this problem, chromatin assembly reactions were supplemented with an extract derived from nuclei of 0-12 h old embryos as a potential source of H2A.V exchange remodelers. This extract is transcriptionally active and therefore called TRAX. However, in contrast to preblastoderm embryo extract (here called DREX), TRAX is not capable of assembling nucleosomes on DNA. TRAX was added to nucleosome fibers either made of nucleosomes assembled by salt gradient dialysis (Figure 34, left and middle) or by prior DREX assembly (Figure 34, right). Supplementing DREX with TRAX did not increase incorporation of H2A.V into recombinant H2A arrays. In contrast, incorporation in presence of both extracts seemed to be decreased and DREX or TRAX alone showed a higher capability to incorporate H2A.V than both in combination (Figure 34, left). Again, addition of acetyl-CoA and butyrate did not increase the effect (Figure 34, middle).

To visualize the exchange of H2A.V by another H2A.V molecule, a tagged form was generated in which three Flag-tags were fused to the N-terminus of H2A.V and used for octamer assembly. However, the tag perturbed octamer formation and only H3-H4 tetramers and 3xFlag-H2A.V-H2B dimers were obtained (data not shown). Therefore, it was not possible to track the exchange of recombinant, preassembled H2A.V by endogenous H2A.V but only turnover of canonical H2A.

Unexpectedly, we observed that H2A.V incorporated by TRAX was not phosphorylated, as the typical H2A.V double band can only be detected on chromatin assembled with DREX and missing in chromatin assembled with TRAX (Figure 34, left and middle). This observation could be explained either by a strong phosphatase, which efficiently removes the phosphorylation mark from H2A.V, by an effective turnover mechanism, which removes phosphorylated H2A.V from chromatin, or by lack of kinase activity in TRAX. To solve this question, chromatin was reconstituted first *in vitro* from endogenous histones and then incubated with either DREX or TRAX. Remarkably, incubation of chromatin containing phosphorylated H2A.V with TRAX, did not remove the phosphorylation mark (Figure 34, right). Therefore, the first two possibilities pointing towards the removal of the phosphorylation mark seemed to be disproven. Instead, TRAX does not seem to be capable to phosphorylate H2A.V and the ability to recognize free DNA ends and initiate the damage response seems to be exclusive for DREX. However, each experiment shown in Figure 34 was only performed once and need further investigation to confirm this hypothesis.

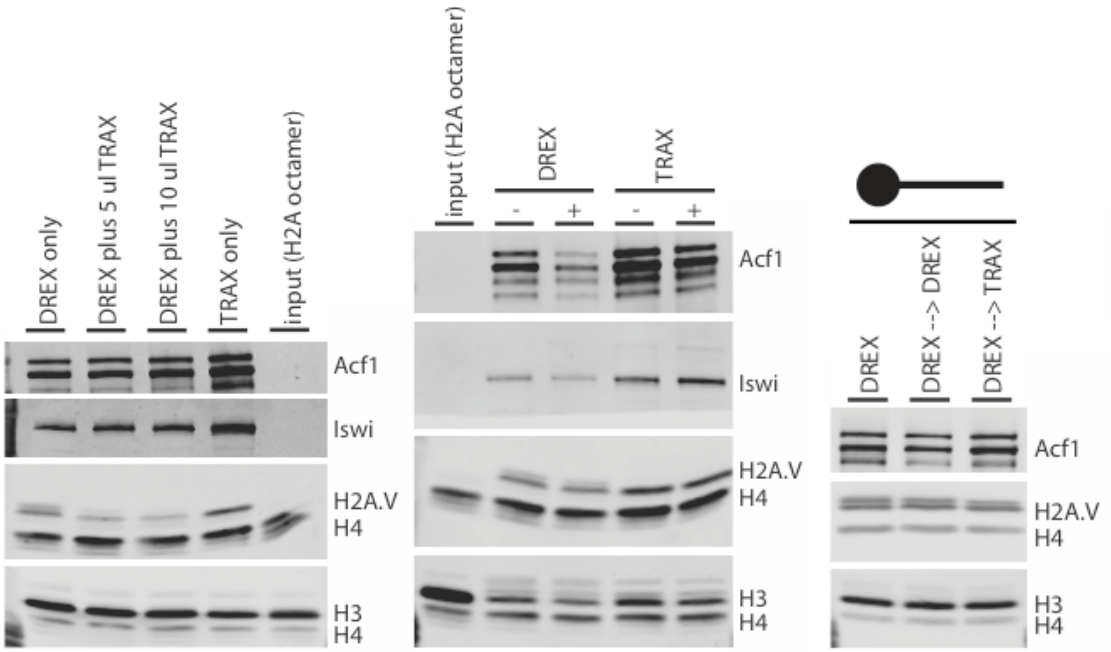

FIGURE 34: CHROMATIN ASSEMBLY WITH PREBLASTODERM *DROSOPHILA* EMBRYO EXTRACT (DREX) OR NUCLEAR TRANSCRIPTION EXTRACT (TRAX). LEFT: DREX ONLY OR INCREASING AMOUNTS OF TRAX OR TRAX ONLY WERE ADDED TO RECOMBINANT H2A-BEARING NUCLEOSOME ARRAYS. MIDDLE: EITHER DREX OR TRAX WERE ADDED TO RECOMBINANT H2A ARRAYS AND INCUBATED IN PRESENCE OR ABSENCE OF ACETYL-COA AND BUTYRATE. RIGHT: CHROMATIN WAS FIRST RECONSTITUTED ON DNA AND THEN INCUBATED WITH EITHER DREX OR TRAX. AS INPUT, H2A ARRAYS BEFORE CHROMATIN ASSEMBLY WAS LOADED. AFTERWARDS, CHROMATIN WAS ANALYZED BY SDS-PAGE, PROTEINS WERE BLOTTED AND MEMBRANES WERE PROBED WITH ANTIBODIES AGAINST ACF1, ISWI, H2A.V, H4 AND H3.

6. INCORPORATION AND TURNOVER IN A GENOMIC BACKGROUND

To investigate the distribution of H2A and H2A.V in a genomic background, ChIP-Seq experiments were performed against H2A or H2A.V on recombinant arrays of H2A or H2A.V nucleosomes before and after addition of extract. For this purpose, recombinant arrays of H2A or H2A.V nucleosomes were assembled on FlyFosmids. After sequencing, normalization was performed by Tamás Schauer to the total number of reads (Figure 35).

Panel (1) and (2) show the distribution of H2A or H2A.V nucleosomes after SGD in absence of extract. As expected, these profiles are highly similar, as dialysis does not differentiate between the two types of nucleosomes. Panel (3) and (4) show profiles after addition of DREX to the recombinant arrays, leading to differences in nucleosome distribution (subtracting the signals from panel (3) and (4) from panels (1) and (2), respectively [shown in (1) – (3) and (2) – (4)]). The similarity of the difference patterns shows that nucleosome remodeling activity in the extract changes nucleosome positions independent of the type of H2A variant.

To visualize turnover reactions, where H2A nucleosomes are exchanged by H2A.V nucleosomes or vice versa, tracks before addition of extract were compared to tracks after addition of extract, detecting potentially exchanged nucleosome (H2A in case of H2A.V arrays and vice

versa) [(1) – (4) and (2) – (5)]. The similarity of all difference profiles suggests, that the DREX cannot perform H2A- or H2A.V-specific turnover reactions. In addition to this, incorporation of H2A.V by the extract did not resemble the genomic organization described by Zhang and Pugh (Zhang & Pugh 2011), presumably because the extract is deficient in transcription, which might be required for re-organization of H2A.V by chromatin remodelers. Altogether, it appears that DREX is not capable to distinguish and specifically incorporate histone variant H2A.V, but rather deposits H2A.V-containing nucleosomes in parallel to H2A-containing nucleosomes. This random distribution resembles the incorporation of H2A.X, which is distributed along the genome as a DNA damage sensor. Specific enrichment to regulate transcription similar to H2A.Z was not observed here and might require transcription. Nevertheless, the reorganization of nucleosomes is highly consistent among the different arrays and seems to be sequence-dependent. However, we were not able to identify a correlation to genic or intergenic regions or other connections to explain this observation.

FIGURE 35 (NEXT PAGE): CHIP-SEQ PROFILES OF RECOMBINANT ARRAYS OF H2A [PANEL (1, 3), AND (4)] OR H2A.V [PANEL (2, 5), AND (6)] NUCLEOSOMES BEFORE [PANEL (1) AND (2)] AND AFTER [PANEL (3) TO (6)] CHROMATIN ASSEMBLY. CHIP WAS PERFORMED AGAINST H2A [PANEL (1, 3), AND (5)] OR H2A.V [PANEL (2, 4, 6)]. TO ILLUSTRATE THE DIFFERENCES BETWEEN TRACKS, SIGNAL INTENSITIES ALONG THE TRACKS WERE SUBTRACTED, WITH (1) – (2) SHOWING DIFFERENCES BETWEEN RECOMBINANT ARRAYS AFTER SALT GRADIENT DIALYSIS (SGD, 1) – (3) AND (2) – (4) SHOWING DIFFERENCES BEFORE AND AFTER ASSEMBLY WITH DREX, (3) – (4) AND (5) – (6) SHOWING DIFFERENCES OF H2A AND H2A.V DISTRIBUTION AFTER ASSEMBLY AND (1) – (4) AND (2) – (5) SHOWING TURNOVER AFTER CHROMATIN ASSEMBLY. SIGNALS WERE NORMALIZED TO TOTAL READS.

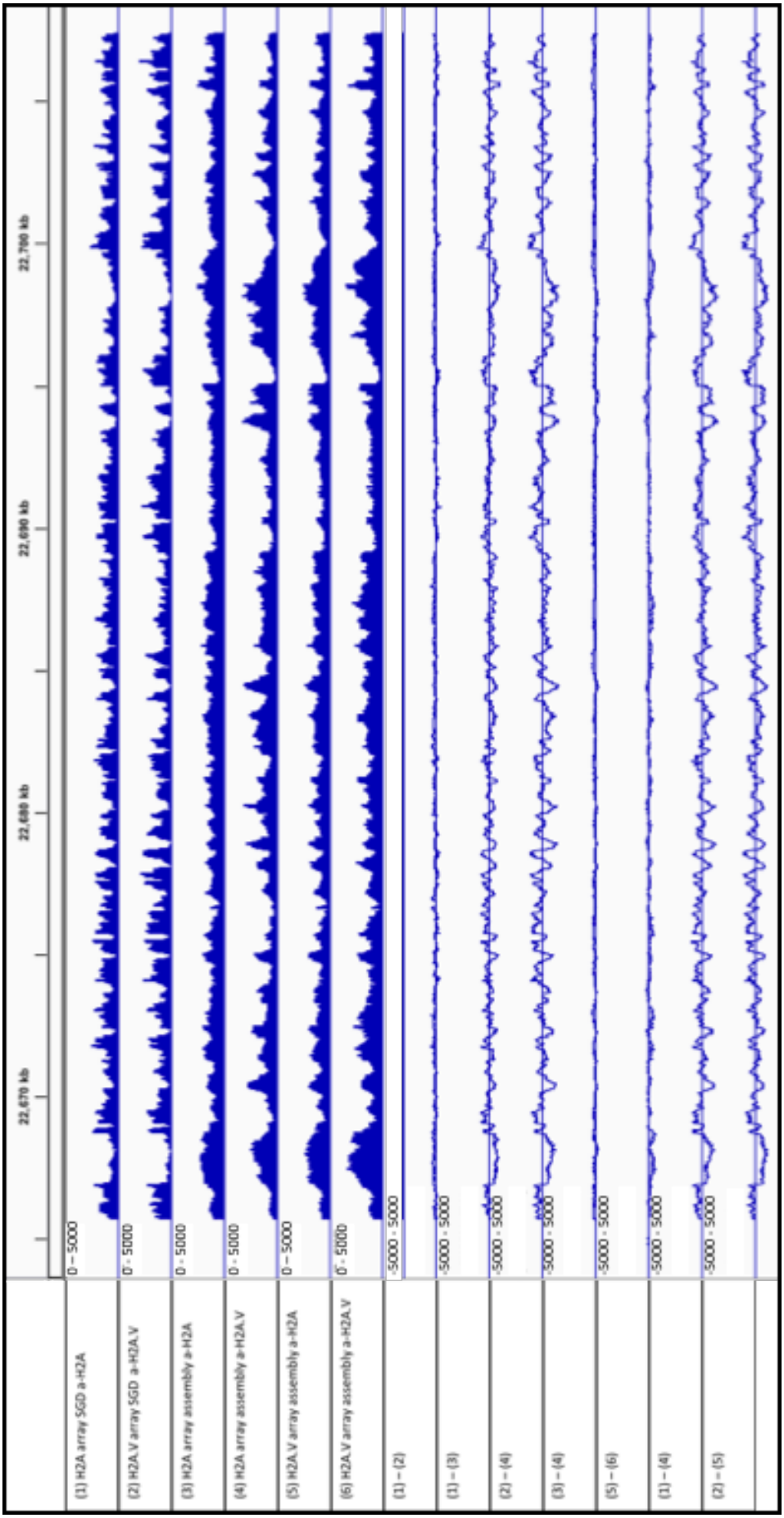
22,670 kb
22,680 kb
22,690 kb
22,700 kb
(1) H2A array SGD a-H2A
(2) H2A.V array SGD a-H2A.V
(3) H2A array assembly a-H2A
(4) H2A array assembly a-H2A.V
(5) H2A.V array assembly a-H2A
(6) H2A.V array assembly a-H2A.V
(1) – (2)
(1) – (3)
(2) – (4)
(3) – (4)
(5) – (6)
(1) – (4)
(2) – (5)
0 – 5000
-5000 - 5000

7. A SEARCH FOR H2A VARIANT-SPECIFIC CHROMATIN INTERACTORS

To investigate, if remodeling factors interact differently with nucleosomes bearing variant H2A, arrays were formed by salt-gradient dialysis with either canonical H2A or H2A.V or mutated forms of H2A.V, immobilized to paramagnetic beads and incubated with DREX. Reconstituted chromatin was then purified and analyzed by mass spectrometry (collaboration with Andreas Schmidt, Protein Analysis Unit ZfP, LMU Munich).

Two sets of experiments were performed: The first data set was performed in triplicates using three different extract preparations and measured after washing with EX-50. However, no significant hits were identified as specific binders for H2A or H2A.V arrays (not shown). Figure 36 shows the enrichment of chromatin-associated factors on arrays composed of H2A nucleosomes or H2A.V nucleosomes compared to embryo extract. In both experiments, ACF (consisting of Acf1 and Iswi) was enriched. In addition, the Ku complex (consisting of Irbp and Ku80) was enriched in response to the free ends of the arrays, which will be investigated in more detail in the next chapter see (VI.B.1 and VI.B.2). Relatedly, Mre11, a component of the MRN complex and shown to be recruited to DSBs (III.D.2), was enriched at chromatin. H2B forms dimers with H2A and H2B and was also enriched. TFAM is a mitochondrial transcription factor (Flybase.org; 22.06.2018), which was recruited to H2A- and H2A.V-containing arrays.

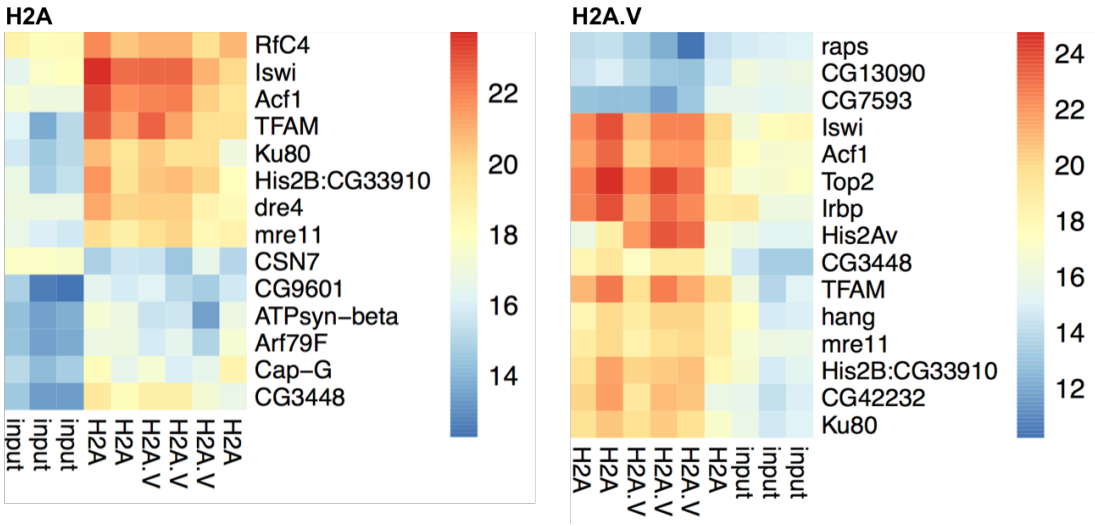

FIGURE 36: ENRICHMENT OF CHROMATIN-ASSOCIATED FACTORS ON ARRAYS COMPOSED OF H2A NUCLEOSOMES OR H2A.V NUCLEOSOMES COMPARED TO EMBRYO EXTRACT (INPUT) MEASURED BY MASS SPECTROMETRY. THE EXPERIMENT WAS PERFORMED IN THREE REPLICATES USING THREE INDEPENDENT EXTRACT PREPARATIONS. HIGH INTENSITIES ARE INDICATED IN RED, LOW INTENSITIES IN BLUE. A FULL LIST OF PROTEINS AND THEIR ENRICHMENT VALUES ARE LISTED IN XI.B.1.A).

Due to phosphorylation of H2A.V triggered by the free end of the array (see III.B.5 and VI.A.3; will be further investigated in VI.B.3), no further analyses of the phospho-mimetic form of H2A.V were performed. Instead, nucleosomes including a C-terminally truncated form of H2A.V was included in the second data set, lacking the phosphorylation motif.

The second experiment included more stringent washing conditions and were measured in collaboration with Andreas Schmidt by a data-independent mass spectrometry analysis named SWATH (Sequential window acquisition of all theoretical fragment ion spectra), which allows a more sensitive, robust and quantitate analysis of complex protein samples (Gillet et al. 2012). As before, three DREX preparations were used in biological replicates. Data after mass spectrometry analysis was analyzed by Tamás Schauer as follows: Protein intensity values were log2-transformed, median normalized and filtered by a low intensity threshold. Statistical analysis was performed by fitting a linear model using the limma R package. Moderated t-statistics were calculated by empirical Bayes moderation. For the identification of significantly enriched proteins, p-value cutoffs and log2-fold change cutoffs were applied as indicated. The heatmap was generated using the pheatmap R package. Under these conditions, only few H2A variant-specific binders were identified, as shown in Figure 37. CG4951, for example, showed a preference for H2A.V nucleosomes relative to the canonical H2A nucleosome. In this experiment the presence or absence of the C-terminus of H2A.V did not make any difference. Unfortunately, CG4951 is not yet described and no information about this protein is available yet. Scully (scu) is a mitochondrial 3-hydroxyacyl-CoA dehydrogenase type-2 (Uniprot: O1840; 29.12.2017) and the interaction of this protein with H2A.V is of unclear significance. CG18067 showed a preference towards H2A or the C-terminally truncated form of H2A.V. It seems therefore, that the C-terminus interfered with binding of this factor to the nucleosome. Unfortunately, CG18067 has also not been characterized so far (Uniprot: A1ZBU8; 29.12.2017) and interaction with nucleosomes is presumably not physiological. We therefore conclude, that the extract does not discriminate considerably among nucleosomes consisting of canonical H2A or its variant, which is in line with the observation obtained after ChIP seq (VI.A.6).

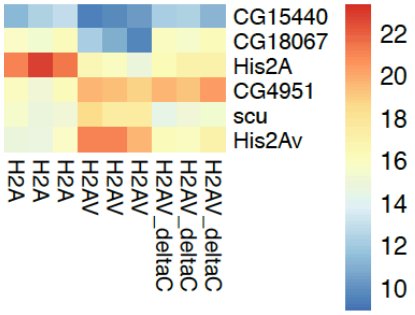

FIGURE 37: COMPARISON OF CHROMATIN-ASSOCIATED FACTORS ON ARRAYS COMPOSED OF H2A NUCLEOSOMES, H2A.V NUCLEOSOMES, AND H2A.VΔC NUCLEOSOMES MEASURED BY MASS SPECTROMETRY. THE EXPERIMENT WAS PERFORMED IN THREE REPLICATES USING THREE INDEPENDENT EXTRACT PREPARATIONS. HIGH INTENSITIES ARE INDICATED IN RED, LOW INTENSITIES IN BLUE. A FULL LIST OF PROTEINS AND THEIR ENRICHMENT VALUES ARE LISTED IN XI.B.1.B).

B. CHARACTERIZATION OF A DNA DAMAGE RESPONSE INITIATED BY DNA BREAKS

Unless indicated otherwise, all mass spectrometry analyses in this chapter were performed in collaboration with Andreas Schmidt by data-independent mass spectrometry analysis (SWATH). Data after mass spectrometry analysis was analyzed by Tamás Schauer as follows: Protein intensity values were log2-transformed, median normalized and filtered by a low

intensity threshold. Statistical analysis was performed by fitting a linear model using the limma R package. Moderated t-statistics were calculated by empirical Bayes moderation. For the identification of significantly enriched proteins, p-value cutoffs and log2-fold change cutoffs were applied as indicated. Gene ontology terms were obtained from the org.Dm.eg.db R package (version: 3.5.0). Scatterplots were plotted by R base graphics and heatmaps using the pheatmap R package.

1. Recruitment of factors to free DNA ends

To test for the recruitment of chromatin-associated factors to free DNA ends during chromatin *in vitro* reconstitution, mass spectrometry analysis was performed after assembly on DNA immobilized at either one end or both ends. To control for unspecific protein binding to beads, a beads-only control without immobilized DNA was included.

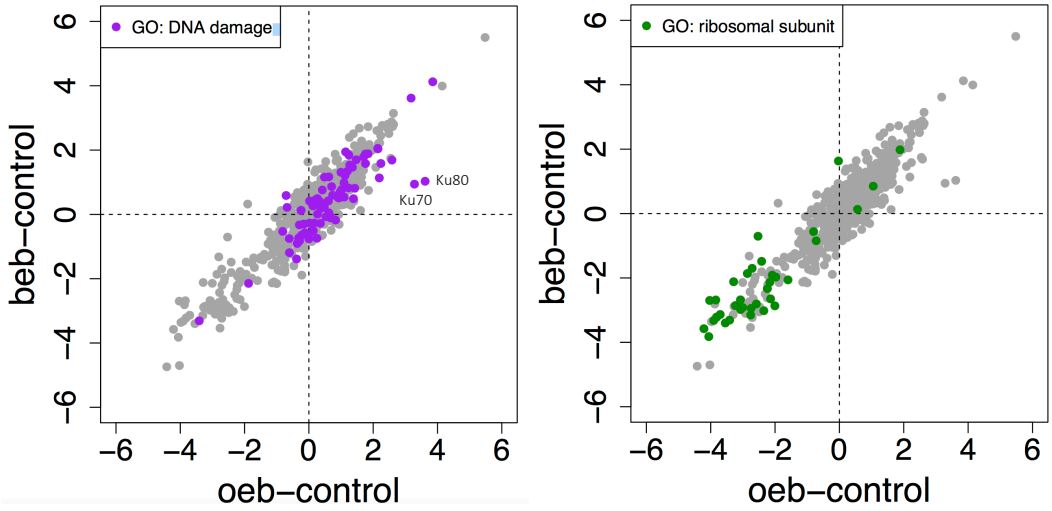

Figure 38: Proteins detected on immobilized DNA by mass spectrometry analysis. Normalized log-transformed values of proteins on DNA immobilized at one end (oeb) and on DNA immobilized on both ends (beb) were plotted against the bead control. Proteins associated with DNA damage are colored in purple (left diagram), and ribosomal proteins are colored in green (right diagram). A full list of proteins and their enrichment values are listed in XI.B.2.a).

After subtraction of bead control, proteins were plotted in Figure 38, with the relative enrichment on the fragment immobilized at one end (y-axis) versus the relative enrichment on the fragment immobilized on both ends (x-axis). The experiment was performed in three biological replicates (three independent extract preparations). Proteins on the top right corner are enriched on both DNA fragments, which are mostly associated with DNA damage (purple data points, left diagram). Of those 77 DNA damage-associated proteins, only two show a preference for the one end bound DNA fragment, namely Ku70 (also known as Irbp) and Ku80. Proteins on the left bottom corner are mainly found in the bead control samples and are mostly

associated with ribosomal proteins (green data points, right diagram), indicating that these proteins were particularly prone to unspecific binding to beads, which is decreased in presence of DNA-coupled beads.

The DNA damage-associated proteins of Figure 38 are listed in Table 5. Amongst those, we found a multitude of DNA damage factors associated with the HR pathway (e.g. the MRN complex consisting of Mre11, Rad50 and Nbs1) and the NHEJ pathway (e.g. Ligase4, Ku complex consisting of Ku70/Irbp and Ku80, see III.D.1).

TABLE 5: DNA DAMAGE-ASSOCIATED FACTORS AND THEIR ENRICHMENT OVER CONTROL BEADS. DNA DAMAGE-ASSOCIATED FACTORS FROM FIGURE 38 ARE LISTED AND ENRICHMENTS OVER CONTROL BEADS WERE DETERMINED BY SUBTRACTION OF NORMALIZED LOG-TRANSFORMED INTENSITIES OF PROTEINS ON DNA IMMOBILIZED AT ONE END (OEB) OR ON DNA IMMOBILIZED AT BOTH ENDS (BEB) MINUS BEAD CONTROL. THE PROTEINS ARE RANKED ACCORDING TO THE HIGHEST DIFFERENCE BETWEEN OEB-CONTROL AND BEB-CONTROL.

FlyBase polypeptide ID	FlyBase symbol	Diff. oeb-control	Diff. beb-control	FlyBase polypeptide ID	FlyBase symbol	Diff. oeb-control	Diff. beb-control
FBpp0080322	**Ku80**	3.62	1.03	**FBpp0087924**	**Cul1**	1.76	1.58
FBpp0081861	**Irbp**	3.28	0.94	**FBpp0309805**	**alien**	0.74	0.60
FBpp0290882	**rad50**	2.19	1.13	**FBpp0311371**	**Jafrac1**	-0.61	-0.75
FBpp0304413	**E(bx)**	0.83	-0.18	**FBpp0082177**	**pic**	-0.16	-0.30
FBpp0089041	**Prosalpha7**	-0.38	-1.39	**FBpp0077927**	**CSN3**	2.15	2.04
FBpp0079437	**Trx-2**	0.25	-0.74	**FBpp0305644**	**Rpn10**	1.09	0.98
FBpp0077263	**gkt**	1.39	0.49	**FBpp0087756**	**FANCI**	2.14	2.06
FBpp0079802	**mre11**	2.58	1.69	**FBpp0088021**	**Rpt1**	-0.30	-0.33
FBpp0076890	**Rpt6**	0.68	-0.11	**FBpp0074246**	**CG8142**	1.84	1.89
FBpp0072041	**DNA-ligI**	0.00	-0.76	**FBpp0079565**	**me31B**	0.34	0.40
FBpp0308486	**Not1**	0.67	-0.08	**FBpp0083399**	**Fancd2**	1.70	1.79
FBpp0306426	**His2Av**	2.24	1.58	**FBpp0311247**	**rept**	1.12	1.21
FBpp0291433	**CG30382**	0.14	-0.51	**FBpp0312066**	**RpS3**	-3.41	-3.31
FBpp0082987	**14-3-3 epsilon**	0.36	-0.28	**FBpp0078478**	**Gnf1**	1.35	1.47
FBpp0078449	**Prosbeta7**	0.00	-0.61	**FBpp0311114**	**RfC38**	1.76	1.88
FBpp0076312	**Mcm7**	1.43	0.81	**FBpp0308680**	**Ald**	0.12	0.26
FBpp0309113	**Dsor1**	0.53	-0.07	**FBpp0079609**	**RfC3**	1.19	1.34
FBpp0085703	**FK506-bp2**	-0.60	-1.19	**FBpp0290448**	**CSN4**	0.71	0.87
FBpp0086223	**Fen1**	0.62	0.05	**FBpp0079641**	**cdc2**	0.27	0.49
FBpp0305067	**ben**	1.10	0.54	**FBpp0087583**	**Uba1**	1.47	1.70
FBpp0297182	**nbs**	-0.36	-0.91	**FBpp0075277**	**DNApol-delta**	0.18	0.42
FBpp0081820	**Tctp**	-0.29	-0.82	**FBpp0288389**	**eIF4G**	0.16	0.41
FBpp0073989	**Prosalpha4**	-0.12	-0.57	**FBpp0312031**	**Rpt3**	0.21	0.46
FBpp0089395	**PCNA**	0.17	-0.27	**FBpp0071172**	**Caf1-180**	1.27	1.53
FBpp0311982	**Rpt2**	0.93	0.51	**FBpp0304598**	**Top2**	3.85	4.12
FBpp0075382	**Prosbeta2**	-0.23	-0.64	**FBpp0305164**	**Dek**	-0.81	-0.53
FBpp0071117	**Trxr-1**	-0.32	-0.73	**FBpp0073120**	**RfC4**	1.00	1.31
FBpp0078756	**Hel25E**	1.23	0.82	**FBpp0311276**	**Uev1A**	0.42	0.76
FBpp0080787	**Top3alpha**	0.91	0.52	**FBpp0087821**	**CSN7**	-0.25	0.12
FBpp0078331	**Snr1**	0.08	-0.29	**FBpp0112608**	**Parp**	-0.24	0.13
FBpp0082180	**timeout**	0.02	-0.27	**FBpp0079710**	**Nup107**	0.02	0.42
FBpp0303628	**eIF-4a**	0.97	0.70	**FBpp0288680**	**Rrp1**	3.18	3.62
FBpp0300790	**wds**	-1.88	-2.15	**FBpp0082511**	**Caf1**	0.62	1.17
FBpp0086400	**Prosbeta1**	0.48	0.22	**FBpp0310470**	**spel1**	1.24	1.85
FBpp0306599	**Rpn2**	0.27	0.01	**FBpp0072658**	**CG12018**	0.49	1.16
FBpp0073678	**Lig4**	1.02	0.78	**FBpp0081704**	**pont**	1.14	1.94
FBpp0076804	**Txl**	0.61	0.42	**FBpp0110174**	**tefu**	-0.68	0.22
FBpp0078631	**Marcal1**	0.37	0.19	**FBpp0289675**	**cdc2c**	-0.71	0.59
FBpp0083658	**CSN6**	0.60	0.42				

To test for the kinetics of the recruitment of factors to DNA ends, the experiment described in Figure 38 was repeated including an early and late time point (15 min versus 3 h assembly time) with DNA fragments immobilized at either one end (oeb) or both ends (beb) to streptavidin-coated paramagnetic beads. The experiment was performed in seven biological replicates from seven independent extract preparations. To evaluate the reproducibility among the seven replicates, a principle component analysis was performed (Figure 40).

We then investigated the changes of factor recruitment as a function of time, here focusing on the one-side-immobilized fragment only, which is similar to the analysis by Völker-Albert et al to identify the kinetics of factors during chromatin assembly (Völker-Albert et al. 2016). The volcano blot in Figure 39 shows early chromatin binders on the left (blue) and late chromatin binders on the right (red).

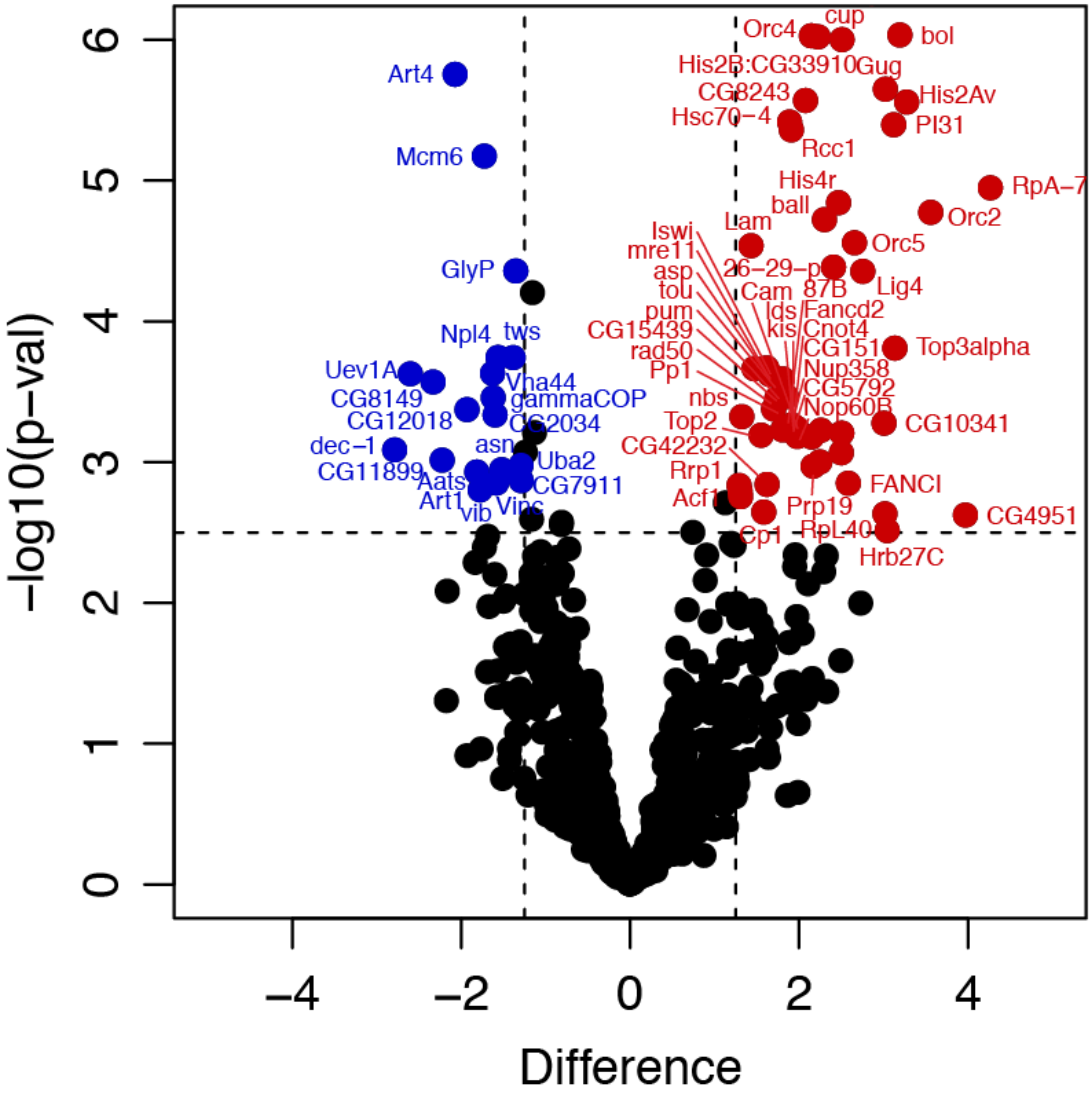

FIGURE 39: CHROMATIN PROTEINS ENRICHED ON DNA IMMOBILIZED AT ONE END AFTER 15 MIN (BLUE) VERSUS AFTER 3 H (RED) OF ASSEMBLY. A FULL LIST OF PROTEINS (ALSO INCLUDING PROTEINS ENRICHED ON DNA IMMOBILIZED AT BOTH ENDS) AND THEIR ENRICHMENT VALUES ARE LISTED IN XI.B.2.B).

Consistent with the data published, the DNA repair proteins Lig4, RpA-70 and H2A.V/H2B were identified as late binders. The late enrichment of H2A.V and H2B is intriguing. As discussed before, H2A.V does not seem to be incorporated in a targeted and remodeler-dependent manner. However, it might be that H2A.V and H2B, which have been shown to be incorporated as dimers like H2A.Z-H2B in yeast and mammals (Kusch et al. 2014; G. Mizuguchi 2004; Luk et al. 2010) are already associated to chromatin for later incorporation. H2A.Z-H2B dimers are generally associated to chaperones like Chz1 or Swr2 in yeast or Yl1 in mammals (Billon & Côté 2012; Obri et al. 2014; Latrick et al. 2016; Liang et al. 2016).

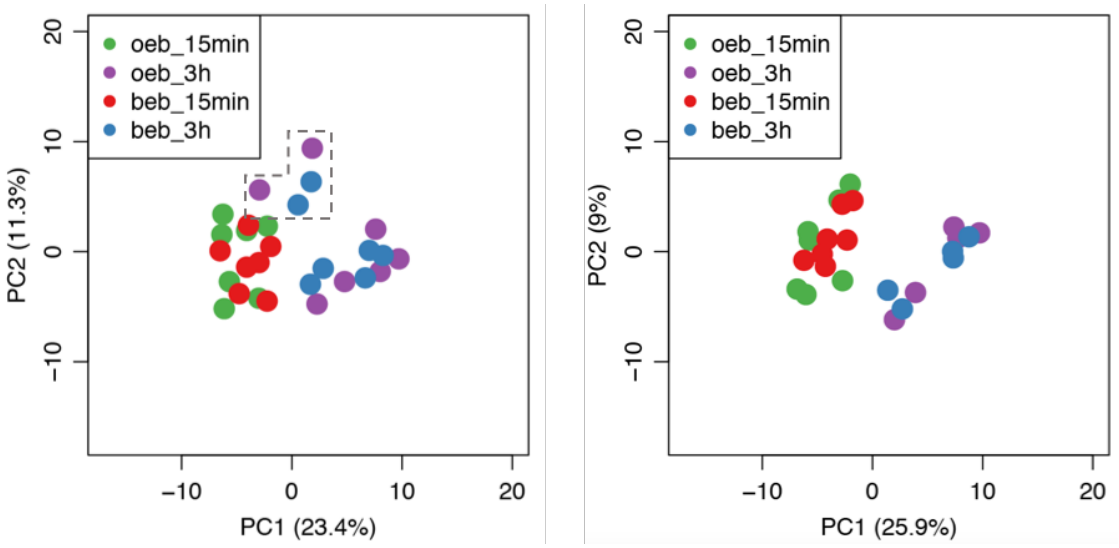

FIGURE 40: PRINCIPAL COMPONENT ANALYSIS OF CHROMATIN SAMPLES ON DNA IMMOBILIZED AT EITHER ONE END (OEB) OR BOTH ENDS (BEB) AFTER 15 MIN OR AFTER 3 H ASSEMBLY TIME. CHROMATIN SAMPLES AFTER 15 MIN, OR AFTER 3 H FORM ONE CLUSTER, WITH THE EXCEPTION OF FOUR OUTLIERS (LEFT, MARKED WITH DASHED LINE), WHICH WERE EXCLUDED IN FURTHER ANALYSES (RIGHT). A FULL LIST OF PROTEINS AND THEIR ENRICHMENT VALUES ARE LISTED IN XI.B.2.B).

The majority of the samples (24 out of 28) were distributed in two main clusters, one composed of the data from the 15 min assembly time point (red and green), and one from the data derived from 3 h assembly (blue and violet). The four samples outside of these clusters were not included in the analysis (see box in grey dashed lines, Figure 40).

The MRN complex consisting of Mre11, Rad50 and Nbs, however, as well as the ACF complex consisting of Acf1 and Iswi, were identified as early binders (after 15 min) in Völker-Albert et al. (Völker-Albert et al. 2016), but were enriched after 3 h in our mass spectrometry data under comparable reaction conditions. In contrast, Western blot analysis revealed the strongest enrichment of ACF at 5 min and a decreased recruitment at later time points (Figure 41 and Figure 42). However, the decrease of ACF only seems to occur within the first 30 minutes and only moderately. It could therefore be, that the sensitivity and the temporal resolution is not sensitive enough, leading to the observed discrepancies. I contrast to this, the increase of H2A.V was consistent and striking in both mass spectrometry experiments as well as in the Western blot analysis. In our data, the Ku complex was associated to chromatin very early and remaining associated over hours. In our mass spectrometry analysis, Irbp and Ku80 were not

significant in Figure 39 using a stringent p-value cut-off of 0.003. However, using a p-value cut-off of 0.01 would identify the Ku complex as late binders. In Völker-Albert et al. (Völker-Albert et al. 2016). Ku was categorized as a late binder and only recruited at late time points. In our experiments, chromatin assembly was performed in presence of β-glycerophosphate to inhibit dephosphorylation of H2A.V. It cannot be excluded that addition of this phosphatase inhibitor has an effect on the kinetics of Ku. The association of Ku to free DNA will be discussed in more detail in VII.B.

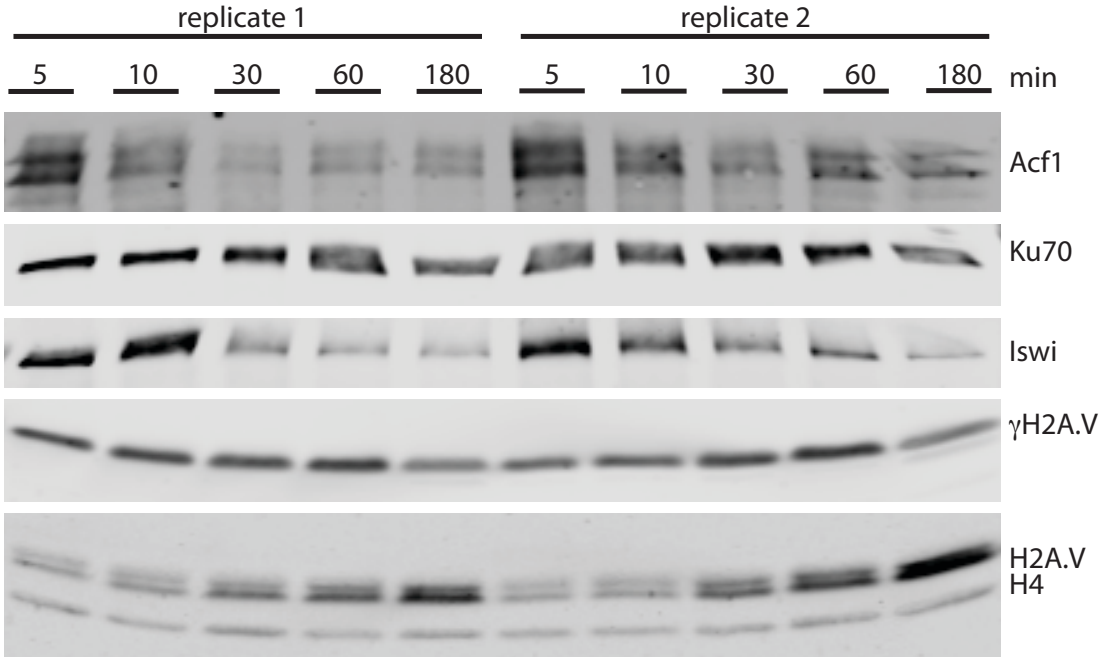

FIGURE 41: CHROMATIN ASSEMBLY ON DNA IMMOBILIZED AT ONE END FOR 5 MIN, 10 MIN, 30 MIN, 60 MIN, OR 180 MIN. THE EXPERIMENT WAS PERFORMED IN TWO REPLICATES, USING TWO INDEPENDENT CHROMATIN PREPARATIONS. AFTER SDS-PAGE, PROTEINS WERE BLOTTED AND MEMBRANES WERE PROBED WITH ANTIBODIES AGAINST ACF1, KU70, ISWI, γH2A.V, H2A.V, AND H4.

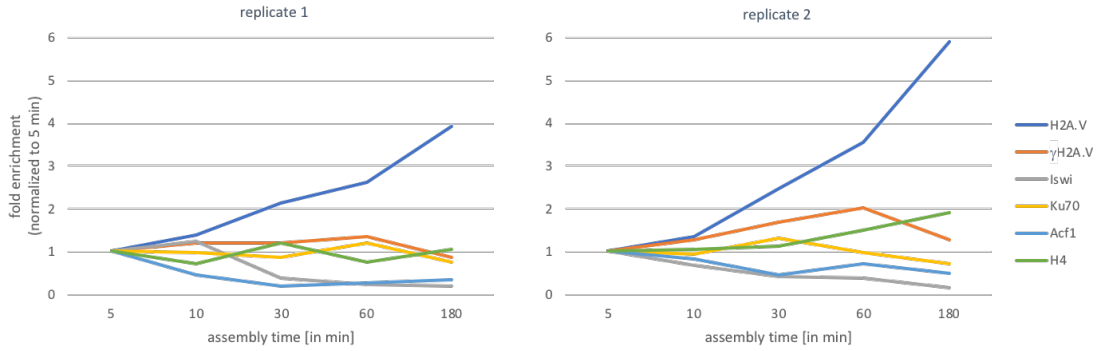

FIGURE 42: RELATIVE ENRICHMENT OF SIGNAL INTENSITIES OF ACF1, KU70, ISWI, γH2A.V, H2A.V, AND H4 AFTER 5 MIN, 10 MIN, 30 MIN, 60 MIN, OR 180 MIN ASSEMBLY ON DNA IMMOBILIZED AT ONE END IN REFERENCE TO THE INTENSITIES AFTER 5 MIN. SIGNAL INTENSITIES WERE QUANTIFIED FROM FIGURE 41 BY IMAGE STUDIO™ LITE SOFTWARE, LI-COR BIOSCIENCES.

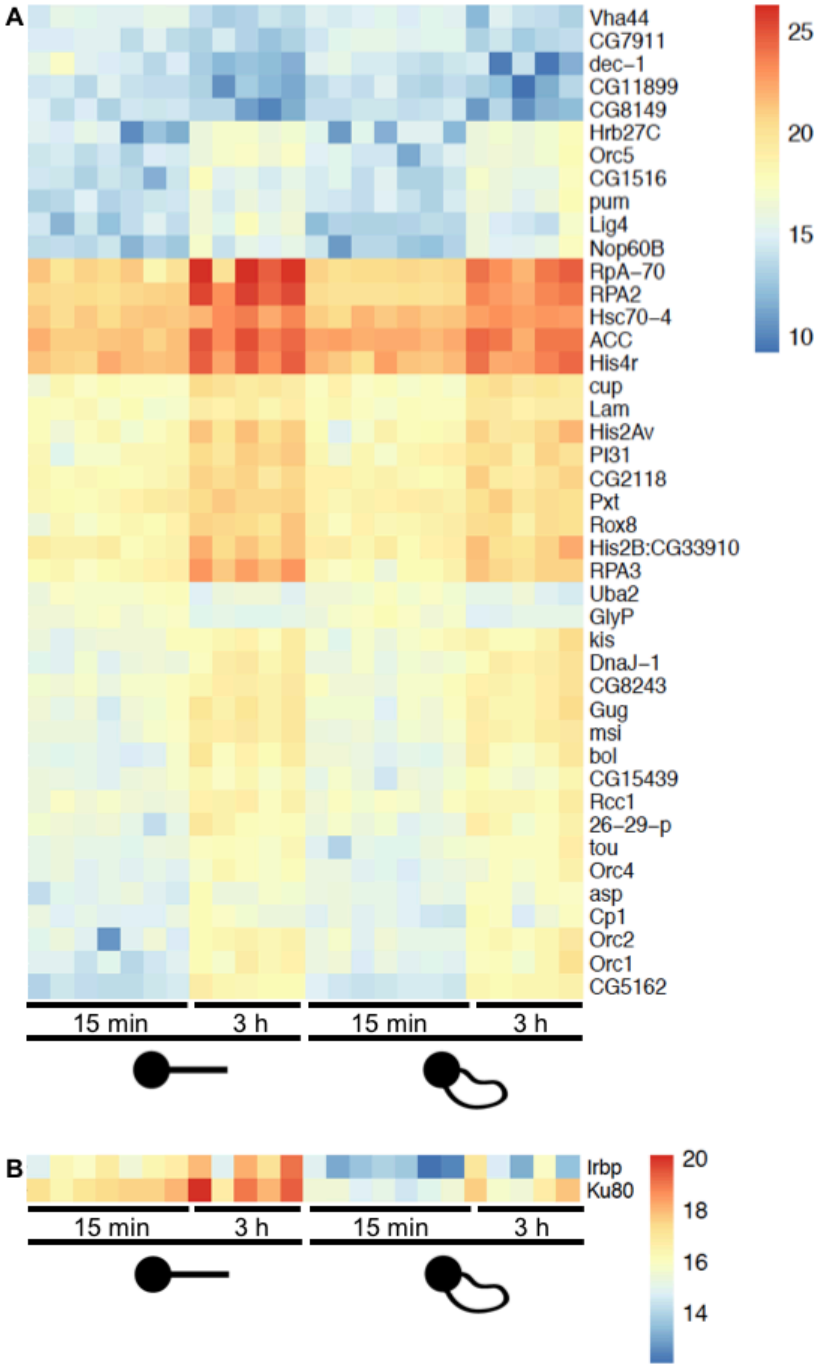

FIGURE 43: ENRICHMENT OF CHROMATIN-ASSOCIATED FACTORS AFTER 15 MIN OR AFTER 3 H ON DNA IMMOBILIZED AT ONE END OR AT BOTH ENDS FROM SEVEN BIOLOGICAL REPLICATES. OUTLIERS INDICATED IN FIGURE 40 WERE REMOVED. HIGH INTENSITIES ARE INDICATED IN RED, LOW INTENSITIES IN BLUE. A FULL LIST OF PROTEINS AND THEIR ENRICHMENT VALUES ARE LISTED IN XI.B.2.B). HEATMAP A SHOWS SIGNIFICANTLY ENRICHED PROTEINS (USING THE STATISTICAL PARAMETERS INDICATED IN VI.B) AFTER COMPARISON OF THE DIFFERENCES BETWEEN 3 H VERSUS 15 MIN ON DNA IMMOBILIZED AT ONE END VERSUS BOTH ENDS, HEATMAP B SHOWS SIGNIFICANTLY ENRICHED PROTEINS (USING THE STATISTICAL PARAMETERS INDICATED IN VI.B) AFTER COMPARISON OF THE DIFFERENCES BETWEEN ONE END VERSUS BOTH ENDS AFTER 15 MIN VERSUS AFTER 3 H.

As already observed in Figure 38 the Ku complex was significantly enriched at both time points, after 15 min and 3 h assembly on DNA immobilized at one end. In addition, we observed that

the RPA complex showed a substantial enrichment after 3 h, but not after 15 min. An explanation for the late enrichment of RPA might be the fact, that RPA binds ssDNA (Liptak & Loria 2015). DNA resection, however, is a well-controlled and time-consuming process, which might not be accomplished after 15 min. Ku, however, has been shown to be able to interact with ssDNA and dsDNA, with a preference for dsDNA (Mimori & Hardin 1986).

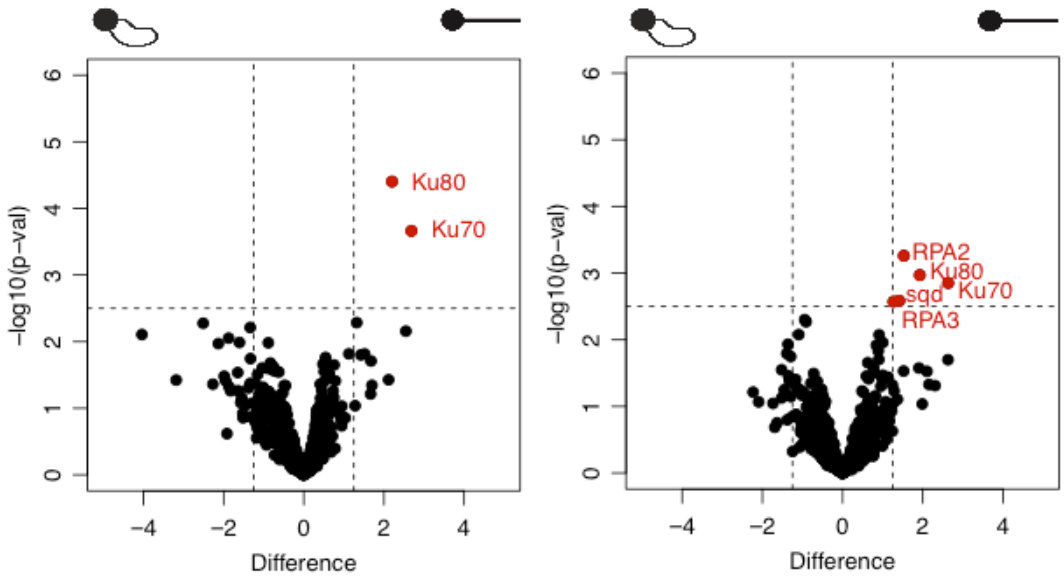

FIGURE 44: VOLCANO PLOT WITH LOG10 P VALUES (Y-AXIS) AND LOG FOLD DIFFERENCE (X-AXIS) AFTER COMPARISON OF CHROMATIN-ASSOCIATED FACTORS ON DNA IMMOBILIZED AT ONE END OR AT BOTH ENDS FROM SEVEN BIOLOGICAL REPLICATES. INTENSITIES WERE MEASURED BY MASS SPECTROMETRY AFTER 15 MIN ASSEMBLY (LEFT) AND AFTER 3 H ASSEMBLY (RIGHT). OUTLIERS INDICATED IN FIGURE 40 WERE REMOVED. A FULL LIST OF PROTEINS AND THEIR ENRICHMENT VALUES ARE LISTED IN XI.B.2.B).

2. GENERATION AND CHARACTERIZATION OF KU ANTIBODIES

To confirm Ku enrichment by Western blot analysis, monoclonal antibodies against Ku70 and Ku80 were generated in collaboration with Elisabeth Kremmer (Helmholtz Center Munich, Germany).

For the identification of suitable immunogens to generate monoclonal antibodies, the amino acid sequences of Ku70 (Flybase: Irbp, FBpp0081861, 07.06.2018) and Ku80 (Flybase Ku80, FBpp0080322, 07.06.2018) were screened by Dr. Anette Jacob (Peps 4 LS GmbH, Heidelberg, Germany). Two peptides for each protein were chosen for the generation of monoclonal rat antibodies and designed by Peps 4 LS GmbH for rat immunization:

Ku70-1:	SEDEEDVSMKRDYHG
Ku70-2:	QDWNNTENTADEQK
Ku80-1:	TLRDTQQPRPWAQN
Ku80-2:	YDNDKEDKMLKDKN

Elisabeth Kremmer (Helmholtz Zentrum Munich) then generated 126 primary tissue cultures of single hybridoma cell lines, with supernatants against peptides Ku70-1, Ku70-2, Ku80-1, and Ku80-2 (Table 6).

TABLE 6: GENERATION OF RAT MONOCLONAL ANTIBODIES. 126 PRIMARY TISSUE CULTURES OF HYBRIDOMA CELLS AFTER RAT IMMUNIZATION WITH KU70-1, KU70-2, KU80-1, AND KU80-2 WERE OBTAINED AND SCREENED IN WESTERN BLOT ANALYSIS. TWO OF EACH PEPTIDE WERE SELECTED AND SUBCLONED AS STABLE CELL LINES. OF THOSE, FIVE STABLE CELL LINES WERE GENERATED.

	Ku70-1	Ku70-2	Ku80-1	Ku80-2
obtained primary tissue cultures	58	10	34	24
subcloned as stable cell lines	2	2	2	2
stable cell lines	2 (6B2, 12B8)	1 (5H4)	1 (8E7)	1 (8B11)

After an initial screening of supernatants obtained from these 126 primary tissue cultures by Western blot using DREX (not shown), the two most specific ones for each peptide were selected and subcloned as stable cell lines for antibody production. Of those, five stable cell lines were maintained for antibody production. Specificity and sensitivity of those antibodies was then tested using DREX, *in vitro*-assembled chromatin on DNA immobilized either at one or at both ends, wt Schneider cell extract and Schneider cell extract after Ku70 RNAi or Ku80 RNAi treatment (Figure 45).

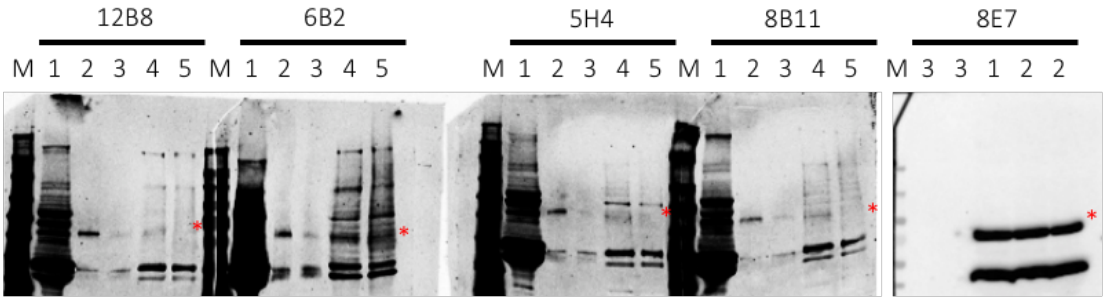

FIGURE 45: WESTERN BLOT ANALYSIS TO INVESTIGATE THE SPECIFICITY AND SENSITIVITY OF MONOCLONAL ANTIBODIES AGAINST KU70 AND KU80. M: MARKER; 1: DREX; 2, 3: *IN VITRO*-ASSEMBLED CHROMATIN ON DNA IMMOBILIZED EITHER AT ONE (2) OR AT BOTH (3) ENDS; 4, 5: *DROSOPHILA* S2 WHOLE CELL EXTRACTS FROM EITHER WT (4) OR KD (5) CELLS. KU70 KD CELLS WERE USED TO TEST 12B8, 6B2, AND 5H4, KU80 KD CELLS WERE USED TO TEST 8B11 AND 8E7. MEMBRANES WERE PROBED WITH SUPERNATANTS FROM STABLE CELL LINES 12B8, 6B2, 5H4, 8B11, AND 8E7. ASTERISKS INDICATE BANDS OF KU70 AND KU80.

A prominent low-molecular weight signal was detected with all supernatants, which could be a degradation product of Ku70 or 80 or an abundant and chromatin-associated low-molecular weight protein, which is recognized by the antibodies. However, these antibodies specifically recognized the subunits of the Ku complex associated to chromatin or in whole cell extracts and were used for all Western blot analyses in this thesis. Furthermore, these antibodies were able to detect Ku in ChIP (Figure 51). The most specific antibodies were used for Western blot analysis and chromatin immunoprecipitation in the following experiments. First, Western blot

analysis was performed to analyze Ku enrichment at DSBs in a time course of chromatin assembly/maturation. Consistent with the mass spectrometry result, enrichment of Ku was limited to the fragment with the free end and almost completely absent when DNA was immobilized at both ends. Furthermore, it remained associated to the fragment at constant levels over the time course of 15 min to 240 min.

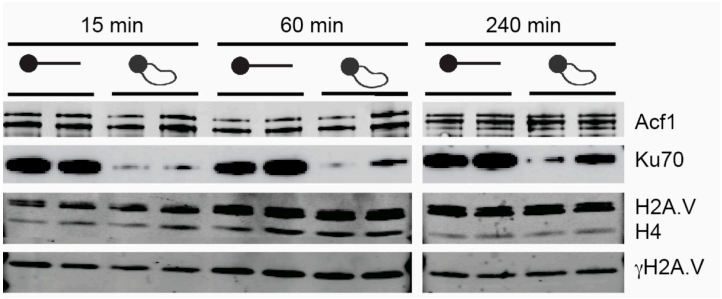

FIGURE 46: CHROMATIN ASSEMBLY ON DNA IMMOBILIZED AT ONE END OR BOTH ENDS FOR THE INDICATED TIMES. THE EXPERIMENT WAS PERFORMED IN TWO BIOLOGICAL REPLICATES, USING TWO INDEPENDENT EXTRACT PREPARATIONS. AFTER SDS-PAGE, PROTEINS WERE BLOTTED AND MEMBRANES WERE PROBED WITH ANTIBODIES AGAINST ACF1, KU70, H2A.V, H4, AND γH2A.V.

As shown in Figure 46 and Figure 47, immobilization of DNA triggered the phosphorylation of H2A.V, despite of the immobilization of the biotinylated fragment to the beads.

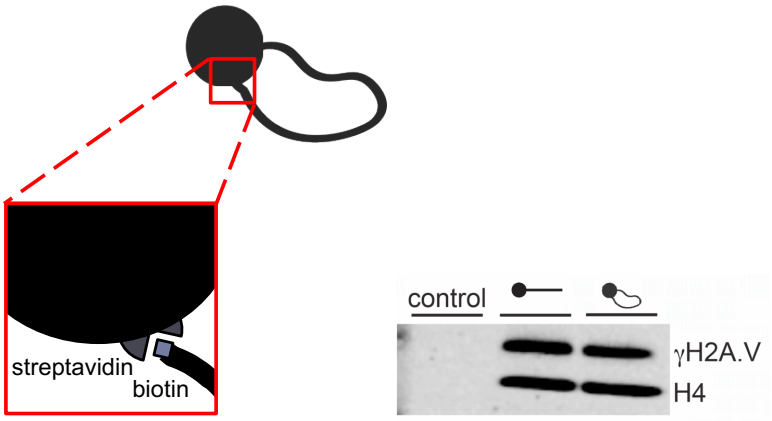

FIGURE 47: LEFT: ILLUSTRATION OF BIOTINYLATED DNA COUPLED TO STREPTAVIDIN-COATED BEADS;

RIGHT: CHROMATIN ASSEMBLY ON DNA IMMOBILIZED AT ONE END OR BOTH ENDS. AFTER SDS-PAGE, PROTEINS WERE BLOTTED AND MEMBRANES WERE PROBED WITH ANTIBODIES AGAINST γH2A.V AND H4.

At early time points (here: 15 min), phosphorylation of H2A.V was decreased in the both-sided-immobilized fragment compared to the one-side-immobilized fragment. However, at later time points, phosphorylation levels among the two fragments were equal (Figure 48).

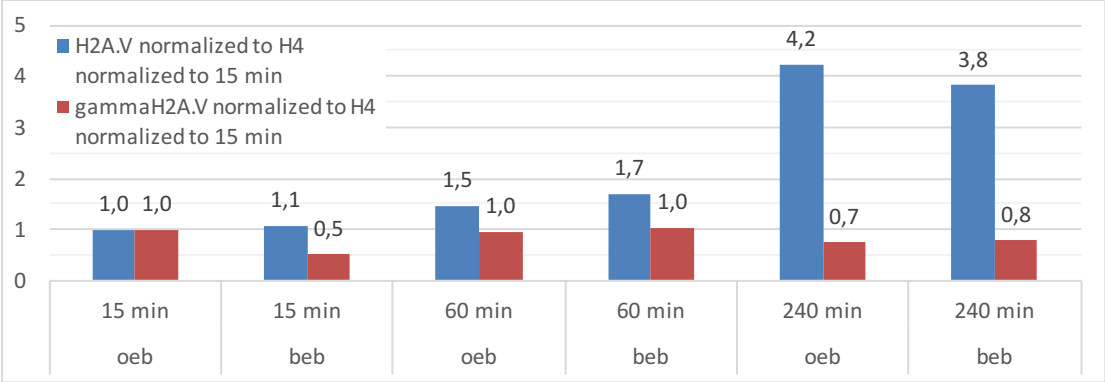

FIGURE 48: RELATIVE ENRICHMENT OF SIGNAL INTENSITIES OF H2A.V AND γH2A.V AFTER 15 MIN, 60 MIN, OR 240 MIN ASSEMBLY ON DNA IMMOBILIZED AT ONE END OR BOTH ENDS NORMALIZED TO H4 IN REFERENCE TO THE INTENSITIES AT ONE END IMMOBILIZED DNA AFTER 15 MIN FROM FIGURE 46 QUANTIFIED BY IMAGE STUDIO™ LITE SOFTWARE, LI-COR BIOSCIENCES.

We suspect, that biotinylation itself already initiated the phosphorylation as insertion of biotinylated nucleotides into intact plasmids by nick translation triggered phosphorylation of H2A.V (Figure 49). Here, the Biotin-Nick Translation Mix (Sigma) was used using different amounts of circular plasmid DNA per reaction to aim for optimal levels of incorporated biotinylated nucleotides. After biotinylation DNA was immobilized to streptavidin-coupled beads and the supernatant after coupling was tested to determine the efficiency of biotinylation (Figure 49, top). Immobilized DNA was then used for chromatin assembly *in vitro* and probed by Western blot analysis to investigate the phosphorylation of H2A.V (Figure 49, bottom). Unfortunately, efficient immobilization was only possible with high levels of nick translation-mediated biotinylation, which led to the phosphorylation of H2A.V.

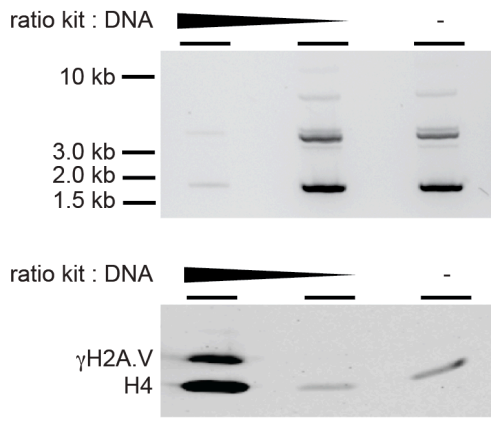

FIGURE 49: TOP: AGAROSE GEL OF CIRCULAR DNA IN THE SUPERNATANT AFTER COUPLING TO STREPTAVIDIN-COATED BEADS. BEFORE, BIOTINYLATED NUCLEOTIDES WERE INSERTED USING A NICK TRANSLATION KIT AND TWO DIFFERENT AMOUNTS OF DNA PER REACTION. AS A NEGATIVE CONTROL, UNTREATED DNA WAS INCUBATED WITH BEADS TO CONTROL FOR UNSPECIFIC BINDING OF DNA TO BEADS. BOTTOM: CHROMATIN ASSEMBLY ON DNA IMMOBILIZED AFTER INSERTION OF BIOTINYLATED NUCLEOTIDES BY NICK TRANSLATION. AFTER SDS-PAGE, PROTEINS WERE BLOTTED AND MEMBRANES WERE PROBED WITH ANTIBODIES AGAINST γH2A.V AND H4.

In addition to this, other approaches to isolate intact DNA without obvious damage (e.g. circular chromatin) without induction of H2A.V phosphorylation were not successful, impeding the investigation of chromatin-associated factors to damaged DNA in relation to intact DNA (see VII.D).

To localize the Ku complex at break sites and visualize the distribution of γH2A.V, both features were mapped by ChIP-Seq on chromatin assembled on two FlyFosmids including different *Drosophila* genomic sequences (Figure 50): One FlyFosmid, in this case FlyFos019829, was intact in the control and in the damage reaction. FlyFos019611 was either circular (control reaction) or cut by FseI (damage reaction).

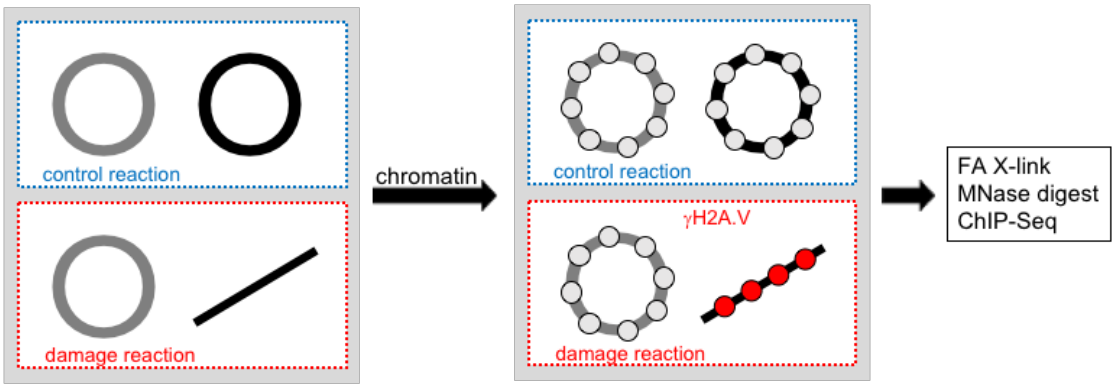

FIGURE 50: EXPERIMENTAL SETUP TO CAPTURE H2A.V PHOSPHOYLATION AND KU RECRUITMENT AT DSBS. FLYFOSMIDS WERE INCUBATED WITH DREX. IN EACH REACTION, ONE OF THE FLYFOSMIDS REMAINED CIRCULAR (CONTROL FLYFOSMID), WHILE THE OTHER FLYFOSMID WAS EITHER CIRCULAR (CONTROL REACTION, BLUE) OR LINEARIZED (DAMAGE REACTION, RED).

In addition to the break introduced into the genomic region of FlyFos1096611, another break was introduced into the backbone, which was not mapped in the following sequencing data (Figure 51). After formaldehyde-crosslinking and MNase fragmentation to fragments of mainly mono-nucleosomes and few di-nucleosomes, samples were analyzed by ChIP-Seq with antibodies against H3, H2A.V, γH2A.V and Ku as described in V.C.3 and V.C.4.

Histones H3 and H2A.V were evenly distributed along both FlyFosmids in the control and damage reactions. Only around the break sites, signals in a region of about 2 kb decreased after 120 min assembly. This loss of signal could be a result of nucleosome removal, as it has been proposed for yeast and mammals (Goldstein et al. 2013; Tsukuda, Fleming, Nickoloff & Osley 2005; Shroff et al. 2004; Morrison & Shen 2009). On the other hand, the loss of signal could also result from DNA degradation, either by random nucleases degrading the accessible DNA or by DNA damage-associated nucleases, which generate regions of ssDNA during the progress of DNA repair. Considering the loss of signal in the input, it is likely that it is indeed a loss of DNA rather than nucleosome removal. However, the loss of DNA will be discussed in more detail in VI.B.5.

Interestingly, at early time points (15 min), Ku was specifically enriched in close proximity to the break site. This enrichment was no longer detected after 2 h, even though Ku remained bound to the DNA fragment with the free end up to 4 h (Figure 46). However, ChIP-seq of Ku was only performed once and requires additional replicates to confirm this observation. In addition to this, phosphorylation of H2A.V was highly increased after 10 min over the entire mapped FlyFosmid including the FseI cut and remained high. Remarkably, no phosphorylation was detected on the circular control FlyFosmid in the same reaction, suggesting that the

phosphorylation signal only spreads along the DNA in *cis*, but is not transferred to intact DNA in the same reaction. Unfortunately, H3 ChIP was generally not highly efficient, leading to a diminished quality of sequencing profiles for H3, particularly in the control reaction (Figure 51).

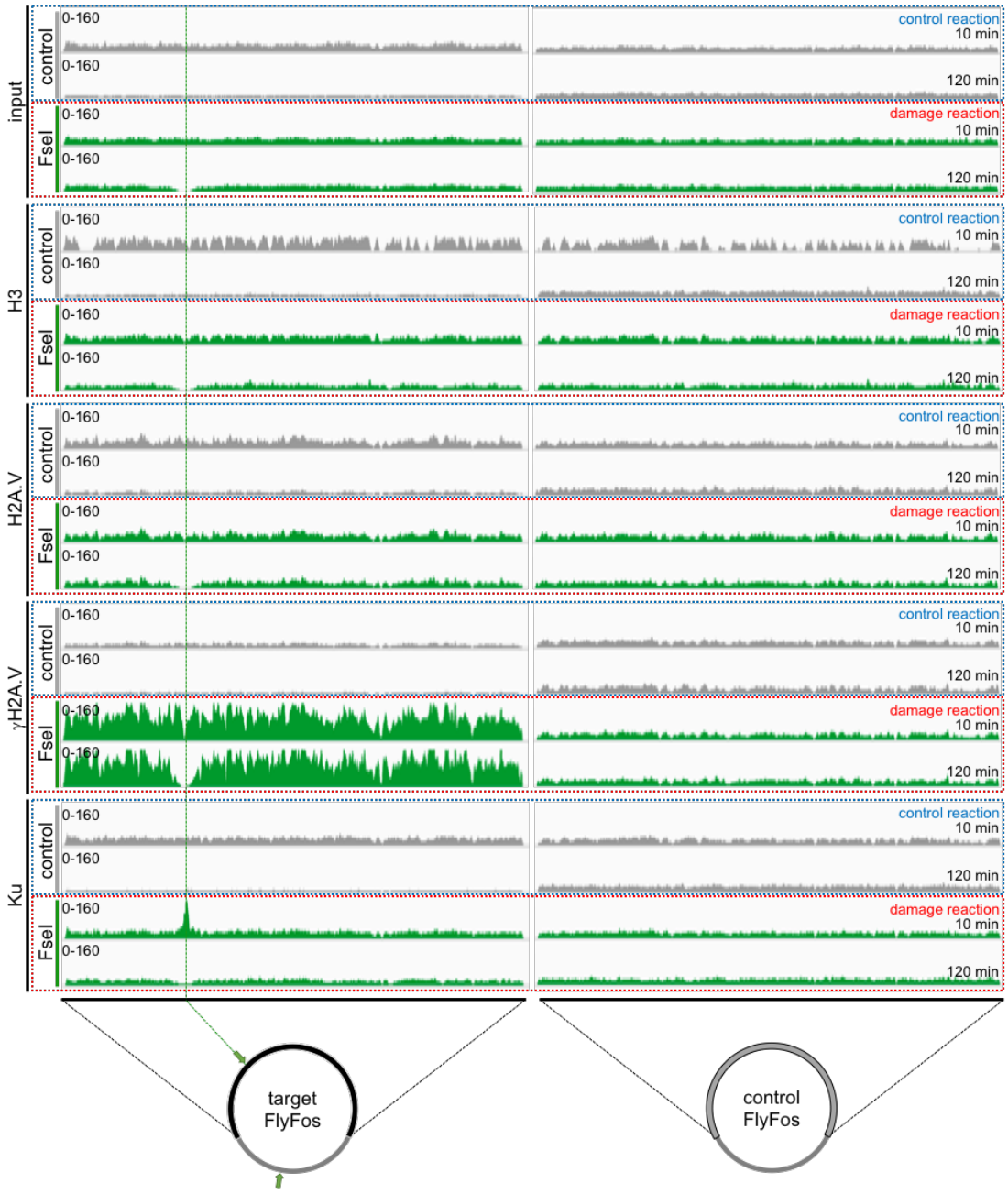

FIGURE 51: CHIP-SEQ ON CHROMATIN ASSEMBLED FOR 10 MIN OR 120 MIN ON A MIX OF CIRCULAR CONTROL FLYFOSMIDS AND ON TARGET FLYFOSMIDS, WHICH ARE EITHER CIRCULAR (CONTROL) OR LINEARIZED BY RESTRICTION WITH FSEI. CHIP WAS DONE WITH ANTIBODIES AGAINST H3, H2A.V, γH2A.V, AND KU. THE GREEN ARROWS INDICATE THE FSEI CLEAVAGE SITES IN THE TARGET FLYFOSMID. READS WERE NORMALIZED TO THE CONTROL FLYFOS.

Enrichment of Ku in proximity to the break site was also confirmed by qPCR. Enrichment was normalized to a control region on the intact control FlyFosmid. In this experiment, both break

sites were addressed, the break in the genomic region and the break in the FlyFosmid vector backbone. Assembly was performed for 2 h (Figure 52).

The upper panel shows the control conditions with both FlyFosmids intact. As expected, signals of H3 and H2A.V ChIP are evenly distributed along the target FlyFosmid and neither signals of H2A.V phosphorylation or Ku are increased. In contrast to this, in the lower panel, showing the damage reaction, Ku is clearly enriched at the sites close to the break site and γH2A.V signals are augmented at 1500 bp to 3000 bp distances from the break site, but also at the more fare located control region, due to spreading along the DNA from the break site. Surprisingly, H2A.V signal around the break site is increased compared to the control region (here at 1500 and 300 bp from cut'). Interestingly, however, signals of H2A.V and γH2A.V, but also of H3 are lost at loci close to the break site, which might be due to DNA resection (VI.B.5, Figure 72). Analogous observations were made in additional ChIP experiments with similar conditions (not shown).

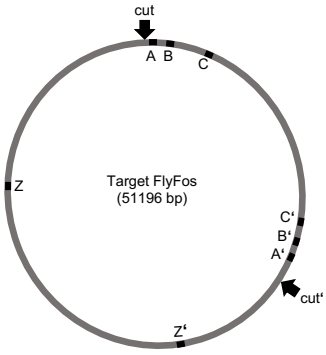

	position	distance to break (in bp)
cut	0	-
A	490	490
B	1480	1480
C	3680	3680
Z	12060	12060
cut'	18090	-
A'	16710	1370
B'	15800	2280
C'	14700	3380
Z'	24700	6600

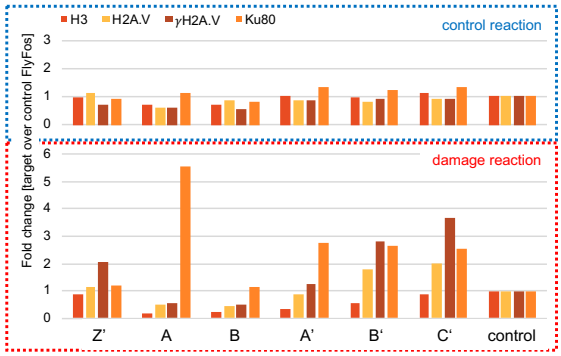

FIGURE 52: CHIP-QPCR ON CHROMATIN ASSEMBLED FOR 2 H ON CIRCULAR CONTROL FLYFOSMIDS AND ON TARGET FLYFOSMIDS, WHICH ARE EITHER CIRCULAR (CONTROL REACTION) OR LINEARIZED (DAMAGE REACTION). ANTIBODIES AGAINST H3, H2A.V, γH2A.V, AND KU80 WERE USED. % OF INPUT WAS DETERMINED AND NORMALIZED TO THE CONTROL FLYFOSMID. THE EXPERIMENT WAS PERFORMED IN ONE BIOLOGICAL REPLICATE.

To investigate the kinetics of factors recruited to *in vitro* reconstituted chromatin, I performed Western blot analysis after 2 min, 15 min, 45 min, 120 min and 240 min assembly time. As a control, beads lacking DNA were incubated with DREX under assembly conditions to control for unspecific binding of proteins to beads (Figure 53). H2A.V and H4 signals constantly increased from 2 min to 45 min and remain at a constant level until 240 min, monitoring the kinetics of the assembly reaction. Acf1 and Ku70 association followed the same kinetics on the DNA with one free end. Ku70 was not associated to DNA with both ends tethered to the beads, consistent with the mass spectrometry analysis (Figure 44).

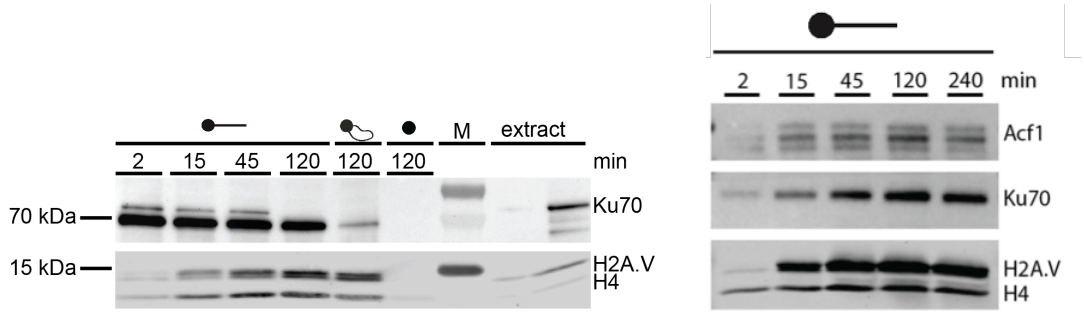

FIGURE 53: TIME COURSE OF ASSOCIATION OF ACF1, KU AND HISTONES H2A.V AND H4 TO *IN VITRO* RECONSTITUTED CHROMATIN OVER TIME ON DNA BEARING A FREE END. 120-MIN TIME POINTS WITH BEB CHROMATIN AND BEADS LACKING DNA SERVE AS REFERENCE. ASSEMBLY WAS PERFORMED FOR 2 MIN, 15 MIN, 45 MIN, 120 MIN, AND 240 MIN AND CHROMATIN WAS THEN ISOLATED VIA PARAMAGNETIC STREPTAVIDIN BEADS. KU70 IS RECRUITED ALREADY AFTER 2 MIN AND REMAINS ASSOCIATED FOR AT LEAST 240 MIN. ASSOCIATION OF ACF1 AND HISTONES H2A.V AND H4 INCREASE OVER TIME. DREX (EXTRACT) WAS USED AS INPUT IN TWO DIFFERENT AMOUNTS OF APPROXIMATELY 60 µG AND 300 µG TOTAL PROTEIN. A PROTEIN STANDARD WAS LOADED (M), WITH PROTEIN SIZES INDICATED ON THE LEFT.

3. CHARACTERIZATION OF H2A.V PHOSPHORYLATION IN RESPONSE TO DNA DSBS

As already mentioned in VI.A.2 and VI.A.3 Western blot analysis of H2A.V, which is incorporated into recombinant DNA, reveals a double band in chromatin assembled on DNA with a free end, pointing to C-terminal phosphorylation.

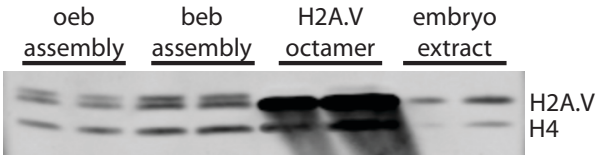

FIGURE 54: WESTERN BLOT ANALYSIS OF *IN VITRO* RECONSTITUTED CHROMATIN ON DNA IMMOBILIZED AT ONE END (OEB) OR BOTH ENDS (BEB). RECOMBINANT HISTONE OCTAMERS CONTAINING HOMOGENOUS H2A.V AND DREX SERVE AS CONTROLS. THE MEMBRANE WAS PROBED WITH ANTIBODIES AGAINST H2A.V AND H4.

To confirm that the slower-migrating band was indeed due to phosphorylation, immobilized chromatin was incubated with alkaline phosphatase. After SDS-PAGE and blotting, the membrane was probed with antibody specific for the C-terminal phosphorylation of H2A.V. As expected, γH2A.V was exclusively detected on chromatin, and not in DREX. Additionally, this mark disappeared completely after treatment with alkaline phosphatase.

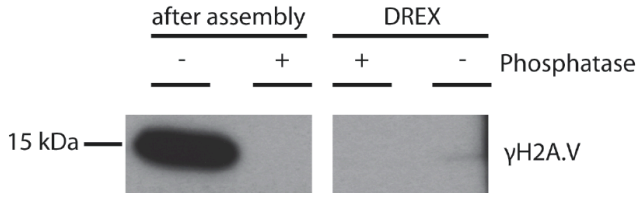

FIGURE 55: WESTERN BLOT ANALYSIS OF *IN VITRO* RECONSTITUTED CHROMATIN AND DREX WITH AND WITHOUT TREATMENT WITH ALKALINE PHOSPHATASE. THE MEMBRANE WAS PROBED WITH γH2A.V SPECIFIC ANTIBODY.

To evaluate the specificity of H2A.V phosphorylation, we performed assembly reactions linear or circular plasmid, or on linear DNA coupled to paramagnetic beads with one end. In the absence of DNA or in chromatin assembled on circular DNA, H2A.V phosphorylation was not detected (Figure 56, lane 1 and 3). However, in presence of linear DNA, either free or immobilized on beads, approximately 30-50% of incorporated H2A.V became phosphorylated (Figure 56, lane 4, 6 and 7). In lane 4 and 7, excess unphosphorylated H2A.V present in DREX was not separated from H2A.V incorporated into nucleosomes and contributes to a higher ratio of unphosphorylated H2A.V compared to lane 6, were chromatin was purified on the magnet and thus only separated from un-incorporated H2A.V (Figure 56, lane 5).

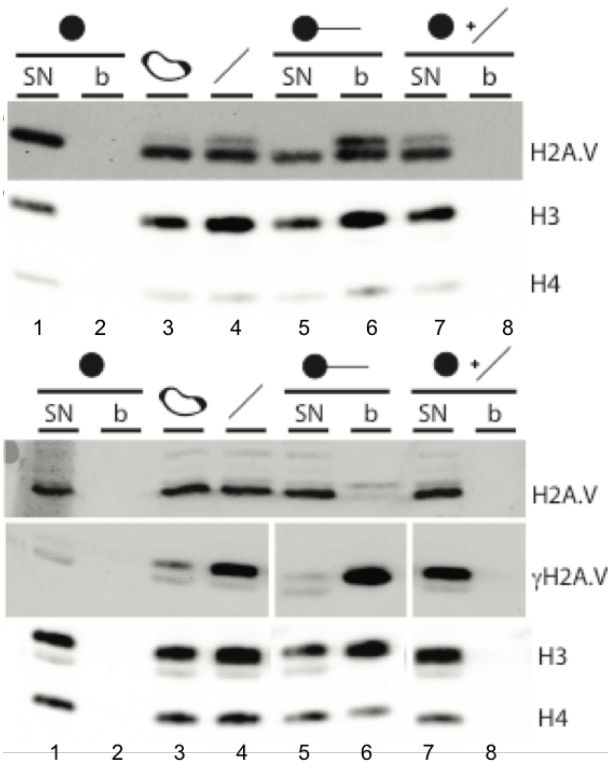

FIGURE 56: WESTERN BLOT ANALYSIS OF *IN VITRO* RECONSTITUTED CHROMATIN ON LINEAR OR CIRCULAR PLASMID, OR ON LINEAR DNA COUPLED TO PARA-MAGNETIC BEADS WITH ONE END. AS CONTROL, CHROMATIN ASSEMBLY WAS PERFORMED WITH BEADS ONLY. MEMBRANES WERE PROBED WITH ANTIBODIES AGAINST H2A.V, H3, H4, AND γH2A.V. LANE NUMBERS ARE INDICATED BELOW. SN: SUPERNATANT; B: BEADS; THE FOLLOWING SAMPLES WERE LOADED: LANES 1 AND 2: BEADS ONLY CONTROL REACTION, WITH SN IN LANE 1 AND B IN LANE 2; LANE 3 AND 4: CIRCULAR (LANE 3) OR LINEARIZED (LANE 4) PLASMID DNA; LANE 5 AND 6: CHROMATIN ASSEMBLY ON IMMOBILIZED DNA WITH SN IN LANE 5 AND B IN LANE 6; CHROMATIN ASSEMBLY ON SOLUBLE LINEARIZED DNA AND BEADS WITH SN IN LANE 7 AND B IN LANE 8; THE EXPERIMENT WAS PERFORMED IN TWO BIOLOGICAL REPLICATES USING EXTRACTS FROM INDEPENDENT PREPARATIONS (REPLICATE 1: TOP; REPLICATE 2: BOTTOM)

According to the previous observations, phosphorylation of H2A.V can only be initiated in the presence of DNA breaks. However, after initiation of H2A.V phosphorylation, it has been shown in yeast and mammals, that an activation cascade leads to amplification and spreading of the γH2A.V signal around the break site (J.-A. Kim et al. 2007; Savic et al. 2009; J. Li et al. 2012; C.-S. Lee et al. 2014). To investigate if H2A.V bearing a phospho-mimetic amino acid in place of SQAY can trigger further H2A.V phosphorylation in absence of free DNA ends, I pre-assembled nucleosomes consisting of H2A.V or a phospho-mimetic form of H2A.V in different ratios on circular DNA. The portion of spiked in H2A.VE were 0%, 1%, 5%, 10% and 100%. However, incorporation of phospho-mimetic nucleosomes did not lead to phosphorylation of H2A.V, leading to the conclusion that the phosphorylation mark by itself is not sufficient to initiate the spreading event.

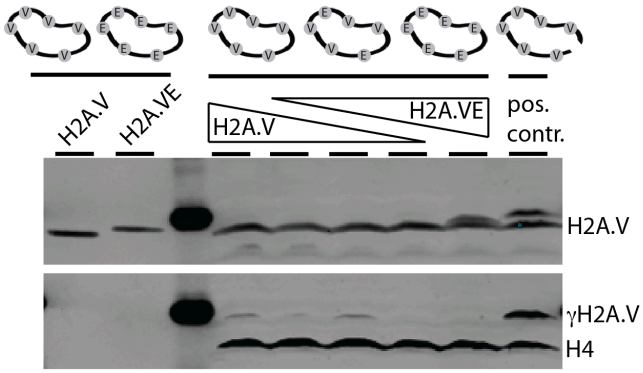

FIGURE 57: WESTERN BLOT ANALYSIS OF *IN VITRO* RECONSTITUTED CHROMATIN ON CIRCULAR DNA WITH PREASSEMBLED NUCLEOSOME ARRAYS CONSISTING OF H2A.V NUCLEOSOMES OR PHOSPHO-MIMETIC H2A.V NUCLEOSOMES IN DIFFERENT RATIOS. AS POSITIVE CONTROL, CHROMATIN ASSEMBLY WAS PERFORMED ON LINEARIZED DNA WITH PREASSEMBLED NUCLEOSOME ARRAYS CONSISTING OF H2A.V. MEMBRANES WERE PROBED WITH ANTIBODIES AGAINST H2A.V, γH2A.V AND H4.

As observed in Figure 51, the phosphorylation signal in response to free DNA ends spreads over several kilobases along the DNA in *cis* but was not transferred to DNA fragments lacking free ends in the same reaction. To confirm this observation, chromatin was assembled on DNA immobilized at one end with either circular or linear soluble DNA in the same reaction. After separating immobilized DNA from the DNA in the supernatant, the phosphorylation status of H2A.V on beads and in the supernatant (containing soluble chromatin and excess H2A.V) was analyzed (Figure 58, left). The appearance of H2A.V phosphorylation was strictly correlated to the presence of free DNA ends. Additionally, consistent with the result obtained in Figure 51, the phosphorylation signal was only detected in the supernatants containing linear, but not circular DNA. Altogether, these results led to the hypothesis illustrated in Figure 58 (right), suggesting that spreading of the H2A.V phosphorylation mark only spreads along DNA in *cis*, but not in *trans* onto intact DNA.

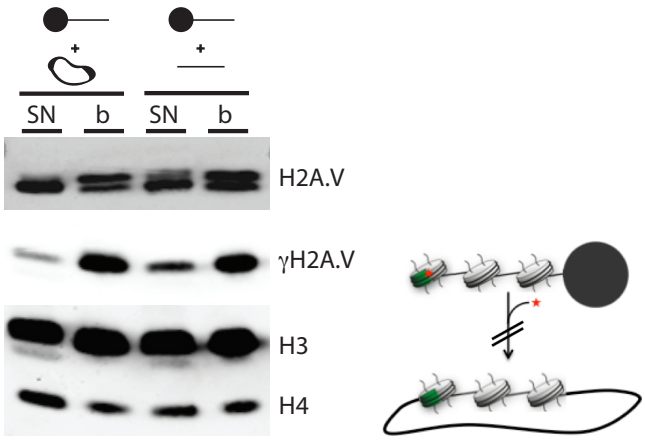

FIGURE 58: LEFT: WESTERN BLOT ANALYSIS OF *IN VITRO* RECONSTITUTED CHROMATIN ON FREE CIRCULAR OR LINEAR AND IMMOBILIZED DNA IN ONE REACTION. MEMBRANES WERE PROBED WITH ANTIBODIES AGAINST H2A.V, γH2A.V, H3 AND H4. RIGHT: H2A.V PHOSPHORYLATION (RED STAR) DOES NOT SPREAD IN *TRANS* FROM IMMOBILIZED DNA ONTO FREE CIRCULAR DNA.

To elucidate, if spreading *in trans* can be triggered by DNA cross-bridging proteins, I preincubated two different FlyFosmids with BAF (kind gift from the Gerlich laboratory in Vienna, Austria, see Samwer et al. 2017) or ParB (kind gift from the Gruber laboratory in Lausanne, Switzerland, see Gruber & Errington 2009) prior to chromatin assembly. BAF is a DNA- and protein-binding factor, which is implicated in processes like chromatin structure, gene regulation, and nuclear assembly (reviewed in Segura-Totten & Wilson 2004). ParB is a bacterial DNA-binding protein (Gruber & Errington 2009).

For each reaction one circular control FlyFosmid and one either circular or linearized target FlyFosmid, was pre-incubated with 0.1 µM or 1 µM ParB or BAF (or in absence of cross-binding protein as a control). To demonstrate DNA-coupling efficiencies of both proteins, immobilized DNA was incubated with soluble DNA fragments and incubated with ParB or BAF. As binding of ParB was reported to be diminished in high salt conditions, beads were washed with 200 mM NaCl buffer. Beads and supernatant, as well as the eluate after incubation with ParB were then analyzed on agarose gels (Figure 59). In presence of 1 µM ParB, soluble DNA was coupled to immobilized DNA and was eluted after washing with 200 mM NaCl. For BAF, DNA was already coupled to immobilized DNA by 0.1 µM BAF, but efficiency was increased by addition of 1 µM BAF. However, after addition of BAF, DNA bands unclear, pointing to a degradation of DNA upon addition of BAF.

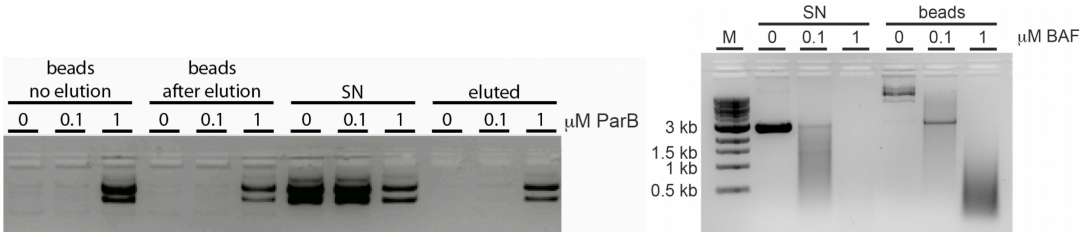

FIGURE 59: DNA CROSS-BRIDGING EFFICIENCIES TESTED WITH PARB (LEFT) AND BAF (RIGHT) WITH EITHER 0.1 μM OR 1 μM PROTEIN (OR IN ABSENCE OF PROTEIN AS A CONTROL). DNA IMMOBILIZED TO BEADS WAS INCUBATED WITH SOLUBLE DNA. SUPERNATANT AFTER INCUBATION WITH PROTEIN (SN) AND BEADS WERE LOADED AFTER PROTEIN DIGESTION. IN CASE OF PARB, AN ELUTION WITH 200 MM NACL BUFFER WAS PERFORMED. FOR PARB, BINDING WAS PERFORMED WITH CIRCULAR PLASMID DNA, LEADING TO A SUPERCOILED AND RELAXED CONFORMATION OF THE PLASMID (LEFT). FOR BAF, LINEARIZED SOLUBLE DNA WAS USED (RIGHT). HOWEVER, COUPLING EFFICIENCIES WERE REPEATED WITH CIRCULAR AND LINEARIZED DNA IN BOTH CASES WITH SIMILAR COUPLING EFFICIENCIES.

To investigate the spreading of H2A.V phosphorylation, assemblies were analyzed by SDS-PAGE and Western blot analysis (Figure 60). Assemblies performed on circular FlyFosmids did not lead to the induction of H2A.V phosphorylation, independent from the addition of BAF. However, in the assemblies performed on circular and linear FlyFosmid, addition of cross-bridging protein led to a concentration-dependent increase of the phosphorylation signal, indicating that the cross-bridging activity of ParB and BAF led to the spreading of the H2A.V phosphorylation signal from the linear to the circular DNA fragment.

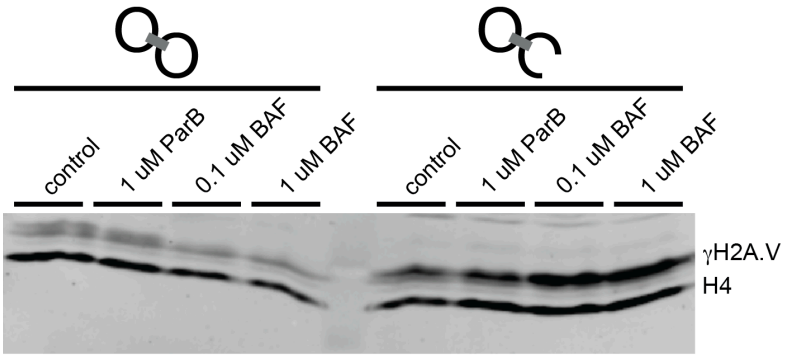

FIGURE 60: CHROMATIN ASSEMBLY AFTER INCUBATION WITH DNA CROSS-BRIDGING BAF OR PARB. EACH ASSEMBLY REACTION WAS PERFORMED ON ONE CIRCULAR CONTROL FLYFOSMID AND ONE EITHER CIRCULAR OR LINEARIZED TARGET FLYFOSMID, WHICH WERE INCUBATED WITH 1 μM PARB, 0.1 μM BAF, OR 1 μM BAF PRIOR TO ASSEMBLY. AS A CONTROL, BOTH SCENARIOS WERE PERFORMED IN ABSENCE OF CROSS-BINDING PROTEIN. THE MEMBRANE WAS. PROBED WITH ANTIBODIES AGAINST γH2A.V AND H4.

To confirm this hypothesis, ChIP-Seq analysis was performed with antibodies against H2A.V and γH2A.V. Because of the slightly stronger increase in phosphorylation upon addition of BAF compared to ParB, the following ChIP-Seq experiment was performed with BAF using the same concentrations as before (Figure 61). Profiles obtained after H2A.V ChIP showed evenly distributed incorporation of H2A.v along both FlyFosmids. In addition to this, chromatin assembled on circular FlyFosmids did not show phosphorylation of H2A.V, neither in presence nor in absence of BAF. In the damage reaction including the linearized FlyFosmid, γH2A.V signals increased and upon addition of BAF, H2A.V phosphorylation was detected on the

control FlyFosmid. This observation indicates, that spreading of the H2A.V phosphorylation mark can spread in *trans* to circular DNA in presence of cross-binding proteins.

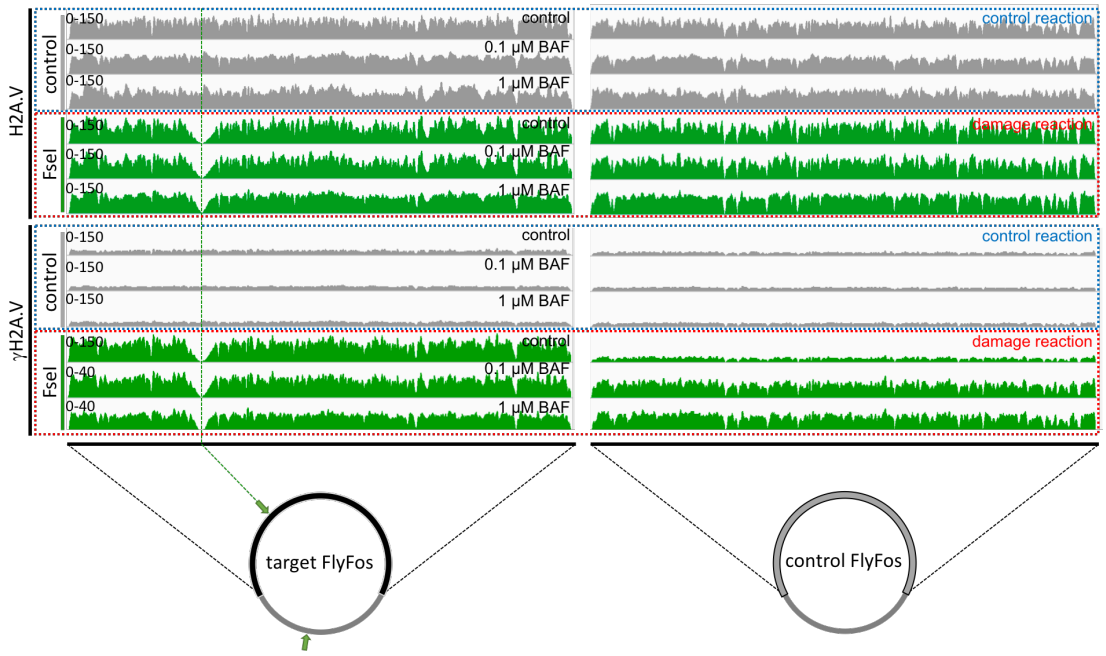

FIGURE 61: CHIP-SEQ ON CHROMATIN ASSEMBLED ON A MIX OF CIRCULAR CONTROL FLYFOSMIDS AND ON TARGET FLYFOSMIDS, WHICH ARE EITHER CIRCULAR (CONTROL) OR LINEARIZED BY RESTRICTION WITH FSEI AND PRE-INCUBATED WITH 0.1 µM OR 1 µM BAF (OR NO BAF AS A CONTROL). CHIP WAS DONE WITH ANTIBODIES AGAINST H2A.V AND γH2A.V. THE GREEN ARROWS INDICATE THE FSEI CLEAVAGE SITES IN THE TARGET FLYFOSMID. SIGNALS WERE NORMALIZED TO THE NUMBERS OF READS. FOR H2A.V, ALL PROFILES ARE SHOWN IN THE SAME DATA RANGE. FOR γH2A.V ADJUSTED DATA SCALES WERE USED FOR BACKGROUND SIGNAL (CONTROL REACTION) AND FOR PHOSPHORYLATION SIGNAL AFTER RESTRICTION (FSEI) AS INDICATED. ALL γH2A.V PROFILES BEFORE DATA RANGE ADJUSTMENTS ARE SHOWN IN XI.C.

However, these experiments are preliminary and need to be confirmed in further replicates. In addition to this, BAF purification should be optimized to avoid uncontrolled DNA damage by nucleases. To allow proper normalization, ChIP experiments in presence of standard DNA should be performed.

Due to the lower increase of phosphorylation observed in presence of ParB compared to the increase observed in BAF, spreading of H2A.V phosphorylation in *trans* in presence of ParB has not yet been investigated. However, as DNA degradation was not observed in presence of ParB, spreading of H2A.V phosphorylation in *trans* in presence of ParB should be repeated to complement this study.

I observed the presence of γH2A.V phosphorylation at the earliest assembly time (10 min, see Figure 51), suggesting that the recognition of the free end is very fast. A precise kinetics of this reaction cannot be performed since the chromatin assembly reaction is slow by comparison. To capture early events in DNA damage recognition, we preassembled nucleosome arrays consisting of H2A.V nucleosomes. This allowed us to monitor the kinetics of γH2A.V appearance during the first few minutes of incubation in DREX. Western blot analysis against C-terminal

phosphorylation revealed, that H2A.V phosphorylation can be detected with this antibody about 6 min after addition of extract (Figure 62).

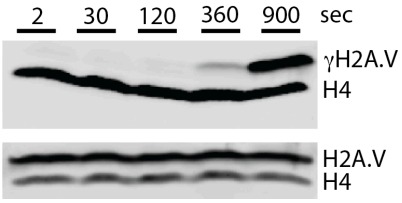

FIGURE 62: H2A.V PHOSPHORYLATION ON PREASSEMBLED H2A.V ARRAYS AFTER 2 SEC, 30 SEC, 120 SEC, 360 SEC, AND 900 SEC AFTER ADDITION OF DREX. MEMBRANES WERE PROBED WITH ANTIBODIES AGAINST γH2A.V, H4, AND H2A.V.

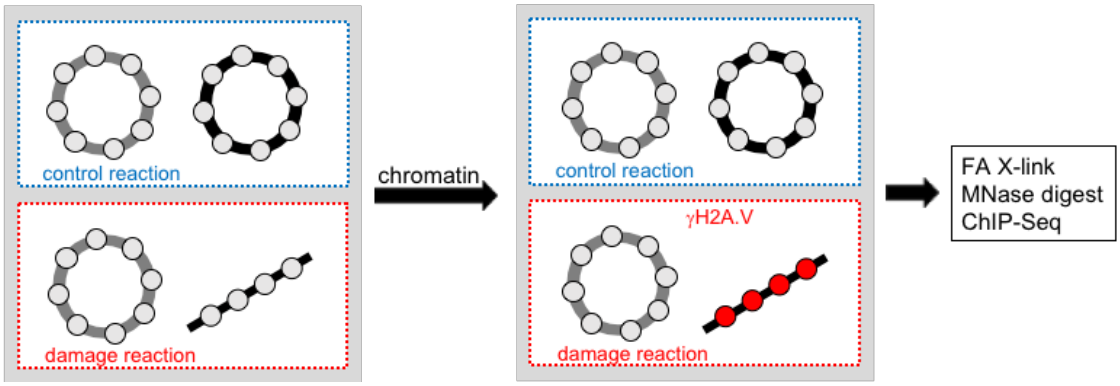

FIGURE 63: EXPERIMENTAL SETUP TO CAPTURE THE EARLY ONSET OF H2A.V PHOSPHORYLATION. PREASSEMBLED NUCLEOSOME ARRAYS CONSISTING OF H2A.V NUCLEOSOMES WERE INCUBATED WITH DREX AND PHOSPHORYLATION WAS STOPPED BY FORMALDEHYDE CROSSLINKING. IN EACH REACTION, ONE OF THE FLYFOSMIDS REMAINED CIRCULAR (CONTROL FLYFOSMID), WHILE THE OTHER FLYFOSMID WAS EITHER CIRCULAR (CONTROL REACTION, BLUE) OR LINEARIZED (DAMAGE REACTION, RED).

To capture the very rapid phosphorylation of H2A.V, conditions to efficiently stop the spreading process at early time points were optimized. Inhibition of phosphorylation by wortmannin, apyrase, and AMP-PNP did not immediately stop the phosphorylation, as tested by Western blot, therefore, a fast and efficient cross-linking step with formaldehyde was performed. This procedure enabled the analysis of phosphorylation at early time points after addition of extract. In addition to this, reactions with different restriction enzymes were performed to obtain spreading profiles of the H2A.V phosphorylation, which were initiated at different sites. In contrast to Figure 62, time points were adjusted to 30 sec, 120 sec, and 600 sec, to disseminate the early H2A.V phosphorylation events. The experimental setup is illustrated in Figure 63: In each reaction, one of the FlyFosmids remained circular (control FlyFosmid), while the other FlyFosmid was either linearized using RsrII (two target sites in the genomic insert of FlyFosmid 019611), FseI (one target site in the genomic insert and one target site in the backbone, which was not mapped), or SgrDI (two target sites in the genomic insert of FlyFosmid 019829). In parallel to the described damage reactions (red), a control reaction was performed, with both FlyFosmids intact (blue). Induction of H2A.V phosphorylation was tested by Western blot analysis and showed an increase of H2A.V phosphorylation over time, but no signal in the negative control using circular FlyFosmids (Figure 64).

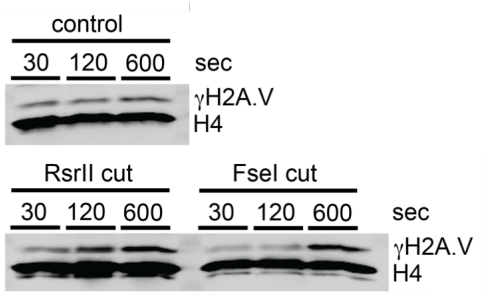

FIGURE 64: H2A.V PHOSPHORYLATION ON PRE-ASSEMBLED H2A.V ARRAYS ON A CIRCULAR CONTROL FLYFOSMID AND A LINEARIZED TARGET FLYFOSMID AFTER 30 SEC, 120 SEC, AND 600 SEC AFTER ADDITION OF DREX. IN THE CONTROL REACTION, BOTH FLYFOSMIDS WERE CIRCULAR. DIFFERENT RESTRICTION ENZYMES WERE USED TO DISSEMINATE PHOSPHORYLATION INITIATED AT DSBS IN DIFFERENT LOCATIONS (ALSO SEE FIGURE 65). MEMBRANES WERE PROBED WITH ANTIBODIES AGAINST γH2A.V AND H4.

Profiles of these samples obtained by ChIP-Seq against γH2A.V are shown in Figure 65. As before, H2A.V ChIP was performed in parallel to confirm the equal assembly of H2A.V nucleosomes (not shown). As expected, no phosphorylation was observed in the control reaction with two circular FlyFosmids and in the damage reactions on the circular control FlyFosmids. On the linearized FlyFosmids, H2A.V phosphorylation signals increased after 120 sec, with different profiles according to the location of the break: RsrII treated FlyFosmids showed an increase in proximity to the RsrII target sites, and FseI treated FlyFosmids showed an increase in proximity to the FseI target site, respectively. Considering the spreading models of the H2A.V phosphorylation signal along DNA (described in III.D.4), this observation speaks in favor of a phosphorylation spreading event, which is initiated at the break site and propagates along DNA (see Figure 11, model A).

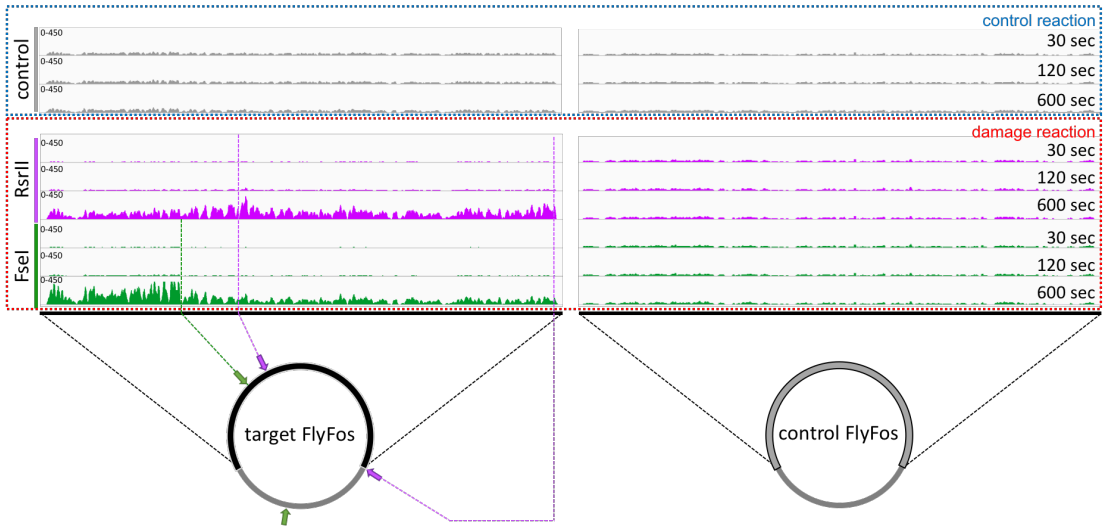

FIGURE 65: CHIP-SEQ OF H2A.V PHOSPHORYLATION AFTER 30 SEC, 120 SEC, AND 600 SEC AFTER ADDITION OF DREX TO PREASSEMBLED H2A.V ARRAYS ON A CIRCULAR CONTROL FLYFOSMID AND A LINEARIZED TARGET FLYFOSMID. IN THE CONTROL REACTION, BOTH FLYFOSMIDS WERE CIRCULAR. DIFFERENT RESTRICTION ENZYMES WERE USED TO DISSEMINATE THE PHOSPHORYLATION INITIATED AT DSBS IN DIFFERENT LOCATIONS INDICATED WITH ARROWS. READS WERE NORMALIZED TO THE CONTROL FLYFOS.

Unfortunately, we were not able to address the kinetics of H2A.V phosphorylation, as phosphorylation increased rapidly from 120 sec to 600 sec. In addition, a previous experiment performed in comparable conditions, displayed a high extent of phosphorylation after 120 sec,

leading to the assumption that the increase of phosphorylation after initiation proceeds very fast. Therefore, to draw conclusions about the kinetics of H2A.V phosphorylation, additional replicates with more resolved time points are required.

In *Drosophila*, two kinases have been identified, which phosphorylate H2A.V in response to DNA damage, Tefu and Mei-41, which are the orthologues of ATM and ATR, respectively (Madigan et al. 2002). An orthologue of DNA-PK has not yet been identified in *Drosophila* so far (Sekelsky et al. 2000; Sekelsky 2017).

To investigate whether the recruitment of DNA damage factors like the Ku complex depend on the γH2A.V signal, I added kinase-specific inhibitors to the extract prior to assembly which prevent H2A.V phosphorylation. The following inhibitors were used in a final concentration of 10 µM (kind gifts from Gyula Timinszky, Ludwig-Maximilians-Universität München, Germany):

- ATMi (KU55933)
- ATRi (VE-821)
- DNA-PKi (NU7441)

These inhibitors were added, alone or in combination, prior to addition of DNA to the chromatin assembly reaction. The phosphorylation was monitored after 15 min or 60 min of the assembly reaction. As a control, chromatin assembly was performed in presence of an equivalent volume of DMSO, which was used to dissolve the inhibitors (Figure 66).

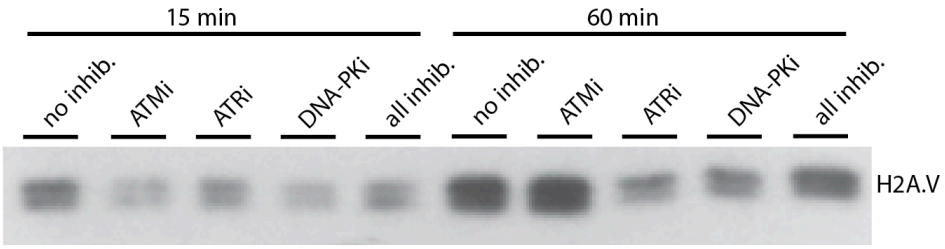

FIGURE 66: CHROMATIN ASSEMBLY IN PRESENCE OF KINASE INHIBITORS FOR 15 MIN OR 60 MIN. AS CONTROL, CHROMATIN WAS ASSEMBLED IN PRESENCE OF DMSO.

However, none of the inhibitors were able to prevent the phosphorylation of H2A.V, as concluded from the appearance of the double band in all samples. This observation could either be explained by either inactive or unfunctional inhibitors, which might not be functional for the *Drosophila* orthologues or by another kinase, which could exist in *Drosophila* and might bear redundant functions in DNA damage signaling. However, it is likely, that these inhibitors, which are specific against the human orthologues, fail to inhibit the not well conserved *Drosophila* kinases, as it has already been shown for KU55933 (Mitchell & Friesen 2012). Unfortunately, inhibitors against *Drosophila* kinases are not yet available.

Therefore, H2A.V phosphorylation was inhibited by wortmannin, a broad-range PI3K inhibitor (Paull et al. 2000). In presence of wortmannin, no phosphorylation of H2A.V was detected (Figure 67). Analysis of factors associated to chromatin revealed that Ku recruitment does not depend on H2A.V phosphorylation. To confirm this observation nucleosome arrays were

assembled from histone octamers containing a C-terminally truncated version of H2A.V, which cannot be phosphorylated in response to DNA damage (H2A.VΔC), and with nucleosomes containing H2A. In both cases, Ku70 was recruited to the same extent in response to free DNA ends in the absence of H2A.V phosphorylation (Figure 68). Likewise, the association of Acf1 and Iswi, components of the ACF complex, and for Dom, a component of the Dom/Tip60 complex did not depend on the H2A.V C-terminus.

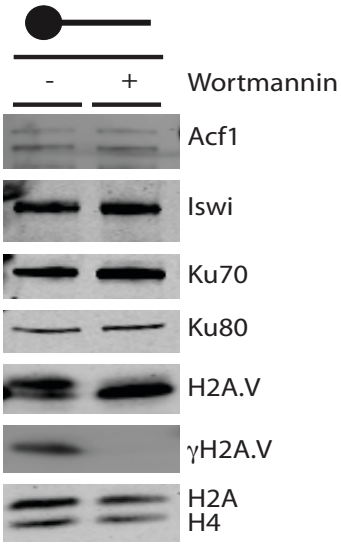

FIGURE 67: CHROMATIN ASSEMBLY IN ABSENCE (-) OR PRESENCE (+) OF WORTMANNIN, A BROAD-RANGE PI3K INHIBITOR. THE NEGATIVE CONTROL WAS SUPPLIED WITH DMSO, WHICH WAS USED TO DISSOLVE WORTMANNIN. MEMBRANES WERE PROBED WITH ANTIBODIES AGAINST ACF1, ISWI, KU70, KU80, H2A.V, γH2A.V, H2A, AND H4.

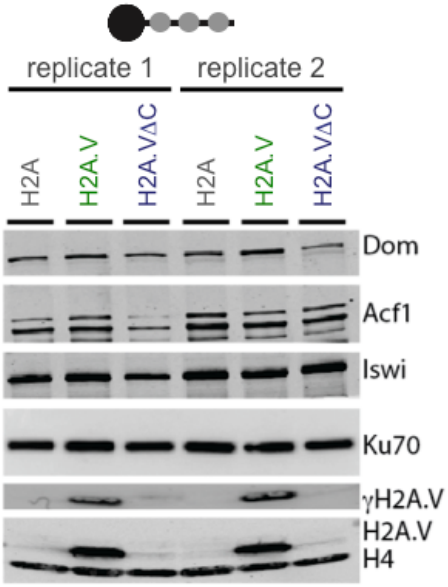

FIGURE 68: RECRUITMENT OF PROTEINS FROM DREX TO NUCLEOSOME ARRAYS UNIFORMLY CONSISTING EITHER OF H2A OR H2A.V OR H2A.VΔC NUCLEOSOMES. MEMBRANES WERE PROBED WITH ANTIBODIES AGAINST DOMB, ACF1, ISWI, KU70, γH2A.V, H2A.V, AND H4.

4. DNA DSBs CAN BE SPECIFICALLY INTRODUCED INTO GENOMIC DNA OF S2 CELLS

All of the experiments performed so far describe the damage-associated processes *in vitro*, where DSBs are represented by free DNA ends. However, the damage reaction is performed in a cell-free system and outside of the nucleus. In addition of this, cellular proteins, which are not present in the nucleus under physiological conditions, could interfere with processes leading to false conclusions. Therefore, we aimed to recapitulate processes in response to DNA DSBs *in vivo*.

The Laboratory of Gaelle Legube in Toulouse developed a system to introduce DNA DSBs in a time-resolved manner and at specific sites in the genome. For this purpose, the endonuclease AsiSI was expressed under a copper sulfate ($CuSO_4$)-inducible promoter and fused to an estrogen receptor hormone binding domain. After induction of expression by $CuSO_4$, addition of 4-hydroxytamoxifen (4-OHT) initiated the translocation of otherwise cytoplasmic endonuclease into the nucleus to generate DNA DSBs at its target sites. A further feature of the system is that the nuclease has been furnished with an Auxin-inducible-degron (AID). This allows to induce rapid degradation of the endonuclease to stop generation of DNA DSBs by Auxin addition (described in Massip et al. 2010).

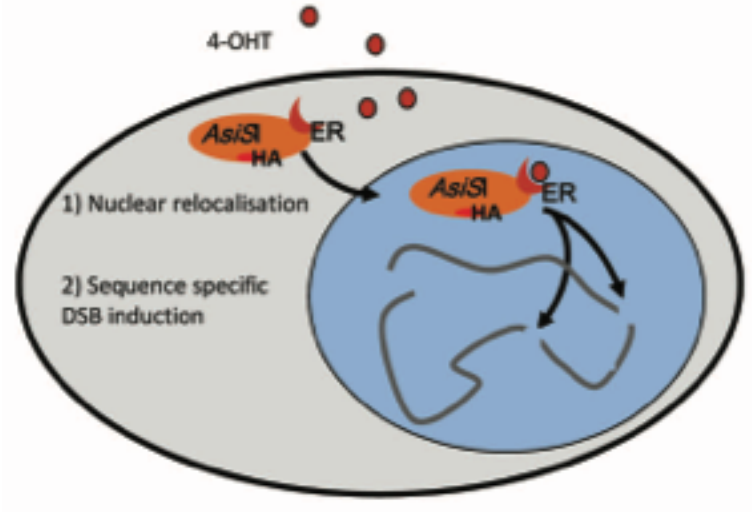

FIGURE 69: DSBS INDUCED BY TRANSLOCATION OF ASISI INTO THE NUCLEUS (FIGURE ADAPTED FROM MASSIP ET AL. 2010). ADDITION OF 4-HYDROXYTAMOXIFEN (4-OHT), WHICH BINDS TO THE ESTROGEN (ER) RECEPTOR HORMONE BINDING DOMAIN FUSED TO ASISI, LEADS TO ITS TRANSLOCATION INTO THE NUCLEUS, WHERE IT SPECIFICALLY CLEAVES AT THE TARGET SITES.

The target site of AsiSI GCGATCGC is CpG methylation-sensitive, so that many of the sites in mammalian cells are not cleaved due to methylation. However, *Drosophila* SL2 cells lack this DNA modification. The AsiSI target motif GCGATCGC occurs 1632 times in the *Drosophila* genome, and potentially, all of these sites can be targeted by AsiSI, leading to a dramatic induction of DNA damage.

To trigger conditions, in which DSBs are efficiently induced but do not lead to apoptosis, we aimed to tune the cleavage by regulating the expression and translocation of AsiSI in different conditions:

- SL2 AsiSI cells untreated were not supplied with $CuSO_4$ and 4-OHT
- SL2 AsiSI cells + 4-OHT were only supplied with 300 nM 4-OHT and incubated for 1 h to induce translocation of leaky expressed AsiSI into the nucleus
- SL2 AsiSI cells +4-OHT +$CuSO_4$ were supplied with 5 mM $CuSO_4$ and incubated over night to induce expression of AsiSI and then supplied with 300 nM 4-OHT and incubated for 1 h to induce translocation of AsiSI into the nucleus

As a control, cells were treated in parallel with ethanol, which was used to solve 4-OHT. As expected, cell viability decreased upon introduction of DSBs, from 92% for control cells to 88% for cells only treated with 4-OHT and particularly in the case of induced expression of AsiSI and 4-OHT treatment, with a viability of 62%. Introduction of DNA DSBs were visualized by immunostaining using γH2A.V as a marker for damaged chromatin.

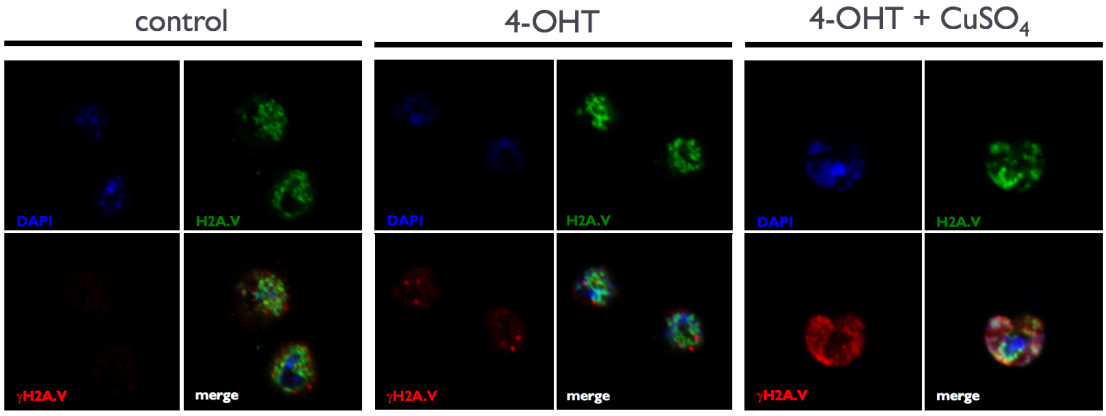

FIGURE 70: IMMUNOFLUORESCENCE OF CELLS TREATED WITH ETHANOL (CONTROL), 4-OHT, OR 4-OHT AND $CuSO_4$ USING ANTIBODIES AGAINST H2A.V (GREEN) AND γH2A.V (RED). NUCLEI WERE STAINED WITH HOECHST.

As expected, the cells showed an induction-dependent damage response, with background signal in untreated cells. A small number of damage foci were induced in the presence of 4-OHT suggesting that the promoter was not tightly repressed in the absence of $CuSO_4$. This indicates that leaky expression of AsiSI already leads to sufficient levels to trigger DNA damage dependent γH2A.V foci. In contrast to this, induction of expression with $CuSO_4$ prior to induction of translocation into the nucleus led to a fulminant DNA damage response and enormous levels of H2A.V phosphorylation. These observations correlated with cell viability.

In parallel to the generation and characterization of the stable AsiSI cell line, I aimed to elucidate the role of Acf1, Ku70, or Ku80 in DNA damage signaling. For this purpose, I generated dsRNA and tested the knock down efficiencies by RNA interference (RNAi) in wt S2 cells. Successful RNAi construct would then be used in combination with AsiSI-transfected cells after induction of DSBs. As a control, cells were either treated in parallel but without addition of dsRNA or with GST RNAi. The viability of these cell populations before induction of DSBs decreased from 95% in control cells in absence of RNAi to 83% in Acf1 RNAi cells, 74% in GST RNAi cells, 77% in Ku70 RNAi cells, and 78% in Ku80 RNAi cells.

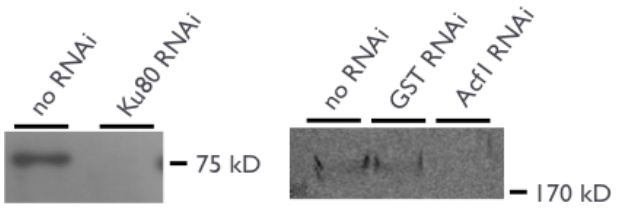

FIGURE 71: KNOCK DOWN OF KU80 AND ACF1 IN *DROSOPHILA* SCHNEIDER CELLS USING KU80 RNAI AND ACF1 RNAI. GST RNAI SERVED AS A NEGATIVE CONTROL.

The generation of DSBs in the stably transfected AsiSI cell line was performed once. To confirm the observations shown in Figure 70 and to fine-tune the induction settings, I performed replicates using different titrations of induction with 4-OHT and $CuSO_4$. Unexpectedly, the detection of γH2A.V foci was no longer possible with this cell line, regardless of the fact that the cell line was stably transfected. We suspect, that the generated cell line was not sustainable due to the leaky expression of AsiSI and the continual generation of breaks, which might have led to the silencing of the AsiSI locus to protect the genome. Due to this technical issue, we were not able to continue this *in vivo* approach.

5. INVESTIGATION OF RESECTION AT DNA ENDS

As previously mentioned, the ChIP signal of histones decreases close to the break site, suggesting the removal of nucleosomes as has been proposed for yeast and mammals (Goldstein et al. 2013; Tsukuda, Fleming, Nickoloff & Osley 2005; Shroff et al. 2004; Morrison & Shen 2009). However, the fact that the DNA at this position is also reduced in the ChIP input rather suggests that the DNA is being lost during the incubation an DREX for extended times.

It is not clear if this DNA is degraded, either by random nucleases degrading the accessible DNA or by DNA damage-associated nucleases, which generate regions of ssDNA during the process of 'resection' associated with homologous recombination.

The resection process is initiated by the CtIP-MRN complex (Sartori et al. 2007) and extended by exo1 and dna2 nucleases leading to 3' overhangs (Symington & Gautier 2011). These overhangs are then immediately bound by single-strand-binding proteins like RPA and later on by rad51 (Wyatt & West 2014). Next-generation sequencing of input DNA after fragmentation with Covaris focused acoustics (to avoid DNA degradation by MNase), loss of DNA was detected in regions of 0.4 kb - 1 kb flanking each DNA end. However, due to the nature of Illumina sequencing sample preparation, dsDNA is favored over ssDNA, which might lead to a loss of signal from ssDNA fragments. This hypothesis is in line with the fact that DNA at these sites was detectable at later time points with qPCR, which allows amplification of ssDNA.

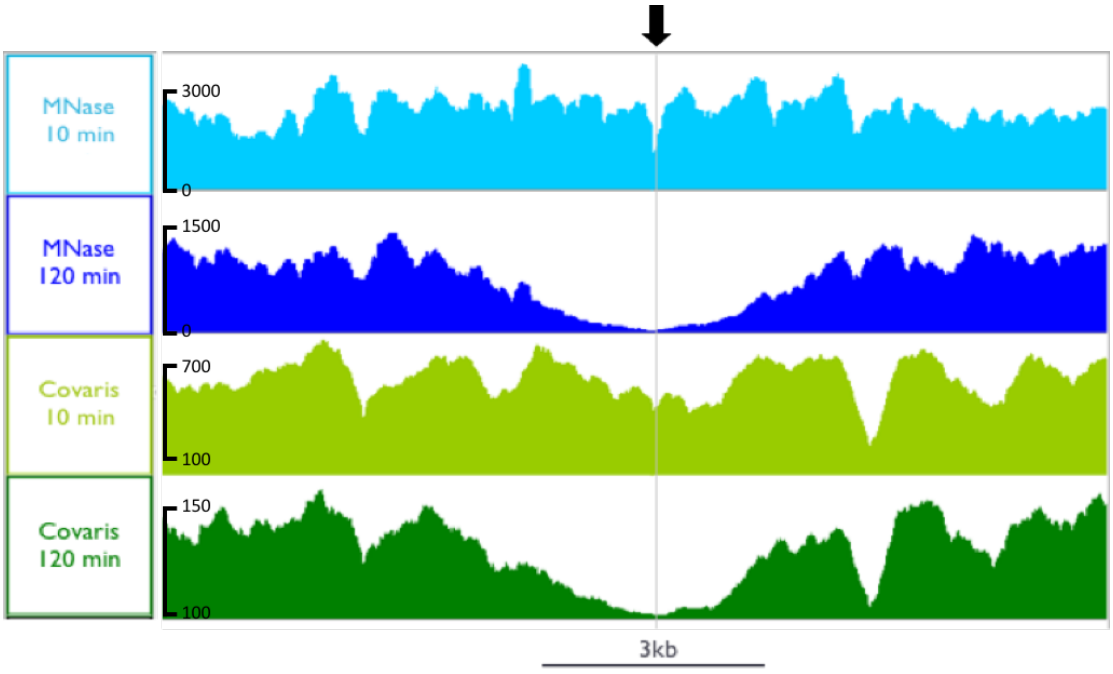

FIGURE 72: RESECTION OF CHROMATIN FLANKING FREE DNA ENDS ANALYZED BY SEQUENCING OF MNASE- OR COVARIS-SHEARED CHROMATIN AFTER 10 MIN OR 120 MIN ASSEMBLY. COVARIS SHEARING WAS PERFORMED FOR 25 MIN AT 100 WATTS IN 12X12 FIBRE TUBES USING THE COVARIS S220 SYSTEM.

To explore this question further, I performed various experiments to identify ssDNA using either single-strand-specific nucleases or recombinant single-strand-binding proteins. Unfortunately, all attempts failed but, as further discussed in VII.A. Due to the lack of appropriate controls, the existence of ssDNA could not be excluded. I therefore applied an approach published by Langerak et al (Langerak et al. 2011), where ssDNA and dsDNA is treated with the double-strand-specific restriction enzyme ApoI, leaving ssDNA intact. Subsequent amplification of regions including the ApoI target site only leads to amplification if the site is not cleaved in case of ssDNA. dsDNA, however, cannot be amplified as the amplicon is cleaved by ApoI (Figure 73).

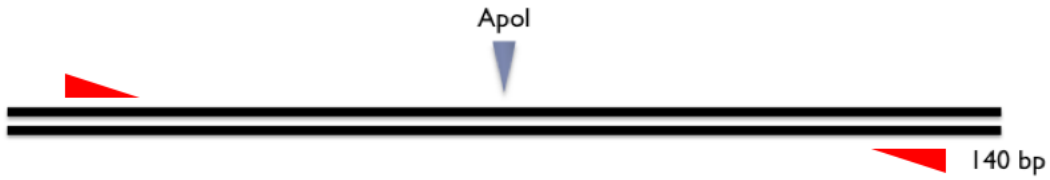

FIGURE 73: QPCR AMPLICON OF 140 BP INCLUDING THE APOI TARGET SITE. AFTER CLEAVAGE WITH APOI, AMPLIFICATION WITH PRIMERS (RED ARROWS) IS NOT POSSIBLE. SSDNA IS NOT CLEAVED BY APOI AND CAN BE AMPLIFIED BY QPCR.

To confirm the specificity and efficiency of ApoI digest, DNA fragments of about 200 bp including the ApoI target site were generated as either dsDNA or ssDNA and incubated with ApoI under the same conditions that were lateron used for the experiment. As shown in Figure 74, ssDNA was not affected upon ApoI treatment, however, dsDNA was cleaved.

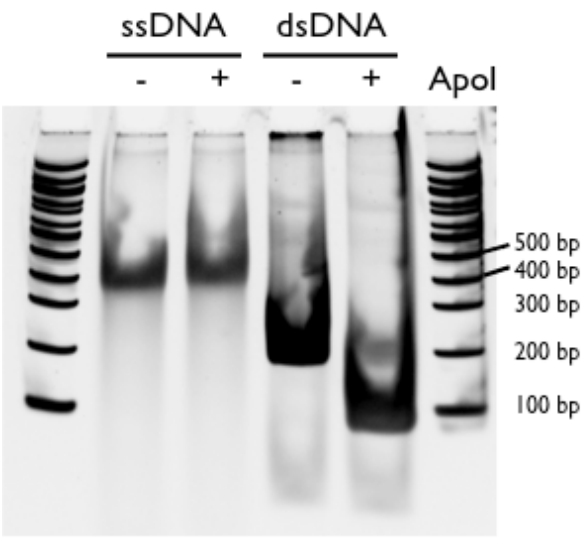

FIGURE 74: ACRYLAMIDE GEL OF SSDNA AND DSDNA BEFORE (-) AND AFTER (+) APOI TREATMENT TO CONFIRM THE SPECIFICITY OF APOI FOR DSDNA.

Linearized plasmid DNA including ApoI target sites proximal to the DNA ends before or after incubation with DREX to potentially generate ssDNA was treated with ApoI or buffer only as a negative control. Amplification of purified DNA after assembly with primers flanking the break site or a more distal site including the ApoI site (No 1 control) was performed. As a negative control, another control site lacking the ApoI target site was analyzed in parallel (No 2 control). Signal intensities were normalized to the No 2 control site and plotted in Figure 75. To our surprise, ApoI treatment prevented amplification of all templates, with or without treatment with DREX, suggesting that no ssDNA was introduced in proximity to the break, and that all target regions remained double-stranded.

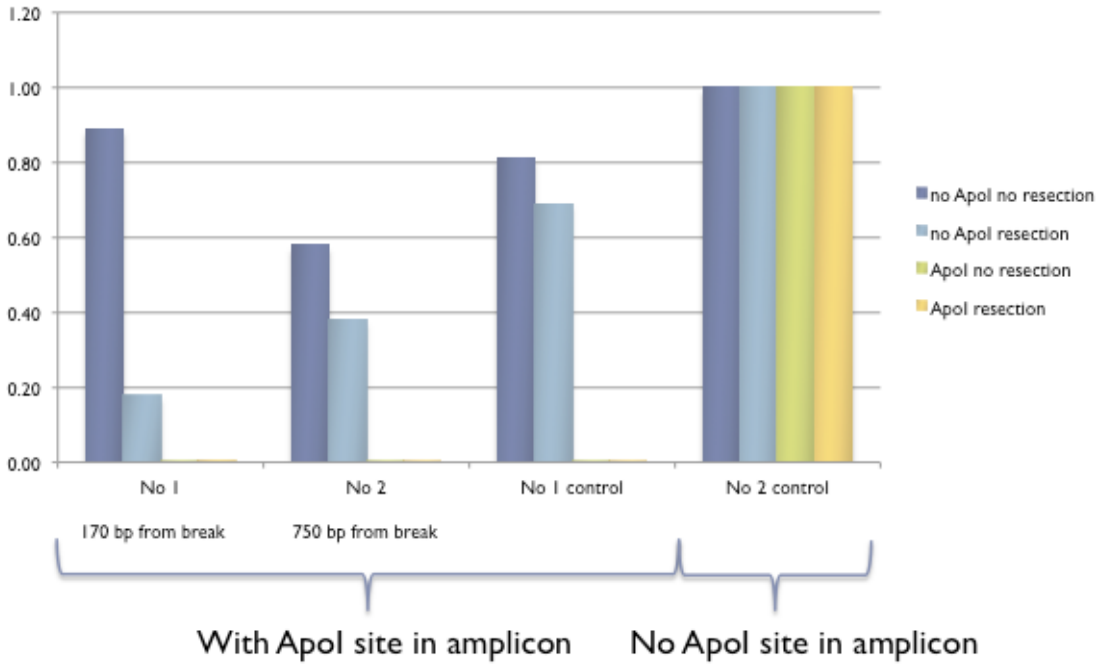

FIGURE 75: QPCR ANALYSIS OF REGIONS 170 BP AND 750 BP FROM THE BREAK SITE BEFORE (NO RESECTION) AND AFTER (RESECTION) INCUBATION OF LINEARIZED DNA WITH DREX BEFORE OR AFTER TREATMENT WITH APOI.

Due to the previous control experiment to control specific and efficient restriction at ApoI sites only at dsDNA, we conclude that the ApoI target site remained double-stranded without generation of ssDNA. It is possible, that DNA resection is performed on both strands, or that resected DNA ends consisting of ssDNA are processed by (unspecific) nucleases. However, discrepancies with the data obtained before suggesting the existence of ssDNA in proximity to the break are further investigated in VII.A.

6. Recruitment of the remodeling factor Acf1 to DNA breaks

As discussed in the previous chapter, during DNA repair nucleosomes are removed from the break site to generate space for DNA repair. This process is mediated by chromatin remodeling factors, which have the ability to shift nucleosomes, remove nucleosomes from chromatin or replace histones for specific histone variants in an ATP-dependent manner. Indeed, all four chromatin remodeling families, namely the Swi/Snf, Chd, Ino80, and Iswi families, have already been implicated in the DNA damage response (reviewed in Price & D'Andrea 2013).

Acf1, a *Drosophila* remodeling component of the ACF complex, which belongs to the ISWI family, has been found to be implicated in the DNA damage response as well. Interestingly, as mentioned in the introduction, Acf1 has been shown to interact with DNA damage proteins, to mention the Ku complex as one example. The interaction of Acf1 with Ku80, a component of the Ku complex, has been shown in our lab by a former PhD student Dhawal Jain in immunoprecipitation experiments using nuclear extract prepared from *Drosophila* embryos. In addition to that, I also observed Acf1 co-immunoprecipitated using monoclonal antibodies against Ku70 and Ku80 (Figure 76), which is in line with data obtained in mammalian cells, where Acf1 was shown to directly interact with Ku70 (Lan et al. 2010).

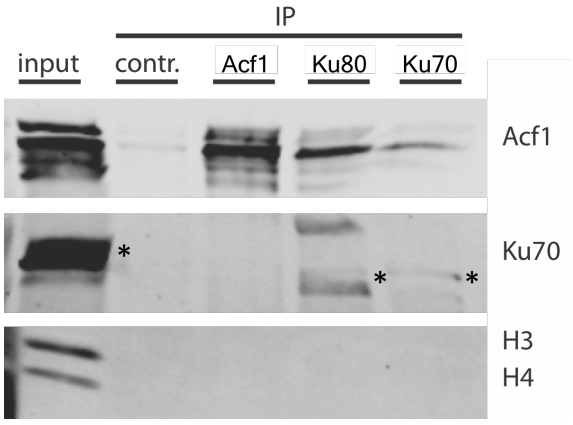

Figure 76: Co-Immunoprecipitation of Acf1, Ku80, and Ku70. As negative control, extract was incubated with beads only (contr.) and extract before immunoprecipitation was used as input. Membranes were probed with antibodies against Acf1, Ku70, Ku80, H3, and H4. Asterisks indicate the band for Ku70, which was consistently detected at higher molecular weight in all extract samples compared to IP or chromatin samples.

We therefore wondered if Acf1 might be enriched at break sites, as it could potentially be recruited by Ku to remove nucleosomes at the break site. Unfortunately, Dhawal Jain, a former PhD student in our lab, revealed that attempts to localize binding sites of chromatin remodelers by chromatin immunoprecipitation are prone to yield false positive signals, henceforth called "phantom peaks" (Jain, Baldi, Zabel, Straub & Becker 2015). These artefactual ChIP peaks arise,

when the crosslinking of protein to a target site is not efficient. It is possible, however, that Acf1 binds tighter to DNA break site, which I have tested in the following experiments.

The specificity of the Acf1 antibodies for immunoprecipitation has been established before (Jain, Baldi, Zabel, Straub & Becker 2015). I performed ChIP with monoclonal or polyclonal antibodies directed against the C-terminus of Acf1 on either control DREX or on an extract from which Acf1 had been depleted by multiple rounds of antibody-bead adsorption. Chromatin assembly was performed on a linearized FlyFosmid (here FlyFos019611) for 15 min, as Acf1 recruitment was shown to be higher at earlier time points (compare Figure 41). Formaldehyde cross-linking was performed for 10 min at 0.1% and chromatin was fragmented to mono-nucleosomes by MNase digestion. After ChIP, immunoprecipitated DNA was purified and analyzed by qPCR using primers defining amplicons at defined distances from the break site of a linearized FlyFosmid (Figure 77). As expected, ChIP yielded 7-15 times less DNA upon Acf1 depletion, depending on the antibody used for ChIP, suggesting that ACF1-chromatin interactions can indeed be monitored in this *in vitro* experiment. However, ChIP-qPCR signals were comparable for the different loci, suggesting that Acf1 binding is not promoted by a close distance to the break, at least not within 3 kb around the break.

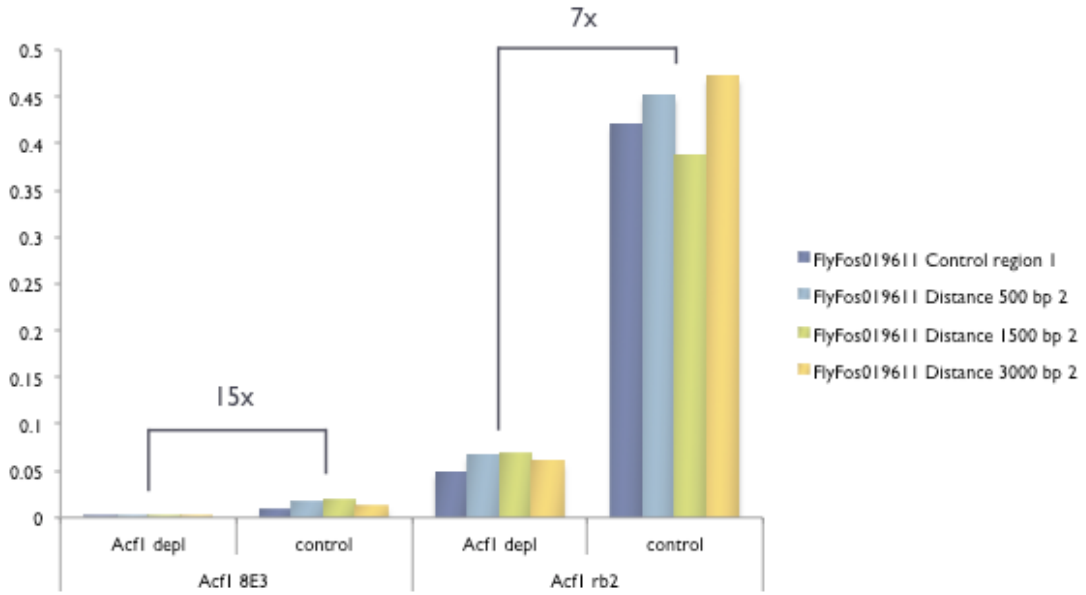

FIGURE 77: QPCR ANALYSIS OF REGIONS 500 BP, 1500 BP, 3000 BP, OR DISTAL TO THE BREAK SITE AFTER CHIP AGAINST ACF1 USING MONOCLONAL (8E3) OR POLYCLONAL (RB2) ANTIBODIES AFTER CHROMATIN ASSEMBLY WITH ACF1-DEPLETED EXTRACT (ACF1 DEPL) OR CONTROL EXTRACT (CONTROL).

However, in Western blot analysis probing chromatin-associated Acf1 versus unbound factor, I observed that only a small fraction of Acf1 is associated to chromatin (compare Figure 28). We therefore considered that, due to excess Acf1 in the extract all chromatin binding sites are saturated with the remodeler, precluding the detection of any additional enrichment at the DNA ends. To avoid this, I titrated the volume of DREX in chromatin reconstitution between 20 - 60 µL of extract per 1 µg DNA. Figure 78 shows yields normalized to input after chromatin immunoprecipitation with monoclonal or polyclonal anti-Acf1 antibody for the corresponding extract titrations relative to the distal control region on the linearized FlyFosmid distant from the break.

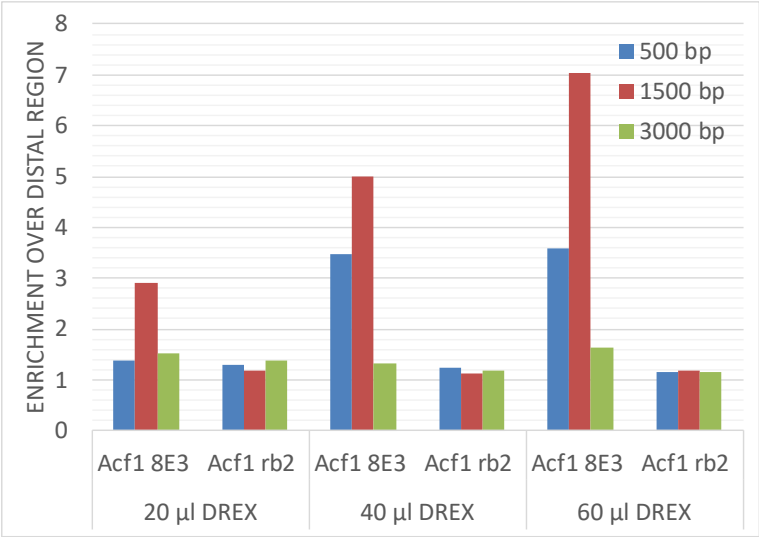

FIGURE 78: RELATIVE ENRICHMENTS AFTER QPCR ANALYSIS OF REGIONS 500 BP, 1500 BP OR 3000 BP FROM THE BREAK SITE IN RELATION TO A DISTAL REGION ON THE SAME FLYFOSMID. CHROMATIN ASSEMBLY WAS PERFORMED WITH 20 µL, 40 µL, OR 60 µL DREX AND MONOCLONAL (8E3) OR POLYCLONAL (RB2) ANTIBODIES AGAINST ACF1 WERE USED FOR CHIP.

Interestingly, in immunoprecipitations performed with the monoclonal antibody 8E3, Acf1 seemed to be about 3 to 7 times enriched 1500 bp away from the break for all tested titrations and about 3.5 times enriched 500 bp away from the break for 40 µL and 60 µL extract per 1 µg DNA. However, this enrichment was not reproduced in immunoprecipitations performed with the polyclonal antibody, were only minor, but consistent enrichments over the control regions were observed (about 1.2 – 1.4 x).

Unfortunately, Acf1 ChIP is very inefficient and signals not robust, presumably due to the particularly short residence time below 500 ms of Iswi chromatin remodelers in chromatin (Erdel & Rippe 2012). To overcome this issue and improve the robustness of Acf1 ChIP, I used different cross-linking strategies by varying formaldehyde concentrations and adding additional protein-protein cross-linking reagents prior to formaldehyde to capture transient and complex interactions. However, these attempts did not improve the yields nor consistency of results.

In conclusion, Acf1 seems to show a preference towards DNA ends with a potential role in DNA repair, supported by the interaction with the Ku complex. However, due to its very general function of chromatin assembly and nucleosome spacing in the early phases of development (Chioda et al. 2010). Acf1 is assumed to be evenly distributed along chromatin and only seems to be marginally enriched at particular sites under specific conditions.

7. FURTHER POST-TRANSLATIONAL HISTONE MODIFICATIONS AROUND DNA BREAKS

As introduced before, other post-translational histone modifications besides the C-terminal phosphorylation of H2A.V (H2A.X in mammals) have been connected to the DNA damage response.

However, only few of them have been studied in *Drosophila*. One example is the N-terminal acetylation of H2A.V, which is required for efficient turnover of phosphorylated H2A.V after the DNA damage response (Kusch 2004). To obtain a general information about damage-dependent post-translational histone modifications in this *in vitro* system, I collaborated with

Christian Feller (ETH Zurich) who analyzed my samples by advanced mass spectrometry. I performed two types of experiments: first, I assembled chromatin on either circular or linearized plasmids in DREX adding lowest-possible amounts of DREX for assembly so that a maximal fraction of soluble histones would be assembled into nucleosomes. In a second experiment I assembled histone octamers on the plasmids containing exclusively the H2A.V variant, or H2A.VΔC, lacking the 'gamma' phosphorylation epitope by salt gradient dialysis. All plasmids, either protein-free or bearing nucleosomes were incubated for 15 min or 3 h in DREX under chromatin assembly conditions. The experiments were done with three independent extract preparations as biological replicates.

Figure 79 and Figure 80 show relative enrichments of histone peptides bearing defined modifications as indicated on linearized versus circular DNA after normalization to their intensities in the sample 'H2A.V preassembled on circular DNA, 15 min'. In Figure 79 nucleosomes were assembled from endogenous factors contained in DREX and in Figure 80 DNA was preassembled with nucleosomes bearing H2A.V on the left side, or the H2A.VΔC, on the right side, respectively. 15 min and 3 h time points are indicated in pink and, purple, respectively, representing early and late time points.

Remarkably, the histone methylation marks H3K9me3, H3K27me2, H3K36me2 and H4K20me2 showed a substantial enrichment of about 5- to 12-fold on linear DNA after assembly with endogenous histones at 15 min assembly time, all decreasing after 3 h assembly time. Only the H4K20me1 mark did not decrease at later time points but increased about 2-fold in both samples. H4K20me1 has already been described in embryo extract by Scharf et al. (Scharf et al. 2008), where it was linked to chromatin maturation and let to deacetylation of H4.

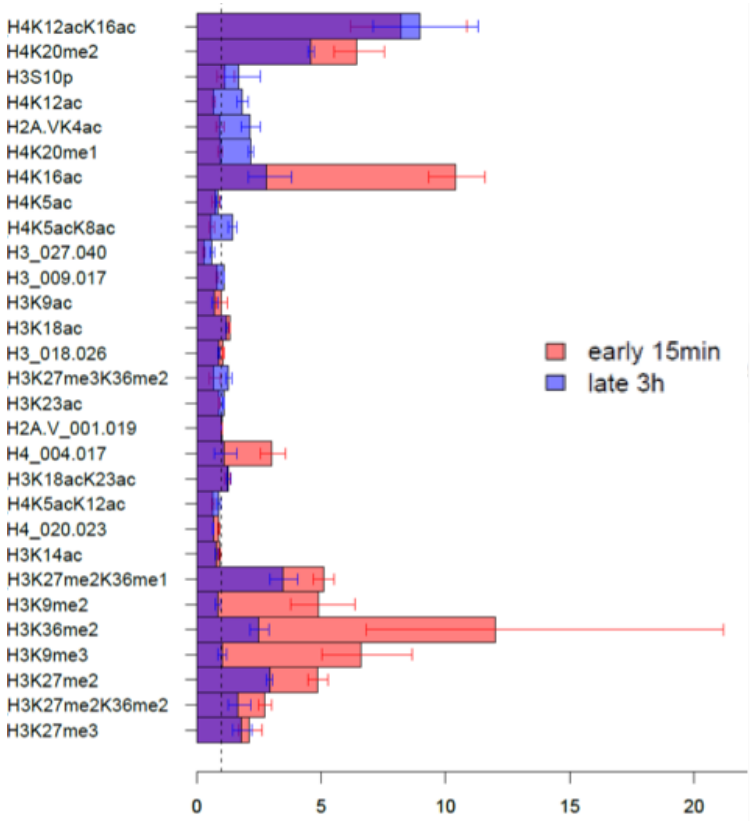

FIGURE 79: RELATIVE ENRICHMENT OF HISTONE MODIFICATIONS AFTER CHROMATIN ASSEMBLY ON FREE LINEARIZED DNA OVER CIRCULAR DNA AFTER 15 MIN (RED) OR AFTER 3 H (PURPLE). ALL INTENSITIES ARE NORMALIZED TO THE INTENSITY OF H2A.V ON CIRCULAR DNA AFTER 15 MIN ASSEMBLY.

A similar situation was detected on nucleosome arrays after incubation in chromatin assembly extract (Figure 80). Here, H3K36me2, H3K9me2/me3, H3K27me2 and H4K20me2 were enriched in both cases, with enrichments scored for H2A.V nucleosomes (with approximately 2.5- to 8.5-fold for 15 min) versus H2A.VΔC nucleosomes (with approximately 1.5- to 3-fold for 15 min). After 3 h assembly, most of the methylation marks decreased again, in parts even more than the reference intensity of H2A.V at 15 min. Remarkably, H2A.VK4ac was decreased to approximately 0.5-fold on full length H2A.V after 15 min but increased after 3 h on full length H2A.V as well as on C-terminally truncated H2A.V at both time points (Figure 80). This observation would argue for a constraining role of the C-terminus on this modification, indicating that the absence of the C-terminus or a C-terminal modification leads to an increase of N-terminal acetylation of H2A.V, in particular at early time points. Interestingly, a dependency of H2A.V acetylation of H2A.V on damage-dependent C-terminal phosphorylation was described in Kusch et al (Kusch 2004). Other modifications with a striking dependency on the C-terminus are H3K36me2, H3K9me2/me3, H3K27me2 and H4K20me2, with a higher abundance in presence of the C-terminus, particularly at the early time point. H3K36me2 has already been linked to DNA damage in mammals, and is deposited by Metnase/SETMAR and is beneficial for the recruitment of Nbs1 and Ku70 (Fnu et al. 2011).

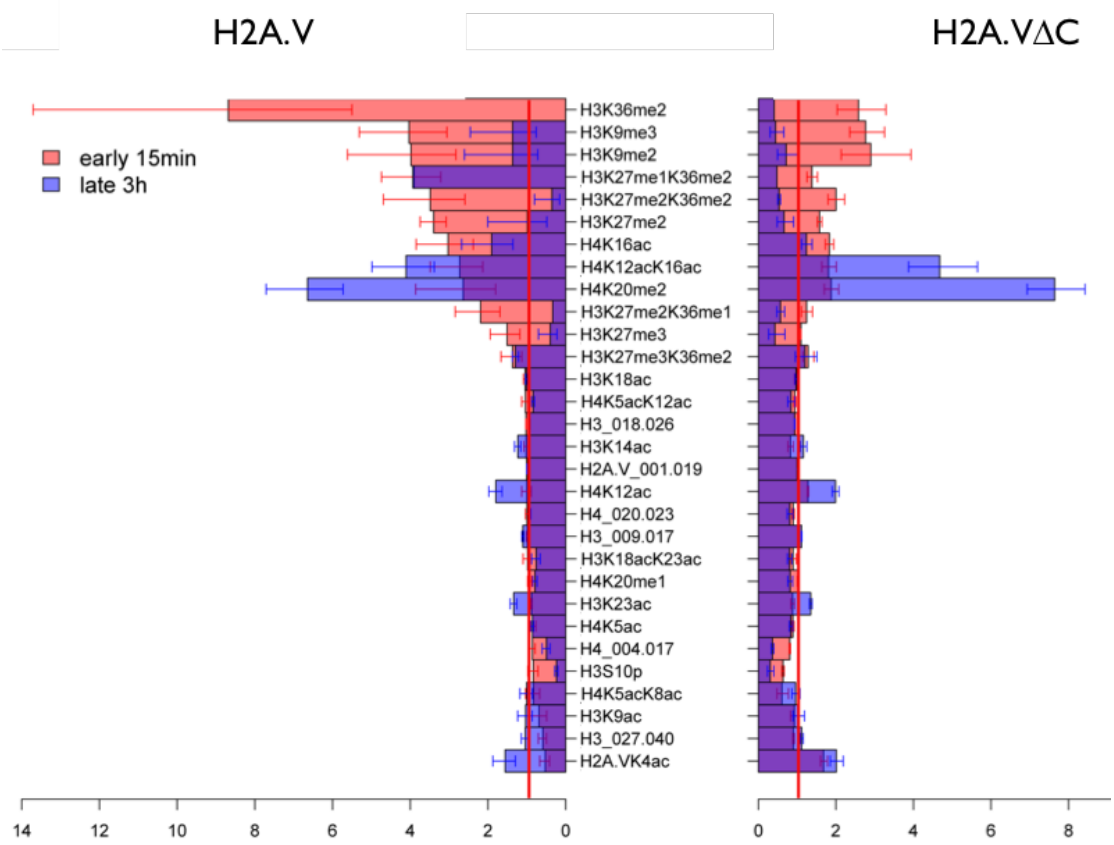

FIGURE 80: RELATIVE ENRICHMENT OF HISTONE MODIFICATIONS AFTER CHROMATIN ASSEMBLY ON LINEARIZED ARRAYS WITH PREASSEMBLED H2A.V OR H2A.VΔC NUCLEOSOMES OVER CIRCULAR ARRAYS AFTER 15 MIN (RED) OR AFTER 3 H (PURPLE). ALL INTENSITIES ARE NORMALIZED TO THE INTENSITY OF H2A.V ON CIRCULAR DNA AFTER 15 MIN ASSEMBLY.

Surprisingly, several damage-dependent histone modifications seem to appear only very transiently, despite the persisting H2A.V phosphorylation mark, which might be explained by the presumably either missing or very inefficient repair of DSBs in the system. However, these methylation marks could have a very general impact on chromatin formation, which might be harmful if maintained over longer time periods compared to the maybe more specific phosphorylation mark, which seems to be more tolerable over the time course of 3 h.

All intensities for free DNA and nucleosome arrays on circular and linearized DNA for 15 min and 3 h normalized to 'H2A.V preassembled on circular DNA, 15 min' are summarized in Figure 79 and Figure 80 with appropriate scales.

FIGURE 81 (NEXT PAGE): RELATIVE INTENSITIES OF HISTONE MODIFICATIONS AFTER CHROMATIN ASSEMBLY ON FREE CIRCULAR (PLASMID, BRIGHT BLUE) OR LINEARIZED (DARK BLUE) DNA, WHICH WAS EITHER FREE (WHITE) OR PREASSEMBLED WITH RECOMBINANT H2A.V (GREEN) OR H2A.VΔC (YELLOW) NUCLEOSOMES AFTER 15 MIN (BRIGHT RED) OR AFTER 3 H (DARK RED). ALL INTENSITIES ARE NORMALIZED TO THE INTENSITY OF H2A.V ON CIRCULAR H2A.V ARRAYS AFTER 15 MIN ASSEMBLY.

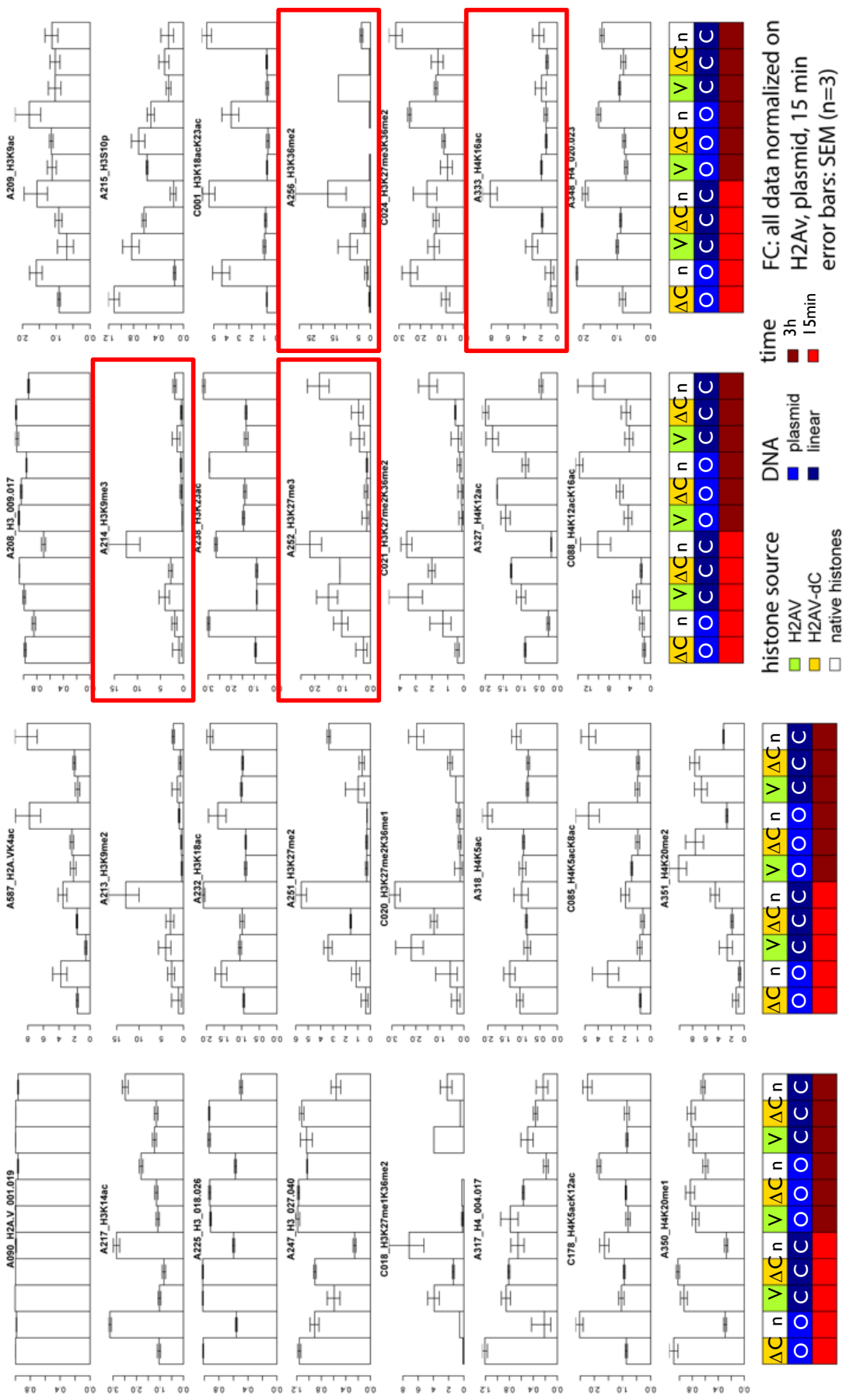
A090_H2A.V_001.019
A217_H3K14ac
A225_H3_018.026
A247_H3_027.040
C018_H3K27me1K36me2
A317_H4_004.017
C178_H4K5acK12ac
A350_H4K20me1
A587_H2A.VK4ac
A213_H3K9me2
A232_H3K18ac
A251_H3K27me2
C020_H3K27me2K36me1
A318_H4K5ac
C085_H4K5acK8ac
A351_H4K20me2
A208_H3_009.017
A214_H3K9me3
A239_H3K23ac
A252_H3K27me3
C021_H3K27me2K36me2
A327_H4K12ac
C088_H4K12acK16ac
A209_H3K9ac
A215_H3S10p
C001_H3K18acK23ac
A256_H3K36me2
C024_H3K27me3K36me2
A333_H4K16ac
A348_H4_020.023
ΔC n V ΔC n V ΔC n V ΔC n
O O C C C O O O C C C C
histone source
H2AV
H2AV-dC
native histones
DNA
plasmid
linear
time
3h
15min
FC: all data normalized on
H2Av, plasmid, 15 min
error bars: SEM (n=3)

C. Influence of ISWI remodeling complexes on chromatin reconstitution

All mass spectrometry analyses in this chapter were performed in collaboration with Andreas Schmidt by data-independent mass spectrometry analysis (SWATH). Data after mass spectrometry analysis of Acf1 interactors was analyzed by Tamás Schauer as follows: Protein intensity values were log2-transformed, median normalized and filtered by a low intensity threshold. Statistical analysis was performed by fitting a linear model using the limma R package. Moderated t-statistics were calculated by empirical Bayes moderation. For the identification of significantly enriched proteins, p-value cutoffs and log2-fold change cutoffs were applied as indicated. Heatmaps were generated using the pheatmap R package.

1. Identification of Acf1 interactors by co-immunoprecipitation

To identify Acf1 interactors, rat monoclonal antibodies raised against an epitope in the Acf1 N-terminus (3F1) or C-terminus (8E3) were coupled to protein G beads and incubated with DREX. After gentle washes, bound protein was analysed by mass spectrometry. The experiment was performed in seven replicates using seven different extract preparations. As a control, DREX was incubated with beads only. Figure 82 shows a principle component analysis, demonstrating a high reproducibility among the biological replicates, but striking differences between the depletions performed with the different antibodies.

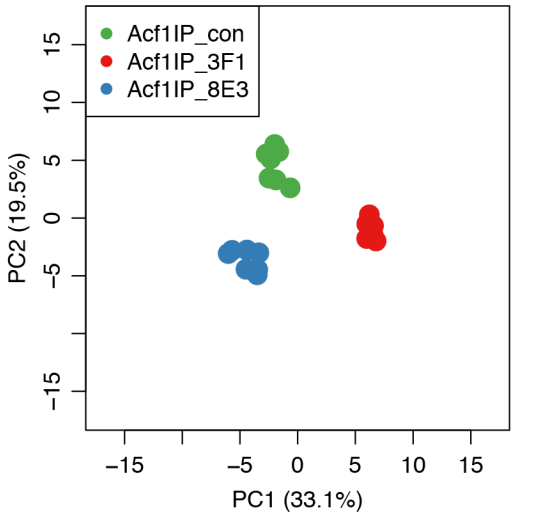

Figure 82: Principal component analysis of DREX immunoprecipitations with antibodies against the N-terminus (3F1) or the C-terminus (8E3) of Acf1. As control, beads only were incubated with DREX.

The proteins enriched after the immunoprecipitations characterized in Figure 82 are shown in the following heatmaps (Figure 83 and Figure 85). The Venn diagram illustrated proteins identified as common or antibody-specific interactors (Figure 84).

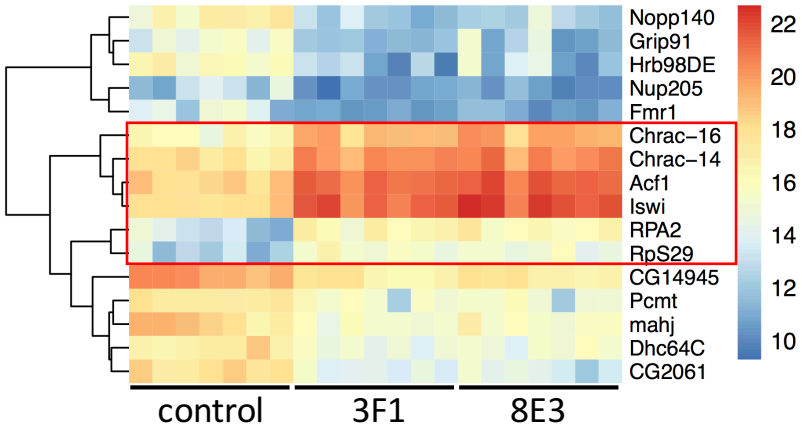

FIGURE 83: ENRICHMENT OF PROTEINS IMMUNOPRECIPITATED WITH ANTIBODIES AGAINST THE N-TERMINUS (3F1) AND THE C-TERMINUS (8E3) OF ACF1. AS CONTROL, BEADS LACKING ANTIBODY WERE INCUBATED WITH EMBRYO EXTRACT. INTENSITIES WERE MEASURED BY MASS SPECTROMETRY FROM SEVEN BIOLOGICAL REPLICATES. HIGH INTENSITIES ARE INDICATED IN RED, LOW INTENSITIES IN BLUE. THE RED BOX MARKS THE SIX COMMON INTERACTORS OF FIGURE 84. A FULL LIST OF PROTEINS AND THEIR ENRICHMENT VALUES ARE LISTED IN XI.B.3.A).

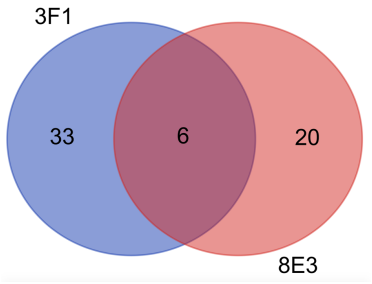

FIGURE 84: VENN DIAGRAM ILLUSTRATING PROTEINS IDENTIFIED BY IMMUNOPRECIPITATIONS WITH ANTIBODIES AGAINST THE N-TERMINUS (3F1) OR THE C-TERMINUS (8E3) OF ACF1. 33 PROTEINS WERE IDENTIFIED AS SPECIFIC INTERACTORS WITH ANTIBODY 3F1, 20 PROTEINS AS SPECIFIC INTERACTORS WITH 8E3. 6 PROTEINS WERE IDENTIFIED AS INTERACTORS WITH BOTH ANTIBODIES. IDENTIFIED PROTEINS ARE LISTED IN TABLE 7.

As expected, the CHRAC complex consisting of Acf1, Iswi, Chrac14 and Chrac16 (Varga-Weisz et al. 1997) was pulled down with both antibodies. In addition to this, RPA2, a component of the RPA complex, and Ribosomal protein S29 (RpS29) were identified as common interactor in both immunoprecipitations (Figure 83, red box). RpS29 is a small ribosomal protein, which is located in the cytoplasm and in the endoplasmic reticulum. Its interaction with Acf1 therefore does not seem to a physiological phenomenon, as Acf1 is a nuclear protein. However, the interaction with Rpa2 might be physiologically relevant, as Acf1 might be able to interact with Ku (see VI.B) and Ku has been shown to interact with RPA in *Drosophila* (Guruharsha et al. 2011). However, Ku proteins were not found enriched in the Acf1 immunoprecipitants in this experiment.

In addition to the six common interactors, many interactors exclusive for the N-terminal or C-terminal specific antibodies were identified and listed in Table 7 (also see Figure 85).

TABLE 7: IDENTIFIED INTERACTORS BY MASS SPECTROMETRY USING ANTIBODIES AGAINST THE N-TERMINUS (3F1) OR THE C-TERMINUS (8E3) OF ACF1.

Common interactors			
Acf1		RPA2	
Iswi		RPS29	
Chrac14			
Chrac16			
3F1 specific interactors		8E3 specific interactors	
atms	hyx	Bruce	ida
Atu	Kap-alpha1	Cdc16	kis
CG13175	Karybeta3	Cdc27	PPP4R2r
CG2091	Klp10A	CG12391	puf
CG3542	mdlc	CG13185	RanBPM
CG3909	mod	CG30122	row
CG4119	msn	CG4751	timeout
CG4849	Nap1	CG6617	tou
Ctr9	Phf7	Dyak\GE13051	Ubqn
Dyak\Ef1beta	pont	Fcp1	woc
Dyak\Ef1gamma	Prp8		
ecd	Ran		
eEF1alpha1	Ranbp9		
eEF1delta	sle		
Etl1	Tailor		
His2A	Vta1		
His3			

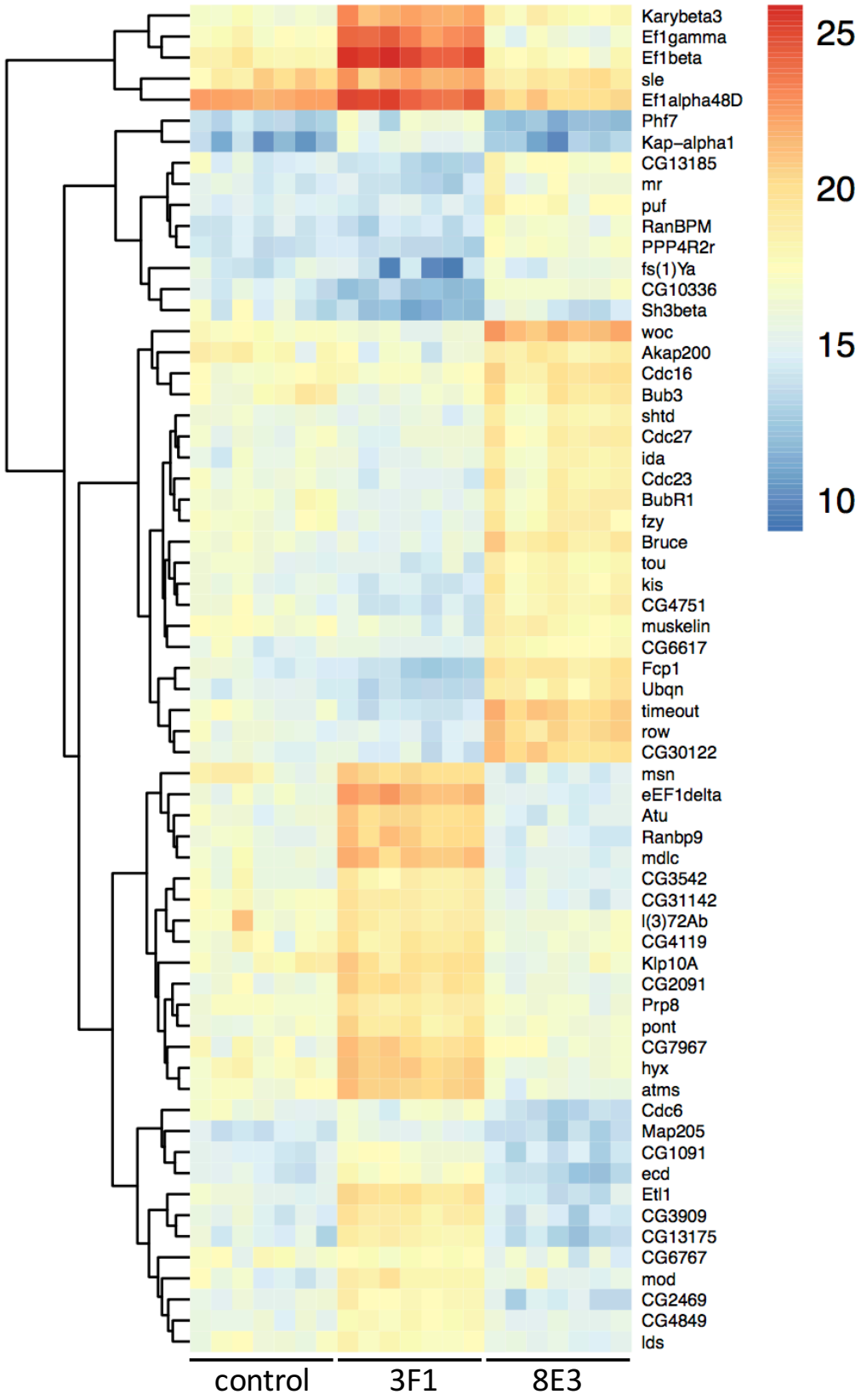

FIGURE 85: ENRICHMENT OF PROTEINS IMMUNOPRECIPITATED WITH ANTIBODIES AGAINST THE N-TERMINUS (3F1) OR THE C-TERMINUS (8E3) OF ACF1. AS CONTROL, BEADS ONLY WERE INCUBATED WITH DREX. INTENSITIES WERE MEASURED BY MASS SPECTROMETRY FROM SEVEN BIOLOGICAL REPLICATES. HIGH INTENSITIES ARE INDICATED IN RED, LOW INTENSITIES IN BLUE. A FULL LIST OF PROTEINS AND THEIR ENRICHMENT VALUES ARE LISTED IN XI.B.3.A).

To evaluate these findings, GO term analyses were performed. Common interactors (Acf1, Iswi, Chrac14, Chrac16) define the CHRAC complex (Varga-Weisz et al. 1997; Eberharter et al. 2001). In addition to that, some interactors involved in chromatin organization were identified as interactors with N-terminal binding antibodies, leading to the assumption that these proteins may rather bind to more C-terminal Acf1 sequences. One example is Nap1, a core histone chaperone, which has already been functionally connected to Acf1 (genetic interaction described in Fyodorov et al. 2004). As Nap1 is known to interact with core histones, the identified interactions with histones H2A and H3 might be due to indirect interactions via Nap1 (Ito et al. 1996). Etl1 (Smarcad1 in mammals, Fun30 in yeast) is an ATP dependent helicase of the SNF2/SWI2 family (Fnu et al. 2011). In yeast, it has been associated with DNA damage and promotes DNA end resection at DSBs during DNA repair (Costelloe et al. 2012). Previous mass spectrometry analysis identified Atms, Ctr9 and Hyx to interact with each other in *Drosophila* (Guruharsha et al. 2011) and might therefore act in a complex to regulate transcription. Furthermore, other GO-terms associated with Acf1 interactors isolated with the N-terminus-specific antibody were 'nucleic acid metabolism'/'(m)RNA metabolism', 'gene expression' and 'splicing'. On the other hand, the GO term associated with Acf1 interactors isolated with the C-terminus-specific antibody was 'ubiquitin-mediated proteolysis'. The significance of this in unclear and cross-reactivity of antibodies with proteins including similar sequences cannot be excluded.

Unfortunately, in this experiment Ku70 and Ku80 were not detected. However, in a previous experiment performed in triplicates, where beads coupled to monoclonal Acf1 antibody 8E3 against the C-terminus were analysed by mass spectrometry, Ku70 and Ku80 were identified and Ku80 was enriched compared to the control reaction with beads only, but due to the high variability among replicates, this enrichment was not significant (Figure 86). Besides this, the identified interactors were largely consistent with the interactors in the previous experiment.

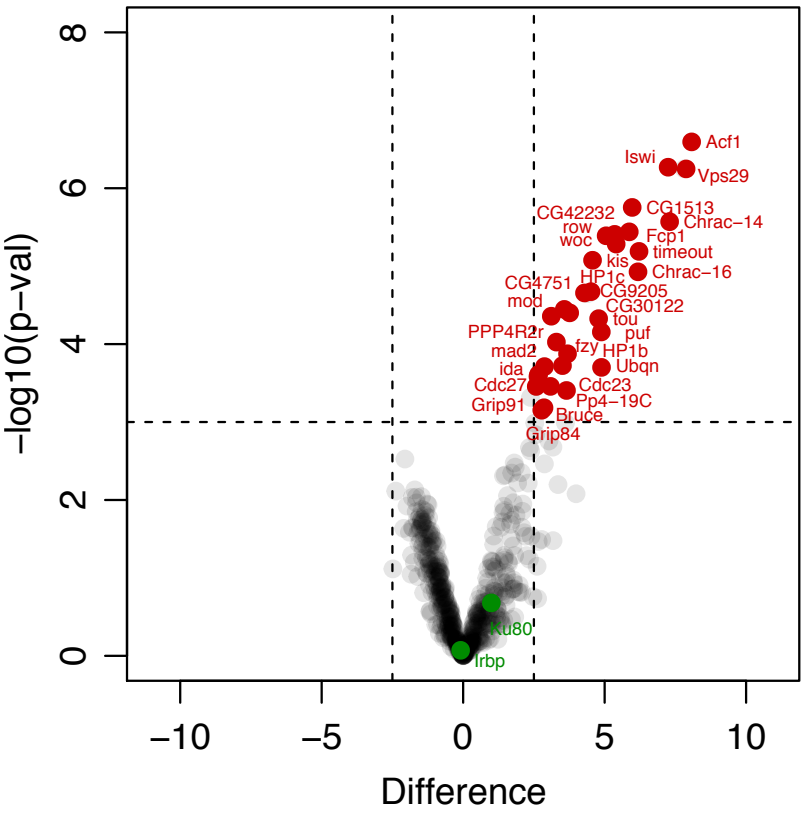

FIGURE 86: VOLCANO PLOT WITH LOG10 P VALUES (Y-AXIS) AND LOG FOLD DIFFERENCE (X-AXIS) AFTER COMPARISON OF PROTEINS IMMUNOPRECIPITATED WITH ANTI-ACF1 ANTIBODY 8E3 VERSUS CONTROL FROM THREE BIOLOGICAL REPLICATES. KU70 (IRBP) AND KU80 ARE MARKED IN GREEN. A FULL LIST OF PROTEINS AND THEIR ENRICHMENT VALUES ARE LISTED IN XI.B.3.B).

This discrepancy might be due to a very weak interaction between Ku and Acf1, why may be detected or not depending on the washing stringency or sample preparation. However, it has been shown that Ku interacts with the RPA complex, therefore the detection of Rpa2 might be due to some indirect interaction of RPA with Acf1 via Ku.

2. DEPLETION OF ACF1 FROM DREX

To investigate the role of Iswi remodelling complexes in chromatin reconstitution, I performed assembly reactions with extract, which was depleted from the remodelling factor of interest, either by immunoprecipitating the factor of interest from wildtype DREX or by preparation of DREX from mutant embryos. In the following experiments, we are focusing on the accessory subunits of the chromatin remodelling complexes ACF and RSF, namely Acf1, and Rsf1, respectively.

DREX was depleted from Acf1 by immunodepletion using rat monoclonal antibody (8E3), which detects and epitope in the Acf1 C-terminus (obtained from E. Kremmer (Helmholtz Center Munich). Depletion was performed by two rounds of immunoaffinity adsorption of extract protein with antibodies coupled to Protein G Sepharose 4 Fast Flow beads (GE Healthcare). As control, DREX of the same batch was treated in the same way, except that the beads lacked antibody. Figure 87 and Figure 88 shows that two rounds of immunodepletion, lead to an almost complete depletion of Acf1. This extract was used in the following chromatin assemblies to investigate the role of Acf1 in chromatin reconstitution.

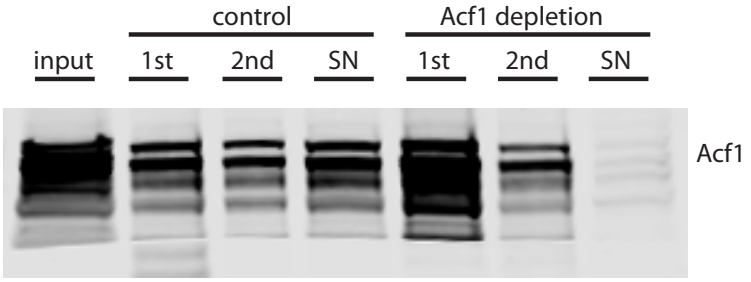

FIGURE 87: DEPLETION OF DREX AS DESCRIBED IN THE TEXT. AS INPUT, EXTRACT BEFORE DEPLETION WAS LOADED, AS WELL AS BEADS FROM THE 1ST ROUND AND 2ND ROUND OF DEPLETION, AND EXTRACT AFTER TWO ROUNDS OF DEPLETION (SN). THE MEMBRANE WAS PROBED WITH ANTIBODY AGAINST ACF1.

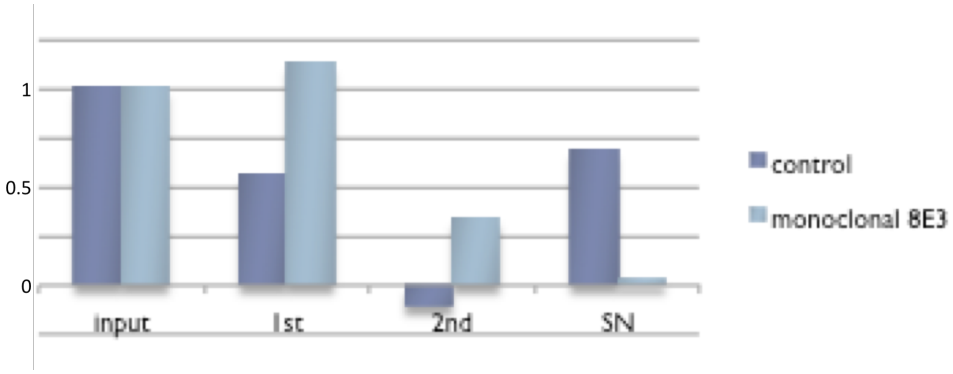

FIGURE 88: SIGNAL INTENSITIES OF ACF1 DEPLETION WITH MONOCLONAL 8E3 ANTIBODIES OR BEADS ONLY (CONTROL) FROM FIGURE 87 QUANTIFIED BY IMAGE STUDIO™ LITE SOFTWARE, LI-COR BIOSCIENCES NORMALIZED TO THE INPUT.

3. CHROMATIN RECONSTITUTION USING DREX IMMUNODEPLETED FROM ACF1

To investigate the role of Acf1 chromatin was assembled using DREX depleted from Acf1 as described in VI.C.2.

Figure 89 shows a supercoiling assay performed with control extract (+Acf1) and Acf1-depleted extract (-Acf1) as described in VI.A.1. In both conditions, the transformation of different states from relaxed to supercoiled plasmid DNA was observed over time, suggesting that Acf1 depletion does not prevent reconstitution of nucleosomes *in vitro*.

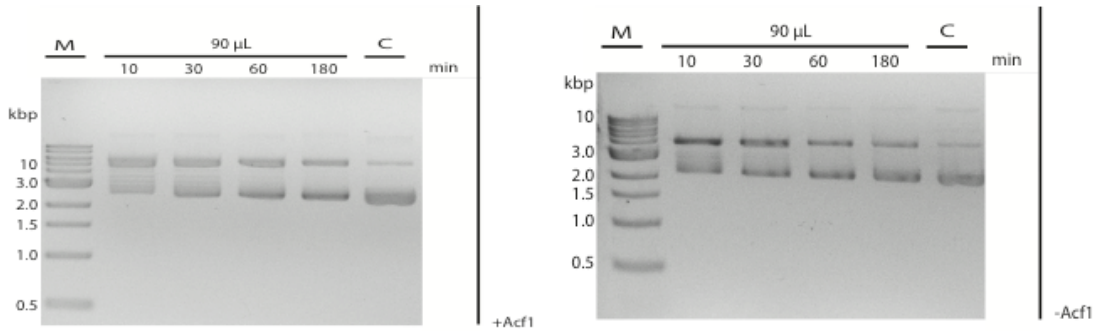

FIGURE 89: SUPERCOILING ASSAY AFTER *IN VITRO* CHROMATIN ASSEMBLY WITH ACF1-DEPLETED DREX FOR 10 MIN, 30 MIN, 60 MIN, AND 180 MIN. FOR INPUT, SUPERCOILED PLASMID DNA WAS USED (C). AFTER 10 MIN, PLASMID DNA IS IN A RELAXED STATE DUE TO TOPOISOMERASES IN THE EXTRACT.

Previous analyses have shown by supercoiling analysis that Acf1 facilitates depositions of nucleosomes and considerably enhances nucleosome reconstitution in an *in vitro* reaction composed of recombinant DNA, purified histone octamers, and recombinant Nap1 in presence or absence of recombinant Acf1 (Ito et al. 1999; Khuong et al. 2017; Fei et al. 2015; Torigoe et al. 2013). However, this effect was not observed here after Acf1 depletion, which might indicate that either the function of Acf1 was taken over by another factor in the extract or residual Acf1 after depletion was sufficient to deposit nucleosomes to a similar extent onto the recombinant DNA. To investigate the regularity of the nucleosome fiber after chromatin reconstitution with Acf1-depleted extract as described in VI.C.2, I performed limited MNase digestion. However, the quality of MNase 'ladders' obtained for control extract, as well as for Acf1-depleted extract, were poor. It is possible, that unspecific binding of Acf1 or another factor to the control beads leads to its depletion in the control extract, which results in a restrained formation of properly spaced nucleosome fibers.

To see, if Acf1 has an effect on the incorporation of H2A.V, I preformed chromatin reconstitution with control or depleted extract on either preassembled arrays of recombinant H2A-bearing nucleosomes or on nucleosome-free DNA, both immobilized to paramagnetic beads, to enable chromatin purification after assembly. Western blot analysis against incorporated H2A.V did not show significant differences in the levels of H2A.V incorporation, neither in the case of free DNA, where chromatin is reconstituted from endogenous factors, nor in the case of preassembled H2A arrays, where H2A-containing nucleosomes could potentially be replaced by H2A.V-containing nucleosomes. Similarly, no difference in H2A.V turnover was observed after incubation with preassembled H2A.VE, the phospho-mimetic form of H2A.V.

In addition to this, phosphorylation levels were not altered on chromatin assembled with Acf1-depleted extract, either because Acf1 is not involved in turnover of H2A.V after phosphorylation as suggested by previous experiments (discussed in III.B.6) or because phosphorylation of newly incorporated unphosphorylated H2A.V happens to the same extent as phosphorylated H2A.V is removed from chromatin. Unfortunately, as already mentioned in VI.A.5, it was not possible to distinguish preassembled recombinant and newly deposited endogenous H2A.V from the extract, as the reconstitution of 3xFlag-tagged H2A.V nucleosomes failed.

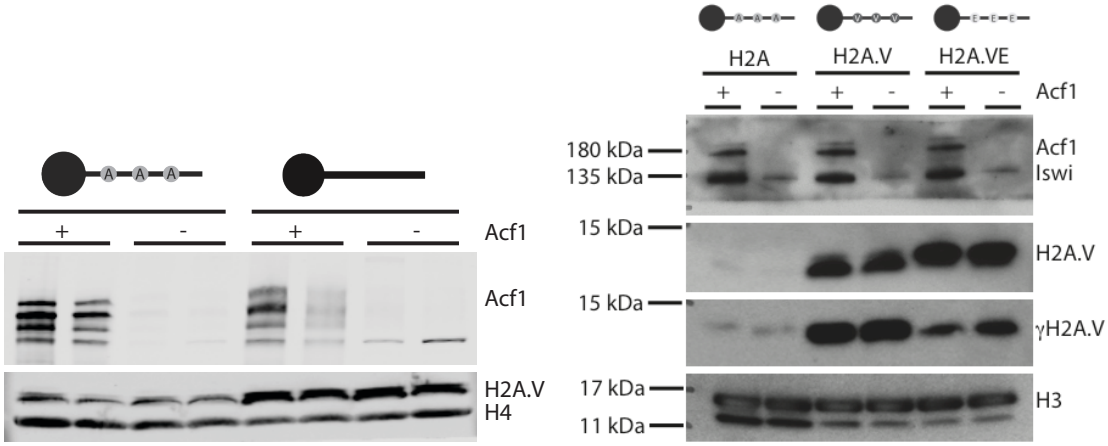

FIGURE 90: CHROMATIN ASSEMBLY WITH ACF1-DEPLETED EXTRACT (- ACF1) OR CONTROL EXTRACT (+ACF1) ON FREE DNA (LEFT) OR ON PREASSEMBLED ARRAYS OF RECOMBINANT H2A (LEFT AND RIGHT), H2A.V OR H2A.VE NUCLEOSOMES (RIGHT). MEMBRANES WERE PROBED WITH ANTIBODIES AGAINST ACF1, ISWI, H2A.V, γH2A.V, H3, AND H4.

In contrast to this bulk analysis, however, ChIP-qPCR on chromatin assembled by Acf1-depleted extract showed an effect on H2A.V levels upon Acf1 depletion (Figure 91). Here, levels of H2A.V and γH2A.V were decreased on chromatin reconstituted with Acf1 depleted extract versus chromatin reconstituted with control extract after normalization to input DNA. The experiment was performed in triplicates using three independent extract preparations as biological replicates and isolated DNA was analysed by qPCR targeting different loci at the control FlyFos019829 or at the linearized FlyFos019611. To our surprize, H2A.V and γH2A.V levels were increased upon Acf1 depletion at all tested loci. To exclude the possibility of a general effect due to altered ChIP efficiencies caused by changes in chromatin structure upon Acf1 depletion, I examined the levels of histone H4 acetylation on lysine 16 (H4K16ac) upon Acf1 depletion, as this modification is assumed to be Acf1-independent. As expected, levels of H4K16ac were comparable in both conditions (Figure 92). It is therefore possible that Acf1 has modest effects on the H2A.V levels in chromatin, but Western Blot analysis might not be sensitive enough to identify the effect. The mechanism, through which Acf1 could influence the amount of incorporated H2A.V is still elusive.

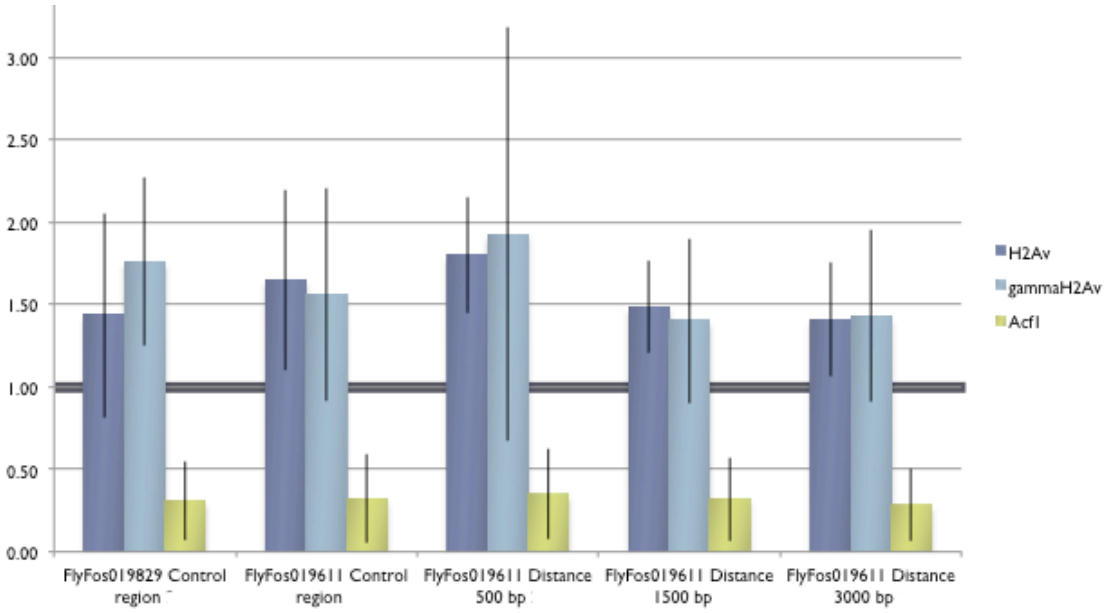

FIGURE 91: CHIP-QPCR ON CHROMATIN ASSEMBLED WITH ACF1-DEPLETED EXTRACT AND WITH CONTROL EXTRACT ON CIRCULAR CONTROL FLYFOS019829 AND ON LINEARIZED FLYFOS019611. REGIONS 500 BP, 1500 BP, AND 3000 BP FROM THE BREAK AS WELL AS A DISTAL REGION ON THE LINEAR FLYFOS019611 WERE ANALYZED. AS A CONTROL, A REGION ON THE CIRCULAR FLYFOS019829 WAS INCLUDED. ANTIBODIES AGAINST H2A.V, γH2A.V, AND ACF1 WERE USED. % OF INPUT WAS DETERMINED AND RATIOS OF ACF1-DEPLETED EXTRACT TO CONTROL EXTRACT WERE PLOTTED. ERROR BARS SHOW STANDARD DEVIATIONS FROM THREE BIOLOGICAL REPLICATES USING THREE DIFFERENT EXTRACT PREPARATIONS.

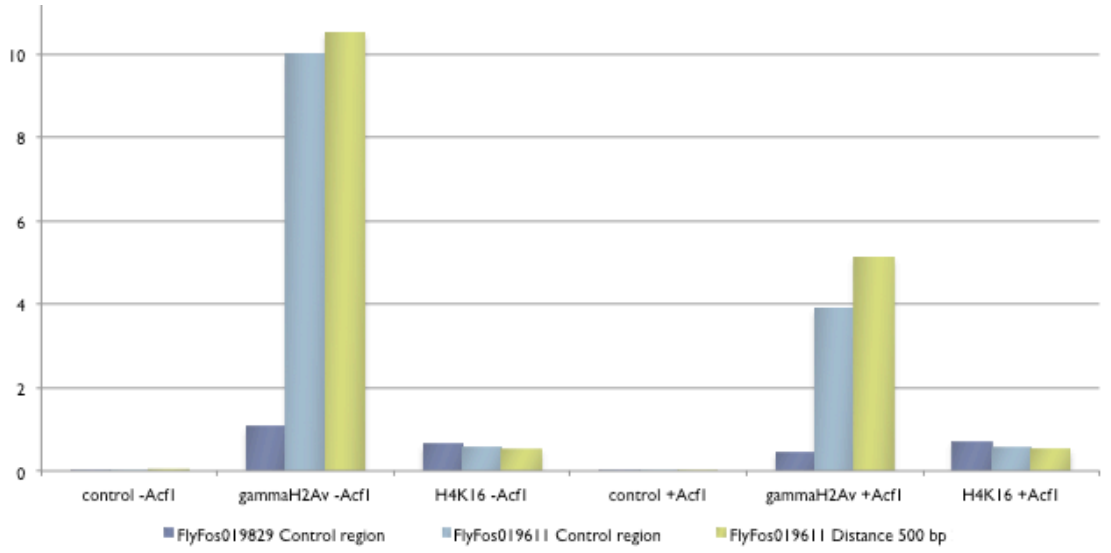

FIGURE 92: CHIP-QPCR ON CHROMATIN ASSEMBLED WITH ACF1-DEPLETED EXTRACT AND WITH CONTROL EXTRACT ON CIRCULAR CONTROL FLYFOS019829 AND ON LINEARIZED FLYFOS019611. % OF INPUT IS SHOWN ANALYZING A REGION 500 BP FROM THE BREAK AS WELL AS A DISTAL REGION ON THE LINEAR FLYFOS019611. AS A CONTROL, A REGION ON THE CIRCULAR FLYFOS019829 WAS INCLUDED. ANTIBODIES AGAINST γH2A.V AND H4K16AC WERE USED. TO CONTROL FOR UNSPECIFIC BINDING TO THE BEADS, A BEAD-ONLY CONTROL WITHOUT ANTIBODY WAS INCLUDED.

To analyse the effect of Acf1 depletion on chromatin composition, chromatin was reconstituted on immobilized DNA in control extract or Acf1-depleted extract, purified on the magnet and bound proteins analysed by mass spectrometry. As an input reference, control extract and Acf1-depleted extract were analysed before addition of DNA. Figure 93 shows a sector of a heatmap after clustering similarly affected hits together. All measurements were performed in duplicates, using different extract preparations as biological replicates. As expected, Iswi, the ATPase subunit of ACF, was strongly co-depleted in the input as well as in the chromatin samples. In addition to this, in both replicates DNApol-α180, was strongly depleted in the input samples. DNApol-α180 is a polymerase, which has been linked to the NHEJ repair pathway (Flybase.org; 27.12.2017), like the Ku complex, which is consistent with our hypothesis, that Acf1 might have a functional interaction with Ku and might be involved in DNA damage repair. Co-depletion of CG5757 (unknown function), CG14476 (Glucosidase subunit) and rump (mRNA localization) was consistent in both replicates, however, there was no obvious functional connection (Flybase.org; 27.12.2017).

Analysis of chromatin-associated factors revealed that ACF (consisting of Acf1 and Iswi), CG8142, Gnf1, and the Ku complex (Irbp and Ku80) were decreased on chromatin samples. CG8142 and Gnf1 are involved in replication (Flybase.org; 27.12.2017). Interestingly, while the reduced recovery of Acf1 and Iswi in chromatin is due to their depletion in the input extract, the reduced association of the Ku complex with chromatin cannot be explained in this way since the co-depletion is not efficient. This leads to the assumption that Ku association to chromatin might be connected to Acf1. It might be possible that the remodelling function of ACF is required for efficient recruitment of Ku, as already postulated in mammals (Lan et al. 2010). In contrast, some factors, which are depleted in the input samples, are recruited to chromatin at similar levels. Examples are CG14476, CG5757 and rump, and also recruitment of DNApol-α180 to chromatin was not significantly affected upon Acf1 depletion. This observation might be explained by a saturated pool of these factors at this embryonic stage, where most chromatin factors are available in excess to be equipped for the very rapid initial preblastodermal replication cycles during embryo development (Mahowald & Hardy 1985).

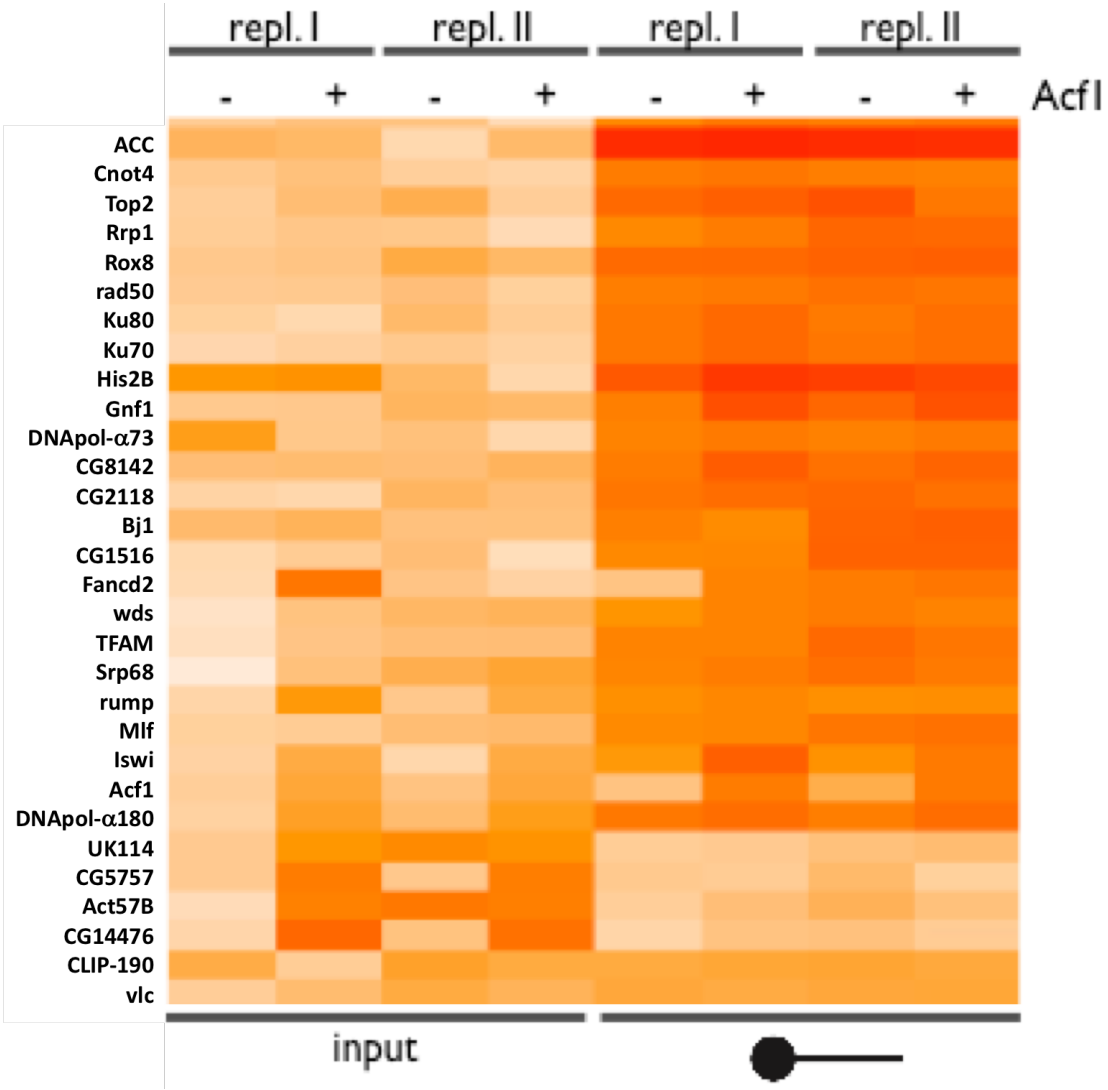

FIGURE 93: HEAT MAP OF PROTEINS ASSOCIATED WITH CHROMATIN ASSEMBLED FROM ACF1-DEPLETED EXTRACT (-ACF1) OR CONTROL EXTRACT (+ACF1). AS INPUT, EXTRACT BEFORE ASSEMBLY WAS ANALYZED. INTENSITIES WERE MEASURED BY MASS SPECTROMETRY FROM TWO BIOLOGICAL REPLICATES.

RSF, a complex consisting of Iswi and Rsf1, has been shown to be involved in the incorporation of H2A.V during heterochromatin formation (Hanai et al. 2008). To test, if Rsf1, the accessory subunit, has an influence on H2A.V incorporation in the *in vitro* system, chromatin was reconstituted with an extract prepared of Rsf1-mutant embryos (Rsf1-mutant DREX). Figure 94 shows a Western blot analysis of Rsf1-mutant DREX in comparison with wt DREX and Schneider cell extract. In Rsf1 mutant DREX, no band for Rsf1 was detected. However, lower bands in the Rsf1-mutant extract were recognized, which could be unspecific or degradation products of Rsf1.

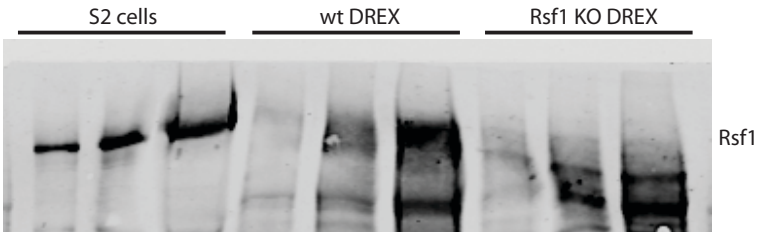

FIGURE 94: EXTRACT OBTAINED FROM *DROSOPHILA* SCHNEIDER CELLS (S2 CELLS), DREX FROM WILDTYPE (WT DREX) AND FROM RSF1 MUTANT EMBRYOS (RSF1 KO DREX) WAS ANALYZED BY WESTERN BLOT IN THREE DIFFERENT CONCENTRATIONS. THE MEMBRANE WAS PROBED WITH ANTIBODY AGAINST RSF1.

However, incorporation of H2A.V *in vitro* was not altered in the absence of Rsf1. To exclude, that the Iswi-containing complexes ACF and RSF could exhibit redundant functions, Rsf1 mutant extract was depleted of Acf1 as described before. However, chromatin assembly using Rsf1 mutant extract depleted from Acf1 did not show any differences in H2A.V levels, suggesting that neither Rsf1 nor Acf1 are involved in H2A.V incorporation and that both remodelling factors do not exhibit redundant functions in the incorporation of H2A.V.

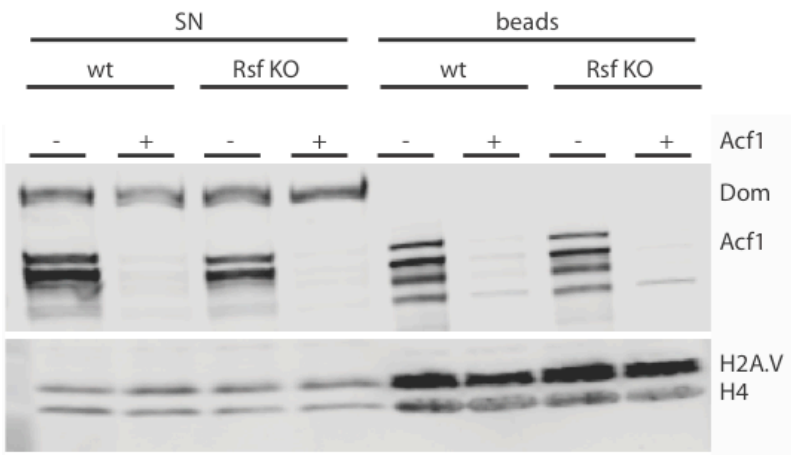

FIGURE 95: CHROMATIN ASSEMBLY USING WILDTYPE (WT) OR RSF1 MUTANT (RSF KO) EXTRACT EITHER DEPLETED FROM ACF1 (-ACF1) OR IN PRESENCE OF ACF1 (+ACF1). SUPERNATANT (SN) AND CHROMATIN (BEADS) WERE LOADED. MEMBRANES WERE INCUBATED WITH ANTIBODIES AGAINST DOMB, ACF1, H2A.V, AND H4.

4. CHROMATIN ASSEMBLY USING DREX PREPARED FROM ACF1$^-$ MUTANT EMBRYOS

For a better interpretation of the function of Acf1 on chromatin and to eliminate the influence of co-depleted factors, DREX from acf1 null mutant embryos were prepared. As expected and already shown for Acf1-depleted extract, limited MNase digestion revealed a lack of nucleosome fiber regularity in the absence of Acf1, confirming that Acf1, and not any co-immunoprecipitated factor is responsible for the establishment of regular chromatin arrays. This was confirmed in a rescue experiment, were addition of recombinant ACF rescued the

regularity to some extent. However, in contrast to this, DREX prepared from Rsf1- embryos did not show a defect in the establishment of regular nucleosome arrays.

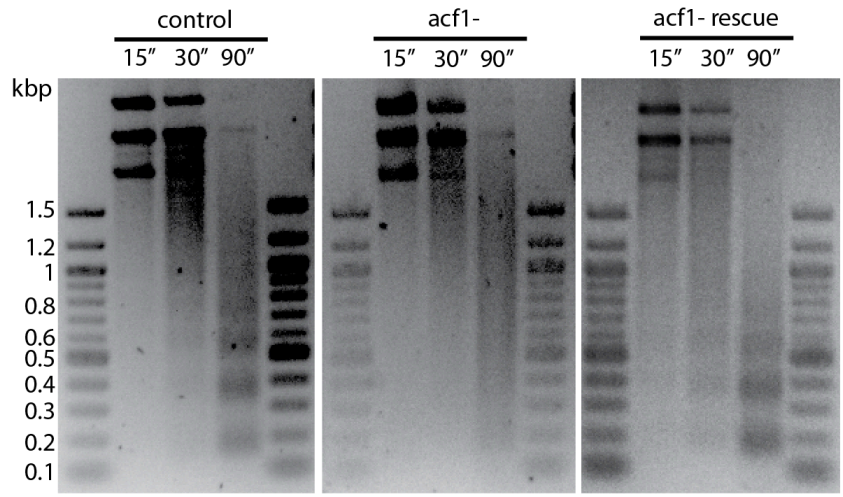

FIGURE 96: LIMITED MNASE DIGESTION FOR 15 SEC, 30 SEC, AND 90 SEC AFTER *IN VITRO* CHROMATIN RECONSTITUTION WITH CONTROL EXTRACT, ACF1 MUTANT EX-TRACT (ACF1-) OR ACF1 MUTANT EXTRACT SUPPLIED WITH RECOMBINANT ACF (ACF1 RESCUE) AND ANALYSIS OF PURIFIED DNA AFTER GEL ELECTROPHORESIS.

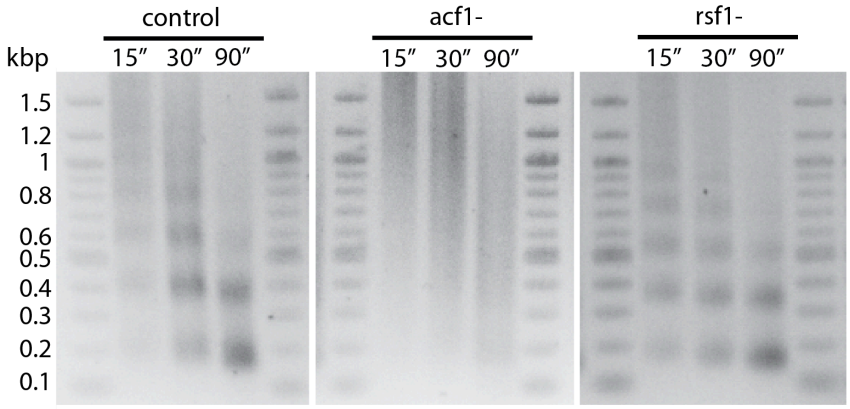

FIGURE 97: LIMITED MNASE DIGESTION FOR 15 SEC, 30 SEC, AND 90 SEC AFTER *IN VITRO* CHROMATIN RECONSTITUTION WITH CONTROL EXTRACT, ACF1 MUTANT EXTRACT (ACF1-) OR RSF1 MUTANT EXTRACT (RSF1-) AND ANALYSIS OF PURIFIED DNA AFTER GEL ELECTROPHORESIS.

Dhawal Jain, a former PhD student in our lab, identified regions of regularly phased nucleosome arrays in the *Drosophila* genome and discovered, that some of these regions depend on the presence of Acf1. These regions share a common motif, characterized by a central ATACG sequence (Baldi et al. 2018). To see, if this data from *in vivo* analysis of 2-8 h old embryos can be reproduced *in vitro*, I performed chromatin reconstitution on genomic DNA with wt and acf1- DREX. After assembly, DNA was fragmented by MNase digestion and purified. Sando Baldi in our lab established a nucleosome dyad density map by NGS. The following results were pre-

published in Baldi et al. 2018. In Figure 98 reads obtained from Next generation sequencing were aligned around the ATACG motifs. Chromatin assembled by wt DREX showed extensive regular phased nucleosome arrays around the motif with about 4-5 nicely positioned nucleosomes on either site. In absence of Acf1, however, the nucleosomes flanking the motif remained well positioned but the remaining nucleosomes did no longer form regularly spaced arrays. This effect was partially rescued by addition of recombinant ACF, leading to well positioned regions around the motif with about 2-3 nucleosomes on each site.

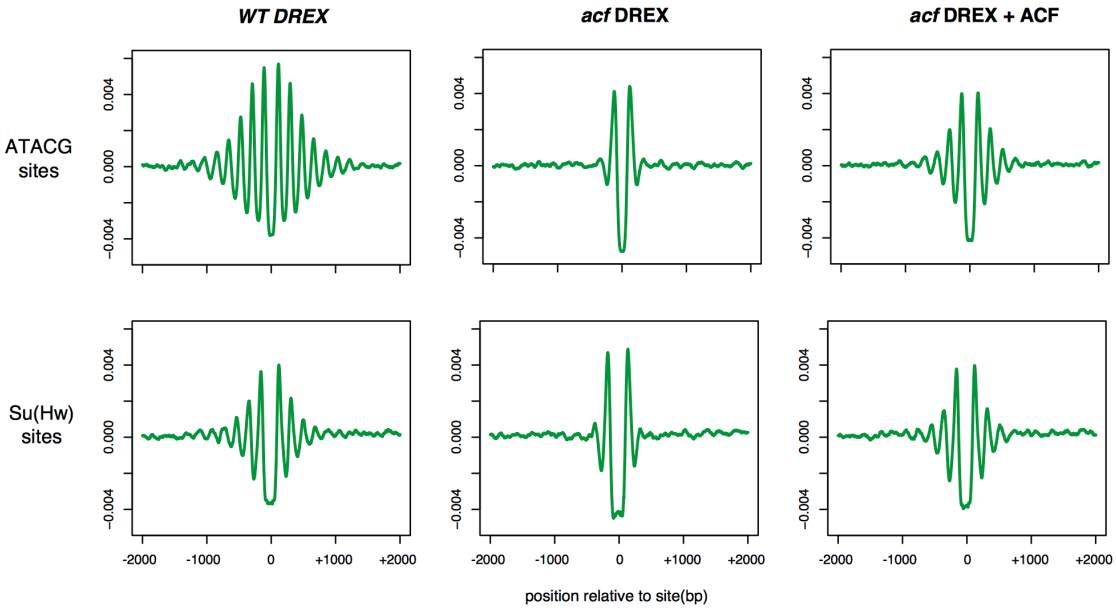

FIGURE 98: CHROMATIN ASSEMBLY ON GENOMIC DNA FROM *DROSOPHILA* BG3-C2 CELLS USING DREX FROM WILDTYPE EMBRYOS (WT DREX) OR FROM ACF1 MUTANT EMBRYOS IN ABSENCE (ACF1 DREX) OR PRESENCE (ACF1 DREX + ACF) OF RECOMBINANT ACF. READS AFTER MNASE-SEQ WERE ALIGNED TO THE ATACG SITES (TOP) OR TO SU(HW) BINDING SITES (BOTTOM). FIGURE FROM BALDI ET AL. 2018.

The mechanism of nucleosome spacing is not yet fully understood. however, it is assumed that insulator proteins act as alignment to position nucleosomes in respect to the insulator protein (Fu et al. 2008). Examples for *Drosophila* insulators are Su(Hw), Ctcf, Beaf and Gaga (J. Yang & Corces 2012). Figure 98 shows the reads after MNase-Seq from chromatin assembled in presence or absence of Acf1 were aligned to the binding motif of Su(Hw). Interestingly, a similar effect as for the alignment to the ATACG motif can be observed: nucleosome arrays are obtained in an Acf1-dependent manner and the decline in regularity of nucleosome arrays in acf1- mutants can be rescued by addition of recombinant ACF. Furthermore, similar to the situation at the ATACG motif, nucleosomes flanking the Su(Hw) binding site are not affected and remain positioned in wt and acf1- conditions. To summarize, Acf1 seem to be required for the formation of regularly spaced nucleosome arrays.

However, the respective protein which binds to the ATACG motif and constitutes a boundary against which ACF can phase nucleosomes is not yet known. To identify this protein, recombinant DNA including the ATACG motif was prepared by Sandro Baldi and immobilized to paramagnetic beads. Subsequently, chromatin assembly reactions were performed and chromatin assembled on these motifs was isolated for mass spectrometry in collaboration with Falk Butter in Mainz. As a negative control, recombinant DNA with mutated ATACG regions was

used. Interestingly, one hit was identified as an ATACG binding protein, CG7372 (termed Phaser), a zinc finger-containing protein. To confirm the obtained data, Sandro Baldi performed knock down experiments in *Drosophila* Schneider cells and analysed the effect of nucleosome array formation at Su(Hw) and ATACG sites upon knock down of Su(Hw), and Phaser, respectively. Interestingly, he observed that array formation around Su(Hw) binding sites, and ATACG motif sites, depends on Su(Hw), and Phaser, respectively (Figure 99). In addition to this, in both cases, knock down of Acf1 remarkably dampened the establishment of regular arrays around these sites (not shown).

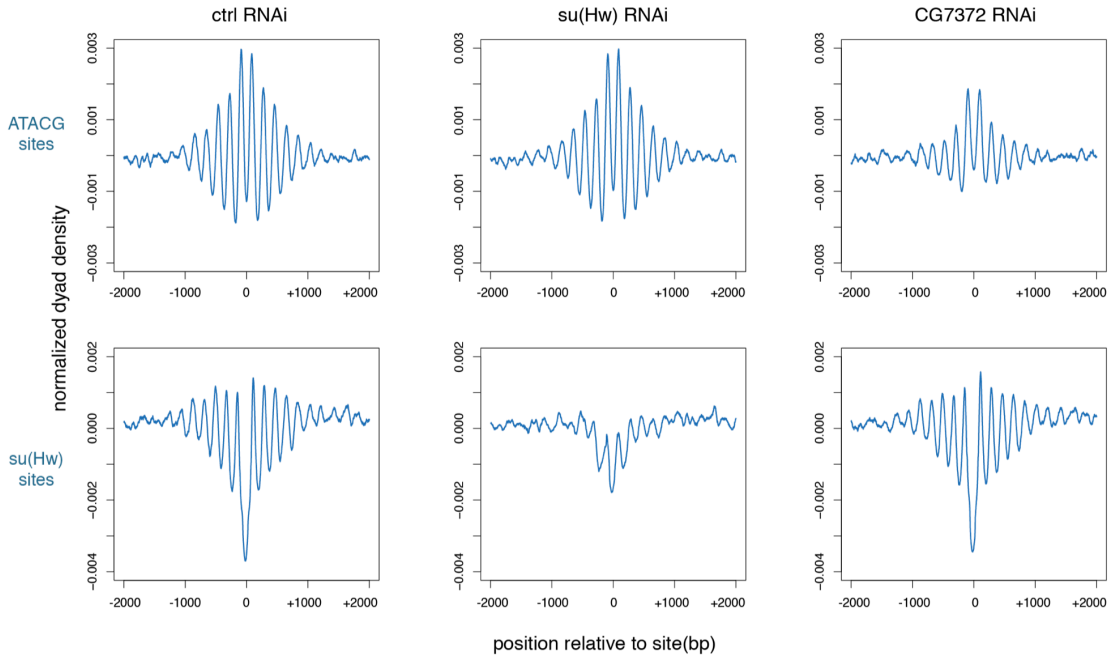

FIGURE 99: MNASE-SEQ PROFILES FROM *DROSOPHILA* SCHNEIDER CELLS AFTER KNOCK DOWN (KD) OF GST AS A CONTROL, AS WELL AS SU(HW) AND CG7372. READS AFTER MNASE-SEQ WERE ALIGNED TO THE ATACG SITES (TOP) OR TO SU(HW) BINDING SITES (BOTTOM) FIGURE FROM BALDI ET AL. 2018.

VII. DISCUSSION

A. DNA REPAIR IN *DROSOPHILA* EMBRYOS

Preblastoderm *Drosophila* embryos contain high levels of maternally deposited factors, which have the ability to reconstitute chromatin *in vitro* on recombinant DNA in presence of an ATP-regenerating buffer (Becker & Wu 1992). The *in vitro* chromatin assembly system has been useful to uncover novel principles once before; the nucleosome sliding factors NURF, CHRAC and ACF have been identified in it and purified from it (Tsukiyama & Wu 1995; Varga-Weisz et al. 1997; Ito et al. 1997). In this thesis, I applied this *in vitro* chromatin assembly approach to dissect processes at free DNA ends. I showed, that this system is able to recognize free DNA ends and to initiate a DNA damage response.

To efficiently repair DNA by NHEJ, the Ku complex and DNA-PKcs were shown to be essential to join and Lig4, Xrcc4, and Xlf to ligate the DNA ends in mammals. These factors are called the core factors, which are required for efficient DNA ligation *in vitro* (Ogiwara & Kohno 2011). Besides this, an alternative NHEJ pathway exists, also named microhomology-mediated end joining, which can occur in the absence of Ku and DNA-PK (Katsura et al. 2007). However, in this pathway, besides the presence of short homology stretches of a few base pairs, other factors are required, namely Fen1, Lig3, Mre11, Nbs1, Parp1 and Xrcc1 (Sharma et al. 2015). For HR, important factors in mammals are the MRN complex, CtIP, Exo1, Blm, and Dna2 (Liu & J. Huang 2016). In this *in vitro* system, I was able to identify Lig4, Fen1, Mre11, Nbs1 and Parp1 enriched at free ends. However, Xrcc4, Lig3, Xlf, Exo1, Dna2 and Xrcc1 were not identified in this study, even though these proteins exist in *Drosophila* (flybase.org, 05.06.2018). Furthermore, DNA-PKcs and CtIP have not been identified in *Drosophila*. Blm was shown to be required for HR in *Drosophila* (Adams et al. 2003). In our experiments, Blm was identified as an interactor with H2A.V nucleosomes (but not recruited to H2A.VΔC) but was not enriched at DNA breaks. It is possible that (the C-terminus of) H2A.V presents a recruitment platform of Blm but requires additional damage-associated factors to be stably recruited at the break site in *Drosophila*. In mammals, Blm was shown to be recruited in two phases, in an early phase together with the MRN complex, ATM, and γH2A.X and in a late phase with Xrcc4 and Rad51. Furthermore, recruitment of Blm was shown to be dependent on MRN and ATM (Tripathi et al. 2018). In our mass spec data, MRN was only enriched after 3 h and only showed a slight preference for free ends (which might be due to the damage reaction initiated by H2A.V phosphorylation on the fragment immobilized at both ends, discussed in VII.D). ATM (Tefu in *Drosophila*) was not enriched at breaks. In *Drosophila*, the recruitment of Blm is not yet well understood. However, it is possible, that in *Drosophila* Blm recruitment to breaks depends on ATM and MRN and was therefore not observed in our study.

In contrast to extracts obtained from *Drosophila*, *Xenopus* extracts are obtained from oocytes (Glikin et al. 1984). In addition, *Xenopus* extracts exhibit autonomous cell cycles (Hara et al. 1980; Blow & Laskey 1986; Hutchison et al. 1987; Murray & Kirschner 1989). *Drosophila* preblastodermal embryo extracts represent a combination of cell cycle states. These are in

particular M- and S-phase, as G-phases are omitted in the first cell divisions during *Drosophila* development (reviewed in Farrell & O'Farrell 2014). This implies that cell cycle-dependent processes like the DNA repair pathway choice cannot be reproduced in this *in vitro* system. Instead, it can be assumed, that combinations of repair processes occur in parallel, which would be separated *in vivo*. For example, resection performed as a step prior to HR is regulated by cyclin-dependent kinases (reviewed in Kakarougkas & Jeggo 2014; Aparicio et al. 2014; Chapman et al. 2012; Shibata 2017; Ceccaldi et al. 2016)). In mammals, it has been shown that the damage-associated complexes Ku and MRN are recruited to DSBs with in the first seconds to minutes (Aleksandrov et al. 2018; Kochan et al. 2017; G. Yang et al. 2018) and it has been shown that MRN and Ku can accumulate at the same break (Britton et al. 2013).

If DNA repair is accomplished by HR, Ku, which generally initiates the NHEJ pathway, is removed from DSBs by post-translational modification and proteasomal (K.-J. Lee et al. 2016; Shibata 2017). However, in our mass spectrometry analysis, we detected Ku associated to DNA for hours and additionally observed an enrichment of the ssDNA-binding protein RPA at the free ends, which is recruited to resected DNA during HR. This co-occupation of HR-and NHEJ-specific complexes at the same time suggests that the cell-cycle-dependent pathway choice is not accomplished in this *in vitro* system. Strikingly, Ku was shown to inhibit resection and is therefore believed to have a regulatory function in the initiation of resection (Mimitou & Symington 2010). However, if DNA end resection was inhibited by Ku, RPA binding would have been constrained. Nevertheless, it is possible, that instead of Ku dissociation, the postulated translocation of Ku away from the break allowed DNA end resection.

Preblastodermal *Drosophila* embryos undergo rapid cell divisions, with the first 14 cell divisions performed in about 1.5 hours. To achieve this, the cell cycle is shortened by omitting the gap phases and shortening the S phases (Farrell & O'Farrell 2014). Therefore, the processes have to be highly efficient and it could be assumed, that the cell does not spend much time on elaborate repair processes but eliminates nuclei affected by DNA damage via apoptosis.

Intriguingly, the H2A.V phosphorylation signal was not removed within the investigated time frames of up to six hours. It has been shown, that H2A.X phosphorylation persists if DSBs are not repaired (Chowdhury et al. 2005; Goodarzi et al. 2008; Eberlein et al. 2015). We therefore hypothesized, that DSBs were not efficiently repaired in this *in vitro* system. For this purpose, chromatin was assembled on linearized DNA fragments and purified for further analysis by gel electrophoresis and PCR. To answer this, I performed PCR-based experiments to identify ligation products after chromatin assembly on linearized DNA fragments. I then isolated the DNA and performed PCR reactions with primers flanking the break site and only amplifying after re-ligation of the linearized fragment. However, I was not able to detect an amplification product, either because ligation was not accomplished by the extract, or because resection of the free ends by the extract prevented primer annealing or amplification of the PCR product. Intriguingly, Lig4 was detected in our analysis and was reported to be highly flexible and able to detect DNA ends in any composition (Lieber 2010), but may be inactive in DREX. It has also been suggested that the removal of the H2A.X phosphorylation mark may signal the accomplishment of a certain repair step and to regulate the process of repair, instead of representing the successful repair (Keogh et al. 2006; Moon et al. 2010). Further work is

required to determine how far the repair process proceeds in the preblastoderm chromatin system.

B. THE ROLE OF KU IN THE DNA DAMAGE RESPONSE

Besides the MRN complex, Ku is an important DSB sensor and recruited to break sites within seconds (G. Yang et al. 2018; Aleksandrov et al. 2018), where it serves as a scaffold protein for other damage-associated proteins and helps to link broken DNA ends together. Furthermore, there is increasing evidence, that Ku also has functions in the regulation of the DNA damage response by influencing the activity of ATM or affecting apoptosis (reviewed in Fell & Schild-Poulter 2015). Ku was shown to be loaded onto DNA as a ring composed of the Ku70 and Ku80 subunits. However, how Ku is associated to DNA is not clear. One hypothesis, resulting from *in vitro* studies and the ring-shaped structure of Ku, suggests that Ku is loaded at the break and slides along DNA away from the break (de Vries et al. 1989; Walker et al. 2001). With this mechanism, sequential loading of several Ku proteins per break site would be possible. However, high-resolution immunofluorescence imaging in mammalian cells revealed, that only one Ku complex per break site is loaded and joined quickly to connect the DSB (Britton et al. 2013). To investigate the importance of Ku in the DNA damage response, I tried to deplete the extract from Ku by immunodepletion with monoclonal antibodies generated in this thesis or by incubating the extract with an excess of immobilized DNA fragments including free DNA ends.

However, both approaches were not efficient enough to remove considerable amounts of Ku from the extract. It was therefore not possible to investigate the Ku-dependence of processes in the DNA damage response. However, it has been shown in previous studies that Ku binding to DNA ends is required for the recruitment of many factors, like DNA-PKcs or Lig4, Xlf and Xrcc forming the ligase complex, or other proteins like Mdc1 or Nbs1 of the MRN complex or Parp1 (reviewed in Fell & Schild-Poulter 2015). In addition to this, Ku was shown to interact with Acf1 (Lan et al. 2010; Chiu et al. 2017).

It is likely that this interaction facilitates the recruitment of remodeling complexes to the DSB to remodel chromatin at the break site. The recruitment of chromatin remodelers to DSBs, which function in the sliding or eviction of nucleosomes, in the exchange of histones and its variants have been investigated in several studies (reviewed in Rother & van Attikum 2017; Jeggo et al. 2017). To investigate, if, due to this interaction, Acf1 is enriched at DSBs *in vitro*, I performed ChIP-qPCR analysis using monoclonal and polyclonal antibodies against the C-terminus of Acf1, but no enrichment of Acf1 at DNA ends was observed. However, ACF is highly abundant in the extract and only a fraction of approximately one sixth to one seventh is incorporated into chromatin. We therefore wondered, if this excess of Acf1 could conceal a possible specific recruitment and repeated the CHIP experiment after titration of DREX. With this approach, we observed a significant enrichment of Acf1 at DNA ends (500 bp and 1500 bp from the break, see Figure 78), but this observation was not reproducible with the polyclonal antibody, which only showed a minor enrichment. *In vivo*, Acf1 enrichment at breaks has been observed in mammals (Lan et al. 2010). It may be, that binding of Acf1 to DNA ends is not direct

but mediated through other proteins. However, Acf1 is known as a general nucleosome spacing factor (Jain, Baldi, Zabel, Straub & Becker 2015; Scacchetti et al. 2018) and is therefore presumably also recruited to interior sites away from DNA breaks.

Removal of Ku is mediated via ubiquitylation and degradation via the proteasome (Postow 2011; Brown et al. 2015). In our *in vitro* system, Ku remained associated to the DNA, as demonstrated by Western blot analysis. However, ChIP-Seq profiles revealed, that the accumulation of Ku in proximity to the break is no longer detectable after 3 h. This striking observation could be either due to a possible translocation of Ku away from the break site (see above) or due to decreased ChIP efficiencies after epitope-masking by ubiquitylation.

C. DNA END RESECTION AND THE INVESTIGATION OF SSDNA *IN VITRO*

In this thesis, I showed by ChIP-qPCR, that Ku can be detected at regions 500 bp away from the break site and ChIP-seq analysis confirmed a sharp peak of Ku at early time points (10 min after addition of DREX). This finding is in line with previous findings, showing that Ku forms sharp peaks at break sites (Britton et al. 2013). However, histones H3 and H2A.V decreased at these sites, suggesting that nucleosomes were removed by remodeling or eviction, which is in line with previous findings, showing that Ku binds to nucleosome-depleted regions (Britton et al. 2013).

It is also possible, that the loss of signal for H2A.V and H3 is due to the loss of DNA through nucleases in the extract that may degrade one DNA strand in reactions reminiscent of resection, or both strands. The wrapping of ssDNA around histone octamers has been observed *in* vitro (Palter et al. 1979; Adkins et al. 2017), but the existence of nucleosomes on ssDNA *in vivo* is still controversial (Adkins et al. 2017; T.-H. Huang et al. 2018).

Interestingly, I reproducibly identified the RPA complex specifically enriched at free ends after 3 h of incubation, but not after 15 min. A plausible explanation for this would be that nucleases in the extract resect the DNA ends, leading to the recruitment of RPA to the remaining ssDNA. The delayed enrichment of RPA at free ends indicates that this is a slow and maybe well controlled event, which serves the purpose to prepare the DNA ends for the homologous recombination repair pathway. Analysis of linearized purified DNA after assembly by gel electrophoresis also revealed a smear instead of a clear band, suggesting that DNA ends were processed by endogenous nucleases.

In line with this, ChIP-Seq data of input DNA after fragmentation with MNase or Covaris showed a loss of signal covering a region of 0.8-2 kb around the break site. Due to the nature of library preparation for DNA sequencing, where adapters are ligated to double-stranded DNA fragments only, signals can only be obtained from dsDNA, not from ssDNA. Possibly, the discrepancies between qPCR data of Ku, where signals were obtained 500 bp from the break, and sequencing data, where input signals are decreased at this area, can be explained by the differential detection of single-stranded DNA with either method. Therefore, it could also be possible, that the generation of ssDNA counteracts the existence of nucleosomes, but still

allows Ku to bind. However, it has been shown, that the affinity of Ku to ssDNA is much lower compared to dsDNA (Ono et al. 1994).

To test for the presence of ssDNA around the break sites, I purified chromatin from embryo extract and treated it with several ss-specific exonucleases, like Mung bean nuclease and ExoI. Afterwards, fragments were probed by PCR, only amplifying fragments, which were not targeted by the nucleases (dsDNA). With this approach, no difference compared to the input DNA before resection and therefore no enrichment of ssDNA around the break was identified. I then performed ChIP experiments after addition of recombinant RPA (kind gift from Christoph Kurat, BMC Munich), to isolate ssDNA. Again, no ssDNA was identified. In *Drosophila melanogaster*, 48 genes are annotated with the GO term 'single strand-binding', encoding for proteins like Brca2, subunits of DNApol-alpha, Ercc1, Rad50, Rad51, RPA, Xpc (mus201 in *Drosophila*), or Xrcc2 (flybase.org, 29.05.2018). Of those, I detected Rad50 and RPA at breaks and found mus201 generally associated with chromatin (but not at breaks) after *in vitro* reconstitution. Therefore, it may well be that these proteins shield the ssDNA and therefore prevent binding of RPA to DNA. To circumvent this problem, DNA was purified after incubation with DREX, fragmented with AluI, and incubated with recombinant RPA. However, ChIP using calmodulin-coupled beads to isolate the calmodulin-binding tag fused to RPA did not lead to the isolation of ssDNA fragments. However, due to the lack of true positive controls, I could not exclude that the RPA prep was non-functional under the applied conditions.

As an alternative approach, I used ApoI as a double-strand-specific nuclease (Langerak et al. 2011). Using amplicons consisting of either dsDNA or ssDNA, I was able to confirm the functionality and specificity of the enzyme. However, unexpectedly, no ssDNA could be detected. To sum up, ChIP data (ChIP-qPCR and ChIP-seq) as well as the detection of a single-strand-specific protein complex RPA support the hypothesis of DNA end resection, creating ssDNA around the break site. Experiments to specifically detect ssDNA did not confirm this observation. One possibility is that the data supporting the presence of ssDNA were misleading. Another possibility could be that ssDNA cannot be detected *in vitro*, due to secondary structures or other technical issues.

D. DETECTION OF DAMAGE-SPECIFIC CHANGES IN RECONSTITUTED CHROMATIN

To analyze chromatin-associated factors, recombinant DNA was immobilized to facilitate purification of chromatin after assembly *in vitro*. I tethered a linear plasmid either by one end (oeb) or at both ends (beb) through a biotin-streptavidin linkage, hoping that the tethered ends would be inaccessible to the DNA damage recognition system as described (Postow et al. 2008). While this was true for Ku binding, the beb chromatin still collected γH2A.V, showing that the end was still recognized. As a control for proteomic analysis one would ideally like to use a circular DNA. However, it was not possible to tag intact circular DNA for chromatin purification, as insertion of biotinylated nucleotides already resulted in the initiation of a DNA damage response, revealed by the phosphorylation of H2A.V. Other approaches to purify chromatin on circular plasmids were tried, for example isolation via GST-LexA using a plasmid with a LexA

binding site (Hamperl et al. 2014). However, isolation of chromatin with via GST-LexA was inefficient, either due to poor binding of LexA to its binding site or due to inefficient purification of GST-LexA on glutathione beads. Another approach was to immunopurify chromatin with antibodies against histones. However, this approach was also very inefficient, most likely due to the excess of a soluble histone pool competing for the incorporated histone pool. Precipitation of chromatin with $MgCl_2$ (Ritzi et al. 1998) or absorption to hydroxylapatite (Hilbrig & Freitag 2011) did not lead to the desired result as high protein concentrations in the extract led to enormous co-precipitation of proteins. Another approach tried was size-exclusion chromatography using columns prepared of Sephacryl from S-400 to S-1000. Chromatin reconstituted on plasmids exhibit a molecular weight of about 4 MDa (calculation performed on the assumption of 15 nucleosomes on a pUC18 plasmid of about 2.7 kb with 262 kDa per nucleosome (PlopperRensselaer Polytechnic Institute George Plopper 2014); no additional chromatin-associated proteins included). However, chromatin remodeling complexes are huge and have been shown to exhibit molecular weights in a similar range (e.g. Dom/Tip60 with > 2 MDa (Ruhf et al. 2001) leading to a vast amount of background, as judged from the control SEC lacking a chromatinized plasmid. Another limitation of this approach was the volume, which should not exceed 10% of the column volume for good resolution. Chromatin assembly reactions contain 1 µg DNA in 120 µL volume. It turned out that fractions containing the DNA did not contain sufficient concentrations of nucleosomes for further analysis by mass spectrometry, shown by Coomassie staining of gels containing the fractions of interest.

To summarize, it was not possible to isolate chromatin for mass spectrometry analysis in a way other than coupling via biotin-streptavidin linkage. This means, that it was not possible to generate a purified chromatin sample which did not induce H2A.V phosphorylation. However, this drawback allowed us to distinguish between a phosphorylation-dependent or a DNA end-dependent recruitment.

E. THE ROLE OF H2A.V PHOSPHORYLATION

The initial phosphorylation of H2A.X is performed by ATM, which is recruited by the DSB sensor complex MRN, or DNA-PK, which consists of the early DSB sensor complex Ku and DNA-PKcs (Barnum & O'Connell 2015; Kinner et al. 2008; J.-S. Kim et al. 2005). Phosphorylation of H2A.X is reported to be one of the first marks at DSBs and believed to serve as an anchor for DNA damage protein containing the BRCT domain, which recognizes phosphorylated proteins like γH2A.X (Kobayashi 2004). Examples for proteins with BRCT domains are Parp1, Brca1, 53BP1, Mdc1 or Nbs1 (Leung & Glover 2011). Indeed, Parp1 and Nbs1 were identified on *in vitro* reconstituted chromatin. Mdc1 (mu2 in *Drosophila*) is present in DREX but was not identified as a chromatin-associated factor, conceivably because it is recruited only transiently or in low stoichiometry (House et al. 2014; Blackford & Jackson 2017), also see Figure 8).

However, it has been shown in mammals, that in the absence of (phosphorylated) H2A.X, Nbs1, 53BP1 and Brca1 are still recruited to the break (Celeste, Fernandez-Capetillo, et al. 2003). In addition to this, Ku was also reported to be recruited to free DNA *in vitro* (Blier et al. 1993;

Downs & Jackson 2004; Radhakrishnan & Lees-Miller 2017; Anisenko et al. 2017), which is consistent with my observations, that Ku recruitment does not depend on histone modifications or variants. Therefore, it can be assumed that Ku recruitment does not depend on γH2A.V. For the other proteins, however, we were not able to address this question, as it was not possible to satisfactorily purify intact DNA without inducing the phosphorylation cascade (see above).

ATM was shown to be activated after addition of phospho-mimetic H2A.XE, a mutant, which mimics the phosphorylated form of H2A.X and can constitutively activate the DNA damage response (Kobayashi et al. 2009). To see, whether the phosphorylation mark is sufficient to trigger the initiation of the damage response including the spreading of H2A.V phosphorylation, we investigated the phosphorylation of nucleosome arrays on circular (undamaged) DNA, which consisted of nucleosomes bearing recombinant H2A.V mixed in increasing ratios with nucleosomes bearing the phospho-mimetic form of H2A.V (H2A.VE), after incubation with DREX. However, the H2A.V phosphorylation mimic provided as a 'seed' did not trigger the amplification of the signal by further H2A.V phosphorylation in the absence of free DNA (Figure 57). This may be because the phospho-mimetic form was not recognized as a damage signal, or because a component of the amplification cascade was lacking in our system. Even though the exchange of serine for negatively charged glutamic acid is a commonly employed to mimic phosphorylation in various systems (Kotova et al. 2011; Celeste, Difilippantonio, et al. 2003; Celeste, Fernandez-Capetillo, et al. 2003; Kobayashi et al. 2009), it is not clear, if the H2A.V phospho-mimetic form H2A.VE of *Drosophila* was recognized as a DNA damage signal mark by proteins in DREX. For example, Celeste et al showed, that BRCA1, 53BP1, and Nbs1 were not recruited to the sites of damage, when H2A.X was replaced by its mimetic form (Celeste, Difilippantonio, et al. 2003; Celeste, Fernandez-Capetillo, et al. 2003). It is possible, that the phosphorylation mark itself is not sufficient to trigger a complete damage response. On the other hand, it may be that the point mutation cannot entirely mimic the phosphorylation mark.

Inhibition of phosphorylation by wortmannin or the replacement of H2A.V by its C-terminally truncated form did not affect the recruitment levels of Ku. Ku binding occurs independently from H2A.V phosphorylation and even independent from H2A.V nucleosomes. Furthermore, H2A.V phosphorylation in the absence of free DNA ends did not lead to Ku recruitment. These findings are in line with the current literature, suggesting that Ku binding only depends on free DNA ends (Downs & Jackson 2004; G. Yang et al. 2018; Emerson et al. 2018; Radhakrishnan & Lees-Miller 2017). Our detailed investigation of post-translational histone modifications in nucleosomes including H2A.V or H2A.VΔC revealed the enrichment of some modifications depended on the H2A.V C terminus. These post-translational histone modifications usually serve as targets to recruit specific factors to chromatin, which can perform specific functions (reviewed in Rothbart & Strahl 2014; Yun et al. 2011; Musselman et al. 2012; Swygert & Peterson 2017). Mdc1, for example, recognizes and is recruited by phosphorylated H2A.X through its BRCT domain in mammals (Stucki et al. 2005). This recruitment is important for the spreading and amplification of the γH2A.X signal, as described in III.D.4 and VII.E. Other examples for histone modifications, which are recognized by readers are lysine methylations, which are recognized by proteins including domains like Tudor, Chromo, PHD, or WD40 (Yun et al. 2011). As an example, 53BP1 bears a Tudor domain, that can bind to methylated lysine 79

on histone H3 or to methylated lysine 20 on histone H4 at DSBs (Huyen et al. 2004; Iwabuchi et al. 2006).

Despite the lack of a general investigation on histone modifications in preblastodermal *Drosophila* embryos, epigenetic modifications are not expected to be highly abundant in early stages of development as they are believed to be erased to reset the epigenetic memory. As an example, heterochromatin is only established after the syncytial state and preblastoderm embryos only contain few modifications like acetylation marks on H3K27 and H4. (discussed in Lindeman et al. 2011; Sarmento et al. 2004; Zheng et al. 2016). In addition to this, methylation of H3K27 was shown to be maternally transmitted and can be detected in preblastoderm embryos (Zenk et al. 2017).

Methylation as well as acetylation on H3K9 was only detected at later stages (Yuan & B. Zhu 2012). Furthermore, the onset of dosage compensation including the acetylation of H4K16 only occurs after the syncytial state (Meller 2003). Therefore, it can be assumed that chromatin of preblastoderm embryos are not yet diversified and histone marks are not yet highly abundant. Accordingly, intensities identified for histone modifications in *in vitro* reconstituted chromatin were not high, but to our surprise, differences observed between different samples were highly reproducible among replicates. Sensitive mass spectrometrical analyses of our collaborator, Christian Feller (ETH Zurich) detected DNA damage-dependent histone modifications in addition to the C-terminal H2A.V phosphorylation, for example the methylation of H3 (H3K27me3, H3H36me2 and H3K9me3) in a time-resolved manner.

However, mass spectrometry analysis of factors recruited to nucleosomes consisting of H2A, H2A.V, or H2A.VΔC, however, did not reveal many specific interactors. It Is not clear, if this result is a consequence of high variability between replicates, leading to a low number of significant hits, or due to the nature of the extract, which might not be able to distinguish among the variants. The latter argument would be in line with the observation, that incorporation of H2A.V does not seem to be specific, as it has been described in Zhang & Pugh 2011). Parp1 is an important repair factor, which is recruited to sites of damage and deposits Poly-(ADP-ribose) units to decondense chromatin. The PARylation mark is recognized by proteins including macro domains, like the remodeler Alc1 (Ahel et al. 2009; Gottschalk et al. 2009). In *Drosophila*, Parp1 was shown to be recruited by H2A.V and becomes activated upon H2A.V phosphorylation (Kotova et al. 2011). In our studies, we were able to identify Parp1 by mass spectrometry on immobilized chromatin. However, using an anti-poly(ADP-ribose) antibody, which is commonly used in the field, no PARylation of *in vitro*-reconstituted chromatin was detected. A positive control reaction included Parp1, NAD as a substrate/coenzyme and DNA to activate the enzyme, leading to auto-PARylation of Parp1 (Dawicki-McKenna et al. 2015; Langelier et al. 2012; Steffen et al. 2016). We were able to detect PARylated Parp1 in our positive control, but no PARylation marks after *in vitro* assembly. We therefore speculated, that Parp1 was inactive in our system, despite the availability of (phosphorylated) H2A.V. It is possible, that the activity of Parp1 is regulated by different levels, preventing the PARylation of chromatin. As this step is a critical event In the DNA damage response, the lack of PARylation goes in line with our hypothesis, that DNA repair is not performed in this *in vitro* system.

F. The role of the Dom/Tip60 complex in H2A.V incorporation and turnover

Drosophila H2A.V combines features of mammalian H2A.Z and H2A.X and including functions of H2A.X in DNA damage signaling and of H2A.Z in promoter definition and the regulation of transcription (reviewed in Baldi & Becker 2013). To fulfill these functions, H2A.V should be distributed along the genome like H2A.X, to guard the genome, but also has to be specifically incorporated into promotor regions like H2A.Z. However, it is not clear, how the distinction between these two roles are accomplished.

In yeast and mammals, H2A.Z was shown to be removed from regions around the DSB by Ino80 (Papamichos-Chronakis et al. 2011; Alatwi & Downs 2015; Gursoy-Yuzugullu et al. 2015). In contrast to this, other studies in yeast and mammals observed incorporation of H2A.Z and H2A.X at break sites (Kalocsay et al. 2009; Horigome et al. 2014; Fukuto et al. 2018; Ikura et al. 2016). It therefore seems obvious, that H2A variants have an important role in the regulation of chromatin around DNA breaks. The following model to explain the function of H2A.Z has been proposed: First, H2A.Z is believed to be incorporated into chromatin around break sites by NuA4-Tip60 to bind the H4 tail of the nucleosome by the acidic patch of H2A.Z and prevent its acetylation to keep chromatin in a repressed state. Then, H2A.Z is removed by Ino80 and the H4 tail is released and acetylated by Tip60, which leads to a decondensation of chromatin to facilitate repair (Gursoy-Yuzugullu, House & Price 2016).

Strikingly, I observed an enrichment of H2A.V on DNA presenting a free end versus fragments where both ends were occluded by immobilization (Table 5). This could be in line with the model, suggesting the incorporation of H2A.V to trigger a repressed chromatin state, as it was already reported (Swaminathan 2005; Hanai et al. 2008). H2A.V enrichment at free ends was particularly high after 3 h, compared to the early time point of 15 min (Table 5, also see XI.B.2.a) and XI.B.2.b)). However according to the model described by Gursoy-Yuzugullu, the first condensation phase including H2A.Z incorporation is reported to be within the first minutes, and subsequently reversed by Ino80 (Gursoy-Yuzugullu, House & Price 2016), which was not reproduced in our analysis and may be explained our inability to detect Ino80 in our chromatin analyses. However, the mechanism as well as the responsible factors responsible for the incorporation of H2A.V were not identified.

As discussed in the previous chapters, Dom/Tip60 was reported to be vital for H2A.V incorporation and turnover (Kusch 2004; Lu et al. 2007; Kusch et al. 2014). In our lab, it has been shown that the different splice forms of Dom, DomA and DomB, have different functions in the incorporation or exchange of H2A.V. These functions are not redundant and specific mutants of either of the variants are embryonic lethal (Börner & Becker 2016). To disseminate the distinct functions of the splice forms, the study was performed in the *Drosophila* germarium with splice variant-specific knock down in different cells of oogenesis. With this approach, a DomB-dependent incorporation of H2A.V was demonstrated in germline and somatic cells, as well as a Dom-independent incorporation for endoreplicating germline nurse cells (Börner & Becker 2016). In contrast to this, removal of H2A.V was performed in a DomA-dependent manner from chromatin of nurse cells.

To follow up on these and other studies on the role of Dom/Tip60 (Kusch 2004; Lu et al. 2007; Kusch et al. 2014), I aimed to perform chromatin assembly reactions in the absence of Dom/Tip60. However, the Dom/Tip60 complex is essential and Dom mutants are not viable (Ruhf et al. 2001), precluding extract preparation of Dom/Tip60 mutants. In addition, immunodepletion of embryonic extract from Domino or Tip60 did not work efficiently, neither using antibodies against the protein itself nor using antibodies against tagged Domino, after preparation of extract from embryos homozygous for tagged Domino. Consequently, chromatin assembly reactions in the absence of Dom/Tip60 were not possible and I could not address the role of Dom/Tip60 in this system.

G. CONCLUDING EVALUATION OF THE *IN VITRO* SYSTEM TO INVESTIGATE DNA DAMAGE AND OUTLOOK

In this work, I demonstrated that damage-associated events can be reproduced in this *in vitro* system, making it a powerful tool to investigate the DNA damage response under defined conditions. However, some aspects were not solved due to technical issues, like the comparison of 'damaged' versus 'intact' chromatin, as isolation of chromatin without inducing H2A.V phosphorylation was not successful. Also, cell cycle- or transcription-dependent events or processes, which are not active in preblastoderm embryos cannot be investigated with this tool and might require additional approaches. Despite these drawbacks, many aspects were elucidated in this project, like the recruitment of chromatin remodelers in reconstituted chromatin, the identification of Acf1 interactors, as well as the role of Iswi remodeling complexes on chromatin reconstitution, the identification of H2A variant-specific chromatin interactors and the characterization of a DNA damage response by analyzing the recruitment of factors to free DNA ends, the H2A.V phosphorylation in response to DNA DSBs, and additional post-translational histone modifications around DNA breaks. As a conclusion, chromatin *in vitro* reconstitution with *Drosophila* embryo extract was proven to be a powerful tool to analyze chromatin changes upon recognition of DNA DSBs in a time- and locus-resolved manner. However, some questions remain to be addressed. For instance, in the field of damage recognition and repair, it is still unclear how γH2A.V spreading is performed. Also, can repair by this extract be performed after addition of missing factors? If yes, is it possible to influence the repair pathway? What is the mechanism of repair in cells lacking relevant factors like DNA-PK? Is Ku required? How is enrichment of Acf1 at DNA breaks achieved and what is its role? Is H2A.V specifically incorporated at DNA breaks? And if so, how is this information transmitted and which factors are relevant for this process? Furthermore, can the extract be supplemented with factors to specifically incorporate H2A.V at promotor regions?

Altogether, many aspects are still unsolved, and the potential of this extract can be challenged with more questions to be addressed in the future.

VIII. References

Adams, M.D., McVey, M. & Sekelsky, J.J., 2003. Drosophila BLM in double-strand break repair by synthesis-dependent strand annealing. *Science*, 299(5604), pp.265–267.

Adkins, N.L. et al., 2017. Nucleosome-like, Single-stranded DNA (ssDNA)-Histone Octamer Complexes and the Implication for DNA Double Strand Break Repair. *Journal of Biological Chemistry*, 292(13), pp.5271–5281.

Ahel, D. et al., 2009. Poly(ADP-ribose)-dependent regulation of DNA repair by the chromatin remodeling enzyme ALC1. *Science*, 325(5945), pp.1240–1243.

Alatwi, H.E. & Downs, J.A., 2015. Removal of H2A.Z by INO80 promotes homologous recombination. *EMBO reports*, 16(8), pp.986–994.

Alberts, B., 2017. *Molecular Biology of the Cell*, Garland Science.

Aleksandrov, R. et al., 2018. Protein Dynamics in Complex DNA Lesions. *Molecular Cell*, 69(6), pp.1046–1061.e5.

Almouzni, G. & Méchali, M., 1988. Assembly of spaced chromatin promoted by DNA synthesis in extracts from Xenopus eggs. *The EMBO Journal*, 7(3), pp.665–672.

Almouzni, G., Méchali, M. & Wolffe, A.P., 1990. Competition between transcription complex assembly and chromatin assembly on replicating DNA. *The EMBO Journal*, 9(2), pp.573–582.

American Association for Cancer Research Human Epigenome Task ForceEuropean Union, Network of Excellence, Scientific Advisory Board, 2008. Moving AHEAD with an international human epigenome project. *Nature*, 454(7205), pp.711–715.

Anisenko, A.N. et al., 2017. Human Ku70 protein binds hairpin RNA and double stranded DNA through two different sites. *Biochimie*, 132(C), pp.85–93.

Aparicio, T., Baer, R. & Gautier, J., 2014. DNA double-strand break repair pathway choice and cancer. *DNA Repair*, 19, pp.169–175.

Aydin, Ö.Z., Vermeulen, W. & Lans, H., 2014. ISWI chromatin remodeling complexes in the DNA damage response. *Cell Cycle*, 13(19), pp.3016–3025.

Ayrapetov, M.K. et al., 2014. DNA double-strand breaks promote methylation of histone H3 on lysine 9 and transient formation of repressive chromatin. *Proceedings of the National Academy of Sciences*, 111(25), pp.9169–9174.

Baldi, S. & Becker, P.B., 2013. The variant histone H2A.V of Drosophila—three roles, two guises. *Chromosoma*, 122(4), pp.245–258.

Baldi, S. et al., 2018. Genome-wide rules of nucleosome phasing. *bioRxiv*, pp.1–29.

Bao, Y., 2011. Chromatin response to DNA double-strand break damage. *Epigenomics*, 3(3), pp.307–321.

Barnum, K.J. & O'Connell, M.J., 2015. Molecular mechanisms involved in initiation of the DNA damage response. *Molecular & Cellular Oncology*, 2(1), p.e970065.

Becker, P.B. & Workman, J.L., 2013. Nucleosome remodeling and epigenetics. *Cold Spring Harbor perspectives in biology*, 5(9), p.a017905.

Becker, P.B. & Wu, C., 1992. Cell-free system for assembly of transcriptionally repressed chromatin from Drosophila embryos. *Molecular and Cellular Biology*, 12(5), pp.2241–2249.

Billon, P. & Côté, J., 2012. Biochimica et Biophysica Acta. *BBA - Gene Regulatory Mechanisms*, 1819(3-4), pp.290–302.

Blackford, A.N. & Jackson, S.P., 2017. ATM, ATR, and DNA-PK: The Trinity at the Heart of the DNA Damage Response. *Molecular Cell*, 66(6), pp.801–817.

Blier, P.R. et al., 1993. Binding of Ku protein to DNA. Measurement of affinity for ends and demonstration of binding to nicks. *Journal of Biological Chemistry*, 268(10), pp.7594–7601.

Blow, J.J. & Laskey, R.A., 1986. Initiation of DNA replication in nuclei and purified DNA by a cell-free extract of Xenopus eggs. *Cell*, 47(4), pp.577–587.

Bönisch, C. & Hake, S.B., 2012. Histone H2A variants in nucleosomes and chromatin: more or less stable? *Nucleic Acids Research*, 40(21), pp.10719–10741.

Böhmdorfer, G. & Wierzbicki, A.T., 2015. Control of Chromatin Structure by Long Noncoding RNA. *Trends in Cell Biology*, 25(10), pp.623–632.

Bönisch, C. et al., 2008. Chromatin proteomics and epigenetic regulatory circuits. *Expert Review of Proteomics*, 5(1), pp.105–119.

Börner, K. & Becker, P.B., 2016. Splice variants of the SWR1-type nucleosome remodeling factor Domino have distinct functions during Drosophila melanogaster oogenesis. *Development*, 143(17), pp.3154–3167.

Brahma, S. et al., 2017. INO80 exchanges H2A.Z for H2A by translocating on DNA proximal to histone dimers. *Nature Communications*, 8, pp.15616–12.

Brandsma, I. & Gent, D.C., 2012. Pathway choice in DNA double strand break repair: observations of a balancing act. *Genome Integrity*, 3(1), pp.1–1.

Britton, S., Coates, J. & Jackson, S.P., 2013. A new method for high-resolution imaging of Ku foci to decipher mechanisms of DNA double-strand break repair. *The Journal of Cell Biology*, 202(3), pp.579–595.

Brown, J.S. et al., 2015. Neddylation promotes ubiquitylation and release of Ku from DNA-damage sites. *CELREP*, 11(5), pp.704–714.

Buschbeck, M. & Hake, S.B., 2017. Variants of core histones and their roles in cell fate decisions, development and cancer. *Nature Publishing Group*, 18(5), pp.299–314.

Caridi, C.P. et al., 2018. Nuclear F-actin and myosins drive relocalization of heterochromatic breaks. *Nature*, 33, p.86.

Caridi, P.C. et al., 2017. And yet, it moves: nuclear and chromatin dynamics of a heterochromatic double-strand break. *Philosophical Transactions of the Royal Society B: Biological Sciences*, 372(1731), pp.20160291–14.

Caron, P. et al., 2012. Cohesin Protects Genes against γH2AX Induced by DNA Double-Strand Breaks M. Grelon, ed. *PLoS Genetics*, 8(1), pp.e1002460–17.

Ceccaldi, R., Rondinelli, B. & D'Andrea, A.D., 2016. Repair Pathway Choices and Consequences at the Double-Strand Break. *Trends in Cell Biology*, 26(1), pp.52–64.

Celeste, A., Difilippantonio, S., et al., 2003. H2AX Haploinsufficiency Modifies Genomic Stability and Tumor Susceptibility. *Cell*, 114(3), pp.371–383.

Celeste, A., Fernandez-Capetillo, O., et al., 2003. Histone H2AX phosphorylation is dispensable for the initial recognition of DNA breaks. *Nature Cell Biology*, 5(7), pp.675–679.

Chailleux, C. et al., 2010. Physical interaction between the histone acetyl transferase Tip60 and the DNA double-strand breaks sensor MRN complex. *Biochemical Journal*, 426(3), pp.365–371.

Chakravarthy, S. et al., 2004. Structural Characterization of Histone H2A Variants. *Cold Spring Harbor Symposia on Quantitative Biology*, 69(0), pp.227–234.

Chang, H.H.Y. et al., 2017. Non-homologous DNA end joining and alternative pathways to double-strand break repair. *Nature Publishing Group*, 18(8), pp.495–506.

Chapman, J.R., Taylor, M.R.G. & Boulton, S.J., 2012. Playing the End Game: DNA Double-Strand Break Repair Pathway Choice. *Molecular Cell*, 47(4), pp.497–510.

Chioda, M. et al., 2010. Developmental role for ACF1-containing nucleosome remodellers in chromatin organisation. *Development*, 137(20), pp.3513–3522.

Chiolo, I. et al., 2011. Double-Strand Breaks in Heterochromatin Move Outside of a Dynamic HP1a Domain to Complete Recombinational Repair. *Cell*, 144(5), pp.732–744.

Chiu, L.-Y., Gong, F. & Miller, K.M., 2017. Bromodomain proteins: repairing DNA damage within chromatin. *Philosophical Transactions of the Royal Society B: Biological Sciences*, 372(1731), pp.20160286–12.

Chowdhury, D. et al., 2005. γ-H2AX Dephosphorylation by Protein Phosphatase 2A Facilitates DNA Double-Strand Break Repair. *Molecular Cell*, 20(5), pp.801–809.

Ciccia, A. & Elledge, S.J., 2010. The DNA Damage Response: Making It Safe to Play with Knives. *Molecular Cell*, 40(2), pp.179–204.

Clapier, C.R. & Cairns, B.R., 2009. The Biology of Chromatin Remodeling Complexes. *Annual Review of Biochemistry*, 78(1), pp.273–304.

Clarkson, M.J. et al., 1999. Regions of variant histone His2AvD required for Drosophila development. *Nature*, 399(6737), pp.694–697.

Costelloe, T. et al., 2012. The yeast Fun30 and human SMARCAD1 chromatin remodellers promote DNA end resection. *Nature*, 489(7417), pp.581–584.

Cutter, A.R. & Hayes, J.J., 2015. A brief review of nucleosome structure. *FEBS Letters*, 589(20 Pt A), pp.2914–2922.

Dawicki-McKenna, J.M. et al., 2015. PARP-1 Activation Requires Local Unfolding of an Autoinhibitory Domain. *Molecular Cell*, 60(5), pp.755–768.

De Bont, R., 2004. Endogenous DNA damage in humans: a review of quantitative data. *Mutagenesis*, 19(3), pp.169–185.

de Vries, E. et al., 1989. HeLa nuclear protein recognizing DNA termini and translocating on DNA forming a regular DNA-multimeric protein complex. *Journal of Molecular Biology*, 208(1), pp.65–78.

de Wit, E. & de Laat, W., 2012. A decade of 3C technologies: insights into nuclear organization. *Genes & Development*, 26(1), pp.11–24.

Denker, A. & de Laat, W., 2016. The second decade of 3C technologies: detailed insights into nuclear organization. *Genes & Development*, 30(12), pp.1357–1382.

Dhar, S. et al., 2017. The tale of a tail: histone H4 acetylation and the repair of DNA breaks. *Philosophical Transactions of the Royal Society B: Biological Sciences*, 372(1731), p.20160284.

Dickinson, B.C. & Chang, C.J., 2011. Chemistry and biology of reactive oxygen species in signaling or stress responses. *Nature Chemical Biology*, 7(8), pp.504–511.

Dixon, J.R., Gorkin, D.U. & Ren, B., 2016. Chromatin Domains: The Unit of Chromosome Organization. *Molecular Cell*, 62(5), pp.668–680.

Do, A.T. et al., 2014. Double-Strand Break Repair Assays Determine Pathway Choice and Structure of Gene Conversion Events in Drosophila melanogaster. *G3: Genes, Genomes, Genetics*, 4(3), pp.425–432.

Doil, C. et al., 2009. RNF168 Binds and Amplifies Ubiquitin Conjugates on Damaged Chromosomes to Allow Accumulation of Repair Proteins. *Cell*, 136(3), pp.435–446.

Dorafshan, E., Kahn, T.G. & Schwartz, Y.B., 2017. Hierarchical recruitment of Polycomb complexes revisited. *Nucleus*, 8(5), pp.496–505.

Downs, J.A. & Jackson, S.P., 2004. A means to a DNA end: the many roles of Ku. *Nature Reviews Molecular Cell Biology*, 5(5), pp.367–378.

Earnshaw, W.C. et al., 1980. Assembly of nucleosomes: the reaction involving X. laevis nucleoplasmin. *Cell*, 21(2), pp.373–383.

Eberharter, A. et al., 2001. Acf1, the largest subunit of CHRAC, regulates ISWI-induced nucleosome remodelling. *The EMBO Journal*, 20(14), pp.3781–3788.

Eberlein, U. et al., 2015. Calibration of the γ-H2AX DNA double strand break focus assay for internal radiation exposure of blood lymphocytes. *PLoS ONE*, 10(4), p.e0123174.

Ejsmont, R.K. et al., 2009. A toolkit for high-throughput, cross- species gene engineering in Drosophila. *Nature Publishing Group*, 6(6), pp.435–437.

Emerson, C.H. et al., 2018. Ku DNA End-Binding Activity Promotes Repair Fidelity and Influences End-Processing During Nonhomologous End-Joining in Saccharomyces cerevisiae. *Genetics*, 209(1), pp.115–128.

Erdel, F., 2017. How Communication Between Nucleosomes Enables Spreading and Epigenetic Memory of Histone Modifications. *BioEssays*, 33, p.1700053.

Erdel, F. & Greene, E.C., 2016. Generalized nucleation and looping model for epigenetic memory of histone modifications. *Proceedings of the National Academy of Sciences of the United States of America*, 113(29), pp.E4180–9.

Erdel, F. & Rippe, K., 2012. Quantifying transient binding of ISWI chromatin remodelers in living cells by pixel-wise photobleaching profile evolution analysis. *Proceedings of the National Academy of Sciences*, 109(47), pp.E3221–E3230.

Farrell, J.A. & O'Farrell, P.H., 2014. From Egg to Gastrula: How the Cell Cycle Is Remodeled During the DrosophilaMid-Blastula Transition. *Annual review of genetics*, 48(1), pp.269–294.

Fei, J. et al., 2015. The prenucleosome, a stable conformational isomer of the nucleosome. *Genes & Development*, 29(24), pp.2563–2575.

Fell, V.L. & Schild-Poulter, C., 2015. The Ku heterodimer: function in DNA repair and beyond. *Mutation Research-Reviews in Mutation Research*, 763, pp.15–29.

Filion, G.J., van Bemmel, J.G., Braunschweig, U., Talhout, W., Kind, J., Ward, L.D., Brugman, W., de Castro, I.J., Kerkhoven, R.M., Bussemaker, H.J. & van Steensel, B., 2010. Systematic protein location mapping reveals five principal chromatin types in Drosophila cells. *Cell*, 143(2), pp.212–224.

Fnu, S. et al., 2011. Methylation of histone H3 lysine 36 enhances DNA repair by nonhomologous end-joining. *Proceedings of the National Academy of Sciences of the United States of America*, 108(2), pp.540–545.

Fu, Y. et al., 2008. The insulator binding protein CTCF positions 20 nucleosomes around its binding sites across the human genome. *PLoS Genetics*, 4(7), p.e1000138.

Fukuto, A. et al., 2018. SUMO modification system facilitates the exchange of histone variant H2A.Z-2 at DNA damage sites. pp.1–9.

Furey, T.S., 2012. ChIP–seq and beyond: new and improved methodologies to detect and characterize protein–DNA interactions. *Nature Reviews Genetics*, 13(12), pp.840–852.

Fyodorov, D.V. & Kadonaga, J.T., 2002. Binding of Acf1 to DNA Involves a WAC Motif and Is Important for ACF-Mediated Chromatin Assembly. *Molecular and Cellular Biology*, 22(18), pp.6344–6353.

Fyodorov, D.V. et al., 2004. Acf1 confers unique activities to ACF/CHRAC and promotes the formation rather than disruption of chromatin in vivo. *Genes & Development*, 18(2), pp.170–183.

Gaillard, P.H. et al., 1997. Initiation and bidirectional propagation of chromatin assembly from a target site for nucleotide excision repair. *The EMBO Journal*, 16(20), pp.6281–6289.

Georgoulis, A. et al., 2017. Genome Instability and γH2AX. *International Journal of Molecular Sciences*, 18(9), p.1979.

Gilbert, N., Gilchrist, S. & Bickmore, W.A., 2005. Chromatin organization in the mammalian nucleus. *International review of cytology*, 242, pp.283–336.

Gillet, L.C. et al., 2012. Targeted data extraction of the MS/MS spectra generated by data-independent acquisition: a new concept for consistent and accurate proteome analysis. *Molecular & cellular proteomics : MCP*, 11(6), p.O111.016717.

Glikin, G.C., Ruberti, I. & Worcel, A., 1984. Chromatin assembly in Xenopus oocytes: in vitro studies. *Cell*, 37(1), pp.33–41.

Goldstein, M. et al., 2013. Nucleolin mediates nucleosome disruption critical for DNA double-strand break repair. *Proceedings of the National Academy of Sciences of the United States of America*, 110(42), pp.16874–16879.

Goodarzi, A.A. et al., 2008. ATM signaling facilitates repair of DNA double-strand breaks associated with heterochromatin. *Molecular Cell*, 31(2), pp.167–177.

Gottschalk, A.J. et al., 2009. Poly(ADP-ribosyl)ation directs recruitment and activation of an ATP-dependent chromatin remodeler. *Proceedings of the National Academy of Sciences of the United States of America*, 106(33), pp.13770–13774.

Gruber, S. & Errington, J., 2009. Recruitment of Condensin to Replication Origin Regions by ParB/SpoOJ Promotes Chromosome Segregation in B. subtilis. *Cell*, 137(4), pp.685–696.

Gursoy-Yuzugullu, O., Ayrapetov, M.K. & Price, B.D., 2015. Histone chaperone Anp32e removes H2A.Z from DNA double-strand breaks and promotes nucleosome reorganization and DNA repair. *Proceedings of the National Academy of Sciences*, 112(24), pp.7507–7512.

Gursoy-Yuzugullu, O., House, N. & Price, B.D., 2016. Patching Broken DNA: Nucleosome Dynamics and the Repair of DNA Breaks. *Journal of Molecular Biology*, 428(9), pp.1846–1860.

Guruharsha, K.G. et al., 2011. A Protein Complex Network of Drosophila melanogaster. *Cell*, 147(3), pp.690–703.

Hamperl, S. et al., 2014. Compositional and structural analysis of selected chromosomal domains from Saccharomyces cerevisiae. *Nucleic Acids Research*, 42(1), pp.e2–e2.

Hanai, K. et al., 2008. RSF Governs Silent Chromatin Formation via Histone H2Av Replacement A. Akhtar, ed. *PLoS Genetics*, 4(2), pp.e1000011–15.

Hansen, A.S. et al., 2018. Recent evidence that TADs and chromatin loops are dynamic structures. pp.1–14.

Hara, K., Tydeman, P. & Kirschner, M., 1980. A cytoplasmic clock with the same period as the division cycle in Xenopus eggs. *Proceedings of the National Academy of Sciences*, 77(1), pp.462–466.

Hartlerode, A.J. et al., 2012. Impact of Histone H4 Lysine 20 Methylation on 53BP1 Responses to Chromosomal Double Strand Breaks Z. Zhou, ed. *PLoS ONE*, 7(11), pp.e49211–11.

Hilbrig, F. & Freitag, R., 2011. Isolation and purification of recombinant proteins, antibodies and plasmid DNA with hydroxyapatite chromatography. *Biotechnology Journal*, 7(1), pp.90–102.

Hiom, K., 2010. Coping with DNA double strand breaks. *DNA Repair*, 9(12), pp.1256–1263.

Hogan, C. & Varga-Weisz, P., 2007. The regulation of ATP-dependent nucleosome remodelling factors. *Mutation Research/Fundamental and Molecular Mechanisms of Mutagenesis*, 618(1-2), pp.41–51.

Horigome, C. et al., 2014. SWR1 and INO80 Chromatin Remodelers Contribute to DNA Double-Strand Break Perinuclear Anchorage Site Choice. *Molecular Cell*, 55(4), pp.626–639.

House, N.C.M., Koch, M.R. & Freudenreich, C.H., 2014. Chromatin modifications and DNA repair: beyond double-strand breaks. *Frontiers in Genetics*, 5(2084), pp.15966–18.

Huang, T.-H. et al., 2018. The Histone Chaperones ASF1 and CAF-1 Promote MMS22L-TONSL-Mediated Rad51 Loading onto ssDNA during Homologous Recombination in Human Cells. *Molecular Cell*, 69(5), pp.879–892.e5.

Huen, M.S.Y. et al., 2007. RNF8 Transduces the DNA-Damage Signal via Histone Ubiquitylation and Checkpoint Protein Assembly. *Cell*, 131(5), pp.901–914.

Hutchison, C.J. et al., 1987. Periodic DNA synthesis in cell-free extracts of Xenopus eggs. *The EMBO Journal*, 6(7), pp.2003–2010.

Huyen, Y. et al., 2004. Methylated lysine 79 of histone H3 targets 53BP1 to DNA double-strand breaks. *Nature*, 432(7015), pp.406–411.

Iacovoni, J.S. et al., 2010. High-resolution profiling of γH2AX around DNA double strand breaks in the mammalian genome. *The EMBO Journal*, pp.1–12.

Ikura, M. et al., 2016. Coordinated Regulation of TIP60 and Poly(ADP-Ribose) Polymerase 1 in Damaged-Chromatin Dynamics. *Molecular and Cellular Biology*, 36(10), pp.1595–1607.

Ito, T. et al., 1999. ACF consists of two subunits, Acf1 and ISWI, that function cooperatively in the ATP-dependent catalysis of chromatin assembly. *Genes & Development*, 13(12), pp.1529–1539.

Ito, T. et al., 1997. ACF, an ISWI-containing and ATP-utilizing chromatin assembly and remodeling factor. *Cell*, 90(1), pp.145–155.

Ito, T. et al., 1996. Drosophila NAP-1 is a core histone chaperone that functions in ATP-facilitated assembly of regularly spaced nucleosomal arrays. *Molecular and Cellular Biology*, 16(6), pp.3112–3124.

Iwabuchi, K. et al., 2006. 53BP1 contributes to survival of cells irradiated with X-ray during G1 without Ku70 or Artemis. *Genes to cells : devoted to molecular & cellular mechanisms*, 11(8), pp.935–948.

Jain, D., Baldi, S., Zabel, A., Straub, T. & Becker, P.B., 2015. Active promoters give rise to false positive "Phantom Peaks" in ChIP-seq experiments. *Nucleic Acids Research*, 43(14), pp.6959–6968.

Jeggo, P.A., Downs, J.A. & Gasser, S.M., 2017. Chromatin modifiers and remodellers in DNA repair and signalling. *Philosophical transactions of the Royal Society of London. Series B, Biological sciences*, 372(1731), p.20160279.

Jin, Y. et al., 1999. JIL-1: a novel chromosomal tandem kinase implicated in transcriptional regulation in Drosophila. *Molecular Cell*, 4(1), pp.129–135.

Jorgensen, S., Schotta, G. & Sorensen, C.S., 2013. Histone H4 Lysine 20 methylation: key player in epigenetic regulation of genomic integrity. *Nucleic Acids Research*, 41(5), pp.2797–2806.

Jost, D. & Vaillant, C., 2018. Epigenomics in 3D: importance of long-range spreading and specific interactions in epigenomic maintenance. *Nucleic Acids Research*, 46(5), pp.2252–2264.

Joyce, E.F. et al., 2011. Drosophila ATM and ATR have distinct activities in the regulation of meiotic DNA damage and repair. *The Journal of Cell Biology*, 195(3), pp.359–367.

Kakarougkas, A. & Jeggo, P.A., 2014. DNA DSB repair pathway choice: an orchestrated handover mechanism. *The British Journal of Radiology*, 87(1035), pp.20130685–8.

Kalocsay, M., Hiller, N.J. & Jentsch, S., 2009. Chromosome-wide Rad51 Spreading and SUMO-H2A.Z-Dependent Chromosome Fixation in Response to a Persistent DNA Double-Strand Break. *Molecular Cell*, 33(3), pp.335–343.

Kassis, J.A., Kennison, J.A. & Tamkun, J.W., 2017. Polycomb and Trithorax Group Genes in Drosophila. *Genetics*, 206(4), pp.1699–1725.

Katsura, Y. et al., 2007. Involvement of Ku80 in microhomology-mediated end joining for DNA double-strand breaks in vivo. *DNA Repair*, 6(5), pp.639–648.

Keller, W., 1975. Characterization of purified DNA-relaxing enzyme from human tissue culture cells. *Proceedings of the National Academy of Sciences*, 72(7), pp.2550–2554.

Keogh, M.-C. et al., 2006. A phosphatase complex that dephosphorylates γH2AX regulates DNA damage checkpoint recovery. *Nature*, 439(7075), pp.497–501.

Khorasanizadeh, S., 2004. The nucleosome: from genomic organization to genomic regulation. *Cell*, 116(2), pp.259–272.

Khuong, M.T. et al., 2017. A simple and versatile system for the ATP-dependent assembly of chromatin. *Journal of Biological Chemistry*, 292(47), pp.19478–19490.

Kim, J.-A. et al., 2007. Heterochromatin is refractory to gamma-H2AX modification in yeast and mammals. *The Journal of Cell Biology*, 178(2), pp.209–218.

Kim, J.-S. et al., 2005. Independent and sequential recruitment of NHEJ and HR factors to DNA damage sites in mammalian cells. *The Journal of Cell Biology*, 170(3), pp.341–347.

Kim, S.-T., Xu, B. & Kastan, M.B., 2002. Involvement of the cohesin protein, Smc1, in Atm-dependent and independent responses to DNA damage. *Genes & Development*, 16(5), pp.560–570.

Kinner, A. et al., 2008. Gamma-H2AX in recognition and signaling of DNA double-strand breaks in the context of chromatin. *Nucleic Acids Research*, 36(17), pp.5678–5694.
Klinker, H., Haas, C., et al., 2014. Rapid Purification of Recombinant Histones A. Dean, ed. *PLoS ONE*, 9(8), p.e104029.
Klinker, H., Mueller-Planitz, F., et al., 2014. ISWI remodelling of physiological chromatin fibres acetylated at lysine 16 of histone H4. *PLoS ONE*, 9(2), p.e88411.
Kobayashi, J., 2004. Molecular mechanism of the recruitment of NBS1/hMRE11/hRAD50 complex to DNA double-strand breaks: NBS1 binds to gamma-H2AX through FHA/BRCT domain. *Journal of radiation research*, 45(4), pp.473–478.
Kobayashi, J. et al., 2009. Histone H2AX participates the DNA damage-induced ATM activation through interaction with NBS1. *Biochemical and Biophysical Research Communications*, 380(4), pp.752–757.
Kobor, M.S. et al., 2004. A Protein Complex Containing the Conserved Swi2/Snf2-Related ATPase Swr1p Deposits Histone Variant H2A.Z into Euchromatin Peter Becker, ed. *PLoS Biology*, 2(5), pp.e131–13.
Kochan, J.A. et al., 2017. Meta-analysis of DNA double-strand break response kinetics. *Nucleic Acids Research*, 45(22), pp.12625–12637.
Kolas, N.K. et al., 2007. Orchestration of the DNA-damage response by the RNF8 ubiquitin ligase. *Science*, 318(5856), pp.1637–1640.
Kornberg, R.D., 1974. Chromatin structure: a repeating unit of histones and DNA. *Science*, 184(4139), pp.868–871.
Kotova, E. et al., 2011. Drosophila histone H2A variant (H2Av) controls poly(ADP-ribose) polymerase 1 (PARP1) activation in chromatin. *Proceedings of the National Academy of Sciences*, 108(15), pp.6205–6210.
Krude, T. & Knippers, R., 1993. Nucleosome assembly during complementary DNA strand synthesis in extracts from mammalian cells. *Journal of Biological Chemistry*, 268(19), pp.14432–14442.
Krude, T., de Maddalena, C. & Knippers, R., 1993. A nucleosome assembly factor is a constituent of simian virus 40 minichromosomes. *Molecular and Cellular Biology*, 13(2), pp.1059–1068.
Kusch, T., 2004. Acetylation by Tip60 Is Required for Selective Histone Variant Exchange at DNA Lesions. *Science*, 306(5704), pp.2084–2087.
Kusch, T., Mei, A. & Nguyen, C., 2014. Histone H3 lysine 4 trimethylation regulates cotranscriptional H2A variant exchange by Tip60 complexes to maximize gene expression. *Proceedings of the National Academy of Sciences*, 111(13), pp.4850–4855.
Lademann, C.A. et al., 2017. The INO80 Complex Removes H2A.Z to Promote Presynaptic Filament Formation during Homologous Recombination. *Cell Reports*, 19(7), pp.1294–1303.
Lake, C.M. et al., 2013. The development of a monoclonal antibody recognizing the Drosophila melanogaster phosphorylated histone H2A variant (γ-H2AV). *G3: Genes, Genomes, Genetics*, 3(9), pp.1539–1543.
Lan, L. et al., 2010. The ACF1 Complex Is Required for DNA Double-Strand Break Repair in Human Cells. *Molecular Cell*, 40(6), pp.976–987.
Langelier, M.-F. et al., 2012. Structural basis for DNA damage-dependent poly(ADP-ribosyl)ation by human PARP-1. *Science*, 336(6082), pp.728–732.
Langerak, P. et al., 2011. Release of Ku and MRN from DNA Ends by Mre11 Nuclease Activity and Ctp1 Is Required for Homologous Recombination Repair of Double-Strand Breaks G. P. Copenhaver, ed. *PLoS Genetics*, 7(9), pp.e1002271–15.
LaRocque, J.R. et al., 2007. Drosophila ATR in double-strand break repair. *Genetics*, 175(3), pp.1023–1033.
Laskey, R.A. & Earnshaw, W.C., 1980. Nucleosome assembly. *Nature*, 286(5775), pp.763–767.

Laskey, R.A., Mills, A.D. & Morris, N.R., 1977. Assembly of SV40 chromatin in a cell-free system from Xenopus eggs. *Cell*, 10(2), pp.237–243.

Latrick, C.M. et al., 2016. Molecular basis and specificity of H2A.Z–H2B recognition and deposition by the histone chaperone YL1. *Nature Structural & Molecular Biology*, 23(4), pp.309–316.

Längst, G. & Becker, P.B., 2001. ISWI induces nucleosome sliding on nicked DNA. *Molecular Cell*, 8(5), pp.1085–1092.

Leach, T.J. et al., 2000. Histone H2A.Z Is Widely but Nonrandomly Distributed in Chromosomes of Drosophila melanogaster. *Journal of Biological Chemistry*, 275(30), pp.23267–23272.

Lee, C.-S. et al., 2014. Dynamics of yeast histone H2A and H2B phosphorylation in response to a double-strand break. *Nature Structural & Molecular Biology*, 21(1), pp.103–109.

Lee, K.-J. et al., 2016. Phosphorylation of Ku dictates DNA double-strand break (DSB) repair pathway choice in S phase. *Nucleic Acids Research*, 44(4), pp.1732–1745.

Lee, S.-H. & Kim, C.-H., 2002. DNA-dependent protein kinase complex: a multifunctional protein in DNA repair and damage checkpoint. *Molecules and cells*, 13(2), pp.159–166.

Leung, C.C.Y. & Glover, J.N.M., 2011. BRCT domains: easy as one, two, three. *Cell Cycle*, 10(15), pp.2461–2470.

Li, J. et al., 2012. Regulation of budding yeast mating-type switching donor preference by the FHA domain of Fkh1. *PLoS Genetics*, 8(4), p.e1002630.

Li, X. et al., 2010. MOF and H4 K16 Acetylation Play Important Roles in DNA Damage Repair by Modulating Recruitment of DNA Damage Repair Protein Mdc1. *Molecular and Cellular Biology*, 30(22), pp.5335–5347.

Li, Z. et al., 2012. Lipid Droplets Control the Maternal Histone Supply of Drosophila Embryos. *Current Biology*, 22(22), pp.2104–2113.

Li, Z. et al., 2017. Drosophila Lipid Droplets Buffer the H2Av Supply to Protect Early Embryonic Development. *Current Biology*, pp.1–7.

Liang, X. et al., 2016. Structural basis of H2A.Z recognition by SRCAP chromatin-remodeling subunit YL1. *Nature Structural & Molecular Biology*, 23(4), pp.317–323.

Lieber, M.R., 2010. The Mechanism of Double-Strand DNA Break Repair by the Nonhomologous DNA End-Joining Pathway. *Annual Review of Biochemistry*, 79(1), pp.181–211.

Lindeman, L.C. et al., 2011. Prepatterning of developmental gene expression by modified histones before zygotic genome activation. *Developmental Cell*, 21(6), pp.993–1004.

Liptak, C. & Loria, J.P., 2015. Movement and Specificity in a Modular DNA Binding Protein. *Structure (London, England : 1993)*, 23(6), pp.973–974.

Liu, T. & Huang, J., 2016. DNA End Resection: Facts and Mechanisms. *Genomics, Proteomics & Bioinformatics*, 14(3), pp.126–130.

Lowary, P.T. & Widom, J., 1998. New DNA sequence rules for high affinity binding to histone octamer and sequence-directed nucleosome positioning. *Journal of Molecular Biology*, 276(1), pp.19–42.

Lu, J. et al., 2007. A genome-wide RNA interference screen identifies putative chromatin regulators essential for E2F repression. *Proceedings of the National Academy of Sciences*, 104(22), pp.9381–9386.

Luger, K. et al., 1997. Crystal structure of the nucleosome core particle at 2.8 A resolution. *Nature*, 389(6648), pp.251–260.

Luger, K., Dechassa, M.L. & Tremethick, D.J., 2012. New insights into nucleosome and chromatin structure: an ordered state or a disordered affair? *Nature Publishing Group*, 13(7), pp.436–447.

Luijsterburg, M.S. & van Attikum, H., 2011. Chromatin and the DNA damage response: The cancer connection J. Bartek, ed. *Molecular Oncology*, 5(4), pp.349–367.

Luk, E. et al., 2010. Stepwise Histone Replacement by SWR1 Requires Dual Activation with Histone H2A.Z and Canonical Nucleosome. *Cell*, 143(5), pp.725–736.
Madigan, J.P., Chotkowski, H.L. & Glaser, R.L., 2002. DNA double-strand break-induced phosphorylation of Drosophila histone variant H2Av helps prevent radiation-induced apoptosis. *Nucleic Acids Research*, 30(17), pp.3698–3705.
Mahowald, A.P. & Hardy, P.A., 1985. Genetics of Drosophila embryogenesis. *Annual review of genetics*, 19(1), pp.149–177.
Maier, V.K. et al., 2008. ACF catalyses chromatosome movements in chromatin fibres. *The EMBO Journal*, 27(6), pp.817–826.
Mailand, N. et al., 2007. RNF8 Ubiquitylates Histones at DNA Double-Strand Breaks and Promotes Assembly of Repair Proteins. *Cell*, 131(5), pp.887–900.
Marin-Vicente, C. et al., 2015. RRP6/EXOSC10 is required for the repair of DNA double-strand breaks by homologous recombination. *Journal of Cell Science*, 128(6), pp.1097–1107.
Massip, L. et al., 2010. Deciphering the chromatin landscape induced around DNA double strand breaks. *Cell Cycle*, 9(15), pp.3035–3044.
Mavrich, T.N. et al., 2008. Nucleosome organization in the Drosophila genome. *Nature*, 453(7193), pp.358–362.
Meller, V.H., 2003. Initiation of dosage compensation in Drosophila embryos depends on expression of the roX RNAs. *Mechanisms of development*, 120(7), pp.759–767.
Mimitou, E.P. & Symington, L.S., 2010. Ku prevents Exo1 and Sgs1-dependent resection of DNA ends in the absence of a functional MRX complex or Sae2. *The EMBO Journal*, 29(19), pp.3358–3369.
Mimori, T. & Hardin, J.A., 1986. Mechanism of interaction between Ku protein and DNA. *Journal of Biological Chemistry*, 261(22), pp.10375–10379.
Mitchell, J.K. & Friesen, P.D., 2012. Baculoviruses modulate a proapoptotic DNA damage response to promote virus multiplication. *Journal of virology*, 86(24), pp.13542–13553.
Mizuguchi, G., 2004. ATP-Driven Exchange of Histone H2AZ Variant Catalyzed by SWR1 Chromatin Remodeling Complex. *Science*, 303(5656), pp.343–348.
Mizuguchi, T., Barrowman, J. & Grewal, S.I.S., 2015. Chromosome domain architecture and dynamic organization of the fission yeast genome. *FEBS Letters*, 589(20PartA), pp.2975–2986.
Moon, S.-H. et al., 2010. Dephosphorylation of γ-H2AX by WIP1: An important homeostatic regulatory event in DNA repair and cell cycle control. *Cell Cycle*, 9(11), pp.2092–2096.
Morrison, A.J. & Shen, X., 2009. Chromatin remodelling beyond transcription: the INO80 and SWR1 complexes. *Nature Publishing Group*, 10(6), pp.373–384.
Moyal, L. et al., 2011. Requirement of ATM-Dependent Monoubiquitylation of Histone H2B for Timely Repair of DNA Double-Strand Breaks. *Molecular Cell*, 41(5), pp.529–542.
Murray, A.W. & Kirschner, M.W., 1989. Cyclin synthesis drives the early embryonic cell cycle. *Nature*, 339(6222), pp.275–280.
Musselman, C.A. et al., 2012. Perceiving the epigenetic landscape through histone readers. *Nature Structural & Molecular Biology*, 19(12), pp.1218–1227.
Nelson, T., Hsieh, T.S. & Brutlag, D., 1979. Extracts of Drosophila embryos mediate chromatin assembly in vitro. *Proceedings of the National Academy of Sciences*, 76(11), pp.5510–5514.
O'Sullivan, R.J. & Karlseder, J., 2010. Telomeres: protecting chromosomes against genome instability. *Nature Reviews Molecular Cell Biology*, 11(3), pp.171–181.
Obri, A. et al., 2014. ANP32E is a histone chaperone that removes H2A.Z from chromatin. *Nature*, pp.1–18.
Ogiwara, H. & Kohno, T., 2011. Essential factors for incompatible DNA end joining at chromosomal DNA double strand breaks in vivo. *PLoS ONE*, 6(12), p.e28756.

Ono, M., Tucker, P.W. & Capra, J.D., 1994. Production and characterization of recombinant human Ku antigen. *Nucleic Acids Research*, 22(19), pp.3918–3924.
Oppikofer, M. et al., 2017. Expansion of the ISWI chromatin remodeler family with new active complexes. *EMBO reports*, 18(10), pp.1697–1706.
Palter, K.B., Foe, V.E. & Alberts, B.M., 1979. Evidence for the formation of nucleosome-like histone complexes on single-stranded DNA. *Cell*, 18(2), pp.451–467.
Papamichos-Chronakis, M. et al., 2011. Global Regulation of H2A.Z Localization by the INO80 Chromatin-Remodeling Enzyme Is Essential for Genome Integrity. *Cell*, 144(2), pp.200–213.
Park, P.J., 2009. ChIP–seq: advantages and challenges of a maturing technology. *Nature Reviews Genetics*, 10(10), pp.669–680.
Park, Y.-J. et al., 2004. A New Fluorescence Resonance Energy Transfer Approach Demonstrates That the Histone Variant H2AZ Stabilizes the Histone Octamer within the Nucleosome. *Journal of Biological Chemistry*, 279(23), pp.24274–24282.
Paull, T.T. et al., 2000. A critical role for histone H2AX in recruitment of repair factors to nuclear foci after DNA damage. *Current Biology*, 10(15), pp.886–895.
Plopper, G.Rensselaer Polytechnic Institute George Plopper, 2014. *Principles of Cell Biology, Second Edition Includes Navigate Advantage Access*, Jones & Bartlett Publishers.
Podhorecka, M., Skladanowski, A. & Bozko, P., 2010. H2AX Phosphorylation: Its Role in DNA Damage Response and Cancer Therapy. *Journal of Nucleic Acids*, 2010(5), pp.1–9.
Postow, L., 2011. Destroying the ring: Freeing DNA from Ku with ubiquitin. *FEBS Letters*, 585(18), pp.2876–2882.
Postow, L. et al., 2008. Ku80 removal from DNA through double strand break–induced ubiquitylation. *The Journal of Cell Biology*, 182(3), pp.467–479.
Prakash, K. & Fournier, D., 2018. Evidence for the implication of the histone code in building the genome structure. *Biosystems*, 164, pp.49–59.
Preston, C.R., Flores, C. & Engels, W.R., 2006. Age-Dependent Usage of Double-Strand-Break Repair Pathways. *Current Biology*, 16(20), pp.2009–2015.
Price, B.D. & D'Andrea, A.D., 2013. Chromatin Remodeling at DNA Double-Strand Breaks. *Cell*, 152(6), pp.1344–1354.
Radhakrishnan, S.K. & Lees-Miller, S.P., 2017. DNA requirements for interaction of the C-terminal region of Ku80 with the DNA-dependent protein kinase catalytic subunit (DNA-PKcs). *DNA Repair*, 57, pp.17–28.
Ranjha, L., Howard, S.M. & Cejka, P., 2018. Main steps in DNA double-strand break repair: an introduction to homologous recombination and related processes. pp.1–28.
Ravi, D. et al., 2009. A Network of Conserved Damage Survival Pathways Revealed by a Genomic RNAi Screen A. Kiger, ed. *PLoS Genetics*, 5(6), pp.e1000527–18.
Reeves, R., 2015. High mobility group (HMG) proteins: Modulators of chromatin structure and DNA repair in mammalian cells. *DNA Repair*, 36, pp.122–136.
Ritzi, M. et al., 1998. Human minichromosome maintenance proteins and human origin recognition complex 2 protein on chromatin. *Journal of Biological Chemistry*, 273(38), pp.24543–24549.
Rodriguez-Campos, A., Shimamura, A. & Worcel, A., 1989. Assembly and properties of chromatin containing histone H1. *Journal of Molecular Biology*, 209(1), pp.135–150.
Rogakou, E.P. et al., 1998. DNA double-stranded breaks induce histone H2AX phosphorylation on serine 139. *Journal of Biological Chemistry*, 273(10), pp.5858–5868.
Rong, Y.S., 2008. Loss of the Histone Variant H2A.Z Restores Capping to Checkpoint-Defective Telomeres in Drosophila. *Genetics*, 180(4), pp.1869–1875.
Rong, Y.S. & Golic, K.G., 2000. Gene targeting by homologous recombination in Drosophila. *Science*, 288(5473), pp.2013–2018.

Rong, Y.S. & Golic, K.G., 2003. The homologous chromosome is an effective template for the repair of mitotic DNA double-strand breaks in Drosophila. *Genetics*, 165(4), pp.1831–1842.

Rothbart, S.B. & Strahl, B.D., 2014. Interpreting the language of histone and DNA modifications. *Biochimica et biophysica acta*, 1839(8), pp.627–643.

Rother, M.B. & van Attikum, H., 2017. DNA repair goes hip-hop: SMARCA and CHD chromatin remodellers join the break dance. *Philosophical Transactions of the Royal Society B: Biological Sciences*, 372(1731), pp.20160285–13.

Ruhf, M.L. et al., 2001. The domino gene of Drosophila encodes novel members of the SWI2/SNF2 family of DNA-dependent ATPases, which contribute to the silencing of homeotic genes. *Development*, 128(8), pp.1429–1441.

Ruhl, D.D. et al., 2006. Purification of a Human SRCAP Complex That Remodels Chromatin by Incorporating the Histone Variant H2A.Z into Nucleosomes †. *Biochemistry*, 45(17), pp.5671–5677.

Ruiz-Carrillo, A. et al., 1979. In vitro core particle and nucleosome assembly at physiological ionic strength. *Proceedings of the National Academy of Sciences*, 76(7), pp.3284–3288.

Saldivar, J.C., Cortez, D. & Cimprich, K.A., 2017. The essential kinase ATR: ensuring faithful duplication of a challenging genome. *Nature Publishing Group*, 18(10), pp.622–636.

Samwer, M. et al., 2017. DNA Cross-Bridging Shapes a Single Nucleus from a Set of Mitotic Chromosomes. *Cell*, 170(5), pp.956–972.e23.

Sandaltzopoulos, R., Blank, T. & Becker, P.B., 1994. Transcriptional repression by nucleosomes but not H1 in reconstituted preblastoderm Drosophila chromatin. *The EMBO Journal*, 13(2), pp.373–379.

Sarmento, O.F. et al., 2004. Dynamic alterations of specific histone modifications during early murine development. *Journal of Cell Science*, 117(Pt 19), pp.4449–4459.

Sartori, A.A. et al., 2007. Human CtIP promotes DNA end resection. *Nature*, 450(7169), pp.509–514.

Sati, S. & Cavalli, G., 2016. Chromosome conformation capture technologies and their impact in understanding genome function. *Chromosoma*, 126(1), pp.33–44.

Savic, V. et al., 2009. Formation of Dynamic γ-H2AX Domains along Broken DNA Strands Is Distinctly Regulated by ATM and MDC1 and Dependent upon H2AX Densities in Chromatin. *Molecular Cell*, 34(3), pp.298–310.

Sánchez-Molina, S. et al., 2011. Role for hACF1 in the G2/M damage checkpoint. *Nucleic Acids Research*, 39(19), pp.8445–8456.

Scacchetti, A. et al., 2018. CHRAC/ACF contribute to the repressive ground state of chromatin. *Life Science Alliance*, 1(1), p.e201800024.

Scharf, A.N.D. et al., 2008. Monomethylation of Lysine 20 on Histone H4 Facilitates Chromatin Maturation. *Molecular and Cellular Biology*, 29(1), pp.57–67.

Schuettengruber, B. et al., 2017. Genome Regulation by Polycomb and Trithorax: 70 Years and Counting. *Cell*, 171(1), pp.34–57.

Schwartz, Y.B. & Cavalli, G., 2017. Three-Dimensional Genome Organization and Function in Drosophila. *Genetics*, 205(1), pp.5–24.

Segura-Totten, M. & Wilson, K.L., 2004. BAF: roles in chromatin, nuclear structure and retrovirus integration. *Trends in Cell Biology*, 14(5), pp.261–266.

Sekelsky, J., 2017. DNA Repair in Drosophila: Mutagens, Models, and Missing Genes. *Genetics*, 205(2), pp.471–490.

Sekelsky, J.J., Brodsky, M.H. & Burtis, K.C., 2000. DNA repair in Drosophila: insights from the Drosophila genome sequence. *The Journal of Cell Biology*, 150(2), pp.F31–6.

Sharma, S. et al., 2015. Homology and enzymatic requirements of microhomology-dependent alternative end joining. *Cell Death and Disease*, 6(3), p.e1697.

Shibata, A., 2017. Regulation of repair pathway choice at two-ended DNA double-strand breaks. *Mutation Research/Fundamental and Molecular Mechanisms of Mutagenesis*, 803-805, pp.51–55.

Shiloh, Y., 2014. ATM: expanding roles as a chief guardian of genome stability. *Experimental cell research*, 329(1), pp.154–161.

Shrivastav, M., De Haro, L.P. & Nickoloff, J.A., 2008. Regulation of DNA double-strand break repair pathway choice. *Cell Research*, 18(1), pp.134–147.

Shroff, R. et al., 2004. Distribution and Dynamics of Chromatin Modification Induced by a Defined DNA Double-Strand Break. *Current Biology*, 14(19), pp.1703–1711.

Sibon, O.C. et al., 1999. The Drosophila ATM homologue Mei-41 has an essential checkpoint function at the midblastula transition. *Current Biology*, 9(6), pp.302–312.

Siino, J.S. et al., 2002. Photobleaching of GFP-labeled H2AX in chromatin: H2AX has low diffusional mobility in the nucleus. *Biochemical and Biophysical Research Communications*, 297(5), pp.1318–1323.

Smeenk, G. et al., 2010. The NuRD chromatin–remodeling complex regulates signaling and repair of DNA damage. *The Journal of Cell Biology*, 190(5), pp.741–749.

Smerdon, M.J., 1991. DNA repair and the role of chromatin structure. *Current Opinion in Cell Biology*, 3(3), pp.422–428.

Soria, G., Polo, S.E. & Almouzni, G., 2012. Prime, Repair, Restore: The Active Role of Chromatin in the DNA Damage Response. *Molecular Cell*, 46(6), pp.722–734.

Steffen, J.D., McCauley, M.M. & Pascal, J.M., 2016. Fluorescent sensors of PARP-1 structural dynamics and allosteric regulation in response to DNA damage. *Nucleic Acids Research*, 44(20), pp.9771–9783.

Stein, A., Whitlock, J.P. & Bina, M., 1979. Acidic polypeptides can assemble both histones and chromatin in vitro at physiological ionic strength. *Proceedings of the National Academy of Sciences*, 76(10), pp.5000–5004.

Stewart, G.S. et al., 2003. MDC1 is a mediator of the mammalian DNA damage checkpoint. *Nature*, 421(6926), pp.961–966.

Ström, L. et al., 2004. Postreplicative recruitment of cohesin to double-strand breaks is required for DNA repair. *Molecular Cell*, 16(6), pp.1003–1015.

Stucki, M. et al., 2005. MDC1 directly binds phosphorylated histone H2AX to regulate cellular responses to DNA double-strand breaks. *Cell*, 123(7), pp.1213–1226.

Swaminathan, J., 2005. The role of histone H2Av variant replacement and histone H4 acetylation in the establishment of Drosophila heterochromatin. *Genes & Development*, 19(1), pp.65–76.

Swygert, S.G. & Peterson, C.L., 2017. Biochimica et Biophysica Acta. pp.1–9.

Symington, L.S. & Gautier, J., 2011. Double-strand break end resection and repair pathway choice. *Annual review of genetics*, 45(1), pp.247–271.

Talbert, P.B. & Henikoff, S., 2010. Histone variants — ancient wrap artists of the epigenome. *Nature Reviews Molecular Cell Biology*, 11(4), pp.264–275.

Thomas, C.J. et al., 2014. Kinase-mediated changes in nucleosome conformation trigger chromatin decondensation via poly(ADP-ribosyl)ation. *Molecular Cell*, 53(5), pp.831–842.

Tommasino, F. et al., 2015. Induction and Processing of the Radiation-Induced Gamma-H2AX Signal and Its Link to the Underlying Pattern of DSB: A Combined Experimental and Modelling Study. *PLoS ONE*, 10(6), p.e0129416.

Torigoe, S.E. et al., 2013. ATP-dependent chromatin assembly is functionally distinct from chromatin remodeling. *eLife*, 2, pp.2767–14.

Torigoe, S.E., Urwin, D.L., Ishii, H., Smith, D.E. & Kadonaga, J.T., 2011. Identification of a Rapidly Formed Nonnucleosomal Histone-DNA Intermediate that Is Converted into Chromatin by ACF. *Molecular Cell*, 43(4), pp.638–648.

Tripathi, V. et al., 2018. MRN complex-dependent recruitment of ubiquitylated BLM helicase to DSBs negatively regulates DNA repair pathways. *Nature Communications*, 9(1), p.1016.
Tsompana, M. & Buck, M.J., 2014. Chromatin accessibility: a window into the genome. *Epigenetics & Chromatin*, 7(1), p.33.
Tsukiyama, T. & Wu, C., 1995. Purification and properties of an ATP-dependent nucleosome remodeling factor. *Cell*, 83(6), pp.1011–1020.
Tsukuda, T., Fleming, A.B., Nickoloff, J.A. & Osley, M.A., 2005. Chromatin remodelling at a DNA double-strand break site in Saccharomyces cerevisiae. *Nature*, 438(7066), pp.379–383.
Ünal, E. et al., 2004. DNA Damage Response Pathway Uses Histone Modification to Assemble a Double-Strand Break-Specific Cohesin Domain. *Molecular Cell*, 16(6), pp.991–1002.
van Daal, A. & Elgin, S.C., 1992. A histone variant, H2AvD, is essential in Drosophila melanogaster. *Molecular biology of the cell*, 3(6), pp.593–602.
Varga-Weisz, P.D. et al., 1997. Chromatin-remodelling factor CHRAC contains the ATPases ISWI and topoisomerase II. *Nature*, 388(6642), pp.598–602.
Völker-Albert, M.C. et al., 2016. A Quantitative Proteomic Analysis of In Vitro Assembled Chromatin. *Molecular & cellular proteomics : MCP*, 15(3), pp.945–959.
Wakeman, T.P. et al., 2012. Bat3 facilitates H3K79 dimethylation by DOT1L and promotes DNA damage-induced 53BP1 foci at G1/G2 cell-cycle phases. *The EMBO Journal*, 31(9), pp.2169–2181.
Walker, J.R., Corpina, R.A. & Goldberg, J., 2001. Structure of the Ku heterodimer bound to DNA and its implications for double-strand break repair. *Nature*, 412(6847), pp.607–614.
Wang, H. et al., 2006. Histone H3 and H4 Ubiquitylation by the CUL4-DDB-ROC1 Ubiquitin Ligase Facilitates Cellular Response to DNA Damage. *Molecular Cell*, 22(3), pp.383–394.
Wang, Y. et al., 2001. The JIL-1 Tandem Kinase Mediates Histone H3 Phosphorylation and Is Required for Maintenance of Chromatin Structure in Drosophila. *Cell*, 105(4), pp.433–443.
Ward, I.M. & Chen, J., 2001. Histone H2AX is phosphorylated in an ATR-dependent manner in response to replicational stress. *Journal of Biological Chemistry*, 276(51), pp.47759–47762.
Weber, C.M., Henikoff, J.G. & Henikoff, S., 2010. H2A.Z nucleosomes enriched over active genes are homotypic. *Nature Structural & Molecular Biology*, 17(12), pp.1500–1507.
Weber, C.M., Ramachandran, S. & Henikoff, S., 2014. Nucleosomes Are Context-Specific, H2A.Z-Modulated Barriers to RNA Polymerase. *Molecular Cell*, 53(5), pp.819–830.
Wyatt, H.D.M. & West, S.C., 2014. Holliday Junction Resolvases. *Cold Spring Harbor perspectives in biology*, 6(9), pp.a023192–a023192.
Xie, A. et al., 2010. H2AX post-translational modifications in the ionizing radiation response and homologous recombination. *Cell Cycle*, 9(17), pp.3602–3610.
Xu, Y. et al., 2012. Histone H2A.Z Controls a Critical Chromatin Remodeling Step Required for DNA Double-Strand Break Repair. *Molecular Cell*, 48(5), pp.723–733.
Yang, G. et al., 2018. Super-resolution imaging identifies PARP1 and the Ku complex acting as DNA double-strand break sensors. *Nucleic Acids Research*, 46(7), pp.3446–3457.
Yang, J. & Corces, V.G., 2012. Insulators, long-range interactions, and genome function. *Current Opinion in Genetics & Development*, 22(2), pp.86–92.
Yanisch-Perron, C., Vieira, J. & Messing, J., 1985. Improved M13 phage cloning vectors and host strains: nucleotide sequences of the M13mp18 and pUC19 vectors. *Gene*, 33(1), pp.103–119.
Yuan, G. & Zhu, B., 2012. Biochimica et Biophysica Acta. *BBA - Gene Regulatory Mechanisms*, 1819(3-4), pp.222–229.
Yun, M. et al., 2011. Readers of histone modifications. *Nature Publishing Group*, 21(4), pp.564–578.

Zenk, F. et al., 2017. Germ line-inherited H3K27me3 restricts enhancer function during maternal-to-zygotic transition. *Science*, 357(6347), pp.212–216.

Zhang, Z. & Pugh, B.F., 2011. Genomic Organization of H2Av Containing Nucleosomes in Drosophila Heterochromatin L. Mariño-Ramírez, ed. *PLoS ONE*, 6(6), pp.e20511–9.

Zheng, H. et al., 2016. Resetting Epigenetic Memory by Reprogramming of Histone Modifications in Mammals. *Molecular Cell*, 63(6), pp.1066–1079.

Zhu, P. & Li, G., 2016. Structural insights of nucleosome and the 30-nm chromatin fiber. *Current opinion in structural biology*, 36, pp.106–115.

Zhu, Q. et al., 2011. BRCA1 tumour suppression occurs via heterochromatin-mediated silencing. *Nature*, 477(7363), pp.179–184.

Zink, L.-M. & Hake, S.B., 2016. Histone variants: nuclear function and disease. *Current Opinion in Genetics & Development*, 37, pp.82–89.

Zlatanova, J. & Thakar, A., 2008. H2A.Z: view from the top. *Structure (London, England : 1993)*, 16(2), pp.166–179.

Zou, L. & Elledge, S.J., 2003. Sensing DNA damage through ATRIP recognition of RPA-ssDNA complexes. *Science*, 300(5625), pp.1542–1548.

IX. ABBREVIATIONS

°C	degrees celsius
LC-MS/MS	liquid chromatography-tandem mass spectrometry
3C	chromosome conformation capture
4-OHT	4-hydroxytamoxifen
53BP1	p53-binding protein 1
aa	amino acids
Ac	acetylation
Acetyl-CoA	acetyl coenzyme A
Acf1	ATP-dependent chromatin assembly factor 1
ADP	adenosine diphosphate
AEL	after egg laying
AID	auxin-inducible-degron
Alc1	amplified in liver cancer protein 1
ATF2	activating transcription factor 2
ATM	ataxia telangiectasia mutated protein
atms	antimeros
ATP	adenosine triphosphate
ATR	ataxia telangiectasia and Rad3-related protein
Atrip	ATR-interacting protein
Atu	another transcription unit
Baf	barrier-to-autointegration factor
Baz1A	bromodomain adjacent to zinc finger domain 1a
Beaf	boundary element associated factor
beb	both ends bound
Blm	bloom syndrome protein
bp	base pairs
Brca1/2	breast cancer type 1/2
Brct	Brca1 C-terminal
Bruce	BIR repeat containing ubiquitin-conjugating enzyme
BSA	bovine serum albumin
C	control
$CaCl_2$	calcium chloride
Cdc	cell division cycle protein
Chd	chromodomain-helicase-DNA-binding protein
ChIP	chromatin immunoprecipitation
CHRAC	chromatin accessibility complex
Chz1	chaperone for Htz1
contr	control
Ctcf	corrected total cell fluorescence
CtIP	C-terminal-binding protein interacting protein
Ctr9	RNA polymerase-associated protein CTR9 homolog
Cul4	cullin4
$CuS0_4$	copper sulphate
Da	Dalton
DAPI	4'.6-diamidino-2-phenylindole
dATP	deoxyadenosine triphosphate
dCTP	deoxycytidine triphosphate
Ddb	DNA damage-binding protein

ddH_2O	double distilled H_2O
dGTP	deoxyguanosine triphosphate
DMSO	dimethylsulfoxide
DNA	deoxyribonucleic acid
DNA-PK	DNA-dependent protein kinase
DNA-PKcs	DNA-dependent protein kinase, catalytic subunit
Dna2	DNA replication ATP-dependent helicase/nuclease 2
dNTP	deoxynucleotide triphosphate
Dom	domino
Dot1	disruptor of telomeric silencing
DREX	*Drosophila* embryonic extract
DSB	double strand break
dsDNA	double-stranded DNA
DTT	1.4-dithiothreitol
dTTP	deoxythymidine triphosphate
dUTP	deoxyuridine triphosphate
E. coli	Escherichia coli
ecd	ecdysoneless
EDTA	ethylenediaminetetraacetic acid
eEF1	eukaryotic translation elongation factor 1 alpha 1
Ef1	elongation factor 1
EGTA	ethylene glycol-bis(β-aminoethyl ether)-N,N,N',N'-tetraacetic acid
Elp3	elongator complex protein 3
ER	estrogen receptor
et al.	et alii
Etl1	enhancer trap locus 1
Exo1	exonuclease 1
FAIRE	formaldehyde-assisted Isolation of regulatory elements
FBS	fetal bovine serum
Fcp1	TFIIF-interacting CTD phosphatase 1
Fen1	flap endonuclease 1
FlyFos	fly fosmid
Fun30	function unknown now 30
FV	forward
g	gram
g	gravitational acceleration
G1/G0-phase	gap1/gap0-phase
Gcn5	general control nonderepressible 5
GO	gene ontology
GST	glutathione S-transferase
H2A.V	histone H2A variant
HA	hemagglutinin
HAT	histone acetyltransferase
Hepes	N-(2-hydroxyethyl)piperazine-H´-(2-ethanesulfonic acid)
Hpa2	histone and other protein acetyltransferase 2
HR	homologous recombination
Hsp70	heat shock protein 70 kDa
Hyx	hyrax
I	inhibitor
Ida	imaginal discs arrested
IF	immunofluorescence

IgG	immunoglobulin G
Ino80	inositol-requiring protein 80
IP	immunoprecipitation
IPTG	isopropyl-D-thiogalactopyranoside)
IR	infrared
Irbp	inverted repeat binding protein
Iswi	imitation switch
k	kilo
kb	kilobase
KCl	potassium chloride
KD	knock down
kis	kismet
Klp10A	kinesin-like protein 10A
KO	knock out
L	liter
LB	lysogeny broth
Lig3	ligase 3
Lig4	ligase 4
M	marker
m	milli
M	molar
Mdc1	mediator of DNA damage checkpoint protein 1
mdlc	midlife crisis
me	methyl
Mei-41	meiotic 41
$MgCl_2$	magnesium chloride
MNase	micrococcal nuclease
mod	modulo
Mof	males absent on the first
Mre11	meiotic recombination 11
Mrg15	mortality factor 4 related gene 15
MRN	Mre11-Rad50-Nbs1
msn	mishappen
n	nano
NaCl	sodium chloride
NAD	nicotinamide adenine dinucleotide
NaMBS	sodium m-maleimidobenzoyl-N-hydroxysuccinimide ester
Nap1	nucleosome assembly protein 1
Nbs1	nibrin 1
NDS	normal donkey serum
NFR	nucleosome-free region
NGS	normal goat serum
NHEJ	non-homologous end joining
NuA4	nucleosome acetyltransferase of histone H4
NuRD	nucleosome remodeling deacetylase
oeb	one end bound
P	phosphate
p300 HAT	histone acetyltransferase p300
p400	E1A-associated protein p400
PAR	Poly-(ADP-ribose)
ParB	chromosome-partitioning protein B

Parp1	Poly-(ADP-ribose) polymerase 1
PBS	phosphate buffered saline
Pcaf	P300/CBP-associated factor
PcG	Polycomb Group
PCR	polymerase chain reaction
PEG	polyethylene glycol
PGC	primordial germ cell
pH	potential of hydrogen
PhD	doctor of philosophy
PHD	plant homeodomain
Phf7	PHD Finger Protein 7
PMSF	Phenylmethanesulfonyl fluoride
Pont	pontin
PP2A	protein phosphatase 2
PP4R2r	protein phosphatase 4 regulatory subunit 2-related protein
PRC1	Polycomb repressor complex 1
PRC2	Polycomb repressor complex 2
Prp8	pre-mRNA processing factor 8
PTM	post-translational modification
puf	puffyeye
Rad50	radiation sensitive 50/51
RanBP	Ran-binding protein
Ring	really interesting new gene
RNA	ribonucleic acid
RNA pol II	RNA polymerase II
RNAi	RNA interference
RNAse	ribonuclease
Rnf8	ring finger protein 8
Roc1	homeobox-leucine zipper protein
row	relative of woc
RPA	replication protein A
rpm	revolutions per minute
RpS29	Ribosomal protein S29
rRNA	ribosomal RNA
RSF	remodeling and spacing factor
Rsf1	repressor splicing factor 1
RV	reverse
S-phase	synthesis phase
S2	*Drosophila* Schneider cells
Sae2	sporulation in the absence of spo eleven 2
Sas2	something about silencing 2
Scu	scully
SD	standard deviation
SDS	sodium dodecyl sulphate
SDS-PAGE	SDS-polyacrylamide gel electrophoresis
Seq	sequencing
Set8	SET domain-containing protein 8
SETMAR	SET Domain And Mariner Transposase Fusion Protein
Sf21	Spodoptera frugiperda 21
sle	slender lobes

Smarca5	Swi/Snf -related matrix-associated actin-dependent regulator of chromatin subfamily A member 5
Smarcad1	Swi/Snf -related matrix-associated actin-dependent regulator of chromatin subfamily A containing DEAD/H box 1
SN	supernatant
Snf2h	sucrose nonfermenting-2 homolog
Snf2l	sucrose nonfermenting-2 like
spn-A	spindle A
SRCAP	Snf2-related CBP activator protein
ssDNA	single-stranded DNA
ssh	slingshot
Su(Hw)	suppressor of hairy wing Suv39h1
Suv4-20	suppressor of variegation 4-20 homolog
SWATH	sequential window acquisition of all theoretical fragment ion spectra
Swi/Snf	switch/sucrose non-fermentable
Swr1/2	Swi2/Snf2-related 1/2
TAD	topologically associated domains
TBS	Tris buffered saline
TE	Tris-EDTA
Tefu	telomere fusion
TEMED	N,N,N´,N´-tetramethylethylenediamine
Tip60	tat interactive protein 60kDa
tou	toutatis
TRAX	transcription extract
TSS	transcription start site
U	unit
UAS	upstream activating sequence
Ub	ubiquitin
UV	ultraviolet
v/v	volume per volume
Vta1	vacuolar protein sorting-associated protein 1
w/v	weight per volume
WB	Western blot
Woc	without children
wt	wild type
Xpc	Xeroderma pigmentosum, complementation group C
Xlf	Xrcc4-like factor
Xrcc	X-Ray Repair Cross Complementing
YL1	vacuolar protein sorting-associated protein 72 homolog 1
γH2A.V	phosphorylated H2A.V
µ	micro

X. ACKNOWLEDGEMENTS

First of all, I would like to thank my mentor Prof. Peter Becker, for giving me the chance to pursue this interesting project, for the continual support and the infinite input and ideas.

I am also very grateful to Sandro - it was more than once that I profited from your remarkably optimistic view on unexpected and sometimes also frustrating results.

I certainly profited from all the helpful input and feedback from the institute, in particular the Becker lab, for sharing material, for discussing experiments and also for motivation and encouragement when things did not work out as expected. Especially Catherine, Raffi and Alessandro contributed with many critical, but very fruitful ideas and suggestions, Silke and Angie, who helped a lot with different sample preparations, and Tamás and Tobias were incredibly helpful in sharing their knowledge about informatics and statistics.

Special thanks also go to the ZfP, especially Andreas, who spent so many hours to get the best out of my Mass Spec samples, to Angie, for helping me so much with the sequencing samples, to Stefan Krebs from the Sequencing Unit, and to Dawa, for being a big support for the fly population work.

I would also like to thank the coordinators Elizabeth Schröder-Reiter from the IRTG and Amy Gerc, Hans-Jörg Schäffer, Ingrid Wolf, Maxi Reif and Viktoria Korzhova from the IMPRS-LS, for making the PhD time a nice and eventful experience.

I am also grateful to my PhD representative colleagues Moritz from the IRTG and Alkmini and Yunmin from the IMPRS-LS - it was great fun to work with you!

I deeply appreciated the support of my Thesis advice committee members Axel Imhof and Jürg Müller. I am very grateful for your feedback and support during the last years.

Many thanks also go to the coffee and lunch mates Ale, Andrea, Daniil, Helena, Irina, Magda, Martina, Nadia, Natalia, Nik and Toby. You made the time in the institute so amiable and humorous.

Thank you also to my “old” lunch pals Catherine, Christian, Johanna, Lennart, Nadine, Sabrina and Silke. Thank you for all the enjoyable hours together and for always having an open ear on disappointing days in the lab.

I also would like to thank my parents and family, for their faith in me and their support at all times.

And I want to thank Eva - I definitely miss the great time we had in the lab.

After all, I also want to thank Martin - you were the best inspiration, coach, criticizer, motivator, supporter, guide, role model and friend I could wish for.

XI. APPENDIX

A. PLASMID SEQUENCES

pRSET-A-H2A.V

GATCTCGATCCCGCGAAATTAATACGACTCACTATAGGGAGACCACAACGGTTTCCCTCTAGAAATAATTTTGTTTAACT
TTAAGAAGGAGATATACATATGGCAGGCGGTAAAGCAGGTAAAGATAGCGGTAAAGCAAAAGCAAAAGCCGTTAGCCGTA
GCGCACGTGCAGGTCTGCAGTTTCCGGTTGGTCGTATTCATCGTCATCTGAAAAGCCGTACCACCAGTCATGGTCGTGTT
GGTGCAACCGCAGCAGTTTATAGCGCAGCAATTCTGGAATATCTGACCGCAGAAGTTCTGGAACTGGCAGGTAATGCAAG
CAAAGATCTGAAAGTGAAACGTATTACACCGCGTCATCTGCAGCTGGCAATTCGTGGTGATGAAGAACTGGATAGCCTGA
TTAAAGCAACCATTGCCGGTGGTGGTGTTATTCCGCATATTCATAAAAGCCTGATTGGCAAAAAAGAAGAAACCGTTCAG
GACCCGCAGCGTAAAGGTAATGTTATTCTGAGCCAGGCCTATTAAGGATCCGAGCTCGAGATCTGCAGCTGGTACCATGG
AATTCGAAGCTTGATCCGGCTGCTAACAAAGCCCGAAAGGAAGCTGAGTTGGCTGCTGCCACCGCTGAGCAATAACTAGC
ATAACCCCTTGGGGCCTCTAAACGGGTCTTGAGGGGTTTTTTGCTGAAAGGAGGAACTATATCCGGATCTGGCGTAATAG
CGAAGAGGCCCGCACCGATCGCCCTTCCCAACAGTTGCGCAGCCTGAATGGCGAATGGGACGCGCCCTGTAGCGGCGCAT
TAAGCGCGGCGGGTGTGGTGGTTACGCGCAGCGTGACCGCTACACTTGCCAGCGCCCTAGCGCCCGCTCCTTTCGCTTTC
TTCCCTTCCTTTCTCGCCACGTTCGCCGGCTTTCCCCGTCAAGCTCTAAATCGGGGGCTCCCTTTAGGGTTCCGATTTAG
TGCTTTACGGCACCTCGACCCCAAAAAACTTGATTAGGGTGATGGTTCACGTAGTGGGCCATCGCCCTGATAGACGGTTT
TTCGCCCTTTGACGTTGGAGTCCACGTTCTTTAATAGTGGACTCTTGTTCCAAACTGGAACAACACTCAACCCTATCTCG
GTCTATTCTTTTGATTTATAAGGGATTTTGCCGATTTCGGCCTATTGGTTAAAAAATGAGCTGATTTAACAAAAATTTAA
CGCGAATTTTAACAAAATATTAACGCTTACAATTTAGGTGGCACTTTTCGGGGAAATGTGCGCGGAACCCCTATTTGTTT
ATTTTTCTAAATACATTCAAATATGTATCCGCTCATGAGACAATAACCCTGATAAATGCTTCAATAATATTGAAAAAGGA
AGAGTATGAGTATTCAACATTTCCGTGTCGCCCTTATTCCCTTTTTTGCGGCATTTTGCCTTCCTGTTTTTGCTCACCCA
GAAACGCTGGTGAAAGTAAAAGATGCTGAAGATCAGTTGGGTGCACGAGTGGGTTACATCGAACTGGATCTCAACAGCGG
TAAGATCCTTGAGAGTTTTCGCCCCGAAGAACGTTTTCCAATGATGAGCACTTTTAAAGTTCTGCTATGTGGCGCGGTAT
TATCCCGTATTGACGCCGGGCAAGAGCAACTCGGTCGCCGCATACACTATTCTCAGAATGACTTGGTTGAGTACTCACCA
GTCACAGAAAAGCATCTTACGGATGGCATGACAGTAAGAGAATTATGCAGTGCTGCCATAACCATGAGTGATAACACTGC
GGCCAACTTACTTCTGACAACGATCGGAGGACCGAAGGAGCTAACCGCTTTTTTGCACAACATGGGGGATCATGTAACTC
GCCTTGATCGTTGGGAACCGGAGCTGAATGAAGCCATACCAAACGACGAGCGTGACACCACGATGCCTGTAGCAATGGCA
ACAACGTTGCGCAAACTATTAACTGGCGAACTACTTACTCTAGCTTCCCGGCAACAATTAATAGACTGGATGGAGGCGGA
TAAAGTTGCAGGACCACTTCTGCGCTCGGCCCTTCCGGCTGGCTGGTTTATTGCTGATAAATCTGGAGCCGGTGAGCGTG
GGTCTCGCGGTATCATTGCAGCACTGGGGCCAGATGGTAAGCCCTCCCGTATCGTAGTTATCTACACGACGGGGAGTCAG
GCAACTATGGATGAACGAAATAGACAGATCGCTGAGATAGGTGCCTCACTGATTAAGCATTGGTAACTGTCAGACCAAGT
TTACTCATATATACTTTAGATTGATTTAAAACTTCATTTTTAATTTAAAAGGATCTAGGTGAAGATCCTTTTTGATAATC
TCATGACCAAAATCCCTTAACGTGAGTTTTCGTTCCACTGAGCGTCAGACCCCGTAGAAAAGATCAAAGGATCTTCTTGA
GATCCTTTTTTTCTGCGCGTAATCTGCTGCTTGCAAACAAAAAAACCACCGCTACCAGCGGTGGTTTGTTTGCCGGATCA
AGAGCTACCAACTCTTTTTCCGAAGGTAACTGGCTTCAGCAGAGCGCAGATACCAAATACTGTTCTTCTAGTGTAGCCGT
AGTTAGGCCACCACTTCAAGAACTCTGTAGCACCGCCTACATACCTCGCTCTGCTAATCCTGTTACCAGTGGCTGCTGCC
AGTGGCGATAAGTCGTGTCTTACCGGGTTGGACTCAAGACGATAGTTACCGGATAAGGCGCAGCGGTCGGGCTGAACGGG
GGGTTCGTGCACACAGCCCAGCTTGGAGCGAACGACCTACACCGAACTGAGATACCTACAGCGTGAGCTATGAGAAAGCG
CCACGCTTCCCGAAGGGAGAAAGGCGGACAGGTATCCGGTAAGCGGCAGGGTCGGAACAGGAGAGCGCACGAGGGAGCTT
CCAGGGGGAAACGCCTGGTATCTTTATAGTCCTGTCGGGTTTCGCCACCTCTGACTTGAGCGTCGATTTTTGTGATGCTC
GTCAGGGGGGCGGAGCCTATGGAAAAACGCCAGCAACGCGGCCTTTTTACGGTTCCTGGCCTTTTGCTGGCCTTTTGCTC
ACATGTTCTTTCCTGCGTTATCCCCTGATTCTGTGGATAACCGTATTACCGCCTTTGAGTGAGCTGATACCGCTCGCCGC
AGCCGAACGACCGAGCGCAGCGAGTCAGTGAGCGAGGAAGCGGAAGAGCGCCCAATACGCAAACCGCCTCTCCCCGCGCG
TTGGCCGATTCATTAATGCAG

pFBDM-6xHis-Iswi-Acf1-Flag to express recombinant ACF in Sf21 cells

AAAGTAGCCGAAGATGACGGTTTGTCACATGGAGTTGGCAGGATGTTTGATTAAAAACATAACAGGAAGAAAAATGCCCC
GCTGTGGGCGGACAAAATAGTTGGGAACTGGGAGGGGTGGAAATGGAGTTTTTAAGGATTATTTAGGGAAGAGTGACAAA
ATAGATGGGAACTGGGTGTAGCGTCGTAAGCTAATACGAAAATTAAAAATGACAAAATAGTTTGGAACTAGATTTCACTT
ATCTGGTTCGGATCTCCTAGGCTCAAGCAGTGATCAGATCCAGACATGATAAGATACATTGATGAGTTTGGACAAACCAC
AACTAGAATGCAGTGAAAAAAATGCTTTATTTGTGAAATTTGTGATGCTATTGCTTTATTTGTAACCATTATAAGCTGCA
ATAAACAAGTTAACAACAACAATTGCATTCATTTTATGTTTCAGGTTCAGGGGGAGGTGTGGGAGGTTTTTTAAAGCAAG
TAAAACCTCTACAAATGTGGTATGGCTGATTATGATCCTCTAGTACTTCTCGACTCACTTCTTCTTCTTTTTCGAGTTGG
AACTGGTTGCCACCACCTCGCTCTTCCGCTTTTGACTGGCCTTCGGTTGGGGCGCGGGTGCTGGAGTGTTCGAGCTGGCA
CTTCCACTTCCAGCGGACACGCTGCCCTTTGGTGCCTTTTTCTTTTTTCTCGGCGCGTTCTTTCTCTTCCAGCTCAATGTT
TTCACGTTCAATAAGGGTAATCAACGTGTTGCAGCGACGCTGTAGCTCCAAAGCGGTTCTAGATTTGATGAACCAGTCAA
AGCGGAATTGCGGAGAAGCTCTTATAGCCGCTCGCAGCTCTTCGTAGACATTCTCCTTGTCAAAGCCCAACTTGTGAAGC
ATGCATACCAGAAAGCGATCCTCTATTTCAGTGTAATTCTTGCCCTTGTTATTACCATATTGCAGCCGCAACTGATGGAA
GGGGGCGCGATACCGCGACATCTTTTGATCCAAAGCCTTCTTAATAGACAATCGCCGTTGAATCTTGCCCTCTCCACGCT
CAATCTGTCCCATTATTCGCTCAATATCCTGCAACTCAGTGCATCGCTCCCAAAACACGGCGTTGTACTCGATAACCTCC
TCCGGAGTCTTGCCCTCCACGTCCTTGGCAATGTTGTCAATATCATCCCGACCGTACTTTTCGTTAGCCTTGATGAACTG
GTTGAAATCGCGCTTGGTCCAGGCAGTGAAACCCTGTGAGAGTAGATTCTCCTTCTCCTGGATCTCTTCCTCGGTAAGCG
GCTCTGCCTCATCGATCTTGCGCTGCTCCTCGCGCTGCACTTTGGTGGCATCCGATCCTAGTTCCGTGTTCTTGGGCACC
TTGTAACCAACAGTCTTGCGGAAATAGTAGATTTCCTGGTCGAGCAGCTCAAACAGACGGGGTGGGAAGAACTGAAAGTC

CTGAACGATAGGCTGCTTGGGTGGGCGGGGAGCCTTCGGTGCCTTGGGTTCGGAGACACGGAGAGCCTCGCGGAAATAGG
CATCCACAGCATAGTTGGCTTTGCGTTCACGCTTCGGTGGCTCGATCCAGTTGCCCAGCGCATTTAGCTTTTGCTTCTCG
CGCCAATCCTCACCCTCGAATTGATATACGGAAGAAGTTCCTGCCTCGCCGTTTGTGTCCATTGTGAACGTCCGCAGCGA
ACTCTCGCCCAGACTGTCCAGTGCTGCCTTTTGCTCGGCCGTCTTGGCCTCACCGCGCTCCAAAATAACATCGATGTCCT
CATCGGTAATGTCTGTCTCCTTAGAGCTGAACACTTGGTTAGCTCCAAAACGGATTATATTAAGCATTTCATCCTTGTTC
AACTGATTGGAGCGGTTGTCAACCAATCTGCCCCCCTGGATGACCATCTTGTCCAGACGGAGCTTGACCTCTGCTCTCTC
CACGATCTTCTCCTCCACTGTACTTTCGGTGATCAGCCGGAAAACGCGCACTTGCTTCTTTTGACCAATACGATGAGCAC
GATCCATAGCTTGCAAATCCATTTGAGGATTCCAATCCGAGTCGTAAATGATGACAACATCAGCGGTAGCCAAATTGATA
CCCAAACCACCGGCTCGGGTGGACAACATGAAGAGAAACTTGGCGCTGTTGTCCATGTTAAATTCCTGAATCTGCCTGTT
ACGATCTTCGTGCGGCGTCTGACCATCCAGGCGGCAATAGTTGTAGTTGCGCCAGTGACAGTAGTCCTCGAGGATATCCA
ACATCCTCGTCATTTGTGAGAAAATCAACACACGCGATCCCTGCTCTTGGAGCTTGGGCAGCAGCTTGTCCAGAATAGCC
ATCTTTCCGGAGTTATACACCAAATGCGTGTCCGTGGTGTATGGCGGACCGGGCTCGGCGCCATCAAACAAATATGGGTG
GTTGGTGCACTTGCGGAGCTGCATAAGGATGTTCTGCAGTCGCATCTTCTCCACTTTGCCAGCACCGTTCACTACATCAA
TGTCCTTAAGCAGCACCTTGGTGTACCAGTCGCGTTGCATCTTGGATAGACCCACAAATATTTTCATCTCCTTCTTCGGC
TTCAGACGCTTCTCCACTTCGGCCTTTAGACGACGGAGCAGGAAAGGTTTCAGCACGGCATGCAAACGCGTAATCAATGC
ATCGTCACCCAGGCAGGTGTTCGTGTTGAACCATTCGTCAAAATCCTCTGACGAATTAAACACATCGGGCAGCAGGAAAT
TAAGCAGGGCCCACAGCTCGTGGAGGTTATTCTGCAGCGGAGTACCCGTGATAAGTAGACGATTAGCGGTCTTAAACTCT
CGCAGAATCTCCGACAGCTTCGACTTCTCGTTCTTGATACGATGCGCCTCGTCGATGACCAAATAGCGCCAGTTGAACTT
CTTGAATACAGACTTCTCGCGGATACACATCTCATAGGAGGTCACGCAAACGTCCCACTCGCCAGGCATGAGCACATCTC
TAATGAAGGTGTTACGGGTGTCCTGGTCACCAATAAGGCAGACGGCTCTGAGGGAAGGACACCACTTTTTAAACTCATTT
ACCCAATTCTGAAGCGTTGACTTTGGCACGATGACGATGTGTGGTCCAGCTTGATTTTTGAAATGCTTGAGGTAACCCAG
CAGAGATATGGTCTGCAGGGTCTTTCCTAGACCCATTTCATCGGCCAGAATTCCATTGATACCATTTTCGTAAAGCGAAA
TCATCCAGTTAAGGCCGCGAATCTGGTAGTCACGCATCTCTCCACTTTTGATGTAGGCGGGTGAGGCATCGAAGCGAAAG
ATCTCCTTGGTGGCCGAGTCTTCCGCCAGCAACTCCTCATCCTCCTCCTGCTCTGTCTTGCGATGACGATGATCGGCCAC
ATCCTTTTCCTTGTCCTTGTCTTTGATCTTCTTGGGTCTACCCTTAGGCTTCGTGGGACTCTTAGCGCTGTTAGTCATGA
AGTGGGTGAATATCTCCGTCTGCTTTAGCAGGAAATCAAAGCGCCTACTGCGATCAGCCTCGATTTTGTTGTCGAACTCA
GCCTCCTTTTCACCGGATGAACTGGTGGCCGCATCTGAAGTCGTCTCGTTCGAGTTCTCTTCGGTTGCCTCCACGGCAGC
TGTATCTGTTTTGGACATGCCCTGAAAATACAGGTTTTCGGTCGTTGGGATATCGTAATCGTGATGGTGATGGTGATGCA
TGCGCCCGATGGTGGGACGGTATGAATAATCCGGAATATTTATAGGTTTTTTTATTACAAAACTGTTACGAAAACAGTAA
AATACTTATTTATTTGCGAGATGGTTATCATTTTAATTATCTCCATGATCTATTAATATTCCGGAGTAGGTCGCGAATCG
ATACTAGTATACGGACCTTTAATTCAACCCAACACAATATATTATAGTTAAATAAGAATTATTATCAAATCATTTGTATA
TTAATTAAAATACTATACTGTAAATTACATTTTATTTACAATCACTCGACGAAGACTTGATCACCCGGGATCTCGAGATG
GCTGGTGGCCTCAACGACATCTTCGAGGCCCAGAAGATCGAGTGGCATGAAGATACTGGTGGATCAGAGAATTTGTATTT
TCAGGGTGCGGCCGCTATGCCCATTTGCAAGCGGGAAGGATTCGACCTGAATCAGAAGGAGGGCAAGAACGAAACATTCC
ACGACAACGACCAGGTCTTCTGCTGCTACATCACTAAGCGCATTTTTCGCGACTATGAACACTACTTCCGGCACGTGATG
GTGATCAACTCAACGGTGTGGCAGTGCGAGGCCACCGGCAAGGAGAACCTCACCTACGAGGAGGCGGTCAAAAGTGAGCG
GGCGGCTCGCAAGAAGATGGAGCAGTTCAAACAGAGCCTTCGGGCACCCGTCCTTCTGGTTGTGGAGCACGCCCAACAGT
CGGCGGTCAACACCTTGAACATGATAGTGGCCAAGTTTCTGCGCAAGCGCTACTTTATCGGCGAGGAGGTGTCGGTGCAA
GCTAAGAAGAACGCCACGTACACGGTGTTGGGTGTCAAGTTGGACAAAAATATGCCGGAACCACTCAATGGTATCTATGA
GGACACGGACAACCTGGTCTACAGACTACGACCAAACAAGGGCGATCCCAGTGCAGAGCTTGATCTGCCCTTTAGGCAAT
TACGTCGCTCGCGCATGGAGTTTAACCTGGAAAACCTGAGTATGTTTATAAAGAGCAATGTATCGCGGGTGGATGGACTT
CTTCGACCCAAGCCAGAGGCATACAAGCAGTACGTGACGGACCCTGGCGTAAACTTCTCCACAATTTTCATTGGCAAAAT
GCCACGTTATTCTCCCGCTAAGATTAAAAAACCTGACGGCAAGAAGCAATCCACTCTCAACAAATATATTGTCGCCGGTG
AAGCAACGGCTGCAAAGTCAAAGGCGAAGGCCAAGTCTGATGCTAAATCTCTGGCAGAGGAATTGGAGCGGGTTAAGCGA
GAAAAAGAGGCCAAGCTTATTGAGTTGGAAAAACAAAAGGCGGAAAAGAAGGCACAGTTGATTGAACGCGTTGAAAACGA
ATGTAATTTACTGCTTCAAAAGACGGACGACCTGGAGAGAACCGACCAAAAAGTCCTGCCCCGCTACAGACAGATCGTCA
CATTGCTGCCTGAGCACCTCCTGGGTGATGCCTTCATGATGCGCGAGTTTATGCACACTTACACAGGATTGCTGTCCGGC
ATCGAGGTGTTCCGTCAGAACCTCAGTTTCTACGAGATGACACGTGCACTGACTGCTCGTGAGATTGCGGGCCCACTATC
GGACATCCTCCTCGTTCTGCTTGGCACTGTTTTCGATCTGCAAAAAGAAGAGGAGGAGGAATGCGCAGTGACCTACCTCG
ATCGGGCTGCACAAACTCAGGAGCCCTATTGGAGTATGGCGCAGGCCGCCAAAAGTCACCTTTACGCCAAGAGGCACTTT
TCCTTTAAGGTAAATGAACTACCATTAGATGCACTGACTCTCAGTGAAGTGCTACGACTGCATCTACTTGGATCCGGAGC
TTTTGTAAATGAAAAGGCGGAGCGCTGGAGAGTCATGTACCGGAATGGCTACTCGTCAAAAGAAGACCCTGGTCTGGAAC
TACGTCTGGAACACTCGCACATCCTGCGCATTCTCAAAAATCATTCCGTATATCAGCTAAAGTTTAAGGATATAATGCTC
CTGATTCGCTGCCTGATGTCCCAAATTATGACATACTCGGGCACGATTAACTTGATTGAGGAGCGTATGGAGCAAACAGC
AAAGGCCAGGCAAGATCTACGAGCTCTAGTTGTCGGGGAAAATAAGAGATTAGCCGCCGTAGAGATAAACAGGAAAAAAC
TCACGCAAATGCACCACCTGGAGGTAAATGGCGTTGAGCCTGAAAAGAGGGAAGCGTTGGTCGAGAAATTAAAGAAGAGT
ATTGCCGAGCTACACGCCCAATCGGATCAGCAACATCGCAAGCACGAGTTGCAGATGCTTAAGTTGCATTCGCAGCTTTT
CAATTTTTTGGTTTACTTGGGCATGGATAGGTGCTACAGGAAATATTACGTTTTGGAGTCTATGCCTGGGATCTTTGTCG
AGCATTCGCCGGACAGCCTTGACACTTGTTTGGAGCAACCAATAACAAATAAGTCCCAAATAGAAATTCGTCAGCAGTCT
GCATTGCCAAAGAATCGCAAGGACCTAAGGGTATATCTACTCAAACTCTACGGAGACGACGAAAAGAAAACTAAGAAAAA
GGCCAAGCACTCTCTAGAGAACAAGGAGAACCAAGAGCATCGCCTTAACGGCAGTGCAGAACCCATGGATGTCGAATCTG
ATTCTCCAGAGGCTCCCACTCATTTTGAGCTCTTGATGTGCAGTGGTGACAAACGATCTTGTATTGTGCATGATTCAAGA
AATGGGCAACGGCAGCGTTGGGCATATATTTACAAAGCCGAGGAGATCGATGAATTAATTAAGGCTCTCAATCCCAATGG
TCTCCGTGAATATGAACTCCTTCAAGAGCTATCCGTTCTGCGTTCCTTAATCGAACAGCATGCTAAGACCTGCCCAGTAG
ACTTGCTAAGTCTAGAAAACGAAACAATGCGCAAGAAGTTTATGGCGGCGATGGAATCTGAAACTAACCGTAAATACGGA
GAAGCAAACTTTGGGTTACCGAATGGGACCGATCTAAACGAAGTGATGCGCTTGCATTTAGTGGATCGAATTATTCAATT
TGAAAATGATATTTACACTGGTGATCTCGGCCGCCTGAAAGTTAAGGATATGGAAAAGTGGCGAAGTGACTTGCTTGGAG
GCAATTACGACGCTCAGTGCAAGTTGCAGTGGGGCCCGGGTGGCAAGTTGGAAGATGAAGCTGGTTCTGACAACGAATCC
CACGAAACTCACGAGGAGGACGATGGCGCACTATTAGGTAAATATGCCAGGAAACCATATCGCGATCCTGGCATGTATTT
GGCAGCTTCTGCAGACACAAAACCCCTACCAGACAGCGACGATGAGGAGGATCAGCATACGAATGCCGTCTCGATTCCTA
TCGCCGTGCATAACATGGCCTCGGCCCTTCTGCAAGTGGAGCAGGCTATTGGAAAACGGTTTCTGAAGGAACCCTACGGC
ATGAAGAAGTGGGACCCCAAGCAGGAGGCTTTAAAACTTGCCTGCGACTCGCGTTTGCACCAGTGGGAAGTTTCGCTAAT
GGAAAGTACAAGCTTTGCTCAAGTCTTTCTGCACCTAAACATCTTGCACGACTGTATTCAGTGGAGGCGTTCCACCAATA
AGTCATTATGCAAGGTCTGCAGGCGTGGCAGCGATCCGGAGAAGATGCTGCTGTGCGATGAATGCAACGCTGGCACTCAC
ATGTTCTGCCTGAAGCCTAAGCTGAGGTCTGTACCCCCGGGCAACTGGTATTGCAATGATTGCGTAAAGAGTCTGGGTCT
CAGCAATGGTCAAAACGAAAAGGATAAAAAGCAGGCGACAAAGAAGAAACGCAAGTTTATCGTAGAAGAGGAGGATGATG
AAGCTACAGACGAAGAAGAGGAAGAGAAAAAGGATGACGATATGACCGATGAGGATGCGGAGCACGAGAACGAAAAACAC
GATGAGGACGTTGAGGACGACGAAAGTGTGACCTCTACCCCCTCATCTTCCAGAGTCAATGGGCGAATTTTAAGGCGACC

CCGCACACGGCCAACAAGCAGAAGACTTACTTCGAAAGAGATCGAAGAACATGCTCAGGAAGACGTTGACAGCGGAGACG
TCAGCGATGACGCATCCTTAACCGCCGGTGAAGATACGATCGAAGACGAGTCAGATGAGGAAAAGGTGTGTCAGAAGTGT
TTCTACGATGGCGGTGAAATCAAATGTGTGCAATGCAGGCTATTCTTTCACCTGGAATGTGTTCACCTCAAGCGACCGCC
TCGCACAGATTTCGTTTGTAAAACCTGCAAGCCGATGCCACAACGACCTAGGCGCCGGCACAGTAACATGAATGGTGATC
ATGACCGCGATGAGGAGGAGCCAAAAGCAAAGCGACCACGTAACTCTTTGCGCCTATCTATCGACAAGACCGCCCGCCCA
AGCAACGGCAACAACAACAACAATAATAACAACAGCAGCGTCAATAACAACAACCATCGCAGAAGCGGGCGTCGGACGAA
CGAGCACATGCCGTTGAACAGTGCCGCCTTGTACGATCTGCTTGAGCAGATCATGAAGCACAAGGCCGCTTGGCCGTTTC
TGCGACCAGTGCTGACATCGGAGGTTCCCGACTACCATCAGATCATCAAAACGCCCATGGATCTAGCTAAAATCAAATCC
AAGCTAAACATGGGCGCCTACCAGCTAAACGAGGAGCTGCTCAGCGACATTCAGTTGGTGTTTAGAAACTGCGATTTGTA
CAACGTAGAAGGCAACGAAATATACGACGCTGGTTGTCAACTAGAACGATTCGTGATCGATCGATGTAGGGACATGCAGC
TACCGTTTAGGCCTAGCGATATGAACGGGGAAGTCAAAGCTTGCGACTACAAGGACGACGACGACAAGACCGGTTGATGC
TAGCAGCTGATGCATAGCATGCGGTACCGGGAGATGGGGGAGGCTAACTGAAACACGGAAGGAGACAATACCGGAAGGAA
CCCGCGCTATGACGGCAATAAAAAGACAGAATAAAACGCACGGGTGTTGGGTCGTTTGTTCATAAACGCGGGGTTCGGTC
CCAGGGCTGGCACTCTGTCGATACCCCACCGAGACCCCATTGGGACCAATACGCCCGCGTTTCTTCCTTTTCCCCACCCC
AACCCCCAAGTTCGGGTGAAGGCCCAGGGCTCGCAGCCAACGTCGGGGCGGCAAGCCCTGCCATAGCCAGCTTTGTTTAA
ACAAAGCTGTAGCCAACCACTAGAACTATAGCTAGAGTCCTGGGCGAACAAACGATGCTCGCCTTCCAGAAAACCGAGGA
TGCGAACCACTTCATCCGGGGTCAGCACCACCGGCAAGCGCCGCGACGGCCGAGGTCTACCGATCTCCTGAAGCAAGGGC
AGATCCGTGCACAGCACCTTGCCGTAGAAGAACAGCAAGGCCGCCAATGCCTGACGATGCGTGGAGACCGAAACCTTGCG
CTCGTTCGCCAGCCAGGACAGAAATGCCTCGACTTCGCTGCTGCCCAAGGTTGCCGGGTGACGCACACCGTGGAAACGGA
TGAAGGCACGAACCCAGTTGACATAAGCCTGTTCGGTTCGTAAACTGTAATGCAAGTAGCGTATGCGCTCACGCAACTGG
TCCAGAACCTTGACCGAACGCAGCGGTGGTAACGGCGCAGTGGCGGTTTTCATGGCTTGTTATGACTGTTTTTTTGTACA
GTCTATGCCTCGGGCATCCAAGCAGCAAGCGCGTTACGCCGTGGGTCGATGTTTGATGTTATGGAGCAGCAACGATGTTA
CGCAGCAGCAACGATGTTACGCAGCAGGGCAGTCGCCCTAAAACAAAGTTAGGTGGCTCAAGTATGGGCATCATTCGCAC
ATGTAGGCTCGGCCCTGACCAAGTCAAATCCATGCGGGCTGCTCTTGATCTTTTCGGTCGTGAGTTCGGAGACGTAGCCA
CCTACTCCCAACATCAGCCGGACTCCGATTACCTCGGGAACTTGCTCCGTAGTAAGACATTCATCGCGCTTGCTGCCTTC
GACCAAGAAGCGGTTGTTGGCGCTCTCGCGGCTTACGTTCTGCCCAAGTTTGAGCAGCCGCGTAGTGAGATCTATATCTA
TGATCTCGCAGTCTCCGGCGAGCACCGGAGGCAGGGCATTGCCACCGCGCTCATCAATCTCCTCAAGCATGAGGCCAACG
CGCTTGGTGCTTATGTGATCTACGTGCAAGCAGATTACGGTGACGATCCCGCAGTGGCTCTCTATACAAAGTTGGGCATA
CGGGAAGAAGTGATGCACTTTGATATCGACCCAAGTACCGCCACCTAACAATTCGTTCAAGCCGAGATCGGCTTCCCGGC
CGCGGAGTTGTTCGGTAAATTGTCACAACGCCGCGAATATAGTCTTTACCATGCCCTTGGCCACGCCCCTCTTTAATACG
ACGGGCAATTTGCACTTCAGAAAATGAAGAGTTTGCTTTAGCCATAACAAAAGTCCAGTATGCTTTTTCACAGCATAACT
GGACTGATTTCAGTTTACAACTATTCTGTCTAGTTTAAGACTTTATTGTCATAGTTTAGATCTATTTTGTTCAGTTTAAG
ACTTTATTGTCCGCCCACACCCGCTTACGCAGGGCATCCATTTATTACTCAACCGTAACCGATTTTGCCAGGTTACGCGG
CTGGTCTATGCGGTGTGAAATACCGCACAGATGCGTAAGGAGAAAATACCGCATCAGGCGCTCTTCCGCTTCCTCGCTCA
CTGACTCGCTGCGCTCGGTCGTTCGGCTGCGGCGAGCGGTATCAGCTCACTCAAAGGCGGTAATACGGTTATCCACAGAA
TCAGGGGATAACGCAGGAAAGAACATGTGAGCAAAAGGCCAGCAAAAGGCCAGGAACCGTAAAAAGGCCGCGTTGCTGGC
GTTTTTCCATAGGCTCCGCCCCCCTGACGAGCATCACAAAAATCGACGCTCAAGTCAGAGGTGGCGAAACCCGACAGGAC
TATAAAGATACCAGGCGTTTCCCCCTGGAAGCTCCCTCGTGCGCTCTCCTGTTCCGACCCTGCCGCTTACCGGATACCTG
TCCGCCTTTCTCCCTTCGGGAAGCGTGGCGCTTTCTCATAGCTCACGCTGTAGGTATCTCAGTTCGGTGTAGGTCGTTCG
CTCCAAGCTGGGCTGTGTGCACGAACCCCCCGTTCAGCCCGACCGCTGCGCCTTATCCGGTAACTATCGTCTTGAGTCCA
ACCCGGTAAGACACGACTTATCGCCACTGGCAGCAGCCACTGGTAACAGGATTAGCAGAGCGAGGTATGTAGGCGGTGCT
ACAGAGTTCTTGAAGTGGTGGCCTAACTACGGCTACACTAGAAGAACAGTATTTGGTATCTGCGCTCTGCTGAAGCCAGT
TACCTTCGGAAAAAGAGTTGGTAGCTCTTGATCCGGCAAACAAACCACCGCTGGTAGCGGTGGTTTTTTTGTTTGCAAGC
AGCAGATTACGCGCAGAAAAAAAGGATCTCAAGAAGATCCTTTGATCTTTTCTACGGGGTCTGACGCTCAGTGGAACGAA
AACTCACGTTAAGGGATTTTGGTCATGAGATTATCAAAAAGGATCTTCACCTAGATCCTTTTAAATTAAAAATGAAGTTT
TAAATCAATCTAAAGTATATATGAGTAAACTTGGTCTGACAGTTACCAATGCTTAATCAGTGAGGCACCTATCTCAGCGA
TCTGTCTATTTCGTTCATCCATAGTTGCCTGACTCCCCGTCGTGTAGATAACTACGATACGGGAGGGCTTACCATCTGGC
CCCAGTGCTGCAATGATACCGCGAGACCCACGCTCACCGGCTCCAGATTTATCAGCAATAAACCAGCCAGCCGGAAGGGC
CGAGCGCAGAAGTGGTCCTGCAACTTTATCCGCCTCCATCCAGTCTATTAATTGTTGCCGGGAAGCTAGAGTAAGTAGTT
CGCCAGTTAATAGTTTGCGCAACGTTGTTGCCATTGCTACAGGCATCGTGGTGTCACGCTCGTCGTTTGGTATGGCTTCA
TTCAGCTCCGGTTCCCAACGATCAAGGCGAGTTACATGATCCCCCATGTTGTGCAAAAAAGCGGTTAGCTCCTTCGGTCC
TCCGATCGTTGTCAGAAGTAAGTTGGCCGCAGTGTTATCACTCATGGTTATGGCAGCACTGCATAATTCTCTTACTGTCA
TGCCATCCGTAAGATGCTTTTCTGTGACTGGTGAGTACTCAACCAAGTCATTCTGAGAATAGTGTATGCGGCGACCGAGT
TGCTCTTGCCCGGCGTCAATACGGGATAATACCGCGCCACATAGCAGAACTTTAAAAGTGCTCATCATTGGAAAACGTTC
TTCGGGGCGAAAACTCTCAAGGATCTTACCGCTGTTGAGATCCAGTTCGATGTAACCCACTCGTGCACCCAACTGATCTT
CAGCATCTTTTACTTTCACCAGCGTTTCTGGGTGAGCAAAAACAGGAAGGCAAAATGCCGCAAAAAAGGGAATAAGGGCG
ACACGGAAATGTTGAATACTCATACTCTTCCTTTTTCAATATTATTGAAGCATTTATCAGGGTTATTGTCTCATGAGCGG
ATACATATTTGAATGTATTTAGAAAAATAAACAAATAGGGGTTCCGCGCACATTTCCCCGAAAAGTGCCACCTAAATTGT
AAGCGTTAATATTTTGTTAAAATTCGCGTTAAATTTTTGTTAAATCAGCTCATTTTTTAACCAATAGGCCGAAATCGGCA
AAATCCCTTATAAATCAAAAGAATAGACCGAGATAGGGTTGAGTGTTGTTCCAGTTTGGAACAAGAGTCCACTATTAAGA
ACGTGGACTCCAACGTCAAAGGGCGAAAAACCGTCTATCAGGGCGATGGCCCACTACGTGAACCATCACCCTAATCAAGT
TTTTTGGGGTCGAGGTGCCGTAAAGCACTAAATCGGAACCCTAAAGGGAGCCCCCGATTTAGAGCTTGACGGGGAAAGCC
GGCGAACGTGGCGAGAAAGGAAGGGAAGAAAGCGAAAGGAGCGGGCGCTAGGGCGCTGGCAAGTGTAGCGGTCACGCTGC
GCGTAACCACCACACCCGCCGCGCTTAATGCGCCGCTACAGGGCGCGTCCCATTCGCCATTCAGGCTGCAAATAAGCGTT
GATATTCAGTCAATTACAAACATTAATAACGAAGAGATGACAGAAAAATTTTCATTCTGTGACAGAGAA

B. INTENSITIES IDENTIFIED BY MASS SPECTROMETRY

1. H2A VARIANT-SPECIFIC CHROMATIN INTERACTORS (see VI.A.7)

a) H2A – H2A.V – input

Flybase polypeptide ID	Flybase symbol	differences		p-values		Flybase polypeptide ID	Flybase symbol	differences		p-values	
		H2A.V-input	H2A-input	H2A.V-input	H2A-input			H2A.V-input	H2A-input	H2A.V-input	H2A-input
FBpp0085065	-	0.93	0.40	0.10	0.45	FBpp0307711	HnRNP-K	-1.22	-0.56	0.01	0.18
FBpp0300412	-	0.51	-0.08	0.24	0.85	FBpp0307465	hoip	-0.13	0.30	0.73	0.44
FBpp0304169	-	-0.95	0.26	0.20	0.71	FBpp0297875	Hrb27C	-0.33	0.92	0.41	0.04
FBpp0304431	-	-0.35	1.69	0.77	0.17	FBpp0084672	Hrb98DE	-0.42	-0.67	0.38	0.17
FBpp0304748	-	-1.36	-1.29	0.01	0.01	FBpp0311376	Hsc70-3	1.02	1.35	0.07	0.02
FBpp0308925	-	0.23	0.62	0.64	0.22	FBpp0307982	Hsc70-4	0.19	0.30	0.64	0.47
FBpp0082990	14-3-3epsilon	-0.17	0.65	0.78	0.29	FBpp0305265	Hsc70Cb	0.12	0.09	0.76	0.82
FBpp0305137	14-3-3zeta	1.16	0.91	0.02	0.06	FBpp0312157	Hsp26	-0.85	-0.97	0.05	0.03
FBpp0075508	26-29-p	-0.25	-0.62	0.52	0.13	FBpp0312159	Hsp27	-1.15	-1.35	0.01	0.00
FBpp0085204	Acf	4.34	4.41	0.00	0.00	FBpp0073291	Hsp60A	0.75	-0.08	0.16	0.88
FBpp0071448	Act57B	-6.80	-4.87	0.05	0.14	FBpp0305095	Hsp83	-1.28	-2.25	0.03	0.00
FBpp0311818	Act5C	-0.69	0.97	0.65	0.52	FBpp0308671	hyd	1.06	1.44	0.01	0.00
FBpp0100051	Adh	-1.37	-1.81	0.02	0.01	FBpp0113041	Idh	0.70	-0.02	0.17	0.96
FBpp0112333	Adi1	-0.81	-0.34	0.23	0.60	FBpp0078152	IleRS	1.61	0.80	0.05	0.29
FBpp0072072	Adk2	-1.38	-0.95	0.03	0.11	FBpp0311679	IM33	0.25	-0.52	0.80	0.60
FBpp0082816	AdSL	-0.43	-0.57	0.33	0.20	FBpp0308804	IMPPP	1.61	1.00	0.08	0.26
FBpp0083395	AdSS	-0.82	-0.82	0.21	0.21	FBpp0088368	Inos	0.76	-0.04	0.21	0.95
FBpp0086845	AGBE	0.94	0.17	0.10	0.75	FBpp0084842	IntS11	-1.21	-1.23	0.09	0.09
FBpp0312000	Ahcy	0.36	-0.22	0.37	0.57	FBpp0076094	iPLA2-VIA	-1.73	-0.50	0.01	0.40
FBpp0087757	AIMP1	1.85	1.22	0.03	0.12	FBpp0081861	Irbp	5.10	4.69	0.00	0.00
FBpp0075318	AIMP2	0.78	0.97	0.09	0.04	FBpp0081736	Irp-1B	0.39	-1.41	0.55	0.05
FBpp0309215	Akap200	1.88	0.89	0.07	0.35	FBpp0086956	Iswi	4.62	4.64	0.00	0.00
FBpp0089366	AlaRS	-0.55	-0.93	0.35	0.12	FBpp0311371	Jafrac1	-0.07	0.21	0.89	0.66
FBpp0308680	Ald	0.05	0.00	0.90	1.00	FBpp0081931	Jupiter	1.22	0.72	0.09	0.29
FBpp0084610	ALiX	-0.16	-0.62	0.78	0.28	FBpp0307568	Karybeta3	-1.49	-1.31	0.16	0.21
FBpp0084812	alph	-0.57	-0.62	0.17	0.14	FBpp0086328	Khc	-1.14	-0.21	0.02	0.63
FBpp0071138	alpha-PheRS	0.54	-0.46	0.32	0.39	FBpp0303946	Klc	0.21	-0.04	0.56	0.92
FBpp0072694	alphaCOP	-0.82	-1.42	0.10	0.01	FBpp0312027	Klp10A	-1.78	-0.83	0.01	0.13
FBpp0074609	alphaSnap	0.53	0.45	0.39	0.46	FBpp0309092	Klp3A	-0.11	0.34	0.85	0.54
FBpp0076122	alphaTub67C	-0.17	-0.40	0.75	0.46	FBpp0072616	Klp61F	0.61	0.04	0.25	0.93
FBpp0081153	alphaTub84B	-1.09	-0.66	0.12	0.33	FBpp0078399	kra	-2.06	-1.83	0.03	0.05
FBpp0309387	AMPdeam	-0.58	-0.48	0.41	0.49	FBpp0080322	Ku80	4.77	3.91	0.00	0.00
FBpp0311374	Amun	0.46	0.29	0.43	0.62	FBpp0307248	l(2)09851	-2.86	-0.48	0.03	0.67
FBpp0291143	AnxB10	1.40	0.21	0.07	0.76	FBpp0080906	La	-0.51	-0.05	0.24	0.91
FBpp0307770	AnxB9	-0.80	-1.69	0.19	0.01	FBpp0312110	Lam	-0.58	-0.06	0.25	0.90
FBpp0082065	Aos1	-1.46	-0.74	0.09	0.36	FBpp0081255	lds	-0.10	-0.02	0.77	0.95

FBpp0074558	AP-1-2beta	-0.83	0.60	0.55	0.67	FBpp0311704	LeuRS	2.02	2.03	0.00	0.00
FBpp0081592	AP-1mu	-1.49	-0.53	0.10	0.54	FBpp0073551	lic	-2.34	-1.42	0.01	0.05
FBpp0293470	ApepP	0.53	0.17	0.22	0.69	FBpp0303481	lig	0.50	1.86	0.56	0.05
FBpp0311464	apolpp	-1.71	-1.01	0.09	0.29	FBpp0293289	Lis-1	2.42	3.01	0.04	0.02
FBpp0303606	APP-BP1	0.87	0.08	0.27	0.92	FBpp0079621	LManII	0.86	0.52	0.21	0.44
FBpp0304364	Arf79F	1.92	3.23	0.00	0.00	FBpp0311512	lolal	1.11	1.25	0.13	0.09
FBpp0304160	ArfGAP3	1.15	2.00	0.10	0.01	FBpp0078561	lost	-1.58	-1.44	0.01	0.01
FBpp0076271	Argk	-1.32	-1.49	0.02	0.01	FBpp0288789	lqfR	0.82	1.02	0.22	0.14
FBpp0073965	ArgRS	1.97	1.97	0.01	0.01	FBpp0073784	Lsd-2	-2.47	-2.46	0.11	0.11
FBpp0082121	Arp1	-0.88	-1.42	0.06	0.01	FBpp0071553	LSm1	-0.22	-1.53	0.64	0.01
FBpp0302793	Arp2	-0.17	0.14	0.66	0.72	FBpp0289873	LSm3	0.35	-0.27	0.66	0.73
FBpp0306212	Arp3	-0.66	-2.02	0.51	0.06	FBpp0310328	LSm7	0.35	0.32	0.39	0.43
FBpp0080147	Arpc1	-2.75	-4.00	0.10	0.02	FBpp0301732	lwr	2.33	0.90	0.09	0.49
FBpp0312086	Arpc2	-0.43	-2.49	0.63	0.02	FBpp0292593	LysRS	2.62	1.80	0.00	0.02
FBpp0078831	Arpc4	-1.32	0.12	0.15	0.89	FBpp0293270	mahj	-0.79	-1.33	0.25	0.07
FBpp0081780	Art1	0.20	0.61	0.60	0.14	FBpp0292313	Mal-B2	1.08	0.67	0.29	0.51
FBpp0082589	Art3	-0.70	-2.26	0.65	0.16	FBpp0306414	Map205	2.03	1.33	0.06	0.20
FBpp0305840	Art4	0.06	-0.17	0.92	0.78	FBpp0087613	Map60	2.53	1.73	0.02	0.09
FBpp0291576	asf1	-1.66	-0.13	0.15	0.90	FBpp0289639	Mapmodulin	1.23	0.18	0.36	0.89
FBpp0304830	AsnRS	-1.03	0.01	0.15	0.99	FBpp0303170	mbf1	2.54	2.15	0.02	0.04
FBpp0308483	AspRS	2.14	1.46	0.03	0.12	FBpp0081317	Mcm2	-1.54	-0.66	0.02	0.25
FBpp0085891	Atg7	0.45	0.00	0.47	0.99	FBpp0309417	Mcm3	-1.12	-1.16	0.04	0.04
FBpp0303150	Atox1	1.04	1.11	0.18	0.16	FBpp0081756	Mcm5	-0.61	-1.52	0.19	0.01
FBpp0289825	ATPCL	-0.64	-1.17	0.14	0.02	FBpp0070913	Mcm6	-0.65	-0.56	0.28	0.35
FBpp0311086	ATPsynbeta	1.05	3.11	0.12	0.00	FBpp0076312	Mcm7	-1.88	-1.65	0.01	0.02
FBpp0312191	awd	0.27	-0.53	0.53	0.23	FBpp0293887	MCTS1	-0.89	-2.01	0.11	0.00
FBpp0300517	B52	-0.46	-0.88	0.21	0.03	FBpp0311560	Mdh1	-0.24	-0.82	0.72	0.23
FBpp0307124	Bacc	1.79	2.40	0.00	0.00	FBpp0079565	me31B	-0.95	-0.55	0.15	0.39
FBpp0305308	baf	1.18	0.86	0.05	0.12	FBpp0288779	MEP-1	2.41	1.81	0.01	0.03
FBpp0071235	Bap111	2.65	2.36	0.01	0.01	FBpp0085809	MetRS	2.29	1.90	0.02	0.05
FBpp0086115	Bap55	1.56	0.91	0.08	0.28	FBpp0081882	mgr	0.05	-0.74	0.94	0.30
FBpp0073572	Bap60	1.92	1.35	0.02	0.08	FBpp0304462	Mi-2	1.14	0.89	0.07	0.15
FBpp0310394	barr	2.55	2.37	0.02	0.03	FBpp0300803	Mlc-c	1.08	1.71	0.07	0.01
FBpp0306433	bel	-0.88	-1.03	0.17	0.11	FBpp0303950	Mo25	-1.63	-1.91	0.26	0.19
FBpp0305067	ben	-2.35	-2.18	0.01	0.02	FBpp0301951	mod	-2.41	-0.91	0.09	0.49
FBpp0084021	beta-PheRS	-0.96	-0.82	0.07	0.11	FBpp0083470	mod(mdg4)	2.55	2.31	0.01	0.02
FBpp0074348	betaCOP	-0.50	-0.66	0.45	0.33	FBpp0300514	Moe	-1.09	-1.11	0.11	0.11
FBpp0085720	betaTub56D	0.71	0.53	0.07	0.16	FBpp0075450	mop	0.20	-0.29	0.77	0.66
FBpp0086896	bic	1.80	1.77	0.07	0.07	FBpp0291706	mor	1.60	1.40	0.02	0.03
FBpp0082428	BigH1	0.20	0.52	0.69	0.30	FBpp0079802	mre11	3.25	3.02	0.00	0.00
FBpp0071794	blw	-0.31	0.07	0.81	0.96	FBpp0075399	Msh6	-0.62	-0.70	0.27	0.22
FBpp0074430	bnb	1.56	1.77	0.02	0.01	FBpp0076408	msk	-1.25	-0.21	0.35	0.87
FBpp0305757	brm	1.96	1.92	0.02	0.02	FBpp0293342	msps	1.12	0.82	0.27	0.41
FBpp0308293	Bub3	1.89	1.57	0.05	0.10	FBpp0304737	Mtor	-0.18	0.21	0.75	0.70
FBpp0310411	bur	-1.35	-2.12	0.09	0.02	FBpp0310063	mts	-2.27	-1.13	0.11	0.39
FBpp0087402	Caf1-105	4.71	4.64	0.03	0.03	FBpp0073648	mus101	0.22	-0.37	0.82	0.71
FBpp0071172	Caf1-180	3.15	2.47	0.02	0.05	FBpp0311887	Naa15-16	-2.02	-1.05	0.00	0.08
FBpp0082511	Caf1-55	0.93	1.14	0.05	0.02	FBpp0084827	Naa40	-3.09	-1.82	0.00	0.04
FBpp0306685	Calr	-0.64	-0.45	0.37	0.53	FBpp0297132	Nap1	-0.47	-1.40	0.39	0.02
FBpp0311269	Cam	3.15	3.33	0.02	0.02	FBpp0306828	NAT1	0.67	1.17	0.28	0.08
FBpp0079795	cana	-0.61	1.69	0.59	0.16	FBpp0311231	ncd	2.30	2.33	0.02	0.02
FBpp0304507	Cand1	-1.78	0.33	0.02	0.60	FBpp0076693	ndl	0.61	0.35	0.27	0.51
FBpp0290540	Cap-G	1.93	3.10	0.01	0.00	FBpp0309711	Nedd8	-0.73	0.30	0.40	0.72
FBpp0304563	capt	-0.58	0.08	0.33	0.89	FBpp0306756	Nlp	0.82	0.18	0.21	0.77
FBpp0308803	casp	-0.57	1.12	0.44	0.15	FBpp0076451	Nmt	-0.85	0.51	0.39	0.60

FBpp0309380	Cbs	0.66	0.37	0.15	0.41	FBpp0309175	NO66	2.75	2.13	0.00	0.01
FBpp0290166	Ccs	-0.38	0.20	0.40	0.64	FBpp0072839	Non2	1.18	1.90	0.05	0.00
FBpp0083684	CCT1	-1.04	-0.61	0.20	0.43	FBpp0078997	nop5	-3.57	-0.68	0.12	0.75
FBpp0071226	CCT2	-0.42	-0.85	0.31	0.06	FBpp0083625	Nop56	-2.84	-1.23	0.03	0.31
FBpp0291566	CCT3	-0.49	-1.01	0.29	0.05	FBpp0112220	Nph	0.99	-0.24	0.24	0.76
FBpp0079992	CCT4	-0.96	-0.94	0.25	0.26	FBpp0289954	Npl4	0.06	0.12	0.92	0.83
FBpp0087095	CCT5	-0.32	-1.98	0.68	0.03	FBpp0073438	Nrd1	-0.76	-0.14	0.22	0.81
FBpp0073902	CCT6	-0.56	-1.64	0.22	0.00	FBpp0311095	Nsf2	0.56	-0.71	0.65	0.57
FBpp0081401	CCT7	-0.73	-1.16	0.07	0.01	FBpp0075699	nst	0.54	1.04	0.39	0.12
FBpp0087764	CCT8	-0.76	-1.18	0.08	0.01	FBpp0070637	Nsun2	-0.89	0.31	0.27	0.69
FBpp0072660	Cdc37	0.06	-0.13	0.89	0.76	FBpp0305904	Ntf-2	-1.02	-1.11	0.09	0.07
FBpp0079641	Cdk1	0.45	0.18	0.41	0.74	FBpp0297079	nudC	-0.73	-1.45	0.23	0.03
FBpp0082085	CG10038	0.22	-0.10	0.55	0.77	FBpp0309144	Nup153	-2.02	-0.15	0.09	0.89
FBpp0305296	CG10077	-1.34	-0.19	0.32	0.88	FBpp0071905	Nup214	-0.13	-0.45	0.74	0.26
FBpp0306293	CG10237	-3.32	-2.09	0.01	0.05	FBpp0084188	Nup358	-1.40	-0.90	0.01	0.05
FBpp0306810	CG10254	-0.43	0.61	0.40	0.24	FBpp0087861	Nup50	-0.87	-0.39	0.07	0.39
FBpp0073440	CG10347	-2.99	-1.76	0.01	0.09	FBpp0087063	Nup54	-2.42	-1.41	0.00	0.04
FBpp0075686	CG10418	0.15	0.29	0.83	0.68	FBpp0083195	Nup58	-0.39	-1.22	0.70	0.25
FBpp0074800	CG10424	1.33	0.63	0.02	0.22	FBpp0309066	Nup62	0.77	1.36	0.17	0.03
FBpp0293954	CG10565	1.11	1.62	0.02	0.00	FBpp0073659	Nup93-1	0.36	0.91	0.46	0.08
FBpp0311825	CG10576	-0.89	-0.98	0.23	0.20	FBpp0306915	Nup98-96	1.56	2.08	0.04	0.01
FBpp0311505	CG10638	0.55	0.02	0.30	0.97	FBpp0072250	Nurf-38	0.49	-0.31	0.36	0.55
FBpp0304491	CG10680	2.21	2.19	0.04	0.04	FBpp0309320	Obp19c	0.39	0.56	0.55	0.40
FBpp0073028	CG10863	0.71	-0.22	0.33	0.75	FBpp0300672	p23	-0.43	-0.77	0.45	0.18
FBpp0077583	CG10869	0.17	0.93	0.73	0.09	FBpp0080111	p38b	0.44	-0.04	0.43	0.94
FBpp0099759	CG10973	0.14	-0.15	0.88	0.86	FBpp0088069	p47	0.21	0.46	0.53	0.20
FBpp0292528	CG11089	0.13	-0.24	0.75	0.57	FBpp0083127	P5cr	1.21	0.54	0.03	0.27
FBpp0304097	CG11134	-1.24	-0.64	0.25	0.54	FBpp0085919	pAbp	-0.19	-0.44	0.78	0.53
FBpp0309343	CG11164	0.74	0.29	0.19	0.58	FBpp0073976	Paf-AHalpha	-0.45	-1.58	0.24	0.00
FBpp0306623	CG11334	0.27	0.15	0.50	0.70	FBpp0305933	Paics	-0.11	-0.30	0.78	0.44
FBpp0084190	CG11858	1.40	1.23	0.01	0.02	FBpp0112608	Parp	1.81	3.11	0.05	0.00
FBpp0084759	CG11899	0.00	-0.24	1.00	0.55	FBpp0082124	Past1	-1.67	-1.10	0.04	0.15
FBpp0081444	CG11980	0.97	0.07	0.11	0.90	FBpp0308430	pch2	-1.96	-0.75	0.20	0.61
FBpp0072658	CG12018	-1.91	-1.16	0.19	0.41	FBpp0089395	PCNA	1.54	0.23	0.17	0.83
FBpp0087483	CG12129	-1.36	-1.32	0.23	0.25	FBpp0075238	PDCD-5	0.45	0.12	0.50	0.86
FBpp0078357	CG12171	-0.25	-1.14	0.64	0.05	FBpp0079527	Pen	-2.60	-2.07	0.03	0.07
FBpp0078279	CG1218	-1.47	-0.17	0.14	0.86	FBpp0078852	Pfas	0.29	-0.17	0.50	0.69
FBpp0082125	CG12279	0.57	0.42	0.12	0.24	FBpp0309825	Pfdn1	0.73	0.43	0.09	0.29
FBpp0083036	CG12321	-1.12	-0.99	0.03	0.05	FBpp0304954	Pfdn2	1.08	0.47	0.18	0.54
FBpp0078370	CG1236	0.42	-0.42	0.42	0.42	FBpp0076858	Pfdn4	0.28	1.52	0.66	0.03
FBpp0312072	CG12702	-1.16	0.62	0.10	0.35	FBpp0290701	Pfdn5	0.52	0.10	0.18	0.79
FBpp0087406	CG12896	0.76	0.25	0.13	0.60	FBpp0303214	Pfdn6	0.33	0.40	0.46	0.37
FBpp0307859	CG1354	-0.73	-1.44	0.08	0.00	FBpp0293464	Pfk	-1.19	-1.01	0.15	0.21
FBpp0085260	CG1416	-0.92	-1.34	0.06	0.01	FBpp0303827	Pgd	-0.19	-0.44	0.69	0.36
FBpp0311833	CG14207	0.34	-0.91	0.80	0.51	FBpp0087762	Pgi	0.80	0.32	0.12	0.49
FBpp0083124	CG14286	0.30	0.20	0.52	0.66	FBpp0306279	Pgk	0.42	0.04	0.27	0.91
FBpp0308525	CG1440	1.06	0.28	0.12	0.67	FBpp0099920	Pglym78	-0.59	-0.92	0.21	0.07
FBpp0311823	CG14434	-0.62	-0.89	0.28	0.13	FBpp0075247	Pgm	0.17	-0.30	0.73	0.55
FBpp0307945	CG14894	0.29	0.85	0.50	0.07	FBpp0072932	PHGPx	0.02	-0.37	0.97	0.40
FBpp0074368	CG15047	2.13	1.98	0.00	0.01	FBpp0082177	pic	0.95	0.83	0.06	0.10
FBpp0308695	CG1532	1.07	0.76	0.21	0.37	FBpp0084559	pins	-3.03	-0.73	0.00	0.31
FBpp0077145	CG15439	2.75	2.81	0.01	0.01	FBpp0076285	pix	-2.06	-1.11	0.03	0.19
FBpp0310939	CG15717	-1.67	-1.08	0.03	0.13	FBpp0307466	Pka-C1	-0.60	0.34	0.28	0.53
FBpp0311370	CG1578	0.44	0.56	0.42	0.30	FBpp0087524	Pka-R2	-2.41	-1.86	0.07	0.15
FBpp0308869	CG1640	0.55	0.15	0.18	0.70	FBpp0310466	Plap	-0.74	-1.07	0.10	0.03
FBpp0310240	CG1703	-1.61	-1.00	0.04	0.16	FBpp0075693	Pmm2	0.16	-0.82	0.77	0.15
FBpp0082059	CG17202	1.46	1.28	0.04	0.06	FBpp0305301	poe	-1.86	-1.59	0.04	0.07
FBpp0298837	CG17266	-1.24	-0.78	0.19	0.40	FBpp0307818	Pol32	1.52	1.63	0.03	0.02
FBpp0073235	CG17333	-0.33	0.61	0.71	0.50	FBpp0099722	polo	-0.67	0.23	0.21	0.65

FBpp0085374	CG17337	0.46	-0.28	0.38	0.59	FBpp0292357	poly	-1.16	-0.66	0.06	0.26
FBpp0072956	CG17746	0.34	-0.89	0.63	0.22	FBpp0081704	pont	0.12	-0.15	0.77	0.71
FBpp0080448	CG17904	-0.38	-0.95	0.45	0.08	FBpp0082067	Pp1-87B	2.41	1.93	0.02	0.04
FBpp0271746	CG18190	-0.99	-1.12	0.25	0.20	FBpp0293227	Pp2A-29B	-1.55	-1.27	0.03	0.06
FBpp0303935	CG18815	-2.09	-2.29	0.04	0.03	FBpp0301546	Pp2B-14D	-0.92	-0.53	0.10	0.32
FBpp0085195	CG1890	1.16	0.48	0.08	0.44	FBpp0312200	Pp4-19C	0.42	-0.29	0.35	0.51
FBpp0085198	CG1910	-4.35	-3.09	0.07	0.19	FBpp0304082	PpD3	0.23	0.90	0.61	0.07
FBpp0306729	CG1943	1.95	0.85	0.12	0.47	FBpp0307839	PPP4R2r	-0.88	-1.01	0.06	0.04
FBpp0311995	CG2004	-0.05	0.08	0.92	0.85	FBpp0293248	Prat	1.43	1.20	0.04	0.07
FBpp0078327	CG2091	-1.96	-1.75	0.01	0.02	FBpp0099895	primo-1	0.28	-0.52	0.64	0.39
FBpp0309262	CG2200	0.70	-0.14	0.19	0.78	FBpp0082062	Prosalpha 2	0.66	0.56	0.10	0.15
FBpp0307424	CG2246	-0.32	0.22	0.49	0.64	FBpp0071451	Prosalpha 3	0.92	0.38	0.22	0.60
FBpp0081312	CG2767	1.20	-0.37	0.14	0.63	FBpp0073989	Prosalpha 4	0.16	0.53	0.66	0.18
FBpp0311613	CG2852	-0.33	0.28	0.54	0.61	FBpp0086067	Prosalpha 5	0.43	0.56	0.23	0.13
FBpp0307127	CG2862	0.04	0.16	0.93	0.76	FBpp0310201	Prosalpha 6	1.08	0.37	0.13	0.59
FBpp0086057	CG30105	1.64	2.40	0.01	0.00	FBpp0089041	Prosalpha 7	0.89	-0.12	0.33	0.89
FBpp0291433	CG30382	0.75	0.31	0.22	0.60	FBpp0086400	Prosbeta1	0.82	1.44	0.06	0.00
FBpp0301728	CG30499	-0.55	-0.02	0.42	0.97	FBpp0075382	Prosbeta2	1.42	1.19	0.01	0.02
FBpp0300161	CG31075	0.38	0.01	0.34	0.98	FBpp0081488	Prosbeta3	0.55	0.16	0.22	0.71
FBpp0084237	CG31098	-1.02	-0.82	0.30	0.40	FBpp0307141	Prosbeta4	0.56	0.98	0.19	0.03
FBpp0307202	CG31549	-0.22	-0.93	0.61	0.05	FBpp0087320	Prosbeta5	1.25	0.60	0.05	0.31
FBpp0308642	CG31673	0.59	0.63	0.14	0.12	FBpp0075119	Prosbeta6	0.92	0.60	0.13	0.30
FBpp0303949	CG32164	-0.84	-1.30	0.05	0.01	FBpp0078449	Prosbeta7	0.73	0.03	0.27	0.97
FBpp0070953	CG3226	-1.55	-0.97	0.02	0.11	FBpp0085902	Prp19	1.36	1.34	0.02	0.02
FBpp0082211	CG32473	1.00	1.45	0.27	0.12	FBpp0100080	Prx5	0.37	-0.11	0.56	0.87
FBpp0309368	CG32549	-0.53	-2.48	0.57	0.02	FBpp0077368	Prx6005	0.70	-0.31	0.16	0.52
FBpp0311482	CG33722	-0.03	-0.64	0.95	0.14	FBpp0072583	Psa	0.76	-0.03	0.20	0.96
FBpp0078978	CG3430	-1.89	-1.39	0.00	0.01	FBpp0086222	Psi	0.78	1.53	0.27	0.05
FBpp0076204	CG3448	4.60	4.29	0.00	0.00	FBpp0083238	psidin	-1.39	-1.46	0.04	0.03
FBpp0303858	CG3609	1.40	1.15	0.15	0.22	FBpp0077277	Ptpa	-1.98	-0.43	0.06	0.66
FBpp0301181	CG3760	1.22	0.29	0.14	0.71	FBpp0082932	Pxt	-0.08	0.05	0.84	0.90
FBpp0310197	CG3939	-1.89	-0.87	0.09	0.41	FBpp0083611	PyK	0.92	-0.22	0.17	0.72
FBpp0110481	CG40045	-2.62	0.56	0.16	0.75	FBpp0304178	pzg	1.78	3.40	0.09	0.01
FBpp0075697	CG4069	-0.61	-0.55	0.44	0.49	FBpp0076788	QC	-0.19	-0.37	0.88	0.78
FBpp0291627	CG4199	1.34	0.66	0.04	0.26	FBpp0309142	r	0.16	-0.36	0.80	0.58
FBpp0288574	CG42232	5.26	4.34	0.00	0.01	FBpp0083440	r-l	-1.11	-1.48	0.01	0.00
FBpp0080392	CG4278	2.38	0.93	0.03	0.34	FBpp0083503	Rab1	-0.51	-0.12	0.23	0.77
FBpp0292832	CG42813	-0.27	-0.13	0.64	0.82	FBpp0083414	Rab11	-1.63	-1.77	0.07	0.06
FBpp0083246	CG4390	1.81	0.97	0.02	0.17	FBpp0307641	Rab2	-0.30	1.98	0.74	0.05
FBpp0308683	CG4408	0.04	-0.14	0.94	0.80	FBpp0303520	Rab5	-0.69	1.79	0.45	0.07
FBpp0309989	CG4593	-0.69	-0.97	0.18	0.07	FBpp0311572	Rack1	0.26	0.17	0.65	0.76
FBpp0304189	CG4603	-0.94	-0.49	0.05	0.26	FBpp0305835	Rad23	-0.43	-0.06	0.52	0.93
FBpp0311588	CG4646	1.02	-0.76	0.43	0.55	FBpp0293866	rad50	4.20	3.30	0.01	0.02
FBpp0071743	CG4752	0.98	1.29	0.04	0.01	FBpp0071600	Rae1	2.24	2.72	0.01	0.00
FBpp0084626	CG4849	-0.77	0.31	0.32	0.68	FBpp0309151	Ran	-0.84	-1.13	0.10	0.03
FBpp0074113	CG4872	0.08	0.19	0.87	0.71	FBpp0309478	Ranbp21	-1.25	-0.37	0.10	0.60
FBpp0303029	CG5098	3.12	3.51	0.01	0.00	FBpp0307011	RanBP3	-1.26	-0.57	0.08	0.39
FBpp0085863	CG5174	0.78	0.67	0.19	0.26	FBpp0312218	Ranbp9	-0.46	-0.93	0.32	0.06
FBpp0079637	CG5355	0.22	0.48	0.62	0.29	FBpp0306292	RanGAP	-1.72	-1.35	0.01	0.02
FBpp0311410	CG5515	-1.57	-0.22	0.02	0.71	FBpp0309791	ras	-1.17	-1.67	0.02	0.00
FBpp0076733	CG5568	-0.29	-0.52	0.70	0.49	FBpp0304602	Rat1	0.66	0.91	0.55	0.41
FBpp0303030	CG5757	-0.97	-0.41	0.11	0.48	FBpp0076784	Rcc1	4.27	5.17	0.01	0.00
FBpp0083584	CG6028	0.98	0.71	0.04	0.11	FBpp0076452	RecQ4	-1.37	-0.31	0.12	0.71
FBpp0303937	CG6084	0.64	-0.05	0.29	0.93	FBpp0302766	REG	-0.99	-0.65	0.17	0.35

FBpp0079979	CG6180	-1.52	-0.24	0.22	0.84	FBpp0073422	regucalcin	0.33	0.78	0.47	0.11
FBpp0083213	CG6195	-1.17	-0.08	0.32	0.94	FBpp0311247	rept	-0.25	0.05	0.52	0.90
FBpp0079809	CG6287	1.10	0.26	0.07	0.64	FBpp0079609	RfC3	1.61	1.59	0.01	0.01
FBpp0080044	CG6523	-0.10	-0.06	0.81	0.89	FBpp0311114	RfC38	1.35	0.69	0.14	0.43
FBpp0074386	CG6617	0.38	-0.02	0.66	0.98	FBpp0073120	RfC4	2.11	2.59	0.00	0.00
FBpp0310703	CG6726	0.42	-0.17	0.36	0.70	FBpp0305320	rhea	-1.02	-0.07	0.11	0.91
FBpp0311284	CG6767	-1.10	-1.80	0.18	0.04	FBpp0089130	Rho1	-0.82	-1.54	0.14	0.01
FBpp0309927	CG6907	-1.35	-1.15	0.16	0.22	FBpp0304185	RhoGDI	-0.96	-1.08	0.17	0.13
FBpp0081996	CG6950	0.40	0.17	0.28	0.64	FBpp0312064	rin	0.09	-0.53	0.88	0.39
FBpp0311665	CG7182	0.83	0.47	0.11	0.34	FBpp0310006	rngo	-0.89	-0.18	0.05	0.66
FBpp0311891	CG7322	-0.04	-1.11	0.96	0.17	FBpp0079648	RnrL	-1.15	-0.27	0.08	0.66
FBpp0309678	CG7332	-1.58	0.17	0.12	0.86	FBpp0087152	RnrS	-0.23	-0.79	0.61	0.11
FBpp0304957	CG7519	-2.11	-0.57	0.01	0.40	FBpp0086076	robl	0.30	0.71	0.42	0.08
FBpp0304452	CG7546	-0.57	-0.13	0.25	0.78	FBpp0085156	rod	-1.94	-2.61	0.27	0.15
FBpp0084849	CG7789	-1.00	0.30	0.26	0.72	FBpp0081356	RpA-70	1.45	1.04	0.17	0.31
FBpp0082183	CG7966	0.03	-0.41	0.96	0.47	FBpp0305226	RPA2	1.22	1.10	0.11	0.14
FBpp0082187	CG8031	1.06	0.87	0.03	0.06	FBpp0310183	RPA3	1.13	1.58	0.03	0.01
FBpp0081371	CG8036	1.15	0.32	0.11	0.63	FBpp0310926	RpII140	-1.95	0.53	0.05	0.55
FBpp0081507	CG8132	1.33	1.76	0.02	0.01	FBpp0309436	RpL11	-1.26	-0.08	0.05	0.89
FBpp0074246	CG8142	3.04	2.19	0.03	0.09	FBpp0311459	RpL17	-1.63	-2.10	0.18	0.10
FBpp0081539	CG8149	2.05	1.50	0.03	0.09	FBpp0071808	RpL23	-1.40	-1.02	0.08	0.19
FBpp0076470	CG8209	-0.50	0.14	0.38	0.80	FBpp0305858	RpL26	-0.05	-1.03	0.95	0.23
FBpp0081398	CG8223	0.61	1.00	0.17	0.04	FBpp0309280	RpL30	-0.87	-0.63	0.34	0.48
FBpp0087116	CG8858	-0.34	-0.77	0.56	0.21	FBpp0078416	RpL35A	-1.86	-1.55	0.21	0.29
FBpp0078684	CG8891	-0.43	-0.63	0.30	0.14	FBpp0084617	RpL4	-2.87	-2.20	0.04	0.10
FBpp0303670	CG8892	-0.45	-0.38	0.45	0.52	FBpp0311121	RpL5	0.52	-0.09	0.52	0.91
FBpp0074128	CG9132	-0.58	-0.60	0.19	0.18	FBpp0310250	RpL7	-2.20	-0.22	0.13	0.87
FBpp0311963	CG9135	1.63	0.30	0.10	0.74	FBpp0072802	RpL8	-1.32	-1.18	0.14	0.18
FBpp0072560	CG9149	0.22	0.00	0.55	1.00	FBpp0309201	RpL9	2.42	2.61	0.05	0.04
FBpp0309269	CG9281	-2.21	-1.41	0.00	0.04	FBpp0306232	RpLP0	-2.00	-0.98	0.01	0.14
FBpp0082298	CG9286	-0.40	-0.91	0.46	0.11	FBpp0304265	RpLP1	0.91	0.31	0.21	0.66
FBpp0296988	CG9391	-0.84	0.44	0.29	0.57	FBpp0086252	RpLP2	0.47	1.01	0.32	0.05
FBpp0085467	CG9436	0.11	-0.46	0.75	0.21	FBpp0074662	Rpn1	-2.27	-2.43	0.00	0.00
FBpp0112123	CG9471	-1.56	-1.13	0.03	0.09	FBpp0305644	Rpn10	-1.16	-1.31	0.02	0.01
FBpp0081343	CG9601	2.18	2.84	0.01	0.00	FBpp0078664	Rpn11	-0.50	0.11	0.30	0.81
FBpp0075103	CG9674	0.08	0.16	0.84	0.69	FBpp0075068	Rpn12	-0.04	-0.30	0.92	0.42
FBpp0305784	CG9705	1.04	0.04	0.26	0.96	FBpp0112987	Rpn13	-0.33	-0.34	0.36	0.35
FBpp0071542	CG9752	0.77	-0.14	0.18	0.80	FBpp0306599	Rpn2	-1.28	0.44	0.15	0.60
FBpp0308531	Chc	-2.01	-2.08	0.02	0.02	FBpp0307804	Rpn3	-1.39	-1.76	0.01	0.00
FBpp0301152	chic	0.04	-0.23	0.93	0.63	FBpp0078278	Rpn5	-0.16	-1.10	0.71	0.02
FBpp0083939	CHORD	-2.36	-1.41	0.02	0.14	FBpp0297513	Rpn6	-0.24	-1.39	0.69	0.04
FBpp0099657	Chrac-14	3.58	3.43	0.01	0.01	FBpp0083687	Rpn7	-1.66	-1.33	0.07	0.13
FBpp0308688	Chrac-16	3.42	2.84	0.02	0.04	FBpp0305141	Rpn8	-1.31	-1.47	0.02	0.01
FBpp0086590	Ciao1	0.99	1.00	0.07	0.07	FBpp0083861	Rpn9	-0.72	-1.11	0.17	0.05
FBpp0310070	cib	0.76	0.78	0.18	0.17	FBpp0310720	RpS10b	-1.38	-0.70	0.10	0.37
FBpp0070064	cin	0.67	-0.84	0.49	0.39	FBpp0075612	RpS12	0.17	0.14	0.70	0.76
FBpp0311360	CkIIalpha	-1.65	-2.44	0.21	0.08	FBpp0312104	RpS13	-0.03	-0.10	0.98	0.93
FBpp0079399	Cks30A	1.30	0.64	0.10	0.40	FBpp0311458	RpS14b	0.95	0.54	0.20	0.45
FBpp0303003	cl	0.63	0.04	0.24	0.94	FBpp0290052	RpS15Aa	-0.98	-1.23	0.10	0.05
FBpp0305007	Clc	1.84	1.83	0.00	0.00	FBpp0309759	RpS16	-2.58	-2.47	0.11	0.13
FBpp0305372	clu	0.53	-0.74	0.45	0.31	FBpp0076207	RpS17	-0.13	-0.88	0.86	0.24
FBpp0292516	CNBP	2.52	1.33	0.05	0.27	FBpp0085586	RpS18	-2.16	-1.54	0.03	0.09
FBpp0301625	cnn	0.13	0.47	0.82	0.42	FBpp0311350	RpS19a	-0.62	0.15	0.38	0.83
FBpp0307640	coro	-1.94	-2.04	0.03	0.02	FBpp0311561	RpS2	-1.43	-0.85	0.13	0.35
FBpp0308977	Cp1	0.50	-0.27	0.55	0.75	FBpp0307130	RpS21	0.40	0.15	0.50	0.80
FBpp0071150	Cp36	2.06	2.01	0.02	0.02	FBpp0308991	RpS23	0.09	-0.35	0.92	0.69
FBpp0071461	cpa	-0.37	-0.29	0.50	0.59	FBpp0071846	RpS24	-4.00	-3.90	0.03	0.03
FBpp0304020	cpb	0.84	0.05	0.08	0.91	FBpp0081846	RpS25	-0.57	-1.15	0.27	0.04
FBpp0080484	Cse1	-0.58	-0.69	0.29	0.22	FBpp0312181	RpS26	0.96	1.76	0.36	0.11
FBpp0074841	CSN1b	-3.07	-1.59	0.07	0.32	FBpp0310057	RpS28b	0.60	0.44	0.19	0.32

FBpp0077927	CSN3	-1.61	-0.78	0.18	0.49	FBpp0312066	RpS3	1.07	0.81	0.10	0.20
FBpp0290448	CSN4	-1.40	-1.90	0.21	0.10	FBpp0300615	RpS3A	0.68	-0.27	0.46	0.77
FBpp0082743	CSN5	-1.35	-0.96	0.01	0.03	FBpp0312080	RpS4	-1.61	-1.37	0.01	0.02
FBpp0083658	CSN6	-0.39	-0.95	0.50	0.12	FBpp0071087	RpS6	-0.94	-1.22	0.07	0.03
FBpp0087821	CSN7	-2.18	-2.54	0.00	0.00	FBpp0308324	RpS7	-2.53	-2.32	0.02	0.03
FBpp0083075	CstF64	1.35	1.27	0.05	0.06	FBpp0311987	RpS8	-0.70	-0.56	0.41	0.51
FBpp0306584	CtBP	-0.55	-0.46	0.16	0.23	FBpp0088021	Rpt1	0.05	0.10	0.89	0.79
FBpp0086732	Ctf4	0.04	0.09	0.93	0.84	FBpp0311982	Rpt2	-0.74	-0.79	0.07	0.05
FBpp0311740	CTPsyn	-0.96	-1.35	0.06	0.01	FBpp0312031	Rpt3	0.48	0.71	0.49	0.32
FBpp0291369	Cul3	-0.78	-0.98	0.54	0.45	FBpp0293948	Rpt4	-0.73	-0.77	0.07	0.06
FBpp0290569	Cul4	-2.45	-1.40	0.11	0.33	FBpp0083843	Rpt5	-0.97	-0.90	0.25	0.29
FBpp0312102	cup	-0.87	-0.29	0.13	0.60	FBpp0076890	Rpt6	-0.60	-1.15	0.17	0.02
FBpp0074017	Cyp1	0.93	0.29	0.07	0.53	FBpp0077362	Rrp1	3.74	2.55	0.05	0.16
FBpp0086373	CysRS	1.04	0.45	0.04	0.32	FBpp0311555	Rrp40	-0.28	-0.34	0.52	0.43
FBpp0290739	D1	1.93	1.53	0.04	0.10	FBpp0081601	rump	-0.43	0.38	0.34	0.40
FBpp0084349	Dak1	-0.80	-0.75	0.06	0.07	FBpp0305462	S6k	-1.17	-0.19	0.36	0.88
FBpp0075498	DCTN1-p150	-1.13	-1.00	0.12	0.16	FBpp0089284	Sar1	2.80	2.55	0.02	0.03
FBpp0087722	DCTN2-p50	0.58	0.01	0.18	0.98	FBpp0074285	scu	2.79	1.31	0.01	0.14
FBpp0071098	dec-01	1.37	1.67	0.06	0.02	FBpp0311988	Sec13	-0.11	0.15	0.80	0.73
FBpp0291138	deltaCOP	-2.04	-0.71	0.01	0.29	FBpp0308424	Sec23	-0.23	0.22	0.57	0.60
FBpp0099688	Df31	1.64	1.38	0.01	0.02	FBpp0303000	Sec24CD	-0.18	0.03	0.85	0.97
FBpp0309535	dgt2	0.12	-0.33	0.81	0.53	FBpp0311417	Sec31	-1.70	-0.46	0.01	0.37
FBpp0305386	dgt4	1.00	1.64	0.16	0.03	FBpp0086691	SelD	-2.23	-1.93	0.01	0.02
FBpp0308700	dgt5	-1.61	-0.53	0.01	0.28	FBpp0076897	Sep 01	-0.51	0.40	0.39	0.50
FBpp0304991	Dhc64C	-1.74	-1.90	0.07	0.05	FBpp0307454	SerRS	-0.25	0.14	0.63	0.80
FBpp0078625	DhpD	-0.12	0.83	0.85	0.20	FBpp0082521	Set	0.53	0.57	0.21	0.18
FBpp0099973	Dhpr	-0.24	-0.26	0.84	0.82	FBpp0293269	SF2	2.32	0.71	0.06	0.53
FBpp0307849	Dhx15	-1.39	-0.92	0.05	0.16	FBpp0072494	Sf3b3	0.39	0.49	0.55	0.45
FBpp0311421	Dip-B	1.49	0.99	0.00	0.03	FBpp0296963	Sgt	0.21	-0.01	0.60	0.98
FBpp0073300	Dlic	-0.48	-0.67	0.31	0.17	FBpp0309359	shi	-0.96	-0.15	0.11	0.79
FBpp0076830	DnaJ-1	-0.75	0.42	0.13	0.39	FBpp0311477	Shmt	0.13	-0.10	0.76	0.82
FBpp0072041	DNAlig1	-1.01	-1.35	0.02	0.00	FBpp0087704	shrb	1.28	0.88	0.17	0.33
FBpp0073678	DNAlig4	0.60	0.55	0.54	0.58	FBpp0081710	sle	1.50	1.60	0.03	0.02
FBpp0083514	DNApol-alpha180	-1.31	-1.81	0.09	0.03	FBpp0086591	SMC2	2.76	2.70	0.00	0.01
FBpp0113035	DNApol-alpha73	-0.19	-0.25	0.82	0.77	FBpp0074065	SMC3	2.00	2.25	0.00	0.00
FBpp0075277	DNApol-delta	-1.19	-0.90	0.13	0.24	FBpp0081234	SmD2	-1.37	-0.54	0.13	0.52
FBpp0311418	Dp1	-0.95	-0.81	0.14	0.20	FBpp0079182	SmE	-0.06	-0.47	0.91	0.33
FBpp0311783	dpa	-0.59	-0.49	0.25	0.33	FBpp0305596	smid	-1.06	-0.82	0.14	0.24
FBpp0083673	Dph5	-0.81	-0.04	0.16	0.94	FBpp0302954	Smn	-1.19	0.53	0.27	0.61
FBpp0081331	DppIII	0.24	-0.12	0.53	0.75	FBpp0312081	Sms	0.03	0.53	0.96	0.49
FBpp0079701	Dpy-30L1	1.26	1.13	0.04	0.06	FBpp0078984	smt3	1.25	-0.05	0.32	0.97
FBpp0072744	dre4	2.85	2.99	0.00	0.00	FBpp0290893	sn	-0.13	-0.83	0.83	0.19
FBpp0082223	Droj2	-0.51	-0.70	0.30	0.17	FBpp0078331	Snr1	1.82	1.60	0.03	0.05
FBpp0307166	Drp1	-1.66	-1.57	0.02	0.02	FBpp0111906	SNRPG	-0.03	0.66	0.94	0.09
FBpp0308813	Dsp1	2.89	2.91	0.01	0.01	FBpp0077206	Snx1	-1.17	0.36	0.14	0.64
FBpp0079746	dUTPase	0.77	-0.41	0.31	0.58	FBpp0297300	Snx6	-2.45	-1.26	0.02	0.16
FBpp0305157	Eb1	0.41	0.58	0.45	0.29	FBpp0075958	Sod1	0.17	0.06	0.65	0.88
FBpp0311273	eEF1alpha 1	-0.66	-0.54	0.12	0.19	FBpp0072164	spag	-0.29	-0.02	0.51	0.97
FBpp0311691	eEF1beta	1.04	0.91	0.04	0.07	FBpp0297149	SpdS	-0.29	-0.64	0.63	0.30
FBpp0079542	eEF1delta	0.13	-0.37	0.81	0.50	FBpp0310470	spel1	-1.43	-0.67	0.11	0.44
FBpp0305182	eEF2	0.09	-0.71	0.85	0.18	FBpp0071184	Sptr	0.24	0.31	0.68	0.59
FBpp0072082	eEF5	0.33	-0.39	0.58	0.51	FBpp0082320	sqd	-0.98	1.32	0.34	0.21
FBpp0307824	eff	-3.72	-2.38	0.04	0.15	FBpp0076244	Srp68	-2.48	-0.54	0.04	0.61
FBpp0310418	eIF1A	0.43	-0.11	0.57	0.88	FBpp0079211	Ssb-c31a	0.03	0.47	0.94	0.31

FBpp0309768	eIF2alpha	-0.79	-0.60	0.06	0.13	FBpp0072151	Ssrp	0.91	0.83	0.06	0.08
FBpp0075700	eIF2beta	0.55	-1.07	0.47	0.18	FBpp0308666	sta	-0.94	-0.48	0.25	0.55
FBpp0307983	eIF2gamma	-0.13	-0.48	0.78	0.32	FBpp0078827	stai	1.24	0.70	0.10	0.34
FBpp0312226	eIF3a	-0.70	-0.81	0.18	0.13	FBpp0077790	Stip1	1.00	1.19	0.05	0.02
FBpp0086098	eIF3b	-0.73	-0.62	0.44	0.51	FBpp0082134	Su(fu)	-2.72	-1.41	0.02	0.19
FBpp0309235	eIF3c	-0.86	-0.66	0.43	0.54	FBpp0079252	Su(var)205	2.41	1.46	0.10	0.30
FBpp0088565	eIF3d1	-1.26	-0.50	0.21	0.61	FBpp0309319	sw	0.96	0.90	0.17	0.20
FBpp0075104	eIF3e	0.69	1.65	0.61	0.23	FBpp0303744	swm	-0.23	-0.35	0.70	0.57
FBpp0070430	eIF3g1	-1.16	-0.32	0.07	0.59	FBpp0085422	sxc	-1.67	-0.26	0.02	0.67
FBpp0089133	eIF3h	-2.66	-1.41	0.05	0.27	FBpp0304719	tacc	1.66	1.75	0.06	0.05
FBpp0078689	eIF3i	0.33	1.43	0.63	0.06	FBpp0072050	Taldo	0.92	1.00	0.04	0.03
FBpp0308512	eIF3j	0.63	0.50	0.14	0.23	FBpp0304616	Tbc1d15-17	-0.42	1.50	0.68	0.16
FBpp0075754	eIF3l	-3.36	-2.69	0.03	0.07	FBpp0085690	TBCB	-0.04	-0.18	0.95	0.78
FBpp0308985	eIF3m	-1.10	-0.71	0.02	0.11	FBpp0081820	Tctp	0.38	0.30	0.29	0.40
FBpp0303628	eIF4A	-0.35	-0.52	0.37	0.19	FBpp0087479	TER94	-0.69	-1.50	0.18	0.01
FBpp0112403	eIF4B	0.66	1.63	0.22	0.01	FBpp0083355	TFAM	6.15	6.17	0.00	0.00
FBpp0306017	eIF4E1	-0.30	-0.68	0.69	0.38	FBpp0304751	TfIIS	2.10	1.18	0.05	0.23
FBpp0288389	eIF4G1	-0.98	-0.17	0.06	0.71	FBpp0312095	ThrRS	-0.24	0.06	0.63	0.90
FBpp0310226	eIF4H1	0.68	-0.04	0.51	0.97	FBpp0082180	timeout	-0.28	-1.52	0.76	0.13
FBpp0089140	eIF5	-0.97	-1.64	0.17	0.03	FBpp0088899	Tm1	1.38	1.93	0.02	0.00
FBpp0301573	eIF5B	-1.39	-0.25	0.05	0.70	FBpp0305273	Tnpo	-3.05	-4.15	0.06	0.02
FBpp0072144	eIF6	-1.54	-1.19	0.12	0.22	FBpp0304598	Top2	6.24	5.12	0.00	0.00
FBpp0311547	Eip55E	0.16	-0.05	0.66	0.89	FBpp0084950	Tpi	0.55	0.08	0.17	0.83
FBpp0083354	EloB	1.44	0.30	0.15	0.75	FBpp0310608	TppII	0.39	0.09	0.61	0.91
FBpp0085725	EloC	0.31	0.85	0.65	0.23	FBpp0304888	tral	0.35	0.85	0.48	0.11
FBpp0079278	emb	-2.70	-1.53	0.02	0.14	FBpp0081461	TrpRS	-1.38	-0.72	0.13	0.41
FBpp0303860	EndoGI	0.68	-0.51	0.31	0.45	FBpp0087398	trsn	-0.56	-1.50	0.39	0.04
FBpp0305267	endos	1.36	0.12	0.20	0.91	FBpp0079437	Trx-2	-0.41	0.29	0.76	0.83
FBpp0077574	Eno	0.90	0.36	0.11	0.50	FBpp0071115	Trxr-1	0.27	0.16	0.50	0.69
FBpp0078891	epsilonCOP	-0.65	-0.68	0.17	0.16	FBpp0310349	Ts	-0.40	0.88	0.46	0.12
FBpp0304201	eRF1	-2.66	-2.02	0.01	0.03	FBpp0312205	Tsf1	0.28	0.30	0.47	0.45
FBpp0311174	eRF3	-1.02	-0.15	0.04	0.73	FBpp0072097	tsr	0.14	0.21	0.72	0.59
FBpp0087164	ERp60	1.23	-0.37	0.16	0.65	FBpp0112273	Ttd14	-1.50	0.41	0.18	0.70
FBpp0099726	fabp	-0.96	-0.96	0.04	0.04	FBpp0087973	TTLL12	-3.30	-1.31	0.03	0.32
FBpp0308326	faf	-1.06	-0.98	0.03	0.04	FBpp0071508	tud	-0.87	-0.67	0.40	0.51
FBpp0307371	FASN1	-0.20	0.48	0.80	0.53	FBpp0304417	Tudor-SN	-1.40	-0.67	0.08	0.38
FBpp0081767	Fdh	0.84	0.26	0.13	0.62	FBpp0082352	twf	-0.65	-0.57	0.15	0.20
FBpp0083551	fit	1.04	0.17	0.36	0.88	FBpp0311386	tws	-0.28	-0.57	0.49	0.18
FBpp0085703	Fkbp12	0.85	-0.04	0.24	0.96	FBpp0076804	Txl	0.98	1.04	0.30	0.28
FBpp0082574	Fkbp39	-0.65	-0.51	0.17	0.27	FBpp0311757	tyf	-0.44	0.39	0.63	0.67
FBpp0309663	Fkbp59	-0.54	-0.11	0.23	0.79	FBpp0075168	TyrRS	0.21	-0.47	0.59	0.23
FBpp0075581	flr	1.27	0.82	0.05	0.18	FBpp0077912	tzn	2.50	2.31	0.01	0.02
FBpp0300445	Fmr1	0.51	1.02	0.35	0.08	FBpp0087583	Uba1	-0.68	-0.71	0.15	0.13
FBpp0304176	fmt	-1.54	-0.51	0.05	0.47	FBpp0076457	Uba2	-0.98	-1.28	0.20	0.11
FBpp0307904	Fnta	0.03	-0.68	0.94	0.12	FBpp0305606	Uba4	-2.71	-1.30	0.00	0.01
FBpp0290502	fon	2.47	1.81	0.02	0.08	FBpp0073354	Uba5	-0.95	-0.09	0.23	0.91
FBpp0294038	Fs(2)Ket	-0.65	-0.25	0.10	0.49	FBpp0088522	Ubc10	-3.05	-1.33	0.08	0.40
FBpp0303129	gammaCOP	-0.96	-1.08	0.20	0.16	FBpp0311673	Ubc4	-0.54	0.33	0.50	0.67
FBpp0304827	gammaTub37C	-0.80	-0.64	0.04	0.08	FBpp0085529	ubl	1.28	0.61	0.13	0.44
FBpp0099914	Gapdh1	0.92	0.92	0.06	0.06	FBpp0309477	Ubqn	-0.37	0.58	0.61	0.42
FBpp0304864	Gapdh2	1.42	1.06	0.01	0.02	FBpp0292511	Uch	-1.03	-0.63	0.11	0.31
FBpp0308722	Gart	0.14	-0.30	0.70	0.40	FBpp0306000	Uch-L5	-0.70	-0.59	0.09	0.15
FBpp0311558	Gdi	0.51	-0.55	0.38	0.35	FBpp0311276	Uev1A	-0.55	1.04	0.46	0.18
FBpp0079819	Ge-1	-0.30	-0.95	0.75	0.33	FBpp0086402	Ufc1	-0.75	-0.20	0.52	0.86

FBpp0071406	Gip	-0.22	-0.67	0.59	0.13	FBpp0075952	Ufd1-like	-0.67	-0.55	0.08	0.14
FBpp0077263	gkt	3.15	2.85	0.01	0.01	FBpp0290913	UGP	-1.47	-1.42	0.01	0.01
FBpp0084240	GlnRS	1.32	0.08	0.01	0.85	FBpp0304650	UK114	0.59	0.62	0.13	0.12
FBpp0088085	Glo1	0.78	0.24	0.08	0.56	FBpp0081284	unc-45	-0.65	-0.15	0.25	0.78
FBpp0310754	glob1	1.35	1.23	0.14	0.17	FBpp0311454	und	-1.68	-1.94	0.01	0.01
FBpp0080489	glu	2.62	2.54	0.01	0.01	FBpp0311664	Unr	-0.39	0.70	0.38	0.13
FBpp0083898	GluProRS	2.23	1.39	0.07	0.23	FBpp0087607	Updo	0.24	0.69	0.76	0.38
FBpp0099923	GlyP	-0.15	-0.58	0.74	0.22	FBpp0304059	Usp14	-1.73	-2.27	0.00	0.00
FBpp0306062	GlyRS	-1.06	-1.32	0.05	0.02	FBpp0298309	Usp5	-0.99	-1.06	0.06	0.05
FBpp0305474	GlyS	-3.23	-1.99	0.07	0.23	FBpp0309600	Usp7	-0.59	-1.12	0.57	0.29
FBpp0071816	Gmer	0.45	1.01	0.41	0.08	FBpp0305353	ValRS	-0.71	-0.66	0.13	0.16
FBpp0099511	Gnf1	3.59	3.13	0.01	0.02	FBpp0311933	Vha13	-2.29	-0.97	0.28	0.64
FBpp0086371	Got1	1.60	0.66	0.03	0.30	FBpp0311965	Vha26	-0.54	-0.67	0.15	0.09
FBpp0077536	Got2	0.42	-0.05	0.38	0.91	FBpp0086468	Vha36-1	-1.24	-1.05	0.01	0.02
FBpp0084623	Gp93	0.55	1.38	0.68	0.32	FBpp0086320	Vha44	-2.14	-1.98	0.02	0.03
FBpp0305432	Gpdh1	-0.18	-1.11	0.66	0.02	FBpp0290875	Vha55	-0.06	-0.33	0.88	0.36
FBpp0080649	Grip71	-2.59	-0.36	0.03	0.73	FBpp0307597	Vha68-2	0.02	-0.28	0.96	0.50
FBpp0308932	gro	-0.09	0.50	0.91	0.50	FBpp0307142	VhaSFD	-0.83	0.24	0.32	0.77
FBpp0310520	grsm	0.18	-0.23	0.67	0.58	FBpp0310907	vib	-0.68	0.08	0.11	0.84
FBpp0290201	Gss2	-0.64	-0.24	0.17	0.59	FBpp0112266	vig2	1.36	2.34	0.06	0.00
FBpp0099824	GstD1	-0.23	0.02	0.70	0.97	FBpp0075690	vih	-1.58	-1.37	0.05	0.08
FBpp0311692	GstE11	-0.65	-0.58	0.70	0.73	FBpp0309623	Vinc	-0.87	-0.98	0.31	0.26
FBpp0291657	GstE13	-1.32	-0.97	0.17	0.30	FBpp0300187	vlc	0.05	1.06	0.92	0.06
FBpp0085855	GstE6	0.20	-1.29	0.70	0.03	FBpp0077625	Vps29	1.30	2.02	0.34	0.15
FBpp0076376	GstO1	0.19	1.43	0.78	0.06	FBpp0309628	Vps4	-2.32	-2.29	0.00	0.00
FBpp0076377	GstO2	0.36	0.89	0.35	0.04	FBpp0305334	Vps60	1.91	2.20	0.01	0.00
FBpp0099646	GstS1	0.35	0.30	0.53	0.59	FBpp0304416	wac	1.73	0.63	0.17	0.60
FBpp0288508	hang	3.98	3.19	0.00	0.00	FBpp0084579	wdb	-2.37	-1.56	0.00	0.02
FBpp0078319	Hat1	-0.59	-1.25	0.18	0.01	FBpp0300790	wds	3.85	2.46	0.01	0.04
FBpp0311793	HBS1	-1.57	-1.01	0.09	0.25	FBpp0112025	wmd	1.35	1.30	0.10	0.11
FBpp0073173	HDAC1	2.31	1.64	0.00	0.02	FBpp0307570	wrd	-0.41	-0.33	0.37	0.46
FBpp0078756	Hel25E	-1.24	-1.14	0.03	0.04	FBpp0083007	WRNexo	1.57	1.26	0.11	0.18
FBpp0305527	Hex-A	-1.40	-0.80	0.13	0.37	FBpp0079472	yip2	1.38	1.38	0.11	0.11
FBpp0305905	HIP-R	0.50	0.58	0.19	0.14	FBpp0073715	yl	-0.14	0.57	0.84	0.41
FBpp0306426	His2Av	7.28	1.45	0.00	0.07	FBpp0312020	Yp1	0.45	0.19	0.24	0.60
FBpp0091155	His2B	4.84	4.19	0.00	0.00	FBpp0308710	Yp2	0.73	1.00	0.10	0.04
FBpp0091112	His3	-1.55	-1.79	0.39	0.32	FBpp0311924	Yp3	0.86	0.43	0.05	0.30
FBpp0309302	His3.3B	-2.12	0.56	0.31	0.78	FBpp0297134	yps	2.84	2.19	0.02	0.05
FBpp0306146	His4r	3.31	3.49	0.02	0.02	FBpp0099896	zip	-1.52	-1.30	0.13	0.19
FBpp0074365	HisRS	-0.33	-1.42	0.56	0.03	FBpp0071277	Zpr1	-3.12	-0.97	0.08	0.55
FBpp0311598	HmgD	2.67	1.23	0.05	0.31						

b) H2A – H2A.V – H2A.VΔC

		differences			p-values		
Flybase polypeptide ID	Flybase symbol	H2AV-H2A	H2AVΔC-H2A	H2AVΔC-H2AV	H2AV-H2A	H2AVΔC-H2A	H2AVΔC-H2AV
FBpp0300412	-	-1.02	0.02	1.04	0.07	0.97	0.07
FBpp0304748	-	0.00	-0.70	-0.70	0.99	0.17	0.17
FBpp0308925	-	0.13	-0.22	-0.35	0.77	0.61	0.43
FBpp0087084	128up	-0.72	-1.05	-0.33	0.35	0.18	0.66
FBpp0082987	14-3-3epsilon	-0.11	0.04	0.15	0.80	0.92	0.73
FBpp0305137	14-3-3zeta	0.59	0.00	-0.59	0.25	0.99	0.24
FBpp0075508	26-29-p	0.22	-0.24	-0.47	0.60	0.56	0.28
FBpp0087947	ACC	-0.35	0.54	0.89	0.47	0.28	0.08
FBpp0085204	Acf	-0.12	-1.07	-0.95	0.79	0.03	0.05

FBpp0307803	Acn	0.69	-0.23	-0.91	0.21	0.67	0.10
FBpp0071448	Act57B	0.88	0.94	0.06	0.22	0.19	0.93
FBpp0311818	Act5C	0.01	0.25	0.24	0.99	0.60	0.61
FBpp0100051	Adh	0.89	0.67	-0.23	0.16	0.28	0.71
FBpp0082816	AdSL	-1.16	-0.21	0.96	0.07	0.74	0.13
FBpp0083395	AdSS	-0.81	-0.90	-0.09	0.18	0.14	0.87
FBpp0075313	AGO2	0.61	0.77	0.16	0.19	0.11	0.73
FBpp0312000	Ahcy	-1.92	0.54	2.46	0.06	0.56	0.02
FBpp0087757	AIMP1	-0.81	-2.56	-1.75	0.23	0.00	0.02
FBpp0075318	AIMP2	-0.99	-2.52	-1.53	0.21	0.01	0.06
FBpp0071969	AIMP3	-0.64	-2.14	-1.50	0.34	0.01	0.04
FBpp0309215	Akap200	-0.89	-0.20	0.69	0.10	0.69	0.19
FBpp0089366	AlaRS	0.04	0.12	0.08	0.93	0.78	0.85
FBpp0308680	Ald	-0.12	0.31	0.43	0.82	0.54	0.41
FBpp0084610	ALiX	-0.16	0.27	0.43	0.72	0.55	0.34
FBpp0072694	alphaCOP	-0.35	-0.42	-0.08	0.45	0.36	0.87
FBpp0076122	alphaTub67C	-0.19	0.33	0.52	0.65	0.44	0.23
FBpp0081153	alphaTub84B	-0.58	-0.09	0.49	0.16	0.82	0.23
FBpp0290266	AMPdeam	-1.41	-0.17	1.24	0.09	0.83	0.13
FBpp0311374	Amun	-0.33	0.31	0.64	0.52	0.54	0.22
FBpp0082065	Aos1	-1.10	-0.80	0.30	0.07	0.18	0.61
FBpp0074558	AP-1-2beta	0.18	-0.01	-0.19	0.80	0.99	0.79
FBpp0305942	AP-1gamma	0.67	-0.16	-0.83	0.35	0.82	0.25
FBpp0301606	APC4	0.68	0.27	-0.41	0.39	0.73	0.60
FBpp0070907	APC7	0.42	0.07	-0.35	0.53	0.92	0.60
FBpp0311464	apolpp	-0.32	-0.47	-0.14	0.42	0.25	0.72
FBpp0305852	Arf102F	0.47	-0.04	-0.52	0.49	0.95	0.45
FBpp0304364	Arf79F	0.25	-0.03	-0.29	0.62	0.95	0.58
FBpp0304398	ArfGAP1	-0.20	-0.49	-0.29	0.76	0.46	0.66
FBpp0076271	Argk	0.61	0.17	-0.44	0.20	0.71	0.35
FBpp0073965	ArgRS	-0.93	-3.82	-2.90	0.12	0.00	0.00
FBpp0304830	AsnRS	1.13	0.73	-0.40	0.07	0.23	0.51
FBpp0308483	AspRS	-0.87	-3.52	-2.64	0.14	0.00	0.00
FBpp0306920	atms	-1.05	0.31	1.36	0.15	0.66	0.07
FBpp0289825	ATPCL	0.67	0.33	-0.35	0.26	0.57	0.55
FBpp0311086	ATPsynbeta	-0.56	-0.15	0.41	0.51	0.86	0.63
FBpp0082555	Atx2	-0.10	0.55	0.65	0.86	0.33	0.26
FBpp0079769	aurB	-0.20	-0.56	-0.36	0.63	0.19	0.39
FBpp0312191	awd	-0.27	-0.03	0.24	0.57	0.96	0.61
FBpp0300517	B52	0.88	0.23	-0.65	0.10	0.65	0.21
FBpp0305308	baf	-0.68	1.49	2.17	0.16	0.01	0.00
FBpp0084466	ball	-0.04	-0.68	-0.64	0.94	0.16	0.19
FBpp0071235	Bap111	0.54	0.01	-0.53	0.26	0.99	0.27
FBpp0086115	Bap55	0.26	-0.20	-0.46	0.56	0.66	0.31
FBpp0073572	Bap60	0.51	0.33	-0.17	0.30	0.49	0.72
FBpp0310394	barr	0.46	-0.56	-1.02	0.50	0.42	0.15
FBpp0305067	ben	0.98	0.31	-0.67	0.07	0.55	0.20
FBpp0085720	betaTub56D	-0.16	0.11	0.26	0.71	0.80	0.53
FBpp0086896	bic	0.46	0.46	0.00	0.45	0.45	1.00
FBpp0082428	BigH1	-0.89	-2.28	-1.40	0.07	0.00	0.01
FBpp0081910	Blm	0.17	-0.82	-0.99	0.74	0.13	0.07
FBpp0071794	blw	-0.55	-1.49	-0.94	0.35	0.02	0.12
FBpp0311234	bol	-0.05	0.43	0.48	0.93	0.42	0.37
FBpp0079417	borr	1.39	0.12	-1.27	0.10	0.88	0.13
FBpp0307610	brat	-0.75	-0.66	0.09	0.27	0.32	0.90
FBpp0305757	brm	0.49	0.20	-0.29	0.31	0.68	0.54
FBpp0304073	Bruce	-0.93	0.88	1.80	0.20	0.22	0.02
FBpp0083988	BRWD3	-0.58	2.30	2.88	0.28	0.00	0.00
FBpp0308293	Bub3	-0.22	-0.05	0.18	0.62	0.92	0.69
FBpp0085368	BubR1	0.22	-0.81	-1.03	0.75	0.25	0.15

FBpp0080450	BuGZ	0.03	0.48	0.45	0.95	0.32	0.35
FBpp0310411	bur	0.54	0.37	-0.17	0.26	0.43	0.72
FBpp0309325	Bx	-0.90	-0.22	0.68	0.18	0.73	0.31
FBpp0087402	Caf1-105	0.18	-0.83	-1.01	0.75	0.16	0.10
FBpp0071172	Caf1-180	-0.40	-1.39	-0.99	0.39	0.01	0.05
FBpp0082511	Caf1-55	0.04	-0.19	-0.23	0.93	0.67	0.60
FBpp0311269	Cam	-0.11	-0.52	-0.41	0.79	0.22	0.33
FBpp0304507	Cand1	0.06	-0.43	-0.49	0.90	0.36	0.30
FBpp0084818	Cap-D2	0.01	-0.71	-0.72	0.98	0.15	0.15
FBpp0288780	Cap-G	-0.38	-1.53	-1.15	0.47	0.01	0.04
FBpp0099391	capt	-0.08	-0.30	-0.22	0.87	0.54	0.66
FBpp0083684	CCT1	0.21	-0.22	-0.43	0.62	0.62	0.33
FBpp0071226	CCT2	0.44	-0.24	-0.68	0.38	0.63	0.18
FBpp0291566	CCT3	-0.02	-0.05	-0.03	0.96	0.92	0.95
FBpp0079992	CCT4	-0.12	-0.55	-0.43	0.82	0.31	0.43
FBpp0087095	CCT5	0.30	-0.09	-0.39	0.50	0.83	0.38
FBpp0073902	CCT6	-0.13	-0.16	-0.03	0.76	0.70	0.94
FBpp0081401	CCT7	0.24	-0.18	-0.42	0.59	0.69	0.35
FBpp0087764	CCT8	0.38	-0.13	-0.51	0.42	0.79	0.29
FBpp0083769	Cdc16	-0.55	-0.53	0.02	0.35	0.36	0.97
FBpp0305185	Cdc23	0.35	0.43	0.08	0.62	0.55	0.92
FBpp0305561	Cdc27	0.55	0.25	-0.29	0.34	0.65	0.60
FBpp0072660	Cdc37	0.57	-0.10	-0.67	0.28	0.85	0.21
FBpp0289951	Cdc5	0.01	-0.09	-0.10	0.99	0.87	0.86
FBpp0076371	Cdc6	-0.01	-1.18	-1.18	0.99	0.02	0.03
FBpp0079641	Cdk1	0.14	-0.28	-0.42	0.73	0.51	0.32
FBpp0303413	CDK2AP1	-0.14	-1.57	-1.43	0.85	0.04	0.06
FBpp0305296	CG10077	0.20	-0.88	-1.08	0.66	0.07	0.03
FBpp0306293	CG10237	0.17	-0.23	-0.39	0.78	0.70	0.52
FBpp0309810	CG10341	0.02	1.10	1.08	0.97	0.07	0.08
FBpp0311825	CG10576	0.15	-0.65	-0.80	0.74	0.16	0.09
FBpp0112044	CG11486	-0.04	0.71	0.74	0.94	0.12	0.11
FBpp0072658	CG12018	0.19	0.12	-0.07	0.69	0.80	0.88
FBpp0078279	CG1218	0.78	0.84	0.06	0.21	0.18	0.92
FBpp0083036	CG12321	0.95	-0.23	-1.19	0.33	0.81	0.23
FBpp0087300	CG12391	-0.75	-0.26	0.49	0.10	0.55	0.27
FBpp0305787	CG13025	-0.15	-1.80	-1.65	0.78	0.00	0.01
FBpp0308521	CG13366	-0.43	0.32	0.74	0.59	0.69	0.35
FBpp0307859	CG1354	-0.54	-0.90	-0.36	0.44	0.21	0.61
FBpp0077750	CG13690	0.74	-0.54	-1.28	0.10	0.21	0.01
FBpp0085260	CG1416	0.03	-0.47	-0.50	0.94	0.30	0.27
FBpp0311267	CG14215	-0.79	-0.30	0.48	0.13	0.54	0.34
FBpp0077145	CG15439	0.58	0.35	-0.23	0.36	0.58	0.71
FBpp0077144	CG15440	-2.37	-0.30	2.07	0.00	0.58	0.00
FBpp0112211	CG1646	-1.15	0.00	1.15	0.07	1.00	0.07
FBpp0312121	CG16772	-0.09	0.69	0.79	0.87	0.22	0.17
FBpp0300672	CG16817	0.35	-0.12	-0.47	0.47	0.80	0.34
FBpp0310240	CG1703	1.10	0.24	-0.86	0.03	0.60	0.08
FBpp0085374	CG17337	0.37	0.68	0.31	0.44	0.17	0.51
FBpp0311847	CG18067	-4.84	0.14	4.99	0.00	0.81	0.00
FBpp0271746	CG18190	0.17	-0.59	-0.76	0.79	0.38	0.26
FBpp0303935	CG18815	1.12	0.11	-1.01	0.05	0.84	0.07
FBpp0304910	CG2034	-0.60	0.34	0.94	0.25	0.50	0.08
FBpp0078327	CG2091	-0.69	0.12	0.81	0.23	0.83	0.16
FBpp0311613	CG2852	-0.77	-0.08	0.70	0.10	0.86	0.13
FBpp0307127	CG2862	-0.71	-1.17	-0.45	0.48	0.26	0.65
FBpp0290146	CG30122	-0.56	0.04	0.61	0.38	0.94	0.35
FBpp0085581	CG30151	0.58	0.95	0.37	0.33	0.12	0.53
FBpp0291433	CG30382	0.38	0.11	-0.27	0.45	0.82	0.59
FBpp0307202	CG31549	-0.04	0.05	0.09	0.96	0.94	0.89

FBpp0303949	CG32164	0.35	-0.64	-0.99	0.55	0.29	0.11
FBpp0073178	CG32243	0.19	-0.13	-0.32	0.76	0.83	0.60
FBpp0070953	CG3226	0.43	-0.20	-0.62	0.51	0.75	0.33
FBpp0078978	CG3430	0.99	0.35	-0.64	0.15	0.59	0.34
FBpp0076204	CG3448	-0.60	-0.58	0.01	0.26	0.27	0.98
FBpp0070273	CG3740	-0.59	0.23	0.82	0.37	0.72	0.22
FBpp0081650	CG3909	-0.37	-1.29	-0.92	0.85	0.50	0.63
FBpp0288574	CG42232	-0.18	-0.37	-0.18	0.68	0.41	0.68
FBpp0083246	CG4390	0.09	0.25	0.16	0.89	0.71	0.82
FBpp0112210	CG4951	3.61	4.13	0.52	0.00	0.00	0.30
FBpp0303029	CG5098	1.41	1.19	-0.22	0.06	0.10	0.75
FBpp0309480	CG5162	-0.42	-0.63	-0.21	0.41	0.23	0.68
FBpp0309317	CG5174	0.16	-0.95	-1.11	0.75	0.08	0.04
FBpp0303961	CG5199	-0.12	0.33	0.45	0.79	0.48	0.33
FBpp0079637	CG5355	-0.34	-0.59	-0.26	0.47	0.21	0.57
FBpp0084281	CG5886	0.24	-1.44	-1.68	0.69	0.03	0.02
FBpp0303937	CG6084	0.10	0.48	0.38	0.85	0.35	0.46
FBpp0079979	CG6180	0.02	0.34	0.32	0.96	0.45	0.48
FBpp0079809	CG6287	-0.63	-0.25	0.38	0.19	0.59	0.42
FBpp0080044	CG6523	0.44	0.80	0.36	0.66	0.43	0.72
FBpp0307760	CG6693	-0.28	-0.50	-0.22	0.55	0.29	0.64
FBpp0311284	CG6767	0.63	0.19	-0.44	0.17	0.67	0.33
FBpp0293610	CG7546	0.12	0.24	0.12	0.84	0.67	0.83
FBpp0087347	CG7637	1.28	2.20	0.92	0.03	0.00	0.10
FBpp0306682	CG7927	-1.34	-0.94	0.40	0.21	0.37	0.70
FBpp0075353	CG7945	-0.38	0.19	0.57	0.57	0.77	0.39
FBpp0302568	CG7946	-0.54	-1.38	-0.84	0.43	0.06	0.22
FBpp0292226	CG7971	-0.30	-0.06	0.25	0.52	0.91	0.60
FBpp0303962	CG8003	-0.05	-0.67	-0.62	0.92	0.18	0.22
FBpp0081371	CG8036	-0.57	-0.23	0.34	0.24	0.62	0.48
FBpp0074246	CG8142	0.06	-0.07	-0.13	0.90	0.87	0.77
FBpp0087733	CG8243	-0.09	0.44	0.53	0.86	0.36	0.28
FBpp0087116	CG8858	-0.30	0.01	0.31	0.60	0.99	0.59
FBpp0309119	CG8963	-0.59	-0.26	0.33	0.39	0.70	0.63
FBpp0311963	CG9135	0.52	-0.09	-0.61	0.26	0.83	0.19
FBpp0072610	CG9184	1.06	1.66	0.59	0.41	0.21	0.64
FBpp0309269	CG9281	0.93	0.34	-0.59	0.07	0.48	0.23
FBpp0082626	CG9590	-0.34	-2.59	-2.25	0.53	0.00	0.00
FBpp0081343	CG9601	-0.23	-1.04	-0.82	0.64	0.04	0.11
FBpp0305785	CG9674	0.49	0.93	0.44	0.49	0.20	0.54
FBpp0308531	Chc	-0.02	-0.51	-0.50	0.97	0.26	0.28
FBpp0074766	Chd3	0.88	1.00	0.12	0.22	0.17	0.86
FBpp0301152	chic	0.73	1.25	0.52	0.24	0.06	0.40
FBpp0308688	Chrac-16	0.11	-1.43	-1.54	0.79	0.00	0.00
FBpp0310070	cib	-0.18	-0.11	0.08	0.70	0.83	0.87
FBpp0311360	CkIIalpha	0.42	0.60	0.18	0.33	0.17	0.67
FBpp0305406	CkIIbeta	-0.96	0.26	1.22	0.12	0.66	0.06
FBpp0079399	Cks30A	-0.58	-1.27	-0.69	0.40	0.08	0.33
FBpp0304514	cmet	-0.75	-0.62	0.14	0.22	0.31	0.82
FBpp0292516	CNBP	0.54	-0.38	-0.92	0.28	0.43	0.07
FBpp0301625	cnn	0.34	-0.03	-0.37	0.46	0.95	0.43
FBpp0304029	Cnot4	-0.12	0.24	0.36	0.79	0.60	0.44
FBpp0076299	Cp15	-1.78	0.05	1.83	0.01	0.93	0.01
FBpp0076300	Cp19	-0.13	0.38	0.51	0.78	0.43	0.30
FBpp0071148	Cp7Fb	-0.23	-0.67	-0.45	0.79	0.43	0.60
FBpp0080484	Cse1	0.02	-0.28	-0.30	0.96	0.53	0.49
FBpp0077927	CSN3	-1.69	-1.10	0.59	0.03	0.12	0.39
FBpp0083658	CSN6	0.47	0.41	-0.06	0.30	0.36	0.89
FBpp0087821	CSN7	0.90	0.60	-0.30	0.20	0.38	0.65
FBpp0086732	Ctf4	0.08	-0.90	-0.98	0.89	0.12	0.09

FBpp0311740	CTPsyn	-0.31	0.21	0.52	0.54	0.68	0.31
FBpp0072562	Ctr9	-0.37	0.17	0.54	0.57	0.79	0.41
FBpp0310479	ctrip	-2.05	-2.20	-0.15	0.02	0.01	0.85
FBpp0087924	Cul1	-1.38	-2.64	-1.25	0.38	0.10	0.42
FBpp0290569	Cul4	0.88	2.41	1.53	0.38	0.03	0.14
FBpp0312102	cup	0.03	-1.13	-1.16	0.96	0.05	0.04
FBpp0071822	CycB	0.86	-0.63	-1.49	0.08	0.19	0.01
FBpp0074017	Cyp1	-0.79	-0.31	0.49	0.08	0.48	0.27
FBpp0086373	CysRS	0.81	0.06	-0.75	0.25	0.93	0.28
FBpp0084349	Dak1	0.24	0.26	0.03	0.61	0.57	0.95
FBpp0112438	Dbp80	0.05	-0.62	-0.68	0.93	0.31	0.27
FBpp0306615	dco	-1.10	-2.00	-0.89	0.11	0.01	0.19
FBpp0071097	dec-1	0.32	-0.16	-0.47	0.53	0.75	0.36
FBpp0305164	Dek	-0.61	1.29	1.90	0.28	0.03	0.00
FBpp0082849	Det	-0.09	-0.62	-0.54	0.92	0.46	0.52
FBpp0099688	Df31	-0.26	0.38	0.64	0.63	0.48	0.24
FBpp0084783	dgt6	0.11	-0.18	-0.29	0.88	0.81	0.70
FBpp0304991	Dhc64C	0.96	-0.05	-1.01	0.08	0.92	0.07
FBpp0311766	dhd	-0.98	0.54	1.52	0.30	0.56	0.12
FBpp0307849	Dhx15	-1.82	-1.72	0.10	0.03	0.04	0.90
FBpp0290598	dl	-0.03	0.17	0.20	0.96	0.81	0.77
FBpp0082996	Dlc90F	1.43	1.36	-0.07	0.05	0.07	0.92
FBpp0073299	Dlic	0.49	0.16	-0.33	0.63	0.87	0.74
FBpp0076830	DnaJ-1	0.38	0.65	0.28	0.46	0.21	0.58
FBpp0072041	DNAlig1	0.20	-0.65	-0.85	0.69	0.21	0.11
FBpp0073678	DNAlig4	-0.38	-0.16	0.22	0.46	0.75	0.66
FBpp0075277	DNApol-delta	-0.49	-0.58	-0.09	0.36	0.29	0.87
FBpp0311418	Dp1	0.00	-0.62	-0.62	1.00	0.37	0.37
FBpp0311783	dpa	0.23	0.22	-0.01	0.61	0.63	0.98
FBpp0081331	DppIII	-1.02	-1.18	-0.16	0.03	0.02	0.72
FBpp0072744	dre4	-0.41	0.72	1.13	0.38	0.14	0.03
FBpp0082223	Droj2	0.04	-0.35	-0.39	0.93	0.43	0.38
FBpp0307166	Drp1	0.30	-0.31	-0.61	0.61	0.59	0.30
FBpp0309113	Dsor1	0.80	0.21	-0.59	0.14	0.69	0.27
FBpp0308813	Dsp1	-0.06	-1.30	-1.24	0.90	0.01	0.02
FBpp0079746	dUTPase	0.88	0.36	-0.52	0.08	0.46	0.29
FBpp0304413	E(bx)	0.63	0.46	-0.18	0.23	0.38	0.73
FBpp0305157	Eb1	0.45	-0.17	-0.62	0.34	0.72	0.20
FBpp0311273	eEF1alpha1	0.05	-0.48	-0.53	0.92	0.34	0.29
FBpp0311691	eEF1beta	0.01	-0.24	-0.25	0.99	0.58	0.57
FBpp0079542	eEF1delta	0.46	-0.01	-0.47	0.33	0.99	0.32
FBpp0305182	eEF2	0.21	0.42	0.21	0.66	0.38	0.66
FBpp0072082	eEF5	-0.05	0.11	0.16	0.89	0.79	0.69
FBpp0307824	eff	-0.51	-0.68	-0.16	0.42	0.29	0.80
FBpp0309768	eIF2alpha	-0.18	-0.64	-0.46	0.69	0.16	0.30
FBpp0291521	eIF2Bdelta	0.40	-1.10	-1.50	0.45	0.05	0.01
FBpp0075700	eIF2beta	1.95	1.45	-0.50	0.01	0.04	0.45
FBpp0307983	eIF2gamma	0.14	-0.57	-0.72	0.75	0.21	0.12
FBpp0309235	eIF3c	-1.15	-1.32	-0.17	0.12	0.08	0.81
FBpp0075104	eIF3e	0.23	0.05	-0.18	0.61	0.91	0.69
FBpp0070430	eIF3g1	-0.22	-0.57	-0.35	0.74	0.40	0.60
FBpp0071587	eIF3k	0.60	0.01	-0.59	0.23	0.98	0.24
FBpp0075754	eIF3l	-0.15	-0.51	-0.36	0.77	0.32	0.47
FBpp0303628	eIF4A	-0.02	-0.20	-0.18	0.96	0.66	0.69
FBpp0306017	eIF4E1	0.46	0.03	-0.43	0.36	0.94	0.39
FBpp0288389	eIF4G1	-0.30	-1.01	-0.71	0.54	0.05	0.16
FBpp0310225	eIF4H1	0.29	-0.62	-0.91	0.54	0.20	0.07
FBpp0089140	eIF5	0.55	0.04	-0.51	0.45	0.96	0.48
FBpp0301573	eIF5B	-0.85	-1.20	-0.35	0.16	0.06	0.55
FBpp0088654	elg1	1.01	0.41	-0.60	0.11	0.50	0.32

FBpp0083354	EloB	-0.44	0.46	0.91	0.36	0.34	0.07
FBpp0085725	EloC	-0.37	-0.30	0.07	0.45	0.55	0.88
FBpp0079278	emb	1.12	0.91	-0.20	0.16	0.25	0.79
FBpp0305267	endos	0.09	0.33	0.24	0.88	0.57	0.67
FBpp0077574	Eno	-0.45	0.29	0.75	0.31	0.50	0.10
FBpp0304201	eRF1	0.49	0.07	-0.42	0.27	0.88	0.34
FBpp0311174	eRF3	0.52	0.39	-0.13	0.26	0.39	0.78
FBpp0099726	fabp	0.07	0.08	0.01	0.88	0.86	0.98
FBpp0308326	faf	-0.15	-1.12	-0.97	0.76	0.03	0.06
FBpp0083399	Fancd2	-0.60	-1.44	-0.84	0.25	0.01	0.12
FBpp0087756	FANCl	-0.56	-1.26	-0.70	0.26	0.02	0.16
FBpp0307371	FASN1	-0.88	-0.85	0.03	0.23	0.25	0.97
FBpp0081767	Fdh	-0.06	0.07	0.13	0.91	0.90	0.81
FBpp0086223	Fen1	-0.39	-2.55	-2.16	0.45	0.00	0.00
FBpp0073266	feo	0.77	0.36	-0.41	0.25	0.59	0.53
FBpp0071892	Fib	0.34	-0.47	-0.81	0.45	0.31	0.09
FBpp0074215	Fim	-0.63	-0.14	0.49	0.34	0.83	0.45
FBpp0271718	Fis1	-0.08	-0.36	-0.28	0.91	0.61	0.69
FBpp0083551	fit	0.25	0.35	0.10	0.54	0.40	0.81
FBpp0082574	FK506-bp1	-0.89	1.02	1.90	0.06	0.03	0.00
FBpp0085703	FK506-bp2	-0.24	0.05	0.29	0.65	0.93	0.58
FBpp0309663	FKBP59	0.43	0.26	-0.17	0.38	0.59	0.73
FBpp0311112	flfl	-0.79	0.22	1.01	0.18	0.69	0.09
FBpp0075581	flr	-0.23	-0.10	0.14	0.70	0.88	0.82
FBpp0300445	Fmr1	0.52	-0.23	-0.75	0.46	0.74	0.29
FBpp0304175	fmt	-0.78	-0.12	0.66	0.22	0.85	0.30
FBpp0290502	fon	-1.69	-1.53	0.16	0.01	0.01	0.77
FBpp0294038	Fs(2)Ket	0.14	-0.54	-0.68	0.79	0.32	0.21
FBpp0290505	gammaCOP	1.03	0.42	-0.62	0.04	0.37	0.20
FBpp0304827	gammaTub37C	-0.27	-0.90	-0.62	0.54	0.06	0.18
FBpp0099914	Gapdh1	-0.71	-1.22	-0.50	0.23	0.05	0.39
FBpp0304864	Gapdh2	-0.50	0.13	0.63	0.29	0.78	0.19
FBpp0311558	Gdi	0.49	0.55	0.06	0.32	0.27	0.89
FBpp0079819	Ge-1	-0.37	0.03	0.40	0.55	0.96	0.52
FBpp0071406	Gip	-1.89	-1.35	0.54	0.01	0.06	0.43
FBpp0077263	gkt	-0.52	-0.23	0.29	0.25	0.61	0.51
FBpp0084240	GlnRS	-0.77	-2.90	-2.14	0.18	0.00	0.00
FBpp0080489	glu	-0.20	-1.26	-1.06	0.67	0.02	0.04
FBpp0083898	GluProRS	-1.05	-3.47	-2.42	0.08	0.00	0.00
FBpp0099923	GlyP	0.75	0.95	0.20	0.11	0.05	0.65
FBpp0306062	GlyRS	-0.17	0.17	0.34	0.79	0.80	0.60
FBpp0082496	GlyS	-0.01	-1.11	-1.09	0.98	0.06	0.06
FBpp0078478	Gnf1	-0.10	-0.27	-0.17	0.83	0.56	0.70
FBpp0075793	Grip163	0.44	1.01	0.57	0.46	0.10	0.34
FBpp0290523	Grip84	-0.49	-0.67	-0.18	0.33	0.19	0.72
FBpp0073672	Grip91	-0.22	-0.27	-0.05	0.73	0.68	0.94
FBpp0099824	GstD1	0.65	0.19	-0.46	0.31	0.76	0.47
FBpp0085855	GstE6	0.12	0.07	-0.05	0.82	0.90	0.92
FBpp0076377	GstO2	-0.43	0.52	0.95	0.34	0.25	0.05
FBpp0099646	GstS1	-0.47	0.13	0.59	0.37	0.80	0.26
FBpp0296978	Gug	0.29	0.76	0.47	0.68	0.29	0.50
FBpp0302680	gw	-0.33	-0.33	0.00	0.49	0.49	1.00
FBpp0310171	hang	0.66	-1.25	-1.91	0.32	0.07	0.01
FBpp0078319	Hat1	0.44	-0.16	-0.60	0.41	0.77	0.27
FBpp0113091	hay	0.25	-1.78	-2.03	0.69	0.01	0.01
FBpp0311451	Hcf	-0.21	-1.13	-0.93	0.63	0.02	0.04
FBpp0073173	HDAC1	0.01	0.52	0.51	0.98	0.28	0.29
FBpp0078756	Hel25E	-0.19	-0.10	0.09	0.73	0.85	0.87
FBpp0312011	heph-RZ	-0.09	-0.77	-0.68	0.90	0.30	0.36
FBpp0072593	hfp	-0.18	0.16	0.34	0.68	0.71	0.44

FBpp0305905	HIP-R	-0.18	0.17	0.35	0.74	0.77	0.54
FBpp0071028	Hira	-0.26	-0.68	-0.42	0.62	0.21	0.44
FBpp0091110	His1:CG33864	-1.04	-3.39	-2.34	0.08	0.00	0.00
FBpp0091111	His2A	-6.04	-5.02	1.01	0.00	0.00	0.10
FBpp0306426	His2Av	5.51	1.28	-4.24	0.00	0.03	0.00
FBpp0091155	His2B	-0.15	-0.04	0.11	0.76	0.93	0.82
FBpp0306146	His4r	-0.24	0.56	0.80	0.64	0.28	0.13
FBpp0305939	HisRS	0.02	0.05	0.03	0.97	0.93	0.96
FBpp0071501	Hmg-2	0.38	0.23	-0.14	0.46	0.65	0.78
FBpp0307711	HnRNP-K	0.15	-0.45	-0.60	0.78	0.40	0.27
FBpp0307465	hoip	0.34	-0.13	-0.47	0.42	0.76	0.27
FBpp0297875	Hrb27C	0.28	0.55	0.27	0.58	0.28	0.59
FBpp0307982	Hsc70-4	-0.23	0.02	0.25	0.58	0.97	0.56
FBpp0305265	Hsc70Cb	-0.54	-0.40	0.13	0.34	0.47	0.81
FBpp0312157	Hsp26	0.00	-0.33	-0.33	0.99	0.54	0.55
FBpp0312159	Hsp27	0.00	-0.14	-0.14	0.99	0.77	0.77
FBpp0305095	Hsp83	0.19	-0.13	-0.32	0.68	0.78	0.49
FBpp0078152	IleRS	-0.99	-3.53	-2.54	0.10	0.00	0.00
FBpp0307848	Incenp	-0.22	-0.57	-0.35	0.63	0.23	0.45
FBpp0081861	Irbp	-0.44	-0.38	0.06	0.37	0.44	0.90
FBpp0086956	Iswi	-0.06	-0.82	-0.76	0.89	0.08	0.10
FBpp0311371	Jafrac1	-0.13	0.25	0.38	0.79	0.59	0.43
FBpp0089165	janA	-0.57	0.32	0.89	0.24	0.51	0.08
FBpp0307568	Karybeta3	0.45	-0.11	-0.56	0.39	0.84	0.29
FBpp0086328	Khc	0.30	-0.06	-0.36	0.56	0.91	0.49
FBpp0289115	kis	0.25	0.14	-0.11	0.60	0.77	0.81
FBpp0303946	Klc	-0.50	0.00	0.51	0.23	0.99	0.23
FBpp0312027	Klp10A	-0.24	-0.75	-0.52	0.67	0.19	0.36
FBpp0309092	Klp3A	-0.02	-0.12	-0.10	0.97	0.80	0.83
FBpp0312148	Klp67A	-2.96	-2.07	0.89	0.01	0.06	0.39
FBpp0078399	kra	0.69	-0.19	-0.88	0.24	0.74	0.14
FBpp0304367	kst	-1.25	-0.05	1.20	0.17	0.95	0.19
FBpp0080322	Ku80	-0.36	-0.41	-0.05	0.44	0.38	0.91
FBpp0080906	La	-0.50	0.05	0.54	0.39	0.93	0.34
FBpp0312110	Lam	-0.13	-0.19	-0.06	0.75	0.65	0.89
FBpp0076556	lark	1.59	1.89	0.30	0.08	0.04	0.72
FBpp0081255	lds	-0.30	-0.50	-0.20	0.52	0.29	0.66
FBpp0311704	LeuRS	-1.13	-3.80	-2.67	0.05	0.00	0.00
FBpp0073551	lic	0.44	-0.34	-0.78	0.29	0.41	0.07
FBpp0303481	lig	-0.06	0.53	0.59	0.91	0.33	0.28
FBpp0311512	lolal	0.72	0.25	-0.47	0.22	0.66	0.42
FBpp0078561	lost	0.26	-0.11	-0.37	0.54	0.80	0.39
FBpp0311908	Lsd-2	-0.01	0.09	0.10	0.98	0.85	0.83
FBpp0309608	lva	0.76	0.95	0.19	0.44	0.33	0.84
FBpp0301732	lwr	0.41	0.60	0.18	0.54	0.38	0.78
FBpp0292593	LysRS	-0.83	-3.65	-2.82	0.16	0.00	0.00
FBpp0087680	Mad1	-0.86	-0.30	0.56	0.14	0.59	0.33
FBpp0076819	mad2	0.24	-0.23	-0.47	0.71	0.73	0.48
FBpp0310551	mahe	-1.95	-2.49	-0.54	0.02	0.00	0.46
FBpp0085235	Map205	0.23	-0.56	-0.79	0.68	0.33	0.17
FBpp0087613	Map60	-1.74	-2.29	-0.54	0.02	0.00	0.40
FBpp0078631	Marcal1	0.23	-1.16	-1.39	0.67	0.04	0.02
FBpp0311207	mars	0.05	-0.12	-0.16	0.94	0.84	0.77
FBpp0293580	mask	-0.61	-0.71	-0.10	0.21	0.15	0.84
FBpp0311400	mats	0.17	-0.43	-0.60	0.76	0.45	0.30
FBpp0082081	MBD-R2	1.82	0.64	-1.17	0.00	0.24	0.04
FBpp0082137	mbo	0.49	0.92	0.43	0.33	0.08	0.40
FBpp0300203	Mccc1	-0.37	0.39	0.76	0.45	0.44	0.14
FBpp0081317	Mcm2	-0.06	0.25	0.32	0.92	0.68	0.61
FBpp0070729	Mcm3	-0.50	-0.42	0.08	0.38	0.46	0.88

FBpp0070913	Mcm6	-0.67	-0.53	0.14	0.36	0.47	0.84
FBpp0076312	Mcm7	0.16	-0.45	-0.61	0.78	0.43	0.29
FBpp0293887	MCTS1	0.51	0.87	0.37	0.26	0.07	0.42
FBpp0311560	Mdh1	0.07	0.27	0.19	0.87	0.56	0.67
FBpp0079565	me31B	0.14	-0.39	-0.53	0.79	0.48	0.34
FBpp0085809	MetRS	-1.09	-3.69	-2.60	0.07	0.00	0.00
FBpp0081882	mgr	0.14	0.86	0.72	0.83	0.20	0.29
FBpp0304462	Mi-2	0.23	0.11	-0.13	0.63	0.82	0.80
FBpp0297606	Mlf	-0.01	0.00	0.01	0.99	1.00	0.99
FBpp0303950	Mo25	-0.35	-0.38	-0.03	0.51	0.47	0.95
FBpp0082692	mor	0.49	0.21	-0.28	0.33	0.67	0.57
FBpp0079802	mre11	-0.25	-0.53	-0.27	0.60	0.29	0.58
FBpp0086340	mrj	0.03	0.40	0.37	0.94	0.39	0.43
FBpp0084256	msi	-0.04	0.20	0.24	0.93	0.65	0.59
FBpp0076408	msk	0.03	-0.71	-0.74	0.95	0.20	0.18
FBpp0293342	msps	-0.33	-1.48	-1.15	0.46	0.01	0.02
FBpp0304737	Mtor	-1.58	0.56	2.14	0.07	0.50	0.02
FBpp0310063	mts	-0.60	-0.66	-0.07	0.31	0.26	0.91
FBpp0305424	mub	-0.02	-1.37	-1.34	0.97	0.02	0.02
FBpp0111603	mute	-0.95	-0.23	0.72	0.13	0.71	0.24
FBpp0311394	Nacalpha	0.05	-0.69	-0.74	0.94	0.33	0.30
FBpp0297132	Nap1	0.12	0.00	-0.12	0.79	1.00	0.79
FBpp0306828	NAT1	-0.06	-0.09	-0.03	0.94	0.92	0.97
FBpp0297182	nbs	0.01	-0.15	-0.16	0.98	0.80	0.79
FBpp0311231	ncd	-0.25	-1.45	-1.20	0.66	0.02	0.05
FBpp0309711	Nedd8	0.91	2.20	1.29	0.17	0.00	0.06
FBpp0305289	NHP2	0.05	1.07	1.02	0.92	0.05	0.06
FBpp0306756	Nlp	0.19	0.51	0.33	0.72	0.33	0.53
FBpp0309175	NO66	0.22	-0.12	-0.34	0.61	0.78	0.43
FBpp0072839	Non2	0.08	0.54	0.46	0.89	0.37	0.45
FBpp0309274	nonA	-1.54	-2.20	-0.66	0.00	0.00	0.12
FBpp0078997	nop5	0.15	-0.66	-0.81	0.77	0.20	0.12
FBpp0290083	Nop60B	-0.84	0.44	1.28	0.12	0.40	0.03
FBpp0112220	Nph	0.14	0.33	0.19	0.81	0.59	0.76
FBpp0312079	Nplp2	-0.33	-0.81	-0.48	0.53	0.13	0.36
FBpp0297079	nudC	0.44	-0.50	-0.93	0.35	0.29	0.06
FBpp0079710	Nup107	-0.15	0.20	0.35	0.78	0.72	0.53
FBpp0310208	Nup160	-1.07	-0.99	0.07	0.08	0.10	0.90
FBpp0074568	Nup205	-0.93	-1.08	-0.15	0.25	0.18	0.85
FBpp0071905	Nup214	-0.11	-0.12	-0.01	0.84	0.83	0.99
FBpp0293235	Nup358	-0.36	0.14	0.50	0.43	0.76	0.29
FBpp0087938	Nup44A	0.17	-1.34	-1.51	0.75	0.03	0.01
FBpp0087063	Nup54	-0.82	0.20	1.02	0.17	0.73	0.09
FBpp0085954	Nup75	-1.16	-1.53	-0.37	0.10	0.04	0.59
FBpp0073659	Nup93-1	0.82	0.17	-0.65	0.13	0.74	0.22
FBpp0306915	Nup98-96	-0.12	0.59	0.71	0.83	0.28	0.20
FBpp0271761	Nurf-38	0.25	0.13	-0.11	0.57	0.76	0.80
FBpp0088033	Orc1	-0.31	-1.08	-0.77	0.55	0.05	0.15
FBpp0082329	Orc2	-0.36	-1.13	-0.77	0.47	0.04	0.14
FBpp0086882	Orc3	-0.01	-1.13	-1.12	0.98	0.02	0.02
FBpp0072330	Orc4	-0.09	-1.27	-1.18	0.85	0.02	0.02
FBpp0080120	Orc5	-0.29	-1.41	-1.12	0.52	0.01	0.02
FBpp0087566	Orc6	0.81	-0.52	-1.33	0.37	0.56	0.15
FBpp0088069	p47	0.88	0.19	-0.70	0.14	0.75	0.24
FBpp0085919	pAbp	0.01	-0.51	-0.51	0.99	0.27	0.26
FBpp0073976	Paf-AHalpha	-2.77	-2.89	-0.12	0.00	0.00	0.88
FBpp0305933	Paics	-1.12	0.04	1.16	0.03	0.93	0.02
FBpp0308411	PAN2	0.57	1.44	0.87	0.30	0.02	0.13
FBpp0112608	Parp	-0.45	-0.25	0.19	0.37	0.61	0.69
FBpp0308299	Patr-1	-0.28	0.49	0.77	0.59	0.36	0.16

FBpp0290074	PCB	-0.26	0.63	0.89	0.61	0.23	0.10
FBpp0308430	pch2	0.29	-0.04	-0.33	0.58	0.94	0.53
FBpp0078405	Pcmt	-0.03	1.25	1.28	0.95	0.04	0.04
FBpp0089395	PCNA	-0.25	-0.16	0.09	0.59	0.73	0.85
FBpp0086647	pea	0.87	-0.10	-0.98	0.09	0.83	0.06
FBpp0079527	Pen	0.09	-0.82	-0.91	0.87	0.14	0.11
FBpp0293516	Pep	-0.33	-0.91	-0.58	0.63	0.20	0.40
FBpp0304954	Pfdn2	-0.29	0.75	1.04	0.56	0.14	0.05
FBpp0306279	Pgk	-0.16	0.27	0.43	0.73	0.56	0.36
FBpp0099920	Pglym78	0.05	-0.14	-0.19	0.91	0.77	0.68
FBpp0087914	phr	1.00	1.21	0.22	0.30	0.21	0.82
FBpp0301844	Pl31	-0.07	0.53	0.60	0.89	0.28	0.23
FBpp0082177	pic	0.17	2.35	2.18	0.73	0.00	0.00
FBpp0310466	Plap	0.31	-0.56	-0.87	0.55	0.29	0.11
FBpp0085618	plu	0.66	0.63	-0.03	0.27	0.29	0.96
FBpp0305301	poe	-1.08	-0.59	0.49	0.11	0.37	0.45
FBpp0099722	polo	0.36	-0.26	-0.62	0.48	0.61	0.23
FBpp0084115	polybromo	0.86	0.82	-0.04	0.17	0.19	0.95
FBpp0081704	pont	-0.06	-0.56	-0.50	0.88	0.17	0.22
FBpp0082067	Pp1-87B	-0.12	-0.68	-0.56	0.79	0.16	0.25
FBpp0293227	Pp2A-29B	0.18	-0.40	-0.58	0.74	0.46	0.30
FBpp0301546	Pp2B-14D	-0.41	0.04	0.45	0.51	0.95	0.47
FBpp0304082	PpD3	-0.61	-0.03	0.59	0.46	0.97	0.48
FBpp0089154	PPP4R2r	-0.50	-0.37	0.13	0.43	0.56	0.84
FBpp0303849	PpV	0.45	0.36	-0.09	0.41	0.50	0.87
FBpp0099895	primo-1	0.81	-0.40	-1.21	0.26	0.57	0.10
FBpp0082062	Prosalpha2	-0.12	0.62	0.74	0.86	0.35	0.27
FBpp0071451	Prosalpha3	0.00	-0.13	-0.13	0.99	0.79	0.80
FBpp0073989	Prosalpha4	0.70	0.58	-0.12	0.33	0.42	0.87
FBpp0086067	Prosalpha5	0.87	0.59	-0.27	0.14	0.30	0.63
FBpp0310201	Prosalpha6	-0.16	0.03	0.19	0.71	0.94	0.65
FBpp0089041	Prosalpha7	0.22	0.18	-0.04	0.72	0.77	0.95
FBpp0086400	Prosbeta1	0.14	-0.85	-0.99	0.79	0.12	0.07
FBpp0075382	Prosbeta2	-0.12	0.01	0.13	0.81	0.98	0.79
FBpp0307141	Prosbeta4	-0.37	-1.15	-0.78	0.49	0.05	0.16
FBpp0087320	Prosbeta5	0.08	-0.78	-0.85	0.88	0.16	0.12
FBpp0075119	Prosbeta6	-0.34	-0.15	0.19	0.44	0.72	0.67
FBpp0078449	Prosbeta7	0.77	0.46	-0.31	0.20	0.43	0.60
FBpp0085902	Prp19	-0.09	0.39	0.47	0.86	0.45	0.35
FBpp0077368	Prx6005	-0.44	-1.28	-0.84	0.42	0.03	0.14
FBpp0305823	pum	-0.28	1.14	1.43	0.72	0.16	0.09
FBpp0082932	Pxt	-0.19	-0.33	-0.14	0.69	0.50	0.78
FBpp0083611	PyK	-0.21	-0.04	0.17	0.64	0.94	0.70
FBpp0304178	pzg	1.05	-0.61	-1.66	0.12	0.36	0.02
FBpp0309142	r	-0.10	1.28	1.39	0.83	0.02	0.01
FBpp0083440	r-l	0.50	0.20	-0.29	0.40	0.73	0.62
FBpp0083503	Rab1	0.36	0.03	-0.34	0.44	0.95	0.48
FBpp0083414	Rab11	0.24	0.25	0.01	0.59	0.57	0.98
FBpp0303520	Rab5	-0.09	-0.08	0.00	0.88	0.88	1.00
FBpp0300836	Rab7	0.65	0.43	-0.22	0.34	0.52	0.75
FBpp0311572	Rack1	-1.01	0.86	1.87	0.06	0.10	0.00
FBpp0290882	rad50	-0.38	-0.49	-0.11	0.46	0.35	0.83
FBpp0071600	Rae1	0.21	0.76	0.55	0.68	0.16	0.30
FBpp0309151	Ran	-0.10	-0.07	0.04	0.82	0.88	0.93
FBpp0309478	Ranbp21	-0.29	-0.20	0.09	0.72	0.80	0.91
FBpp0306292	RanGAP	-0.16	-0.59	-0.43	0.75	0.26	0.41
FBpp0293634	Rbfox1	-0.04	-0.23	-0.19	0.93	0.63	0.69
FBpp0076784	Rcc1	-1.29	-2.29	-0.99	0.01	0.00	0.04
FBpp0073058	Rcd5	0.98	0.78	-0.20	0.24	0.35	0.80
FBpp0081156	Ref1	0.36	1.04	0.68	0.65	0.21	0.40

FBpp0302766	REG	0.78	-0.34	-1.12	0.27	0.62	0.12
FBpp0311247	rept	0.16	-0.42	-0.58	0.74	0.41	0.25
FBpp0079609	RfC3	0.16	-0.37	-0.53	0.69	0.36	0.20
FBpp0311114	RfC38	-0.04	-0.31	-0.27	0.92	0.46	0.52
FBpp0073120	RfC4	0.11	-0.11	-0.22	0.80	0.81	0.62
FBpp0305319	rhea	-0.47	-1.44	-0.97	0.52	0.07	0.20
FBpp0304185	RhoGDI	0.07	-0.21	-0.28	0.89	0.66	0.56
FBpp0291753	Rm62	-1.53	-1.05	0.48	0.01	0.05	0.35
FBpp0310006	rngo	-0.30	-1.51	-1.21	0.63	0.03	0.07
FBpp0079648	RnrL	-0.16	0.22	0.39	0.71	0.60	0.38
FBpp0087152	RnrS	-0.19	-0.60	-0.41	0.74	0.32	0.50
FBpp0085156	rod	-0.65	-0.17	0.48	0.46	0.84	0.59
FBpp0302971	row	0.26	-0.89	-1.16	0.65	0.13	0.06
FBpp0305404	Rox8	-0.24	0.23	0.47	0.60	0.61	0.31
FBpp0081356	RpA-70	-0.51	-1.78	-1.27	0.25	0.00	0.01
FBpp0305226	RPA2	-0.31	-1.86	-1.54	0.46	0.00	0.00
FBpp0310183	RPA3	-0.28	-1.90	-1.62	0.50	0.00	0.00
FBpp0075764	RpL10Ab	-0.92	-0.15	0.77	0.13	0.80	0.20
FBpp0072085	RpL12	0.30	0.41	0.11	0.57	0.44	0.83
FBpp0302626	RpL13	-0.73	0.77	1.50	0.24	0.22	0.03
FBpp0076359	RpL14	-0.58	-0.60	-0.03	0.33	0.30	0.96
FBpp0311286	RpL18	-1.39	-0.68	0.71	0.14	0.46	0.44
FBpp0086103	RpL18A	-1.42	0.14	1.56	0.01	0.77	0.01
FBpp0089141	RpL19	-0.91	-0.59	0.32	0.15	0.34	0.60
FBpp0311640	RpL21	-0.47	-0.05	0.43	0.29	0.92	0.33
FBpp0303780	RpL27	-1.09	-1.18	-0.09	0.21	0.18	0.92
FBpp0311452	RpL27A	-0.73	0.33	1.06	0.12	0.46	0.03
FBpp0307759	RpL3	-2.77	-0.90	1.87	0.01	0.35	0.07
FBpp0309280	RpL30	-0.04	0.35	0.39	0.96	0.65	0.62
FBpp0308319	RpL34b	-1.03	0.24	1.27	0.23	0.77	0.15
FBpp0310250	RpL7	-0.41	-0.75	-0.34	0.49	0.22	0.56
FBpp0072802	RpL8	-0.09	-1.00	-0.91	0.89	0.11	0.15
FBpp0306232	RpLP0	-0.73	-0.41	0.32	0.20	0.46	0.56
FBpp0086252	RpLP2	-0.41	0.03	0.44	0.59	0.97	0.57
FBpp0074662	Rpn1	0.04	0.11	0.07	0.95	0.85	0.90
FBpp0305644	Rpn10	0.61	0.50	-0.11	0.19	0.27	0.81
FBpp0078664	Rpn11	0.11	-0.61	-0.72	0.85	0.30	0.22
FBpp0075068	Rpn12	-0.11	-0.62	-0.51	0.89	0.44	0.53
FBpp0306599	Rpn2	0.33	0.08	-0.25	0.55	0.88	0.65
FBpp0307804	Rpn3	0.22	-0.11	-0.33	0.66	0.83	0.52
FBpp0078278	Rpn5	-0.03	-0.27	-0.25	0.96	0.58	0.62
FBpp0297513	Rpn6	0.12	-0.21	-0.33	0.81	0.67	0.50
FBpp0083687	Rpn7	-0.06	-0.71	-0.65	0.91	0.17	0.20
FBpp0305141	Rpn8	-0.24	-1.90	-1.66	0.65	0.00	0.01
FBpp0083861	Rpn9	0.03	-0.05	-0.08	0.95	0.91	0.86
FBpp0310720	RpS10b	0.40	1.81	1.41	0.38	0.00	0.01
FBpp0087115	RpS11	0.11	2.09	1.97	0.87	0.01	0.01
FBpp0075612	RpS12	-0.52	1.25	1.77	0.25	0.01	0.00
FBpp0312104	RpS13	0.97	2.72	1.74	0.15	0.00	0.02
FBpp0311458	RpS14b	-0.73	0.85	1.58	0.18	0.12	0.01
FBpp0309759	RpS16	-0.29	1.65	1.94	0.53	0.00	0.00
FBpp0076207	RpS17	-0.49	0.28	0.76	0.44	0.65	0.23
FBpp0085586	RpS18	-0.35	1.64	2.00	0.54	0.01	0.00
FBpp0311350	RpS19a	-1.11	0.29	1.40	0.09	0.64	0.04
FBpp0311561	RpS2	0.94	2.62	1.68	0.12	0.00	0.01
FBpp0083371	RpS20	-0.86	1.20	2.05	0.16	0.06	0.00
FBpp0308991	RpS23	0.66	2.38	1.72	0.27	0.00	0.01
FBpp0081846	RpS25	-0.28	1.57	1.85	0.64	0.02	0.01
FBpp0079606	RpS27A	-0.24	0.55	0.79	0.61	0.25	0.11
FBpp0310057	RpS28b	-0.33	1.64	1.97	0.49	0.00	0.00

FBpp0306740	RpS29	0.52	0.48	-0.04	0.44	0.47	0.95
FBpp0312066	RpS3	-0.88	1.03	1.92	0.10	0.06	0.00
FBpp0300615	RpS3A	-2.51	-0.67	1.84	0.00	0.30	0.01
FBpp0312080	RpS4	-0.24	1.81	2.05	0.62	0.00	0.00
FBpp0071087	RpS6	-0.86	1.44	2.30	0.08	0.01	0.00
FBpp0308324	RpS7	0.30	2.19	1.90	0.62	0.00	0.01
FBpp0311987	RpS8	-0.44	1.44	1.88	0.44	0.02	0.01
FBpp0088021	Rpt1	-0.54	-0.79	-0.25	0.31	0.15	0.63
FBpp0311982	Rpt2	0.53	0.43	-0.10	0.27	0.36	0.84
FBpp0312031	Rpt3	0.74	0.92	0.18	0.13	0.06	0.70
FBpp0293948	Rpt4	0.37	-0.38	-0.75	0.46	0.45	0.15
FBpp0083843	Rpt5	0.34	0.15	-0.19	0.50	0.77	0.70
FBpp0076890	Rpt6	0.85	0.20	-0.65	0.09	0.68	0.19
FBpp0288680	Rrp1	-0.17	-1.02	-0.85	0.74	0.06	0.11
FBpp0081601	rump	0.19	-1.00	-1.18	0.77	0.13	0.08
FBpp0089284	Sar1	0.41	-0.37	-0.78	0.43	0.47	0.14
FBpp0297362	SC35	0.55	-0.33	-0.88	0.28	0.51	0.09
FBpp0074285	scu	2.58	-0.28	-2.86	0.00	0.56	0.00
FBpp0082877	sds22	-1.74	-1.08	0.66	0.07	0.23	0.46
FBpp0083932	Sec10	-0.12	-0.20	-0.08	0.79	0.65	0.85
FBpp0311988	Sec13	-0.47	0.20	0.68	0.26	0.62	0.12
FBpp0309105	Sec16	-0.43	-0.01	0.42	0.48	0.99	0.49
FBpp0303000	Sec24CD	-0.73	-0.42	0.31	0.20	0.45	0.58
FBpp0087723	Sec31	0.31	-0.03	-0.35	0.47	0.94	0.43
FBpp0086691	SelD	0.54	-0.17	-0.71	0.30	0.75	0.18
FBpp0307454	SerRS	0.43	0.79	0.36	0.43	0.15	0.50
FBpp0089160	sgg	-0.26	-1.09	-0.84	0.65	0.07	0.15
FBpp0296963	Sgt	0.32	0.64	0.32	0.42	0.12	0.42
FBpp0305484	shep	-0.27	-0.66	-0.39	0.63	0.25	0.49
FBpp0305866	shi	0.44	-0.77	-1.21	0.37	0.14	0.03
FBpp0070792	Shmt	1.65	1.29	-0.36	0.01	0.02	0.49
FBpp0073893	shtd	-0.49	-0.61	-0.11	0.41	0.31	0.85
FBpp0303964	simj	-0.08	0.00	0.08	0.84	1.00	0.85
FBpp0081709	sle	-0.51	0.13	0.64	0.24	0.76	0.15
FBpp0306059	slmb	0.70	0.33	-0.37	0.26	0.59	0.54
FBpp0293061	SmB	0.01	0.36	0.34	0.97	0.42	0.44
FBpp0083926	SMC1	0.34	-1.18	-1.52	0.53	0.04	0.01
FBpp0086591	SMC2	-0.18	-1.01	-0.83	0.69	0.04	0.09
FBpp0075684	SmD1	0.68	-0.29	-0.98	0.16	0.53	0.05
FBpp0081234	SmD2	0.59	0.10	-0.48	0.28	0.84	0.37
FBpp0304234	smid	-0.43	0.18	0.61	0.57	0.81	0.42
FBpp0078984	smt3	-0.38	-0.79	-0.41	0.38	0.08	0.34
FBpp0078331	Snr1	0.03	-0.45	-0.48	0.96	0.44	0.41
FBpp0079247	Snx6	0.26	0.52	0.26	0.71	0.46	0.71
FBpp0075958	Sod1	-0.48	0.29	0.76	0.36	0.58	0.16
FBpp0075122	spd-2	0.46	-0.01	-0.47	0.33	0.99	0.33
FBpp0297149	SpdS	0.12	0.42	0.30	0.86	0.54	0.66
FBpp0310470	spel1	1.39	0.34	-1.04	0.05	0.60	0.13
FBpp0301102	sqd	-0.24	-0.15	0.10	0.66	0.79	0.86
FBpp0079471	Srp54	-0.13	0.22	0.35	0.77	0.63	0.44
FBpp0076872	Srp54k	-0.06	-0.67	-0.61	0.91	0.23	0.27
FBpp0076244	Srp68	0.04	-0.90	-0.95	0.93	0.09	0.08
FBpp0083319	Srp72	0.10	-0.36	-0.46	0.86	0.51	0.41
FBpp0079211	Ssb-c31a	-0.37	-0.64	-0.27	0.42	0.18	0.56
FBpp0072151	Ssrp	-0.44	0.64	1.07	0.32	0.16	0.02
FBpp0308666	sta	1.03	1.85	0.81	0.04	0.00	0.10
FBpp0078827	stai	-0.07	0.34	0.41	0.88	0.48	0.40
FBpp0077790	Stip1	-0.05	-0.16	-0.11	0.92	0.73	0.80
FBpp0307636	Strn-Mlck-RV	-0.76	-0.30	0.46	0.23	0.62	0.47
FBpp0312201	Su(H)	0.12	-2.00	-2.12	0.81	0.00	0.00

FBpp0079252	Su(var)205	-0.02	-0.60	-0.58	0.96	0.17	0.19
FBpp0290871	Su(var)3-7	0.08	-0.69	-0.77	0.90	0.29	0.24
FBpp0078372	Sym	-1.07	-1.09	-0.02	0.08	0.07	0.98
FBpp0304718	tacc	-0.32	-1.56	-1.24	0.48	0.00	0.01
FBpp0073459	Tango4	-1.04	-0.42	0.62	0.07	0.44	0.26
FBpp0080045	Tap42	0.02	-0.26	-0.29	0.97	0.65	0.62
FBpp0081820	Tctp	-0.05	0.10	0.15	0.91	0.82	0.73
FBpp0290143	tea	-0.85	-1.50	-0.65	0.08	0.01	0.18
FBpp0110174	tefu	-0.20	-0.44	-0.23	0.68	0.39	0.64
FBpp0087479	TER94	0.01	-0.23	-0.24	0.99	0.60	0.60
FBpp0081350	tex	-0.61	-1.19	-0.58	0.34	0.08	0.36
FBpp0083355	TFAM	-0.39	-1.52	-1.13	0.49	0.02	0.06
FBpp0084526	TfIIA-L	0.26	1.20	0.94	0.70	0.09	0.18
FBpp0306851	tho2	0.78	0.50	-0.28	0.16	0.36	0.61
FBpp0312095	ThrRS	0.30	-0.22	-0.51	0.49	0.62	0.24
FBpp0082180	timeout	-1.14	-0.52	0.62	0.08	0.39	0.32
FBpp0077346	toc	-0.19	-0.69	-0.50	0.71	0.19	0.33
FBpp0304598	Top2	-0.24	-1.21	-0.97	0.63	0.03	0.06
FBpp0080787	Top3alpha	-0.41	-1.40	-0.99	0.41	0.01	0.06
FBpp0087193	tou	0.02	-0.03	-0.05	0.96	0.96	0.91
FBpp0084948	Tpi	0.17	1.01	0.85	0.75	0.07	0.12
FBpp0310608	TppII	-0.86	-0.45	0.42	0.14	0.43	0.46
FBpp0304887	tral	1.13	0.67	-0.45	0.05	0.22	0.40
FBpp0079437	Trx-2	0.57	0.29	-0.28	0.32	0.60	0.62
FBpp0071117	Trxr-1	-0.09	0.17	0.26	0.87	0.75	0.63
FBpp0312205	Tsf1	-0.40	0.18	0.58	0.40	0.69	0.22
FBpp0072097	tsr	0.04	0.39	0.35	0.94	0.45	0.50
FBpp0304417	Tudor-SN	0.05	-0.01	-0.06	0.91	0.99	0.90
FBpp0083956	twin	0.03	-0.81	-0.84	0.95	0.12	0.11
FBpp0311386	tws	0.71	0.09	-0.62	0.19	0.87	0.25
FBpp0076804	Txl	0.55	0.55	0.00	0.22	0.22	1.00
FBpp0075168	TyrRS	0.02	0.14	0.11	0.96	0.79	0.82
FBpp0077912	tzn	0.37	0.37	0.00	0.51	0.50	1.00
FBpp0305600	U2af38	-1.58	-2.33	-0.75	0.04	0.00	0.29
FBpp0298007	U2af50	0.64	-0.75	-1.38	0.24	0.18	0.02
FBpp0087583	Uba1	0.29	-0.72	-1.01	0.65	0.27	0.13
FBpp0076457	Uba2	-0.39	0.18	0.57	0.54	0.77	0.37
FBpp0311673	Ubc4	-0.16	-0.16	-0.01	0.81	0.80	0.99
FBpp0304449	UbcE2M	0.75	0.66	-0.08	0.29	0.34	0.91
FBpp0309477	Ubqn	0.02	0.12	0.10	0.96	0.79	0.83
FBpp0292511	Uch	0.30	0.23	-0.07	0.59	0.68	0.90
FBpp0306000	Uch-L5	0.04	-0.30	-0.34	0.93	0.48	0.43
FBpp0311276	Uev1A	-0.09	-0.18	-0.09	0.83	0.67	0.83
FBpp0290913	UGP	0.11	-0.87	-0.98	0.85	0.17	0.13
FBpp0081284	unc-45	0.54	0.33	-0.21	0.24	0.46	0.65
FBpp0304059	Usp14	0.75	-0.10	-0.85	0.16	0.84	0.11
FBpp0298309	Usp5	0.17	-0.54	-0.72	0.72	0.28	0.16
FBpp0073474	Usp7	-0.39	0.13	0.52	0.50	0.82	0.37
FBpp0305353	ValRS	0.11	0.17	0.06	0.83	0.74	0.91
FBpp0311965	Vha26	0.82	-0.01	-0.83	0.22	0.99	0.21
FBpp0086468	Vha36-1	0.12	0.14	0.03	0.79	0.75	0.95
FBpp0086320	Vha44	-1.01	-0.03	0.98	0.07	0.95	0.07
FBpp0290875	Vha55	-0.73	-0.05	0.67	0.47	0.96	0.50
FBpp0307597	Vha68-2	0.39	0.28	-0.11	0.40	0.54	0.82
FBpp0307142	VhaSFD	-0.34	0.33	0.67	0.65	0.66	0.38
FBpp0310907	vib	-0.52	-1.98	-1.46	0.37	0.00	0.02
FBpp0112266	vig2	1.03	0.68	-0.34	0.06	0.19	0.50
FBpp0309628	Vps4	0.57	0.98	0.41	0.21	0.04	0.36
FBpp0072691	Vta1	-2.45	-1.05	1.40	0.06	0.39	0.25
FBpp0084579	wdb	-0.32	-0.36	-0.05	0.58	0.52	0.93

FBpp0300790	wds	-0.01	0.23	0.24	0.99	0.62	0.61
FBpp0289361	wech	-0.04	-0.74	-0.70	0.94	0.19	0.21
FBpp0306779	woc	-0.54	-0.68	-0.13	0.31	0.21	0.80
FBpp0307569	wrd	0.18	-0.78	-0.97	0.74	0.17	0.10
FBpp0291513	WRNexo	-0.77	-1.01	-0.24	0.10	0.04	0.59
FBpp0304606	x16	0.54	-0.71	-1.26	0.25	0.14	0.02
FBpp0071503	Xpd	0.16	0.06	-0.09	0.83	0.93	0.90
FBpp0071049	Ykt6	0.37	-0.37	-0.73	0.49	0.49	0.18
FBpp0312020	Yp1	-0.03	-0.05	-0.02	0.95	0.91	0.95
FBpp0308710	Yp2	-0.04	-0.05	-0.02	0.93	0.90	0.97
FBpp0311924	Yp3	-0.12	-0.03	0.09	0.78	0.94	0.84
FBpp0309943	ytr	0.79	-0.13	-0.92	0.15	0.80	0.10
FBpp0072306	zip	0.30	-1.26	-1.56	0.73	0.17	0.09
FBpp0085138	Zwilch	-0.92	-1.30	-0.38	0.08	0.02	0.45

2. RECRUITMENT OF FACTORS TO FREE DNA ENDS

(see VI.B.1)

a) OEB – BEB – CONTROL

Flybase polypeptide ID	Flybase symbol	differences			p-values		
		oeb-control	beb-control	(oeb-control)-(beb-control)	oeb-control	beb-control	(oeb-control)-(beb-control)
FBpp0304748	-	0.32	0.07	0.25	0.40	0.85	0.51
FBpp0308925	-	0.99	0.91	0.08	0.03	0.05	0.85
FBpp0087084	128up	0.31	0.74	-0.43	0.52	0.14	0.38
FBpp0082987	14-3-3epsilon	0.36	-0.28	0.64	0.38	0.49	0.13
FBpp0305137	14-3-3zeta	0.58	0.16	0.41	0.17	0.69	0.31
FBpp0075508	26-29-p	0.43	0.21	0.22	0.48	0.73	0.71
FBpp0085204	Acf	2.16	2.20	-0.04	0.00	0.00	0.93
FBpp0311818	Act5C	0.28	0.35	-0.07	0.59	0.50	0.89
FBpp0100051	Adh	1.33	1.53	-0.20	0.00	0.00	0.59
FBpp0086845	AGBE	-0.87	0.12	-0.99	0.18	0.85	0.13
FBpp0075313	AGO2	-0.30	-0.41	0.11	0.56	0.43	0.82
FBpp0312000	Ahcy	0.11	-0.40	0.52	0.88	0.59	0.49
FBpp0087757	AIMP1	0.71	0.51	0.20	0.14	0.28	0.67
FBpp0075318	AIMP2	1.67	1.55	0.12	0.03	0.04	0.86
FBpp0082682	Akt1	0.87	0.66	0.22	0.12	0.23	0.69
FBpp0089366	AlaRS	0.46	0.01	0.45	0.47	0.98	0.49
FBpp0308680	Ald	0.12	0.26	-0.14	0.83	0.65	0.81
FBpp0309805	alien	0.74	0.60	0.14	0.17	0.26	0.78
FBpp0084610	ALiX	-1.77	-1.98	0.21	0.01	0.00	0.71
FBpp0072694	alphaCOP	0.56	0.46	0.10	0.26	0.35	0.83
FBpp0076122	alphaTub67C	-0.90	-0.65	-0.25	0.05	0.14	0.55
FBpp0081153	alphaTub84B	-0.64	-0.99	0.35	0.12	0.03	0.38
FBpp0290266	AMPdeam	-1.90	0.32	-2.23	0.24	0.84	0.17
FBpp0311374	Amun	0.04	-0.39	0.43	0.95	0.59	0.55
FBpp0082065	Aos1	2.55	1.74	0.80	0.00	0.01	0.19
FBpp0074558	AP-1-2beta	0.50	0.35	0.15	0.20	0.36	0.69
FBpp0070907	APC7	0.69	0.96	-0.27	0.27	0.13	0.66
FBpp0311464	apolpp	1.15	1.42	-0.27	0.03	0.01	0.58

FBpp0305852	Arf102F	1.02	1.30	-0.28	0.16	0.08	0.69
FBpp0304364	Arf79F	1.53	1.37	0.16	0.01	0.02	0.76
FBpp0076271	Argk	0.57	0.47	0.10	0.38	0.46	0.87
FBpp0073965	ArgRS	2.46	2.81	-0.35	0.00	0.00	0.47
FBpp0304830	AsnRS	0.12	-0.34	0.46	0.78	0.43	0.30
FBpp0084071	asp	-0.09	0.22	-0.31	0.87	0.70	0.58
FBpp0308483	AspRS	2.49	2.51	-0.02	0.00	0.00	0.96
FBpp0306920	atms	0.84	-0.08	0.92	0.18	0.89	0.14
FBpp0289825	ATPCL	0.18	1.31	-1.13	0.76	0.05	0.08
FBpp0311086	ATPsynbeta	0.83	0.73	0.10	0.21	0.26	0.88
FBpp0082555	Atx2	-2.76	-3.54	0.77	0.00	0.00	0.15
FBpp0079769	aurB	1.42	2.14	-0.72	0.01	0.00	0.17
FBpp0312191	awd	-0.24	-0.89	0.65	0.64	0.10	0.22
FBpp0300517	B52	0.42	0.66	-0.24	0.44	0.24	0.66
FBpp0305308	baf	0.11	-0.29	0.40	0.81	0.52	0.38
FBpp0085442	Bap170	1.75	2.00	-0.25	0.00	0.00	0.59
FBpp0086115	Bap55	0.31	0.93	-0.62	0.56	0.09	0.25
FBpp0073572	Bap60	1.65	0.96	0.69	0.00	0.05	0.14
FBpp0310394	barr	1.88	2.17	-0.29	0.01	0.01	0.65
FBpp0306433	bel	1.10	0.62	0.48	0.02	0.15	0.26
FBpp0305067	ben	1.10	0.54	0.56	0.09	0.39	0.37
FBpp0084021	beta-PheRS	0.07	0.40	-0.33	0.89	0.41	0.49
FBpp0074348	betaCOP	0.01	0.36	-0.35	0.98	0.56	0.57
FBpp0085720	betaTub56D	-0.15	-0.74	0.59	0.71	0.10	0.18
FBpp0080362	BicC	-1.08	-0.64	-0.44	0.03	0.16	0.32
FBpp0082428	BigH1	2.46	2.65	-0.19	0.00	0.00	0.76
FBpp0071794	blw	-0.59	0.10	-0.70	0.23	0.83	0.16
FBpp0311234	bol	-1.69	-1.65	-0.04	0.00	0.00	0.93
FBpp0079417	borr	1.80	2.05	-0.26	0.00	0.00	0.60
FBpp0305757	brm	0.19	0.33	-0.14	0.68	0.49	0.77
FBpp0304073	Bruce	0.25	-0.14	0.39	0.57	0.75	0.38
FBpp0308293	Bub3	-1.03	-1.13	0.10	0.11	0.08	0.86
FBpp0080450	BuGZ	-2.42	-1.81	-0.61	0.00	0.01	0.33
FBpp0087402	Caf1-105	0.10	0.87	-0.77	0.90	0.27	0.33
FBpp0071172	Caf1-180	1.27	1.53	-0.26	0.03	0.01	0.60
FBpp0082511	Caf1-55	0.62	1.17	-0.55	0.18	0.02	0.23
FBpp0311269	Cam	-1.77	-1.51	-0.26	0.02	0.03	0.69
FBpp0304507	Cand1	0.13	0.30	-0.17	0.78	0.52	0.72
FBpp0084818	Cap-D2	1.68	2.12	-0.44	0.00	0.00	0.31
FBpp0288780	Cap-G	1.52	1.59	-0.07	0.01	0.01	0.90
FBpp0099391	capt	1.11	0.50	0.60	0.02	0.24	0.17
FBpp0308803	casp	0.04	-0.39	0.43	0.96	0.56	0.52
FBpp0083684	CCT1	0.93	0.72	0.21	0.05	0.13	0.63
FBpp0071226	CCT2	0.98	0.56	0.42	0.05	0.23	0.36
FBpp0291566	CCT3	0.44	0.34	0.09	0.34	0.45	0.83
FBpp0079992	CCT4	0.84	0.63	0.21	0.13	0.25	0.69
FBpp0087095	CCT5	0.51	0.20	0.31	0.39	0.73	0.60
FBpp0073902	CCT6	0.44	0.24	0.20	0.45	0.68	0.73
FBpp0081401	CCT7	0.48	0.54	-0.06	0.53	0.48	0.94
FBpp0087764	CCT8	0.96	0.80	0.16	0.04	0.08	0.72
FBpp0083769	Cdc16	0.14	0.08	0.06	0.77	0.87	0.89
FBpp0305185	Cdc23	-0.54	0.11	-0.64	0.52	0.90	0.45
FBpp0305561	Cdc27	0.65	0.45	0.20	0.26	0.42	0.72
FBpp0072660	Cdc37	0.49	0.38	0.11	0.28	0.40	0.80
FBpp0076371	Cdc6	0.48	0.29	0.19	0.34	0.55	0.70
FBpp0079641	Cdk1	0.27	0.49	-0.22	0.53	0.25	0.59
FBpp0289675	Cdk2	-0.71	0.59	-1.30	0.26	0.35	0.05
FBpp0305296	CG10077	-0.76	-0.28	-0.49	0.31	0.71	0.51

FBpp0306293	CG10237	1.38	2.51	-1.13	0.03	0.00	0.07
FBpp0293954	CG10565	0.34	0.39	-0.05	0.50	0.44	0.92
FBpp0311825	CG10576	0.33	-0.08	0.41	0.72	0.93	0.66
FBpp0292528	CG11089	-0.37	0.37	-0.74	0.71	0.72	0.47
FBpp0306623	CG11334	-0.11	-1.06	0.94	0.81	0.04	0.06
FBpp0112044	CG11486	-2.62	-1.97	-0.65	0.00	0.00	0.27
FBpp0072658	CG12018	0.49	1.16	-0.67	0.50	0.12	0.35
FBpp0078279	CG1218	0.63	-0.20	0.83	0.35	0.77	0.23
FBpp0305787	CG13025	0.69	-0.50	1.19	0.20	0.35	0.04
FBpp0304298	CG1344	0.11	-0.25	0.36	0.90	0.77	0.68
FBpp0307859	CG1354	1.37	1.27	0.11	0.01	0.02	0.83
FBpp0085260	CG1416	0.41	0.67	-0.26	0.54	0.32	0.70
FBpp0077144	CG15440	-3.98	-3.36	-0.62	0.00	0.00	0.41
FBpp0112211	CG1646	-4.42	-4.74	0.32	0.00	0.00	0.60
FBpp0312121	CG16772	-3.27	-2.89	-0.39	0.00	0.00	0.48
FBpp0300672	CG16817	0.22	0.02	0.20	0.68	0.97	0.71
FBpp0297346	CG17018	-0.70	-0.08	-0.62	0.52	0.94	0.56
FBpp0310240	CG1703	0.71	0.91	-0.20	0.14	0.07	0.67
FBpp0271746	CG18190	0.89	0.78	0.10	0.03	0.05	0.78
FBpp0303935	CG18815	1.42	1.36	0.06	0.01	0.01	0.89
FBpp0304910	CG2034	-0.45	0.54	-0.99	0.32	0.24	0.04
FBpp0078327	CG2091	1.26	1.24	0.02	0.01	0.01	0.97
FBpp0307423	CG2246	2.08	1.46	0.62	0.00	0.03	0.32
FBpp0311613	CG2852	-0.15	-1.07	0.91	0.77	0.06	0.10
FBpp0307127	CG2862	-0.16	-0.50	0.34	0.85	0.55	0.68
FBpp0290146	CG30122	-0.32	0.35	-0.67	0.49	0.46	0.17
FBpp0291433	CG30382	0.14	-0.51	0.65	0.79	0.33	0.22
FBpp0307202	CG31549	1.61	0.12	1.48	0.10	0.89	0.12
FBpp0303949	CG32164	1.02	0.80	0.22	0.03	0.08	0.60
FBpp0070953	CG3226	1.38	0.93	0.45	0.01	0.06	0.34
FBpp0078978	CG3430	0.62	0.23	0.39	0.17	0.59	0.38
FBpp0070273	CG3740	0.58	1.09	-0.51	0.31	0.07	0.36
FBpp0081650	CG3909	-4.03	-4.70	0.67	0.01	0.00	0.59
FBpp0303976	CG40045	1.97	1.99	-0.02	0.01	0.01	0.97
FBpp0288574	CG42232	2.60	2.73	-0.13	0.00	0.00	0.75
FBpp0079789	CG4751	-0.39	-0.27	-0.12	0.53	0.66	0.85
FBpp0112210	CG4951	1.76	2.10	-0.34	0.00	0.00	0.45
FBpp0309480	CG5162	0.42	1.40	-0.98	0.55	0.07	0.18
FBpp0309317	CG5174	0.56	-0.01	0.57	0.20	0.98	0.19
FBpp0079637	CG5355	-0.36	-1.05	0.69	0.50	0.07	0.21
FBpp0084281	CG5886	-0.27	-0.07	-0.20	0.73	0.93	0.80
FBpp0303937	CG6084	-0.69	-1.13	0.44	0.30	0.10	0.50
FBpp0079979	CG6180	-0.89	-0.29	-0.60	0.18	0.65	0.35
FBpp0079809	CG6287	-1.42	-1.42	0.00	0.06	0.06	1.00
FBpp0080044	CG6523	0.94	-0.31	1.25	0.10	0.56	0.03
FBpp0307760	CG6693	0.40	0.15	0.25	0.44	0.78	0.62
FBpp0311284	CG6767	0.65	0.90	-0.25	0.17	0.07	0.59
FBpp0293610	CG7546	0.40	0.47	-0.07	0.41	0.34	0.89
FBpp0087347	CG7637	-3.00	-2.14	-0.86	0.00	0.00	0.13
FBpp0292226	CG7971	-1.06	-0.09	-0.96	0.16	0.90	0.20
FBpp0303962	CG8003	-0.54	-0.27	-0.27	0.49	0.73	0.73
FBpp0081371	CG8036	-1.14	-2.13	0.99	0.09	0.00	0.13
FBpp0074246	CG8142	1.84	1.89	-0.04	0.00	0.00	0.91
FBpp0081398	CG8223	0.42	-0.26	0.68	0.45	0.63	0.23
FBpp0087733	CG8243	-2.79	-2.84	0.05	0.00	0.00	0.93
FBpp0078684	CG8891	1.60	0.90	0.70	0.02	0.16	0.27
FBpp0311963	CG9135	0.77	-0.24	1.02	0.25	0.71	0.14
FBpp0072610	CG9184	-2.49	-3.06	0.56	0.03	0.01	0.60

FBpp0309269	CG9281	0.70	0.53	0.17	0.18	0.30	0.73
FBpp0074708	CG9330	-1.23	-0.93	-0.30	0.04	0.10	0.58
FBpp0308531	Chc	0.47	0.95	-0.48	0.28	0.04	0.28
FBpp0074766	Chd3	0.72	1.03	-0.30	0.34	0.19	0.69
FBpp0301152	chic	0.91	0.86	0.05	0.17	0.19	0.93
FBpp0310070	cib	-0.61	-1.14	0.53	0.37	0.11	0.43
FBpp0311360	CkIIalpha	0.82	1.29	-0.47	0.06	0.01	0.26
FBpp0305406	CkIIbeta	0.51	0.67	-0.16	0.32	0.20	0.75
FBpp0304514	cmet	-0.05	0.04	-0.09	0.94	0.95	0.89
FBpp0304029	Cnot4	-2.31	-2.50	0.19	0.00	0.00	0.71
FBpp0307640	coro	1.03	0.93	0.11	0.05	0.07	0.83
FBpp0076300	Cp19	-2.92	-3.10	0.19	0.00	0.00	0.79
FBpp0080484	Cse1	1.25	1.16	0.09	0.02	0.03	0.85
FBpp0077927	CSN3	2.15	2.04	0.11	0.00	0.01	0.86
FBpp0290448	CSN4	0.71	0.87	-0.16	0.14	0.08	0.73
FBpp0083658	CSN6	0.60	0.42	0.18	0.25	0.41	0.72
FBpp0087821	CSN7	-0.25	0.12	-0.37	0.77	0.89	0.66
FBpp0086732	Ctf4	0.72	0.86	-0.14	0.10	0.05	0.74
FBpp0072562	Ctr9	-0.19	0.14	-0.33	0.73	0.79	0.54
FBpp0310479	ctrip	-0.04	0.94	-0.98	0.96	0.26	0.24
FBpp0087924	Cul1	1.76	1.58	0.18	0.26	0.31	0.91
FBpp0312102	cup	-0.16	0.76	-0.92	0.82	0.27	0.19
FBpp0074017	Cyp1	-0.53	-1.23	0.70	0.39	0.06	0.27
FBpp0290739	D1	-0.75	-1.22	0.47	0.25	0.07	0.46
FBpp0084349	Dak1	1.07	1.06	0.01	0.11	0.12	0.98
FBpp0112438	Dbp80	0.37	0.50	-0.13	0.47	0.33	0.80
FBpp0306615	dco	-0.23	-0.65	0.42	0.75	0.37	0.56
FBpp0087722	DCTN2-p50	0.72	0.44	0.28	0.13	0.34	0.54
FBpp0305164	Dek	-0.81	-0.53	-0.29	0.17	0.36	0.62
FBpp0291138	deltaCOP	1.22	0.95	0.27	0.01	0.04	0.53
FBpp0082849	Det	0.69	0.42	0.26	0.23	0.45	0.64
FBpp0099688	Df31	-1.01	-1.46	0.44	0.38	0.21	0.69
FBpp0308700	dgt5	0.90	0.36	0.55	0.06	0.42	0.22
FBpp0084783	dgt6	0.53	0.14	0.39	0.22	0.73	0.35
FBpp0304991	Dhc64C	0.51	0.32	0.20	0.24	0.46	0.65
FBpp0099973	Dhpr	-0.03	0.08	-0.11	0.96	0.88	0.83
FBpp0307849	Dhx15	0.58	0.61	-0.03	0.25	0.23	0.96
FBpp0082996	Dlc90F	1.70	1.37	0.33	0.00	0.01	0.49
FBpp0076830	DnaJ-1	-1.95	-1.48	-0.47	0.00	0.02	0.41
FBpp0072041	DNAlig1	0.00	-0.76	0.76	1.00	0.39	0.39
FBpp0073678	DNAlig4	1.02	0.78	0.25	0.13	0.24	0.70
FBpp0075277	DNApol-delta	0.18	0.42	-0.23	0.68	0.36	0.60
FBpp0311418	Dp1	0.83	0.75	0.08	0.05	0.07	0.84
FBpp0311783	dpa	0.35	0.57	-0.21	0.48	0.27	0.67
FBpp0083673	Dph5	1.18	1.19	-0.01	0.02	0.02	0.98
FBpp0072744	dre4	1.32	1.34	-0.02	0.01	0.01	0.96
FBpp0082223	Droj2	0.42	0.28	0.14	0.30	0.49	0.71
FBpp0307166	Drp1	0.58	1.12	-0.54	0.32	0.07	0.35
FBpp0309113	Dsor1	0.53	-0.07	0.60	0.18	0.85	0.13
FBpp0308813	Dsp1	0.49	1.44	-0.95	0.40	0.02	0.11
FBpp0079746	dUTPase	-0.18	-0.77	0.59	0.70	0.12	0.23
FBpp0304413	E(bx)	0.83	-0.18	1.00	0.38	0.85	0.30
FBpp0305157	Eb1	0.96	0.38	0.58	0.15	0.55	0.36
FBpp0311691	eEF1beta	1.06	0.55	0.51	0.03	0.21	0.24
FBpp0079542	eEF1delta	1.62	1.40	0.21	0.00	0.00	0.57
FBpp0305182	eEF2	-0.21	-1.05	0.84	0.77	0.17	0.26
FBpp0072082	eEF5	0.09	-0.85	0.94	0.87	0.16	0.13
FBpp0307824	eff	0.73	1.25	-0.52	0.24	0.06	0.39

FBpp0072908	eIF1	-1.52	-1.39	-0.13	0.08	0.11	0.87
FBpp0309768	eIF2alpha	0.30	0.45	-0.15	0.51	0.34	0.75
FBpp0291521	eIF2Bdelta	1.66	1.60	0.06	0.00	0.00	0.88
FBpp0089217	eIF2Bepsilon	0.56	1.08	-0.52	0.33	0.07	0.36
FBpp0075700	eIF2beta	0.22	0.22	0.00	0.61	0.62	0.99
FBpp0307983	eIF2gamma	0.70	0.95	-0.25	0.10	0.03	0.53
FBpp0312226	eIF3a	-0.96	-0.89	-0.07	0.06	0.08	0.87
FBpp0088565	eIF3d1	-1.15	-1.24	0.09	0.06	0.04	0.87
FBpp0075104	eIF3e	0.39	-0.67	1.06	0.68	0.49	0.28
FBpp0078532	eIF3f1	1.29	0.91	0.38	0.02	0.08	0.44
FBpp0071587	eIF3k	0.18	-0.04	0.22	0.75	0.94	0.70
FBpp0075754	eIF3l	0.12	0.71	-0.59	0.84	0.25	0.34
FBpp0303628	eIF4A	0.97	0.70	0.27	0.03	0.11	0.51
FBpp0306017	eIF4E1	0.72	0.25	0.47	0.32	0.72	0.51
FBpp0288389	eIF4G1	0.16	0.41	-0.24	0.73	0.40	0.61
FBpp0089140	eIF5	1.15	1.56	-0.41	0.08	0.02	0.51
FBpp0301573	eIF5B	0.88	0.59	0.29	0.15	0.32	0.62
FBpp0083354	EloB	-0.26	-0.68	0.42	0.61	0.20	0.41
FBpp0085725	EloC	0.24	0.06	0.18	0.65	0.91	0.73
FBpp0079278	emb	0.56	0.13	0.43	0.22	0.77	0.34
FBpp0305267	endos	-0.22	-1.89	1.67	0.77	0.03	0.04
FBpp0077574	Eno	-1.00	-1.48	0.48	0.05	0.01	0.31
FBpp0304201	eRF1	1.35	1.61	-0.26	0.00	0.00	0.51
FBpp0311174	eRF3	1.05	1.17	-0.12	0.02	0.01	0.75
FBpp0079496	Etl1	1.51	0.94	0.56	0.02	0.12	0.34
FBpp0099726	fabp	0.53	0.53	0.00	0.29	0.29	1.00
FBpp0308326	faf	0.68	1.11	-0.42	0.18	0.04	0.39
FBpp0083399	Fancd2	1.70	1.79	-0.08	0.00	0.00	0.86
FBpp0087756	FANCl	2.14	2.06	0.08	0.00	0.00	0.86
FBpp0307371	FASN1	0.23	-0.47	0.70	0.63	0.33	0.16
FBpp0081767	Fdh	-0.74	-1.14	0.40	0.18	0.05	0.46
FBpp0086223	Fen1	0.62	0.05	0.57	0.28	0.93	0.32
FBpp0073266	feo	0.62	0.76	-0.14	0.44	0.34	0.86
FBpp0071892	Fib	0.13	0.36	-0.23	0.79	0.47	0.65
FBpp0074215	Fim	-0.05	0.70	-0.76	0.93	0.21	0.18
FBpp0271718	Fis1	0.42	1.12	-0.70	0.42	0.05	0.19
FBpp0083551	fit	-0.51	-0.60	0.09	0.57	0.50	0.92
FBpp0082574	FK506-bp1	0.33	0.57	-0.24	0.47	0.23	0.60
FBpp0085703	FK506-bp2	-0.60	-1.19	0.59	0.37	0.09	0.38
FBpp0309663	FKBP59	0.13	-0.47	0.60	0.79	0.34	0.23
FBpp0075581	flr	-0.87	-1.77	0.90	0.22	0.02	0.21
FBpp0300445	Fmr1	0.78	0.21	0.56	0.13	0.66	0.26
FBpp0304175	fmt	0.57	0.15	0.42	0.21	0.73	0.35
FBpp0290502	fon	-0.42	-0.31	-0.11	0.32	0.46	0.79
FBpp0088923	for	0.30	-0.33	0.63	0.65	0.62	0.35
FBpp0070463	fs(1)Ya	1.13	0.32	0.81	0.14	0.66	0.28
FBpp0294038	Fs(2)Ket	0.87	0.52	0.35	0.05	0.20	0.39
FBpp0080391	fzy	0.07	-0.31	0.39	0.90	0.60	0.52
FBpp0290505	gammaCOP	-0.64	-0.12	-0.52	0.34	0.86	0.43
FBpp0304827	gammaTub37C	0.51	0.65	-0.13	0.34	0.23	0.80
FBpp0304864	Gapdh2	-1.08	-2.10	1.02	0.10	0.01	0.13
FBpp0311558	Gdi	0.49	0.25	0.24	0.29	0.59	0.60
FBpp0079819	Ge-1	-0.14	0.50	-0.64	0.80	0.36	0.25
FBpp0077263	gkt	1.39	0.49	0.90	0.00	0.24	0.04
FBpp0084240	GlnRS	1.33	1.74	-0.41	0.01	0.00	0.36
FBpp0080489	glu	1.30	1.87	-0.57	0.02	0.00	0.28
FBpp0083898	GluProRS	2.23	2.45	-0.21	0.00	0.00	0.64
FBpp0099923	GlyP	-0.01	-0.31	0.30	0.98	0.43	0.45

FBpp0306062	GlyRS	0.89	1.12	-0.22	0.05	0.02	0.60
FBpp0082496	GlyS	0.04	0.30	-0.27	0.97	0.79	0.81
FBpp0078478	Gnf1	1.35	1.47	-0.11	0.02	0.01	0.83
FBpp0075793	Grip163	0.59	0.64	-0.05	0.42	0.38	0.94
FBpp0290523	Grip84	0.04	-0.48	0.52	0.93	0.33	0.29
FBpp0073672	Grip91	0.26	0.16	0.10	0.54	0.70	0.82
FBpp0310520	grsm	-0.47	-1.60	1.13	0.41	0.01	0.06
FBpp0099824	GstD1	0.74	-0.10	0.84	0.19	0.85	0.14
FBpp0085855	GstE6	0.70	0.00	0.69	0.36	1.00	0.36
FBpp0290108	Gyf	-0.51	-0.04	-0.47	0.51	0.96	0.54
FBpp0310171	hang	0.89	1.71	-0.82	0.15	0.01	0.18
FBpp0078319	Hat1	1.69	1.41	0.28	0.00	0.01	0.55
FBpp0311451	Hcf	1.15	0.82	0.34	0.05	0.15	0.54
FBpp0073173	HDAC1	-0.38	-0.06	-0.32	0.39	0.90	0.46
FBpp0078756	Hel25E	1.23	0.82	0.41	0.02	0.10	0.38
FBpp0305905	HIP-R	0.15	-0.79	0.93	0.82	0.25	0.18
FBpp0091110	His1:CG33864	1.27	0.76	0.51	0.04	0.20	0.38
FBpp0306426	His2Av	2.24	1.58	0.66	0.06	0.16	0.55
FBpp0091155	His2B	5.48	5.50	-0.02	0.00	0.00	0.97
FBpp0306146	His4r	4.15	3.99	0.15	0.00	0.00	0.73
FBpp0305939	HisRS	0.89	-0.28	1.17	0.09	0.56	0.03
FBpp0071501	Hmg-2	1.36	1.79	-0.43	0.00	0.00	0.28
FBpp0307711	HnRNP-K	0.59	0.54	0.04	0.24	0.28	0.93
FBpp0307465	hoip	0.63	0.61	0.02	0.29	0.30	0.97
FBpp0297875	Hrb27C	-2.60	-3.01	0.41	0.00	0.00	0.51
FBpp0305265	Hsc70Cb	0.45	-0.27	0.72	0.32	0.54	0.13
FBpp0312159	Hsp27	-0.26	-0.13	-0.13	0.57	0.78	0.77
FBpp0073018	ida	-1.50	-1.33	-0.16	0.09	0.12	0.84
FBpp0078152	IleRS	2.28	2.77	-0.48	0.00	0.00	0.26
FBpp0307848	Incenp	1.69	1.91	-0.22	0.01	0.00	0.69
FBpp0076091	iPLA2-VIA	0.65	0.31	0.34	0.23	0.55	0.52
FBpp0081861	Irbp	3.28	0.94	2.34	0.00	0.06	0.00
FBpp0086956	Iswi	1.50	1.92	-0.43	0.01	0.00	0.36
FBpp0311371	Jafrac1	-0.61	-0.75	0.14	0.26	0.17	0.79
FBpp0307568	Karybeta3	0.88	0.76	0.12	0.14	0.20	0.83
FBpp0086328	Khc	1.11	0.63	0.48	0.18	0.44	0.55
FBpp0289115	kis	-1.26	-0.55	-0.71	0.02	0.25	0.15
FBpp0303946	Klc	0.90	0.46	0.43	0.08	0.34	0.37
FBpp0312027	Klp10A	0.95	0.68	0.27	0.04	0.12	0.51
FBpp0309092	Klp3A	0.78	0.31	0.47	0.09	0.48	0.29
FBpp0072616	Klp61F	1.02	0.98	0.04	0.05	0.06	0.94
FBpp0080322	Ku80	3.62	1.03	2.58	0.00	0.05	0.00
FBpp0080906	La	-0.12	-1.06	0.93	0.83	0.08	0.12
FBpp0312110	Lam	-0.72	-0.32	-0.40	0.17	0.53	0.43
FBpp0081255	lds	0.22	0.91	-0.69	0.66	0.09	0.19
FBpp0311704	LeuRS	2.63	2.80	-0.17	0.00	0.00	0.79
FBpp0073551	lic	-0.11	-0.06	-0.04	0.87	0.92	0.95
FBpp0303481	lig	-3.30	-3.14	-0.16	0.00	0.00	0.82
FBpp0088383	lola	1.86	0.75	1.11	0.01	0.23	0.08
FBpp0078561	lost	0.25	0.62	-0.36	0.61	0.23	0.47
FBpp0309608	lva	-0.92	-0.51	-0.40	0.28	0.54	0.63
FBpp0292593	LysRS	2.57	2.88	-0.30	0.00	0.00	0.56
FBpp0076819	mad2	0.74	0.54	0.19	0.18	0.32	0.72
FBpp0310551	mahe	-1.08	-1.01	-0.07	0.05	0.07	0.89
FBpp0085235	Map205	0.41	0.32	0.09	0.55	0.64	0.90
FBpp0078631	Marcal1	0.37	0.19	0.19	0.68	0.84	0.84
FBpp0311207	mars	0.87	0.35	0.52	0.09	0.47	0.29
FBpp0293580	mask	-1.40	-1.36	-0.04	0.03	0.04	0.94

FBpp0311400	mats	0.27	0.27	0.00	0.67	0.67	0.99
FBpp0300535	Mbs	-1.02	-0.66	-0.37	0.41	0.59	0.76
FBpp0081317	Mcm2	1.09	1.21	-0.12	0.01	0.01	0.75
FBpp0070729	Mcm3	0.85	1.66	-0.81	0.11	0.01	0.13
FBpp0081756	Mcm5	1.21	0.90	0.31	0.02	0.06	0.49
FBpp0070913	Mcm6	1.06	1.28	-0.23	0.10	0.05	0.71
FBpp0076312	Mcm7	1.43	0.81	0.61	0.07	0.28	0.42
FBpp0293887	MCTS1	-0.03	1.63	-1.66	0.97	0.09	0.09
FBpp0311560	Mdh1	0.49	0.17	0.32	0.23	0.67	0.42
FBpp0079565	me31B	0.34	0.40	-0.05	0.39	0.32	0.89
FBpp0085809	MetRS	1.64	2.28	-0.65	0.00	0.00	0.18
FBpp0081882	mgr	0.66	0.01	0.65	0.28	0.98	0.29
FBpp0304462	Mi-2	1.01	0.92	0.09	0.04	0.06	0.83
FBpp0297606	Mlf	-3.87	-2.81	-1.06	0.00	0.00	0.14
FBpp0301951	mod	0.67	0.42	0.25	0.10	0.29	0.53
FBpp0083467	mod(mdg4)	-1.00	-2.15	1.15	0.40	0.09	0.33
FBpp0082692	mor	0.98	1.37	-0.39	0.09	0.03	0.48
FBpp0079802	mre11	2.58	1.69	0.89	0.00	0.00	0.06
FBpp0086340	mrj	-2.80	-1.32	-1.48	0.00	0.03	0.02
FBpp0084256	msi	-1.17	-0.96	-0.21	0.01	0.03	0.58
FBpp0076408	msk	0.95	0.42	0.53	0.06	0.36	0.26
FBpp0293342	msps	0.99	1.49	-0.50	0.06	0.01	0.32
FBpp0304737	Mtor	-0.94	-0.65	-0.29	0.11	0.26	0.60
FBpp0310063	mts	-0.21	-0.23	0.02	0.62	0.58	0.95
FBpp0305424	mub	0.24	0.15	0.09	0.69	0.80	0.88
FBpp0111603	mute	-0.20	-0.84	0.64	0.81	0.33	0.46
FBpp0311394	Nacalpha	0.64	0.32	0.32	0.33	0.62	0.62
FBpp0297132	Nap1	0.73	0.70	0.03	0.19	0.21	0.95
FBpp0306828	NAT1	1.71	1.57	0.14	0.01	0.01	0.78
FBpp0297182	nbs	-0.36	-0.91	0.54	0.62	0.23	0.47
FBpp0309711	Nedd8	1.04	0.30	0.74	0.12	0.64	0.25
FBpp0305289	NHP2	-2.24	-2.62	0.38	0.00	0.00	0.47
FBpp0306756	Nlp	-1.27	-1.30	0.02	0.09	0.09	0.97
FBpp0309175	NO66	1.64	2.07	-0.43	0.01	0.00	0.38
FBpp0309274	nonA	-1.38	-1.24	-0.14	0.11	0.15	0.86
FBpp0078997	nop5	0.37	1.09	-0.72	0.41	0.03	0.13
FBpp0290083	Nop60B	-2.48	-2.90	0.43	0.01	0.01	0.62
FBpp0308486	Not1	0.67	-0.08	0.75	0.28	0.90	0.23
FBpp0112220	Nph	-0.10	-0.24	0.13	0.86	0.70	0.83
FBpp0312079	Nplp2	-0.76	-1.58	0.82	0.27	0.04	0.24
FBpp0297079	nudC	0.21	-0.34	0.56	0.84	0.75	0.61
FBpp0079710	Nup107	0.02	0.42	-0.40	0.97	0.51	0.53
FBpp0074568	Nup205	-0.46	0.33	-0.79	0.50	0.63	0.26
FBpp0071905	Nup214	-0.96	-1.73	0.77	0.04	0.00	0.09
FBpp0293235	Nup358	-2.23	-2.21	-0.02	0.00	0.00	0.97
FBpp0087063	Nup54	-0.02	-0.59	0.57	0.97	0.24	0.25
FBpp0073659	Nup93-1	0.50	0.20	0.30	0.21	0.61	0.44
FBpp0306915	Nup98-96	-2.64	-2.08	-0.56	0.00	0.00	0.32
FBpp0271761	Nurf-38	-0.34	0.59	-0.92	0.57	0.33	0.14
FBpp0072061	or	0.21	1.39	-1.17	0.71	0.03	0.06
FBpp0088033	Orc1	1.31	1.13	0.18	0.04	0.06	0.75
FBpp0082329	Orc2	2.20	2.22	-0.02	0.00	0.00	0.97
FBpp0086882	Orc3	1.09	1.14	-0.05	0.05	0.04	0.92
FBpp0072330	Orc4	1.84	2.73	-0.89	0.01	0.00	0.12
FBpp0080120	Orc5	1.25	1.11	0.14	0.03	0.05	0.79
FBpp0309148	p115	-0.91	-0.01	-0.90	0.17	0.98	0.17
FBpp0088069	p47	-0.19	-0.73	0.53	0.79	0.32	0.46
FBpp0085919	pAbp	-0.88	-1.36	0.48	0.05	0.01	0.26

FBpp0305933	Paics	0.35	0.68	-0.34	0.42	0.13	0.44
FBpp0308411	PAN2	-3.16	-2.91	-0.25	0.00	0.00	0.60
FBpp0112608	Parp	-0.24	0.13	-0.37	0.62	0.79	0.45
FBpp0308299	Patr-1	-1.15	-1.57	0.42	0.04	0.01	0.42
FBpp0290074	PCB	-2.80	-2.74	-0.06	0.00	0.00	0.91
FBpp0308430	pch2	0.73	0.32	0.41	0.16	0.52	0.42
FBpp0089395	PCNA	0.17	-0.27	0.44	0.72	0.58	0.37
FBpp0086647	pea	0.52	-0.01	0.53	0.58	0.99	0.58
FBpp0079527	Pen	1.24	0.96	0.28	0.01	0.03	0.47
FBpp0304954	Pfdn2	-1.12	-1.07	-0.05	0.14	0.16	0.94
FBpp0290701	Pfdn5	1.13	0.46	0.67	0.09	0.47	0.30
FBpp0303214	Pfdn6	-0.92	-1.14	0.22	0.22	0.14	0.76
FBpp0293464	Pfk	0.32	0.68	-0.35	0.46	0.13	0.41
FBpp0303827	Pgd	1.31	0.28	1.03	0.14	0.74	0.24
FBpp0306279	Pgk	-0.90	-1.20	0.30	0.08	0.02	0.53
FBpp0099920	Pglym78	0.79	0.91	-0.12	0.08	0.05	0.77
FBpp0082177	pic	-0.16	-0.30	0.14	0.76	0.57	0.79
FBpp0310466	Plap	0.93	0.00	0.93	0.07	0.99	0.07
FBpp0085618	plu	-0.61	-0.25	-0.37	0.36	0.71	0.58
FBpp0305301	poe	1.40	0.41	0.99	0.05	0.54	0.15
FBpp0099722	polo	1.05	1.11	-0.05	0.03	0.02	0.90
FBpp0084115	polybromo	0.38	1.42	-1.04	0.53	0.03	0.11
FBpp0081704	pont	1.14	1.94	-0.80	0.06	0.00	0.17
FBpp0082067	Pp1-87B	0.15	0.51	-0.37	0.69	0.18	0.33
FBpp0293227	Pp2A-29B	1.08	0.56	0.52	0.02	0.17	0.20
FBpp0301546	Pp2B-14D	1.10	0.32	0.77	0.03	0.49	0.12
FBpp0312200	Pp4-19C	-0.08	-0.64	0.56	0.85	0.16	0.22
FBpp0089154	PPP4R2r	-0.63	-0.22	-0.41	0.36	0.74	0.55
FBpp0303849	PpV	0.30	-0.30	0.60	0.64	0.63	0.35
FBpp0099895	primo-1	-0.21	-0.38	0.16	0.70	0.50	0.77
FBpp0082062	Prosalpha2	0.67	-0.11	0.79	0.36	0.87	0.28
FBpp0071451	Prosalpha3	0.23	-0.21	0.44	0.69	0.73	0.46
FBpp0073989	Prosalpha4	-0.12	-0.57	0.45	0.77	0.19	0.30
FBpp0086067	Prosalpha5	0.79	0.02	0.77	0.10	0.96	0.11
FBpp0310201	Prosalpha6	0.41	0.17	0.24	0.47	0.76	0.68
FBpp0089041	Prosalpha7	-0.38	-1.39	1.00	0.59	0.07	0.18
FBpp0086400	Prosbeta1	0.48	0.22	0.26	0.31	0.64	0.57
FBpp0075382	Prosbeta2	-0.23	-0.64	0.42	0.75	0.38	0.56
FBpp0087320	Prosbeta5	-0.09	-0.02	-0.07	0.90	0.98	0.92
FBpp0075119	Prosbeta6	0.19	-0.39	0.58	0.67	0.38	0.20
FBpp0078449	Prosbeta7	0.00	-0.61	0.61	1.00	0.22	0.22
FBpp0085902	Prp19	-3.06	-2.69	-0.37	0.00	0.00	0.58
FBpp0308280	puf	0.37	-0.30	0.67	0.50	0.59	0.23
FBpp0082932	Pxt	-0.06	0.29	-0.35	0.90	0.55	0.47
FBpp0083611	PyK	0.36	0.31	0.05	0.48	0.54	0.93
FBpp0309142	r	-2.22	-1.92	-0.29	0.00	0.00	0.47
FBpp0083440	r-l	0.73	0.80	-0.08	0.24	0.19	0.89
FBpp0083503	Rab1	0.82	1.87	-1.06	0.25	0.02	0.14
FBpp0083414	Rab11	1.26	2.39	-1.13	0.04	0.00	0.07
FBpp0307641	Rab2	0.14	0.83	-0.70	0.83	0.20	0.28
FBpp0303520	Rab5	2.12	2.61	-0.49	0.00	0.00	0.33
FBpp0300836	Rab7	1.15	1.51	-0.36	0.09	0.03	0.58
FBpp0311572	Rack1	-2.98	-2.88	-0.11	0.00	0.00	0.89
FBpp0290882	rad50	2.19	1.13	1.06	0.00	0.04	0.05
FBpp0071600	Rae1	-2.68	-2.64	-0.03	0.00	0.00	0.95
FBpp0309151	Ran	1.05	0.85	0.20	0.04	0.09	0.67
FBpp0312218	Ranbp9	0.28	0.65	-0.37	0.65	0.30	0.55
FBpp0306292	RanGAP	-0.72	-1.16	0.43	0.14	0.03	0.36

FBpp0293634	Rbfox1	-1.27	-0.92	-0.35	0.02	0.08	0.48
FBpp0076784	Rcc1	2.63	3.14	-0.51	0.00	0.00	0.26
FBpp0302766	REG	1.32	1.00	0.32	0.02	0.07	0.53
FBpp0311247	rept	1.12	1.21	-0.09	0.04	0.03	0.86
FBpp0079609	RfC3	1.19	1.34	-0.15	0.02	0.01	0.75
FBpp0311114	RfC38	1.76	1.88	-0.12	0.00	0.00	0.80
FBpp0073120	RfC4	1.00	1.31	-0.31	0.06	0.02	0.53
FBpp0305319	rhea	0.68	0.93	-0.24	0.25	0.13	0.68
FBpp0086441	Rif1	0.62	0.17	0.45	0.58	0.88	0.68
FBpp0310006	rngo	0.64	0.60	0.05	0.49	0.52	0.96
FBpp0079648	RnrL	1.39	1.29	0.11	0.01	0.02	0.83
FBpp0087152	RnrS	0.80	1.00	-0.20	0.09	0.04	0.66
FBpp0302971	row	0.67	0.49	0.17	0.27	0.41	0.77
FBpp0084067	Rpb10	-0.54	-0.06	-0.48	0.25	0.90	0.31
FBpp0296955	Rpi	0.09	-0.69	0.78	0.90	0.32	0.27
FBpp0075764	RpL10Ab	-2.71	-1.70	-1.01	0.02	0.11	0.33
FBpp0302626	RpL13	-2.86	-1.86	-1.00	0.03	0.12	0.39
FBpp0300655	RpL15	-3.07	-2.68	-0.39	0.00	0.00	0.51
FBpp0311286	RpL18	-2.16	-2.13	-0.03	0.11	0.11	0.98
FBpp0089141	RpL19	-2.70	-2.20	-0.50	0.01	0.02	0.55
FBpp0311640	RpL21	-2.35	-3.02	0.67	0.01	0.00	0.36
FBpp0072687	RpL23A	-4.03	-2.70	-1.33	0.00	0.02	0.21
FBpp0311573	RpL24	-2.53	-0.70	-1.82	0.07	0.59	0.17
FBpp0311452	RpL27A	-2.78	-2.43	-0.35	0.00	0.00	0.61
FBpp0309280	RpL30	-0.80	-0.56	-0.24	0.54	0.67	0.85
FBpp0308319	RpL34b	-1.60	-2.06	0.46	0.04	0.01	0.52
FBpp0311481	RpL36	-2.14	-2.65	0.51	0.07	0.03	0.64
FBpp0084617	RpL4	-3.29	-2.12	-1.17	0.00	0.02	0.16
FBpp0311121	RpL5	-1.97	-1.97	0.00	0.03	0.03	1.00
FBpp0310250	RpL7	-2.42	-1.48	-0.93	0.01	0.07	0.23
FBpp0072802	RpL8	-2.09	-1.91	-0.17	0.03	0.04	0.84
FBpp0306232	RpLP0	-0.72	-0.84	0.12	0.29	0.22	0.85
FBpp0074662	Rpn1	0.89	1.20	-0.31	0.07	0.02	0.50
FBpp0305644	Rpn10	1.09	0.98	0.11	0.01	0.02	0.78
FBpp0078664	Rpn11	0.73	1.04	-0.31	0.14	0.05	0.51
FBpp0075068	Rpn12	0.82	0.94	-0.12	0.08	0.05	0.79
FBpp0112987	Rpn13	0.64	0.71	-0.07	0.29	0.24	0.91
FBpp0306599	Rpn2	0.27	0.01	0.26	0.62	0.99	0.63
FBpp0307804	Rpn3	-0.20	0.11	-0.31	0.73	0.86	0.60
FBpp0078278	Rpn5	0.56	0.57	0.00	0.40	0.39	1.00
FBpp0297513	Rpn6	1.64	1.17	0.47	0.00	0.03	0.32
FBpp0083687	Rpn7	0.60	0.78	-0.18	0.25	0.14	0.72
FBpp0305141	Rpn8	1.00	0.80	0.20	0.06	0.13	0.69
FBpp0083861	Rpn9	0.78	0.72	0.06	0.11	0.14	0.90
FBpp0310720	RpS10b	-2.71	-3.23	0.52	0.00	0.00	0.33
FBpp0087115	RpS11	-3.84	-2.68	-1.16	0.00	0.00	0.15
FBpp0075612	RpS12	-3.23	-2.86	-0.38	0.00	0.00	0.54
FBpp0312104	RpS13	-3.16	-2.85	-0.31	0.00	0.00	0.70
FBpp0311458	RpS14b	-3.07	-2.98	-0.09	0.00	0.00	0.87
FBpp0309759	RpS16	-3.55	-3.40	-0.15	0.00	0.00	0.78
FBpp0076207	RpS17	-2.58	-2.81	0.23	0.00	0.00	0.76
FBpp0085586	RpS18	-4.06	-3.82	-0.24	0.00	0.00	0.63
FBpp0311350	RpS19a	-3.00	-2.92	-0.09	0.00	0.00	0.90
FBpp0311561	RpS2	-2.24	-2.33	0.09	0.00	0.00	0.84
FBpp0307130	RpS21	-3.82	-3.22	-0.60	0.00	0.00	0.29
FBpp0081846	RpS25	-2.76	-3.15	0.39	0.00	0.00	0.62
FBpp0079606	RpS27A	1.88	1.98	-0.10	0.27	0.24	0.95
FBpp0312066	RpS3	-3.41	-3.31	-0.10	0.00	0.00	0.86

FBpp0300615	RpS3A	-4.21	-3.58	-0.64	0.00	0.00	0.23
FBpp0312080	RpS4	-3.81	-3.22	-0.60	0.00	0.00	0.16
FBpp0071087	RpS6	-3.91	-3.32	-0.59	0.00	0.00	0.28
FBpp0308324	RpS7	-2.74	-2.94	0.20	0.00	0.00	0.66
FBpp0311987	RpS8	-3.70	-3.13	-0.57	0.00	0.00	0.27
FBpp0088021	Rpt1	-0.30	-0.33	0.03	0.65	0.62	0.96
FBpp0311982	Rpt2	0.93	0.51	0.42	0.07	0.29	0.38
FBpp0312031	Rpt3	0.21	0.46	-0.25	0.64	0.32	0.59
FBpp0293948	Rpt4	0.31	0.07	0.24	0.48	0.87	0.59
FBpp0083843	Rpt5	0.27	0.10	0.18	0.51	0.81	0.66
FBpp0076890	Rpt6	0.68	-0.11	0.78	0.26	0.85	0.20
FBpp0288680	Rrp1	3.18	3.62	-0.44	0.00	0.00	0.33
FBpp0080746	RtcB	1.57	2.68	-1.11	0.28	0.08	0.44
FBpp0081601	rump	-0.47	-0.42	-0.05	0.24	0.29	0.90
FBpp0089284	Sar1	0.90	1.06	-0.17	0.09	0.05	0.73
FBpp0297362	SC35	-1.20	-0.81	-0.39	0.03	0.13	0.45
FBpp0074285	scu	-0.30	-0.63	0.33	0.48	0.16	0.44
FBpp0082877	sds22	0.73	0.35	0.38	0.21	0.54	0.51
FBpp0083932	Sec10	0.53	0.88	-0.35	0.41	0.18	0.58
FBpp0311988	Sec13	-0.88	-0.92	0.04	0.05	0.04	0.92
FBpp0309105	Sec16	-1.72	-1.35	-0.37	0.01	0.03	0.52
FBpp0308424	Sec23	0.88	0.87	0.01	0.16	0.17	0.99
FBpp0087723	Sec31	0.37	0.23	0.14	0.39	0.60	0.74
FBpp0086691	SelD	0.82	0.60	0.22	0.13	0.26	0.66
FBpp0307454	SerRS	0.42	-0.65	1.07	0.50	0.31	0.11
FBpp0089160	sgg	0.52	1.64	-1.12	0.47	0.04	0.14
FBpp0296963	Sgt	-0.20	-0.22	0.01	0.69	0.67	0.98
FBpp0291704	Sh3beta	-0.10	-1.30	1.20	0.87	0.07	0.09
FBpp0305866	shi	1.14	0.67	0.47	0.02	0.12	0.26
FBpp0073893	shtd	-2.14	-1.77	-0.36	0.02	0.04	0.65
FBpp0081709	sle	0.30	0.81	-0.50	0.68	0.28	0.50
FBpp0086591	SMC2	2.18	2.62	-0.44	0.00	0.00	0.36
FBpp0075684	SmD1	0.15	-0.33	0.48	0.73	0.43	0.27
FBpp0081234	SmD2	0.37	0.66	-0.29	0.46	0.19	0.55
FBpp0079182	SmE	0.19	0.79	-0.61	0.73	0.17	0.28
FBpp0288543	smg	-0.70	0.12	-0.81	0.34	0.87	0.27
FBpp0304234	smid	0.37	0.54	-0.18	0.46	0.28	0.72
FBpp0078984	smt3	0.64	0.57	0.06	0.18	0.22	0.89
FBpp0078331	Snr1	0.08	-0.29	0.36	0.91	0.68	0.60
FBpp0079247	Snx6	0.27	0.61	-0.34	0.62	0.28	0.53
FBpp0075958	Sod1	-0.75	-1.79	1.04	0.15	0.00	0.05
FBpp0075122	spd-2	0.05	0.03	0.02	0.92	0.95	0.97
FBpp0297149	SpdS	0.77	0.76	0.02	0.13	0.14	0.97
FBpp0310470	spel1	1.24	1.85	-0.60	0.05	0.01	0.31
FBpp0301102	sqd	0.49	0.37	0.12	0.52	0.63	0.87
FBpp0271779	Srp14	-1.03	-0.72	-0.31	0.08	0.20	0.57
FBpp0079471	Srp54	0.47	0.78	-0.31	0.35	0.13	0.52
FBpp0076872	Srp54k	-0.81	-0.83	0.01	0.09	0.09	0.97
FBpp0076244	Srp68	-0.14	-0.11	-0.03	0.73	0.78	0.95
FBpp0083319	Srp72	0.54	-0.15	0.69	0.39	0.81	0.28
FBpp0079211	Ssb-c31a	0.48	0.11	0.37	0.41	0.85	0.53
FBpp0072151	Ssrp	0.92	0.27	0.64	0.11	0.62	0.25
FBpp0308666	sta	-2.00	-2.87	0.86	0.00	0.00	0.16
FBpp0078827	stai	-0.18	-0.90	0.72	0.80	0.20	0.30
FBpp0077790	Stip1	0.20	-0.36	0.56	0.75	0.58	0.38
FBpp0290871	Su(var)3-7	1.14	1.10	0.04	0.03	0.03	0.93
FBpp0078372	Sym	-0.32	-0.04	-0.28	0.47	0.92	0.53
FBpp0304718	tacc	1.06	0.51	0.55	0.02	0.22	0.18

FBpp0080045	Tap42	0.48	-0.31	0.79	0.39	0.58	0.17
FBpp0081820	Tctp	-0.29	-0.82	0.53	0.53	0.10	0.26
FBpp0110174	tefu	-0.68	0.22	-0.90	0.50	0.83	0.38
FBpp0087479	TER94	1.05	0.99	0.07	0.02	0.02	0.86
FBpp0083355	TFAM	0.94	1.27	-0.34	0.21	0.10	0.64
FBpp0084526	TfIIA-L	0.58	1.34	-0.75	0.22	0.01	0.12
FBpp0312095	ThrRS	0.74	1.19	-0.46	0.12	0.02	0.32
FBpp0082180	timeout	0.02	-0.27	0.29	0.97	0.58	0.55
FBpp0305273	Tnpo	1.52	1.15	0.37	0.00	0.02	0.37
FBpp0077346	toc	-0.27	0.17	-0.44	0.62	0.75	0.43
FBpp0304598	Top2	3.85	4.12	-0.27	0.00	0.00	0.50
FBpp0080787	Top3alpha	0.91	0.52	0.40	0.16	0.41	0.53
FBpp0087193	tou	-0.89	-0.63	-0.26	0.06	0.16	0.54
FBpp0084948	Tpi	-0.93	-1.09	0.15	0.14	0.09	0.80
FBpp0310608	TppII	-0.02	0.05	-0.07	0.96	0.90	0.86
FBpp0304887	tral	-0.54	-0.84	0.30	0.28	0.11	0.54
FBpp0087398	trsn	-0.21	-0.16	-0.05	0.63	0.71	0.91
FBpp0079437	Trx-2	0.25	-0.74	0.99	0.75	0.35	0.22
FBpp0071117	Trxr-1	-0.32	-0.73	0.42	0.58	0.22	0.48
FBpp0310349	Ts	1.50	1.10	0.40	0.04	0.11	0.54
FBpp0312205	Tsf1	-0.74	-1.38	0.64	0.23	0.04	0.29
FBpp0072097	tsr	-0.75	-1.72	0.97	0.19	0.01	0.10
FBpp0304417	Tudor-SN	0.91	1.15	-0.24	0.06	0.02	0.60
FBpp0311386	tws	-0.16	0.17	-0.34	0.75	0.74	0.52
FBpp0076804	Txl	0.61	0.42	0.19	0.54	0.67	0.85
FBpp0077912	tzn	0.22	0.15	0.07	0.81	0.87	0.94
FBpp0298007	U2af50	0.07	0.25	-0.18	0.95	0.81	0.86
FBpp0087583	Uba1	1.47	1.70	-0.22	0.00	0.00	0.60
FBpp0076457	Uba2	0.95	0.96	-0.01	0.11	0.11	0.99
FBpp0073354	Uba5	1.07	0.48	0.59	0.08	0.40	0.31
FBpp0311673	Ubc4	0.27	0.19	0.08	0.78	0.84	0.93
FBpp0309477	Ubqn	-0.40	-0.72	0.32	0.33	0.09	0.44
FBpp0292511	Uch	0.01	-0.18	0.19	0.99	0.82	0.81
FBpp0306000	Uch-L5	-1.95	-1.86	-0.09	0.00	0.00	0.84
FBpp0311276	Uev1A	0.42	0.76	-0.34	0.66	0.43	0.72
FBpp0290913	UGP	1.60	1.47	0.13	0.05	0.07	0.86
FBpp0311454	und	0.34	0.80	-0.45	0.56	0.19	0.44
FBpp0304059	Usp14	0.65	0.85	-0.20	0.16	0.07	0.64
FBpp0298309	Usp5	0.74	0.65	0.09	0.08	0.12	0.82
FBpp0073474	Usp7	0.51	0.49	0.02	0.27	0.29	0.97
FBpp0305353	ValRS	0.71	0.65	0.06	0.07	0.10	0.87
FBpp0086468	Vha36-1	0.21	-0.01	0.23	0.79	0.99	0.77
FBpp0086320	Vha44	0.69	0.86	-0.16	0.17	0.10	0.74
FBpp0290875	Vha55	0.80	-0.02	0.82	0.10	0.97	0.09
FBpp0307597	Vha68-2	0.71	0.50	0.20	0.13	0.26	0.64
FBpp0307142	VhaSFD	0.65	0.15	0.50	0.18	0.75	0.29
FBpp0309628	Vps4	0.68	-0.16	0.84	0.45	0.86	0.35
FBpp0300790	wds	-1.88	-2.15	0.27	0.00	0.00	0.59
FBpp0289361	wech	-0.73	-0.29	-0.43	0.33	0.69	0.55
FBpp0306779	woc	-0.37	-0.43	0.05	0.51	0.45	0.92
FBpp0307569	wrd	0.41	0.54	-0.13	0.31	0.18	0.73
FBpp0291513	WRNexo	1.51	2.05	-0.54	0.00	0.00	0.23
FBpp0304606	x16	-0.84	-0.92	0.08	0.15	0.12	0.89
FBpp0071049	Ykt6	-0.36	0.68	-1.04	0.66	0.40	0.21
FBpp0072306	zip	0.88	0.53	0.35	0.09	0.28	0.47
FBpp0085138	Zwilch	0.34	0.72	-0.38	0.50	0.17	0.46

b) OEB – BEB – 15 min – 3 h

Flybase polypeptide ID	Flybase symbol	differences					p-values				
		oeb_15min-beb_15min	oeb_3h-beb_3h	oeb_3h-oeb_15min	beb_3h-beb_15min	(oeb_15min-beb_15min) - (oeb_3h-beb_3h)	oeb_15min-beb_15min	oeb_3h-beb_3h	oeb_3h-oeb_15min	beb_3h-beb_15min	(oeb_15min-beb_15min) - (oeb_3h-beb_3h)
FBpp0304169	-	0.36	-0.45	0.54	1.36	0.82	0.12	0.10	0.04	0.00	0.03
FBpp0304748	-	0.31	-0.42	0.06	0.80	0.74	0.13	0.08	0.78	0.00	0.02
FBpp0308925	-	0.05	0.03	0.45	0.47	0.01	0.86	0.92	0.12	0.11	0.97
FBpp0312116	-	0.11	-0.01	-1.30	-1.19	0.12	0.82	0.99	0.02	0.03	0.87
FBpp0087084	128up	0.37	-0.69	-0.64	0.42	1.06	0.34	0.13	0.13	0.32	0.08
FBpp0082990	14-3-3epsilon	0.02	0.05	-0.47	-0.50	-0.03	0.92	0.84	0.04	0.03	0.93
FBpp0305137	14-3-3zeta	-0.43	0.24	0.06	-0.60	-0.66	0.20	0.55	0.86	0.11	0.20
FBpp0075508	26-29-p	-0.28	0.22	2.41	1.90	-0.50	0.52	0.67	0.00	0.00	0.46
FBpp0087947	ACC	-0.83	0.62	2.89	1.44	-1.45	0.02	0.13	0.00	0.00	0.01
FBpp0085204	Acf	-0.25	0.01	1.31	1.05	-0.26	0.46	0.98	0.00	0.01	0.62
FBpp0311818	Act5C	0.29	1.20	1.43	0.52	-0.91	0.63	0.10	0.04	0.43	0.34
FBpp0100051	Adh	-0.04	0.10	-0.52	-0.66	-0.14	0.94	0.85	0.33	0.22	0.85
FBpp0082816	AdSL	0.09	0.74	0.47	-0.18	-0.65	0.84	0.17	0.34	0.71	0.35
FBpp0312000	Ahcy	-0.40	0.53	-1.13	-2.06	-0.93	0.44	0.38	0.05	0.00	0.24
FBpp0087757	AIMP1	-0.83	-0.48	0.21	-0.15	-0.36	0.21	0.54	0.77	0.84	0.72
FBpp0075318	AIMP2	-0.49	-0.17	0.15	-0.17	-0.32	0.21	0.71	0.73	0.68	0.59
FBpp0071969	AIMP3	-0.24	-0.49	0.28	0.53	0.25	0.44	0.18	0.41	0.12	0.59
FBpp0309214	Akap200	0.04	0.23	0.16	-0.02	-0.19	0.92	0.64	0.71	0.96	0.77
FBpp0311050	Akt1	0.68	0.35	0.38	0.71	0.33	0.38	0.70	0.65	0.40	0.78
FBpp0089366	AlaRS	-0.45	0.31	0.15	-0.61	-0.76	0.12	0.36	0.63	0.06	0.09
FBpp0308680	Ald	-0.46	0.63	-0.14	-1.22	-1.08	0.05	0.02	0.57	0.00	0.00
FBpp0309805	alien	1.68	0.00	-0.91	0.77	1.67	0.02	1.00	0.23	0.31	0.12
FBpp0084610	ALiX	0.07	-0.34	0.56	0.98	0.41	0.73	0.18	0.02	0.00	0.21
FBpp0071138	alpha-PheRS	-0.73	-1.07	0.62	0.95	0.34	0.50	0.41	0.61	0.43	0.84
FBpp0072694	alphaCOP	0.46	-0.42	-1.13	-0.26	0.87	0.09	0.19	0.00	0.37	0.04
FBpp0076122	alphaTub67C	-0.31	-0.19	-0.31	-0.42	-0.11	0.25	0.54	0.29	0.15	0.78
FBpp0081153	alphaTub84B	-0.24	0.45	-0.26	-0.95	-0.69	0.30	0.11	0.30	0.00	0.06
FBpp0311374	Amun	0.21	-0.19	-1.07	-0.67	0.40	0.54	0.63	0.01	0.08	0.45
FBpp0082065	Aos1	-0.70	0.67	0.86	-0.51	-1.37	0.13	0.22	0.09	0.32	0.06
FBpp0074558	AP-1-2beta	-1.07	0.34	0.64	-0.77	-1.41	0.08	0.62	0.33	0.24	0.13
FBpp0311464	apolpp	-0.06	0.39	-0.53	-0.98	-0.45	0.85	0.27	0.11	0.01	0.33
FBpp0305852	Arf102F	0.44	-0.69	-0.99	0.14	1.14	0.59	0.47	0.27	0.87	0.37
FBpp0304364	Arf79F	-1.83	0.58	1.11	-1.30	-2.40	0.05	0.59	0.27	0.20	0.10
FBpp0304160	ArfGAP3	0.03	-0.43	-0.75	-0.28	0.46	0.96	0.56	0.28	0.68	0.63
FBpp0076271	Argk	0.07	-0.08	-1.24	-1.09	0.15	0.82	0.83	0.00	0.00	0.75
FBpp0073965	ArgRS	-0.52	-0.11	0.28	-0.14	-0.41	0.06	0.73	0.34	0.64	0.32
FBpp0082121	Arp1	0.48	-0.31	-0.29	0.51	0.79	0.04	0.25	0.26	0.05	0.03
FBpp0081780	Art1	-0.09	-1.02	-1.82	-0.89	0.93	0.85	0.07	0.00	0.08	0.19
FBpp0305840	Art4	0.32	-0.62	-2.07	-1.13	0.94	0.29	0.09	0.00	0.00	0.05
FBpp0304830	AsnRS	0.23	-0.38	-1.52	-0.91	0.61	0.54	0.40	0.00	0.04	0.30
FBpp0084071	asp	-0.61	-0.37	1.66	1.41	-0.24	0.09	0.38	0.00	0.00	0.66
FBpp0308483	AspRS	-0.48	-0.11	0.17	-0.21	-0.38	0.10	0.75	0.58	0.51	0.39
FBpp0309030	ATPCL	-0.01	0.75	-0.09	-0.85	-0.76	0.98	0.14	0.84	0.07	0.25
FBpp0311086	ATPsynbeta	0.40	-0.38	-0.38	0.40	0.78	0.49	0.58	0.55	0.53	0.39
FBpp0312191	awd	-1.92	-0.01	0.87	-1.04	-1.91	0.24	1.00	0.62	0.56	0.45

FBpp0307124	Bacc	-0.73	0.02	0.42	-0.33	-0.75	0.23	0.98	0.52	0.62	0.43
FBpp0084466	ball	-0.67	0.49	2.30	1.15	-1.15	0.10	0.30	0.00	0.01	0.07
FBpp0071235	Bap111	-1.34	0.55	0.96	-0.92	-1.88	0.01	0.31	0.06	0.07	0.01
FBpp0085442	Bap170	-0.20	-0.28	0.53	0.61	0.08	0.57	0.52	0.19	0.14	0.89
FBpp0086115	Bap55	-0.32	-0.79	-0.09	0.38	0.47	0.32	0.04	0.80	0.28	0.35
FBpp0073572	Bap60	-1.18	-0.38	0.99	0.20	-0.80	0.28	0.76	0.40	0.87	0.63
FBpp0310394	barr	-0.44	-0.43	-0.27	-0.27	-0.01	0.19	0.27	0.46	0.45	0.99
FBpp0306433	bel	0.00	-0.33	0.06	0.40	0.34	0.99	0.31	0.83	0.19	0.44
FBpp0080048	beta'COP	0.47	0.33	-0.43	-0.29	0.13	0.18	0.41	0.26	0.43	0.80
FBpp0074348	betaCOP	0.36	-0.21	-0.02	0.55	0.58	0.28	0.59	0.95	0.14	0.27
FBpp0085720	betaTub56D	-0.28	0.77	-0.13	-1.19	-1.06	0.31	0.03	0.66	0.00	0.02
FBpp0086896	bic	-0.97	2.30	1.24	-2.03	-3.28	0.31	0.05	0.24	0.06	0.03
FBpp0080362	BicC	0.17	0.26	1.20	1.10	-0.09	0.62	0.52	0.00	0.01	0.86
FBpp0082428	BigH1	-3.18	-1.25	1.99	0.05	-1.94	0.04	0.47	0.22	0.98	0.40
FBpp0071794	blw	0.22	-0.27	0.38	0.87	0.49	0.73	0.72	0.58	0.22	0.62
FBpp0311234	bol	-0.40	0.47	3.19	2.31	-0.88	0.37	0.37	0.00	0.00	0.21
FBpp0079417	borr	-0.86	0.34	2.29	1.09	-1.21	0.22	0.68	0.01	0.17	0.27
FBpp0305757	brm	-0.63	-0.83	0.31	0.51	0.20	0.14	0.10	0.50	0.27	0.76
FBpp0308293	Bub3	0.47	-0.67	0.56	1.70	1.15	0.12	0.06	0.09	0.00	0.02
FBpp0310411	bur	0.03	-0.63	-0.64	0.02	0.66	0.95	0.26	0.21	0.97	0.36
FBpp0087402	Caf1-105	-1.04	-0.41	0.40	-0.22	-0.63	0.02	0.43	0.40	0.64	0.36
FBpp0071172	Caf1-180	-0.44	-0.28	0.34	0.18	-0.17	0.22	0.51	0.38	0.65	0.76
FBpp0082511	Caf1-55	0.18	-0.83	-0.21	0.80	1.00	0.75	0.21	0.73	0.19	0.24
FBpp0311269	Cam	-0.88	0.47	1.91	0.56	-1.35	0.06	0.37	0.00	0.25	0.06
FBpp0301600	CanB2	-0.04	-0.37	-0.51	-0.18	0.33	0.95	0.63	0.48	0.80	0.74
FBpp0304507	Cand1	-0.15	0.21	0.27	-0.09	-0.35	0.58	0.51	0.36	0.77	0.39
FBpp0084818	Cap-D2	0.01	-0.23	-0.33	-0.09	0.24	0.97	0.47	0.27	0.76	0.57
FBpp0288780	Cap-G	-0.03	-0.29	-0.28	-0.02	0.26	0.94	0.56	0.54	0.96	0.69
FBpp0304563	capt	0.32	-0.21	-0.46	0.07	0.53	0.11	0.38	0.04	0.74	0.09
FBpp0308803	casp	1.52	0.98	0.21	0.75	0.54	0.02	0.17	0.74	0.25	0.55
FBpp0083684	CCT1	-0.04	0.26	-0.26	-0.57	-0.31	0.86	0.36	0.33	0.04	0.42
FBpp0071226	CCT2	-0.11	0.08	-0.33	-0.52	-0.19	0.69	0.80	0.27	0.09	0.65
FBpp0291566	CCT3	-0.17	-0.06	-0.73	-0.84	-0.11	0.52	0.86	0.02	0.01	0.78
FBpp0079992	CCT4	-0.04	0.27	-0.58	-0.89	-0.31	0.90	0.43	0.08	0.01	0.49
FBpp0087095	CCT5	-0.12	0.35	-0.50	-0.97	-0.47	0.67	0.28	0.10	0.00	0.27
FBpp0073902	CCT6	0.17	0.40	-0.18	-0.41	-0.22	0.48	0.18	0.49	0.14	0.55
FBpp0081401	CCT7	0.13	0.31	-0.49	-0.67	-0.17	0.54	0.24	0.05	0.01	0.60
FBpp0087764	CCT8	0.05	0.06	-0.45	-0.47	-0.02	0.83	0.81	0.07	0.06	0.96
FBpp0079641	Cdk1	0.26	-0.14	0.00	0.39	0.40	0.23	0.59	0.99	0.10	0.23
FBpp0308475	ced-6	-0.15	-0.30	0.61	0.76	0.15	0.79	0.64	0.31	0.21	0.86
FBpp0305296	CG10077	0.78	-0.99	0.68	2.45	1.77	0.40	0.37	0.50	0.02	0.22
FBpp0080749	CG10237	0.27	-0.67	0.33	1.27	0.94	0.55	0.21	0.50	0.01	0.18
FBpp0306810	CG10254	0.25	0.05	-0.16	0.04	0.20	0.60	0.92	0.76	0.94	0.79
FBpp0309810	CG10341	-0.69	0.71	3.01	1.61	-1.39	0.32	0.39	0.00	0.04	0.20
FBpp0293954	CG10565	0.22	-0.09	0.44	0.74	0.31	0.42	0.78	0.15	0.02	0.46
FBpp0311825	CG10576	-0.68	-0.06	-0.10	-0.72	-0.62	0.29	0.93	0.88	0.30	0.53
FBpp0309343	CG11164	0.32	-1.16	-0.39	1.09	1.48	0.62	0.13	0.58	0.13	0.14
FBpp0084759	CG11899	0.27	0.04	-2.23	-1.99	0.23	0.62	0.95	0.00	0.00	0.78
FBpp0072658	CG12018	1.12	-1.29	-1.93	0.49	2.42	0.02	0.02	0.00	0.31	0.00
FBpp0312072	CG12702	0.25	-0.06	-0.68	-0.36	0.31	0.61	0.92	0.22	0.50	0.68
FBpp0307859	CG1354	0.59	-0.24	-1.69	-0.86	0.83	0.23	0.67	0.00	0.11	0.27
FBpp0085260	CG1416	0.32	0.12	-0.91	-0.71	0.20	0.40	0.79	0.04	0.10	0.73
FBpp0311823	CG14434	0.04	0.35	-0.88	-1.19	-0.31	0.94	0.55	0.11	0.03	0.68
FBpp0077145	CG15439	0.02	0.38	1.74	1.37	-0.36	0.96	0.40	0.00	0.00	0.54
FBpp0084691	CG1646	-0.93	0.42	2.33	0.98	-1.35	0.36	0.72	0.04	0.38	0.39
FBpp0300672	CG16817	-0.15	0.34	-0.18	-0.67	-0.49	0.87	0.76	0.86	0.52	0.74
FBpp0310240	CG1703	-0.07	-0.19	0.14	0.26	0.13	0.88	0.70	0.77	0.58	0.85
FBpp0085374	CG17337	-0.83	0.79	-0.18	-1.80	-1.62	0.22	0.32	0.80	0.02	0.13
FBpp0087367	CG17765	-0.32	0.47	-0.37	-1.16	-0.79	0.60	0.52	0.57	0.09	0.40
FBpp0271746	CG18190	0.62	-0.07	0.34	1.03	0.69	0.03	0.83	0.26	0.00	0.11

FBpp0303935	CG18815	-0.46	-0.51	-0.28	-0.23	0.05	0.40	0.43	0.64	0.70	0.95
FBpp0306729	CG1943	-0.20	0.31	-1.76	-2.27	-0.51	0.84	0.79	0.11	0.04	0.74
FBpp0304910	CG2034	0.44	-0.57	-1.60	-0.59	1.01	0.23	0.19	0.00	0.15	0.08
FBpp0078327	CG2091	0.14	1.22	-0.44	-1.53	-1.09	0.83	0.12	0.53	0.04	0.28
FBpp0307423	CG2246	0.16	0.70	-0.99	-1.53	-0.54	0.69	0.14	0.03	0.00	0.38
FBpp0311613	CG2852	-0.51	0.79	1.38	0.08	-1.30	0.47	0.34	0.08	0.92	0.24
FBpp0307127	CG2862	-1.88	-0.02	0.47	-1.39	-1.86	0.01	0.98	0.52	0.06	0.08
FBpp0086057	CG30105	-0.76	-0.07	1.05	0.36	-0.69	0.21	0.92	0.12	0.58	0.46
FBpp0291433	CG30382	0.23	-0.01	-0.36	-0.13	0.24	0.28	0.97	0.12	0.57	0.46
FBpp0070997	CG3040	0.68	0.78	1.62	1.52	-0.10	0.45	0.47	0.11	0.13	0.94
FBpp0076007	CG32066	-0.27	-1.04	-0.18	0.60	0.78	0.71	0.22	0.82	0.45	0.48
FBpp0311522	CG32165	0.35	-0.52	0.13	0.99	0.86	0.64	0.55	0.87	0.22	0.45
FBpp0070953	CG3226	-0.72	0.00	-0.34	-1.07	-0.73	0.32	1.00	0.66	0.18	0.51
FBpp0311482	CG33722	-0.49	1.09	-1.21	-2.78	-1.57	0.59	0.32	0.23	0.01	0.27
FBpp0310197	CG3939	1.67	0.60	-0.89	0.18	1.07	0.06	0.56	0.35	0.85	0.42
FBpp0303976	CG40045	-0.67	-0.28	-1.69	-2.07	-0.38	0.33	0.72	0.03	0.01	0.71
FBpp0288574	CG42232	-0.18	0.10	1.30	1.02	-0.29	0.59	0.79	0.00	0.01	0.58
FBpp0304189	CG4603	-0.40	-0.28	0.00	-0.12	-0.12	0.17	0.41	0.99	0.70	0.79
FBpp0079789	CG4751	-0.10	-0.59	1.92	2.41	0.49	0.90	0.53	0.04	0.01	0.69
FBpp0112210	CG4951	-2.27	0.75	3.97	0.95	-3.02	0.04	0.55	0.00	0.42	0.08
FBpp0309480	CG5162	-0.49	0.03	4.40	3.88	-0.53	0.05	0.91	0.00	0.00	0.16
FBpp0309317	CG5174	0.01	-0.31	0.49	0.82	0.33	0.95	0.28	0.08	0.01	0.39
FBpp0311410	CG5515	0.24	0.64	-0.38	-0.78	-0.40	0.53	0.17	0.37	0.08	0.51
FBpp0085950	CG5721	0.12	-0.30	-0.94	-0.52	0.42	0.76	0.51	0.04	0.23	0.48
FBpp0084281	CG5886	-0.19	-0.36	0.39	0.56	0.17	0.56	0.36	0.28	0.13	0.74
FBpp0303937	CG6084	-0.62	0.91	0.01	-1.52	-1.53	0.03	0.01	0.98	0.00	0.00
FBpp0079979	CG6180	-1.58	2.15	1.27	-2.45	-3.73	0.08	0.05	0.19	0.02	0.01
FBpp0083213	CG6195	0.50	-0.19	-1.03	-0.33	0.70	0.14	0.63	0.01	0.37	0.19
FBpp0079809	CG6287	-0.45	0.32	-0.50	-1.27	-0.77	0.21	0.45	0.20	0.00	0.17
FBpp0080044	CG6523	-0.09	0.09	0.15	-0.02	-0.17	0.86	0.88	0.78	0.97	0.82
FBpp0311284	CG6767	-0.61	0.56	0.65	-0.51	-1.17	0.23	0.35	0.24	0.35	0.14
FBpp0309927	CG6907	0.63	-0.34	-1.25	-0.28	0.97	0.12	0.48	0.01	0.53	0.13
FBpp0304957	CG7519	0.58	-0.27	-1.41	-0.56	0.85	0.29	0.68	0.03	0.35	0.32
FBpp0302568	CG7946	-0.74	-0.05	0.95	0.27	-0.68	0.20	0.94	0.13	0.66	0.44
FBpp0303962	CG8003	0.34	-0.43	-0.45	0.33	0.78	0.18	0.15	0.11	0.24	0.05
FBpp0081371	CG8036	-0.91	0.21	0.25	-0.87	-1.12	0.06	0.69	0.62	0.09	0.12
FBpp0074246	CG8142	-0.29	0.46	0.96	0.21	-0.75	0.46	0.33	0.03	0.62	0.22
FBpp0081539	CG8149	0.13	0.11	-2.33	-2.31	0.02	0.79	0.85	0.00	0.00	0.98
FBpp0076470	CG8209	0.27	0.32	-0.75	-0.80	-0.05	0.64	0.64	0.24	0.21	0.96
FBpp0081398	CG8223	0.34	-0.02	-0.78	-0.42	0.36	0.52	0.97	0.19	0.47	0.66
FBpp0087733	CG8243	-0.10	0.01	2.08	1.96	-0.12	0.74	0.97	0.00	0.00	0.81
FBpp0087116	CG8858	0.52	0.21	-0.45	-0.14	0.31	0.07	0.52	0.16	0.66	0.48
FBpp0074128	CG9132	0.54	-0.29	-0.36	0.47	0.83	0.02	0.26	0.14	0.05	0.02
FBpp0311963	CG9135	0.35	0.15	0.59	0.80	0.20	0.45	0.79	0.25	0.12	0.78
FBpp0072610	CG9184	-0.36	0.47	2.04	1.21	-0.83	0.62	0.59	0.02	0.14	0.46
FBpp0309269	CG9281	-0.28	0.60	0.07	-0.82	-0.88	0.34	0.09	0.84	0.02	0.06
FBpp0074708	CG9330	-1.33	0.66	1.20	-0.79	-1.99	0.02	0.30	0.05	0.18	0.02
FBpp0081343	CG9601	0.65	1.12	1.41	0.95	-0.47	0.44	0.26	0.13	0.30	0.72
FBpp0088471	chb	-0.13	-0.14	0.84	0.84	0.01	0.84	0.86	0.24	0.24	1.00
FBpp0308531	Chc	0.02	-0.16	-0.52	-0.34	0.18	0.93	0.57	0.06	0.20	0.63
FBpp0301152	chic	-0.18	0.82	-0.03	-1.02	-0.99	0.63	0.07	0.95	0.02	0.09
FBpp0083939	CHORD	0.27	1.13	-0.87	-1.74	-0.87	0.55	0.04	0.08	0.00	0.21
FBpp0099657	Chrac-14	-0.55	-0.02	1.17	0.64	-0.53	0.22	0.97	0.02	0.19	0.44
FBpp0308688	Chrac-16	-0.09	0.13	1.23	1.01	-0.22	0.81	0.75	0.00	0.01	0.69
FBpp0310070	cib	-0.32	0.34	-0.24	-0.91	-0.66	0.25	0.30	0.42	0.01	0.13
FBpp0311360	CkIIalpha	-0.22	-0.58	-0.98	-0.61	0.37	0.61	0.26	0.05	0.20	0.58
FBpp0305406	CkIIbeta	0.26	-0.26	-0.83	-0.31	0.52	0.74	0.79	0.35	0.73	0.68
FBpp0301627	cnn	-0.04	-0.95	0.43	1.34	0.91	0.95	0.22	0.54	0.07	0.36
FBpp0304029	Cnot4	-0.93	0.02	2.51	1.55	-0.95	0.12	0.98	0.00	0.02	0.30
FBpp0086719	Cp1	0.22	0.12	1.58	1.69	0.11	0.60	0.82	0.00	0.00	0.87

FBpp0304020	cpb	1.32	-0.79	-0.23	1.88	2.11	0.01	0.13	0.63	0.00	0.00
FBpp0074329	CrebB	-0.10	-0.50	0.15	0.55	0.40	0.82	0.34	0.75	0.25	0.55
FBpp0080484	Cse1	-0.05	0.25	-0.29	-0.60	-0.31	0.85	0.46	0.36	0.07	0.50
FBpp0077927	CSN3	-0.04	-0.52	-0.74	-0.26	0.48	0.89	0.13	0.02	0.41	0.28
FBpp0290448	CSN4	0.27	-0.25	-0.37	0.16	0.53	0.35	0.45	0.24	0.62	0.24
FBpp0082743	CSN5	0.23	-1.38	-0.50	1.11	1.61	0.78	0.16	0.58	0.22	0.21
FBpp0087821	CSN7	0.27	0.01	-0.97	-0.70	0.27	0.70	1.00	0.22	0.37	0.81
FBpp0306584	CtBP	-0.45	-0.26	-0.17	-0.36	-0.19	0.34	0.64	0.74	0.48	0.79
FBpp0086732	Ctf4	0.23	-0.45	0.88	1.57	0.69	0.54	0.32	0.04	0.00	0.25
FBpp0312102	cup	-0.03	-0.06	2.23	2.25	0.03	0.92	0.87	0.00	0.00	0.96
FBpp0074017	Cyp1	-0.84	1.12	-0.08	-2.05	-1.97	0.06	0.04	0.86	0.00	0.01
FBpp0290739	D1	-0.89	0.74	1.74	0.11	-1.63	0.27	0.43	0.05	0.89	0.19
FBpp0084349	Dak1	-1.21	-0.40	0.18	-0.63	-0.81	0.16	0.69	0.85	0.50	0.54
FBpp0075498	DCTN1-p150	0.14	0.07	0.42	0.49	0.07	0.66	0.86	0.23	0.16	0.88
FBpp0087722	DCTN2-p50	0.23	-0.10	-0.69	-0.36	0.33	0.50	0.80	0.07	0.34	0.53
FBpp0071097	dec-1	0.52	0.39	-2.79	-2.67	0.12	0.44	0.62	0.00	0.00	0.91
FBpp0291138	deltaCOP	-0.17	-0.15	-2.17	-2.19	-0.02	0.81	0.86	0.01	0.01	0.98
FBpp0099688	Df31	-1.95	0.17	0.80	-1.32	-2.12	0.04	0.87	0.42	0.19	0.14
FBpp0304991	Dhc64C	0.14	-0.49	-0.37	0.27	0.64	0.52	0.07	0.13	0.28	0.07
FBpp0311766	dhd	0.16	-0.09	0.45	0.70	0.25	0.81	0.91	0.54	0.34	0.81
FBpp0073299	Dlic	-0.30	-0.47	0.11	0.27	0.16	0.50	0.38	0.83	0.58	0.81
FBpp0076830	DnaJ-1	-0.42	-0.19	2.87	2.65	-0.22	0.26	0.66	0.00	0.00	0.69
FBpp0072041	DNAlig1	0.09	-0.63	-0.15	0.57	0.72	0.73	0.04	0.59	0.05	0.07
FBpp0073678	DNAlig4	0.43	1.24	2.75	1.94	-0.81	0.40	0.05	0.00	0.00	0.31
FBpp0075277	DNApol-delta	0.75	-1.36	-0.65	1.46	2.12	0.09	0.01	0.17	0.00	0.00
FBpp0311418	Dp1	-0.09	-0.29	0.01	0.21	0.20	0.68	0.25	0.96	0.36	0.54
FBpp0311783	dpa	-0.14	0.36	-0.55	-1.04	-0.49	0.64	0.31	0.10	0.00	0.29
FBpp0083673	Dph5	0.19	1.01	-1.04	-1.87	-0.82	0.72	0.12	0.08	0.00	0.32
FBpp0072744	dre4	0.04	0.55	-0.36	-0.86	-0.50	0.89	0.14	0.30	0.02	0.30
FBpp0082223	Droj2	0.16	0.00	0.74	0.91	0.17	0.43	0.99	0.00	0.00	0.61
FBpp0307166	Drp1	0.10	-0.37	0.00	0.46	0.47	0.67	0.19	0.99	0.08	0.21
FBpp0309113	Dsor1	0.94	0.00	-1.30	-0.37	0.93	0.13	1.00	0.06	0.58	0.32
FBpp0308813	Dsp1	-0.15	-0.24	0.97	1.06	0.09	0.79	0.71	0.12	0.09	0.92
FBpp0079746	dUTPase	-0.08	0.67	-0.74	-1.50	-0.76	0.87	0.28	0.20	0.01	0.35
FBpp0304413	E(bx)	-0.29	0.52	1.66	0.85	-0.82	0.73	0.60	0.08	0.36	0.53
FBpp0305157	Eb1	0.45	0.13	-0.11	0.21	0.32	0.05	0.63	0.65	0.40	0.36
FBpp0311273	eEF1alpha1	0.42	0.01	-0.81	-0.40	0.41	0.07	0.97	0.00	0.11	0.24
FBpp0311691	eEF1beta	0.04	0.05	0.60	0.60	-0.01	0.86	0.87	0.04	0.04	0.99
FBpp0079542	eEF1delta	-0.05	0.16	0.27	0.07	-0.20	0.84	0.56	0.28	0.77	0.57
FBpp0305182	eEF2	-0.01	0.52	-0.52	-1.05	-0.53	0.97	0.06	0.05	0.00	0.14
FBpp0072082	eEF5	-0.36	0.76	0.01	-1.10	-1.12	0.48	0.22	0.98	0.06	0.17
FBpp0072908	eIF1	0.61	0.30	-1.30	-0.99	0.32	0.28	0.65	0.04	0.11	0.71
FBpp0309768	eIF2alpha	0.29	-0.17	0.38	0.83	0.45	0.18	0.50	0.11	0.00	0.17
FBpp0291521	eIF2Bdelta	-0.07	-0.41	0.05	0.38	0.33	0.81	0.27	0.88	0.26	0.49
FBpp0075700	eIF2beta	-0.29	0.40	1.14	0.46	-0.68	0.81	0.78	0.39	0.73	0.71
FBpp0307983	eIF2gamma	0.41	-0.04	0.08	0.53	0.45	0.04	0.87	0.71	0.02	0.15
FBpp0312226	eIF3a	0.45	0.95	0.48	-0.02	-0.50	0.38	0.12	0.39	0.98	0.53
FBpp0075104	eIF3e	-0.93	2.63	2.73	-0.83	-3.56	0.31	0.02	0.01	0.40	0.02
FBpp0070430	eIF3g1	-1.33	-0.35	1.93	0.95	-0.98	0.13	0.73	0.05	0.32	0.47
FBpp0071587	eIF3k	0.36	-0.54	-0.59	0.31	0.90	0.22	0.12	0.07	0.32	0.05
FBpp0075754	eIF3l	0.15	-0.17	-0.38	-0.07	0.32	0.59	0.62	0.22	0.83	0.47
FBpp0303628	eIF4A	0.23	-0.20	-0.78	-0.36	0.42	0.45	0.59	0.03	0.29	0.37
FBpp0306959	eIF4B	0.85	0.77	0.14	0.23	0.08	0.11	0.22	0.80	0.69	0.92
FBpp0288389	eIF4G1	0.28	-0.91	0.53	1.72	1.19	0.28	0.01	0.07	0.00	0.01
FBpp0310226	eIF4H1	0.61	-0.72	-1.03	0.30	1.34	0.17	0.17	0.04	0.53	0.06
FBpp0089140	eIF5	0.83	-0.64	-1.50	-0.03	1.47	0.10	0.28	0.01	0.96	0.06
FBpp0301573	eIF5B	0.72	0.62	-0.76	-0.66	0.10	0.26	0.41	0.28	0.34	0.92
FBpp0072144	eIF6	-0.08	-0.74	-1.13	-0.48	0.65	0.80	0.07	0.00	0.20	0.21
FBpp0311547	Eip55E	0.13	1.52	-0.12	-1.50	-1.39	0.81	0.03	0.85	0.02	0.12
FBpp0083354	EloB	-0.01	-0.26	-0.15	0.10	0.25	0.99	0.82	0.89	0.92	0.87

FBpp0079278	emb	-0.19	-0.35	-0.21	-0.05	0.16	0.57	0.38	0.58	0.90	0.76
FBpp0303860	EndoGI	0.46	-0.51	-1.17	-0.20	0.97	0.25	0.28	0.01	0.64	0.12
FBpp0077574	Eno	-0.75	-0.04	-0.69	-1.41	-0.72	0.02	0.93	0.05	0.00	0.15
FBpp0304201	eRF1	-0.43	-0.06	-1.43	-1.80	-0.37	0.59	0.95	0.11	0.05	0.76
FBpp0311174	eRF3	0.22	0.20	-1.09	-1.06	0.02	0.60	0.70	0.03	0.03	0.97
FBpp0079496	Etl1	0.46	-0.65	0.13	1.25	1.12	0.52	0.45	0.87	0.12	0.32
FBpp0099726	fabp	0.36	0.32	-0.73	-0.69	0.04	0.10	0.21	0.00	0.01	0.90
FBpp0308326	faf	-0.05	-0.65	-0.26	0.34	0.60	0.87	0.08	0.44	0.31	0.21
FBpp0083399	Fancd2	-0.12	0.35	2.26	1.78	-0.48	0.81	0.57	0.00	0.00	0.56
FBpp0087756	FANCl	-0.20	0.25	2.58	2.13	-0.45	0.76	0.75	0.00	0.01	0.66
FBpp0307371	FASN1	0.60	-0.34	-1.06	-0.12	0.94	0.11	0.44	0.01	0.76	0.11
FBpp0081767	Fdh	-0.40	0.48	-1.56	-2.44	-0.89	0.56	0.55	0.05	0.00	0.41
FBpp0071892	Fib	0.41	0.17	0.76	1.00	0.24	0.57	0.84	0.34	0.22	0.83
FBpp0074215	Fim	0.43	0.25	-0.19	-0.02	0.18	0.22	0.53	0.61	0.97	0.74
FBpp0083551	fit	-0.02	0.79	0.28	-0.53	-0.81	0.96	0.13	0.55	0.27	0.23
FBpp0082574	FK506-bp1	-1.87	0.77	1.14	-1.49	-2.63	0.05	0.47	0.25	0.14	0.07
FBpp0085703	FK506-bp2	-0.05	0.41	-0.45	-0.92	-0.47	0.83	0.17	0.11	0.00	0.24
FBpp0309663	FKBP59	0.14	-0.30	-0.80	-0.37	0.44	0.57	0.31	0.01	0.18	0.26
FBpp0300445	Fmr1	0.10	0.52	1.15	0.73	-0.42	0.87	0.47	0.09	0.27	0.65
FBpp0304175	fmt	-0.40	0.33	0.66	-0.08	-0.73	0.47	0.61	0.28	0.90	0.40
FBpp0310694	fray	2.12	-2.23	-2.18	2.17	4.35	0.04	0.06	0.05	0.05	0.01
FBpp0294038	Fs(2)Ket	0.22	-0.16	-0.23	0.15	0.38	0.39	0.59	0.42	0.58	0.34
FBpp0303129	gammaCOP	0.58	-0.34	-1.62	-0.70	0.92	0.11	0.42	0.00	0.08	0.11
FBpp0304827	gammaTub37C	0.27	-0.13	0.40	0.80	0.40	0.28	0.66	0.14	0.01	0.30
FBpp0099914	Gapdh1	-0.30	1.37	-0.57	-2.24	-1.67	0.63	0.08	0.41	0.00	0.10
FBpp0304864	Gapdh2	-4.04	0.23	1.86	-2.41	-4.27	0.01	0.89	0.23	0.13	0.06
FBpp0311558	Gdi	-1.18	1.13	0.13	-2.18	-2.31	0.11	0.20	0.87	0.01	0.05
FBpp0307688	Gel	-0.59	-0.02	1.85	1.28	-0.57	0.45	0.98	0.04	0.14	0.63
FBpp0084240	GlnRS	-0.44	-0.36	0.11	0.04	-0.08	0.13	0.28	0.71	0.91	0.86
FBpp0080489	glu	0.00	0.04	0.04	-0.01	-0.04	1.00	0.90	0.91	0.98	0.92
FBpp0083898	GluProRS	-0.48	-0.26	0.30	0.07	-0.23	0.23	0.58	0.49	0.86	0.71
FBpp0099923	GlyP	-0.17	0.04	-1.35	-1.57	-0.21	0.49	0.89	0.00	0.00	0.58
FBpp0306062	GlyRS	-0.20	0.14	-0.75	-1.09	-0.34	0.49	0.69	0.03	0.00	0.46
FBpp0305474	GlyS	0.51	0.09	-1.60	-1.18	0.42	0.31	0.88	0.01	0.04	0.58
FBpp0078478	Gnf1	-0.02	0.12	0.67	0.52	-0.15	0.94	0.73	0.05	0.12	0.76
FBpp0310187	Grip84	-0.46	0.52	0.52	-0.46	-0.98	0.40	0.42	0.38	0.44	0.25
FBpp0073672	Grip91	-0.84	-0.91	0.54	0.62	0.08	0.14	0.17	0.38	0.31	0.93
FBpp0300970	Grx1	-0.61	0.86	0.91	-0.55	-1.47	0.28	0.20	0.15	0.37	0.10
FBpp0290201	Gss2	0.49	0.55	-1.21	-1.27	-0.06	0.36	0.39	0.05	0.04	0.95
FBpp0099824	GstD1	-1.05	0.35	-0.68	-2.08	-1.40	0.10	0.64	0.32	0.01	0.16
FBpp0085855	GstE6	0.51	0.20	-1.16	-0.85	0.31	0.03	0.45	0.00	0.00	0.37
FBpp0305731	GstS1	-0.76	-0.12	-0.47	-1.12	-0.64	0.31	0.89	0.56	0.18	0.57
FBpp0305263	Gug	-0.34	0.23	3.02	2.45	-0.57	0.45	0.66	0.00	0.00	0.41
FBpp0310171	hang	-0.64	-0.01	1.11	0.48	-0.63	0.20	0.99	0.05	0.37	0.41
FBpp0078319	Hat1	-0.03	0.10	-0.88	-1.01	-0.13	0.96	0.87	0.15	0.10	0.88
FBpp0311451	Hcf	-1.00	-0.80	1.88	1.68	-0.20	0.15	0.33	0.02	0.03	0.85
FBpp0073173	HDAC1	-0.07	-1.18	-0.18	0.93	1.11	0.89	0.05	0.73	0.09	0.15
FBpp0078756	Hel25E	0.11	-0.14	-0.38	-0.13	0.25	0.65	0.64	0.17	0.64	0.52
FBpp0305905	HIP-R	0.01	0.02	-0.71	-0.72	-0.01	0.96	0.94	0.03	0.03	0.98
FBpp0071028	Hira	-0.26	-0.54	1.22	1.50	0.28	0.67	0.47	0.09	0.04	0.77
FBpp0091111	His2A	0.33	-2.09	0.59	3.02	2.43	0.74	0.09	0.59	0.01	0.13
FBpp0306426	His2Av	0.02	0.27	3.27	3.03	-0.25	0.96	0.64	0.00	0.00	0.74
FBpp0091155	His2B	-0.10	0.23	2.51	2.18	-0.33	0.78	0.58	0.00	0.00	0.55
FBpp0091112	His3	-0.03	1.99	2.49	0.48	-2.01	0.98	0.09	0.03	0.65	0.19
FBpp0306146	His4r	-0.09	0.53	2.47	1.85	-0.62	0.83	0.29	0.00	0.00	0.34
FBpp0307711	HnRNP-K	1.70	-0.52	-0.78	1.44	2.22	0.05	0.59	0.39	0.11	0.09
FBpp0297875	Hrb27C	-0.12	-0.13	3.04	3.06	0.01	0.89	0.90	0.00	0.00	0.99
FBpp0307982	Hsc70-4	-0.28	0.11	1.89	1.50	-0.38	0.34	0.76	0.00	0.00	0.40
FBpp0305265	Hsc70Cb	-0.44	0.84	-0.25	-1.53	-1.28	0.10	0.01	0.40	0.00	0.00
FBpp0312157	Hsp26	0.41	0.05	0.49	0.85	0.35	0.10	0.86	0.07	0.00	0.35

FBpp0312159	Hsp27	-0.08	0.12	0.89	0.69	-0.20	0.78	0.71	0.01	0.03	0.64
FBpp0073291	Hsp60A	0.19	-0.61	-0.65	0.14	0.79	0.67	0.26	0.19	0.77	0.26
FBpp0305095	Hsp83	0.08	-0.09	-0.63	-0.46	0.17	0.73	0.72	0.02	0.07	0.62
FBpp0305272	Idh	-0.68	-0.33	-0.87	-1.22	-0.35	0.23	0.62	0.17	0.06	0.69
FBpp0078152	IleRS	-0.68	-0.38	0.28	-0.02	-0.30	0.03	0.28	0.38	0.95	0.51
FBpp0307848	Incenp	-1.02	0.81	1.47	-0.35	-1.83	0.05	0.18	0.01	0.52	0.02
FBpp0084842	IntS11	0.11	-0.13	-0.44	-0.19	0.24	0.86	0.86	0.54	0.79	0.81
FBpp0076091	iPLA2-VIA	0.68	-0.64	-0.12	1.20	1.32	0.19	0.30	0.83	0.04	0.11
FBpp0081861	Irbp	2.69	2.63	1.39	1.45	0.05	0.00	0.00	0.05	0.04	0.96
FBpp0086956	Iswi	-0.34	0.05	1.62	1.23	-0.38	0.33	0.91	0.00	0.00	0.47
FBpp0311371	Jafrac1	-0.80	0.41	0.01	-1.20	-1.21	0.02	0.31	0.98	0.00	0.03
FBpp0307568	Karybeta3	0.20	-0.24	-0.64	-0.20	0.44	0.46	0.46	0.04	0.51	0.30
FBpp0086328	Khc	0.30	-0.44	-0.87	-0.12	0.75	0.24	0.16	0.00	0.66	0.07
FBpp0289115	kis	-0.53	-0.33	1.98	1.79	-0.19	0.26	0.55	0.00	0.00	0.79
FBpp0303946	Klc	0.66	0.04	-0.70	-0.07	0.63	0.27	0.96	0.29	0.91	0.50
FBpp0312027	Klp10A	0.39	-0.05	0.42	0.86	0.44	0.09	0.86	0.10	0.00	0.22
FBpp0309092	Klp3A	-0.31	0.12	1.13	0.69	-0.44	0.30	0.73	0.00	0.04	0.35
FBpp0072616	Klp61F	0.26	0.06	-0.48	-0.28	0.20	0.45	0.89	0.20	0.45	0.70
FBpp0078399	kra	-0.07	-0.24	-0.18	-0.01	0.17	0.89	0.67	0.73	0.99	0.81
FBpp0080322	Ku80	2.20	1.92	1.29	1.57	0.28	0.00	0.00	0.01	0.00	0.68
FBpp0307649	l(1)G0156	0.12	-0.70	0.71	1.53	0.82	0.86	0.39	0.35	0.05	0.44
FBpp0080906	La	0.21	-0.46	-0.88	-0.20	0.67	0.49	0.21	0.01	0.54	0.16
FBpp0312110	Lam	-0.16	-0.36	1.43	1.63	0.20	0.53	0.24	0.00	0.00	0.62
FBpp0081255	lds	-0.50	0.19	1.97	1.28	-0.68	0.28	0.73	0.00	0.02	0.34
FBpp0311704	LeuRS	-0.76	-0.05	0.51	-0.21	-0.71	0.03	0.90	0.16	0.57	0.17
FBpp0073551	lic	0.31	-0.10	0.25	0.66	0.41	0.15	0.69	0.29	0.01	0.22
FBpp0088383	lola	-0.68	-0.47	0.74	0.52	-0.22	0.30	0.54	0.31	0.47	0.83
FBpp0078561	lost	0.27	0.03	-0.06	0.18	0.24	0.28	0.92	0.82	0.51	0.53
FBpp0311908	Lsd-2	0.40	-0.06	-0.36	0.10	0.46	0.24	0.88	0.33	0.78	0.38
FBpp0071301	LysRS	-0.92	-0.39	0.19	-0.34	-0.53	0.07	0.51	0.73	0.53	0.49
FBpp0076819	mad2	-0.34	0.69	0.28	-0.75	-1.03	0.66	0.45	0.74	0.38	0.39
FBpp0085235	Map205	-0.74	0.86	1.34	-0.26	-1.60	0.11	0.12	0.01	0.60	0.03
FBpp0087613	Map60	-0.69	0.44	1.15	0.02	-1.13	0.14	0.42	0.03	0.97	0.12
FBpp0289639	Mapmodulin	0.95	0.36	-1.83	-1.24	0.59	0.09	0.58	0.01	0.05	0.49
FBpp0306961	mask	-1.10	-0.99	0.90	0.78	-0.11	0.06	0.15	0.16	0.21	0.90
FBpp0087350	Mat1	-0.13	0.03	1.53	1.38	-0.15	0.84	0.97	0.03	0.04	0.87
FBpp0311400	mats	0.36	-0.48	-0.04	0.81	0.84	0.13	0.09	0.89	0.00	0.03
FBpp0300203	Mccc1	-0.33	0.40	2.29	1.56	-0.73	0.26	0.24	0.00	0.00	0.11
FBpp0081317	Mcm2	-0.64	0.28	-0.52	-1.44	-0.92	0.24	0.66	0.38	0.02	0.27
FBpp0081756	Mcm5	-0.04	-0.47	-1.17	-0.75	0.43	0.92	0.28	0.01	0.07	0.45
FBpp0070913	Mcm6	0.22	-0.59	-1.73	-0.92	0.81	0.43	0.08	0.00	0.01	0.07
FBpp0076312	Mcm7	1.03	0.44	-1.34	-0.75	0.59	0.14	0.59	0.08	0.32	0.58
FBpp0293887	MCTS1	0.21	-0.06	-0.89	-0.63	0.26	0.59	0.90	0.04	0.14	0.65
FBpp0311560	Mdh1	-0.34	0.28	-0.91	-1.53	-0.62	0.31	0.47	0.02	0.00	0.23
FBpp0079565	me31B	0.65	-0.08	-0.77	-0.04	0.73	0.02	0.81	0.02	0.90	0.09
FBpp0288779	MEP-1	0.17	-0.54	1.17	1.88	0.71	0.77	0.44	0.08	0.01	0.44
FBpp0085809	MetRS	-0.58	-0.52	0.15	0.09	-0.05	0.06	0.15	0.65	0.77	0.91
FBpp0304462	Mi-2	-0.29	-0.76	1.27	1.73	0.46	0.48	0.13	0.01	0.00	0.47
FBpp0297604	Mlf	0.15	-0.42	1.09	1.66	0.57	0.78	0.53	0.09	0.01	0.51
FBpp0301951	mod	-0.38	0.13	-0.02	-0.53	-0.51	0.54	0.86	0.98	0.44	0.59
FBpp0083472	mod(mdg4)	-1.99	0.13	2.16	0.05	-2.11	0.03	0.90	0.03	0.96	0.13
FBpp0075450	mop	0.38	1.27	1.61	0.72	-0.89	0.54	0.09	0.02	0.29	0.35
FBpp0291706	mor	-1.15	0.12	0.80	-0.46	-1.26	0.10	0.88	0.28	0.53	0.23
FBpp0079802	mre11	0.19	1.00	1.47	0.66	-0.81	0.53	0.01	0.00	0.06	0.10
FBpp0305821	msi	-0.09	0.29	2.94	2.57	-0.37	0.78	0.43	0.00	0.00	0.44
FBpp0076408	msk	0.15	0.00	0.11	0.25	0.14	0.61	0.99	0.73	0.43	0.75
FBpp0293342	msps	-0.42	-0.14	0.91	0.63	-0.28	0.13	0.66	0.00	0.04	0.50
FBpp0303028	Mtap	0.20	0.96	-0.32	-1.08	-0.76	0.77	0.24	0.67	0.16	0.47
FBpp0304737	Mtor	0.73	0.79	0.84	0.78	-0.06	0.06	0.08	0.05	0.06	0.92
FBpp0310063	mts	-1.52	-1.63	-1.51	-1.39	0.12	0.14	0.18	0.18	0.21	0.94

FBpp0082729	mtSSB	1.28	0.60	1.24	1.92	0.68	0.09	0.50	0.13	0.02	0.55
FBpp0305424	mub	0.36	0.40	1.16	1.12	-0.04	0.35	0.38	0.01	0.01	0.95
FBpp0311946	mus201	-1.02	-0.19	1.55	0.72	-0.83	0.07	0.77	0.01	0.23	0.32
FBpp0311394	Nacalpha	0.31	0.08	-0.84	-0.61	0.23	0.24	0.80	0.01	0.04	0.56
FBpp0297132	Nap1	-0.06	-0.26	-0.67	-0.48	0.19	0.78	0.33	0.01	0.06	0.57
FBpp0306828	NAT1	-0.30	-0.69	0.95	1.34	0.39	0.37	0.08	0.01	0.00	0.44
FBpp0297182	nbs	0.49	0.64	1.32	1.17	-0.16	0.11	0.08	0.00	0.00	0.74
FBpp0311231	ncd	-0.02	0.99	1.99	0.98	-1.01	0.99	0.39	0.07	0.36	0.51
FBpp0309711	Nedd8	-0.49	0.16	1.08	0.43	-0.65	0.51	0.86	0.19	0.59	0.57
FBpp0080867	nesd	-0.15	-0.67	0.34	0.86	0.52	0.81	0.37	0.62	0.22	0.59
FBpp0306756	Nlp	-0.36	0.00	-0.40	-0.77	-0.37	0.17	0.99	0.17	0.01	0.36
FBpp0076451	Nmt	-0.26	0.96	0.75	-0.47	-1.22	0.69	0.23	0.30	0.52	0.24
FBpp0309175	NO66	-0.75	-0.67	0.80	0.72	-0.08	0.16	0.28	0.17	0.21	0.92
FBpp0290083	Nop60B	0.39	-0.45	2.17	3.01	0.84	0.47	0.47	0.00	0.00	0.31
FBpp0112220	Nph	-0.60	-0.17	-1.29	-1.72	-0.43	0.07	0.65	0.00	0.00	0.40
FBpp0289954	Npl4	0.60	-1.09	-1.56	0.13	1.69	0.07	0.01	0.00	0.71	0.00
FBpp0312079	Nplp2	-0.15	-0.09	-0.66	-0.72	-0.06	0.63	0.80	0.06	0.04	0.90
FBpp0311095	Nsf2	0.59	-0.79	-1.09	0.29	1.38	0.24	0.19	0.06	0.59	0.08
FBpp0305904	Ntf-2	0.26	0.31	-0.61	-0.65	-0.04	0.39	0.40	0.08	0.06	0.93
FBpp0297079	nudC	-0.15	-0.33	0.09	0.27	0.18	0.60	0.32	0.77	0.38	0.68
FBpp0079710	Nup107	-0.05	-0.64	0.27	0.86	0.59	0.93	0.36	0.67	0.19	0.52
FBpp0083695	Nup133	0.49	-0.46	0.08	1.02	0.95	0.44	0.54	0.91	0.14	0.33
FBpp0309144	Nup153	0.79	-0.42	-1.17	0.04	1.21	0.04	0.34	0.01	0.93	0.04
FBpp0297623	Nup188	0.41	-0.94	-0.61	0.75	1.35	0.13	0.00	0.04	0.01	0.00
FBpp0074568	Nup205	0.29	-0.53	0.22	1.04	0.82	0.50	0.29	0.63	0.03	0.21
FBpp0071905	Nup214	0.09	-0.90	-0.55	0.44	1.00	0.84	0.10	0.27	0.37	0.16
FBpp0293235	Nup358	-0.22	0.34	2.50	1.94	-0.56	0.71	0.63	0.00	0.01	0.55
FBpp0087861	Nup50	0.22	-0.02	-0.25	-0.01	0.24	0.65	0.98	0.64	0.99	0.75
FBpp0087063	Nup54	2.55	1.24	-0.55	0.75	1.31	0.01	0.23	0.56	0.43	0.34
FBpp0306915	Nup98-96	-1.38	0.96	1.97	-0.37	-2.34	0.05	0.23	0.01	0.62	0.03
FBpp0297127	Nurf-38	-0.65	-0.60	-0.19	-0.23	-0.04	0.21	0.31	0.73	0.68	0.96
FBpp0072061	or	-1.29	0.07	1.54	0.18	-1.35	0.08	0.94	0.06	0.82	0.23
FBpp0088033	Orc1	-0.80	0.07	3.50	2.64	-0.86	0.08	0.90	0.00	0.00	0.21
FBpp0082329	Orc2	-1.13	0.07	3.56	2.37	-1.19	0.07	0.93	0.00	0.00	0.21
FBpp0086882	Orc3	-0.33	0.95	2.32	1.04	-1.28	0.63	0.25	0.00	0.17	0.23
FBpp0072330	Orc4	-0.11	0.14	2.15	1.90	-0.25	0.71	0.70	0.00	0.00	0.59
FBpp0080120	Orc5	-0.04	0.07	2.66	2.54	-0.11	0.93	0.89	0.00	0.00	0.88
FBpp0307031	osa	0.18	-0.12	-0.99	-0.68	0.30	0.84	0.91	0.32	0.49	0.83
FBpp0088069	p47	-0.39	-0.06	0.16	-0.17	-0.33	0.57	0.94	0.83	0.82	0.75
FBpp0085919	pAbp	0.13	-0.53	0.68	1.33	0.65	0.58	0.06	0.01	0.00	0.07
FBpp0073976	Paf-AHalpha	-0.22	0.93	-0.17	-1.32	-1.15	0.73	0.22	0.80	0.06	0.24
FBpp0305933	Paics	0.22	0.53	-0.74	-1.05	-0.31	0.50	0.17	0.05	0.01	0.53
FBpp0112608	Parp	-1.61	-0.25	1.61	0.25	-1.36	0.01	0.72	0.02	0.69	0.14
FBpp0082124	Past1	0.15	-0.25	-0.58	-0.18	0.40	0.67	0.53	0.13	0.63	0.45
FBpp0290074	PCB	-0.53	-0.63	2.15	2.25	0.10	0.30	0.30	0.00	0.00	0.90
FBpp0308430	pch2	0.21	-0.09	-0.97	-0.67	0.30	0.72	0.90	0.15	0.31	0.74
FBpp0089395	PCNA	-1.15	1.07	1.10	-1.12	-2.22	0.03	0.08	0.06	0.05	0.01
FBpp0297204	pds5	-0.33	-0.33	0.21	0.21	0.00	0.72	0.76	0.83	0.83	1.00
FBpp0079527	Pen	-0.04	0.00	0.20	0.16	-0.03	0.89	0.99	0.51	0.59	0.94
FBpp0304954	Pfdn2	-1.04	-0.73	0.76	0.45	-0.31	0.15	0.39	0.34	0.56	0.78
FBpp0303214	Pfdn6	-0.76	-0.48	-0.31	-0.60	-0.29	0.32	0.60	0.71	0.48	0.81
FBpp0293464	Pfk	-0.40	1.04	0.71	-0.73	-1.44	0.45	0.11	0.23	0.22	0.09
FBpp0303827	Pgd	-1.34	0.02	1.41	0.05	-1.35	0.04	0.98	0.05	0.94	0.17
FBpp0306279	Pgk	-0.30	0.65	-0.45	-1.40	-0.95	0.24	0.04	0.11	0.00	0.02
FBpp0099920	Pglym78	0.23	0.05	-0.99	-0.81	0.18	0.50	0.90	0.01	0.03	0.73
FBpp0072932	PHGPx	-0.97	0.14	0.55	-0.57	-1.11	0.13	0.85	0.43	0.41	0.26
FBpp0301844	Pl31	-0.63	0.61	3.12	1.87	-1.25	0.19	0.29	0.00	0.00	0.10
FBpp0088847	Pih1D1	0.16	1.28	2.25	1.13	-1.12	0.77	0.06	0.00	0.07	0.20
FBpp0310466	Plap	0.43	-0.36	-0.20	0.59	0.79	0.08	0.22	0.44	0.04	0.04
FBpp0305301	poe	0.26	-1.17	-0.43	0.99	1.43	0.58	0.04	0.39	0.06	0.05

FBpp0307818	Pol32	-0.03	0.34	-0.01	-0.38	-0.37	0.95	0.49	0.98	0.41	0.57
FBpp0099722	polo	-0.34	-0.21	0.33	0.20	-0.13	0.38	0.65	0.43	0.63	0.82
FBpp0292357	poly	0.20	-0.86	-0.86	0.19	1.05	0.76	0.27	0.23	0.79	0.30
FBpp0084115	polybromo	-0.20	0.00	0.47	0.27	-0.20	0.55	0.99	0.21	0.46	0.71
FBpp0081704	pont	-0.13	-0.22	-0.05	0.04	0.09	0.52	0.36	0.83	0.86	0.78
FBpp0082067	Pp1-87B	-0.39	0.16	1.81	1.26	-0.55	0.36	0.74	0.00	0.01	0.40
FBpp0293227	Pp2A-29B	-0.15	-0.07	-0.01	-0.09	-0.08	0.62	0.85	0.97	0.78	0.86
FBpp0304082	PpD3	-0.61	-1.69	-1.93	-0.85	1.08	0.58	0.21	0.12	0.49	0.53
FBpp0071451	Prosalpha3	0.16	0.77	0.30	-0.30	-0.61	0.88	0.55	0.80	0.80	0.72
FBpp0073989	Prosalpha4	-0.12	-0.97	-1.04	-0.19	0.85	0.77	0.06	0.03	0.68	0.20
FBpp0086067	Prosalpha5	-0.17	-0.73	-1.48	-0.92	0.55	0.75	0.27	0.02	0.13	0.52
FBpp0310201	Prosalpha6	-0.03	0.24	-0.02	-0.30	-0.27	0.88	0.30	0.92	0.18	0.38
FBpp0089041	Prosalpha7	-0.21	-0.07	-0.60	-0.74	-0.14	0.64	0.89	0.24	0.15	0.85
FBpp0086400	Prosbeta1	-0.90	0.43	0.47	-0.86	-1.33	0.06	0.44	0.36	0.10	0.07
FBpp0075382	Prosbeta2	-1.64	0.60	0.87	-1.38	-2.25	0.05	0.54	0.34	0.13	0.09
FBpp0087320	Prosbeta5	-0.65	0.29	0.56	-0.38	-0.94	0.08	0.51	0.17	0.34	0.11
FBpp0075119	Prosbeta6	-0.32	-0.24	-0.02	-0.09	-0.07	0.30	0.50	0.96	0.78	0.87
FBpp0078449	Prosbeta7	-0.26	0.37	0.13	-0.50	-0.62	0.30	0.21	0.64	0.07	0.11
FBpp0085902	Prp19	-0.74	0.11	1.62	0.76	-0.86	0.08	0.82	0.00	0.10	0.19
FBpp0100080	Prx5	0.18	0.48	-0.69	-0.99	-0.30	0.52	0.16	0.03	0.00	0.50
FBpp0077277	Ptpa	0.35	0.26	0.88	0.97	0.09	0.63	0.76	0.27	0.22	0.93
FBpp0305823	pum	-0.29	-0.59	1.85	2.15	0.30	0.48	0.23	0.00	0.00	0.63
FBpp0082932	Pxt	-0.19	0.50	2.24	1.55	-0.69	0.47	0.13	0.00	0.00	0.11
FBpp0083611	PyK	-0.17	0.30	0.73	0.26	-0.47	0.63	0.46	0.06	0.50	0.38
FBpp0309142	r	0.27	0.68	0.28	-0.13	-0.41	0.39	0.08	0.41	0.72	0.40
FBpp0083440	r-l	0.09	0.06	-0.42	-0.38	0.03	0.81	0.90	0.32	0.36	0.96
FBpp0083503	Rab1	0.39	-0.87	-0.74	0.53	1.27	0.41	0.13	0.16	0.31	0.09
FBpp0083414	Rab11	0.31	-0.04	-0.01	0.34	0.34	0.36	0.93	0.99	0.36	0.51
FBpp0307641	Rab2	-0.29	-1.46	-1.36	-0.19	1.17	0.64	0.06	0.05	0.77	0.23
FBpp0303520	Rab5	-0.68	0.44	1.13	0.01	-1.12	0.32	0.58	0.13	0.99	0.29
FBpp0311572	Rack1	-0.63	0.02	-0.48	-1.13	-0.65	0.37	0.98	0.53	0.15	0.55
FBpp0293866	rad50	0.09	0.98	1.70	0.80	-0.90	0.82	0.04	0.00	0.06	0.14
FBpp0071600	Rae1	-0.92	0.43	1.95	0.60	-1.35	0.12	0.53	0.00	0.34	0.14
FBpp0309151	Ran	0.14	0.48	-0.47	-0.81	-0.35	0.51	0.06	0.05	0.00	0.29
FBpp0307011	RanBP3	-2.13	2.10	1.03	-3.21	-4.23	0.01	0.03	0.23	0.00	0.00
FBpp0312218	Ranbp9	0.42	-0.41	-0.63	0.19	0.82	0.13	0.21	0.04	0.52	0.06
FBpp0306292	RanGAP	0.12	-1.35	-0.77	0.70	1.47	0.82	0.03	0.18	0.22	0.08
FBpp0076784	Rcc1	-0.34	0.15	1.91	1.42	-0.49	0.26	0.66	0.00	0.00	0.29
FBpp0302766	REG	-0.14	0.32	0.03	-0.42	-0.45	0.60	0.30	0.91	0.14	0.26
FBpp0311247	rept	-0.04	-0.46	-0.48	-0.06	0.42	0.85	0.08	0.05	0.80	0.22
FBpp0079609	RfC3	-0.12	0.27	0.62	0.22	-0.39	0.71	0.47	0.08	0.52	0.43
FBpp0311114	RfC38	0.12	-0.06	0.63	0.81	0.18	0.66	0.85	0.04	0.01	0.67
FBpp0073120	RfC4	-0.85	0.42	1.28	0.01	-1.27	0.09	0.47	0.02	0.99	0.10
FBpp0305320	rhea	0.15	-0.51	-0.21	0.44	0.65	0.60	0.13	0.49	0.16	0.14
FBpp0304185	RhoGDI	-0.10	0.29	-0.60	-0.99	-0.39	0.87	0.70	0.38	0.15	0.69
FBpp0312064	rin	-0.44	0.07	-0.60	-1.12	-0.51	0.39	0.91	0.29	0.06	0.52
FBpp0310006	rngo	0.04	0.41	1.23	0.85	-0.37	0.97	0.71	0.23	0.40	0.79
FBpp0079648	RnrL	-0.67	0.26	0.05	-0.88	-0.93	0.09	0.57	0.91	0.04	0.13
FBpp0087152	RnrS	0.46	-0.13	-1.17	-0.58	0.59	0.16	0.73	0.00	0.11	0.24
FBpp0302971	row	0.43	0.37	0.70	0.77	0.07	0.53	0.65	0.36	0.31	0.95
FBpp0305404	Rox8	-0.68	0.66	2.86	1.53	-1.33	0.09	0.16	0.00	0.00	0.03
FBpp0081356	RpA-70	-0.24	1.05	4.27	2.97	-1.29	0.73	0.22	0.00	0.00	0.24
FBpp0305226	RPA2	0.48	1.53	4.09	3.04	-1.05	0.15	0.00	0.00	0.00	0.05
FBpp0310183	RPA3	0.50	1.41	3.93	3.02	-0.91	0.17	0.00	0.00	0.00	0.11
FBpp0302626	RpL13	0.10	-0.45	-0.50	0.05	0.55	0.90	0.64	0.57	0.95	0.66
FBpp0311452	RpL27A	-0.35	0.51	0.58	-0.28	-0.86	0.72	0.65	0.59	0.79	0.56
FBpp0306837	RpL40	-1.43	0.54	3.02	1.04	-1.97	0.09	0.58	0.00	0.25	0.13
FBpp0306232	RpLP0	-1.21	0.18	0.58	-0.82	-1.39	0.04	0.79	0.36	0.20	0.12
FBpp0074662	Rpn1	0.16	0.15	-0.67	-0.65	0.02	0.61	0.70	0.06	0.07	0.97
FBpp0305644	Rpn10	-0.24	0.90	0.45	-0.69	-1.14	0.45	0.02	0.19	0.05	0.02

FBpp0078664	Rpn11	0.48	-0.02	-0.06	0.43	0.49	0.02	0.95	0.77	0.05	0.11
FBpp0075068	Rpn12	0.26	-0.48	-1.02	-0.28	0.74	0.41	0.21	0.01	0.43	0.14
FBpp0112987	Rpn13	0.26	0.41	0.07	-0.08	-0.15	0.62	0.51	0.91	0.89	0.86
FBpp0306599	Rpn2	0.09	-0.07	-0.47	-0.31	0.16	0.66	0.79	0.05	0.18	0.62
FBpp0307804	Rpn3	0.04	-0.52	-0.31	0.25	0.57	0.84	0.06	0.20	0.30	0.11
FBpp0078278	Rpn5	-0.34	-0.14	0.39	0.19	-0.20	0.64	0.87	0.63	0.81	0.86
FBpp0297513	Rpn6	-0.06	-0.10	0.23	0.26	0.03	0.85	0.81	0.54	0.48	0.95
FBpp0083687	Rpn7	-0.03	0.31	0.16	-0.19	-0.35	0.90	0.34	0.59	0.54	0.41
FBpp0305141	Rpn8	0.29	0.61	-0.64	-0.96	-0.32	0.61	0.37	0.32	0.14	0.72
FBpp0083861	Rpn9	0.63	0.23	-0.32	0.08	0.40	0.03	0.48	0.30	0.79	0.36
FBpp0087115	RpS11	0.35	-0.93	-1.01	0.27	1.28	0.64	0.29	0.21	0.74	0.27
FBpp0311350	RpS19a	0.09	-0.02	0.51	0.62	0.11	0.92	0.98	0.61	0.53	0.94
FBpp0311561	RpS2	0.24	0.73	-0.08	-0.57	-0.49	0.51	0.10	0.85	0.16	0.39
FBpp0071087	RpS6	-0.71	-1.26	-0.43	0.11	0.54	0.32	0.14	0.58	0.89	0.62
FBpp0311987	RpS8	0.12	-0.27	-0.50	-0.11	0.39	0.73	0.50	0.19	0.76	0.46
FBpp0088021	Rpt1	0.18	-0.04	-0.42	-0.20	0.23	0.36	0.86	0.06	0.37	0.47
FBpp0311982	Rpt2	0.15	0.33	-0.60	-0.79	-0.19	0.61	0.33	0.07	0.02	0.67
FBpp0293948	Rpt4	0.10	0.17	-0.36	-0.44	-0.08	0.74	0.61	0.26	0.17	0.86
FBpp0083843	Rpt5	-0.06	-0.14	-0.95	-0.86	0.08	0.86	0.73	0.02	0.03	0.88
FBpp0076890	Rpt6	0.31	0.95	-0.43	-1.07	-0.65	0.44	0.05	0.33	0.02	0.29
FBpp0288680	Rrp1	-0.20	0.23	1.29	0.86	-0.43	0.55	0.55	0.00	0.02	0.40
FBpp0311555	Rrp40	0.28	-0.48	-1.26	-0.49	0.76	0.73	0.62	0.18	0.59	0.55
FBpp0081601	rump	0.11	-1.04	1.00	2.16	1.16	0.88	0.25	0.23	0.01	0.32
FBpp0089284	Sar1	-0.95	0.85	1.95	0.15	-1.80	0.12	0.23	0.01	0.82	0.06
FBpp0074285	scu	0.15	-0.01	1.44	1.60	0.16	0.78	0.98	0.02	0.01	0.84
FBpp0082877	sds22	0.62	0.52	-0.24	-0.14	0.10	0.12	0.26	0.57	0.73	0.87
FBpp0309105	Sec16	0.30	-0.08	0.86	1.25	0.38	0.72	0.94	0.36	0.19	0.77
FBpp0303000	Sec24CD	0.57	-0.74	-1.14	0.17	1.31	0.20	0.16	0.02	0.72	0.06
FBpp0311417	Sec31	0.34	-1.08	-0.62	0.80	1.42	0.46	0.06	0.22	0.12	0.05
FBpp0086691	SelD	-2.51	-0.96	-1.13	-2.68	-1.56	0.01	0.33	0.22	0.01	0.23
FBpp0307454	SerRS	0.53	0.37	-0.31	-0.15	0.16	0.46	0.66	0.69	0.85	0.89
FBpp0296963	Sgt	0.21	-0.30	-0.47	0.05	0.52	0.50	0.42	0.19	0.89	0.30
FBpp0081351	Sgt1	0.25	-0.18	-0.61	-0.19	0.42	0.53	0.70	0.15	0.65	0.48
FBpp0309359	shi	0.16	-0.09	0.22	0.47	0.25	0.62	0.81	0.53	0.19	0.62
FBpp0311477	Shmt	-1.08	0.49	0.56	-1.01	-1.56	0.08	0.49	0.40	0.13	0.10
FBpp0306437	skap	0.48	0.63	0.30	0.16	-0.14	0.57	0.53	0.74	0.86	0.91
FBpp0311474	SkpA	-0.27	-1.52	-0.60	0.66	1.25	0.70	0.07	0.44	0.39	0.25
FBpp0081710	sle	-0.26	0.56	0.93	0.12	-0.82	0.60	0.34	0.09	0.83	0.29
FBpp0293061	SmB	0.92	-1.05	-1.45	0.52	1.97	0.15	0.17	0.04	0.45	0.05
FBpp0086591	SMC2	0.07	-0.20	0.04	0.31	0.27	0.84	0.62	0.92	0.42	0.61
FBpp0074065	SMC3	0.12	0.04	-0.21	-0.13	0.08	0.81	0.95	0.70	0.82	0.92
FBpp0305647	SMC5	0.30	-0.12	0.67	1.09	0.42	0.49	0.82	0.17	0.03	0.53
FBpp0081234	SmD2	-0.17	0.02	0.37	0.18	-0.19	0.73	0.97	0.50	0.74	0.81
FBpp0078984	smt3	-1.52	-0.41	1.64	0.52	-1.11	0.12	0.72	0.13	0.62	0.45
FBpp0078331	Snr1	-0.86	-0.02	1.47	0.63	-0.84	0.09	0.98	0.01	0.25	0.28
FBpp0082111	Snx3	0.59	-1.33	-1.35	0.56	1.91	0.27	0.04	0.03	0.33	0.03
FBpp0075958	Sod1	-0.27	0.65	-0.71	-1.63	-0.92	0.73	0.48	0.40	0.06	0.44
FBpp0072164	spag	0.59	1.00	0.45	0.04	-0.41	0.13	0.03	0.28	0.92	0.49
FBpp0297149	SpdS	0.13	0.67	-0.76	-1.30	-0.54	0.69	0.09	0.04	0.00	0.28
FBpp0307742	spg	-0.95	0.51	1.16	-0.31	-1.47	0.07	0.39	0.04	0.58	0.07
FBpp0301102	sqd	-0.05	1.27	-0.05	-1.37	-1.32	0.87	0.00	0.89	0.00	0.01
FBpp0076244	Srp68	-0.42	0.13	0.98	0.44	-0.55	0.44	0.84	0.10	0.46	0.51
FBpp0083319	Srp72	0.56	-0.45	0.34	1.35	1.01	0.11	0.27	0.37	0.00	0.07
FBpp0072151	Ssrp	-0.24	0.05	-0.96	-1.25	-0.30	0.55	0.91	0.04	0.01	0.64
FBpp0078827	stai	-1.65	0.15	0.23	-1.58	-1.80	0.03	0.86	0.77	0.05	0.11
FBpp0077790	Stip1	-0.24	0.48	0.56	-0.16	-0.72	0.35	0.13	0.06	0.57	0.08
FBpp0079252	Su(var)205	-0.05	-0.45	0.36	0.75	0.40	0.88	0.24	0.31	0.04	0.42
FBpp0082204	Su(var)3-7	-0.40	0.35	0.87	0.11	-0.76	0.49	0.61	0.18	0.86	0.40
FBpp0309283	Swip-1	0.47	-0.42	0.92	1.81	0.89	0.49	0.60	0.23	0.02	0.40
FBpp0304719	tacc	-0.74	0.52	1.02	-0.25	-1.27	0.19	0.43	0.11	0.68	0.15

FBpp0311865	Taf4	-1.55	-0.51	1.26	0.22	-1.04	0.07	0.60	0.17	0.80	0.42
FBpp0085690	TBCB	0.94	1.17	-0.04	-0.26	-0.22	0.18	0.17	0.96	0.74	0.84
FBpp0081820	Tctp	-0.06	0.05	-1.06	-1.16	-0.10	0.87	0.90	0.01	0.00	0.84
FBpp0110174	tefu	-0.31	-0.67	0.70	1.06	0.36	0.49	0.21	0.16	0.04	0.60
FBpp0087479	TER94	0.29	0.39	-0.40	-0.50	-0.10	0.27	0.21	0.17	0.09	0.80
FBpp0083355	TFAM	-0.46	0.06	1.26	0.75	-0.51	0.45	0.94	0.06	0.26	0.58
FBpp0081216	TfIIFalpha	-0.45	-0.43	1.24	1.22	-0.02	0.46	0.55	0.07	0.07	0.98
FBpp0306851	tho2	-0.55	0.26	0.59	-0.22	-0.81	0.19	0.60	0.20	0.63	0.22
FBpp0312095	ThrRS	0.19	0.18	-0.87	-0.85	0.01	0.48	0.58	0.01	0.01	0.97
FBpp0304598	Top2	-0.23	0.32	1.55	1.00	-0.55	0.53	0.46	0.00	0.02	0.34
FBpp0080787	Top3alpha	-0.17	1.15	3.13	1.81	-1.32	0.79	0.14	0.00	0.02	0.19
FBpp0111979	tou	0.38	-0.08	1.80	2.26	0.46	0.33	0.87	0.00	0.00	0.45
FBpp0084948	Tpi	-0.89	0.07	-0.29	-1.25	-0.96	0.01	0.85	0.41	0.00	0.06
FBpp0304887	tral	-0.44	-0.87	-1.73	-1.29	0.43	0.38	0.15	0.00	0.03	0.58
FBpp0079437	Trx-2	-0.96	0.41	0.27	-1.10	-1.37	0.07	0.49	0.62	0.05	0.09
FBpp0312205	Tsf1	-0.87	0.78	0.74	-0.91	-1.65	0.07	0.17	0.16	0.09	0.03
FBpp0075088	TSG101	0.38	0.18	-0.77	-0.56	0.21	0.44	0.76	0.16	0.30	0.79
FBpp0072097	tsr	-0.48	-0.18	-0.80	-1.09	-0.30	0.24	0.70	0.08	0.02	0.63
FBpp0309672	tud	-0.62	-0.76	0.65	0.79	0.14	0.10	0.09	0.12	0.06	0.81
FBpp0304417	Tudor-SN	0.75	-0.08	-0.93	-0.10	0.82	0.07	0.87	0.04	0.81	0.19
FBpp0311386	tws	0.29	-0.55	-1.38	-0.54	0.84	0.32	0.11	0.00	0.09	0.07
FBpp0076804	Txl	0.13	0.07	-0.41	-0.35	0.06	0.55	0.79	0.09	0.15	0.85
FBpp0075168	TyrRS	-0.45	0.06	-0.51	-1.02	-0.50	0.33	0.92	0.31	0.05	0.48
FBpp0077912	tzn	0.15	-0.21	0.78	1.13	0.35	0.62	0.56	0.03	0.00	0.45
FBpp0087583	Uba1	-0.01	0.27	-0.81	-1.10	-0.28	0.97	0.31	0.00	0.00	0.42
FBpp0076457	Uba2	0.22	0.35	-1.29	-1.43	-0.14	0.50	0.35	0.00	0.00	0.78
FBpp0073354	Uba5	0.57	-0.05	-1.06	-0.44	0.62	0.08	0.89	0.00	0.20	0.20
FBpp0311673	Ubc4	-0.25	-0.23	-0.89	-0.91	-0.02	0.66	0.73	0.16	0.15	0.98
FBpp0304449	UbcE2M	-0.50	0.12	-0.26	-0.88	-0.62	0.43	0.87	0.70	0.21	0.52
FBpp0083740	Ublcp1	-0.40	0.29	-1.31	-2.01	-0.70	0.55	0.71	0.09	0.01	0.51
FBpp0292511	Uch	-1.02	0.25	-0.43	-1.69	-1.26	0.05	0.68	0.43	0.00	0.11
FBpp0306000	Uch-L5	0.16	0.89	0.01	-0.71	-0.72	0.57	0.01	0.97	0.03	0.11
FBpp0311276	Uev1A	1.42	0.06	-2.60	-1.24	1.37	0.02	0.93	0.00	0.05	0.12
FBpp0075952	Ufd1-like	0.26	-0.62	-0.89	-0.01	0.88	0.64	0.36	0.16	0.99	0.32
FBpp0309077	Ufm1	-1.16	-0.05	-0.23	-1.34	-1.11	0.20	0.96	0.81	0.18	0.42
FBpp0290912	UGP	-0.48	0.38	0.20	-0.66	-0.86	0.42	0.59	0.76	0.31	0.36
FBpp0311454	und	0.29	0.90	-1.57	-2.18	-0.61	0.65	0.23	0.03	0.00	0.53
FBpp0311664	Unr	0.47	1.90	-0.31	-1.74	-1.43	0.49	0.03	0.69	0.03	0.19
FBpp0304059	Usp14	-0.18	0.10	-0.51	-0.78	-0.27	0.74	0.87	0.38	0.18	0.73
FBpp0298309	Usp5	-0.03	0.25	-0.14	-0.43	-0.29	0.91	0.48	0.66	0.20	0.54
FBpp0309600	Usp7	0.76	-0.21	-0.67	0.30	0.97	0.02	0.56	0.06	0.38	0.05
FBpp0305353	ValRS	0.50	-0.42	-1.46	-0.55	0.92	0.30	0.46	0.01	0.30	0.22
FBpp0311933	Vha13	-0.11	-1.73	-1.43	0.20	1.62	0.89	0.09	0.13	0.83	0.22
FBpp0311965	Vha26	0.14	0.07	-0.63	-0.55	0.08	0.61	0.84	0.05	0.08	0.86
FBpp0086468	Vha36-1	0.43	0.02	-0.80	-0.38	0.41	0.33	0.97	0.11	0.44	0.55
FBpp0288471	Vha44	0.24	0.01	-1.63	-1.40	0.23	0.48	0.98	0.00	0.00	0.67
FBpp0290875	Vha55	-0.51	0.78	-0.29	-1.58	-1.28	0.09	0.03	0.36	0.00	0.01
FBpp0307597	Vha68-2	0.48	-0.12	-1.42	-0.82	0.59	0.36	0.85	0.02	0.16	0.47
FBpp0307142	VhaSFD	-0.68	-1.29	-0.95	-0.33	0.62	0.25	0.07	0.15	0.60	0.50
FBpp0075794	viaf	-0.59	-0.26	0.63	0.30	-0.33	0.33	0.71	0.35	0.65	0.73
FBpp0310907	vib	0.37	-1.39	-1.78	-0.01	1.76	0.42	0.02	0.00	0.98	0.02
FBpp0112266	vig2	0.05	-1.52	-1.67	-0.10	1.57	0.93	0.03	0.01	0.86	0.08
FBpp0075690	vih	0.00	-0.40	-0.69	-0.28	0.40	1.00	0.31	0.07	0.44	0.44
FBpp0309623	Vinc	-0.21	-0.85	-1.58	-0.94	0.64	0.61	0.08	0.00	0.04	0.31
FBpp0309628	Vps4	0.38	-0.59	-1.58	-0.60	0.98	0.58	0.47	0.05	0.43	0.37
FBpp0084579	wdb	0.34	0.18	0.50	0.66	0.16	0.54	0.79	0.42	0.28	0.85
FBpp0300790	wds	-1.00	-0.28	2.11	1.39	-0.72	0.14	0.72	0.01	0.06	0.49
FBpp0307569	wrd	0.04	-0.75	-0.15	0.64	0.79	0.93	0.13	0.74	0.16	0.22
FBpp0308997	WRNexo	-1.05	0.28	2.08	0.75	-1.33	0.26	0.80	0.05	0.46	0.35
FBpp0071049	Ykt6	0.59	-0.72	0.64	1.95	1.32	0.04	0.03	0.04	0.00	0.00

FBpp0312020	Yp1	-0.40	0.48	0.57	-0.32	-0.89	0.52	0.52	0.41	0.64	0.37
FBpp0308710	Yp2	-0.91	0.55	0.33	-1.13	-1.46	0.03	0.23	0.43	0.01	0.02
FBpp0311924	Yp3	-0.18	0.59	-0.01	-0.79	-0.77	0.42	0.04	0.95	0.00	0.04
FBpp0075111	zetaCOP	-1.08	-0.79	0.04	-0.25	-0.29	0.21	0.43	0.97	0.78	0.82
FBpp0072305	zip	0.34	0.40	0.02	-0.03	-0.05	0.39	0.41	0.96	0.94	0.93

3. IDENTIFICATION OF ACF1 INTERACTORS BY CO-IMMUNOPRECIPITATION (see VI.C.1)

a) 3F1 – 8E3 – control

		differences			p-values		
Flybase polypeptide ID	Flybase symbol	3F1-con	8E3-con	3F1-8E3	3F1-con	8E3-con	3F1-8E3
FBpp0308925	-	6.08	-1.38	7.46	0.00	0.00	0.00
FBpp0082990	14-3-3epsilon	-0.75	-0.47	-0.28	0.03	0.17	0.40
FBpp0085204	Acf	2.68	3.01	-0.32	0.00	0.00	0.30
FBpp0311818	Act5C	-0.98	-1.33	0.35	0.01	0.00	0.28
FBpp0309215	Akap200	-1.93	0.91	-2.84	0.00	0.12	0.00
FBpp0072694	alphaCOP	0.09	-0.28	0.36	0.79	0.39	0.26
FBpp0076122	alphaTub67C	-0.71	-0.18	-0.54	0.28	0.79	0.41
FBpp0081153	alphaTub84B	-0.11	-0.44	0.33	0.77	0.26	0.40
FBpp0086107	APC10	-1.76	-0.43	-1.33	0.00	0.45	0.03
FBpp0301606	APC4	-1.31	0.57	-1.88	0.01	0.21	0.00
FBpp0070907	APC7	-1.25	0.66	-1.91	0.22	0.52	0.07
FBpp0311464	apolpp	-1.52	-1.15	-0.37	0.00	0.00	0.28
FBpp0082121	Arp1	-1.96	-0.56	-1.41	0.00	0.38	0.03
FBpp0084071	asp	0.13	-0.97	1.10	0.78	0.05	0.03
FBpp0306920	atms	3.74	-1.11	4.86	0.00	0.00	0.00
FBpp0311086	ATPsynbeta	0.22	-0.27	0.49	0.81	0.77	0.59
FBpp0078353	Atu	4.23	-1.03	5.26	0.00	0.01	0.00
FBpp0082555	Atx2	-1.00	-0.84	-0.16	0.03	0.07	0.71
FBpp0300517	B52-RO	-1.79	-0.21	-1.57	0.00	0.49	0.00
FBpp0305308	baf	1.11	0.65	0.46	0.33	0.57	0.68
FBpp0306433	bel	-0.47	-0.85	0.37	0.38	0.12	0.49
FBpp0080048	beta'COP	0.58	-0.11	0.69	0.19	0.81	0.12
FBpp0074348	betaCOP	-0.19	-0.27	0.08	0.53	0.37	0.79
FBpp0085720	betaTub56D	-0.29	0.02	-0.32	0.48	0.96	0.45
FBpp0304072	Bruce	-0.75	2.98	-3.73	0.08	0.00	0.00
FBpp0083988	BRWD3	-0.32	-0.66	0.34	0.60	0.29	0.58
FBpp0308293	Bub3	-1.56	1.40	-2.96	0.01	0.01	0.00
FBpp0085368	BubR1	-1.47	1.40	-2.87	0.00	0.00	0.00
FBpp0291059	Caf1-55	-1.84	-1.32	-0.52	0.00	0.01	0.30
FBpp0311269	Cam	0.26	-1.07	1.33	0.69	0.12	0.05
FBpp0304507	Cand1	-1.19	-0.90	-0.30	0.03	0.09	0.56
FBpp0083684	CCT1	-0.54	-0.73	0.19	0.30	0.17	0.72
FBpp0071226	CCT2	-1.56	-1.47	-0.09	0.01	0.01	0.88
FBpp0291566	CCT3	-1.09	-0.85	-0.24	0.07	0.15	0.67
FBpp0079992	CCT4	-0.89	-0.83	-0.06	0.11	0.13	0.92
FBpp0087095	CCT5	-0.14	0.06	-0.21	0.79	0.91	0.70
FBpp0073902	CCT6	-1.79	-1.58	-0.21	0.00	0.01	0.71
FBpp0081401	CCT7	-0.25	-0.04	-0.21	0.80	0.97	0.83
FBpp0087764	CCT8	-0.85	-0.50	-0.35	0.10	0.32	0.49
FBpp0083769	Cdc16	-0.04	2.37	-2.41	0.92	0.00	0.00

FBpp0305185	Cdc23	-1.28	1.91	-3.19	0.01	0.00	0.00
FBpp0305561	Cdc27	-0.30	2.43	-2.73	0.48	0.00	0.00
FBpp0076371	Cdc6	0.27	-2.19	2.46	0.55	0.00	0.00
FBpp0289675	Cdk2	1.65	0.66	0.99	0.01	0.23	0.08
FBpp0305296	CG10077	-0.36	0.50	-0.86	0.40	0.25	0.05
FBpp0271702	CG10336	-2.34	1.87	-4.21	0.00	0.00	0.00
FBpp0087300	CG12391	0.13	2.22	-2.09	0.82	0.00	0.00
FBpp0099493	CG13175	3.67	-1.28	4.95	0.00	0.01	0.00
FBpp0302006	CG13185	-1.61	2.09	-3.69	0.00	0.00	0.00
FBpp0079879	CG14945	-2.74	-2.57	-0.17	0.00	0.00	0.66
FBpp0087535	CG1513	0.29	2.42	-2.13	0.71	0.00	0.01
FBpp0087421	CG18011	-0.74	-0.46	-0.27	0.12	0.33	0.56
FBpp0304657	CG2061	-3.70	-3.95	0.25	0.00	0.00	0.57
FBpp0078327	CG2091	3.69	-0.32	4.02	0.00	0.37	0.00
FBpp0291763	CG2246	0.96	-1.01	1.96	0.11	0.09	0.00
FBpp0290146	CG30122	-0.91	4.68	-5.59	0.03	0.00	0.00
FBpp0083880	CG31142	1.81	-2.05	3.86	0.00	0.00	0.00
FBpp0083372	CG31223	-1.45	-2.17	0.72	0.07	0.01	0.35
FBpp0309501	CG3436	1.83	-0.08	1.91	0.00	0.82	0.00
FBpp0077333	CG3542	2.29	-1.13	3.42	0.00	0.01	0.00
FBpp0307919	CG3679	0.22	0.32	-0.10	0.63	0.48	0.82
FBpp0081650	CG3909	3.82	-0.89	4.71	0.00	0.03	0.00
FBpp0309405	CG4119	2.18	-0.58	2.76	0.00	0.19	0.00
FBpp0288574	CG42232	0.17	1.84	-1.67	0.67	0.00	0.00
FBpp0079789	CG4751	-1.75	2.10	-3.85	0.00	0.00	0.00
FBpp0084626	CG4849	2.07	-0.19	2.26	0.00	0.50	0.00
FBpp0309317	CG5174-RP	-1.56	-1.23	-0.33	0.05	0.13	0.67
FBpp0074386	CG6617	-0.11	2.37	-2.49	0.76	0.00	0.00
FBpp0311284	CG6767	0.65	-1.49	2.14	0.14	0.00	0.00
FBpp0271876	CG7504	-0.36	-0.39	0.03	0.69	0.67	0.98
FBpp0074246	CG8142	0.50	0.02	0.48	0.10	0.96	0.11
FBpp0072518	CG9205	-1.55	0.10	-1.65	0.01	0.86	0.01
FBpp0088471	chb	-1.48	-2.06	0.58	0.02	0.00	0.34
FBpp0308531	Chc	-0.39	-0.24	-0.15	0.41	0.61	0.75
FBpp0099657	Chrac-14	2.54	2.76	-0.22	0.00	0.00	0.56
FBpp0308688	Chrac-16	3.09	3.49	-0.40	0.00	0.00	0.34
FBpp0311360	CkIIalpha	0.81	0.76	0.05	0.09	0.11	0.92
FBpp0305406	CkIIbeta	0.50	0.19	0.31	0.23	0.64	0.45
FBpp0312156	Claspin	-0.36	0.38	-0.74	0.37	0.33	0.07
FBpp0304513	cmet	-1.79	-1.89	0.10	0.00	0.00	0.85
FBpp0311194	coil	-1.94	-1.47	-0.47	0.00	0.01	0.40
FBpp0307637	coro	-2.02	-1.71	-0.31	0.00	0.01	0.63
FBpp0297908	ctp	-1.12	1.16	-2.28	0.15	0.13	0.01
FBpp0072562	Ctr9	2.27	-1.40	3.66	0.00	0.00	0.00
FBpp0312102	cup	-1.30	-0.14	-1.16	0.00	0.58	0.00
FBpp0294012	CycE	0.60	-1.36	1.96	0.19	0.01	0.00
FBpp0075498	DCTN1-p150	-1.53	-1.00	-0.52	0.00	0.02	0.22
FBpp0087722	DCTN2-p50	-2.20	-0.88	-1.32	0.00	0.10	0.02
FBpp0301952	dec-01	-3.28	-2.22	-1.06	0.00	0.02	0.22
FBpp0070355	deltaCOP	-0.53	-0.52	-0.01	0.14	0.15	0.97
FBpp0304991	Dhc64C	-2.39	-2.08	-0.31	0.00	0.00	0.42
FBpp0073299	Dlic	-2.02	-1.53	-0.50	0.00	0.00	0.18
FBpp0072744	dre4	0.83	-0.31	1.14	0.05	0.44	0.01
FBpp0082223	Droj2	0.14	-0.34	0.49	0.59	0.21	0.08
FBpp0304412	E(bx)	-2.47	-1.59	-0.89	0.00	0.04	0.25
FBpp0072781	ecd	2.42	-1.41	3.83	0.00	0.00	0.00
FBpp0311273	eEF1alpha1	2.36	-1.75	4.11	0.00	0.00	0.00
FBpp0311691	eEF1beta	6.67	-0.94	7.61	0.00	0.02	0.00
FBpp0079542	eEF1delta	5.68	-1.16	6.84	0.00	0.00	0.00
FBpp0305182	eEF2	-0.27	-0.29	0.02	0.62	0.59	0.97

FBpp0309768	eIF2alpha	1.73	1.73	0.00	0.00	0.00	1.00
FBpp0075700	eIF2beta	0.66	0.34	0.32	0.03	0.24	0.27
FBpp0307983	eIF2gamma	0.68	0.34	0.34	0.01	0.20	0.20
FBpp0312226	eIF3a	0.92	0.40	0.51	0.01	0.23	0.13
FBpp0086098	eIF3b	1.04	0.72	0.32	0.01	0.04	0.36
FBpp0309235	eIF3c	0.90	0.51	0.39	0.00	0.06	0.15
FBpp0088565	eIF3d1	1.23	0.72	0.51	0.00	0.06	0.17
FBpp0075104	eIF3e	0.23	0.12	0.11	0.39	0.64	0.69
FBpp0078532	eIF3f1	0.51	0.18	0.33	0.05	0.47	0.20
FBpp0070430	eIF3g1	-0.39	-0.06	-0.33	0.20	0.83	0.28
FBpp0089133	eIF3h	0.35	0.26	0.10	0.27	0.42	0.77
FBpp0078689	eIF3i	0.68	0.81	-0.13	0.05	0.02	0.70
FBpp0308512	eIF3j	-0.39	-0.28	-0.12	0.40	0.55	0.80
FBpp0071587	eIF3k	0.76	0.59	0.17	0.06	0.14	0.66
FBpp0075754	eIF3l	0.44	0.38	0.05	0.07	0.11	0.82
FBpp0308985	eIF3m	0.66	0.26	0.40	0.06	0.44	0.24
FBpp0303628	eIF4A	-1.07	-1.34	0.27	0.00	0.00	0.40
FBpp0306017	eIF4E1	-0.88	0.10	-0.98	0.00	0.71	0.00
FBpp0288389	eIF4G1	-1.77	-1.42	-0.35	0.00	0.00	0.22
FBpp0072144	eIF6	-0.43	-0.16	-0.27	0.20	0.64	0.42
FBpp0079496	Etl1	4.16	-1.37	5.52	0.00	0.00	0.00
FBpp0310097	Fcp1	-1.86	4.13	-5.99	0.00	0.00	0.00
FBpp0071892	Fib	-1.09	-1.14	0.05	0.04	0.03	0.93
FBpp0082574	FK506-bp1	-0.23	-0.61	0.38	0.62	0.20	0.42
FBpp0307052	Fmr1	-2.95	-2.72	-0.24	0.00	0.00	0.65
FBpp0304176	fmt	-1.52	-0.65	-0.87	0.05	0.38	0.24
FBpp0307786	fon	-1.46	-1.33	-0.12	0.01	0.02	0.83
FBpp0070463	fs(1)Ya	-2.30	0.92	-3.23	0.01	0.26	0.00
FBpp0294038	Fs(2)Ket	1.04	1.55	-0.50	0.00	0.00	0.12
FBpp0080391	fzy	-1.56	1.54	-3.11	0.00	0.00	0.00
FBpp0290505	gammaCOP	0.11	-0.30	0.42	0.71	0.33	0.18
FBpp0304827	gammaTub37C	-1.49	-0.66	-0.83	0.00	0.09	0.04
FBpp0304864	Gapdh2	-0.17	-0.98	0.82	0.86	0.31	0.40
FBpp0079819	Ge-1	-0.42	-0.73	0.30	0.32	0.09	0.47
FBpp0099923	GlyP	-0.16	0.42	-0.58	0.83	0.58	0.45
FBpp0305474	GlyS	0.33	0.14	0.18	0.45	0.74	0.67
FBpp0078478	Gnf1	0.43	-0.23	0.67	0.16	0.43	0.03
FBpp0080649	Grip71	-1.45	-0.63	-0.82	0.03	0.33	0.21
FBpp0073672	Grip91	-3.03	-2.46	-0.56	0.00	0.00	0.40
FBpp0072593	hfp	-3.76	-2.83	-0.93	0.00	0.00	0.23
FBpp0091111	His2A	2.59	1.78	0.81	0.00	0.00	0.15
FBpp0091155	His2B	0.00	-1.04	1.03	1.00	0.08	0.08
FBpp0091112	His3	2.59	1.52	1.06	0.00	0.00	0.01
FBpp0306146	His4r	0.96	0.07	0.90	0.04	0.88	0.06
FBpp0307465	hoip	-1.21	-1.33	0.12	0.00	0.00	0.74
FBpp0083702	HP1c	-0.53	1.08	-1.61	0.36	0.07	0.01
FBpp0084672	Hrb98DE	-4.34	-3.63	-0.71	0.00	0.00	0.36
FBpp0307982	Hsc70-4	0.01	-0.05	0.06	0.98	0.82	0.81
FBpp0312157	Hsp26	-1.22	-1.46	0.24	0.03	0.01	0.65
FBpp0312159	Hsp27	-1.54	-1.66	0.12	0.00	0.00	0.78
FBpp0305095	Hsp83	-0.05	-0.53	0.48	0.89	0.19	0.23
FBpp0289644	hyx	3.47	-1.15	4.63	0.00	0.00	0.00
FBpp0073018	ida	-0.22	2.30	-2.51	0.63	0.00	0.00
FBpp0293679	Imp	-1.82	-1.46	-0.36	0.00	0.02	0.53
FBpp0086956	Iswi	3.23	3.81	-0.58	0.00	0.00	0.11
FBpp0311371	Jafrac1	-1.47	-1.65	0.18	0.00	0.00	0.63
FBpp0074650	Kap-alpha1	3.58	0.33	3.24	0.00	0.58	0.00
FBpp0307568	Karybeta3	5.37	1.25	4.12	0.00	0.00	0.00
FBpp0300573	kis	-1.31	2.46	-3.77	0.00	0.00	0.00
FBpp0312027	Klp10A	2.28	-1.40	3.68	0.00	0.01	0.00

FBpp0075282	l(3)72Ab	1.48	-1.09	2.57	0.01	0.05	0.00
FBpp0081255	lds	1.11	-1.21	2.32	0.00	0.00	0.00
FBpp0078561	lost	-0.99	-0.92	-0.06	0.11	0.14	0.92
FBpp0309608	lva	-0.40	-1.01	0.61	0.47	0.08	0.27
FBpp0087680	Mad1	-1.61	-1.98	0.36	0.02	0.01	0.59
FBpp0076819	mad2	-1.58	0.78	-2.37	0.02	0.23	0.00
FBpp0293270	mahj	-2.91	-2.53	-0.38	0.00	0.00	0.39
FBpp0306414	Map205	1.23	-0.79	2.02	0.00	0.03	0.00
FBpp0087613	Map60	0.94	0.13	0.81	0.09	0.80	0.14
FBpp0083244	mdlc	4.80	-1.25	6.05	0.00	0.00	0.00
FBpp0079565	me31B	-1.80	-0.07	-1.74	0.00	0.84	0.00
FBpp0070749	Mlc-c	-0.07	-1.26	1.19	0.90	0.03	0.04
FBpp0301951	mod	2.97	0.19	2.78	0.00	0.71	0.00
FBpp0072065	mr	-1.04	1.65	-2.68	0.04	0.00	0.00
FBpp0079802	mre11	-1.17	-0.78	-0.39	0.07	0.22	0.54
FBpp0072830	msn	2.94	-2.49	5.43	0.00	0.00	0.00
FBpp0293343	msps	-1.88	-1.81	-0.07	0.00	0.00	0.82
FBpp0310063	mts	-2.01	-1.52	-0.49	0.00	0.02	0.43
FBpp0290680	mu2	-0.64	-0.74	0.10	0.29	0.22	0.87
FBpp0086999	muskelin	-1.72	1.05	-2.76	0.00	0.01	0.00
FBpp0297132	Nap1	2.24	1.30	0.94	0.00	0.01	0.04
FBpp0306828	NAT1	-0.92	-1.06	0.14	0.21	0.15	0.84
FBpp0309175	NO66	-1.30	-1.08	-0.22	0.00	0.02	0.60
FBpp0305169	nocte	-0.39	-0.63	0.25	0.27	0.08	0.48
FBpp0309274	nonA	-2.62	-1.69	-0.93	0.00	0.02	0.17
FBpp0083625	Nop56	-1.63	-1.74	0.11	0.12	0.10	0.91
FBpp0305035	Nopp140	-4.33	-3.91	-0.42	0.00	0.00	0.43
FBpp0079710	Nup107	-1.34	-2.47	1.12	0.01	0.00	0.03
FBpp0083695	Nup133	0.43	-1.41	1.83	0.29	0.00	0.00
FBpp0074568	Nup205	-2.25	-2.10	-0.15	0.00	0.00	0.78
FBpp0293235	Nup358	-0.34	0.12	-0.46	0.38	0.74	0.23
FBpp0082998	Nup43	0.63	-1.71	2.34	0.38	0.02	0.00
FBpp0087938	Nup44A	0.65	-1.32	1.97	0.22	0.02	0.00
FBpp0085954	Nup75	-0.54	-1.26	0.72	0.31	0.02	0.18
FBpp0085919	pAbp	-0.78	0.02	-0.81	0.03	0.94	0.02
FBpp0078405	Pcmt	-2.32	-2.53	0.21	0.00	0.00	0.70
FBpp0089395	PCNA	-0.15	-1.52	1.37	0.86	0.09	0.12
FBpp0079527	Pen	0.70	1.33	-0.63	0.03	0.00	0.04
FBpp0293516	Pep	-0.38	0.81	-1.19	0.49	0.16	0.04
FBpp0303214	Pfdn6	1.72	0.27	1.46	0.01	0.64	0.02
FBpp0305727	Phf7	2.40	-1.32	3.73	0.00	0.01	0.00
FBpp0082177	pic	1.12	-0.16	1.29	0.01	0.66	0.00
FBpp0305301	poe	-0.80	-1.23	0.43	0.09	0.01	0.36
FBpp0099722	polo	0.82	-0.02	0.84	0.08	0.96	0.07
FBpp0081704	pont	2.96	0.31	2.65	0.00	0.36	0.00
FBpp0082067	Pp1-87B	-0.85	-1.11	0.26	0.05	0.01	0.54
FBpp0308836	Pp2A-29B	-1.46	-1.06	-0.40	0.00	0.03	0.39
FBpp0312200	Pp4-19C	-1.46	-0.08	-1.38	0.02	0.89	0.03
FBpp0089154	PPP4R2r	-0.47	2.72	-3.19	0.13	0.00	0.00
FBpp0085902	Prp19	-0.32	1.59	-1.91	0.65	0.03	0.01
FBpp0087124	Prp8	2.09	-0.44	2.53	0.00	0.13	0.00
FBpp0308280	puf	-0.33	2.64	-2.96	0.42	0.00	0.00
FBpp0082932	Pxt	-1.78	-1.79	0.01	0.00	0.00	0.98
FBpp0083610	PyK	-0.82	-0.91	0.09	0.15	0.11	0.86
FBpp0304178	pzg	-0.06	-0.45	0.40	0.90	0.35	0.41
FBpp0309142	r	-0.29	-0.46	0.17	0.28	0.10	0.53
FBpp0311572	Rack1	1.02	1.06	-0.04	0.00	0.00	0.90
FBpp0293866	rad50	0.79	0.37	0.42	0.02	0.26	0.21
FBpp0305773	RAF2	-2.57	-1.32	-1.25	0.00	0.01	0.01
FBpp0309151	Ran	2.48	1.49	0.99	0.00	0.00	0.03

FBpp0312218	Ranbp9	4.53	-1.23	5.76	0.00	0.00	0.00
FBpp0297357	RanBPM	-0.35	2.17	-2.52	0.35	0.00	0.00
FBpp0306292	RanGAP	-1.19	-0.50	-0.70	0.00	0.17	0.06
FBpp0302766	REG	-1.29	0.46	-1.75	0.01	0.28	0.00
FBpp0311247	rept	0.93	-0.25	1.18	0.01	0.48	0.00
FBpp0079609	RfC3	0.85	0.43	0.42	0.01	0.13	0.14
FBpp0311114	RfC38	0.92	0.41	0.51	0.00	0.11	0.05
FBpp0073120	RfC4	0.49	0.18	0.32	0.09	0.53	0.26
FBpp0085564	rig	1.32	1.47	-0.15	0.01	0.00	0.75
FBpp0312064	rin	-1.07	-0.51	-0.56	0.14	0.48	0.44
FBpp0291753	Rm62	-1.99	-0.80	-1.19	0.01	0.23	0.08
FBpp0085156	rod	-1.07	-0.86	-0.21	0.11	0.20	0.75
FBpp0302971	row	-1.06	4.35	-5.41	0.02	0.00	0.00
FBpp0081356	RpA-70	1.23	0.94	0.28	0.01	0.04	0.52
FBpp0305226	RPA2	3.40	3.20	0.21	0.00	0.00	0.70
FBpp0310183	RPA3	-0.53	-1.38	0.85	0.40	0.04	0.19
FBpp0306039	RpL10	1.56	1.47	0.10	0.02	0.03	0.88
FBpp0075764	RpL10Ab	0.74	0.95	-0.22	0.32	0.20	0.77
FBpp0309436	RpL11	0.25	0.31	-0.06	0.56	0.47	0.89
FBpp0072085	RpL12	0.74	0.74	0.00	0.16	0.16	1.00
FBpp0302626	RpL13	1.17	1.23	-0.06	0.07	0.06	0.92
FBpp0076359	RpL14	0.87	0.99	-0.12	0.16	0.11	0.84
FBpp0300655	RpL15	0.53	0.25	0.29	0.42	0.71	0.67
FBpp0311459	RpL17	-0.57	-0.02	-0.55	0.48	0.98	0.50
FBpp0311286	RpL18	1.53	0.93	0.61	0.04	0.19	0.39
FBpp0086103	RpL18A	0.82	0.74	0.07	0.14	0.18	0.89
FBpp0089141	RpL19	-0.63	-0.36	-0.27	0.28	0.54	0.64
FBpp0311640	RpL21	0.75	0.66	0.09	0.26	0.31	0.89
FBpp0070143	RpL22	0.53	0.64	-0.11	0.40	0.31	0.86
FBpp0071808	RpL23	1.14	1.06	0.08	0.08	0.10	0.89
FBpp0072687	RpL23A	-0.26	0.29	-0.55	0.69	0.66	0.40
FBpp0311573	RpL24	1.03	1.26	-0.23	0.10	0.05	0.71
FBpp0305858	RpL26	1.72	1.66	0.06	0.01	0.01	0.92
FBpp0303780	RpL27	0.80	0.77	0.03	0.24	0.25	0.96
FBpp0311452	RpL27A	1.19	1.39	-0.20	0.10	0.06	0.78
FBpp0297522	RpL28	0.05	-0.13	0.19	0.92	0.81	0.74
FBpp0307759	RpL3	0.55	0.52	0.02	0.32	0.34	0.97
FBpp0309280	RpL30	1.77	1.76	0.01	0.01	0.01	0.99
FBpp0087610	RpL31	-0.49	-0.42	-0.07	0.41	0.47	0.91
FBpp0308319	RpL34b	0.44	1.63	-1.19	0.57	0.04	0.13
FBpp0078416	RpL35A	-0.90	-0.58	-0.32	0.17	0.37	0.62
FBpp0084617	RpL4	0.56	0.86	-0.30	0.30	0.12	0.58
FBpp0306837	RpL40	-0.82	-0.43	-0.39	0.02	0.21	0.26
FBpp0311121	RpL5	0.08	0.58	-0.50	0.89	0.31	0.38
FBpp0085166	RpL6	-0.31	0.29	-0.60	0.70	0.72	0.46
FBpp0310250	RpL7	0.98	1.13	-0.15	0.09	0.05	0.79
FBpp0311460	RpL7A	0.81	1.11	-0.30	0.20	0.09	0.63
FBpp0072802	RpL8	0.36	0.58	-0.22	0.53	0.31	0.70
FBpp0309201	RpL9	0.84	1.05	-0.21	0.21	0.12	0.75
FBpp0306232	RpLP0	-0.29	0.21	-0.50	0.59	0.70	0.36
FBpp0304265	RpLP1	0.26	0.50	-0.24	0.56	0.26	0.58
FBpp0086252	RpLP2	0.01	0.27	-0.26	0.97	0.56	0.58
FBpp0074662	Rpn1	1.34	-0.07	1.41	0.05	0.91	0.04
FBpp0078664	Rpn11	0.19	-0.64	0.83	0.82	0.45	0.32
FBpp0075068	Rpn12	-1.43	-1.94	0.51	0.01	0.00	0.28
FBpp0306599	Rpn2	0.09	0.35	-0.26	0.88	0.57	0.68
FBpp0078278	Rpn5	1.22	1.23	-0.01	0.01	0.01	0.99
FBpp0310720	RpS10b	0.74	0.91	-0.18	0.06	0.02	0.65
FBpp0087115	RpS11	0.63	0.41	0.22	0.12	0.30	0.57
FBpp0075612	RpS12	0.58	0.48	0.10	0.07	0.12	0.74

FBpp0312104	RpS13	0.42	0.35	0.06	0.60	0.66	0.94
FBpp0311458	RpS14b	0.98	0.52	0.46	0.00	0.10	0.14
FBpp0086270	RpS15	0.64	0.62	0.02	0.05	0.06	0.95
FBpp0290052	RpS15Aa	0.87	1.27	-0.39	0.05	0.01	0.35
FBpp0309759	RpS16	0.32	0.34	-0.02	0.34	0.31	0.96
FBpp0076207	RpS17	0.35	0.79	-0.45	0.64	0.29	0.55
FBpp0085586	RpS18	-0.32	-0.36	0.04	0.31	0.25	0.90
FBpp0311350	RpS19a	0.58	0.52	0.06	0.12	0.16	0.88
FBpp0311561	RpS2	1.18	1.06	0.12	0.01	0.02	0.78
FBpp0083371	RpS20	0.44	0.87	-0.43	0.43	0.12	0.44
FBpp0271801	RpS21	1.07	0.92	0.15	0.00	0.00	0.61
FBpp0308991	RpS23	1.29	1.01	0.28	0.00	0.01	0.42
FBpp0071846	RpS24	1.89	1.94	-0.05	0.00	0.00	0.89
FBpp0081846	RpS25	1.05	1.25	-0.20	0.00	0.00	0.54
FBpp0312181	RpS26	0.73	0.38	0.34	0.02	0.19	0.23
FBpp0293236	RpS27	1.10	0.90	0.20	0.01	0.02	0.59
FBpp0310057	RpS28b	0.76	0.70	0.06	0.01	0.02	0.81
FBpp0306740	RpS29	2.88	2.36	0.51	0.00	0.00	0.27
FBpp0312066	RpS3	1.04	0.86	0.17	0.00	0.00	0.54
FBpp0300615	RpS3A	-0.87	-0.98	0.11	0.02	0.01	0.75
FBpp0312080	RpS4	-0.17	0.05	-0.23	0.53	0.85	0.42
FBpp0311353	RpS5a	1.43	0.63	0.80	0.09	0.44	0.33
FBpp0082465	RpS5b	0.12	-0.47	0.58	0.83	0.39	0.28
FBpp0071087	RpS6	1.14	1.04	0.11	0.00	0.00	0.72
FBpp0308324	RpS7	0.35	0.59	-0.23	0.27	0.07	0.46
FBpp0311987	RpS8	0.52	0.60	-0.07	0.08	0.05	0.80
FBpp0309532	RpS9	0.82	0.75	0.06	0.00	0.01	0.80
FBpp0088021	Rpt1	0.52	0.02	0.49	0.24	0.96	0.26
FBpp0293948	Rpt4	-0.99	0.39	-1.39	0.31	0.68	0.16
FBpp0081601	rump	-1.20	-0.16	-1.03	0.00	0.62	0.00
FBpp0311988	Sec13	-0.09	-1.66	1.57	0.88	0.01	0.02
FBpp0311417	Sec31	-0.68	-0.07	-0.62	0.15	0.89	0.19
FBpp0082521	Set	-0.39	-0.15	-0.23	0.66	0.86	0.79
FBpp0293269	SF2	-1.73	-1.36	-0.37	0.01	0.05	0.57
FBpp0291704	Sh3beta	-3.05	-0.41	-2.65	0.00	0.53	0.00
FBpp0073893	shtd	-0.52	1.89	-2.41	0.17	0.00	0.00
FBpp0311474	SkpA	-1.87	-1.80	-0.07	0.00	0.00	0.89
FBpp0081710	sle	2.18	-0.37	2.55	0.00	0.45	0.00
FBpp0081234	SmD2	-2.60	-1.79	-0.81	0.00	0.00	0.07
FBpp0087094	SmD3	1.00	-0.26	1.25	0.05	0.60	0.02
FBpp0079182	SmE	-0.80	-2.42	1.62	0.30	0.00	0.04
FBpp0302954	Smn	0.21	-0.52	0.72	0.79	0.51	0.36
FBpp0078984	smt3	-2.64	-1.45	-1.20	0.00	0.03	0.07
FBpp0075122	spd-2	-1.87	-1.33	-0.54	0.01	0.04	0.38
FBpp0072151	Ssrp	1.42	0.26	1.16	0.00	0.43	0.00
FBpp0308666	sta	1.04	0.86	0.17	0.00	0.01	0.59
FBpp0079252	Su(var)205	1.17	0.42	0.74	0.03	0.42	0.16
FBpp0309241	sub	1.58	0.08	1.50	0.00	0.83	0.00
FBpp0311329	Svil-RW	-0.84	-2.13	1.29	0.09	0.00	0.01
FBpp0309319	sw-RO	-2.29	-1.50	-0.79	0.00	0.05	0.29
FBpp0081154	Tailor	2.10	-0.74	2.84	0.00	0.04	0.00
FBpp0310395	TER94	-3.28	-2.72	-0.57	0.00	0.00	0.50
FBpp0082180	timeout	-2.16	4.46	-6.61	0.00	0.00	0.00
FBpp0305284	tou	-1.01	2.16	-3.17	0.02	0.00	0.00
FBpp0310608	TppII	0.50	0.09	0.41	0.15	0.79	0.24
FBpp0304887	tral	-0.99	0.55	-1.54	0.00	0.04	0.00
FBpp0309477	Ubqn	-1.38	3.73	-5.11	0.00	0.00	0.00
FBpp0290875	Vha55	0.09	-0.57	0.66	0.87	0.31	0.24
FBpp0112266	vig2	0.83	0.50	0.34	0.10	0.31	0.49
FBpp0072691	Vta1	3.72	0.21	3.51	0.00	0.64	0.00

FBpp0308553	wde	-1.28	0.31	-1.59	0.02	0.54	0.00
FBpp0306779	woc	-1.24	4.22	-5.46	0.00	0.00	0.00
FBpp0312020	Yp1	-1.38	-0.99	-0.39	0.01	0.04	0.39
FBpp0308710	Yp2	-1.55	-1.33	-0.23	0.00	0.00	0.58
FBpp0311924	Yp3	-1.83	-1.46	-0.38	0.00	0.00	0.35
FBpp0075759	yps	-0.50	0.96	-1.46	0.21	0.02	0.00
FBpp0070425	Zw10	-2.19	-1.99	-0.20	0.00	0.00	0.75
FBpp0085138	Zwilch	-0.95	-1.83	0.88	0.25	0.03	0.29

b) 8E3 – control

Flybase polypeptide ID	Flybase symbol	difference 8E3-con	p-value 8E3-con	Flybase polypeptide ID	Flybase symbol	difference 8E3-con	p-value 8E3-con
FBpp0085065	**-**	-0.74	0.25	**FBpp0310551**	**mahe**	0.67	0.42
FBpp0300412	**-**	-0.78	0.17	**FBpp0085235**	**Map205**	-0.49	0.53
FBpp0304748	**-**	-1.15	0.03	**FBpp0289639**	**Mapmodulin**	0.01	0.98
FBpp0308925	**-**	-0.86	0.08	**FBpp0293580**	**mask**	-0.39	0.52
FBpp0082987	**14-3-3epsilon**	-0.81	0.09	**FBpp0311400**	**mats**	-0.74	0.12
FBpp0305137	**14-3-3zeta**	-0.13	0.79	**FBpp0300535**	**Mbs**	0.01	0.99
FBpp0075508	**26-29-p**	-0.42	0.58	**FBpp0081317**	**Mcm2**	-0.07	0.88
FBpp0085204	**Acf**	8.08	0.00	**FBpp0081756**	**Mcm5**	-0.61	0.20
FBpp0071448	**Act57B**	-1.44	0.02	**FBpp0070913**	**Mcm6**	-0.18	0.71
FBpp0311818	**Act5C**	-1.35	0.01	**FBpp0290646**	**MCPH1**	0.81	0.39
FBpp0100051	**Adh**	-1.47	0.01	**FBpp0311560**	**Mdh1**	-1.48	0.02
FBpp0086845	**AGBE**	-1.46	0.02	**FBpp0079565**	**me31B**	0.09	0.82
FBpp0312000	**Ahcy**	-1.60	0.03	**FBpp0085809**	**MetRS**	-0.23	0.70
FBpp0087757	**AIMP1**	0.78	0.23	**FBpp0081882**	**mgr**	-1.18	0.27
FBpp0075318	**AIMP2**	0.49	0.34	**FBpp0297606**	**Mlf**	1.71	0.02
FBpp0309215	**Akap200**	3.03	0.00	**FBpp0301951**	**mod**	3.12	0.00
FBpp0308680	**Ald**	-1.20	0.04	**FBpp0082692**	**mor**	1.45	0.06
FBpp0084610	**ALiX**	0.95	0.60	**FBpp0072065**	**mr**	2.38	0.00
FBpp0305102	**alpha-Spec**	0.30	0.71	**FBpp0076408**	**msk**	-0.79	0.18
FBpp0076122	**alphaTub67C**	-0.91	0.06	**FBpp0293342**	**msps**	-0.86	0.17
FBpp0081153	**alphaTub84B**	-0.46	0.29	**FBpp0304737**	**Mtor**	0.54	0.41
FBpp0290266	**AMPdeam**	3.62	0.00	**FBpp0310063**	**mts**	0.07	0.89
FBpp0307770	**AnxB9**	-2.48	0.08	**FBpp0305424**	**mub**	0.22	0.70
FBpp0082065	**Aos1**	-0.87	0.10	**FBpp0111603**	**mute**	-1.05	0.03
FBpp0301606	**APC4**	2.53	0.00	**FBpp0311394**	**Nacalpha**	-0.19	0.67
FBpp0070907	**APC7**	0.17	0.72	**FBpp0297132**	**Nap1**	0.39	0.36
FBpp0311464	**apolpp**	-0.44	0.47	**FBpp0306828**	**NAT1**	-0.06	0.89
FBpp0305852	**Arf102F**	0.07	0.88	**FBpp0311231**	**ncd**	0.99	0.06
FBpp0304364	**Arf79F**	-0.52	0.37	**FBpp0309711**	**Nedd8**	-1.62	0.02
FBpp0076271	**Argk**	-2.38	0.01	**FBpp0305289**	**NHP2**	1.33	0.02
FBpp0073965	**ArgRS**	0.01	0.98	**FBpp0309274**	**nonA**	0.17	0.81
FBpp0079751	**Art8**	-1.13	0.29	**FBpp0078997**	**nop5**	-0.26	0.63
FBpp0304830	**AsnRS**	-0.97	0.05	**FBpp0083625**	**Nop56**	0.86	0.25
FBpp0084071	**asp**	-0.16	0.71	**FBpp0290083**	**Nop60B**	1.52	0.22
FBpp0304013	**AspRS-m**	0.88	0.08	**FBpp0305034**	**Nopp140**	1.05	0.06
FBpp0308483	**AspRS**	-0.38	0.46	**FBpp0308486**	**Not1**	0.19	0.80
FBpp0289825	**ATPCL**	-1.41	0.02	**FBpp0112220**	**Nph**	-1.84	0.09
FBpp0311086	**ATPsynbeta**	1.07	0.03	**FBpp0312079**	**Nplp2**	0.23	0.85
FBpp0082555	**Atx2**	-0.88	0.15	**FBpp0297079**	**nudC**	-1.29	0.04
FBpp0312191	**awd**	-0.22	0.70	**FBpp0310208**	**Nup160**	0.01	0.98
FBpp0300517	**B52**	1.84	0.00	**FBpp0074568**	**Nup205**	0.31	0.65
FBpp0307124	**Bacc**	0.77	0.17	**FBpp0293235**	**Nup358**	-0.24	0.69

FBpp0305308	**baf**	1.61	0.07	**FBpp0073659**	**Nup93-1**	-0.17	0.79
FBpp0086115	**Bap55**	-0.49	0.28	**FBpp0306915**	**Nup98-96**	0.80	0.59
FBpp0306433	**bel**	-0.23	0.65	**FBpp0271761**	**Nurf-38**	-0.80	0.09
FBpp0305067	**ben**	-0.76	0.14	**FBpp0072061**	**or**	-1.39	0.08
FBpp0080048	**beta'COP**	0.92	0.16	**FBpp0082329**	**Orc2**	1.10	0.15
FBpp0074348	**betaCOP**	0.31	0.61	**FBpp0086882**	**Orc3**	2.08	0.02
FBpp0085720	**betaTub56D**	-0.96	0.03	**FBpp0072330**	**Orc4**	1.08	0.04
FBpp0082428	**BigH1**	1.43	0.00	**FBpp0080120**	**Orc5**	2.15	0.03
FBpp0071794	**blw**	-0.42	0.61	**FBpp0300672**	**p23**	-0.49	0.41
FBpp0304073	**Bruce**	3.65	0.00	**FBpp0085919**	**pAbp**	-0.51	0.32
FBpp0308293	**Bub3**	1.93	0.01	**FBpp0073976**	**Paf-AHalpha**	2.63	0.18
FBpp0085368	**BubR1**	2.34	0.00	**FBpp0305933**	**Paics**	0.02	0.98
FBpp0309346	**cactin**	1.19	0.25	**FBpp0308411**	**PAN2**	0.08	0.86
FBpp0071172	**Caf1-180**	0.88	0.11	**FBpp0112608**	**Parp**	2.09	0.01
FBpp0082511	**Caf1-55**	0.20	0.69	**FBpp0078405**	**Pcmt**	-1.52	0.02
FBpp0311269	**Cam**	-0.73	0.22	**FBpp0089395**	**PCNA**	-0.27	0.64
FBpp0304507	**Cand1**	-0.75	0.13	**FBpp0086647**	**pea**	-1.27	0.01
FBpp0084818	**Cap-D2**	0.81	0.14	**FBpp0079527**	**Pen**	-0.13	0.79
FBpp0099391	**capt**	-1.16	0.04	**FBpp0293516**	**Pep**	0.88	0.31
FBpp0083684	**CCT1**	-0.43	0.29	**FBpp0304954**	**Pfdn2**	0.02	0.98
FBpp0071226	**CCT2**	-0.82	0.08	**FBpp0293464**	**Pfk**	-1.19	0.12
FBpp0291566	**CCT3**	-0.44	0.26	**FBpp0303827**	**Pgd**	-0.09	0.93
FBpp0079992	**CCT4**	-0.41	0.34	**FBpp0087762**	**Pgi**	-0.58	0.42
FBpp0087095	**CCT5**	-0.31	0.54	**FBpp0306279**	**Pgk**	-2.10	0.02
FBpp0073902	**CCT6**	-1.39	0.15	**FBpp0099920**	**Pglym78**	-1.80	0.02
FBpp0081401	**CCT7**	-1.10	0.10	**FBpp0075247**	**Pgm**	0.63	0.64
FBpp0087764	**CCT8**	-0.90	0.10	**FBpp0301844**	**PI31**	0.23	0.86
FBpp0083769	**Cdc16**	2.30	0.01	**FBpp0082177**	**pic**	-0.34	0.42
FBpp0305185	**Cdc23**	2.58	0.00	**FBpp0076285**	**pix**	0.95	0.40
FBpp0305561	**Cdc27**	2.67	0.00	**FBpp0310466**	**Plap**	-0.74	0.19
FBpp0076371	**Cdc6**	0.17	0.87	**FBpp0305301**	**poe**	0.48	0.29
FBpp0079641	**Cdk1**	-0.34	0.40	**FBpp0099722**	**polo**	-0.01	0.99
FBpp0308475	**ced-6**	0.28	0.55	**FBpp0081704**	**pont**	-1.16	0.26
FBpp0306293	**CG10237**	-1.06	0.09	**FBpp0082067**	**Pp1-87B**	-0.11	0.81
FBpp0075686	**CG10418**	0.33	0.55	**FBpp0301546**	**Pp2B-14D**	-0.83	0.11
FBpp0311825	**CG10576**	-1.30	0.05	**FBpp0312200**	**Pp4-19C**	3.09	0.00
FBpp0292528	**CG11089**	-0.75	0.40	**FBpp0089154**	**PPP4R2r**	3.30	0.00
FBpp0112044	**CG11486**	-0.63	0.37	**FBpp0303849**	**PpV**	1.01	0.06
FBpp0084759	**CG11899**	0.06	0.95	**FBpp0082062**	**Prosalpha2**	-0.14	0.77
FBpp0072658	**CG12018**	-0.84	0.51	**FBpp0086067**	**Prosalpha5**	0.16	0.70
FBpp0078279	**CG1218**	0.54	0.55	**FBpp0310201**	**Prosalpha6**	0.19	0.69
FBpp0083036	**CG12321**	0.18	0.80	**FBpp0086400**	**Prosbeta1**	-0.31	0.42
FBpp0302006	**CG13185**	1.70	0.34	**FBpp0075382**	**Prosbeta2**	-0.47	0.26
FBpp0070154	**CG13364**	-0.65	0.18	**FBpp0087320**	**Prosbeta5**	0.81	0.30
FBpp0307859	**CG1354**	-1.17	0.03	**FBpp0075119**	**Prosbeta6**	-0.38	0.39
FBpp0085260	**CG1416**	-0.94	0.10	**FBpp0078449**	**Prosbeta7**	2.00	0.15
FBpp0308525	**CG1440**	-0.31	0.82	**FBpp0085902**	**Prp19**	1.39	0.02
FBpp0079879	**CG14945**	-1.45	0.01	**FBpp0087124**	**Prp8**	2.34	0.06
FBpp0087535	**CG1513**	5.97	0.00	**FBpp0308280**	**puf**	4.88	0.00
FBpp0112211	**CG1646**	1.31	0.36	**FBpp0082932**	**Pxt**	-0.99	0.11
FBpp0297346	**CG17018**	-0.14	0.84	**FBpp0083611**	**PyK**	-0.80	0.09
FBpp0085374	**CG17337**	-1.52	0.02	**FBpp0297295**	**qua**	-0.42	0.76
FBpp0311847	**CG18067**	0.89	0.20	**FBpp0309142**	**r**	-0.01	0.98
FBpp0271746	**CG18190**	-0.62	0.21	**FBpp0083414**	**Rab11**	-1.57	0.02
FBpp0072674	**CG2021**	0.54	0.27	**FBpp0303520**	**Rab5**	-0.46	0.32
FBpp0304657	**CG2061**	-1.27	0.03	**FBpp0311572**	**Rack1**	0.70	0.32
FBpp0311613	**CG2852**	-0.87	0.10	**FBpp0071600**	**Rae1**	-0.84	0.15
FBpp0307127	**CG2862**	1.41	0.01	**FBpp0309151**	**Ran**	-1.00	0.06
FBpp0290146	**CG30122**	3.77	0.00	**FBpp0312218**	**Ranbp9**	-0.50	0.41
FBpp0291433	**CG30382**	-0.81	0.14	**FBpp0297357**	**RanBPM**	2.57	0.00

FBpp0307202	**CG31549**	0.04	0.98	**FBpp0306292**	**RanGAP**	0.34	0.44
FBpp0110163	**CG3689**	-0.63	0.13	**FBpp0311247**	**rept**	-0.41	0.42
FBpp0081650	**CG3909**	0.36	0.46	**FBpp0079609**	**RfC3**	1.43	0.01
FBpp0288574	**CG42232**	5.05	0.00	**FBpp0311114**	**RfC38**	0.36	0.58
FBpp0310306	**CG4747**	-0.52	0.40	**FBpp0073120**	**RfC4**	1.01	0.07
FBpp0079789	**CG4751**	3.58	0.00	**FBpp0305319**	**rhea**	0.00	1.00
FBpp0077868	**CG4858**	0.26	0.86	**FBpp0304185**	**RhoGDI**	-0.80	0.08
FBpp0112210	**CG4951**	-0.69	0.22	**FBpp0086441**	**Rif1**	-0.79	0.42
FBpp0309317	**CG5174**	-0.26	0.62	**FBpp0312064**	**rin**	-0.23	0.61
FBpp0084312	**CG5913**	3.18	0.03	**FBpp0291753**	**Rm62**	1.38	0.13
FBpp0303937	**CG6084**	-1.71	0.01	**FBpp0310006**	**rngo**	-0.32	0.68
FBpp0083213	**CG6195**	-0.38	0.50	**FBpp0079648**	**RnrL**	-0.52	0.34
FBpp0079809	**CG6287**	-1.98	0.01	**FBpp0087152**	**RnrS**	-0.81	0.13
FBpp0080044	**CG6523**	-1.38	0.03	**FBpp0085156**	**rod**	1.35	0.17
FBpp0307760	**CG6693**	1.45	0.05	**FBpp0302971**	**row**	5.35	0.00
FBpp0309927	**CG6907**	0.73	0.26	**FBpp0305404**	**Rox8**	-0.74	0.15
FBpp0088545	**CG7730**	1.12	0.13	**FBpp0081356**	**RpA-70**	0.42	0.42
FBpp0303962	**CG8003**	-1.27	0.09	**FBpp0305226**	**RPA2**	0.53	0.38
FBpp0081371	**CG8036**	-1.28	0.02	**FBpp0310183**	**RPA3**	0.57	0.31
FBpp0081398	**CG8223**	-0.75	0.23	**FBpp0084067**	**Rpb10**	2.47	0.17
FBpp0087733	**CG8243**	2.65	0.03	**FBpp0296955**	**Rpi**	-1.22	0.07
FBpp0087116	**CG8858**	0.60	0.56	**FBpp0306039**	**RpL10**	0.67	0.66
FBpp0311963	**CG9135**	-0.96	0.07	**FBpp0075764**	**RpL10Ab**	1.47	0.18
FBpp0072560	**CG9149**	-1.20	0.06	**FBpp0309436**	**RpL11**	1.15	0.29
FBpp0072518	**CG9205**	4.29	0.00	**FBpp0072085**	**RpL12**	0.69	0.36
FBpp0309269	**CG9281**	-0.44	0.32	**FBpp0302626**	**RpL13**	0.34	0.67
FBpp0074708	**CG9330**	0.54	0.66	**FBpp0078354**	**RpL13A**	1.12	0.15
FBpp0071449	**CG9344**	0.60	0.26	**FBpp0076359**	**RpL14**	0.43	0.51
FBpp0305785	**CG9674**	0.31	0.77	**FBpp0300655**	**RpL15**	1.52	0.09
FBpp0088471	**chb**	1.70	0.03	**FBpp0311459**	**RpL17**	1.32	0.32
FBpp0308531	**Chc**	-0.10	0.81	**FBpp0311286**	**RpL18**	0.38	0.72
FBpp0301152	**chic**	-1.40	0.04	**FBpp0086103**	**RpL18A**	0.41	0.71
FBpp0083939	**CHORD**	-0.70	0.59	**FBpp0311640**	**RpL21**	1.10	0.24
FBpp0099657	**Chrac-14**	7.30	0.00	**FBpp0071808**	**RpL23**	-0.08	0.90
FBpp0308688	**Chrac-16**	6.18	0.00	**FBpp0072687**	**RpL23A**	1.79	0.12
FBpp0310070	**cib**	-1.77	0.02	**FBpp0311573**	**RpL24**	1.22	0.26
FBpp0311360	**CkIIalpha**	1.17	0.02	**FBpp0303780**	**RpL27**	1.98	0.12
FBpp0305406	**CkIIbeta**	0.51	0.29	**FBpp0311452**	**RpL27A**	1.72	0.14
FBpp0304514	**cmet**	0.03	0.96	**FBpp0297522**	**RpL28**	0.86	0.40
FBpp0292516	**CNBP**	-0.55	0.23	**FBpp0309280**	**RpL30**	2.61	0.07
FBpp0307640	**coro**	-1.15	0.08	**FBpp0113047**	**RpL32**	1.94	0.15
FBpp0304020	**cpb**	0.70	0.68	**FBpp0308319**	**RpL34b**	1.42	0.15
FBpp0080484	**Cse1**	-0.99	0.08	**FBpp0311481**	**RpL36**	1.06	0.16
FBpp0083658	**CSN6**	0.23	0.72	**FBpp0291726**	**RpL37A**	-0.37	0.61
FBpp0087821	**CSN7**	-0.45	0.48	**FBpp0084617**	**RpL4**	0.93	0.27
FBpp0086732	**Ctf4**	-1.09	0.07	**FBpp0311121**	**RpL5**	1.52	0.11
FBpp0072562	**Ctr9**	-0.34	0.47	**FBpp0310250**	**RpL7**	1.54	0.16
FBpp0312102	**cup**	-1.60	0.10	**FBpp0311460**	**RpL7A**	2.07	0.15
FBpp0074017	**Cyp1**	-1.29	0.02	**FBpp0072802**	**RpL8**	1.77	0.11
FBpp0086373	**CysRS**	1.26	0.15	**FBpp0306232**	**RpLP0**	0.58	0.46
FBpp0290739	**D1**	3.17	0.00	**FBpp0304265**	**RpLP1**	0.96	0.26
FBpp0112438	**Dbp80**	-0.38	0.51	**FBpp0086252**	**RpLP2**	0.51	0.39
FBpp0306615	**dco**	0.05	0.96	**FBpp0074662**	**Rpn1**	-0.89	0.19
FBpp0305164	**Dek**	-0.03	0.95	**FBpp0305644**	**Rpn10**	-0.48	0.27
FBpp0291138	**deltaCOP**	0.33	0.60	**FBpp0078664**	**Rpn11**	-0.55	0.21
FBpp0099688	**Df31**	-1.55	0.02	**FBpp0075068**	**Rpn12**	0.06	0.89
FBpp0084783	**dgt6**	-0.97	0.40	**FBpp0306599**	**Rpn2**	0.64	0.34
FBpp0099973	**Dhpr**	-0.80	0.25	**FBpp0307804**	**Rpn3**	0.40	0.44
FBpp0307849	**Dhx15**	-0.02	0.96	**FBpp0078278**	**Rpn5**	-0.01	0.99
FBpp0082996	**Dlc90F**	2.40	0.03	**FBpp0297513**	**Rpn6**	0.27	0.63

FBpp0076830	**DnaJ-1**	0.12	0.78	**FBpp0083687**	**Rpn7**	-0.39	0.36
FBpp0075277	**DNApol-delta**	0.24	0.59	**FBpp0305141**	**Rpn8**	-0.33	0.49
FBpp0311418	**Dp1**	0.47	0.27	**FBpp0083861**	**Rpn9**	0.55	0.34
FBpp0311783	**dpa**	-0.55	0.21	**FBpp0310720**	**RpS10b**	-0.05	0.92
FBpp0072744	**dre4**	1.77	0.01	**FBpp0087115**	**RpS11**	1.29	0.06
FBpp0086817	**drk**	0.01	0.99	**FBpp0075612**	**RpS12**	0.86	0.38
FBpp0082223	**Droj2**	-0.51	0.26	**FBpp0312104**	**RpS13**	1.67	0.02
FBpp0307166	**Drp1**	-0.47	0.54	**FBpp0311458**	**RpS14b**	0.78	0.20
FBpp0079746	**dUTPase**	-2.06	0.00	**FBpp0086270**	**RpS15**	0.89	0.63
FBpp0311273	**eEF1alpha1**	-1.22	0.02	**FBpp0309759**	**RpS16**	0.19	0.73
FBpp0311691	**eEF1beta**	-0.65	0.14	**FBpp0076207**	**RpS17**	-0.20	0.68
FBpp0079542	**eEF1delta**	-0.80	0.14	**FBpp0085586**	**RpS18**	-0.62	0.53
FBpp0305182	**eEF2**	-1.14	0.02	**FBpp0311350**	**RpS19a**	0.58	0.34
FBpp0072082	**eEF5**	-1.42	0.06	**FBpp0311561**	**RpS2**	1.44	0.12
FBpp0307824	**eff**	1.22	0.40	**FBpp0308991**	**RpS23**	0.89	0.23
FBpp0310418	**eIF1A**	-1.56	0.04	**FBpp0071846**	**RpS24**	1.10	0.17
FBpp0309768	**eIF2alpha**	-0.37	0.37	**FBpp0081846**	**RpS25**	0.07	0.92
FBpp0075700	**eIF2beta**	0.64	0.27	**FBpp0079606**	**RpS27A**	0.48	0.31
FBpp0307983	**eIF2gamma**	-0.22	0.62	**FBpp0310057**	**RpS28b**	1.04	0.48
FBpp0088565	**eIF3d1**	1.80	0.00	**FBpp0306740**	**RpS29**	0.68	0.39
FBpp0075104	**eIF3e**	0.49	0.31	**FBpp0312066**	**RpS3**	0.67	0.28
FBpp0078532	**eIF3f1**	-0.68	0.22	**FBpp0311976**	**RpS30**	0.74	0.42
FBpp0078689	**eIF3i**	-0.67	0.53	**FBpp0300615**	**RpS3A**	1.18	0.08
FBpp0071587	**eIF3k**	-0.19	0.68	**FBpp0312080**	**RpS4**	1.10	0.07
FBpp0075754	**eIF3l**	-0.93	0.08	**FBpp0311353**	**RpS5a**	1.59	0.06
FBpp0303628	**eIF4A**	-0.87	0.07	**FBpp0071087**	**RpS6**	0.55	0.58
FBpp0288389	**eIF4G1**	-1.23	0.06	**FBpp0308324**	**RpS7**	0.24	0.73
FBpp0301573	**eIF5B**	1.20	0.30	**FBpp0311987**	**RpS8**	1.46	0.06
FBpp0311547	**Eip55E**	-1.10	0.15	**FBpp0309532**	**RpS9**	1.18	0.33
FBpp0088654	**elg1**	0.47	0.59	**FBpp0311982**	**Rpt2**	0.20	0.67
FBpp0083354	**EloB**	-0.46	0.25	**FBpp0312031**	**Rpt3**	-0.23	0.59
FBpp0085725	**EloC**	-0.54	0.31	**FBpp0293948**	**Rpt4**	-0.62	0.23
FBpp0307426	**Elp1**	0.43	0.73	**FBpp0083843**	**Rpt5**	-0.61	0.26
FBpp0305267	**endos**	-1.22	0.03	**FBpp0288680**	**Rrp1**	1.76	0.04
FBpp0077574	**Eno**	-1.80	0.01	**FBpp0081601**	**rump**	0.27	0.73
FBpp0304201	**eRF1**	0.06	0.89	**FBpp0081088**	**Sas-4**	0.59	0.64
FBpp0079496	**Etl1**	0.36	0.47	**FBpp0297362**	**SC35**	0.43	0.33
FBpp0099726	**fabp**	-1.44	0.04	**FBpp0306437**	**ScsbetaA**	0.61	0.37
FBpp0307371	**FASN1**	1.37	0.38	**FBpp0074285**	**scu**	-0.54	0.45
FBpp0310097	**Fcp1**	5.87	0.00	**FBpp0082877**	**sds22**	-0.74	0.13
FBpp0081767	**Fdh**	-1.15	0.06	**FBpp0083932**	**Sec10**	0.27	0.55
FBpp0071892	**Fib**	-0.45	0.32	**FBpp0087723**	**Sec31**	0.48	0.28
FBpp0271718	**Fis1**	-0.03	0.96	**FBpp0307454**	**SerRS**	-1.31	0.01
FBpp0083551	**fit**	-1.29	0.06	**FBpp0089160**	**sgg**	-0.12	0.87
FBpp0085703	**Fkbp12**	-0.93	0.12	**FBpp0296963**	**Sgt**	-1.18	0.04
FBpp0082574	**Fkbp39**	1.57	0.01	**FBpp0291704**	**Sh3beta**	2.11	0.01
FBpp0309663	**Fkbp59**	-1.35	0.02	**FBpp0305866**	**shi**	-0.64	0.29
FBpp0311112	**flfl**	2.39	0.00	**FBpp0070792**	**Shmt**	-0.14	0.89
FBpp0075581	**flr**	-1.66	0.01	**FBpp0073893**	**shtd**	2.06	0.00
FBpp0300445	**Fmr1**	0.31	0.70	**FBpp0311474**	**SkpA**	1.19	0.25
FBpp0304175	**fmt**	1.66	0.01	**FBpp0081709**	**sle**	1.48	0.00
FBpp0290502	**fon**	-1.46	0.02	**FBpp0293061**	**SmB**	1.44	0.35
FBpp0070463	**fs(1)Ya**	0.40	0.47	**FBpp0086591**	**SMC2**	0.55	0.19
FBpp0294038	**Fs(2)Ket**	0.62	0.16	**FBpp0075684**	**SmD1**	0.08	0.88
FBpp0080391	**fzy**	3.69	0.00	**FBpp0081234**	**SmD2**	0.15	0.71
FBpp0290505	**gammaCOP**	-0.05	0.91	**FBpp0079182**	**SmE**	-0.40	0.44
FBpp0304827	**gammaTub37**	0.68	0.21	**FBpp0078984**	**smt3**	-1.50	0.03
FBpp0099914	**Gapdh1**	-0.87	0.13	**FBpp0078331**	**Snr1**	0.30	0.65
FBpp0304864	**Gapdh2**	-1.22	0.02	**FBpp0075958**	**Sod1**	-1.34	0.02
FBpp0311558	**Gdi**	-0.92	0.12	**FBpp0075122**	**spd-2**	0.29	0.63

FBpp0079819	**Ge-1**	-0.28	0.51	**FBpp0297149**	**SpdS**	-0.84	0.10
FBpp0077263	**gkt**	-0.16	0.80	**FBpp0301102**	**sqd**	-0.54	0.23
FBpp0084240	**GlnRS**	-0.01	0.99	**FBpp0079471**	**Srp54**	0.20	0.80
FBpp0088858	**glo**	1.09	0.08	**FBpp0076872**	**Srp54k**	0.24	0.54
FBpp0080489	**glu**	0.25	0.60	**FBpp0076244**	**Srp68**	0.31	0.44
FBpp0083898	**GluProRS**	0.03	0.94	**FBpp0079211**	**Ssb-c31a**	-0.03	0.96
FBpp0099923	**GlyP**	-0.64	0.18	**FBpp0072151**	**Ssrp**	2.87	0.00
FBpp0082496	**GlyS**	0.60	0.21	**FBpp0308666**	**sta**	-0.42	0.29
FBpp0078478	**Gnf1**	0.73	0.23	**FBpp0077790**	**Stip1**	-1.20	0.07
FBpp0075793	**Grip163**	0.26	0.73	**FBpp0300967**	**Stlk**	3.99	0.01
FBpp0080649	**Grip71**	1.72	0.00	**FBpp0307636**	**Strn-Mlck-RV**	1.77	0.14
FBpp0290523	**Grip84**	2.86	0.00	**FBpp0079252**	**Su(var)205**	0.83	0.10
FBpp0073672	**Grip91**	2.78	0.00	**FBpp0290871**	**Su(var)3-7**	2.78	0.03
FBpp0310520	**grsm**	0.31	0.57	**FBpp0311334**	**SvilB**	-1.42	0.05
FBpp0085855	**GstE6**	-0.49	0.65	**FBpp0303744**	**swm**	1.01	0.38
FBpp0099646	**GstS1**	-0.59	0.32	**FBpp0078372**	**Sym**	0.59	0.60
FBpp0302680	**gw**	-1.73	0.06	**FBpp0072050**	**Taldo**	-0.75	0.35
FBpp0290108	**Gyf**	-1.43	0.02	**FBpp0081820**	**Tctp**	-1.38	0.03
FBpp0078319	**Hat1**	-0.48	0.40	**FBpp0087479**	**TER94**	-0.75	0.14
FBpp0073173	**HDAC1**	-0.23	0.63	**FBpp0083355**	**TFAM**	1.79	0.14
FBpp0078756	**Hel25E**	-1.02	0.13	**FBpp0312095**	**ThrRS**	-0.99	0.08
FBpp0078162	**Hem**	1.02	0.40	**FBpp0082180**	**timeout**	6.22	0.00
FBpp0072593	**hfp**	0.28	0.52	**FBpp0077346**	**toc**	-0.93	0.17
FBpp0305905	**HIP-R**	-0.81	0.18	**FBpp0087193**	**tou**	4.79	0.00
FBpp0091111	**His2A**	2.24	0.05	**FBpp0084948**	**Tpi**	-1.13	0.07
FBpp0306426	**His2Av**	1.54	0.09	**FBpp0310608**	**TppII**	1.87	0.02
FBpp0091155	**His2B**	0.35	0.38	**FBpp0304887**	**tral**	0.35	0.42
FBpp0306146	**His4r**	1.46	0.01	**FBpp0079437**	**Trx-2**	-0.19	0.78
FBpp0305939	**HisRS**	-1.06	0.04	**FBpp0071117**	**Trxr-1**	-1.90	0.03
FBpp0307711	**HnRNP-K**	-0.05	0.91	**FBpp0310349**	**Ts**	-0.23	0.64
FBpp0307465	**hoip**	-0.40	0.35	**FBpp0312205**	**Tsf1**	-1.11	0.03
FBpp0301605	**HP1b**	3.52	0.00	**FBpp0072097**	**tsr**	-1.11	0.04
FBpp0083702	**HP1c**	4.40	0.00	**FBpp0304417**	**Tudor-SN**	-0.98	0.15
FBpp0297875	**Hrb27C**	-0.91	0.07	**FBpp0083956**	**twin**	0.10	0.90
FBpp0306562	**Hrb87F**	-0.14	0.78	**FBpp0311386**	**tws**	-0.21	0.67
FBpp0084672	**Hrb98DE**	-0.01	0.98	**FBpp0076804**	**Txl**	-0.05	0.91
FBpp0311376	**Hsc70-3**	-1.24	0.01	**FBpp0075168**	**TyrRS**	-0.56	0.24
FBpp0307982	**Hsc70-4**	-0.92	0.04	**FBpp0305600**	**U2af38**	-1.30	0.09
FBpp0308990	**Hsc70-5**	-1.82	0.05	**FBpp0298007**	**U2af50**	-0.36	0.58
FBpp0305265	**Hsc70Cb**	-1.48	0.02	**FBpp0087583**	**Uba1**	-1.06	0.08
FBpp0312157	**Hsp26**	-1.25	0.04	**FBpp0076457**	**Uba2**	-0.60	0.39
FBpp0312159	**Hsp27**	-0.76	0.16	**FBpp0309477**	**Ubqn**	4.89	0.00
FBpp0305095	**Hsp83**	-1.51	0.02	**FBpp0292511**	**Uch**	-1.15	0.08
FBpp0073018	**ida**	2.64	0.00	**FBpp0311276**	**Uev1A**	-0.79	0.15
FBpp0078152	**IleRS**	0.27	0.65	**FBpp0290913**	**UGP**	-0.25	0.62
FBpp0081861	**Irbp**	-0.09	0.85	**FBpp0311454**	**und**	0.56	0.28
FBpp0086956	**Iswi**	7.25	0.00	**FBpp0087607**	**Updo**	-0.05	0.96
FBpp0311371	**Jafrac1**	-1.65	0.01	**FBpp0304059**	**Usp14**	-0.64	0.15
FBpp0307568	**Karybeta3**	-0.90	0.08	**FBpp0298309**	**Usp5**	0.08	0.94
FBpp0289115	**kis**	4.57	0.00	**FBpp0073474**	**Usp7**	0.72	0.20
FBpp0312027	**Klp10A**	-0.11	0.81	**FBpp0311933**	**Vha13**	-0.19	0.82
FBpp0309092	**Klp3A**	1.32	0.10	**FBpp0086468**	**Vha36-1**	-0.90	0.23
FBpp0072616	**Klp61F**	2.20	0.03	**FBpp0290875**	**Vha55**	-0.82	0.07
FBpp0078399	**kra**	-0.38	0.59	**FBpp0307597**	**Vha68-2**	-1.66	0.01
FBpp0080322	**Ku80**	1.00	0.21	**FBpp0112266**	**vig2**	-0.77	0.23
FBpp0080906	**La**	-0.01	0.98	**FBpp0077625**	**Vps29**	7.81	0.00
FBpp0312110	**Lam**	-0.85	0.06	**FBpp0072691**	**Vta1**	3.35	0.01
FBpp0081255	**lds**	-0.90	0.40	**FBpp0300790**	**wds**	-0.09	0.87
FBpp0311704	**LeuRS**	-0.45	0.53	**FBpp0289361**	**wech**	-0.39	0.39
FBpp0073551	**lic**	-0.63	0.18	**FBpp0112025**	**wmd**	1.37	0.40

FBpp0303481	**lig**	-0.37	0.39	**FBpp0306779**	**woc**	5.41	0.00
FBpp0088383	**lola**	1.23	0.61	**FBpp0304606**	**x16**	0.16	0.73
FBpp0078561	**lost**	0.19	0.66	**FBpp0303324**	**yem**	0.32	0.78
FBpp0310328	**LSm7**	1.82	0.05	**FBpp0312020**	**Yp1**	-0.66	0.18
FBpp0309608	**lva**	0.86	0.45	**FBpp0308710**	**Yp2**	-1.09	0.03
FBpp0292593	**LysRS**	0.14	0.78	**FBpp0311924**	**Yp3**	-0.84	0.11
FBpp0087680	**Mad1**	-0.42	0.57	**FBpp0075111**	**zetaCOP**	-0.08	0.95
FBpp0076819	**mad2**	2.87	0.00	**FBpp0085138**	**Zwilch**	-0.63	0.57

C. ChIP-Seq profiles of γH2A.V on BAF-coupled FlyFosmids

(see VI.B.3)

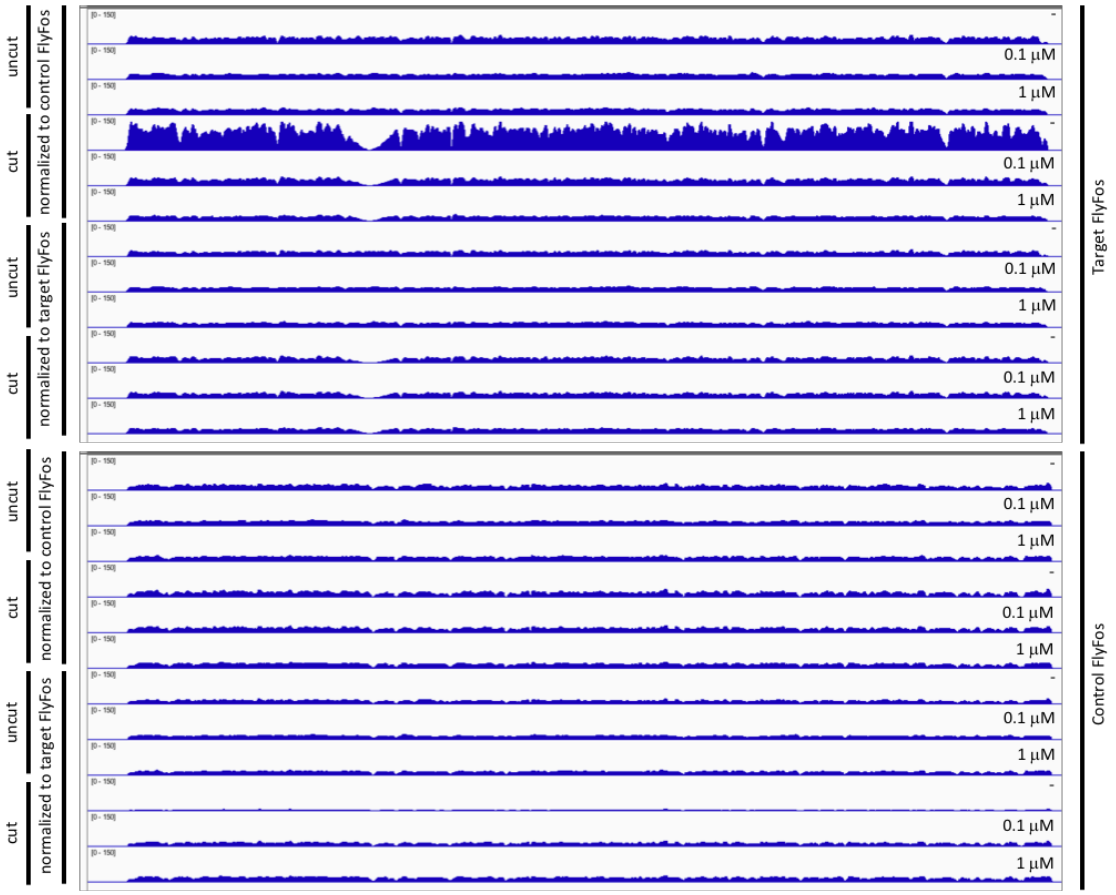

Figure 100: γH2A.V profiles from ChIP-Seq on a mix of circular control FlyFosmid and either circular or liearized target FlyFosmid preincubated with 0.1 µM or 1 µM BAF, or no BAF (-) as a control. Uncut: both FlyFosmid are circular; cut: the control FlyFosmid is circular, the target FlyFosmid is linearized. Signals were either normalized to the reads on the target FlyFosmid or to the control FlyFosmid